Computational & Multiscale Mechanics of Materials

CM3

www.ltas-cm3.ulg.ac.be

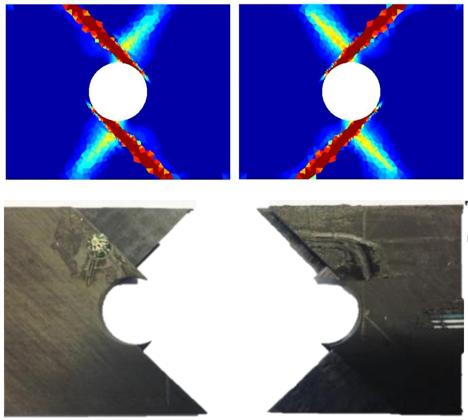

Non-local damage mean-field-homogenization

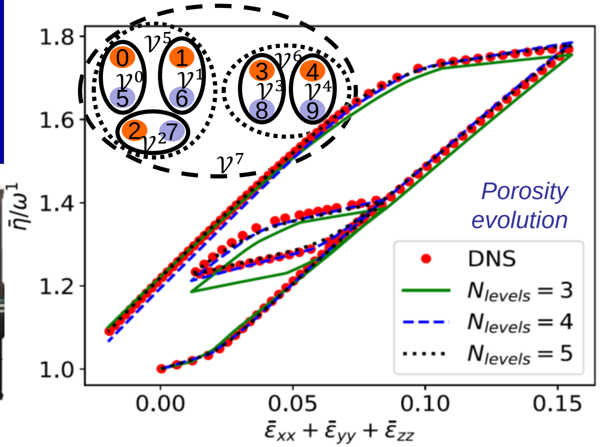

Deep-Material-Networks

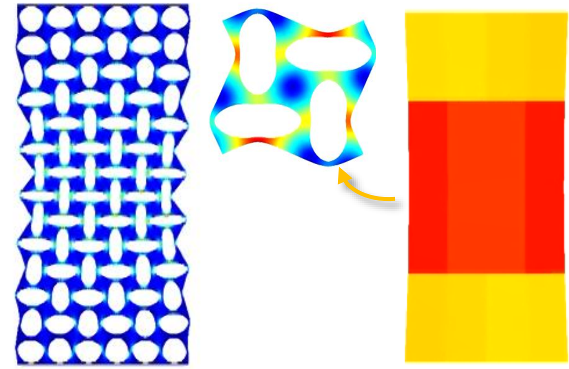

FE2 homogenization of metamaterials

Stochastic multi-scale methods

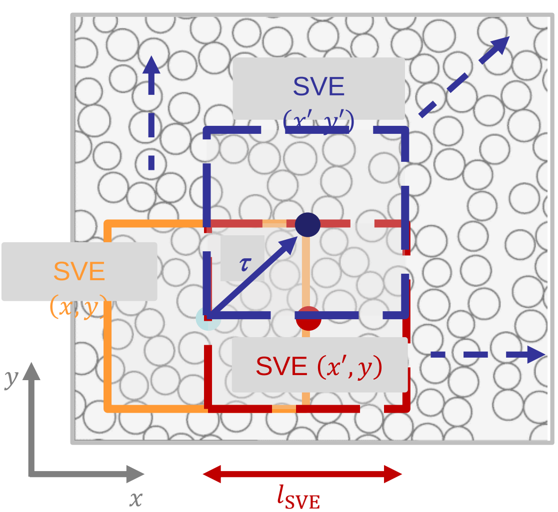

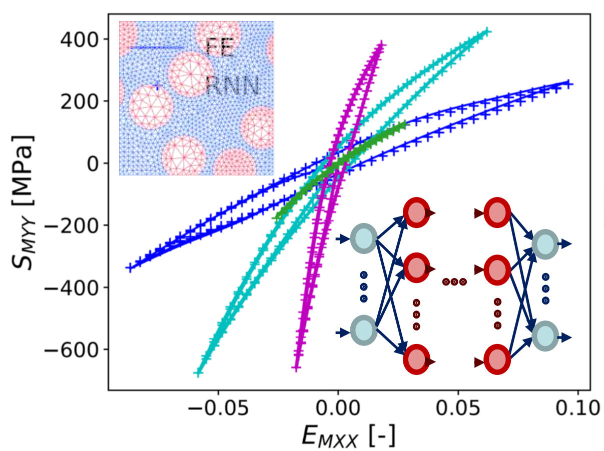

Data-driven multi-scale simulations

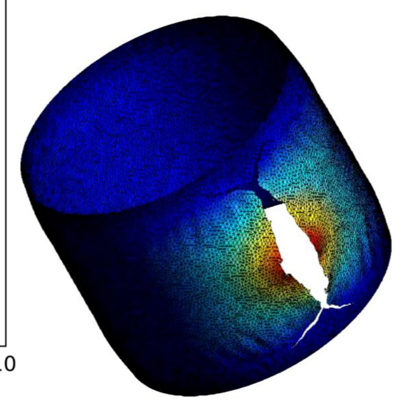

DG-based fracture

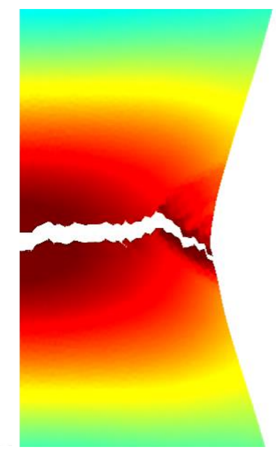

Nonlocal Gurson to crack transition

LIÈGE université

July 2022 - CM3 research projects

Direct links

- Data-driven approaches
  - Deep Material Networks from the interactions viewpoint ;
  - Mean-Field-Based Deep Material Networks for woven composites ;
  - Recurrent Neural Network-accelerated multi-scale simulations in elasto-plasticity ;
  - Recurrent Neural Network with dimensionality reduction and break down ;
  - Bayesian identification of stochastic MFH model parameters ;
- Complex constitutive models for failure prediction under complex loading states
  - Shear and necking coalescence model for porous materials ;
  - Ductile failure of High-Entropy Alloys (HEA) ;
  - Damage-enhanced viscoelastic-viscoplastic finite strain model for crosslinked resin ;
- Homogenization & Multi-Scale methods
  - Second order Computational Homogenization for Honeycombs ;
  - Second order homogenization without RVE size effect for cellular and metamaterials ;
  - Mean-Field-Homogenization for Elasto-Visco-Plastic Composites ;
  - Micro-structural simulation of fiber-reinforced highly crosslinked epoxy ;
  - Non-Local Damage Mean-Field-Homogenization ;
  - Non-Local Damage & Phase-Field-Enhanced Mean-Field-Homogenization ;
  - Stochastic Homogenization of Composite Materials ;
  - Stochastic 3-Scale Models for Polycrystalline Materials ;
  - Boundary conditions and tangent operator in multi-physics FE^2;
  - Stochastic Multi-Scale Model to Predict MEMS Stiction ;
  - Multi-Scale Modeling of Nano-Crystal Grain Boundary Sliding ;
- Fracture Mechanics
  - DG-Based Multi-Scale Fracture, DG-Based Dynamic Fracture ;
  - DG-Based Damage elastic damage to crack transition ;
  - Non-local Gurson damage model to crack transition ;
  - Stochastic Multi-Scale Fracture of Polycrystalline Films ;
- Smart Composite Materials – Shape Memory Effects

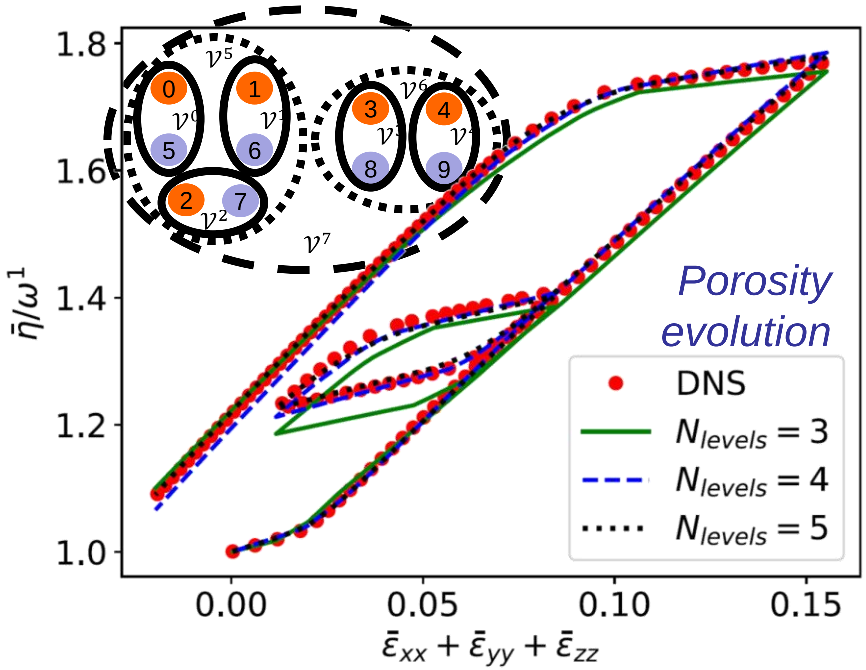

Deep Material Networks from the interactions viewpoint

The authors gratefully acknowledge the financial support from F.R.S-F.N.R.S

Deep Material Networks from the interactions viewpoint

- Architecture of mechanistic building blocks
  - Example for a 2-phase material

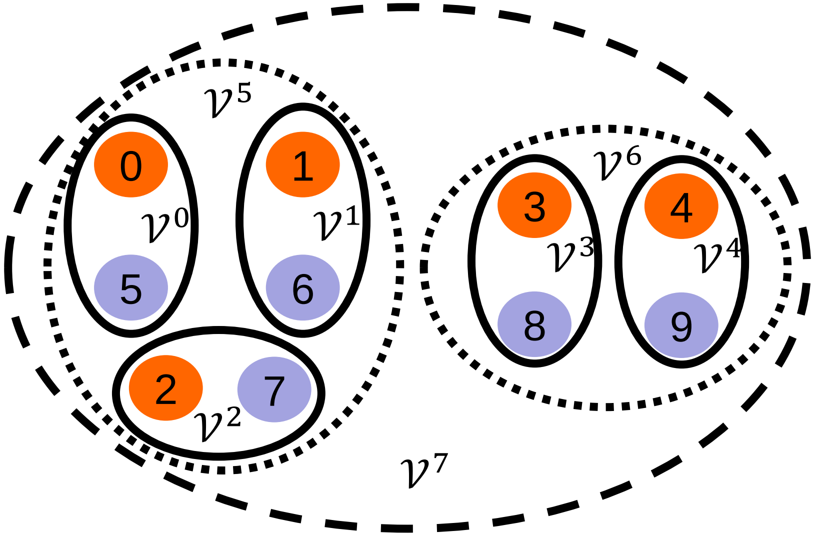

Homogenised behaviour

$$\bar{\boldsymbol{P}}(t) = \bar{\boldsymbol{P}}(\bar{\boldsymbol{F}}(t), z(\tau \leq t))$$

$$\bar{\boldsymbol{P}}(t) = \sum_{i=0}^{9} W^i \, \boldsymbol{P}^i(t)$$

$$\bar{\boldsymbol{F}}(t) = \sum_{i=0}^{9} W^i \, \boldsymbol{F}^i(t)$$

Weight of node i (parameter)

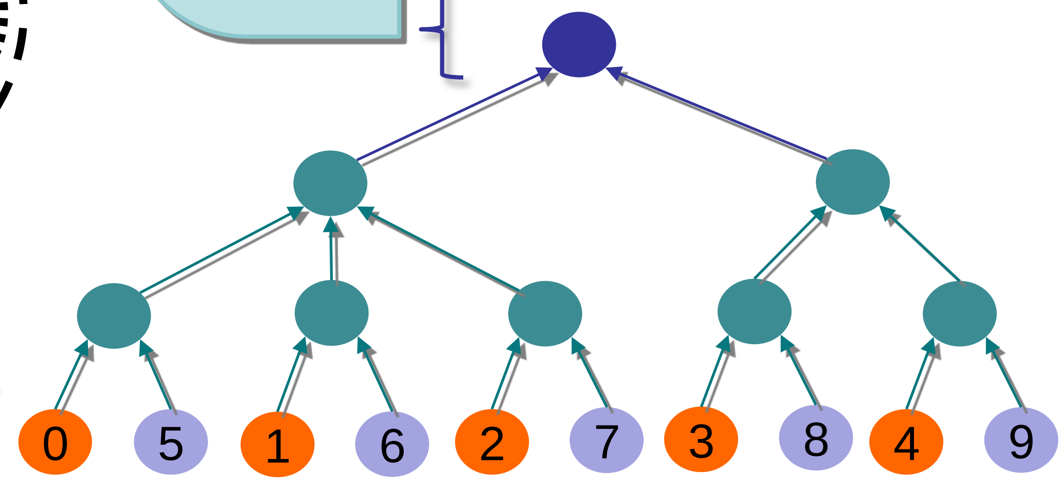

Material node i =0..9, of weight W^i

Constitutive behaviours: $\boldsymbol{P}^p(t) = \boldsymbol{P}^p\left(\boldsymbol{F}^i(t), z(\tau \leq t)\right)$

if node $i \in$ phase p for material p=0 or p=1

Deep Material Networks from the interactions viewpoint

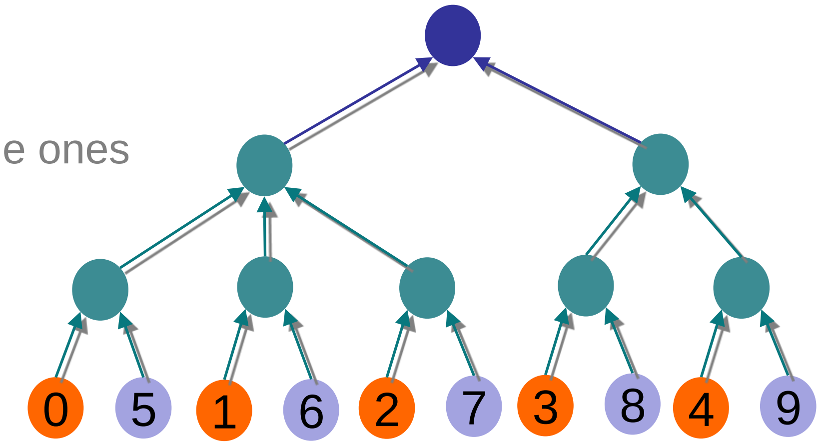

- Mechanism $k=0..M-1$
  - Link homogenised deformation gradient to node ones
    - Construction of a strain fluctuation field

$$\overline{\boldsymbol{F}}+\sum_{k=0}^{M-1}\alpha^{i,k}\,\boldsymbol{a}^{k}\otimes\boldsymbol{G}^{k}=\boldsymbol{F}^{i}\,,\quad i=0..9$$

Contribution of node i in mechanism k (parameter?)

Degrees of freedom of mechanism k definition the strain fluctuation

Direction of mechanism k (parameter)

Weight of node i (parameter)

  - Constraints from strain averaging
    - $\overline{\boldsymbol{F}}=\sum_i W^i\boldsymbol{F}^i$ ⇨ $\sum_k\left(\sum_i W^i\alpha^{i,k}\right)\boldsymbol{a}^{k}\otimes\boldsymbol{G}^{k}=0$ ⇨ $\sum_i W^i\alpha^{i,k}=0$
  - Weak form from Hill-Mandel
    - $\overline{\boldsymbol{P}}:\delta\overline{\boldsymbol{F}}=\sum_i W^i\,\boldsymbol{P}^i:\delta\boldsymbol{F}^i$ ⇨ $\left[\sum_k\left(\sum_i W^i\boldsymbol{P}^i\alpha^{i,k}\right)\cdot\boldsymbol{G}^{k}\right]\cdot\,\delta\boldsymbol{a}^{k}=0$

Deep Material Networks from the interactions viewpoint

- Mechanistic building blocks: Laminate
  - Interaction $\mathcal{V}^j$ as a laminate

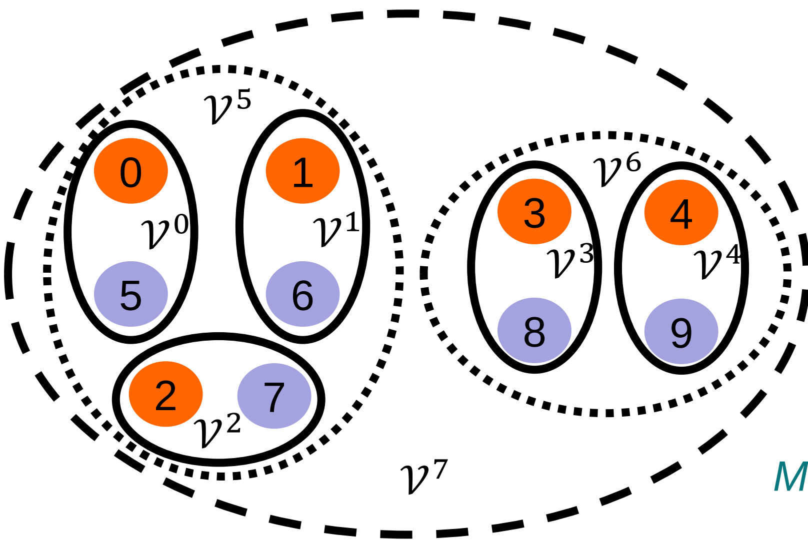

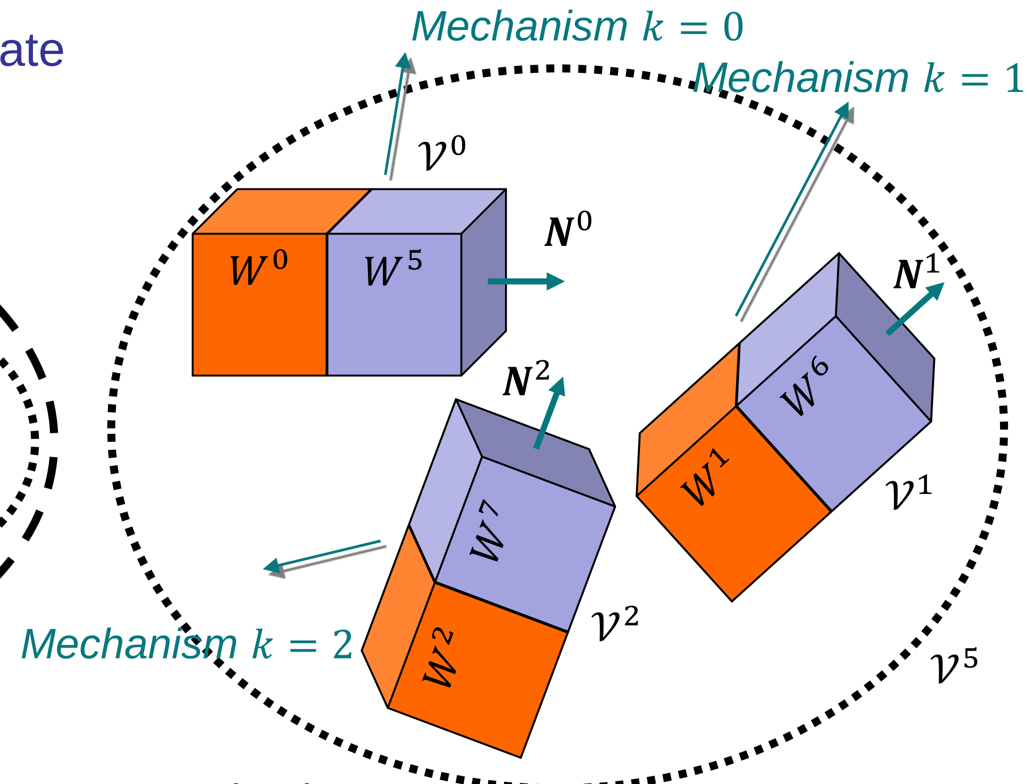

  - Parameters
    - Weight: $W^i,\ i = 0..9$
    - Unique direction for an interaction $\mathcal{V}^j$:

      $\boldsymbol{G}^k \Rightarrow \boldsymbol{N}^j,\ j = 0..7$
  - Constraint
    - $\sum_i W^i \alpha^{i,k} = 0 \Rightarrow \alpha^{i,k}$ from nodes weight in mechanism k

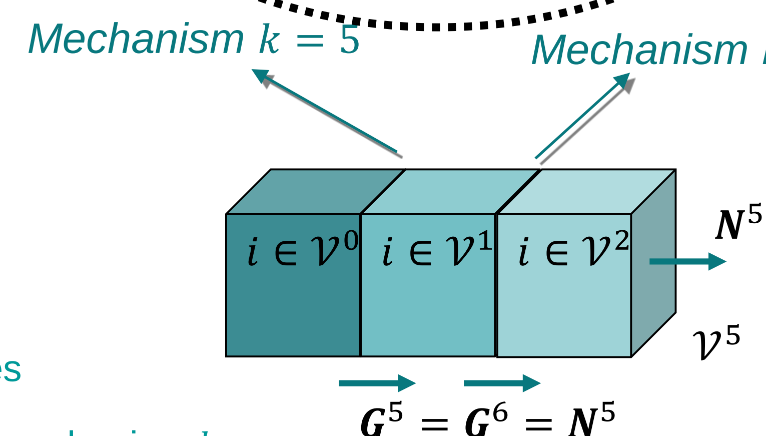

Deep Material Networks from the interactions viewpoint

- Mechanistic building blocks: Laminate
  - Interaction $\mathcal{V}^j$ as a laminate

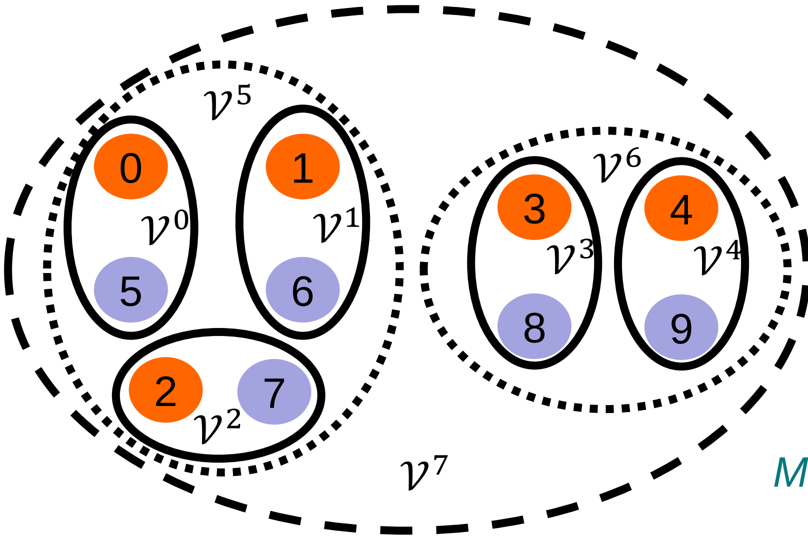

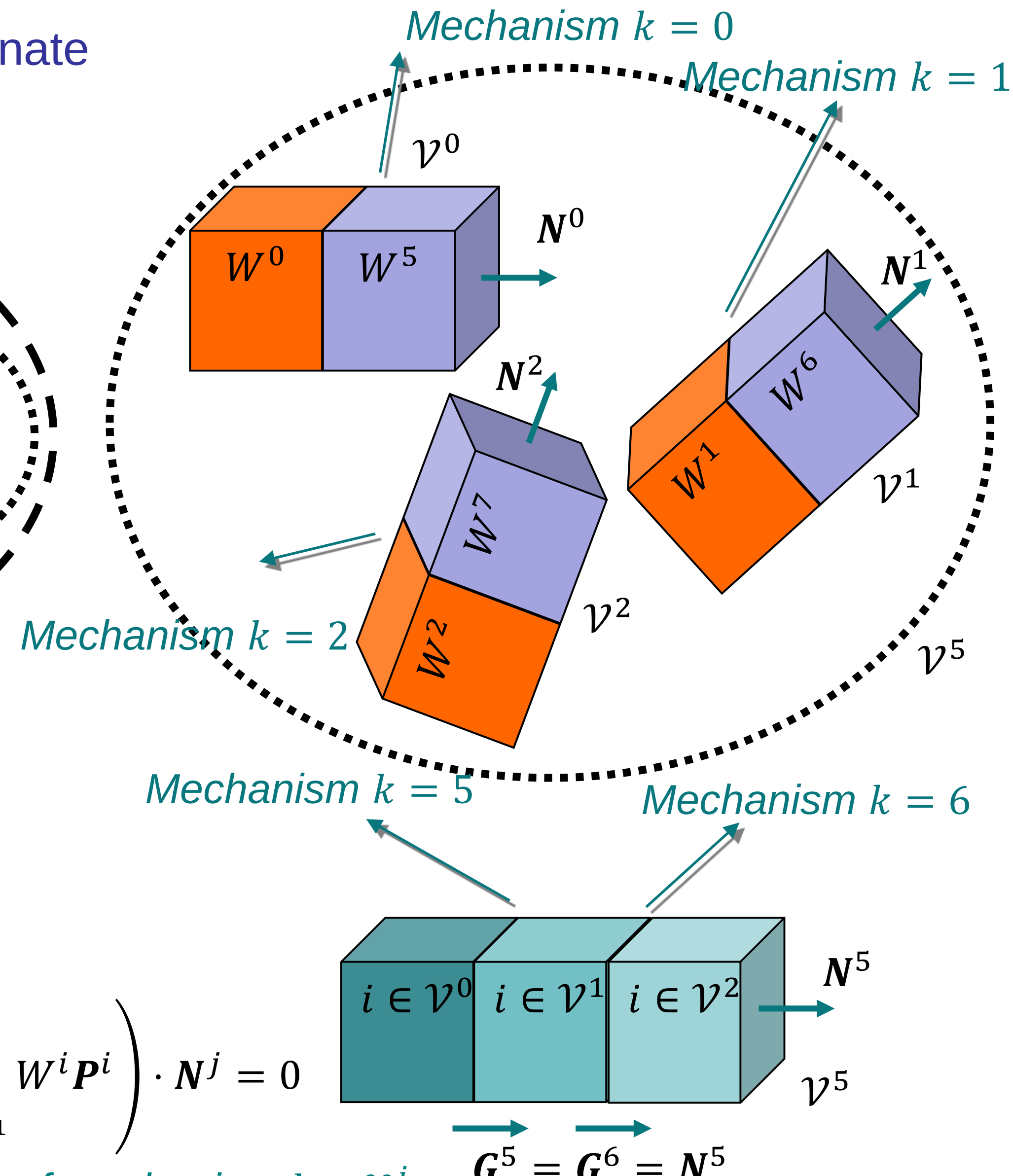

  - Weak form

$$\left[\sum_k \left(\sum_i W^i \boldsymbol{P}^i \alpha^{i,k}\right) \cdot \boldsymbol{G}^k\right] \cdot \delta \boldsymbol{a}^k = 0$$

$$\left(\frac{1}{W(\mathcal{V}^m)} \sum_{i \in \mathcal{V}^m} W^i \boldsymbol{P}^i - \frac{1}{W(\mathcal{V}^{m+1})} \sum_{i \in \mathcal{V}^{m+1}} W^i \boldsymbol{P}^i\right) \cdot \boldsymbol{N}^j = 0$$

$j = 0..7$, $\mathcal{V}^m$ and $\mathcal{V}^{m+1}$ interactions of mechanism $k \in \mathcal{V}^j$

- Offline stage on a p-phase RVE
  - Topological parameters $\boldsymbol{\chi}$
    - Weight: $W^i,\ i = 0..9$
    - Direction of interaction $\mathcal{V}^j$: $\boldsymbol{N}^j, j = 0..7$

      $\chi\ = [W^0, \dots, W^9, \boldsymbol{N}^0, \dots, \boldsymbol{N}^7\,]$
  - Using elastic data
    - Random properties on RVE

      $$\boldsymbol{\gamma} = [E_0,\, \nu_0, E_0,\, \nu_0 \dots E_p,\, \nu_p,]$$

      Direct simulations on RVE $\hat{\mathbb{C}}(\boldsymbol{\gamma})$
    - Cost functions to minimise

      $$L(\hat{\mathbb{C}},\, \bar{\mathbb{C}}(\boldsymbol{\chi})) = \frac{1}{n}\sum_{s=1}^{n} \frac{\|\hat{\mathbb{C}}(\boldsymbol{\gamma}_s) - \bar{\mathbb{C}}(\boldsymbol{\chi}|\boldsymbol{\gamma}_s)\|}{\|\hat{\mathbb{C}}(\boldsymbol{\gamma}_s)\|}$$
    - « stochastic gradient descent (SGD) » algorithm

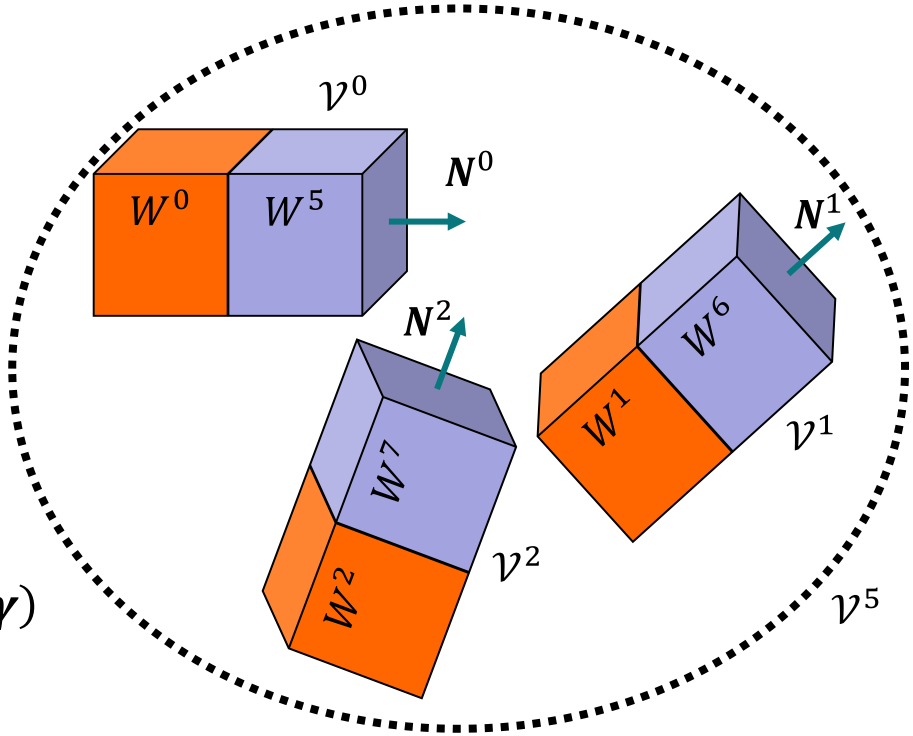

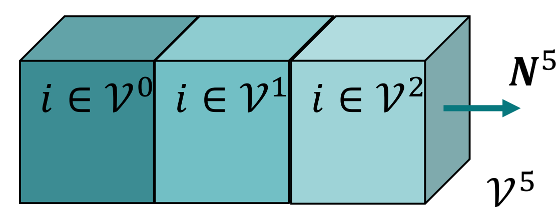

Deep Material Networks from the interactions viewpoint

- Online stage on a particle-reinforced composite
  - Properties
    - Elastic inclusions
    - Elasto-plastic matrix

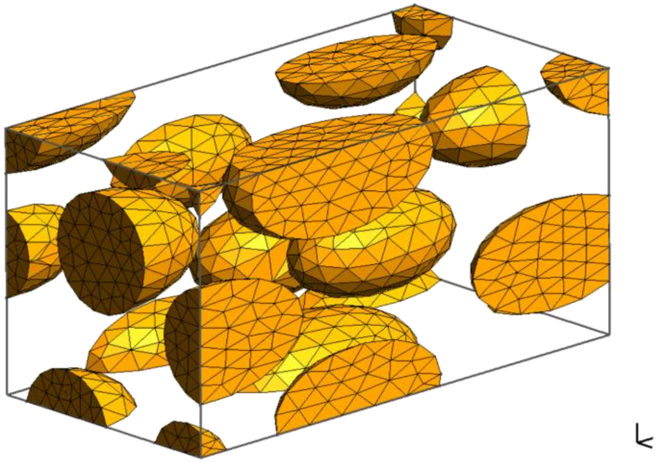

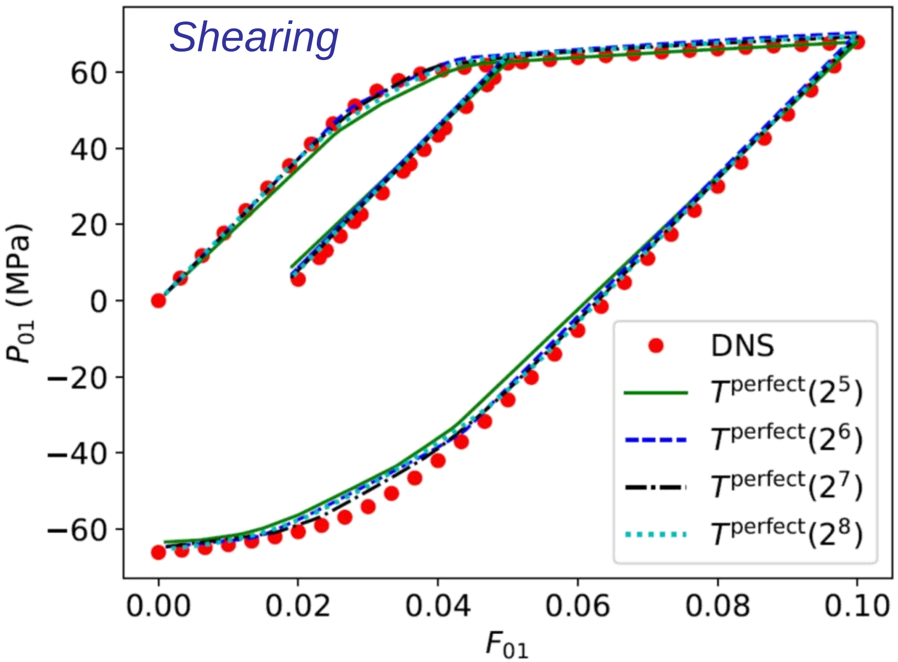

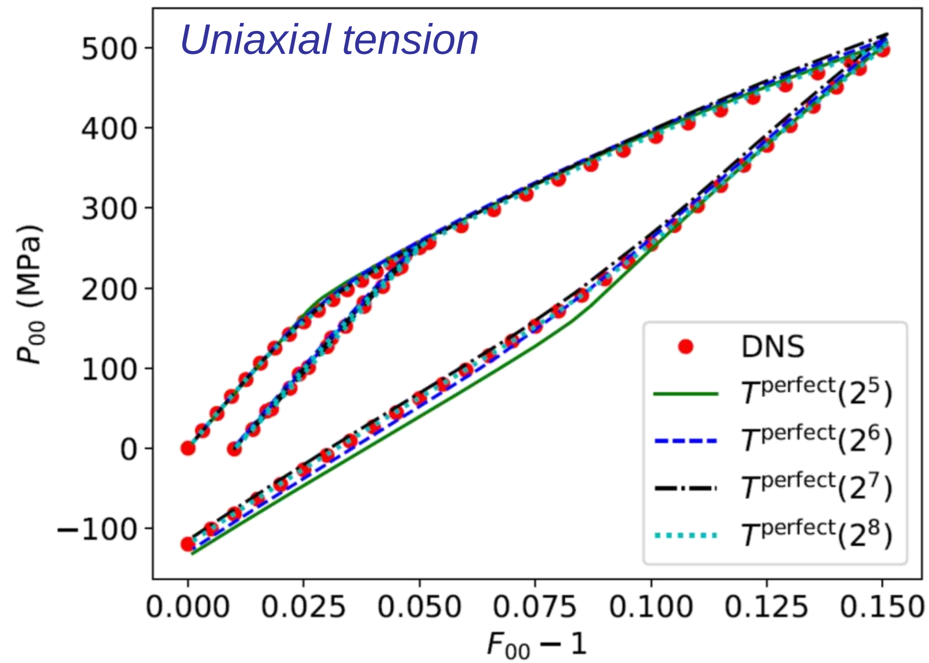

Deep Material Networks from the interactions viewpoint

- Multiscale simulation
  - Elasto-plastic composite RVE
  - Comparison FE² vs. DMN-surrogate

Off-line	FE^2	FE-DMN
Data generation	-	10 min.-cpu
Training	-	2 min.-cpu
On-line	**FE^2**	**FE-DMN**
Simulation	18000 h-cpu	½ to 34 h-cpu

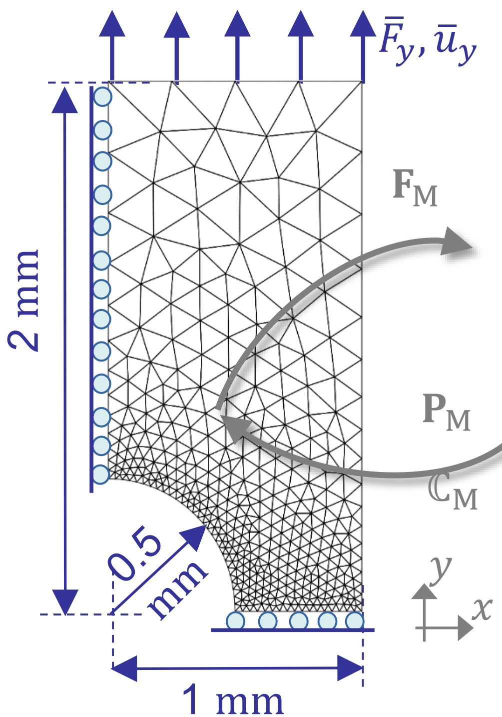

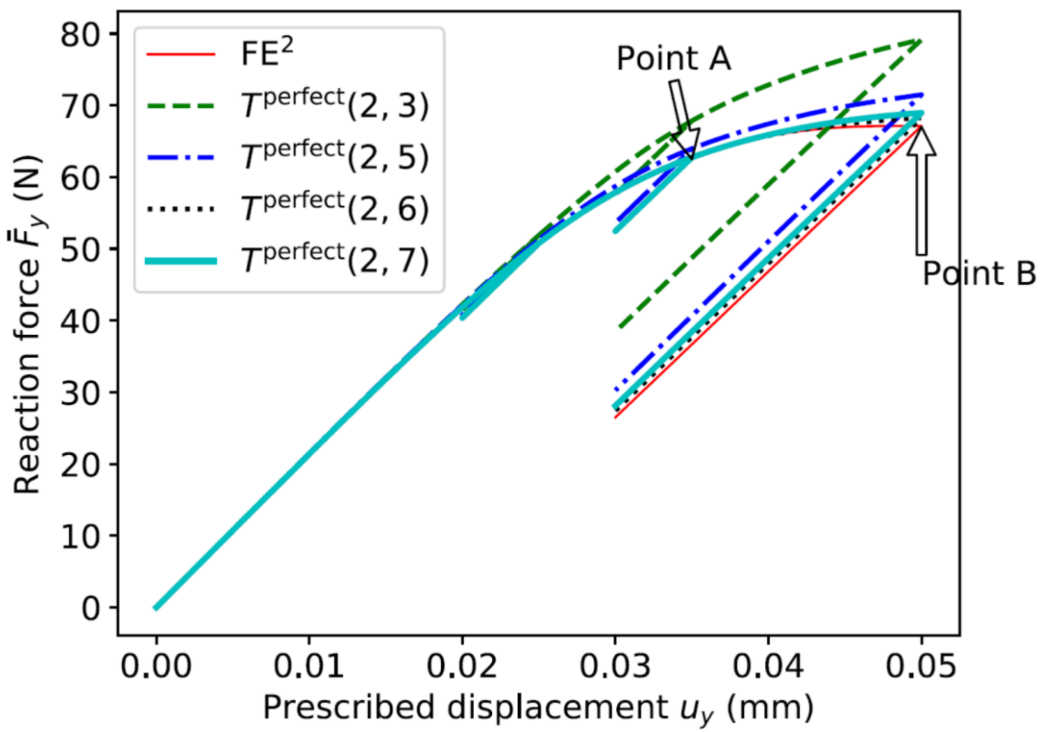

Deep Material Networks from the interactions viewpoint

- Multiscale simulation
  - Stress-strain distribution at point A
  - For 2^7 material nodes

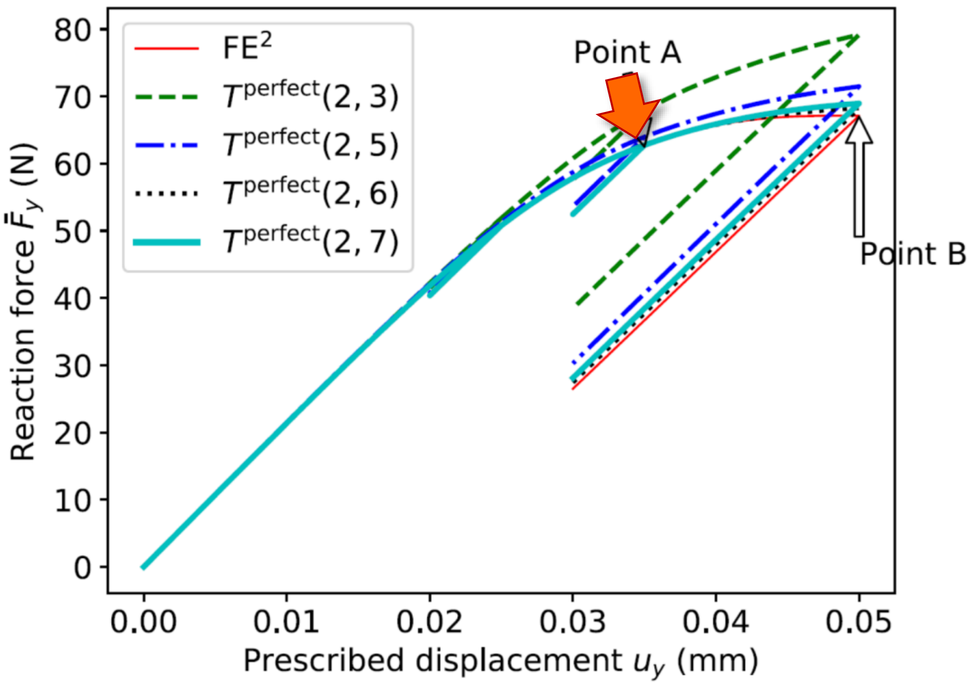

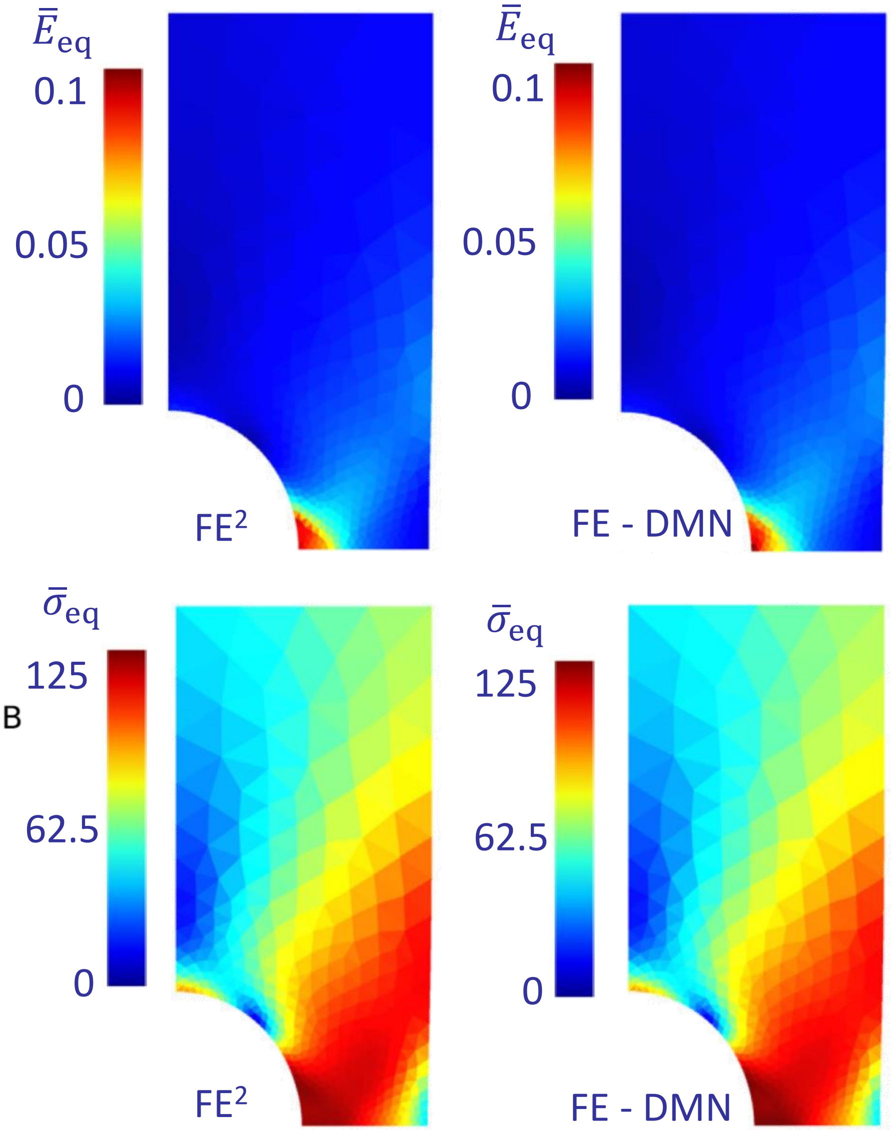

Deep Material Networks from the interactions viewpoint

- Multiscale simulation
  - Stress-strain distribution at point B
  - For 2^7 material nodes

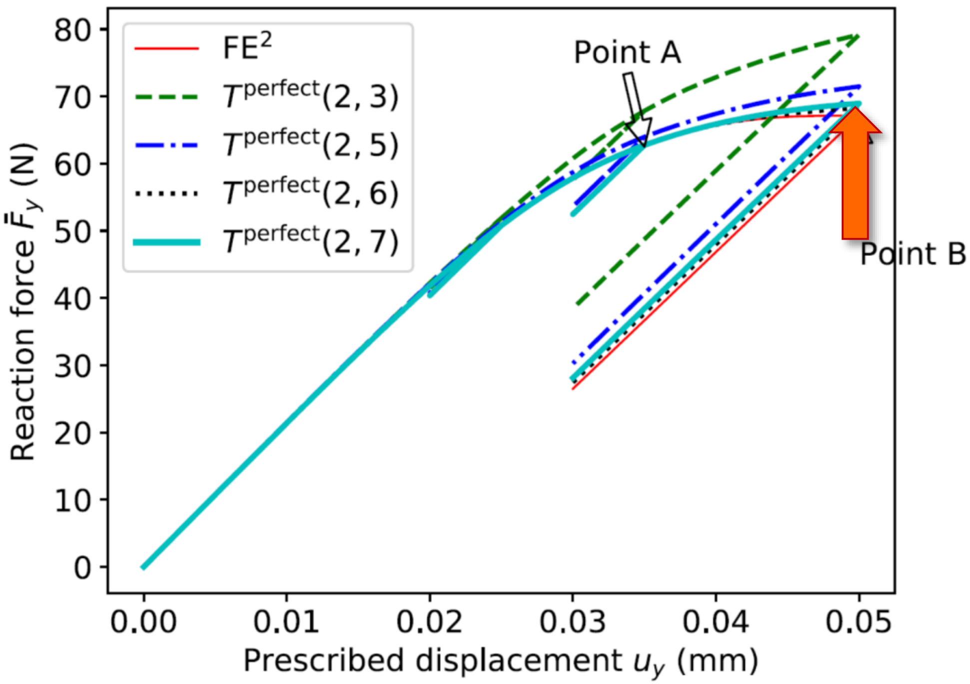

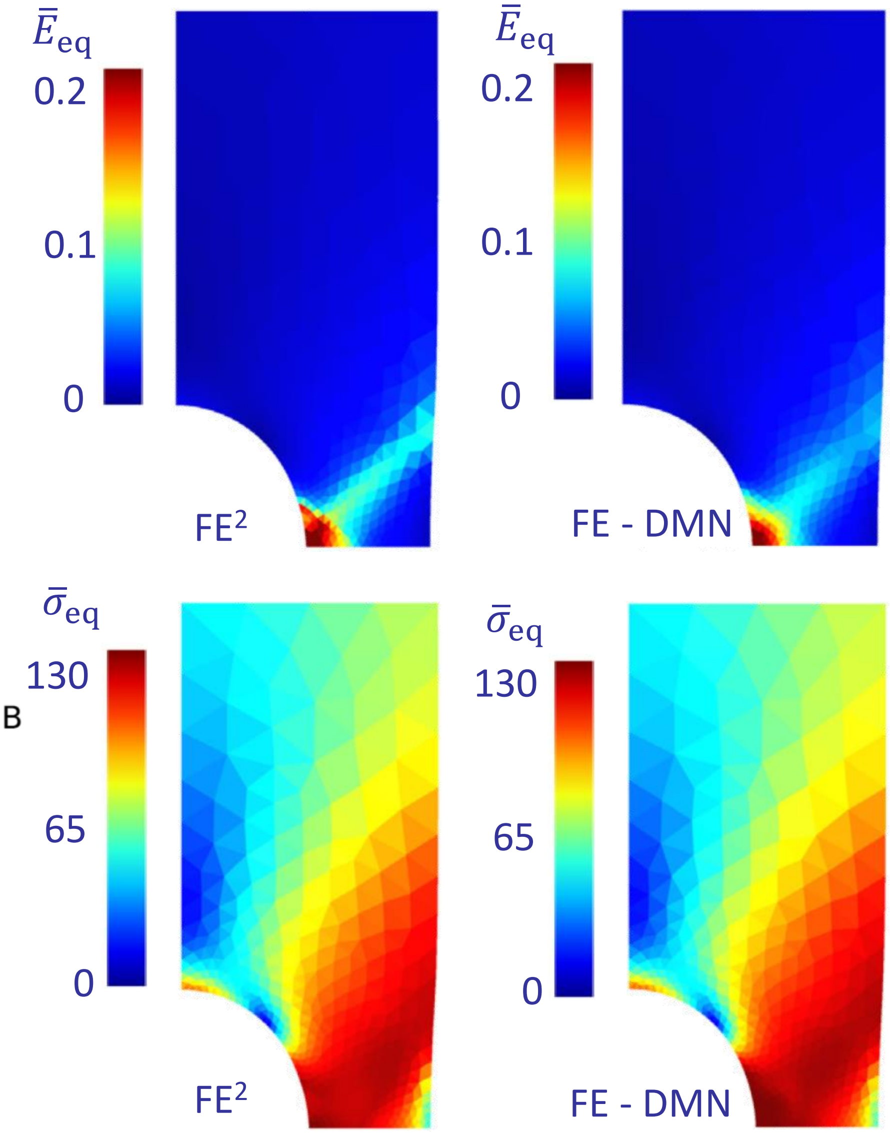

- Multiscale simulation
  - Localisation step
  - For 2^7 material nodes

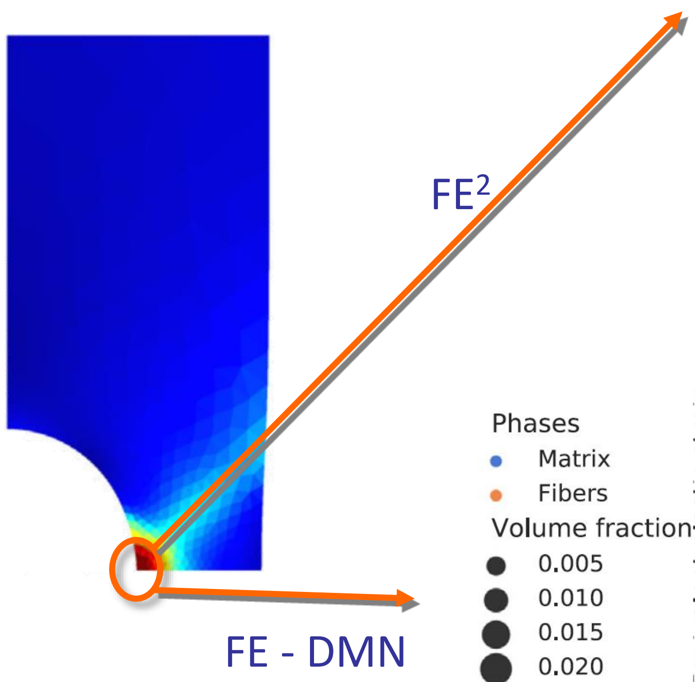

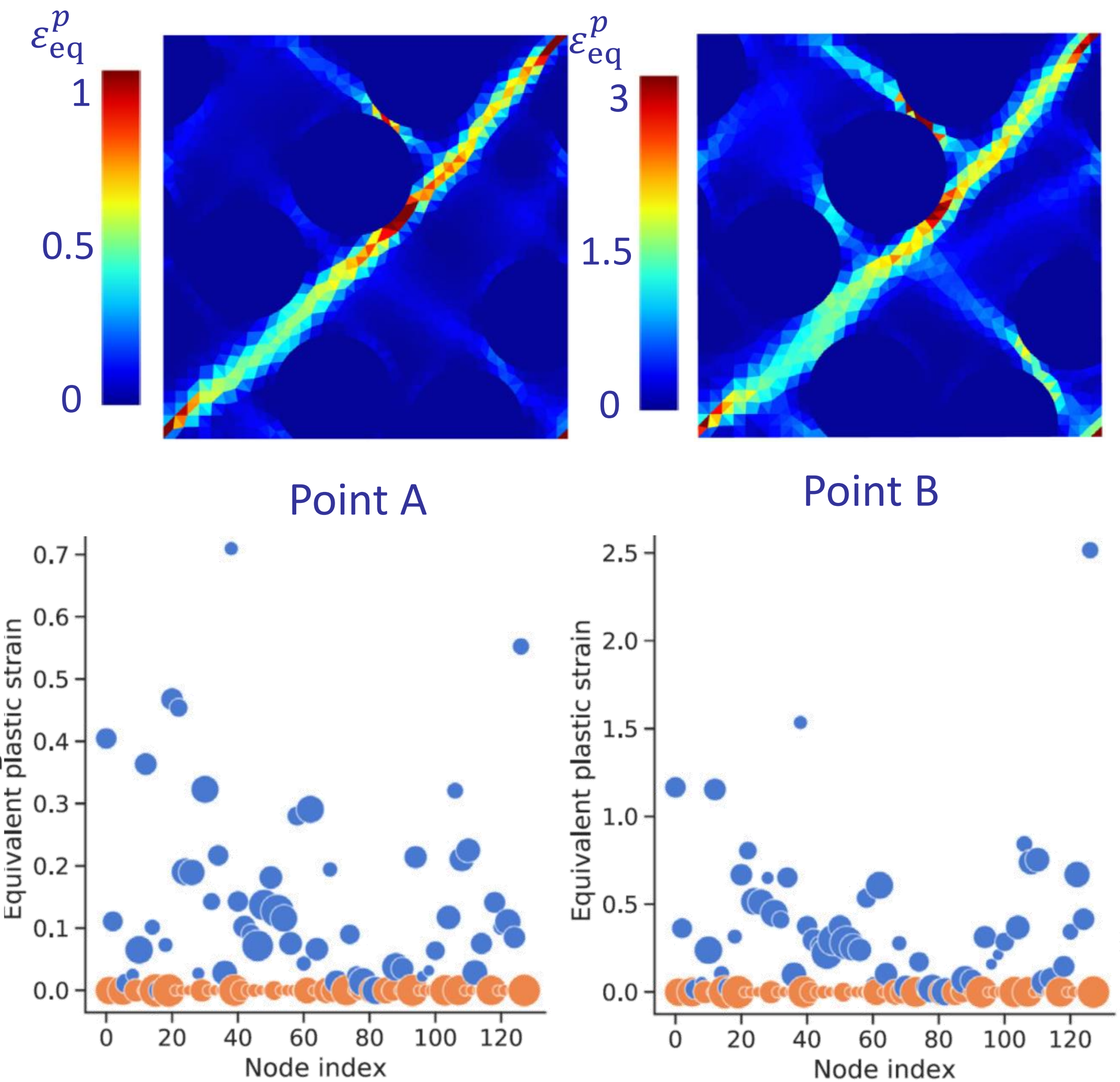

- Alternative to laminate (e.g. for porous material)
- Mechanism $j = 0..M-1$ of interaction $\mathcal{V}^j$
  - Homogenised deformation gradient
    - Construction of a strain fluctuation field

$$\overline{\boldsymbol{F}} + \sum_{j:i\in\mathcal{V}^j} \alpha^{i,j}\, \boldsymbol{a}^j \otimes \boldsymbol{N}^j = \boldsymbol{F}^i\,, \quad j = 0..M-1$$

Contribution of node i in mechanism j (parameter?)

Degrees of freedom of mechanism j definition the strain fluctuation

Direction of mechanism j (parameter)

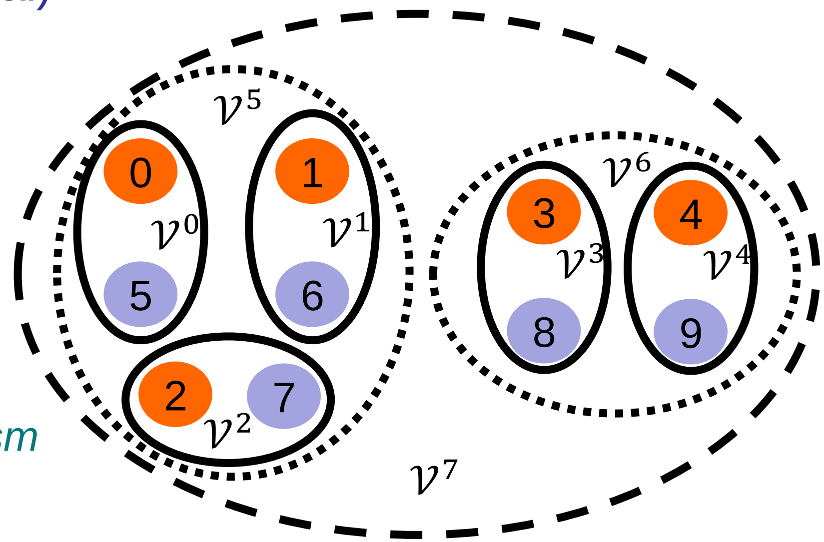

Weight of node i (parameter)

  - Constraints from strain averaging
    - $\overline{\boldsymbol{F}} = \sum_i W^i \boldsymbol{F}^i \Rightarrow \sum_j \left(\sum_{i\in\mathcal{V}^j} W^i \alpha^{i,j}\right) \boldsymbol{a}^j \otimes \boldsymbol{N}^j = 0 \Rightarrow \sum_{i\in\mathcal{V}^j} W^i \alpha^{i,j} = 0$
  - Weak form from Hill-Mandel
    - $\overline{\boldsymbol{P}} : \delta\overline{\boldsymbol{F}} = \sum_i W^i\, \boldsymbol{P}^i : \delta\boldsymbol{F}^i \Rightarrow \left[\sum_j \left(\sum_{i\in\mathcal{V}^j} W^i \boldsymbol{P}^i \alpha^{i,j}\right) \cdot \boldsymbol{N}^j\right] \cdot\, \delta\boldsymbol{a}^j = 0$

- Mechanistic building blocks: Polyhedra
  - Interaction $\mathcal{V}^j$, $j = 0..M-1$

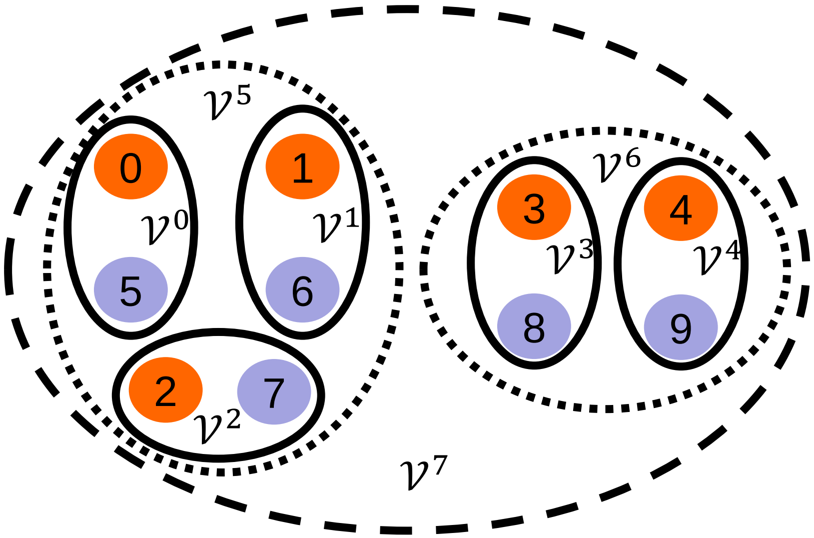

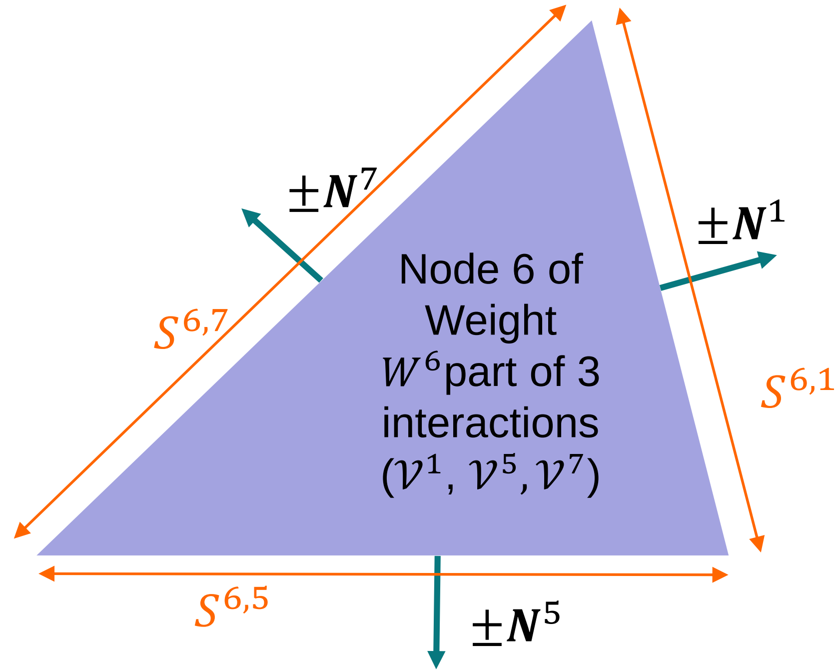

  - Fluctuation field
    - Integration by parts on a polyhedron of volume V^i associated to node i

$$\overline{\boldsymbol{F}} + \frac{1}{V^i}\int_{V^i} w \otimes \nabla \, dV = \boldsymbol{F}^i \quad \Rightarrow \quad \overline{\boldsymbol{F}} + \sum_{j:i\in\mathcal{V}^j} \frac{S^{i,j}}{V^i} w \otimes (\pm \mathbf{N}^j) = \boldsymbol{F}^i$$

    - To be compared with the interactions $\overline{\boldsymbol{F}} + \sum_{j:i\in\mathcal{V}^j} \alpha^{i,j}\, \boldsymbol{a}^j \otimes \boldsymbol{N}^j = \boldsymbol{F}^i$, $\quad j = 0..M-1$

$\Rightarrow$
- $\alpha^{i,j}$ is the weighted surface of a polyhedron face (parameter to be identified)
- $\boldsymbol{N}^j$ is the inward or outward normal of the polyhedron face (parameter to be identified)
- $\boldsymbol{a}^j$ is the fluctuation field (degree of freedom for online simulations)

Deep Material Networks from the interactions viewpoint

- Offline stage on a p-phase RVE
  - Topological parameters χ
    - Nodal weight: $W^{i}, i = 0..9$
    - Direction of interaction $\mathcal{V}^{j}$: $\boldsymbol{N}^{j}, j = 0..7$
    - Interaction weight: $\alpha^{i,j}$

$$\chi = [W^{0}, \ldots, W^{9}, \boldsymbol{N}^{0}, \ldots, \boldsymbol{N}^{7}, \alpha^{0,0}, \ldots \ \alpha^{9\,7}]$$

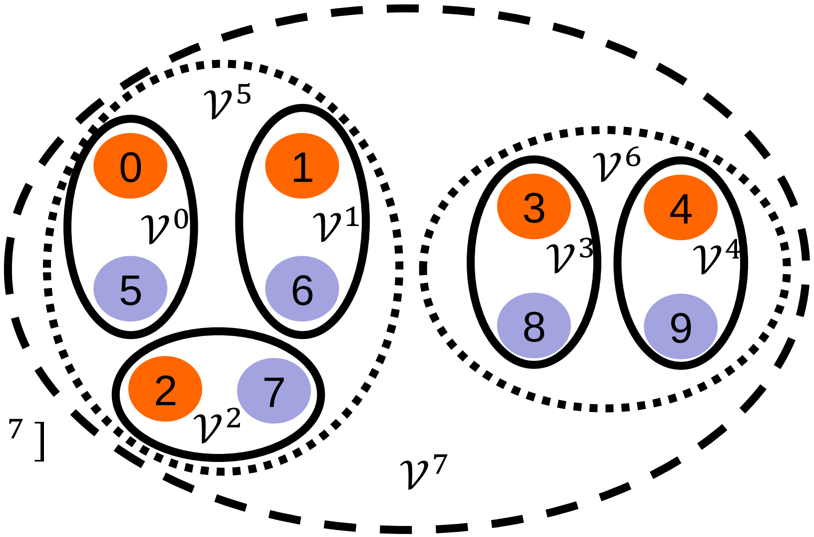

  - Using elastic data
    - Random properties on RVE $\Rightarrow \hat{\mathbb{C}}(\boldsymbol{\gamma})$

$$\boldsymbol{\gamma} = [E_0, \nu_0, E_1, \nu_1 \ldots E_p, \nu_p]$$

    - Cost functions to minimise $L(\hat{\mathbb{C}}, \mathbb{C}(\boldsymbol{\chi})) = \frac{1}{n}\sum_{s=1}^{n} \frac{\|\hat{\mathbb{C}}(\boldsymbol{\gamma}_s) - \bar{\mathbb{C}}\,(\boldsymbol{\chi}|\boldsymbol{\gamma}_s)\|}{\|\hat{\mathbb{C}}(\boldsymbol{\gamma}_s)\|}$
  - Using non-linear response
    - Random loading on RVE (strain sequence $\bar{\mathbf{F}}_s$)
    - Compare stress history $\mathbf{P}(\bar{\mathbf{F}}_s)$ and quantity of interest $Z(\bar{\mathbf{F}}_s)$ (e.g. porosity)
    - Cost function to minimise $L\left(\hat{\mathbf{P}}, \mathbf{P}(\boldsymbol{\chi})\right) = \frac{1}{n}\sum_{s=1}^{n} \frac{\left\|\hat{\mathbf{P}}(\bar{\mathbf{F}}_s) - \bar{\mathbf{P}}(\boldsymbol{\chi}|\bar{\mathbf{F}}_s)\right\|}{\left\|\hat{\mathbf{P}}(\bar{\mathbf{F}}_s)\right\|} + \frac{1}{n}\sum_{s=1}^{n} \frac{\left\|\hat{Z}(\bar{\mathbf{F}}_s) - \bar{Z}\,(\boldsymbol{\chi}|\bar{\mathbf{F}}_s)\right\|}{\left\|\hat{Z}(\bar{\mathbf{F}}_s)\right\|}$
  - By « stochastic gradient descent (SGD) » algorithm

Deep Material Networks from the interactions viewpoint

- Online stage on a porous material
  - Properties
    - Elasto-plastic matrix
    - Small strain
  - Non-linear training
  - Uniaxial tension

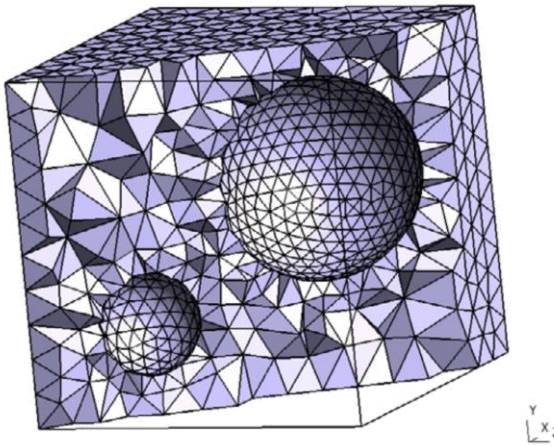

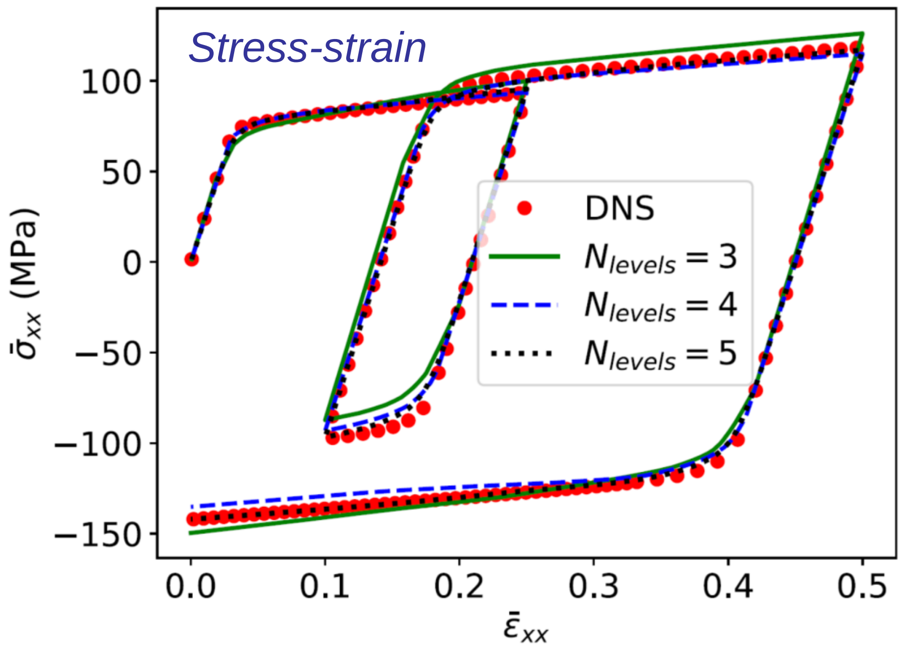

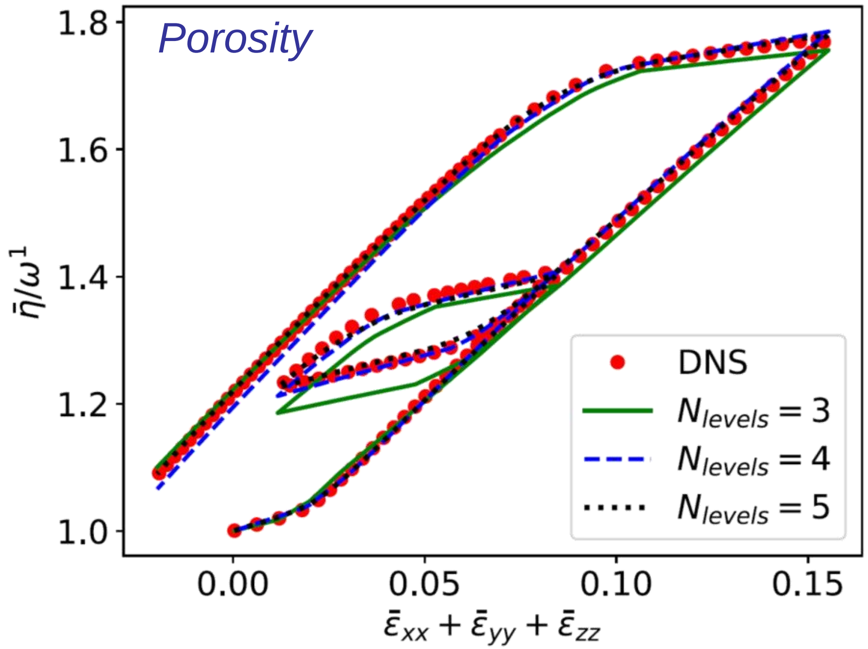

Deep Material Networks from the interactions viewpoint

- Online stage on a porous material
  - Properties
    - Elasto-plastic matrix
    - Small strain
  - Non-linear training with Material 1, on-line material 2
  - Random loading

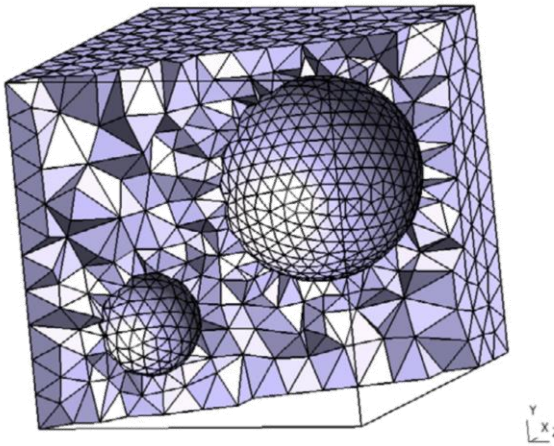

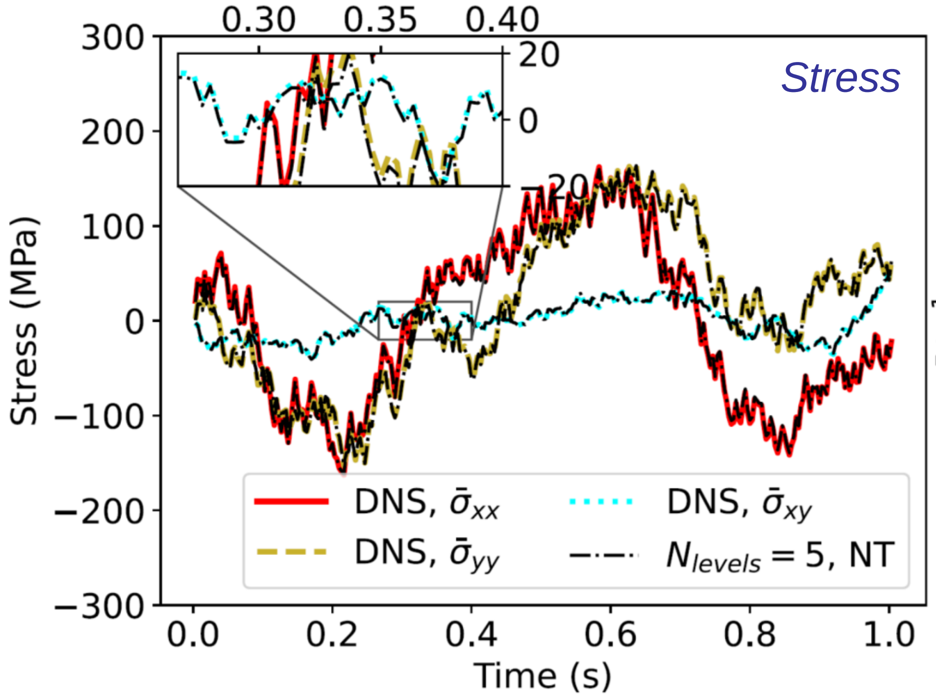

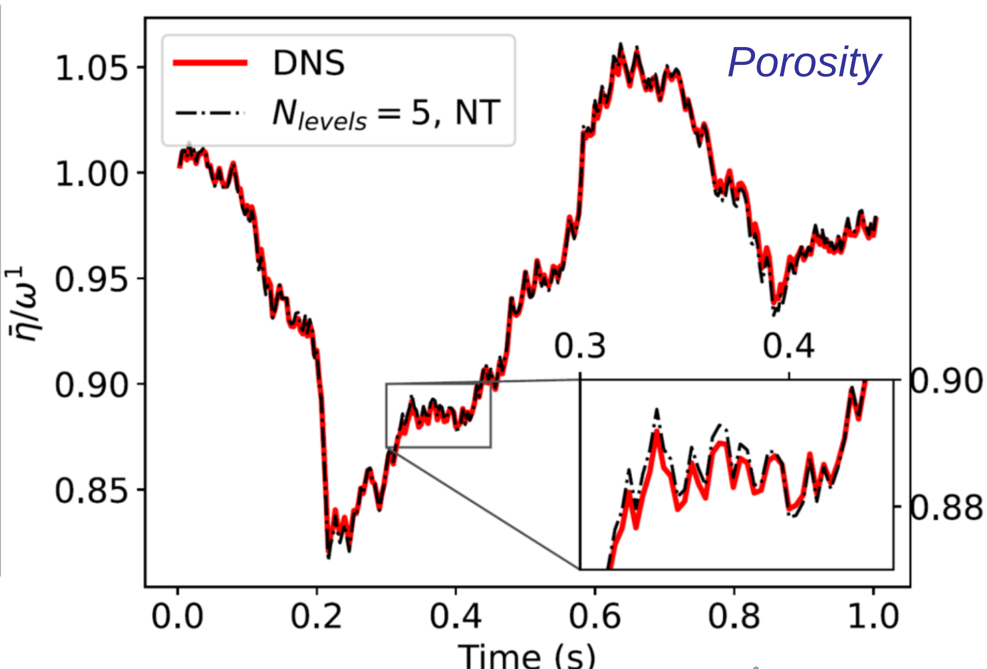

- Online stage on a porous material
  - Properties
    - Elasto-plastic matrix
    - Small strain
  - Non-linear training
  - Thermodynamically consistent

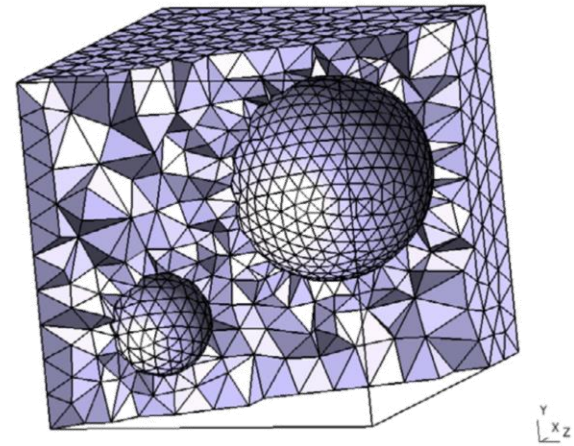

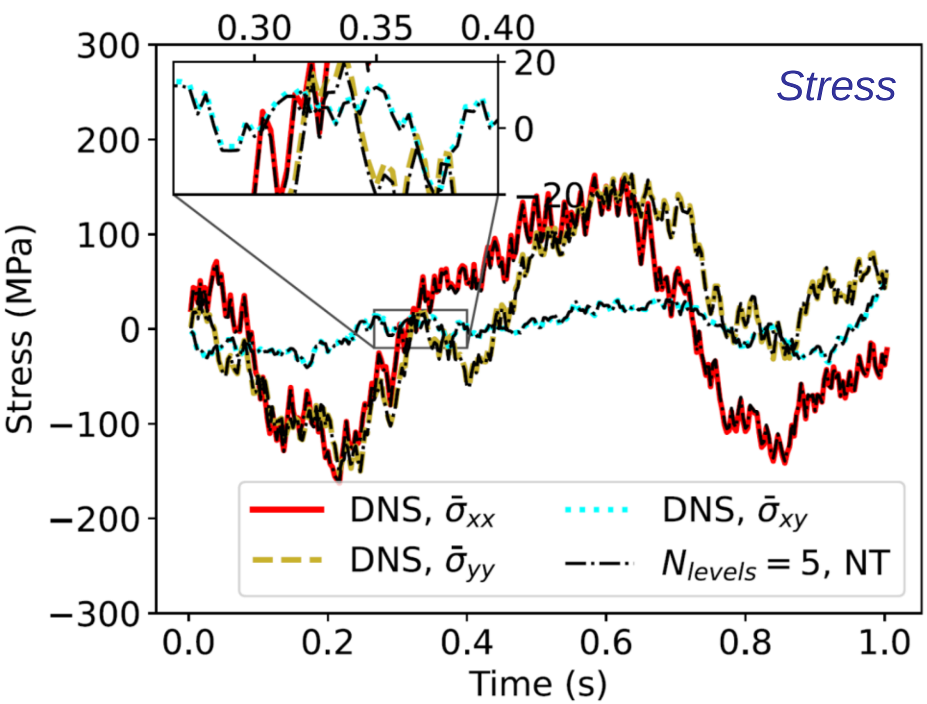

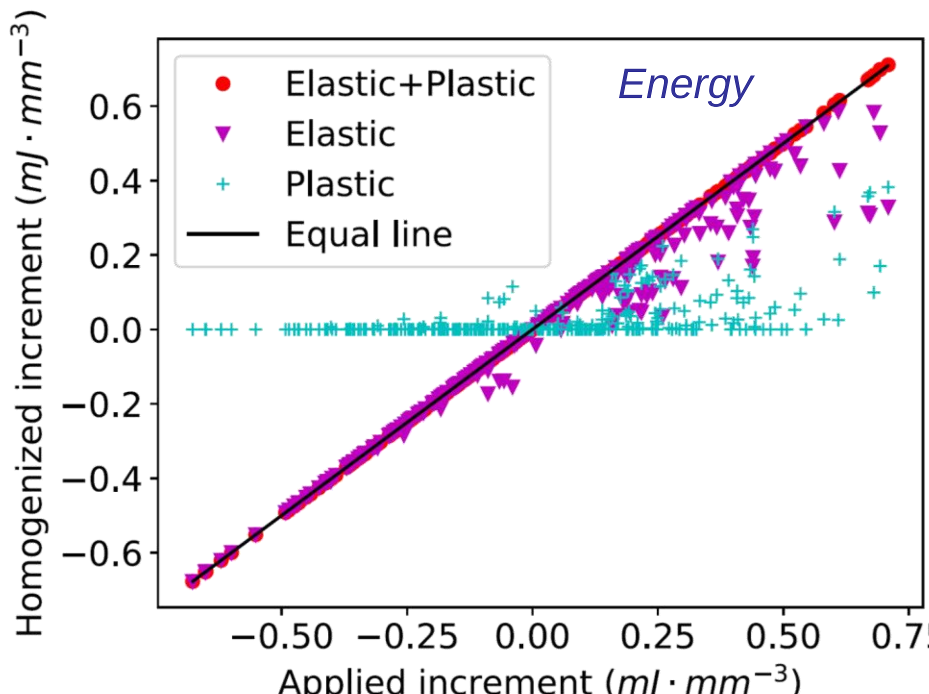

- Multiscale simulation

Off-line	FE^2	FE-DMN
Data generation	-	0.04 (linear) – 3.5 (non-linear) hour.-cpu
Training	-	0.16-20 hours.-cpu
On-line	**FE^2**	**FE-DMN**
Simulation	7200 h-cpu	0.1 to 1 h-cpu

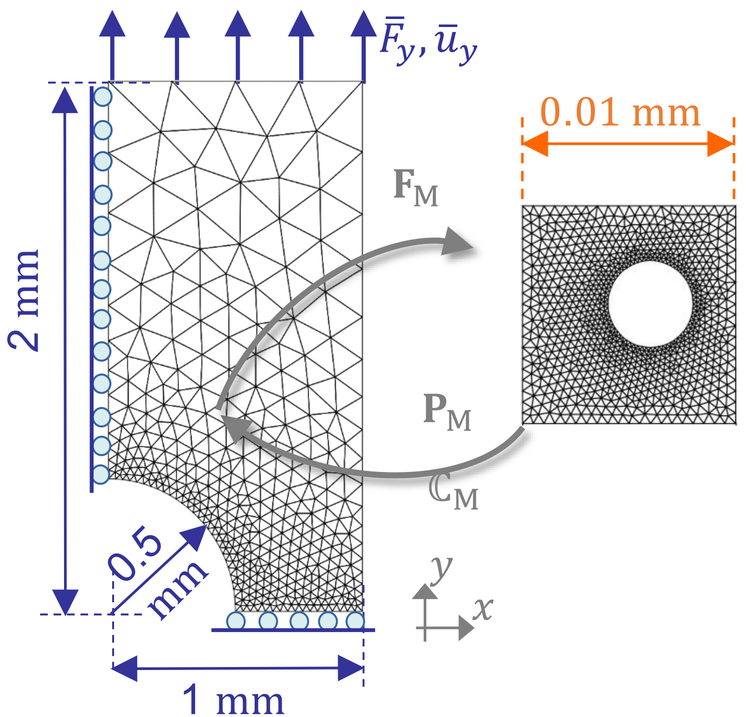

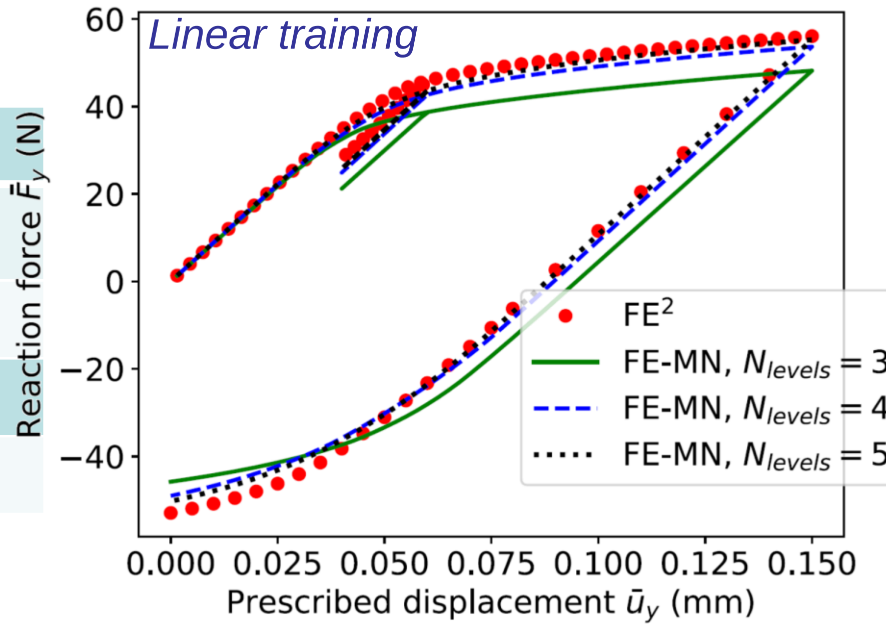

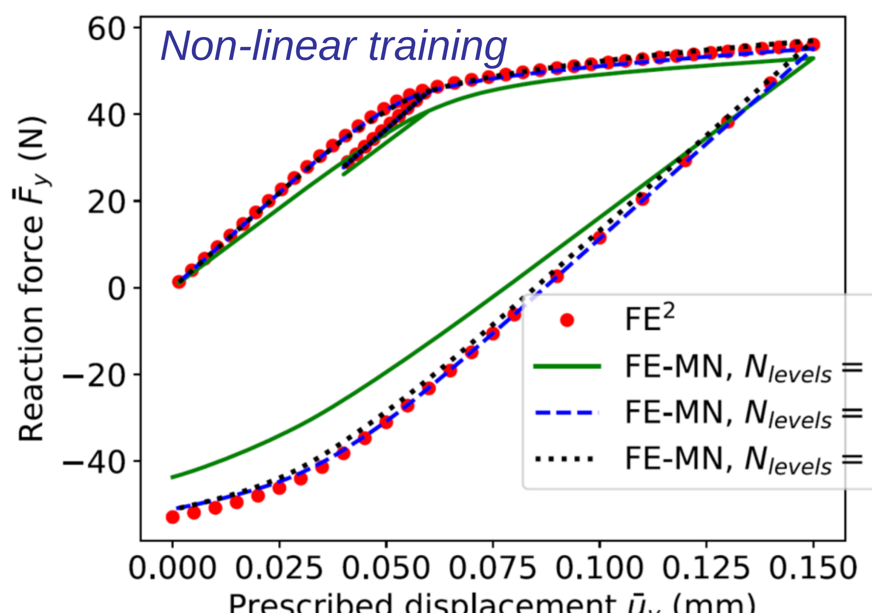

Deep Material Networks from the interactions viewpoint

- Multiscale simulation
  - Stress-strain distribution at point A
  - For 2^5 material nodes
  - Non-linear training

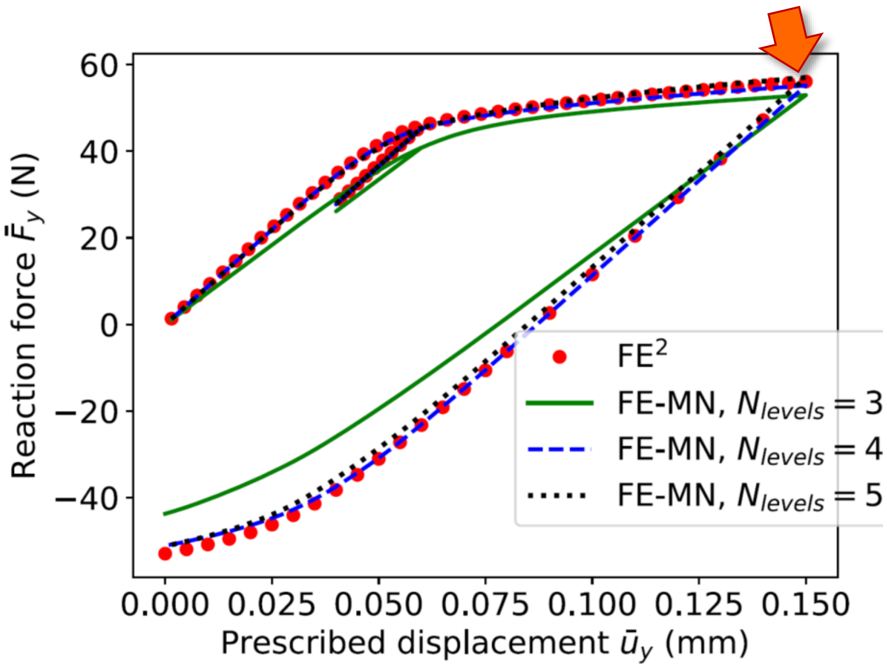

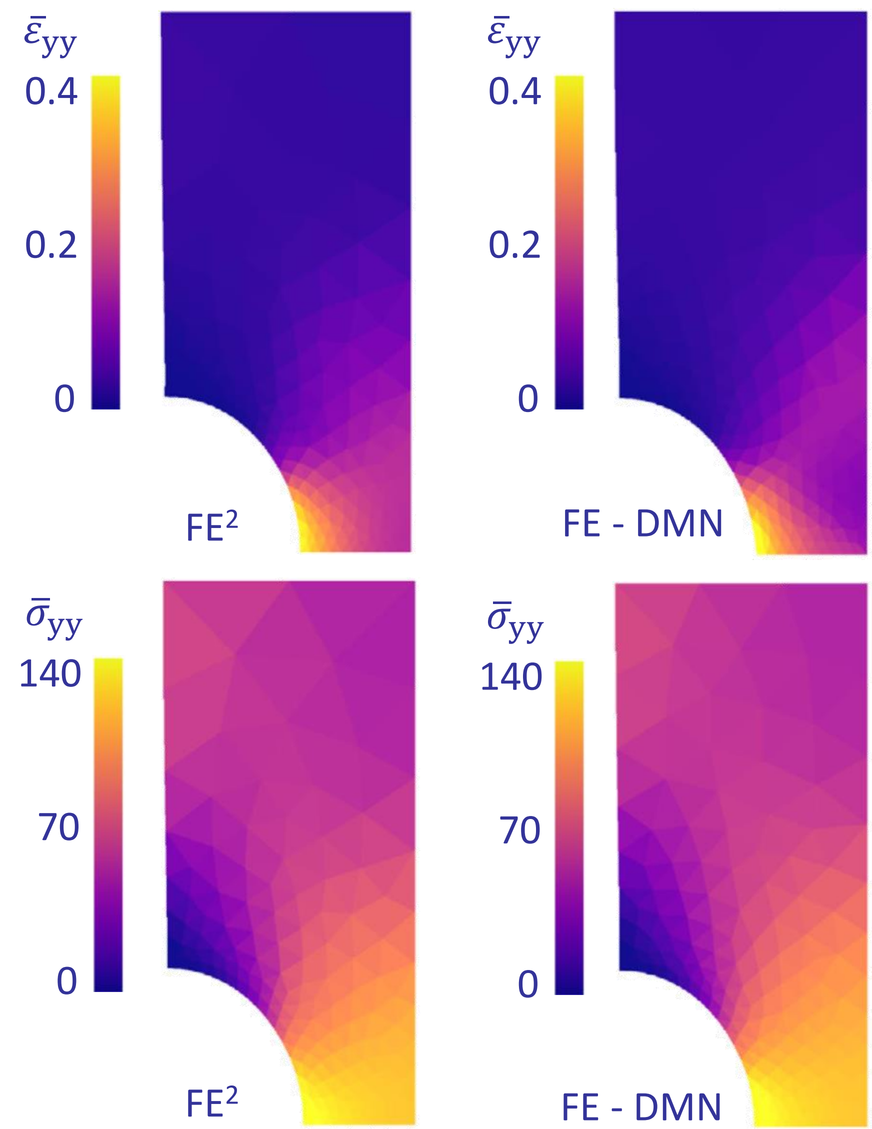

Deep Material Networks from the interactions viewpoint

- Multiscale simulation
  - Stress-strain distribution at point B
  - For 2^5 material nodes
  - Non-linear training

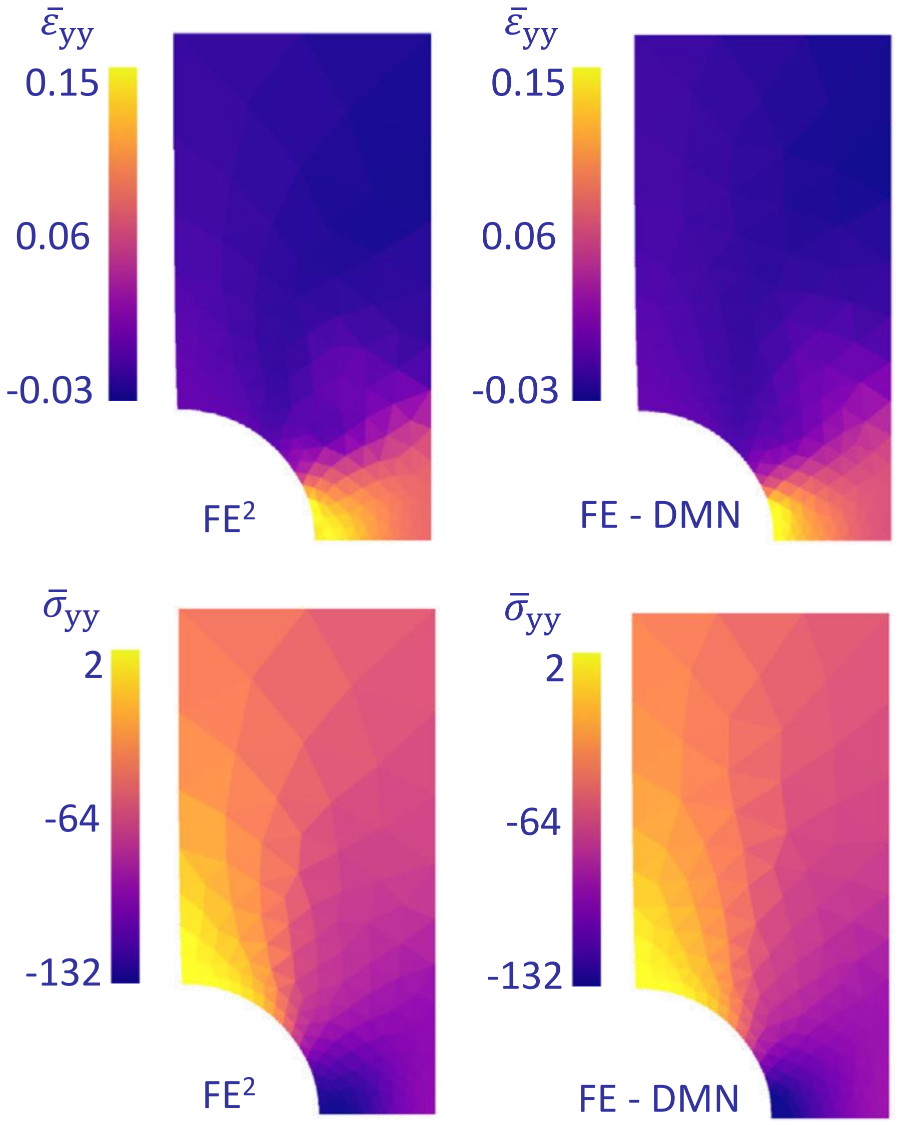

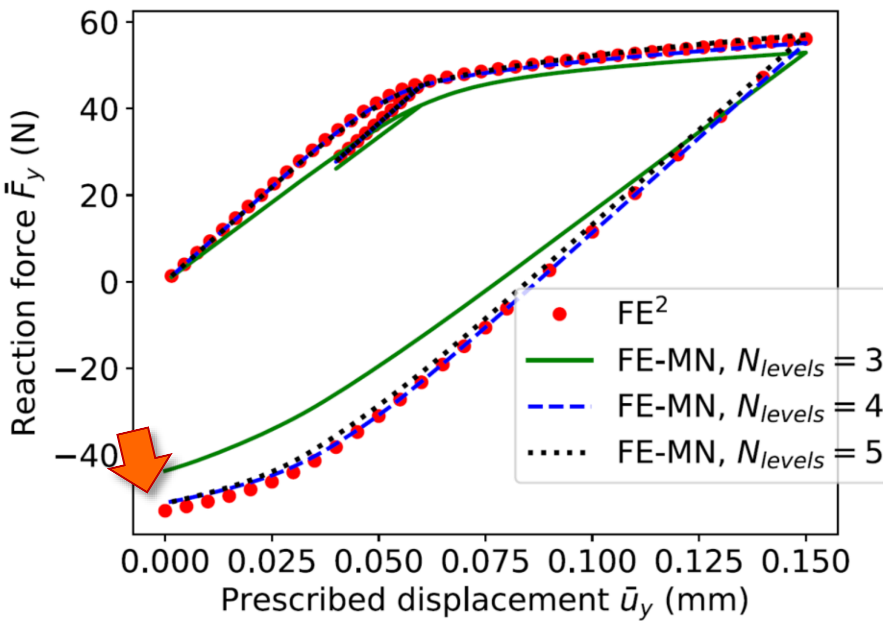

Deep Material Networks from the interactions viewpoint

- Publications (doi)
  - 10.1016/j.cma.2021.114300
    - Open data
  - 10.1016/j.euromechsol.2021.104384
    - Open data

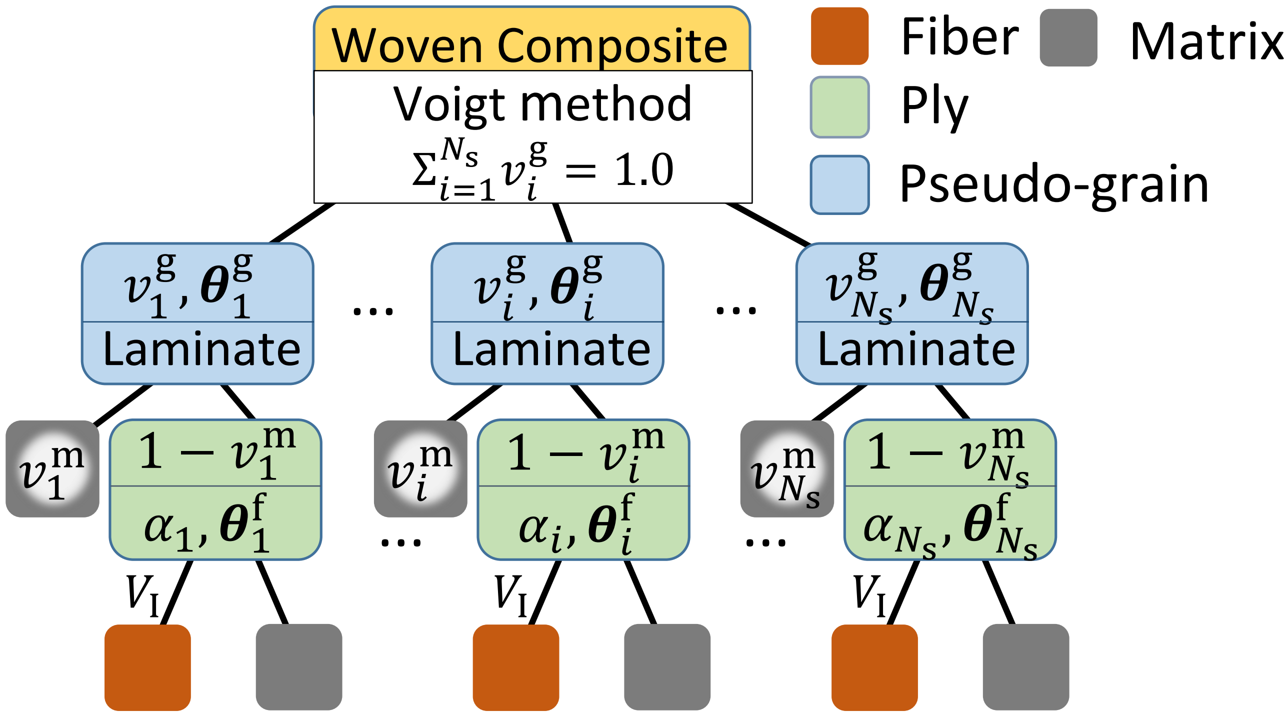

Mean-Field-Based Deep Material Networks for woven composites

The research has been funded by the Walloon Region under the agreement no.7911-VISCOS in the context of the 21st SKYWIN call.

Mean-Field-Based Deep Material Networks for woven composites

- Definition of 3 Reduced-order-models
- Using simple micro-mechanistic grains
  - MFH (short fibre-reinforced matrix)
  - Voigt mixture
  - Laminate theory

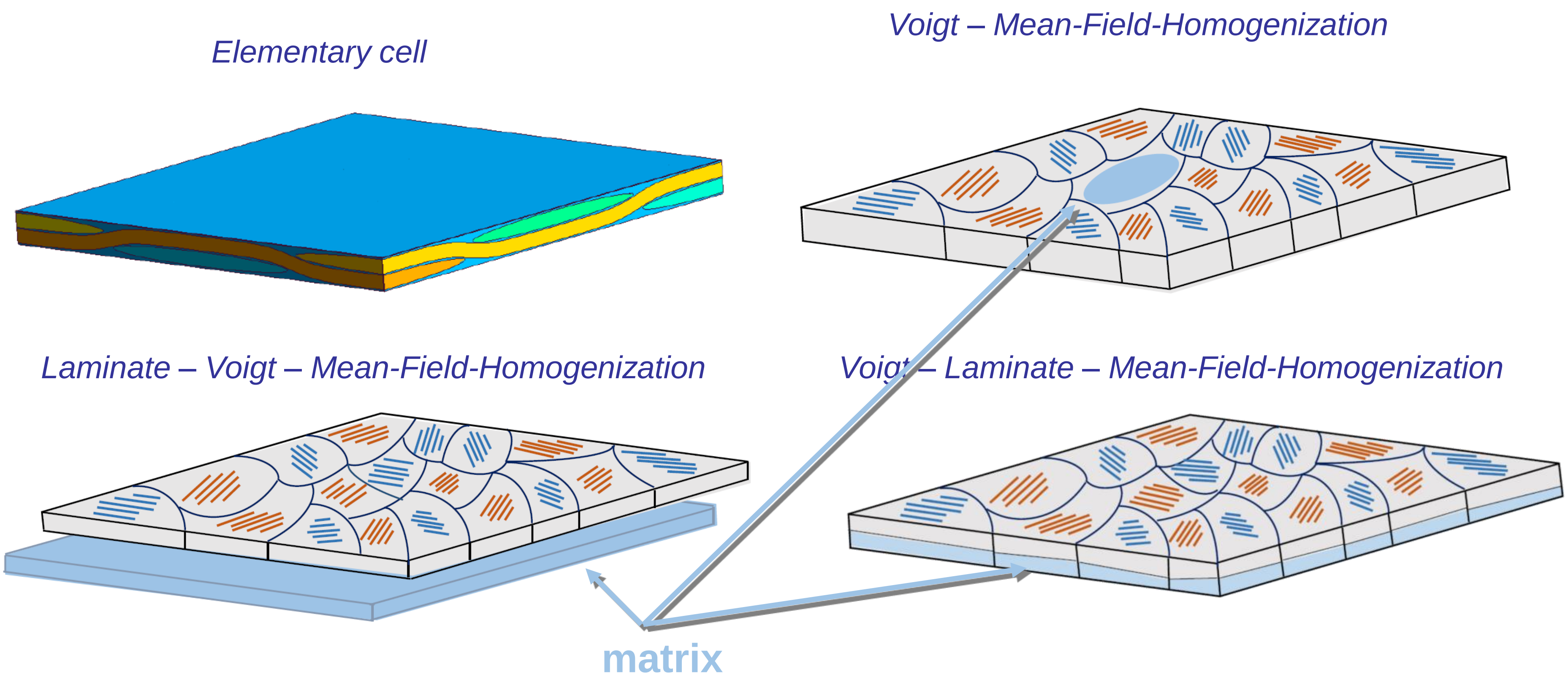

Mean-Field-Based Deep Material Networks for woven composites

- Definition of material networks

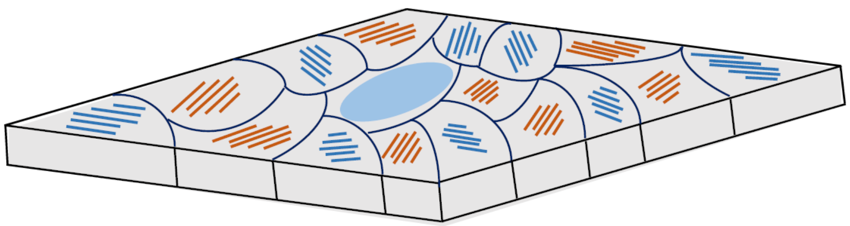

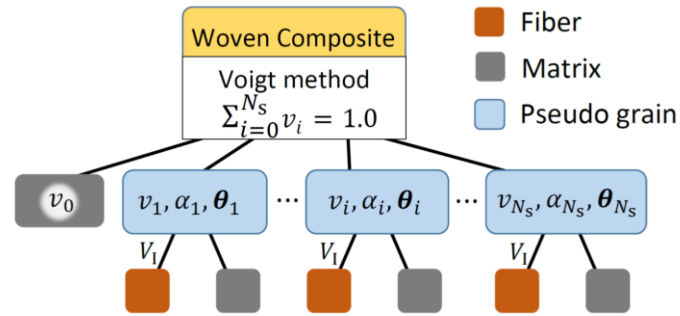

$$\chi^{\mathrm{VM}} = \left\{ v_i,\, \boldsymbol{\theta}_i,\, \alpha_i \mid i = 1, \dots, N_S;\ \sum_{i=1}^{N_S} v_i = 1.0 - v_0 \right\}$$

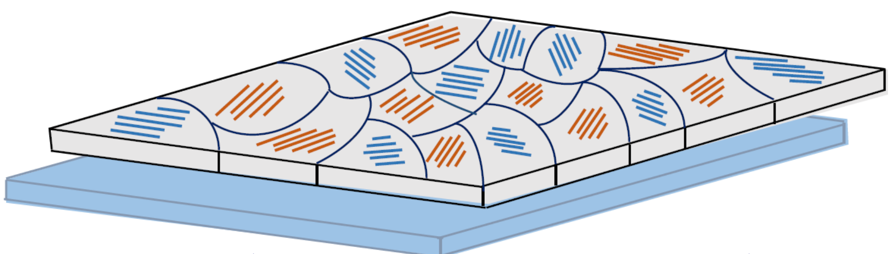

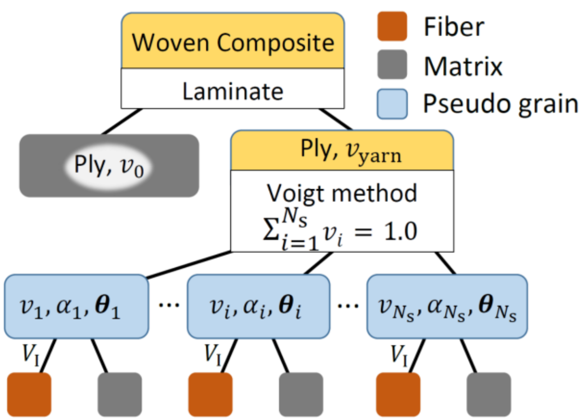

$$\chi^{\mathrm{LVM}} = \left\{ v_i,\, \boldsymbol{\theta}_i,\, \alpha_i \mid i = 1, \dots, N_S;\ \sum_{i=1}^{N_S} v_i = 1.0 \right\}$$

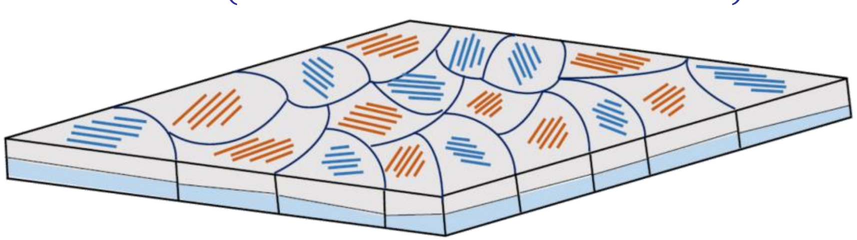

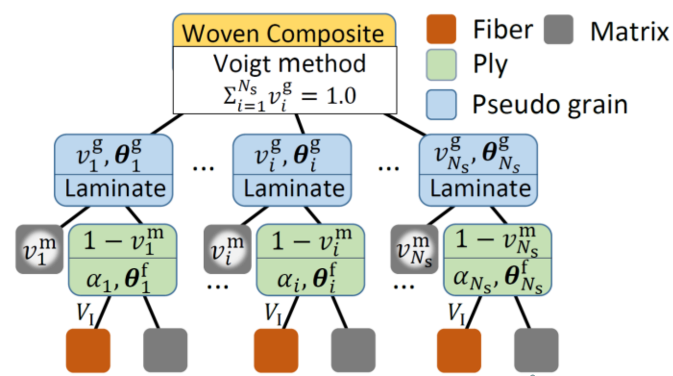

$$\chi^{\mathrm{VLM}} = \left\{ v_i^{\mathrm{g}},\, \boldsymbol{\theta}_i^{\mathrm{g}},\, v_i^{\mathrm{m}},\, \boldsymbol{\theta}_i^{\mathrm{f}},\, \alpha_i \mid i = 1, \dots, N_S;\ \sum_{i=1}^{N_S} v_i^{\mathrm{g}} = 1.0;\ \sum_{i=1}^{N_S} v_i^{\mathrm{g}}\, v_i^{\mathrm{m}} = v_0 \right\}$$

Mean-Field-Based Deep Material Networks for woven composites

- Identification of topological parameters from direct simulations
  - Parameters:

$$\boldsymbol{\chi}^{\mathrm{VM}} = \left\{ v_i,\, \boldsymbol{\theta}_i,\, \alpha_i \mid i = 1, \dots, N_{\mathrm{S}};\ \sum_{i=1}^{N_{\mathrm{S}}} v_i = 1.0 - v_0 \right\}$$

$$\boldsymbol{\chi}^{\mathrm{LVM}} = \left\{ v_i,\, \boldsymbol{\theta}_i,\, \alpha_i \mid i = 1, \dots, N_{\mathrm{S}};\ \sum_{i=1}^{N_{\mathrm{S}}} v_i = 1.0 \right\}$$

$$\boldsymbol{\chi}^{\mathrm{VLM}} = \left\{ v_i^{\mathrm{g}},\, \boldsymbol{\theta}_i^{\mathrm{g}},\, v_i^{\mathrm{m}},\, \boldsymbol{\theta}_i^{\mathrm{f}},\, \alpha_i \mid i = 1, \dots, N_{\mathrm{S}};\ \sum_{i=1}^{N_{\mathrm{S}}} v_i^{\mathrm{g}} = 1.0;\ \sum_{i=1}^{N_{\mathrm{S}}} v_i^{\mathrm{g}} v_i^{\mathrm{m}} = v_0 \right\}$$

  - Using elastic data
    - Random properties on RVE

$$\boldsymbol{\gamma} = \left[E_0,\, \nu_0,\, E_{\mathrm{I}}^{\mathrm{T}},\, E_{\mathrm{I}}^{\mathrm{L}},\, \nu_{\mathrm{I}}^{\mathrm{LT}},\, \nu_{\mathrm{I}}^{\mathrm{TT}},\, G_{\mathrm{I}}^{\mathrm{LT}},\, V_{\mathrm{I}}\right]$$

Direct simulations on RVE

Constraints

    - Cost functions to minimise

$$L(\hat{\mathbb{C}}, \mathbb{C}(\boldsymbol{\chi})) = \frac{1}{n}\sum_{s=1}^{n} \frac{\|\hat{\mathbb{C}}(\boldsymbol{\gamma}_s) - \mathbb{C}(\boldsymbol{\chi}|\boldsymbol{\gamma}_s)\|}{\|\hat{\mathbb{C}}(\boldsymbol{\gamma}_s)\|} + \frac{\lambda}{2} G(\boldsymbol{\chi})$$

    - « stochastic gradient descent (SGD) » algorithm

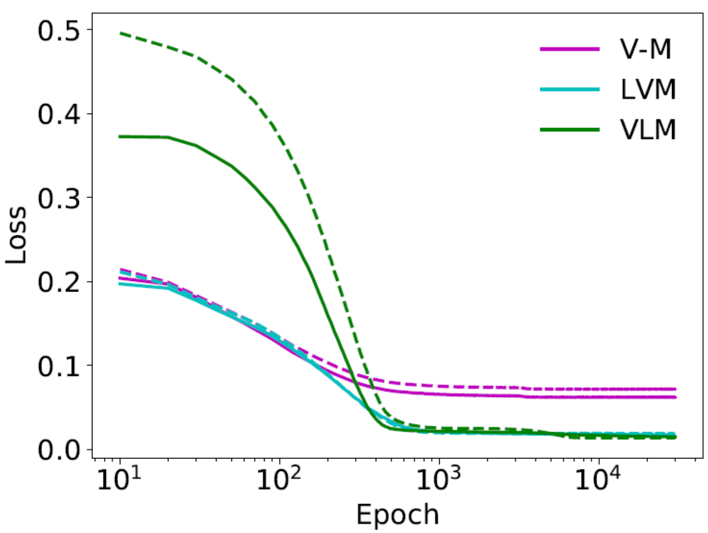

Mean-Field-Based Deep Material Networks for woven composites

- Elasto-plastic matrix case

PBC tension cyclique

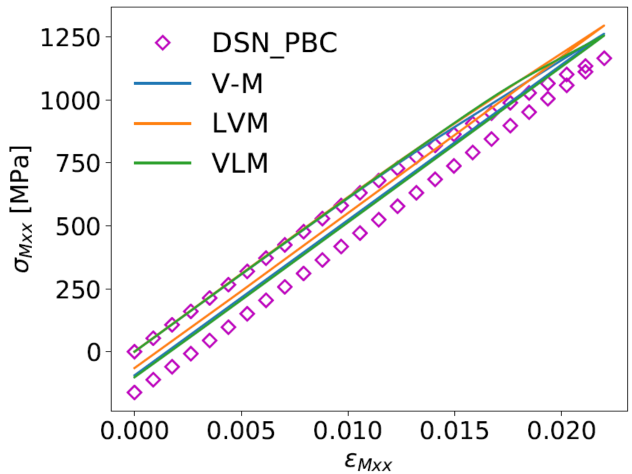

MBC tension cyclique

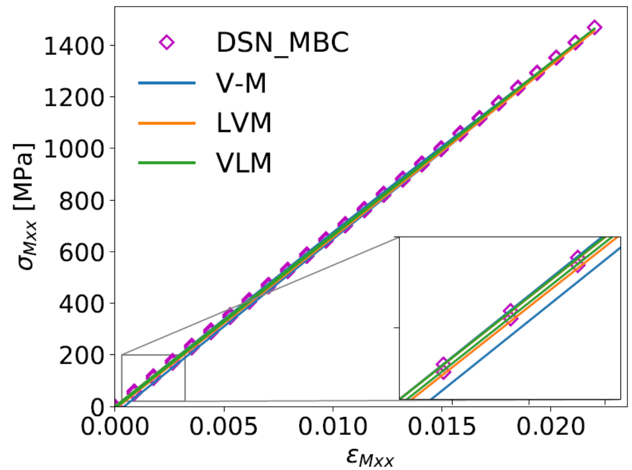

MBC tension

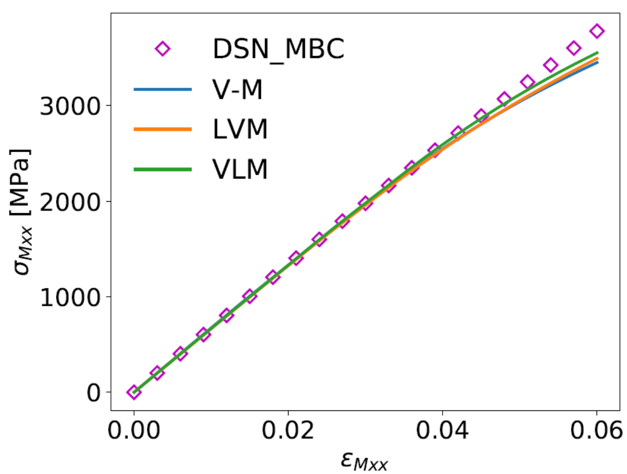

Cisaillement

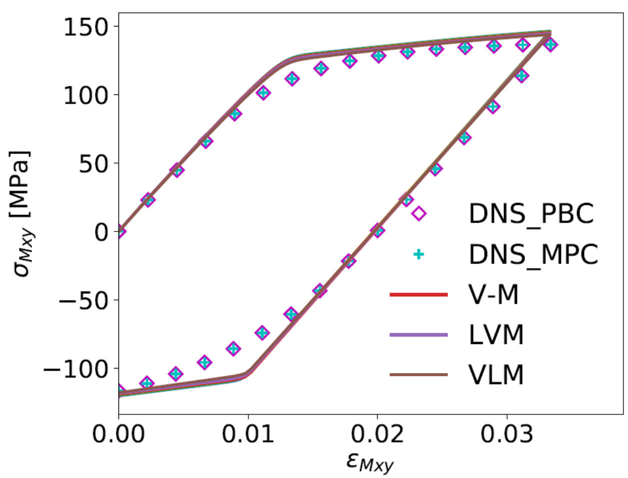

Mean-Field-Based Deep Material Networks for woven composites

- VISCOS project, 21st Call of Skywin
  - SONACA S.A.
  - e-Xstream (Hexagon S.A.)
  - Isomatex S.A.
  - UCL
  - ULiege
- Publications (doi)
  - 10.1016/j.compstruct.2021.114058
    - Open data

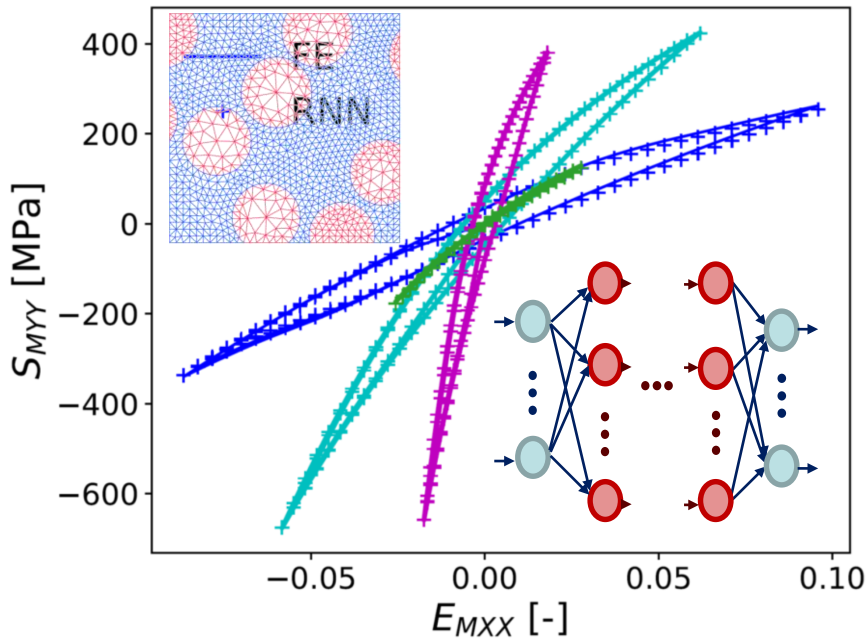

Recurrent Neural Network-accelerated multi-scale simulations in elasto-plasticity

MOAMMM project has received funding from the European Union's Horizon 2020 research and innovation programme under grant agreement No 862015 for the project Multi-scale Optimisation for Additive Manufacturing of fatigue resistant shock-absorbing MetaMaterials (MOAMMM) of the H2020-EU.1.2.1. - FET Open Programme

MOAMMM

Recurrent Neural Network-accelerated multi-scale simulations

- Introduction to non-linear multi-scale simulations
  - FE multi-scale simulations
    - Problems to be solved at two scales
    - Requires Newton-Raphson iterations at both scales
  - Use of surrogate models
    - Train a meso-scale surrogate model (off-line)
      - Requires extensive data
      - Obtained from RVE simulations
    - Use the trained surrogate model during analyses (on-line)
      - Surrogate acts as a homogenised constitutive law
      - Expected speed-up of several orders

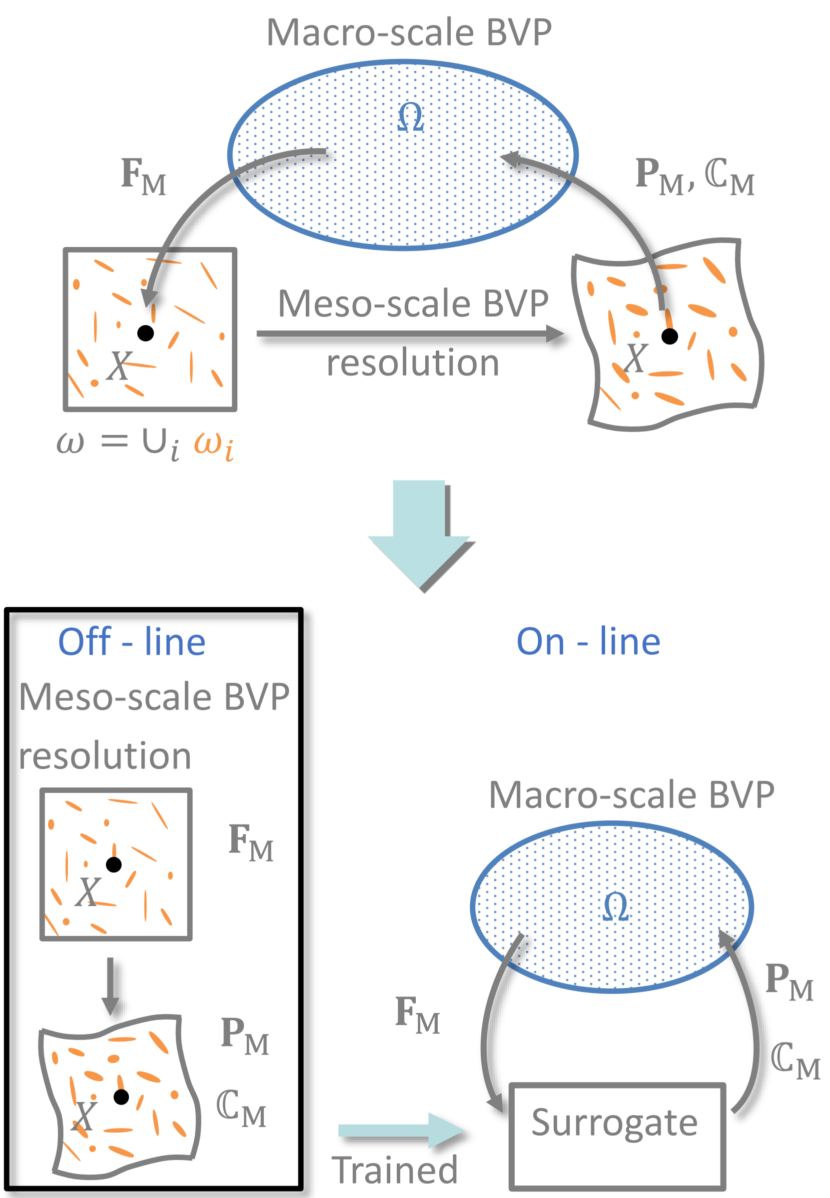

Recurrent Neural Network-accelerated multi-scale simulations

- Definition of the surrogate model
  - Artificial neuron
    - Non-linear function on n_0 inputs u_k
    - Requires evaluation of weights w_k
    - Requires definition of activation function f

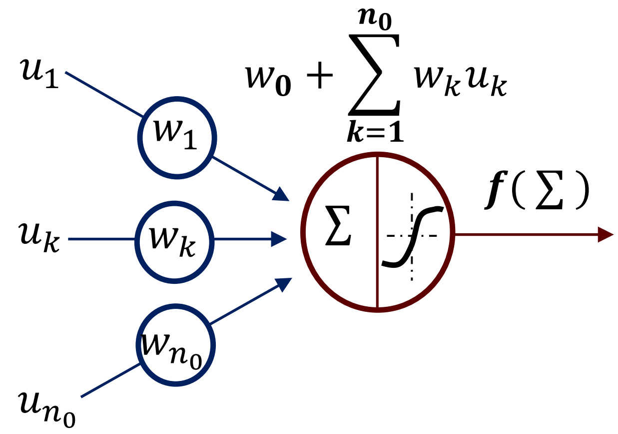

  - Activation functions f

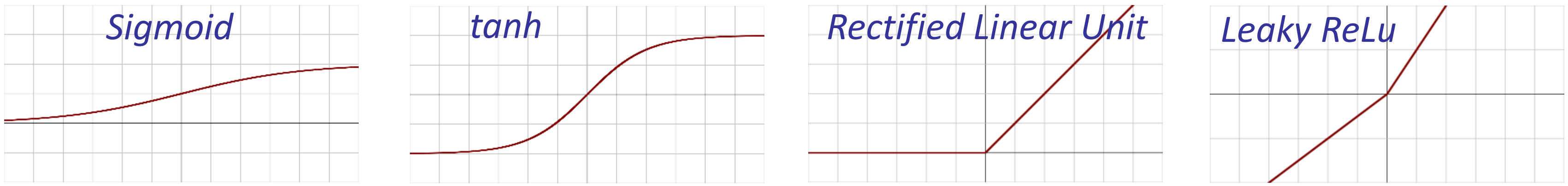

  - Feed-Forward Neuron Network
    - Simplest architecture
    - Layers of neurons
      - Input layer
      - $N-1$ hidden layers
      - Output layers
    - Mapping $\Re^{n_0} \rightarrow \Re^{n_N}: \boldsymbol{v} = \boldsymbol{g}(\boldsymbol{u})$

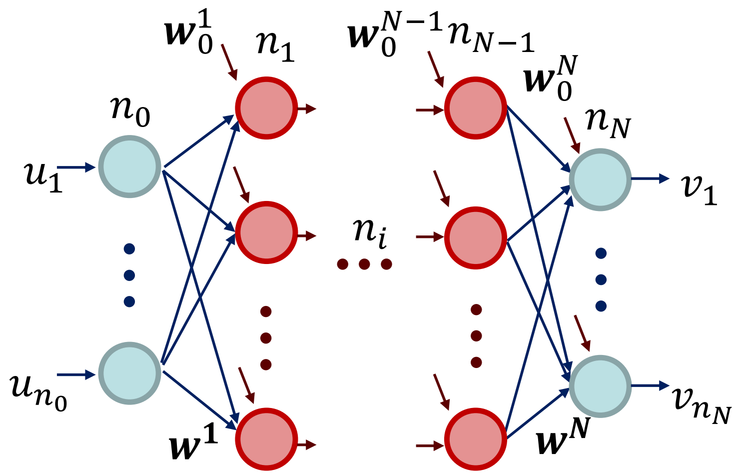

Recurrent Neural Network-accelerated multi-scale simulations

- Training
  - Evaluate
    - The weights w_{kj}^{i}, $k = 1..n_{i-1}, j = 1..n_i$
    - The bias w_0^i
    - Minimise error prediction $\boldsymbol{v}$ vs. real $\boldsymbol{v}^{(p)}$

$$L_{\mathrm{MSE}}\left(\mathbf{W}\right) = \frac{1}{n}\sum_{i}^{n}\left\|\boldsymbol{v}_i(\mathbf{W}) - \boldsymbol{v}_i^{(p)}\right\|^2$$

    - Requires an optimizer: Stochastic Gradient Descent

$$\boldsymbol{\Delta}\mathbf{W} = -\mathcal{F}\left(\frac{\partial L_i(\mathbf{W})}{\partial \mathbf{W}}, \quad \left(\frac{\partial L_i(\mathbf{W})}{\partial \mathbf{W}}\right)^2, \text{batch size}, \ldots\right)$$

  - Training data
    - Input $\boldsymbol{u}^{(p)}$ & Output $\boldsymbol{v}^{(p)}$
- Testing
  - Use new data
    - Input $\boldsymbol{u}^{(p)}$ & Output $\boldsymbol{v}^{(p)}$
    - Verify prediction $\boldsymbol{v}$ vs. real $\boldsymbol{v}^{(p)}$

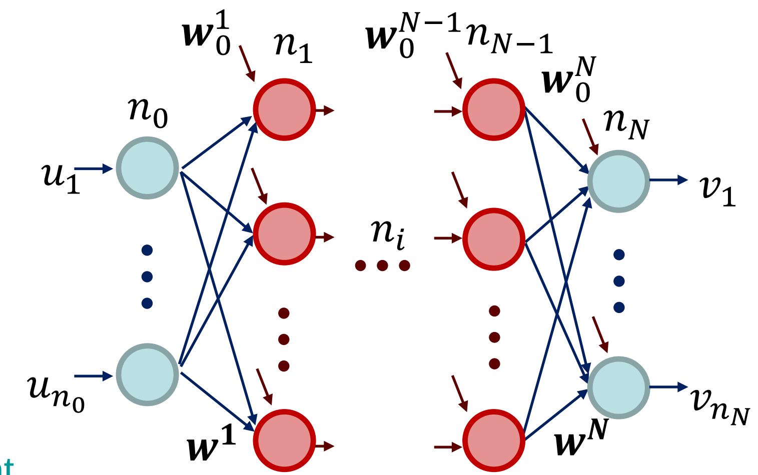

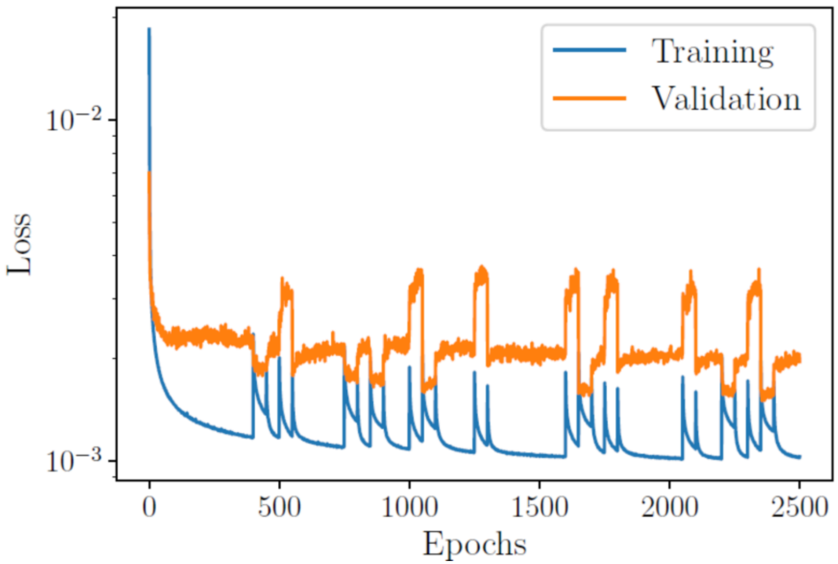

Beginning

Recurrent Neural Network-accelerated multi-scale simulations

- Input / output definition
  - Input: Strain (history): $\mathbf{F}_{\mathrm{M}}$
  - Output: Stress (history): $\mathbf{P}_{\mathrm{M}}$
- Elasto-plastic material behaviour
  - No bijective strain-stress relation
    - Feed-forward NNW cannot be used
    - History should be accounted for

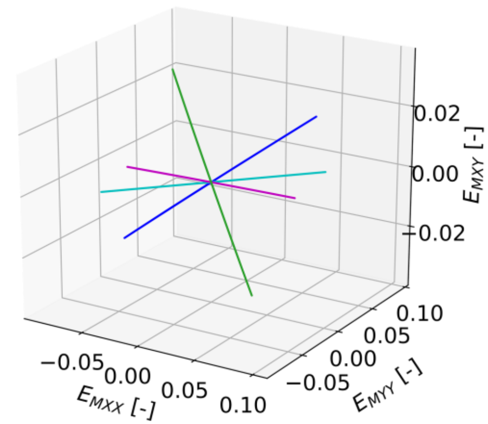

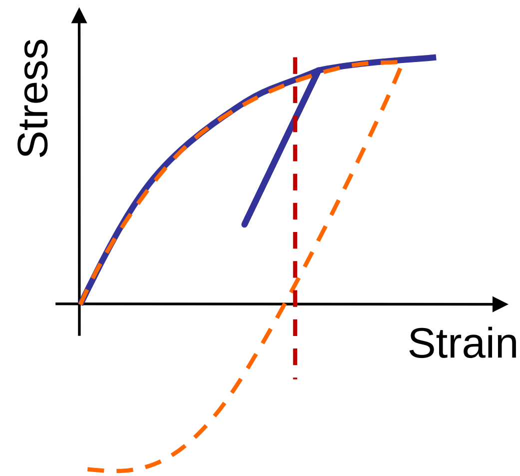

- Recurrent neural network
  - Allows a history dependent relation
    - Input $\boldsymbol{u}_t$
    - Output $\boldsymbol{v}_t = \boldsymbol{g}(\boldsymbol{u}_t, \boldsymbol{h}_{t-1})$
    - Internal variable $\boldsymbol{h}_t = \boldsymbol{g}(\boldsymbol{u}_t, \boldsymbol{h}_{t-1})$
  - Weights matrices $\mathbf{U}, \mathbf{W}, \mathbf{V}$
    - Trained using sequences
      - Inputs $\boldsymbol{u}_{t-n}^{(p)}, \ldots, \boldsymbol{u}_t^{(p)}$
      - Output $\boldsymbol{v}_{t-n}^{(p)}, \ldots, \boldsymbol{v}_t^{(p)}$

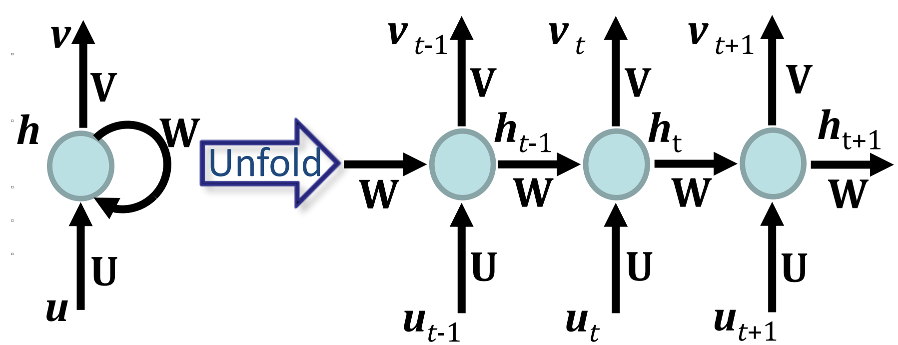

LIÈGE université

- Gated Recurrent Unit (GRU) at a glance

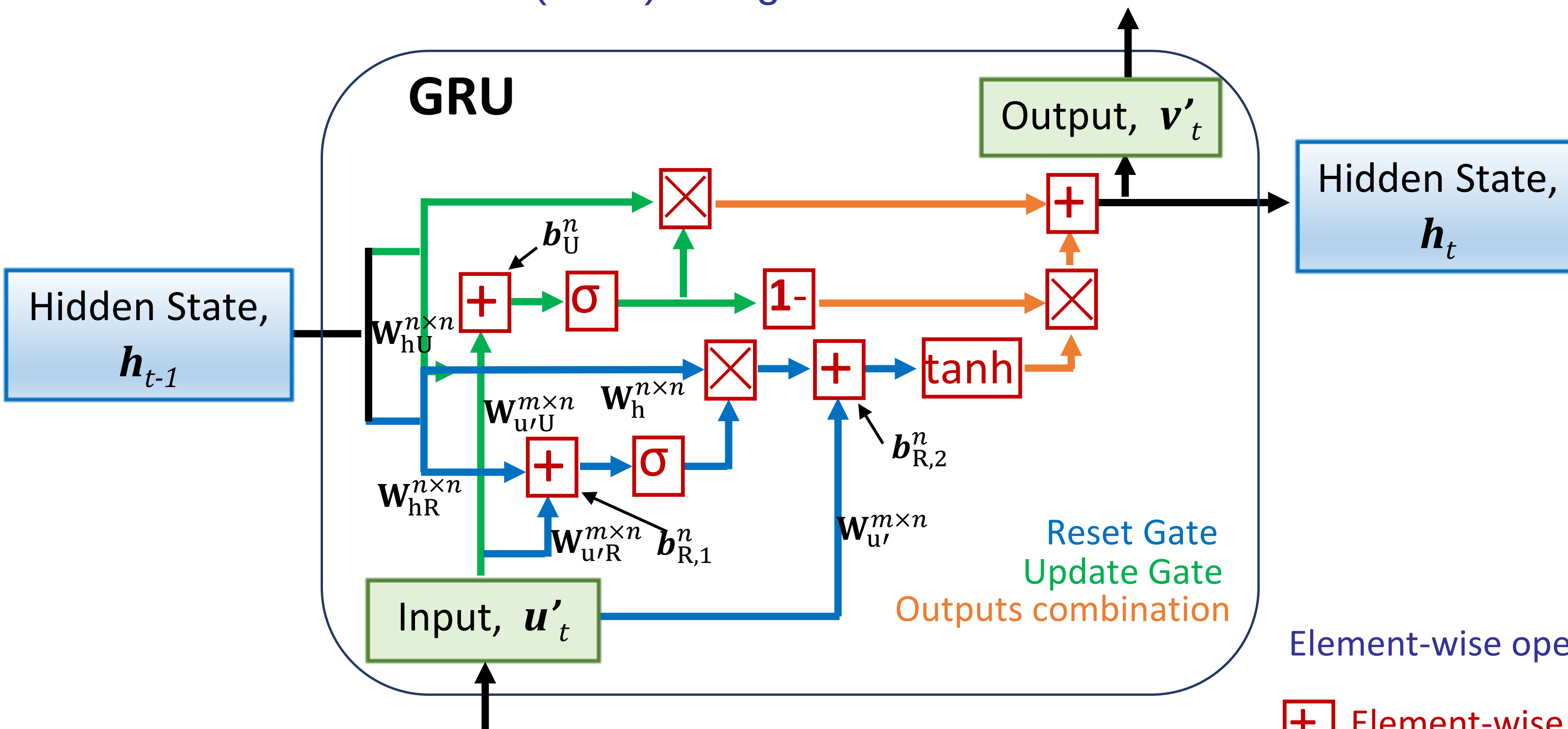

Element-wise operations

- + Element-wise sum
- 1- Element-wise 1-
- ⊠ Element-wise product
- σ Element-wise sigmoid
- tanh Element-wise tanh

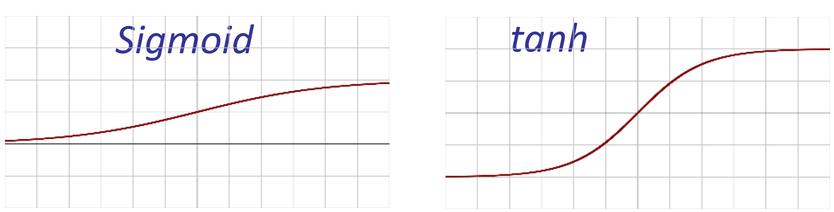

Recurrent Neural Network-accelerated multi-scale simulations

- Recurrent neural network design
  - 1 Gated Recurrent Unit (GRU)
    - Rest gate: select past information to be forgotten
    - Update gate: select past information to be passed along
  - 2 feed-forward NNWs
    - NNW_I to treat inputs $\boldsymbol{u}_t$
    - NNW_O to produce outputs $\boldsymbol{v}_t$
  - Details
    - $\boldsymbol{u}_t$: homogenised GL strain $\mathbf{E}_\text{M}$ (symmetric)
    - $\boldsymbol{v}_t$: homogenised 2nd PK stress $\mathbf{S}_\text{M}$ (symmetric)
    - 100 hidden variables $\boldsymbol{h}_t$
    - NNW_I one hidden layer of 60 neurons
    - NNW_O two hidden layers of 100 neurons

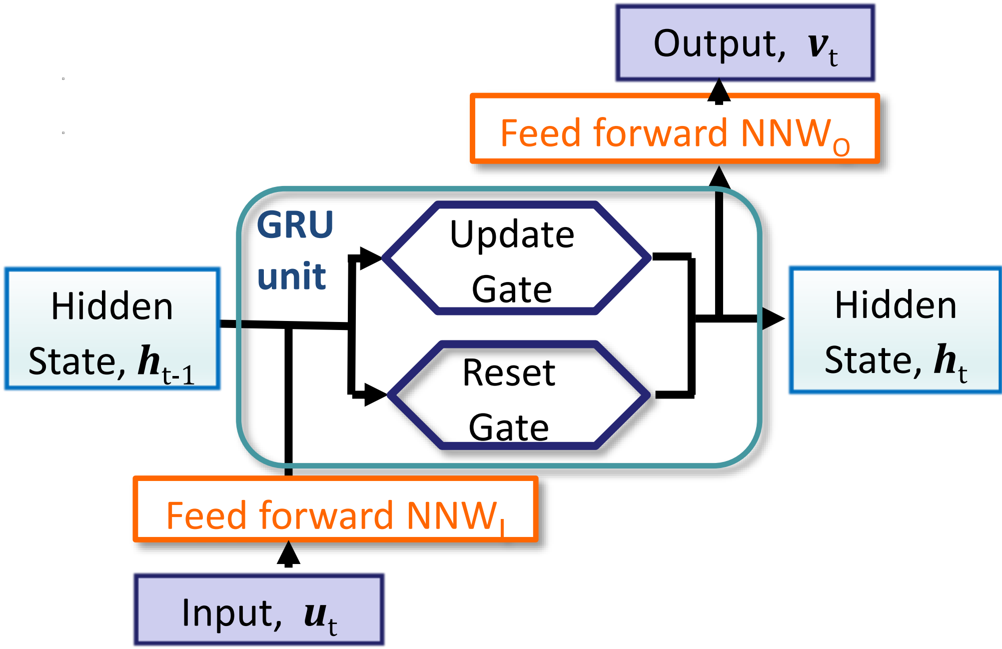

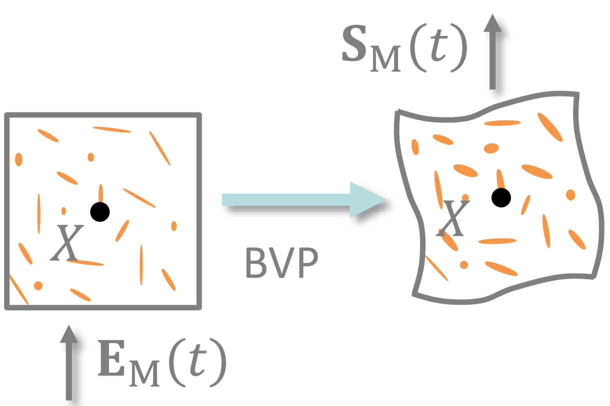

Recurrent Neural Network-accelerated multi-scale simulations

- Data generation
  - Elasto-plastic composite RVE
  - Training stage
    - Should cover full range of possible loading histories
    - Use random walking strategy (thousands)
    - Completes with random cyclic loading (tens)
    - Bounded by a sphere of 10% deformation

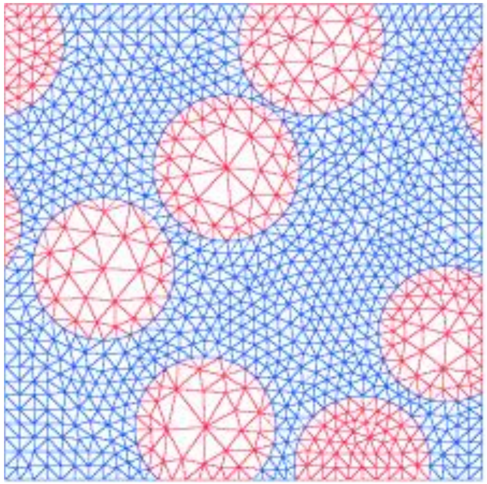

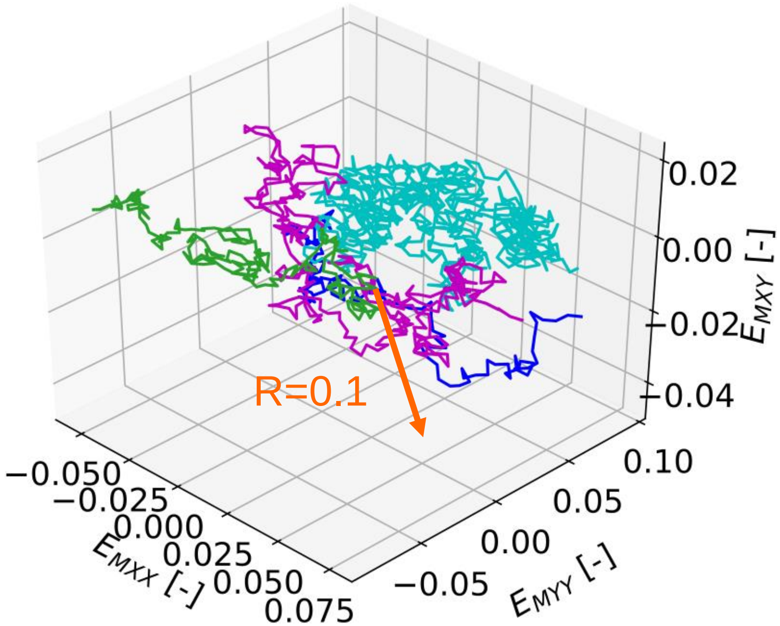

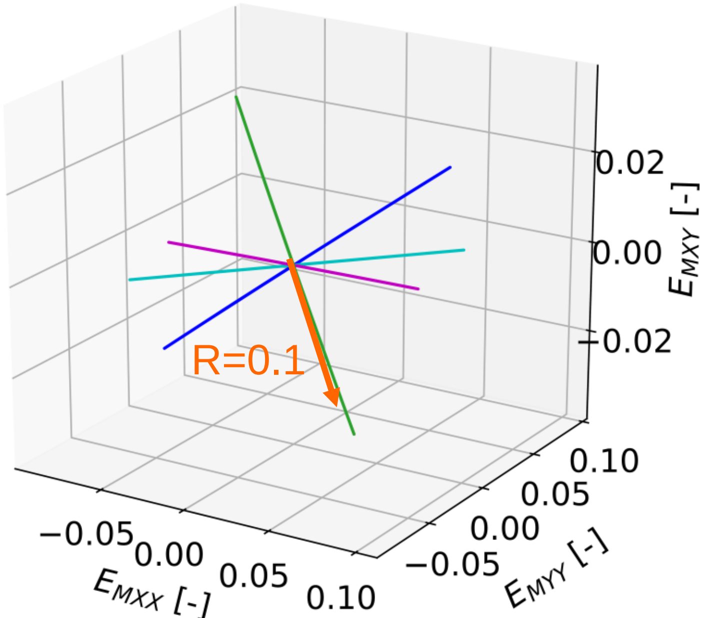

- Testing process (new data)
  - On random walk

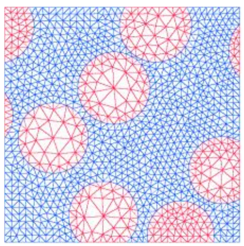

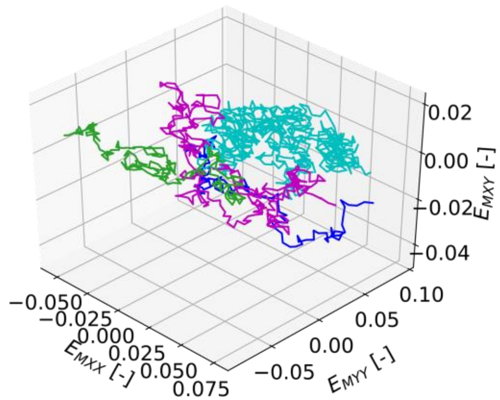

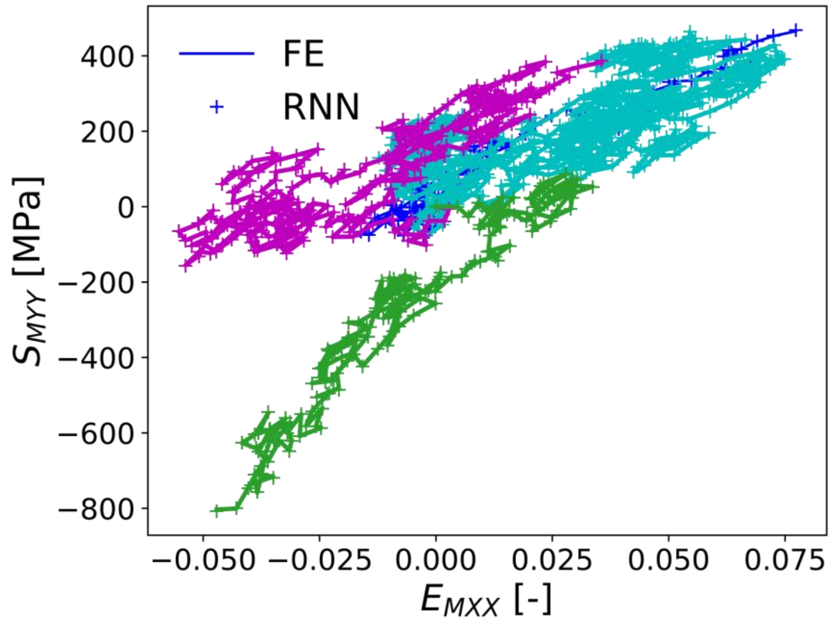

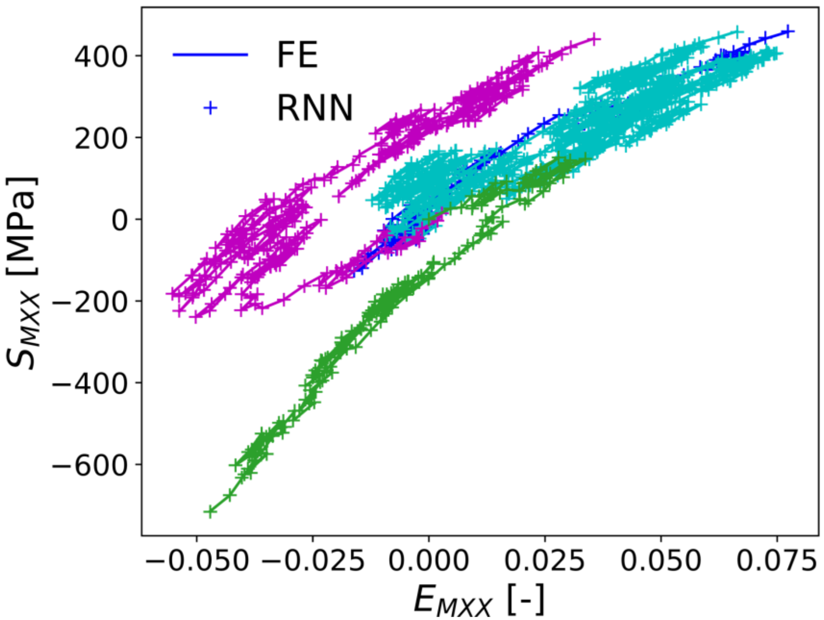

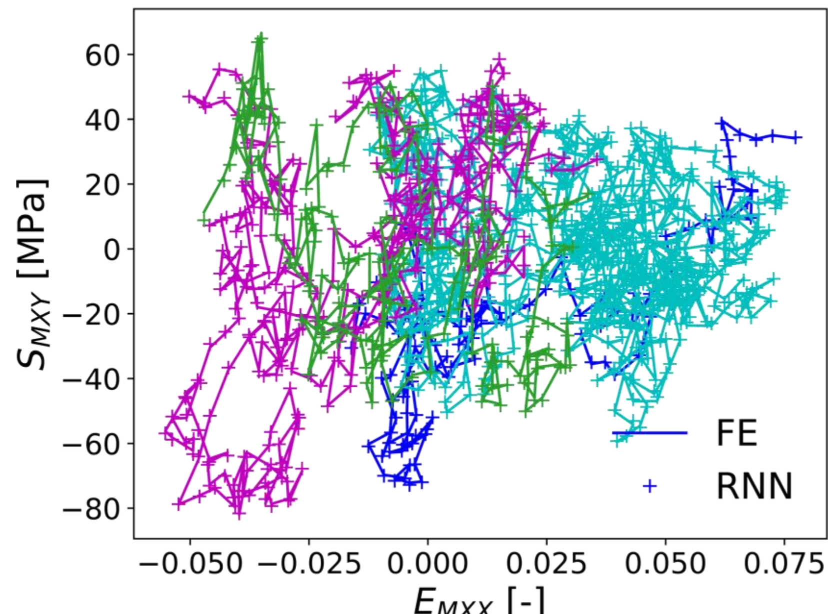

Recurrent Neural Network-accelerated multi-scale simulations

- Testing process (new data)
  - On cyclic loading

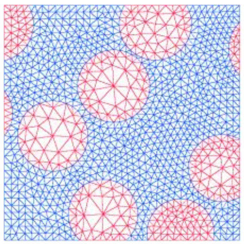

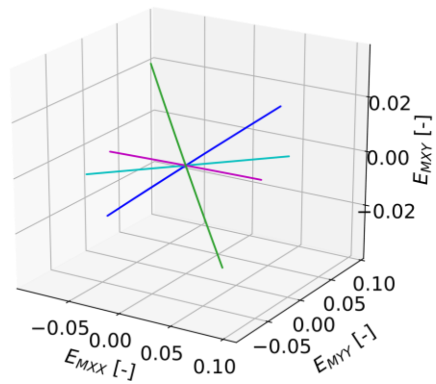

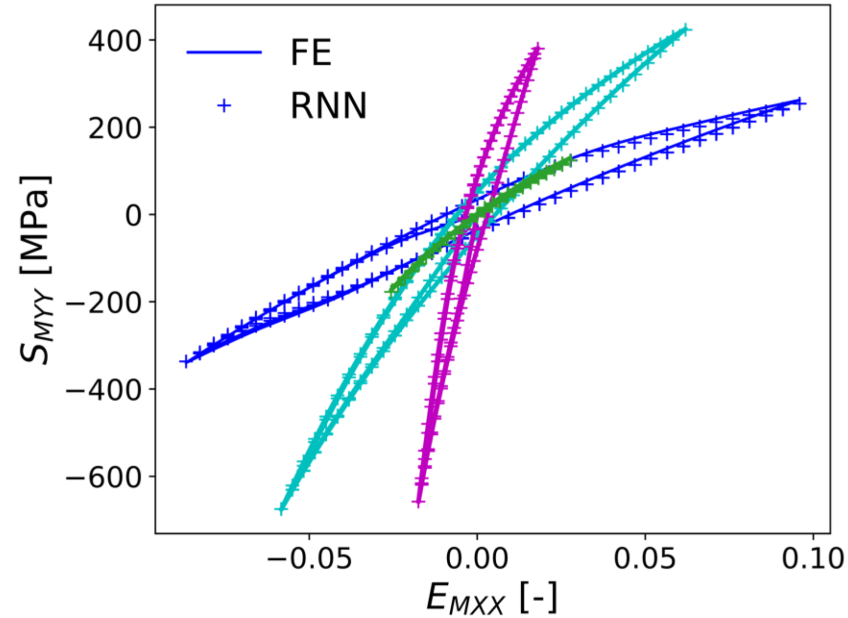

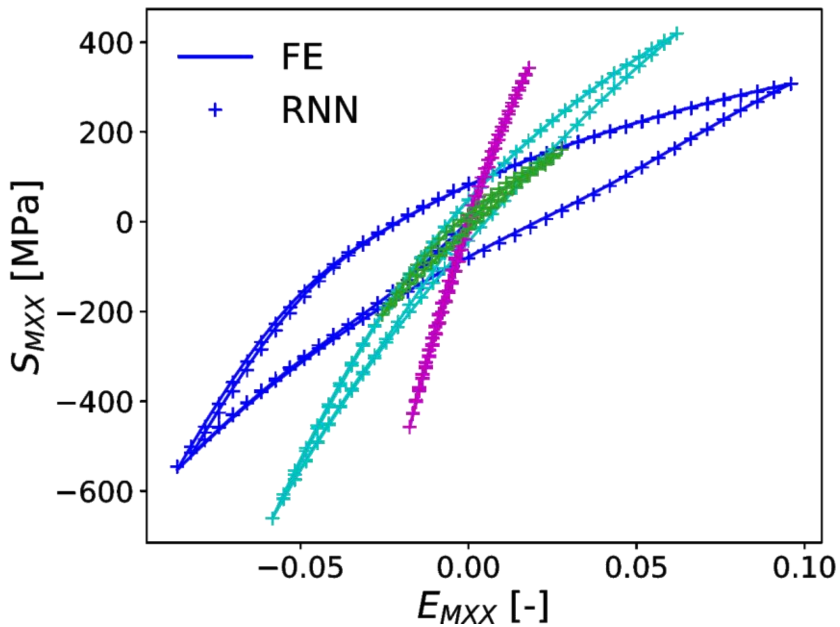

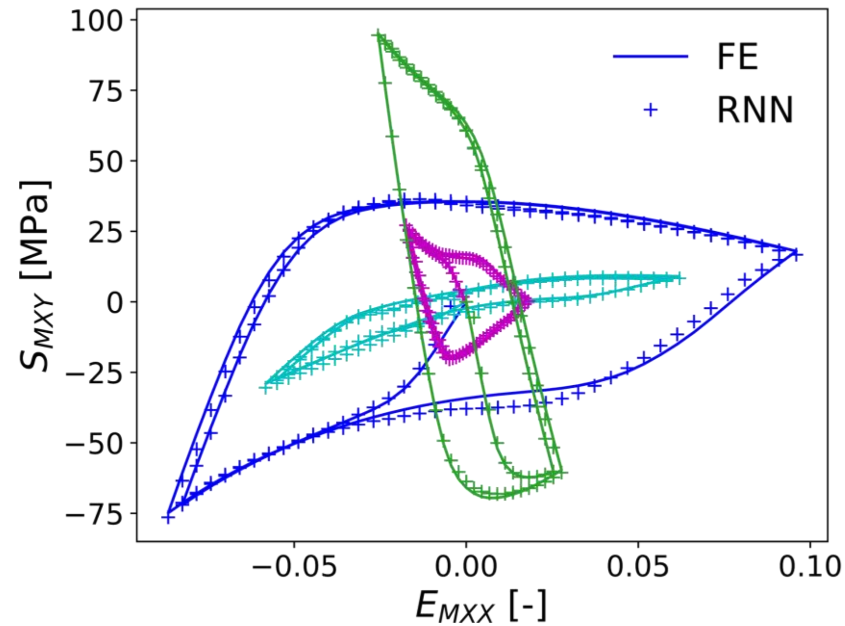

Recurrent Neural Network-accelerated multi-scale simulations

- Multiscale simulation
  - Elasto-plastic composite RVE
  - Comparison FE^2 vs. RNN-surrogate
  - Training data
    - Bounded at 10% deformation

Off-line	FE^2	FE-RNN
Data generation	-	9000 x 2 h-cpu
Training	-	3 day-cpu
On-line	**FE^2**	**FE-RNN**
Simulation	18000 h-cpu	0.5 h-cpu

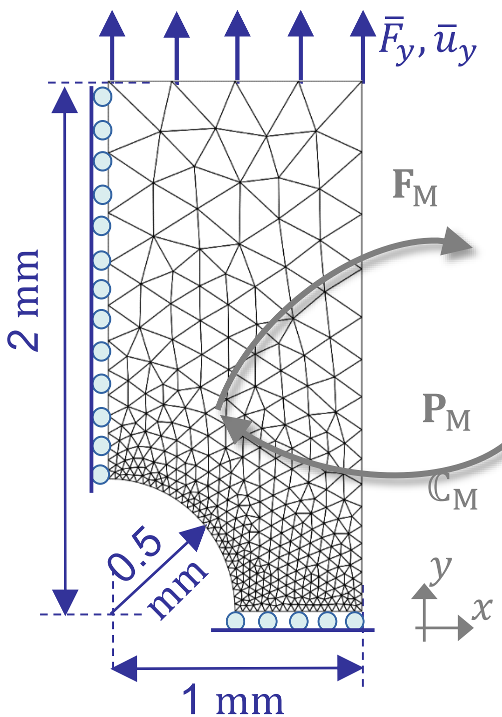

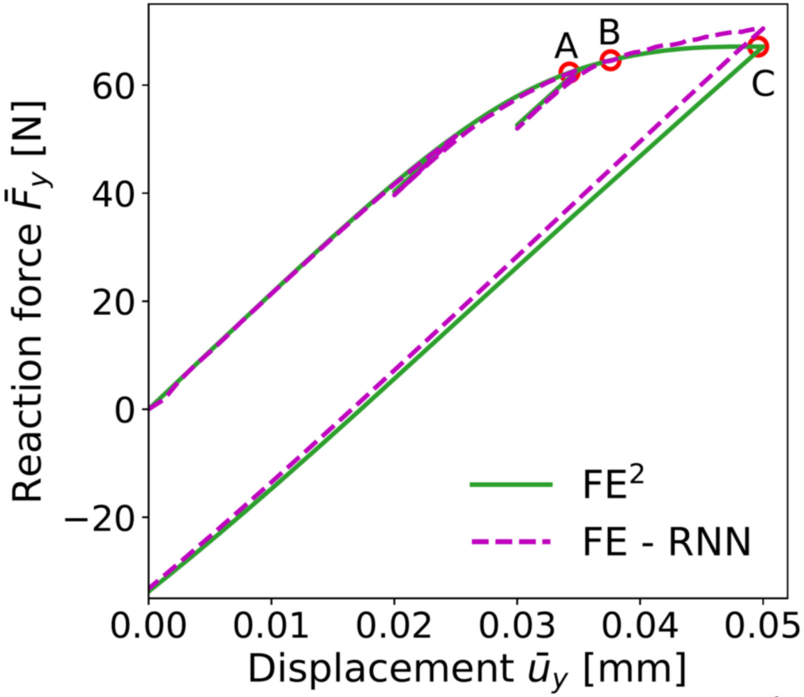

- Multiscale simulation
  - Stress-strain distribution at point A
  - Strain within the 10% training range

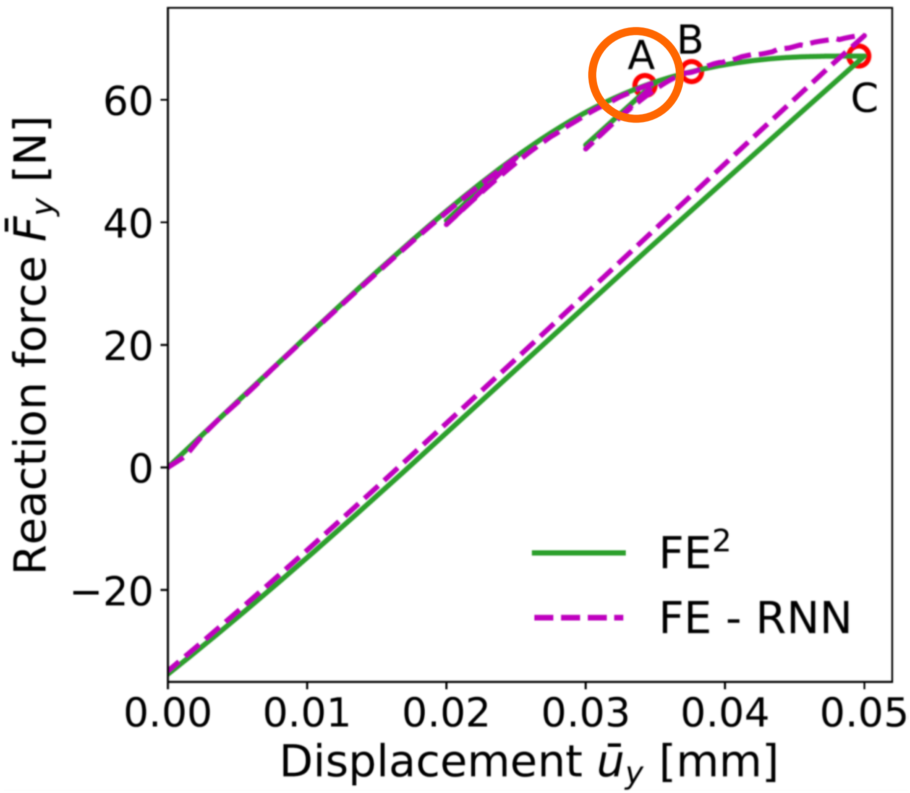

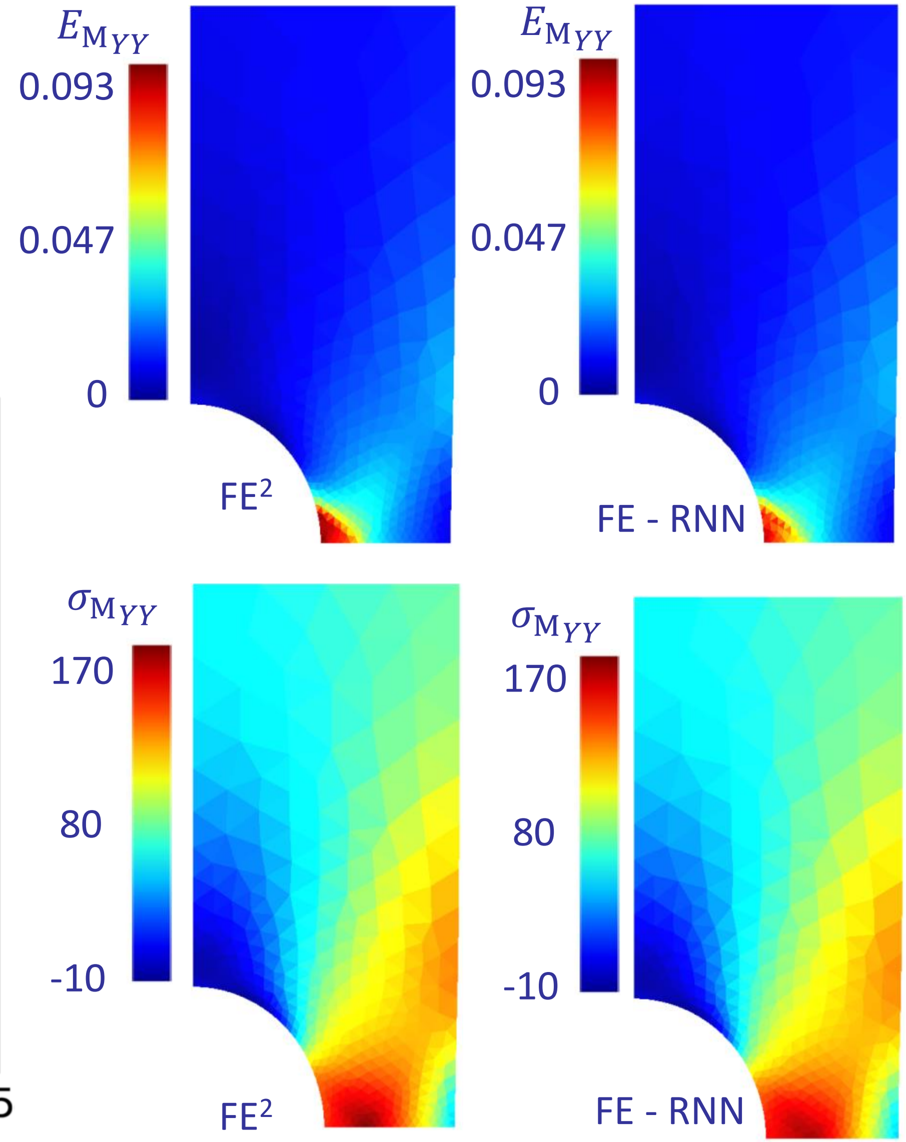

Recurrent Neural Network-accelerated multi-scale simulations

- Multiscale simulation
  - Stress-strain distribution at point B
  - Strain just at 10% training range

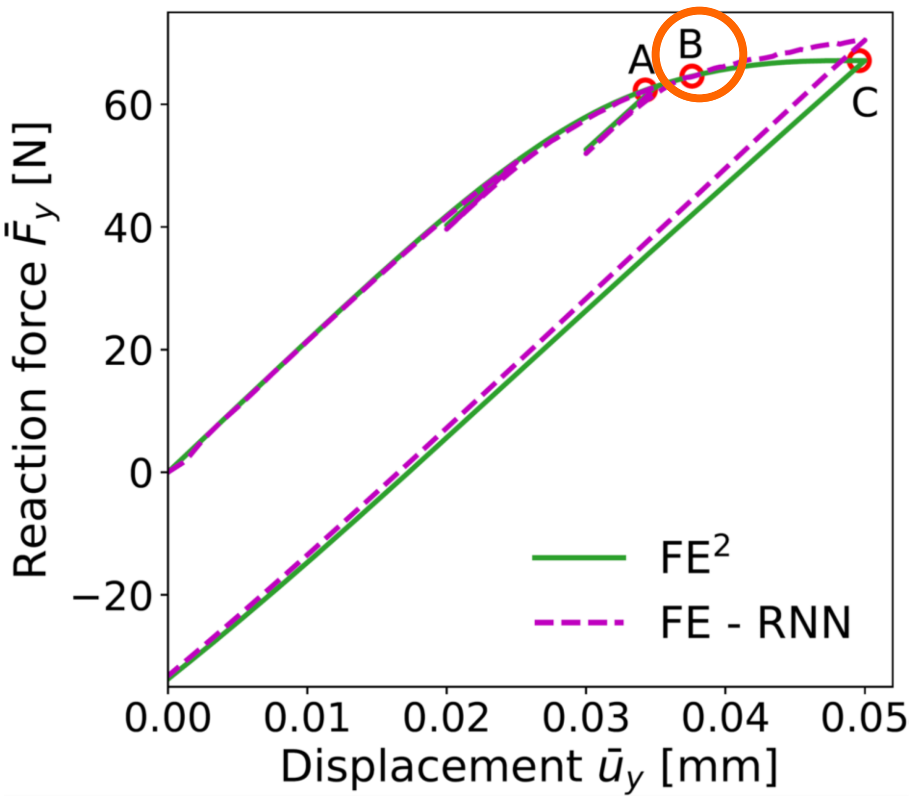

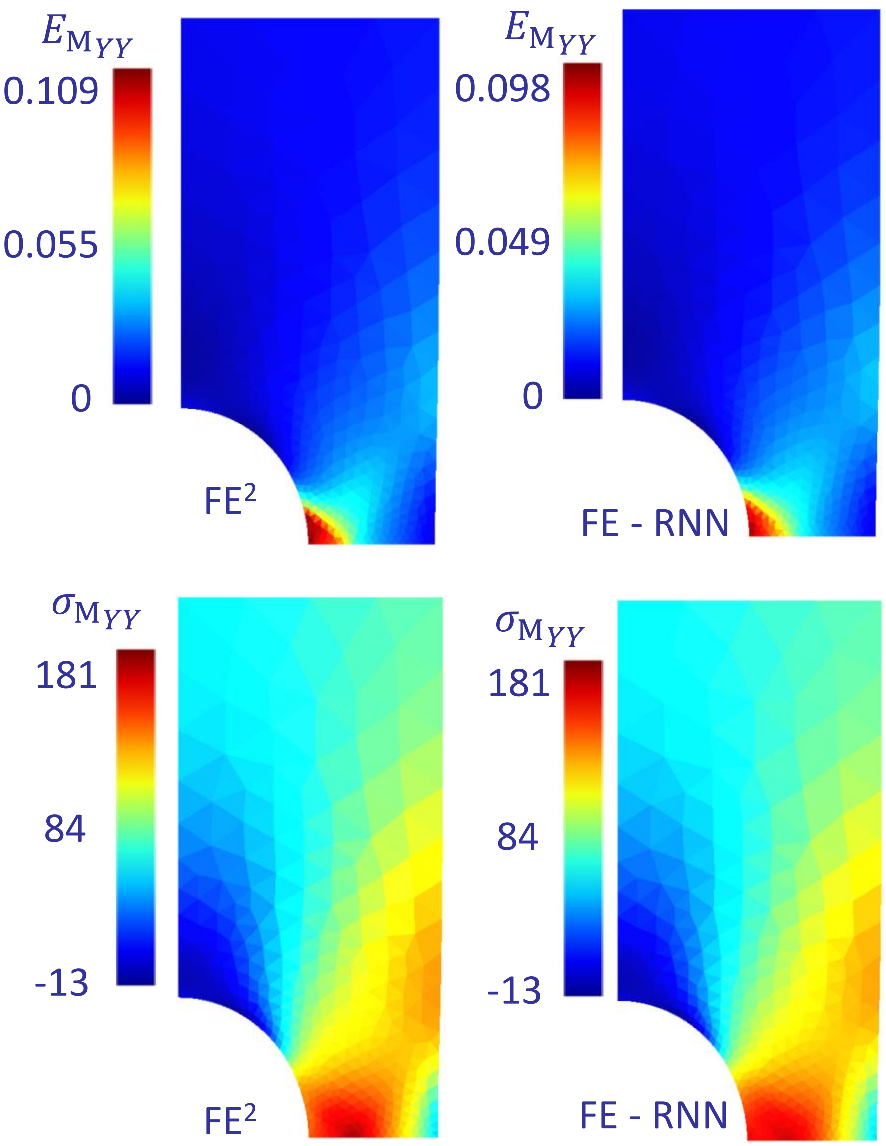

- Multiscale simulation
  - Stress-strain distribution at point C
  - Strain out of 10% training range

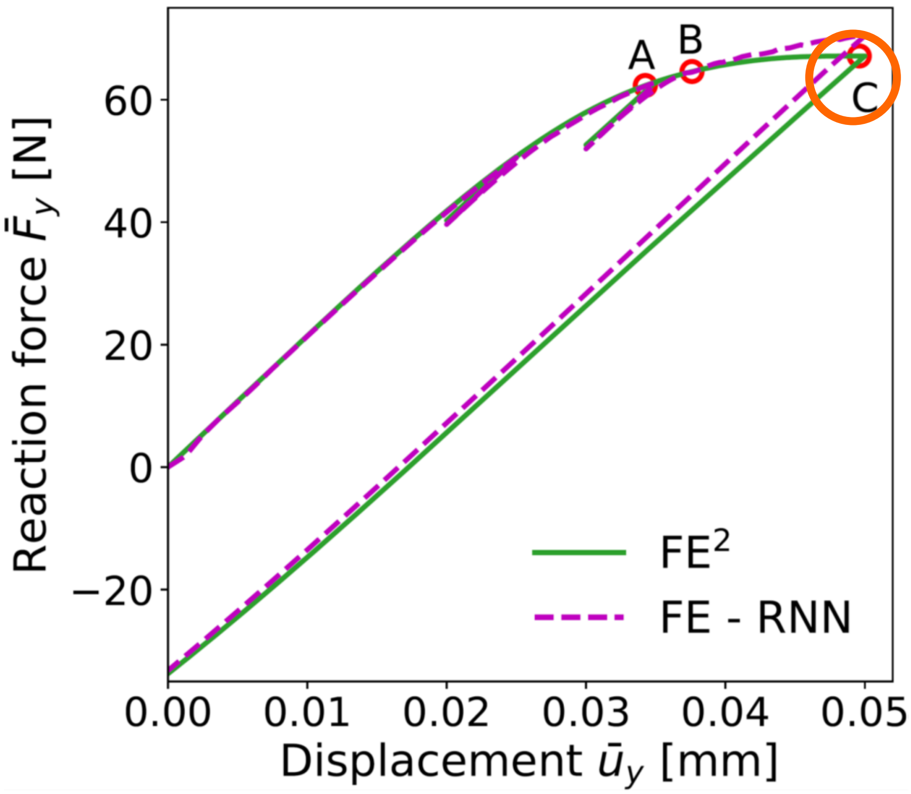

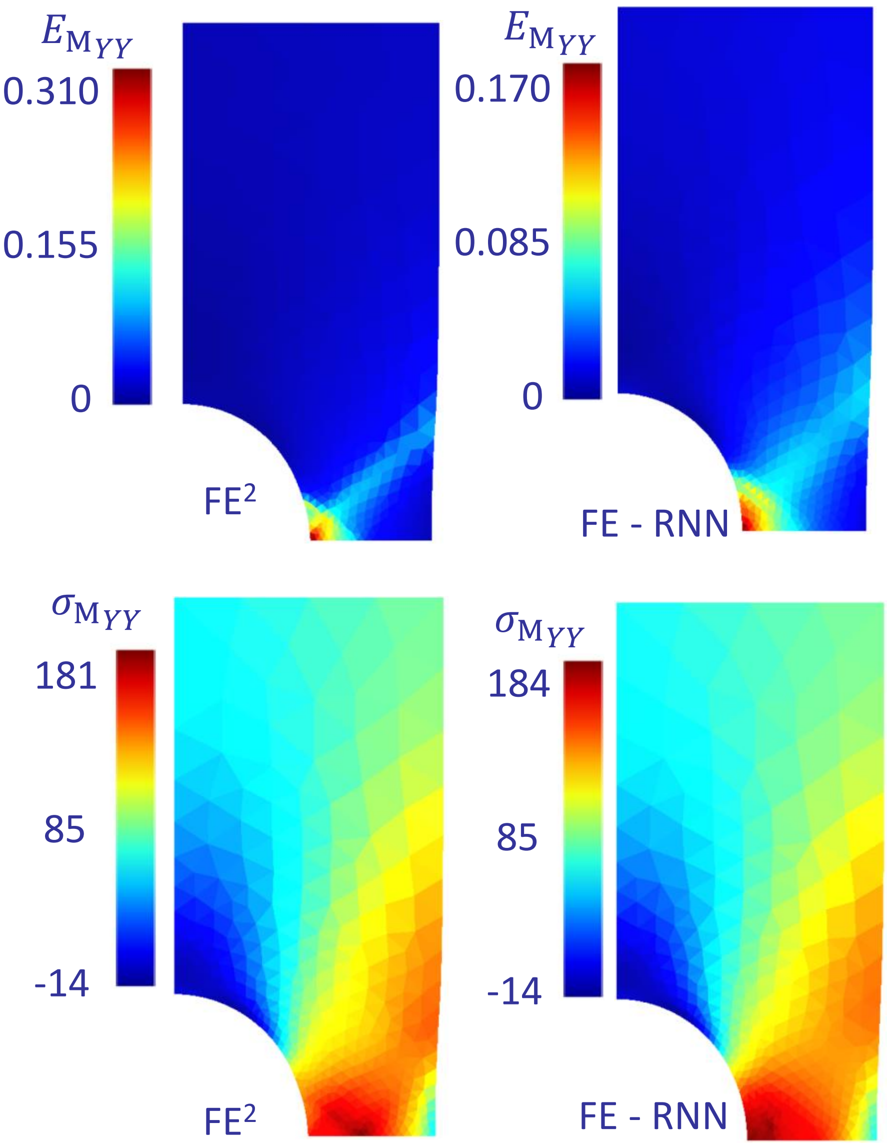

Recurrent Neural Network-accelerated multi-scale simulations

- MOAMMM FET-OPEN project (https://www.moammm.eu/)
  - ULiège, UCL (Belgium)
  - IMDEA Materials (Spain)
  - JKU (Austria)
  - cirp GmbH (Germany)

- Publications (doi)
  - 10.1016/j.cma.2020.113234
    - Open Data: 10.5281/zenodo.3902663
  - 10.1016/j.cma.2021.114476
    - Open Data: 10.5281/zenodo.5668390

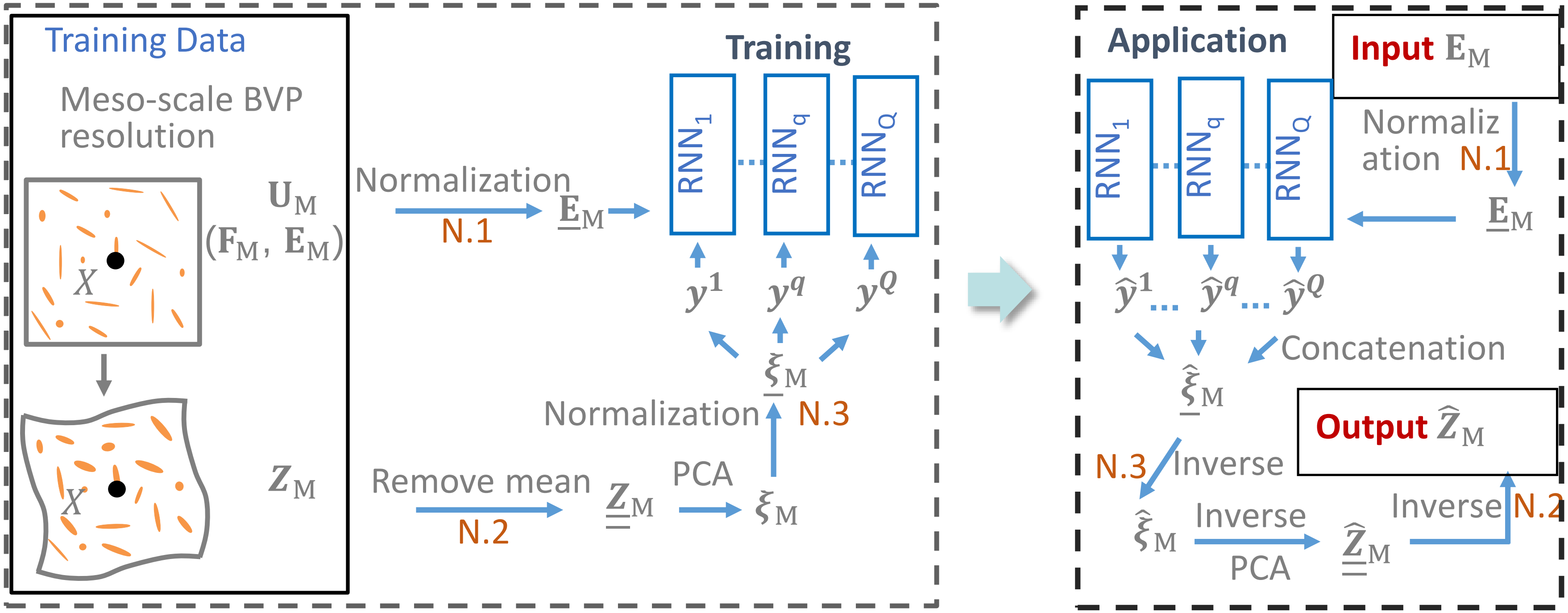

Recurrent Neural Network with dimensionality reduction and break down

MOAMMM project has received funding from the European Union's Horizon 2020 research and innovation programme under grant agreement No 862015 for the project Multi-scale Optimisation for Additive Manufacturing of fatigue resistant shock-absorbing MetaMaterials (MOAMMM) of the H2020-EU.1.2.1. - FET Open Programme

MOAMMM

LIÈGE université

RNN with dimensionality reduction and break down

- Recurrent neural network-accelerated multi-scale simulations
  - FE multi-scale simulations
    - Problems to be solved at two scales
    - Requires Newton-Raphson iterations at both scales
  - Use of surrogate models
    - Train a meso-scale surrogate model (off-line)
      - Requires extensive data
      - Obtained from RVE simulations
    - Use the trained surrogate model during analyses (on-line)
      - Surrogate acts as a homogenised constitutive law
      - Expected speed-up of several orders

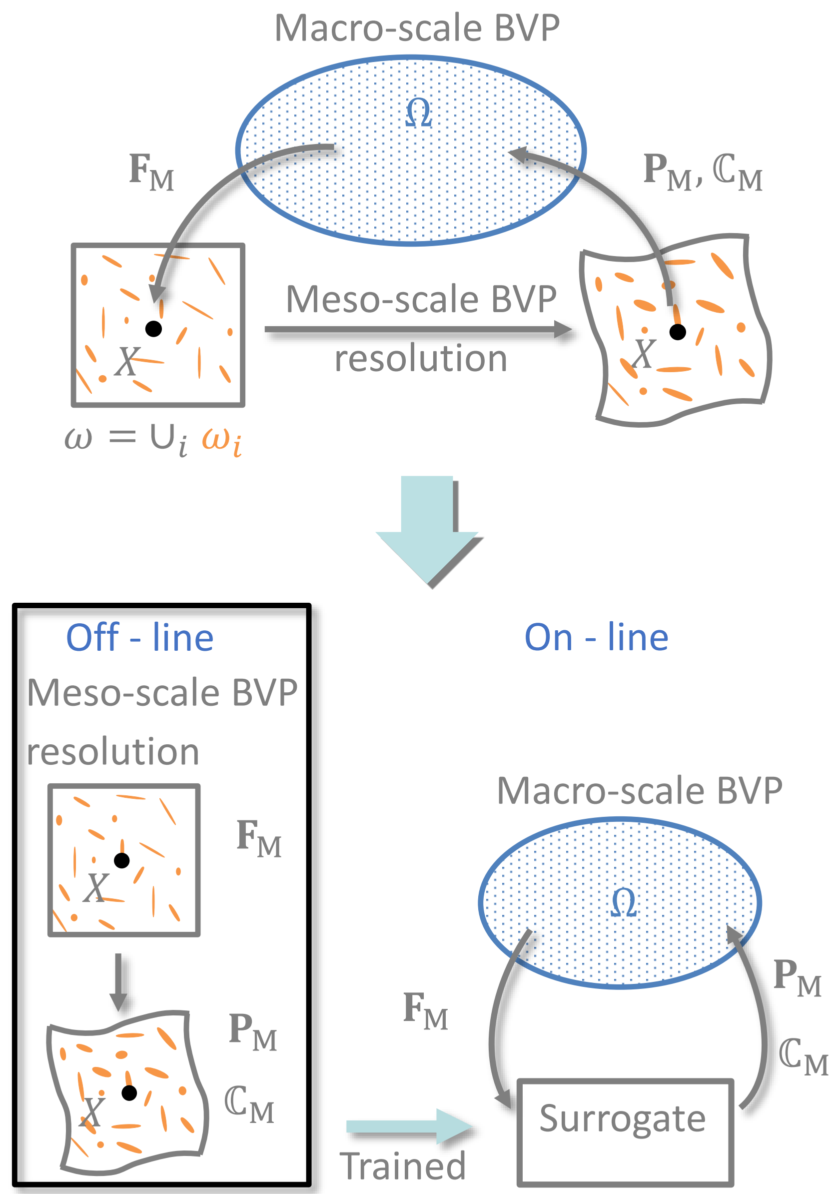

RNN with dimensionality reduction and break down

- Accurate surrogate of homogenised behaviour

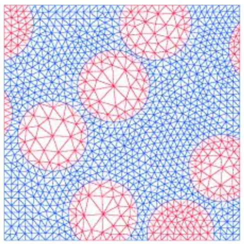

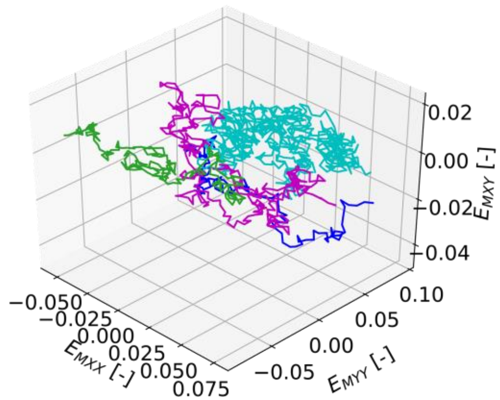

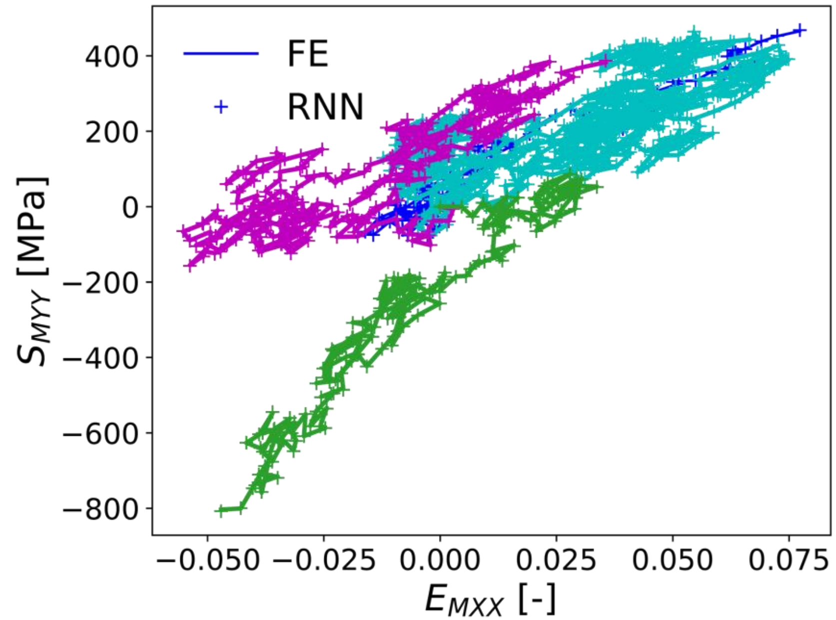

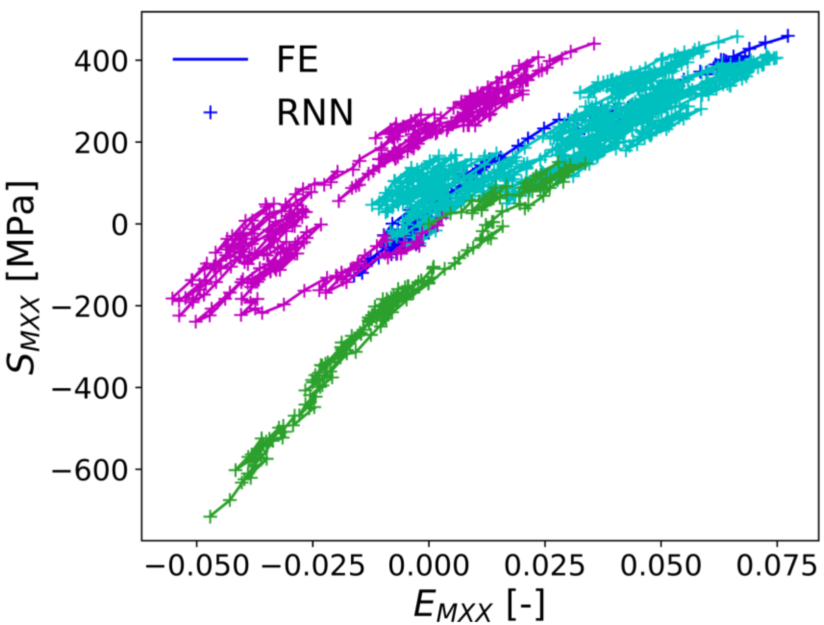

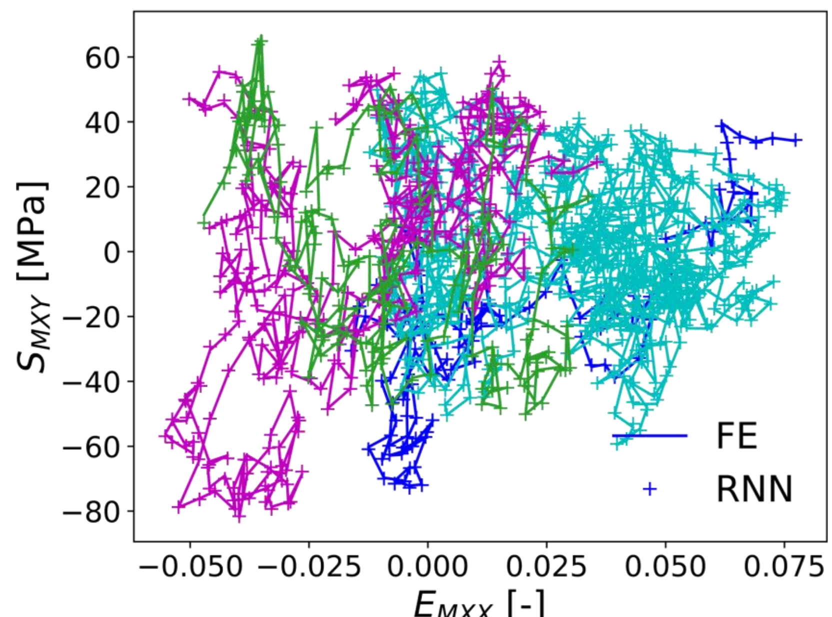

RNN with dimensionality reduction and break down

- Only homogenised output is predicted
  - On random walk

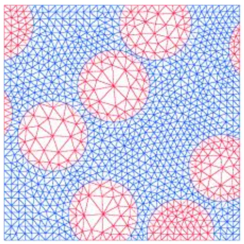

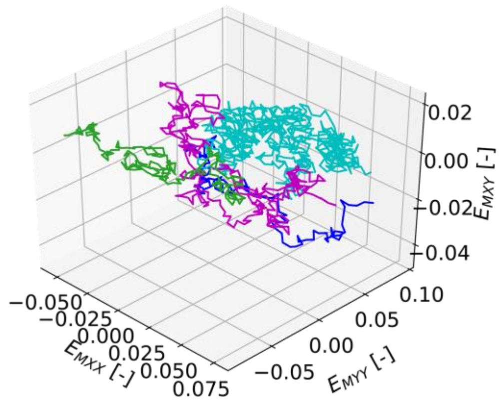

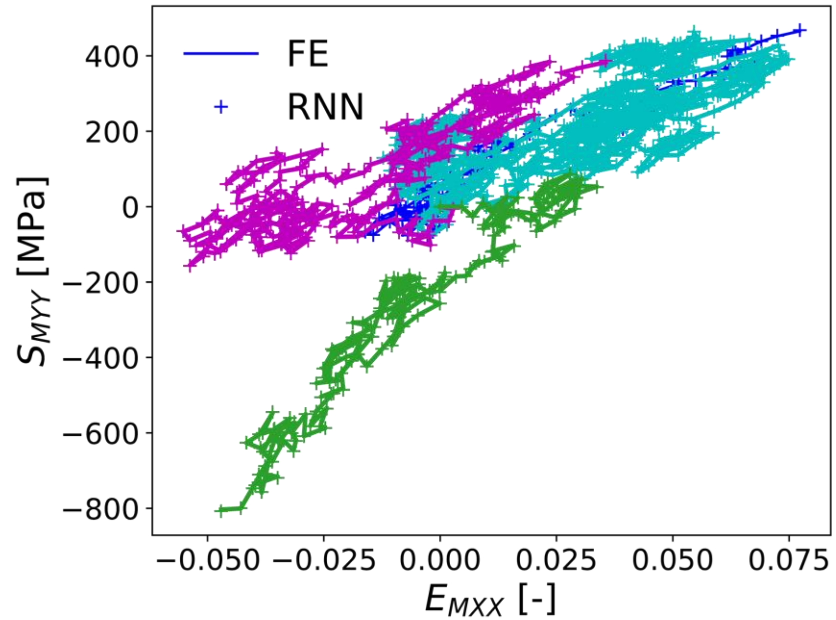

- Quid of local fields?
  - This is an advantage of multiscale methods
  - Useful to predict failure, fatigue etc.
  - Can we get it back at low cost?

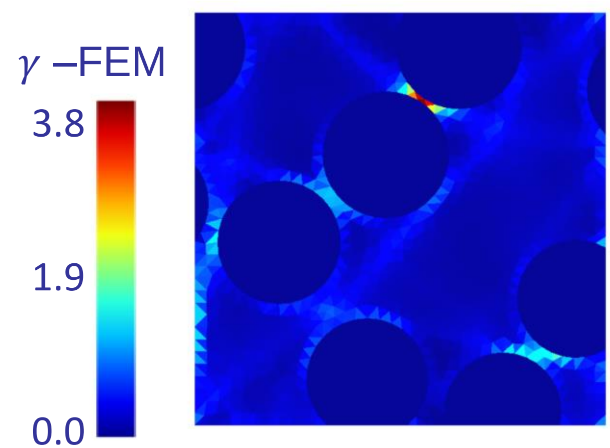

RNN with dimensionality reduction and break down

- Also build a surrogate model of the internal variables

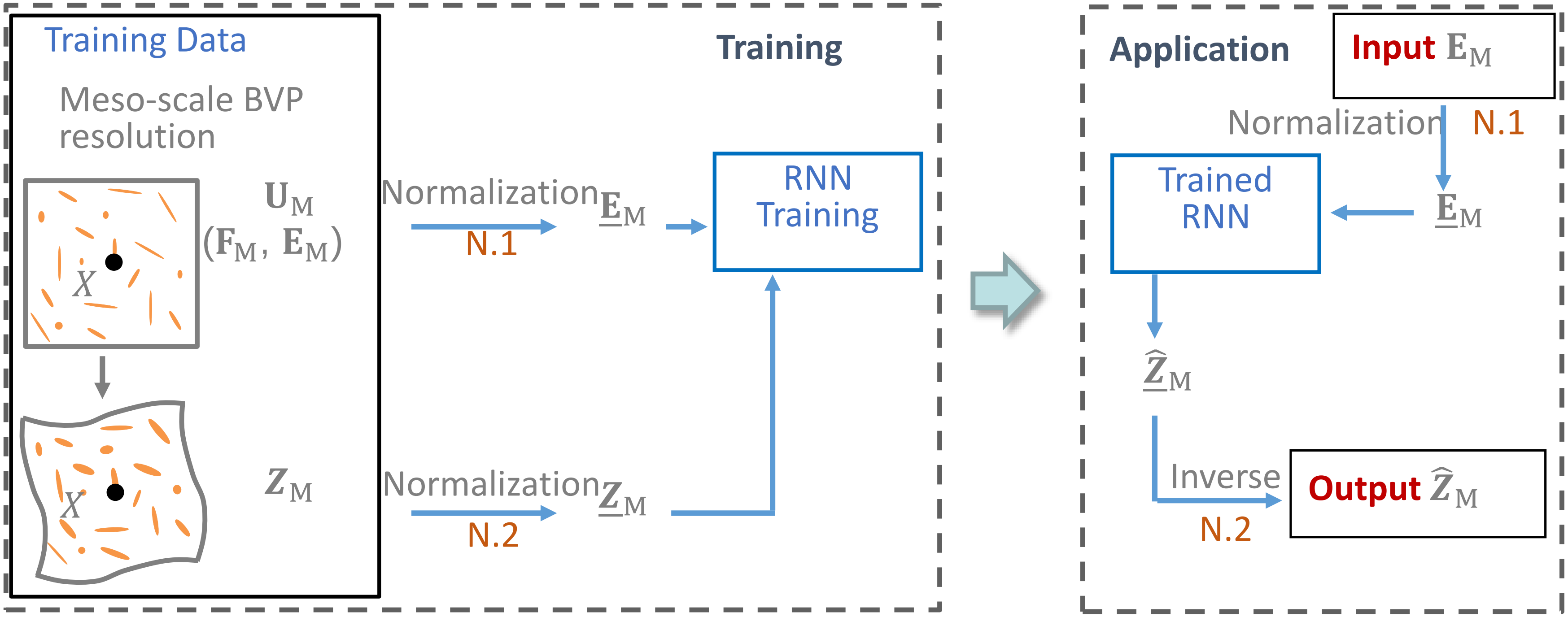

  - Problem: The size of $\underline{\boldsymbol{Z}}_\mathrm{M}$ is large
    - $\underline{\boldsymbol{Z}}_\mathrm{M}$ of size d the number of Gauss points of the RVE × internal variables by Gauss point

⇨ overwhelming cost

- Optimise the method: reduce the size of the internal variables

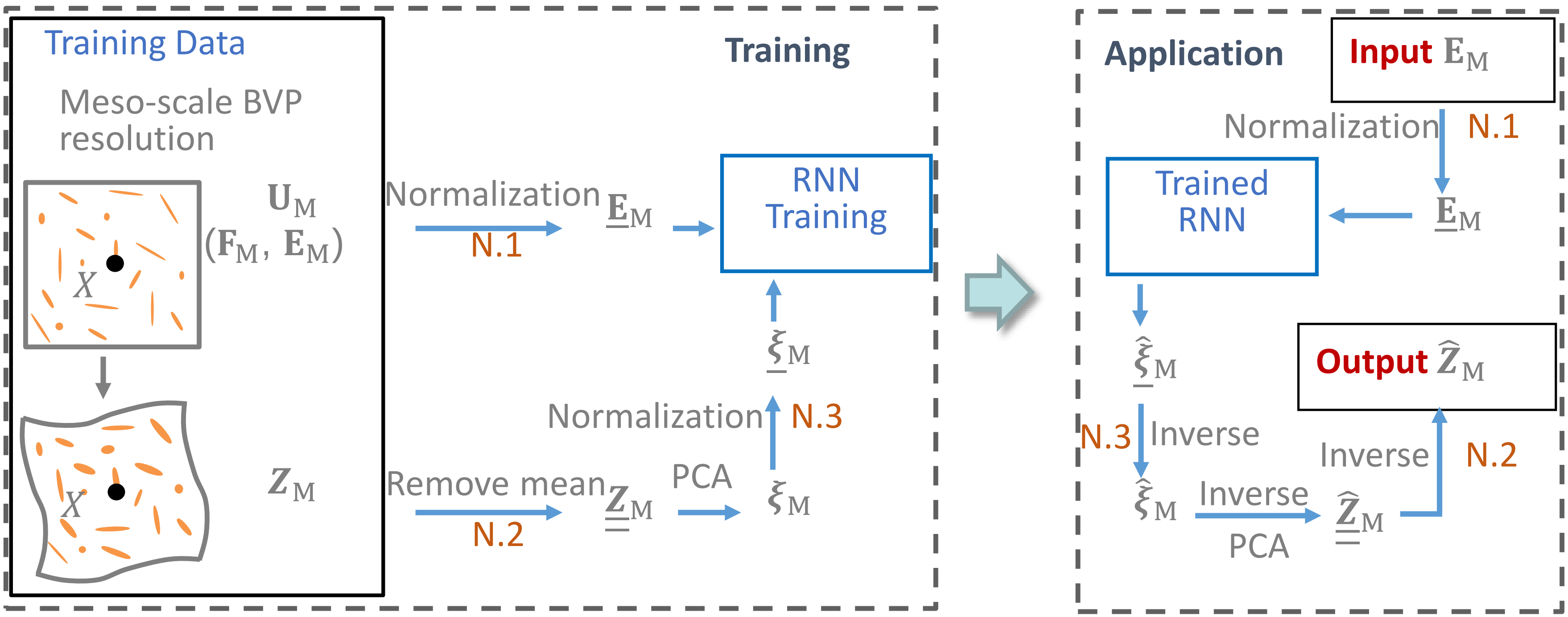

  – Principal Component Analysis (PCA) applied on $\boldsymbol{Z}_{\mathrm{M}}$ to reduce the output of RNN
    - Construct matrix $\mathbf{Z}_{\mathbf{M}} = \left[\underline{\underline{Z}}_{\mathrm{M}_1}\ \underline{\underline{Z}}_{\mathrm{M}_2}\ \ldots \underline{\underline{Z}}_{\mathrm{M}_n}\right]_{d\times n}$ from n observations (1% from all data)
    - Extract n ordered eigenvalues Λ_i and eigen vector $\underline{v}_i$ of $\mathbf{Z}_{\mathrm{M}}^T\mathbf{Z}_{\mathrm{M}}$
    - Build reduced basis $\mathbf{V} = \left[\ \underline{v}_1\ \underline{v}_2\ \ \ldots \underline{v}_p\ \right]_{d\times p}$ and reduced data $\boldsymbol{\xi}_{\mathrm{M}} = \mathbf{V}^T\underline{\underline{\boldsymbol{Z}}}_{\mathrm{M}}$ of size $p < d$
    - Reconstruction $\underline{\underline{\hat{\boldsymbol{Z}}}}_{\mathrm{M}} = \mathbf{V}\boldsymbol{\xi}_{\mathrm{M}}$
    - But not enough

RNN with dimensionality reduction and break down

- Dimensionality reduction & break down

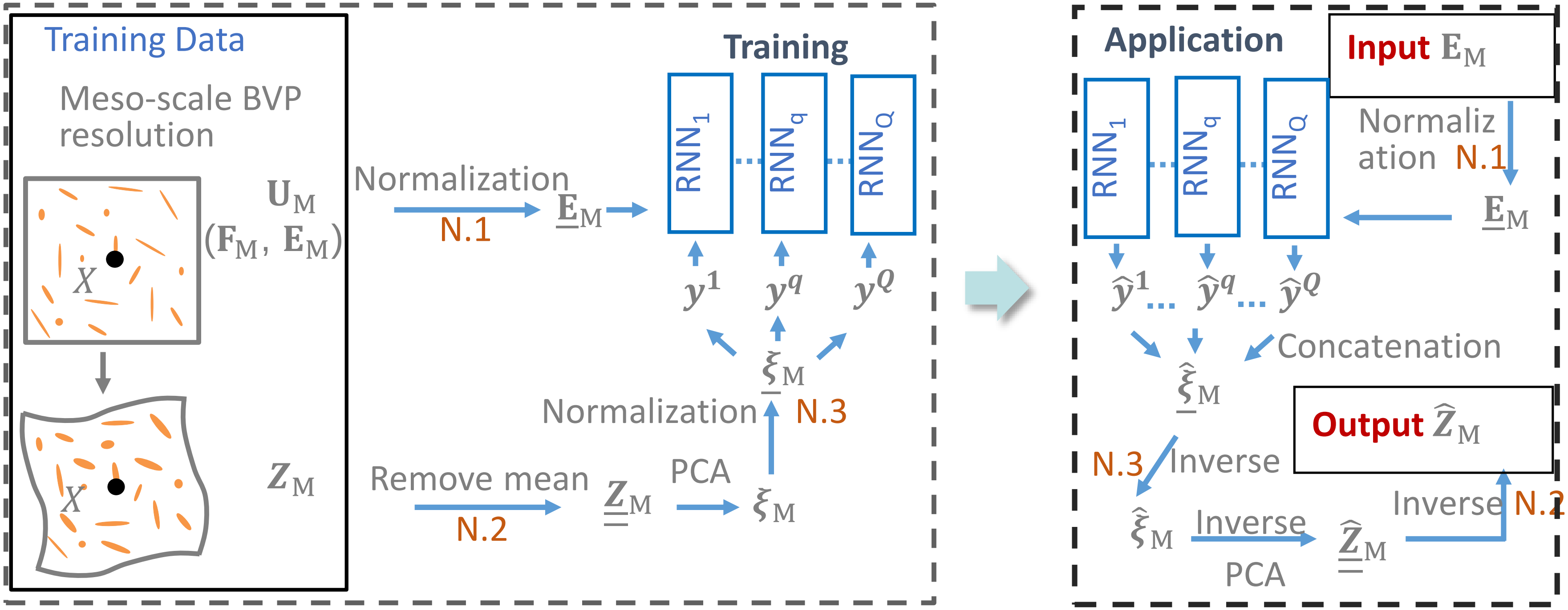

  - To further reduce the output dimension of RNN
    - The surrogate modelling is carried out by a few small RNNs, instead of one big RNN
    - The high dimension output is divided into Q groups, and each RNN is used to reproduce only a part of output
  - PCA reduces $\boldsymbol{Z}_\mathrm{M}$ to 180 outputs and we use Q=6

RNN with dimensionality reduction and break down

- Effect of dimensionality reduction and number of hidden variables

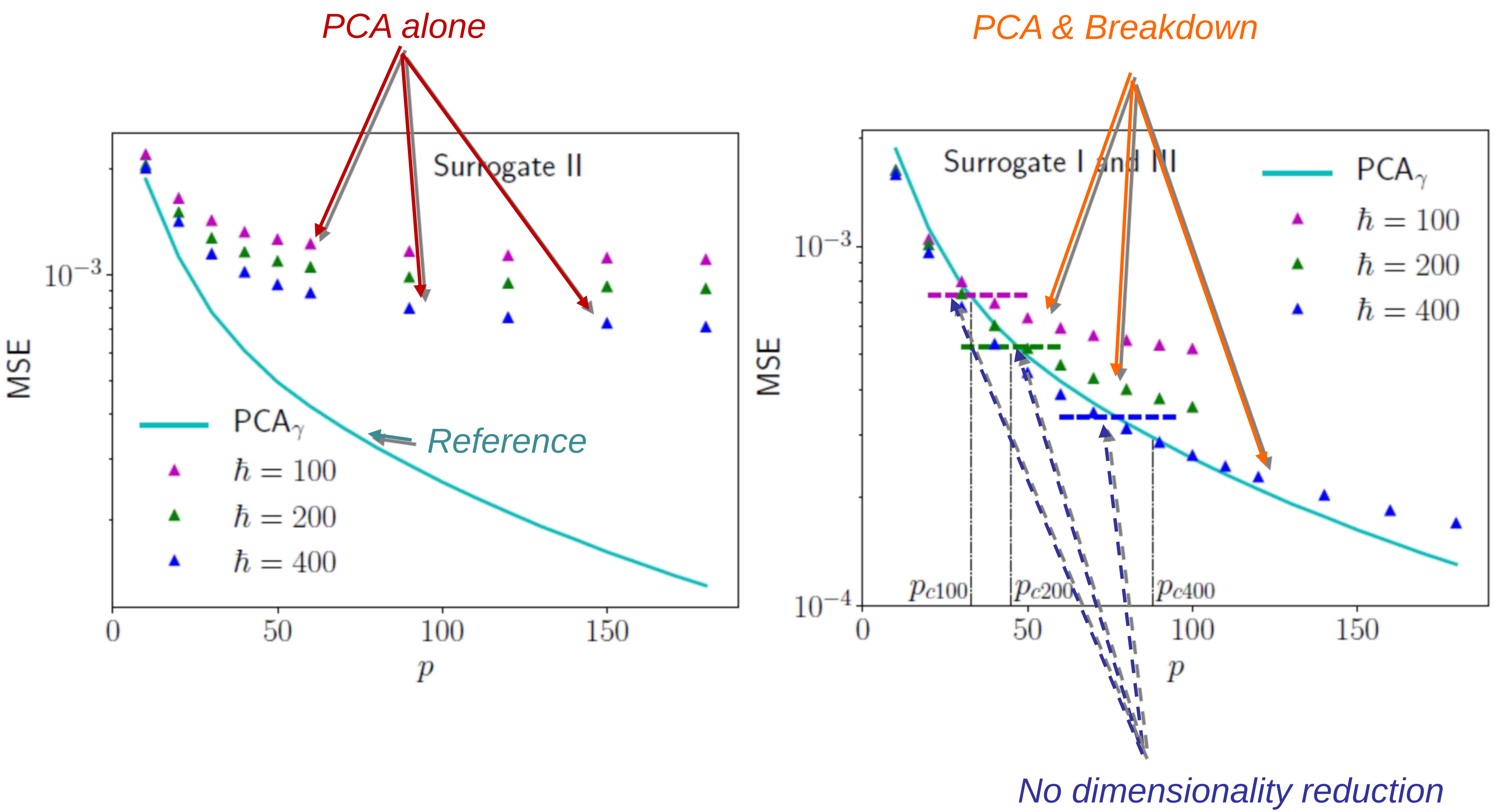

Beginning

RNN with dimensionality reduction and break down

- Evaluation of equivalent plastic strain γ: Random loading (testing data)

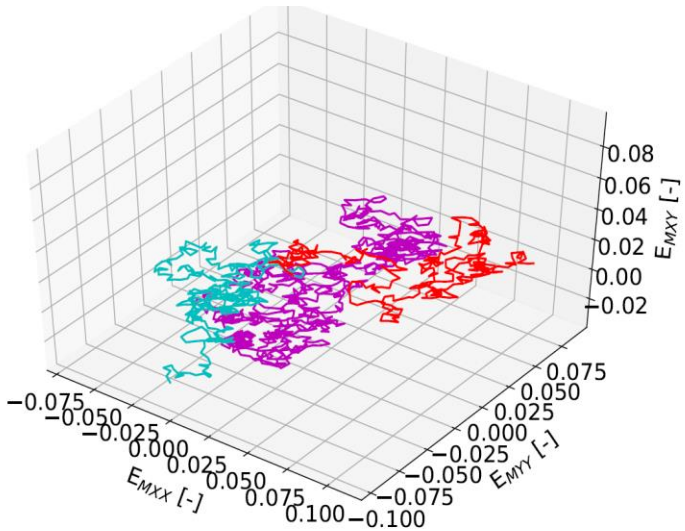

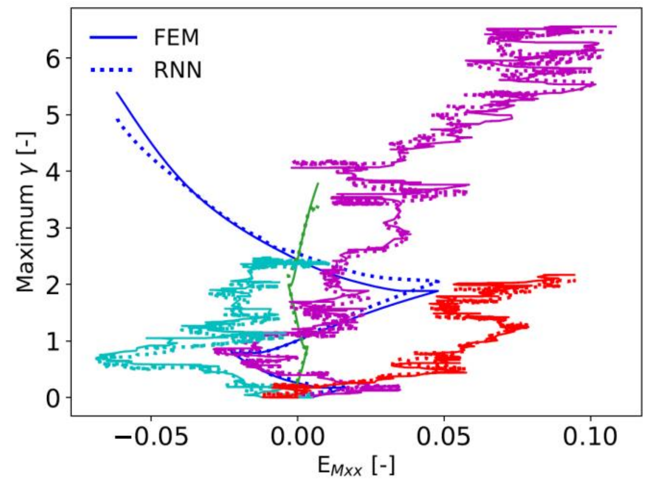

Purple loading – step 500

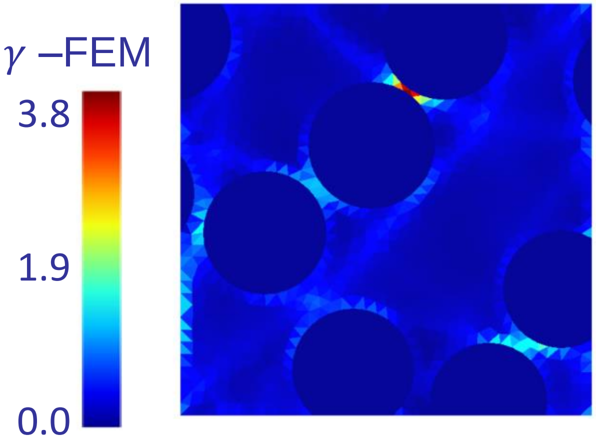

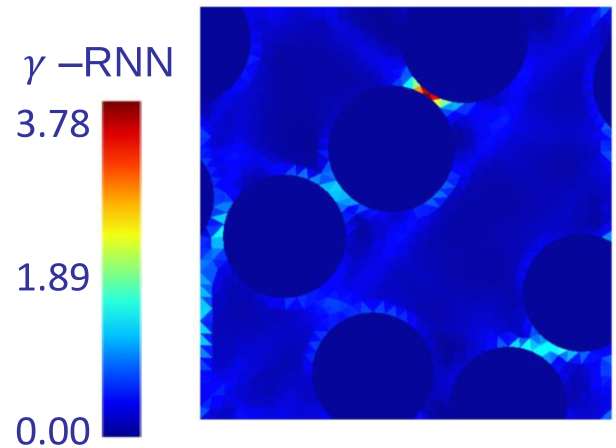

RNN with dimensionality reduction and break down

- Evaluation of equivalent plastic strain γ: Cyclic loading (testing data)

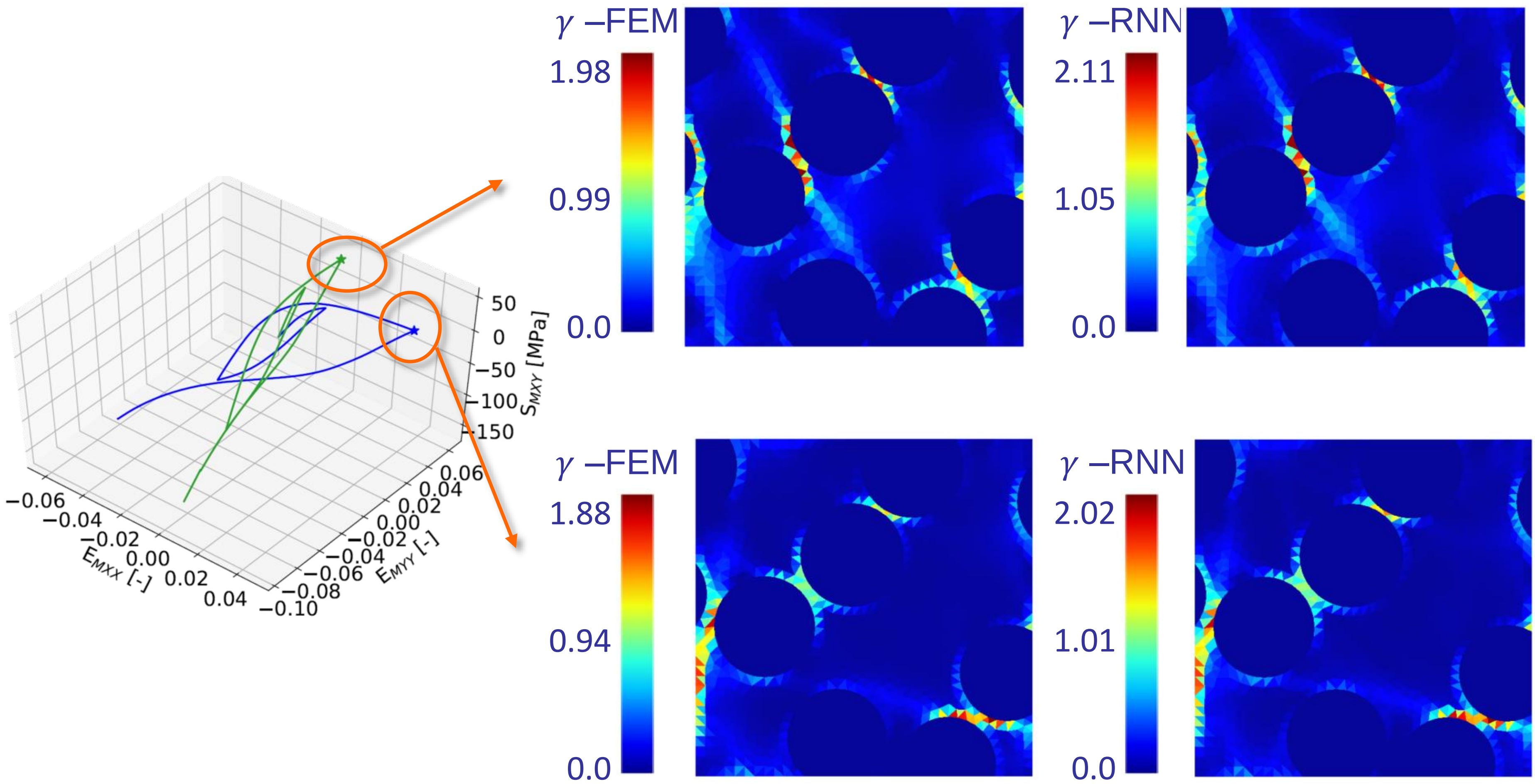

RNN with dimensionality reduction and break down

- MOAMMM FET-OPEN project (https://www.moammm.eu/)
  - ULiège, UCL (Belgium)
  - IMDEA Materials (Spain)
  - JKU (Austria)
  - cirp GmbH (Germany)

- Publications (doi)
  - 10.1016/j.cma.2020.113234
    - Open Data: 10.5281/zenodo.3902663
  - 10.1016/j.cma.2021.114476
    - Open Data: 10.5281/zenodo.5668390

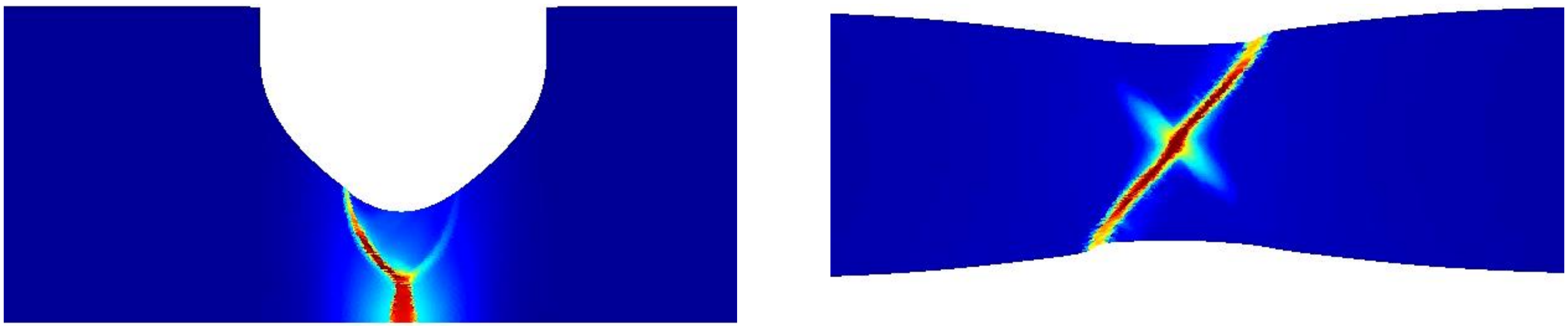

Shear and necking coalescence mechanisms for porous materials

The research has been funded by the Walloon Region under the agreement no. 1610154- EntroTough in the context of the 2016 WalInnov call

Shear and necking coalescence mechanisms for porous materials

- Objective:
  - To develop a non-local ductile failure model accounting for complex loading stress states
- Porous plasticity

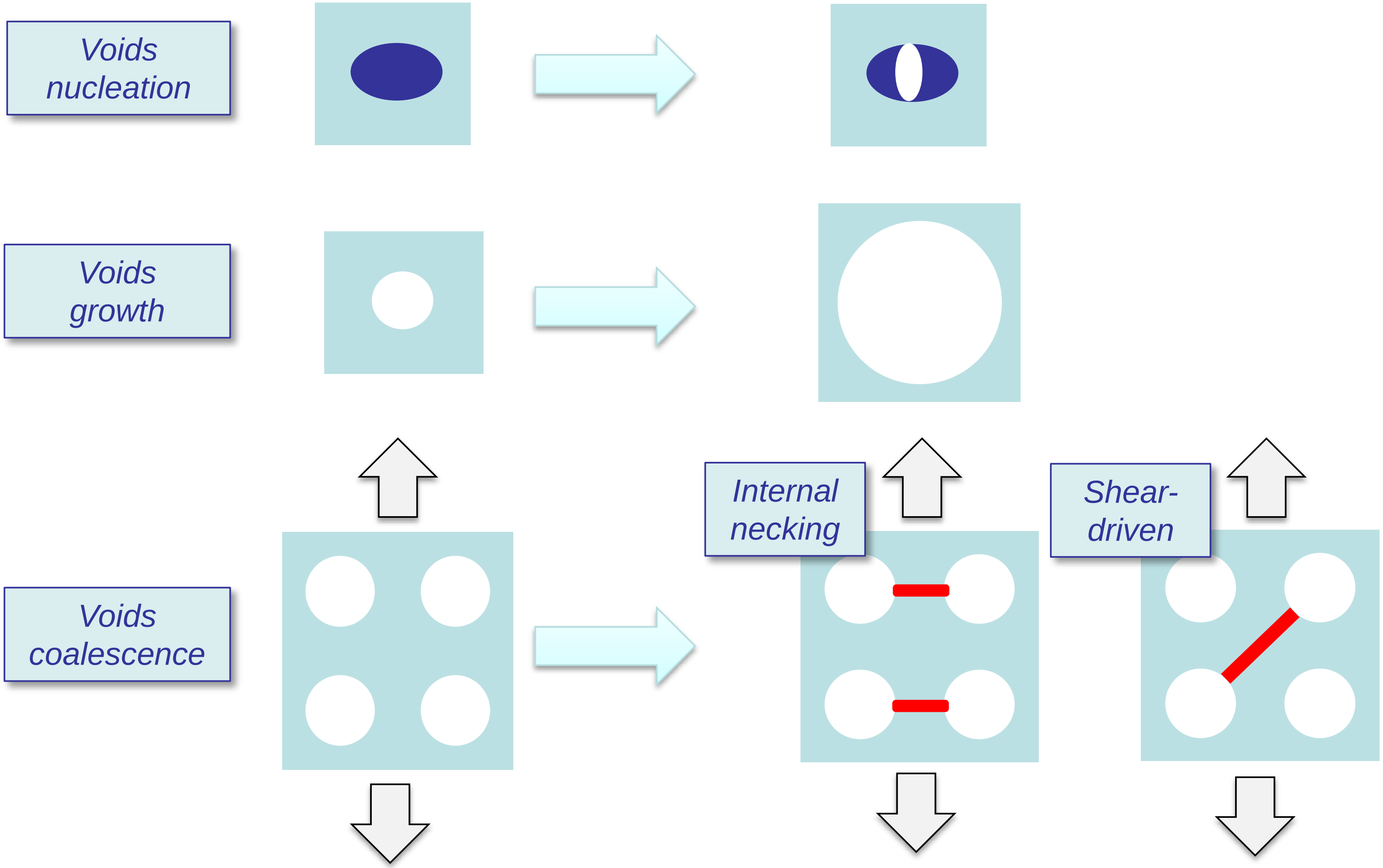

- Ductile failure: stress-state dependent fracture strain
  - Stress triaxiality dependent

$$\eta = \frac{p'}{\sigma_{eq}} \in]-\infty\ \infty[\qquad p = \frac{\mathrm{tr}\,(\boldsymbol{\sigma})}{3} \qquad \sigma_{eq} = \sqrt{\frac{3}{2}\mathrm{dev}(\boldsymbol{\sigma}):\mathrm{dev}(\boldsymbol{\sigma})}$$

  - Lode dependent

$$\theta = \frac{1}{3}\arccos\left(\frac{27 J_3}{2{\sigma_{eq}}^3}\right) \qquad J_3 = \det(\mathrm{dev}(\boldsymbol{\sigma})\,)$$

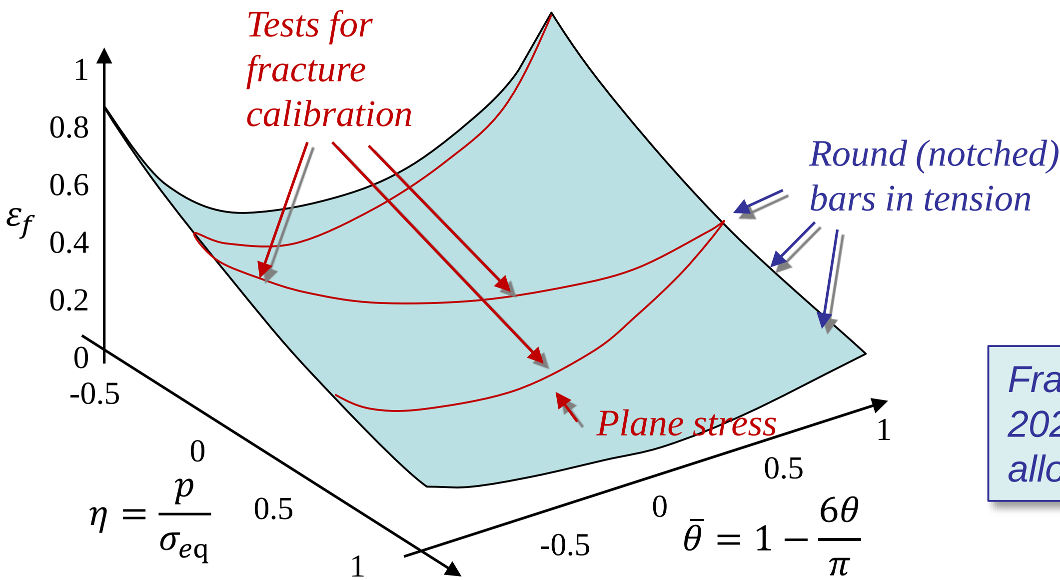

Fracture locus for 2024-T351 aluminum alloy

(Bai & Wierzbicki 2010)

Shear and necking coalescence mechanisms for porous materials

- Hyperelastic-based formulation
  - Multiplicative decomposition
    $\mathbf{F} = \mathbf{F}^{\mathrm{e}} \cdot \mathbf{F}^{\mathrm{p}},\quad \mathbf{C}^{\mathrm{e}} = \mathbf{F}^{\mathrm{e}^T} \cdot \mathbf{F}^{\mathrm{e}},\quad J^e = \det(\mathbf{F}^{\mathrm{e}})$
  - Stress tensor definition
    - Elastic potential $\psi(\mathbf{C}^{\mathrm{e}})$
    - First Piola-Kirchhoff stress tensor

$$\mathbf{P} = 2\mathbf{F}^{\mathrm{e}} \cdot \frac{\partial \psi(\mathbf{C}^{\mathrm{e}})}{\partial \mathbf{C}^{\mathrm{e}}} \cdot \mathbf{F}^{\mathrm{p}^{-T}}$$

    - Kirchhoff stress tensors
      - In current configuration

$$\boldsymbol{\kappa} = \mathbf{P} \cdot \mathbf{F}^T = 2\mathbf{F}^{\mathrm{e}} \cdot \frac{\partial \psi(\mathbf{C}^{\mathrm{e}})}{\partial \mathbf{C}^{\mathrm{e}}} \cdot \mathbf{F}^{\mathrm{e}^T}$$

      - In co-rotational space

$$\boldsymbol{\tau} = \mathbf{C}^{\mathrm{e}} \cdot \mathbf{F}^{\mathrm{e}^{-1}} \cdot \boldsymbol{\kappa} \cdot \mathbf{F}^{\mathrm{e}^{-T}} = 2\mathbf{C}^{\mathrm{e}} \cdot \frac{\partial \psi(\mathbf{C}^{\mathrm{e}})}{\partial \mathbf{C}^{\mathrm{e}}}$$

- Logarithmic deformation
  - Elastic potential ψ:

$$\psi(\mathbf{C}^{\mathrm{e}}) = \frac{K}{2} \ln^2(J^e) + \frac{G}{4} (\ln(\mathbf{C}^{\mathrm{e}}))^{\mathrm{dev}} : (\ln(\mathbf{C}^{\mathrm{e}}))^{\mathrm{dev}}$$

  - Stress tensor in co-rotational space

$$\boldsymbol{\tau} = \underbrace{K \ln(J^e)}_{p}\, \mathbf{I} + G (\ln(\mathbf{C}^{\mathrm{e}}))^{\mathrm{dev}}$$

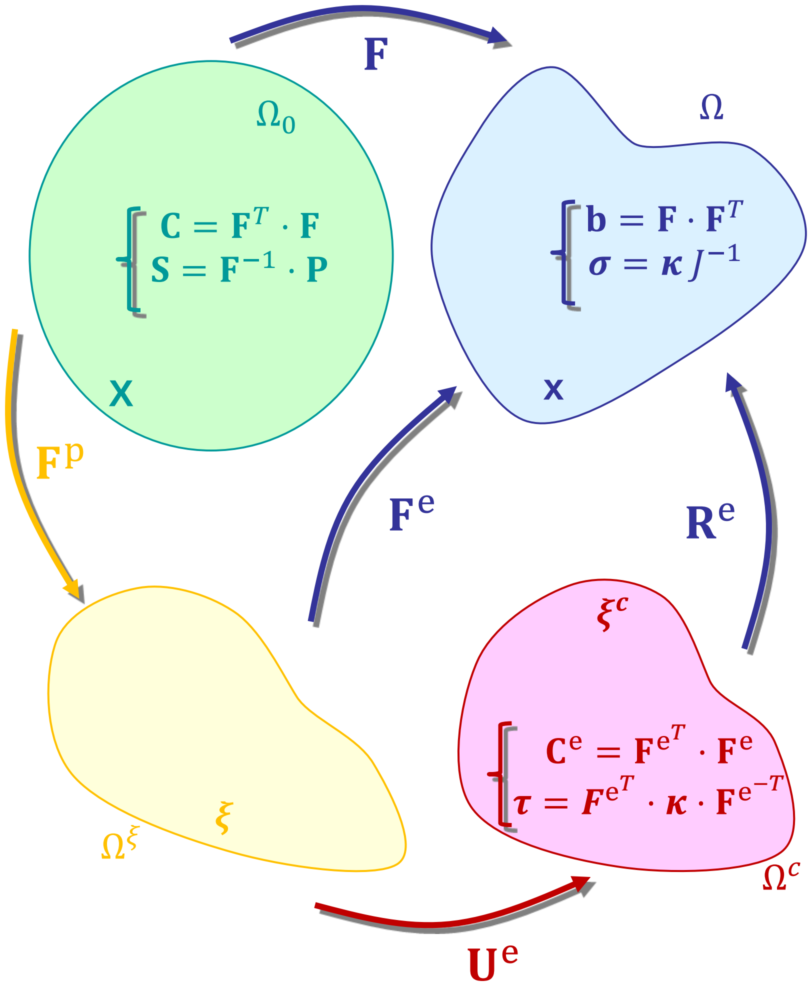

Shear and necking coalescence mechanisms for porous materials

- Material changes represented via internal variables
  - Constitutive law $\boldsymbol{\sigma}\big(\boldsymbol{\varepsilon}; \boldsymbol{Z}(t')\big)$
  - Internal variables $\boldsymbol{Z}(t')$
    - Plastic flow normal to yield surface Φ

$$\mathbf{D}^{\mathrm{p}} = \dot{\mathbf{F}}^{\mathrm{p}} \mathbf{F}^{\mathrm{p}-1} = \dot{\mu} \frac{\partial \Phi}{\partial \boldsymbol{\sigma}}$$

    - Matrix plastic strain rate $\dot{\varepsilon}_m = \dfrac{\boldsymbol{\sigma} : \mathbf{D}^{\mathrm{p}}}{(1-f)\sigma_Y}$
    - Volumetric plastic deformation $\dot{\varepsilon}_v = \mathrm{tr}\,(\mathbf{D}^{\mathrm{p}})$
    - Deviatoric plastic deformation $\dot{\varepsilon}_d = \sqrt{\dfrac{2}{3} \mathrm{dev}(\mathbf{D}^{\mathrm{p}}) : \mathrm{dev}(\mathbf{D}^{\mathrm{p}})}$
  - Voids characteristics **Y**
    - Porosity : f
    - Void ligament ratio: χ
    - Void aspect ratio: W
    - Void spacing ratio: λ

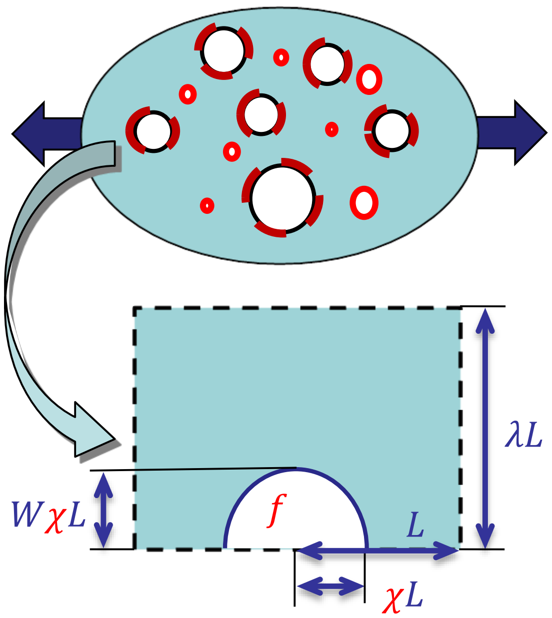

Shear and necking coalescence mechanisms for porous materials

- Non-local formalism
  - Local form
    - Mesh dependency
  - Requires non-local form [Bažant 1988]
    - Introduction of characteristic length l_c
    - Weighted average: $\tilde{Z}_k(\boldsymbol{x}) = \int_{V_C} W(\boldsymbol{y};\boldsymbol{x},l_c)\ Z_k(\mathbf{y})d\boldsymbol{y}$
  - Implicit form [Peerlings et al. 1998]
    - New degrees of freedom: $\tilde{Z}_k$
    - New Helmholtz-type equations: $\tilde{Z}_k - l_c^2\ \Delta\tilde{Z}_k = Z_k$
  - Constitutive law $\boldsymbol{\sigma}\left(\boldsymbol{\varepsilon},\widetilde{\boldsymbol{Z}}(t');\boldsymbol{Z}(t')\right)$

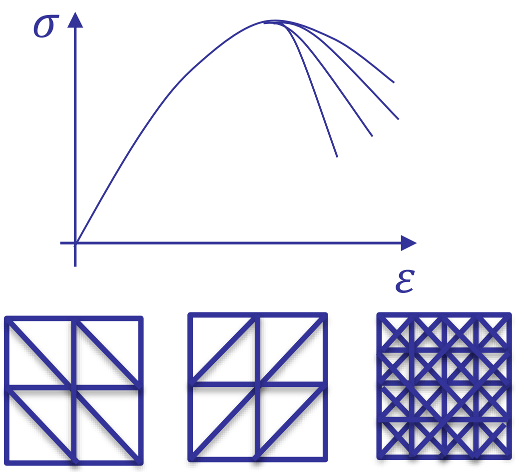

The numerical results change without convergence

- Non-local multi-mechanisms

$$\begin{cases} \dot{\varepsilon}_m = \dfrac{\boldsymbol{\sigma}:\mathbf{D}^{\mathrm{p}}}{(1-f)\sigma_Y} \\ \dot{\varepsilon}_v = \mathrm{tr}\,(\mathbf{D}^{\mathrm{p}}) \\ \dot{\varepsilon}_d = \sqrt{\dfrac{2}{3}\mathrm{dev}(\mathbf{D}^{\mathrm{p}}):\mathrm{dev}(\mathbf{D}^{\mathrm{p}})} \end{cases} \Rightarrow \begin{cases} \tilde{\varepsilon}_m - l_c^2\ \Delta\tilde{\varepsilon}_m = \varepsilon_m \\ \tilde{\varepsilon}_v - l_c^2\ \Delta\tilde{\varepsilon}_v = \varepsilon_v \\ \tilde{\varepsilon}_d - l_c^2\ \Delta\tilde{\varepsilon}_d = \varepsilon_d \end{cases}$$

- Different yield surfaces: void growth
  - Classical GTN model
    - Non-local porosity evolution

$$\dot{f} = \dot{f}_{\mathrm{gr}} + \dot{f}_{\mathrm{nu}} + \dot{f}_{\mathrm{sh}}$$

$$\begin{cases} \dot{f}_{\mathrm{gr}} = (1-f)\dot{\tilde{\varepsilon}}_v \\ \dot{f}_{\mathrm{nu}} = A_n(\tilde{\varepsilon}_m)\dot{\tilde{\varepsilon}}_m \\ \dot{f}_{\mathrm{sh}} = k_w \phi_\eta\left(\frac{p}{\sigma_{\mathrm{eq}}}\right)\phi_\omega(\cos 3\theta) f \dot{\tilde{\varepsilon}}_d \end{cases}$$

    - Yield surface

$$\phi_{\mathrm{G}} = \frac{\sigma_{\mathrm{eq}}^2}{\sigma_{\mathrm{Y}}^2} + 2q_1 f \cosh\left(\frac{q_2 p}{2\sigma_{\mathrm{Y}}}\right) - 1 - q_3^2 f^2 \leq 0$$

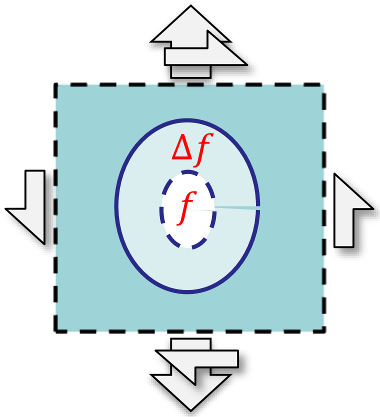

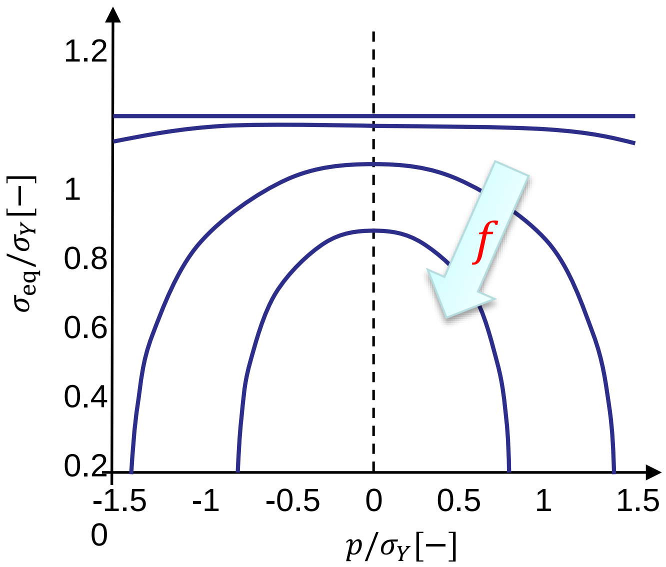

Shear and necking coalescence mechanisms for porous materials

- Different yield surfaces: coalescence
  - Coalescence by necking
    - Yield surface

$$\phi_\mathrm{T} = \frac{2}{3}\sigma_\mathrm{eq}\cos\theta + |p| - C_\mathrm{T}^f(\chi, \mathrm{W})\sigma_\mathrm{Y} \leq 0$$

Max Principal Stress

    - Limit load factor

$$C_\mathrm{T}^f(\chi, W) = (1-\chi^2)\left[h\left(\frac{1-\chi}{W\chi}\right)^2 + g\sqrt{\frac{1}{\chi}}\right]$$

    - Cavities evolution

$$\begin{cases} \dot{\lambda} = \kappa\lambda\dot{\hat{\varepsilon}}_d \\ \dot{\chi} = \dfrac{3\lambda}{4W}\left(\dfrac{3}{2\chi^2} - 1\right)\dot{\hat{\varepsilon}}_d \\ \dot{W} = \dfrac{9\lambda}{4\chi}\left(1 - \dfrac{1}{2\chi^2}\right)\dot{\hat{\varepsilon}}_d \\ \dot{f} = f\left(\dfrac{3\dot{\chi}}{\chi} + \dfrac{\dot{W}}{W} - \dfrac{\dot{\lambda}}{\lambda}\right) \end{cases}$$

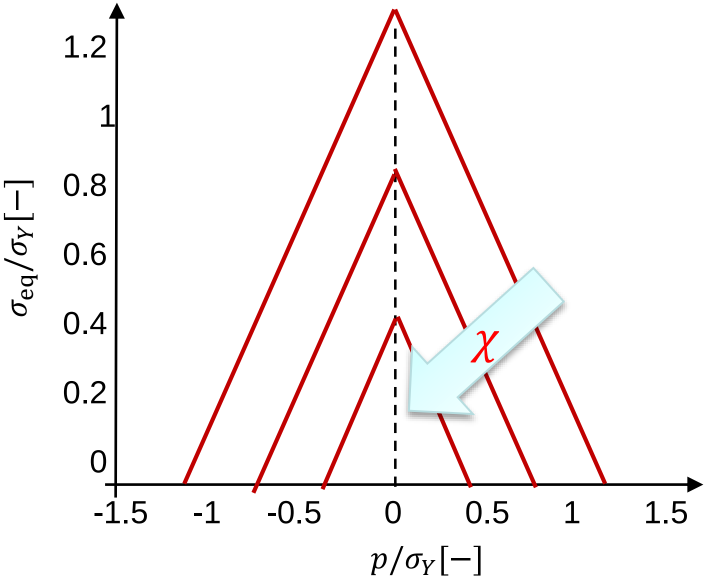

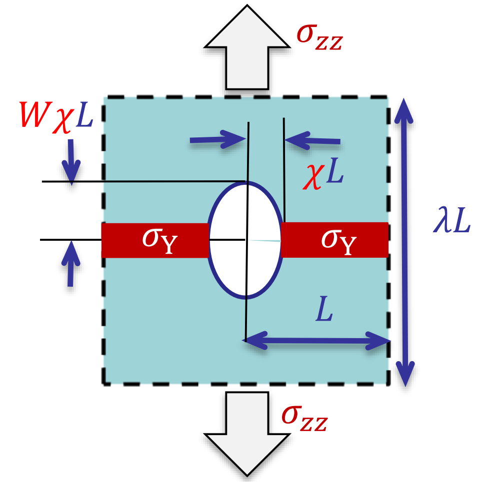

- Different yield surfaces: coalescence
  - Coalescence by shearing
    - Yield surface

$$\phi_{\mathrm{T}} = \frac{2}{3}\sigma_{\mathrm{eq}}\cos\theta + |p| - C_{\mathrm{T}}^{f}(\chi, W)\sigma_{\mathrm{Y}} \leq 0$$

Max Principal Stress

    - Limit load factor

$$C_{\mathrm{T}}^{f}(\chi, W) = (1-\chi^2)\left[h\left(\frac{1-\chi}{W\chi}\right)^2 + g\sqrt{\frac{1}{\chi}}\right]$$

    - Cavities evolution

$$\begin{cases} \dot{\chi} = K_{\chi}\dot{\hat{\varepsilon}}_d \\ \dot{\lambda} = 3\lambda\frac{\dot{\chi}}{\chi} \\ \dot{W} = 0 \\ \dot{f} = 0 \end{cases}$$

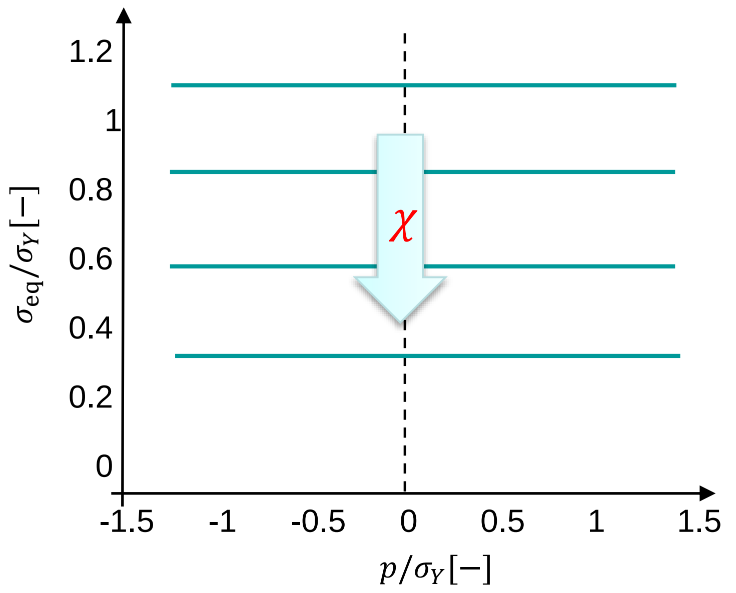

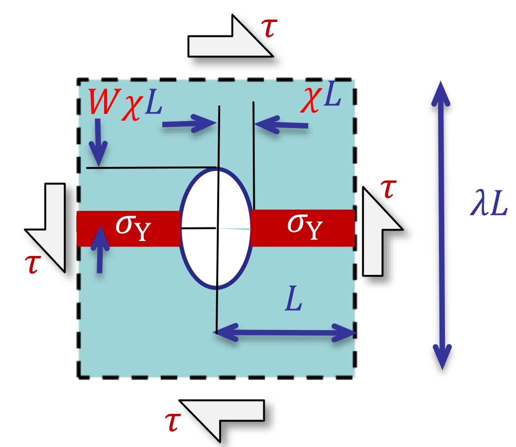

Shear and necking coalescence mechanisms for porous materials

- Multi-surface model
  - Effective yield surface

$$\phi_e = \begin{pmatrix} (\phi_G + 1)^m + \\ (\phi_T + 1)^m + \\ (\phi_S + 1)^m \end{pmatrix}^{1/m}$$

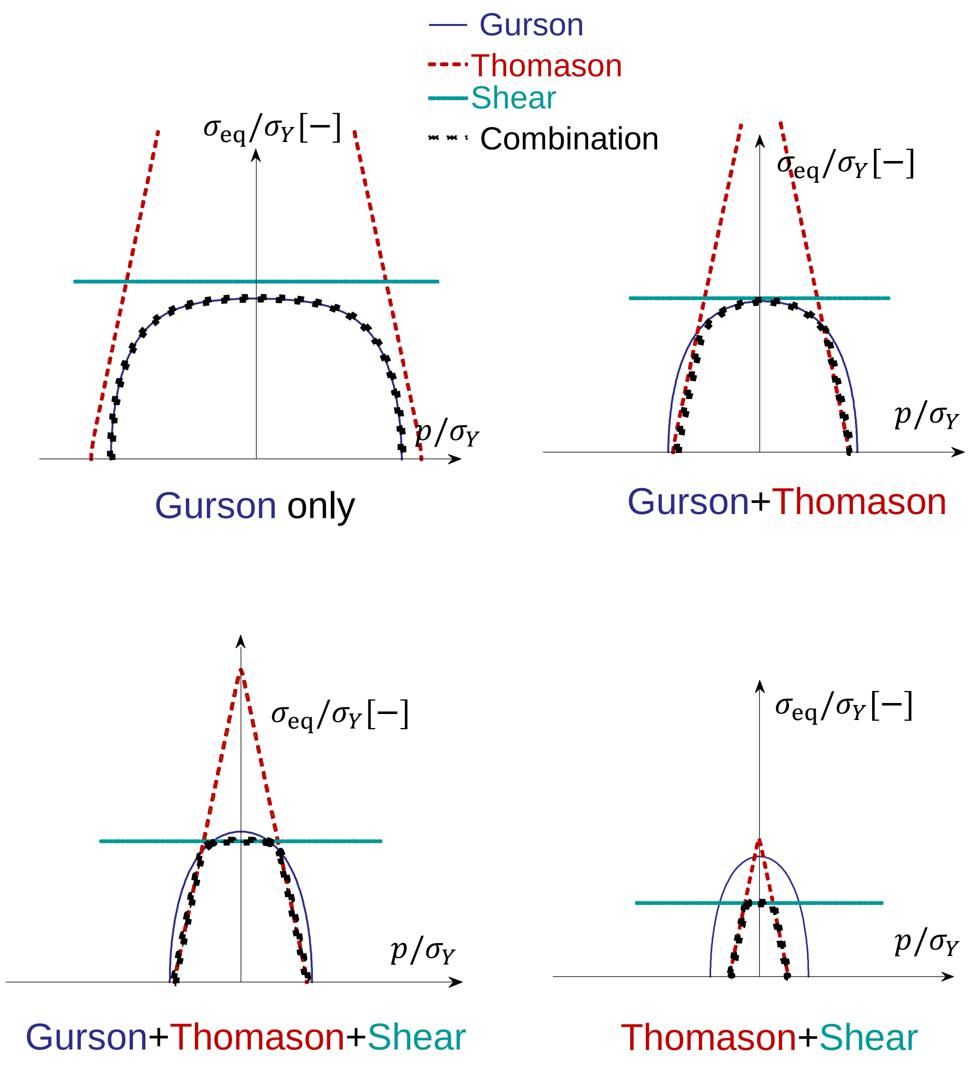

Shear and necking coalescence mechanisms for porous materials

- Solution under proportional loadings
  - Constant
    - Stress triaxiality ($\frac{p}{\sigma_{\text{eq}}}$); and
    - Normalized Lode angle ($\bar{\theta} = 1 - \frac{6\theta}{\pi}$)
  - ε_{dc}- ductility = plastic deformation at coalescence onset

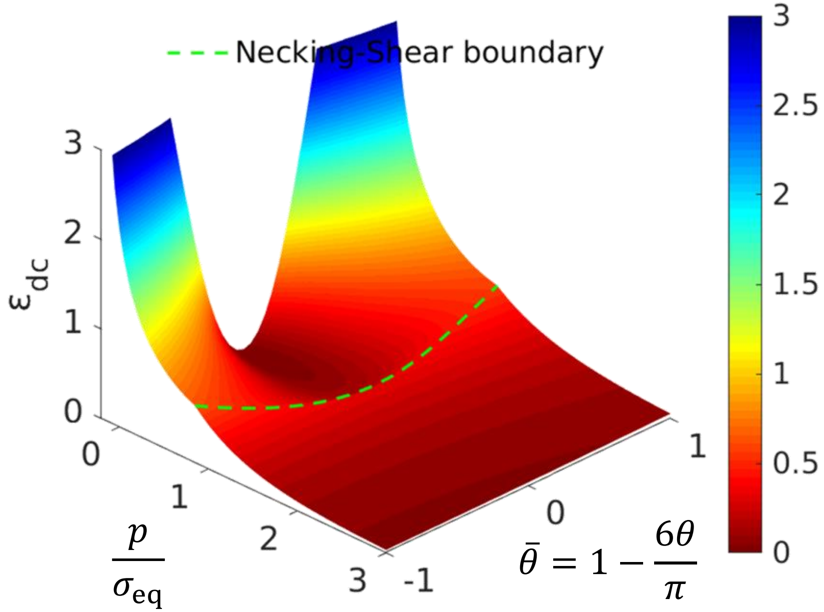

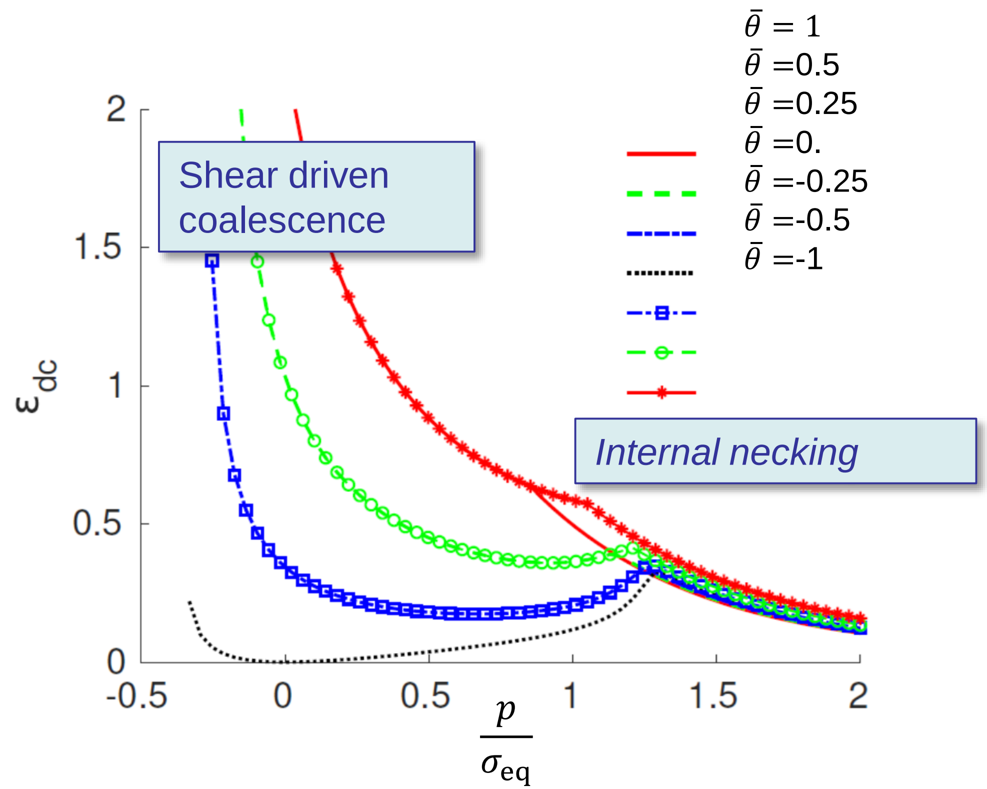

Beginning

Shear and necking coalescence mechanisms for porous materials

- Plane strain smooth specimen under tensile loading
  - Verification of the nonlocal model: mesh convergence

$L = 12.5$ mm
$e_0 = 3$ mm
$\xi = 1.015$ ($\varepsilon_{ds} = 0.95$)

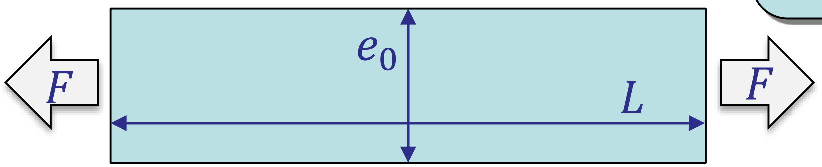

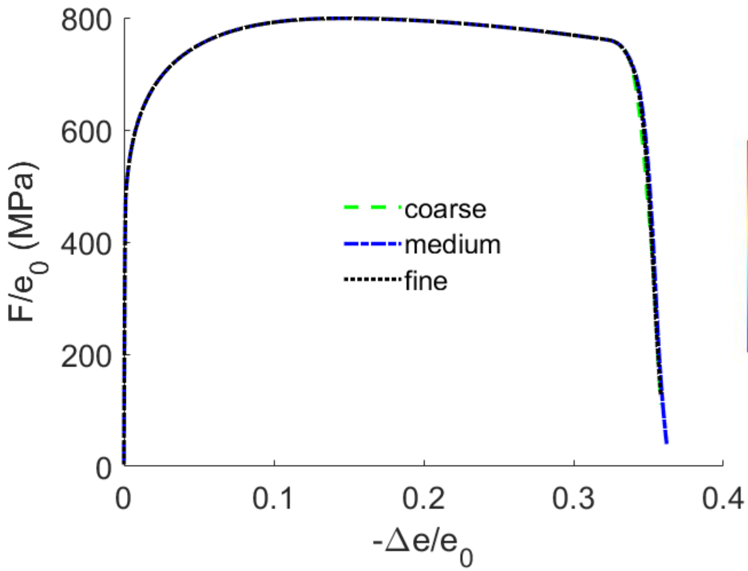

Distribution of void ligament ratio χ

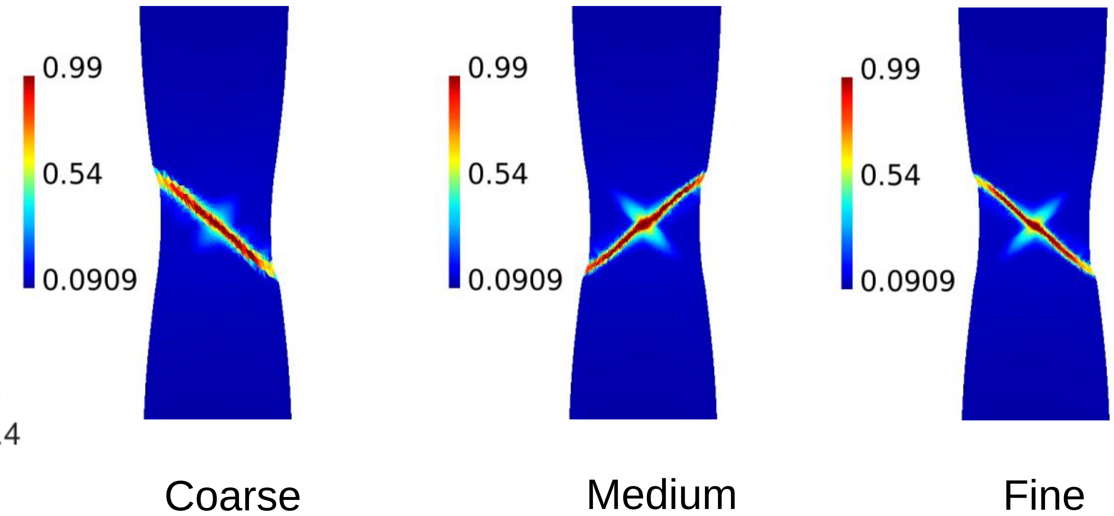

Capture slant fracture

Shear and necking coalescence mechanisms for porous materials

- Plane strain smooth specimen under tensile loading
  - Effect of ξ

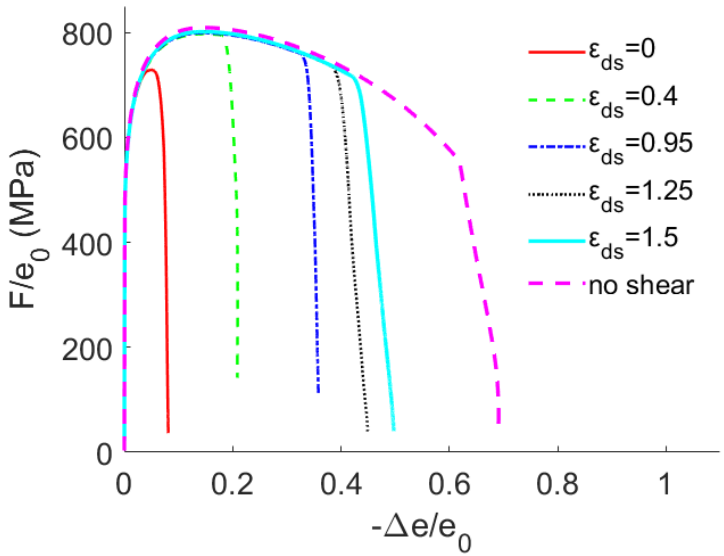

$L = 12.5$ mm
$e_0 = 3$ mm

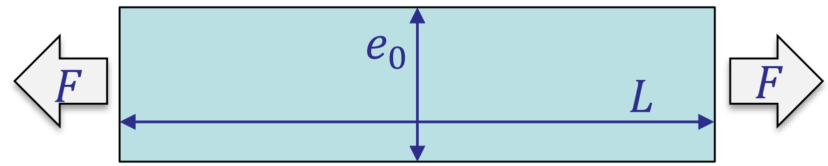

Distribution of void ligament ratio χ

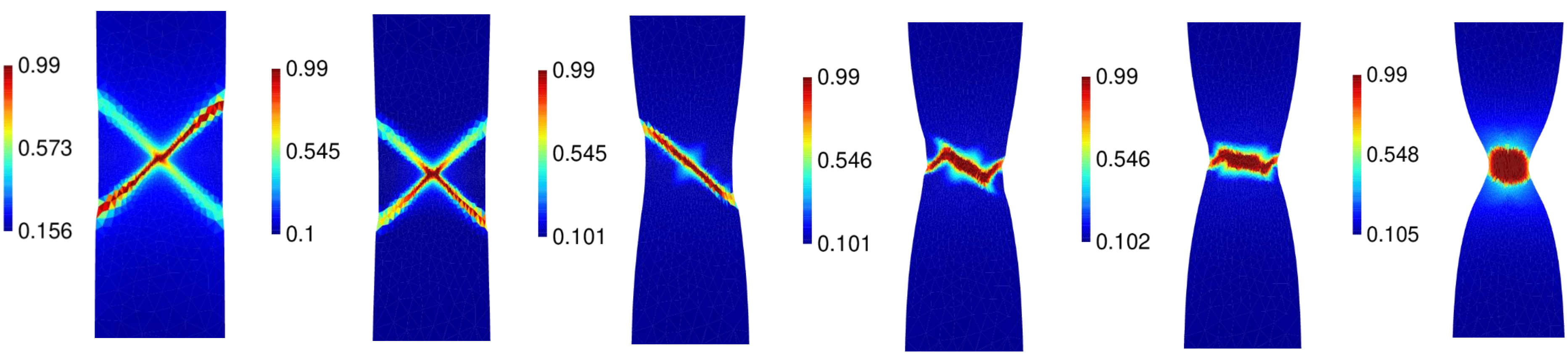

$\varepsilon_{ds} = 0$ | $\varepsilon_{ds} = 0.4$ | $\varepsilon_{ds} = 0.95$ | $\varepsilon_{ds} = 1.25$ | $\varepsilon_{ds} = 1.5$ | no shear

Shear and necking coalescence mechanisms for porous materials

- Axisymmetric (notched) specimens under tensile loading
  - Different notch radii: $R_0/R_n = 0, 0.2, 0.6, 1, 1.5$

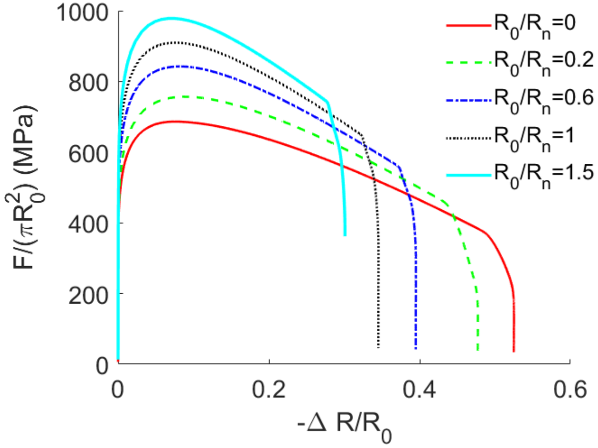

$R_0 = 3$ mm
$R_1 = 6$ mm
$L = 25$ mm
$\xi = 1.015$ ($\varepsilon_{ds} = 0.95$)

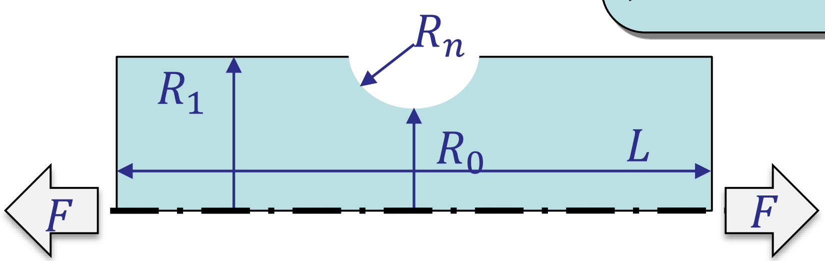

Distribution of void ligament ratio χ

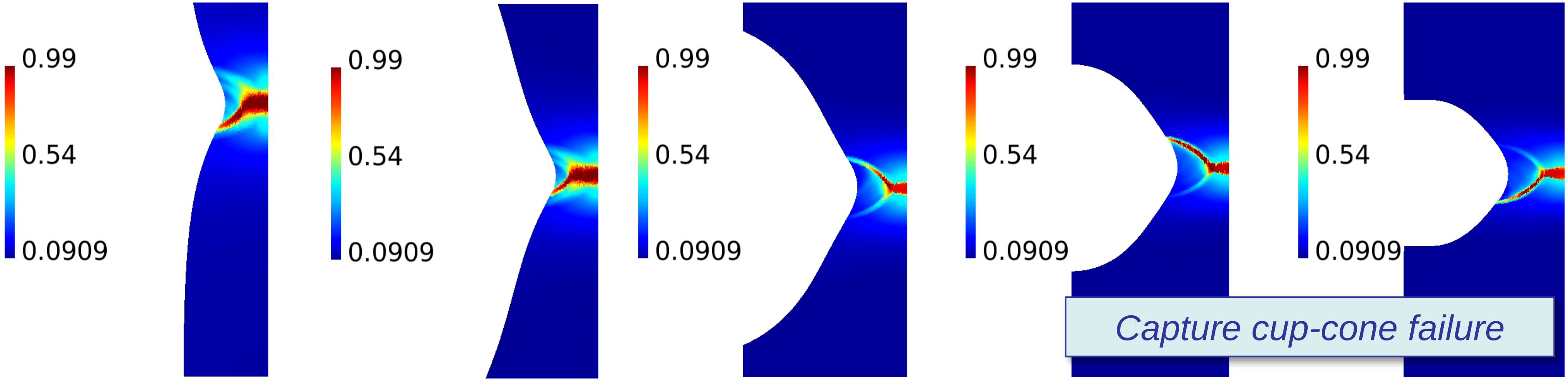

Capture cup-cone failure

Shear and necking coalescence mechanisms for porous materials

- EntroTough WalInnov project
  - UCL, ULB, ULiege (Belgium)
- Publication (doi)
  - 10.1016/j.jmps.2020.103891
  - 10.1016/j.engfracmech.2022.108844

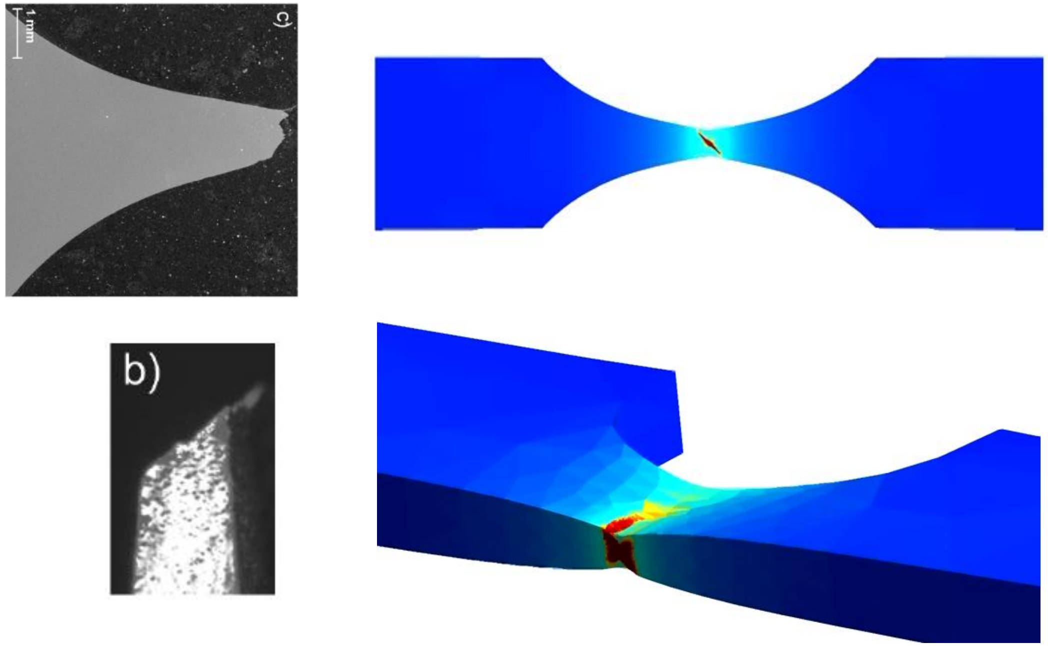

Ductile failure of High-Entropy Alloys (HEA)

The research has been funded by the Walloon Region under the agreement no. 1610154- EntroTough in the context of the 2016 WalInnov call

Ductile failure of High-Entropy Alloys (HEA)

- Design of experimental campaign on CoCrNi ternary HEA
  - Cover wide range of stress states
    - Triaxiality $\eta = \frac{p}{\sigma_{eq}}$
    - Lode angle: $\theta = \frac{1}{3}\arccos\left(\frac{27\det(\mathrm{dev}(\boldsymbol{\sigma}))}{2{\sigma_{eq}}^3}\right)$

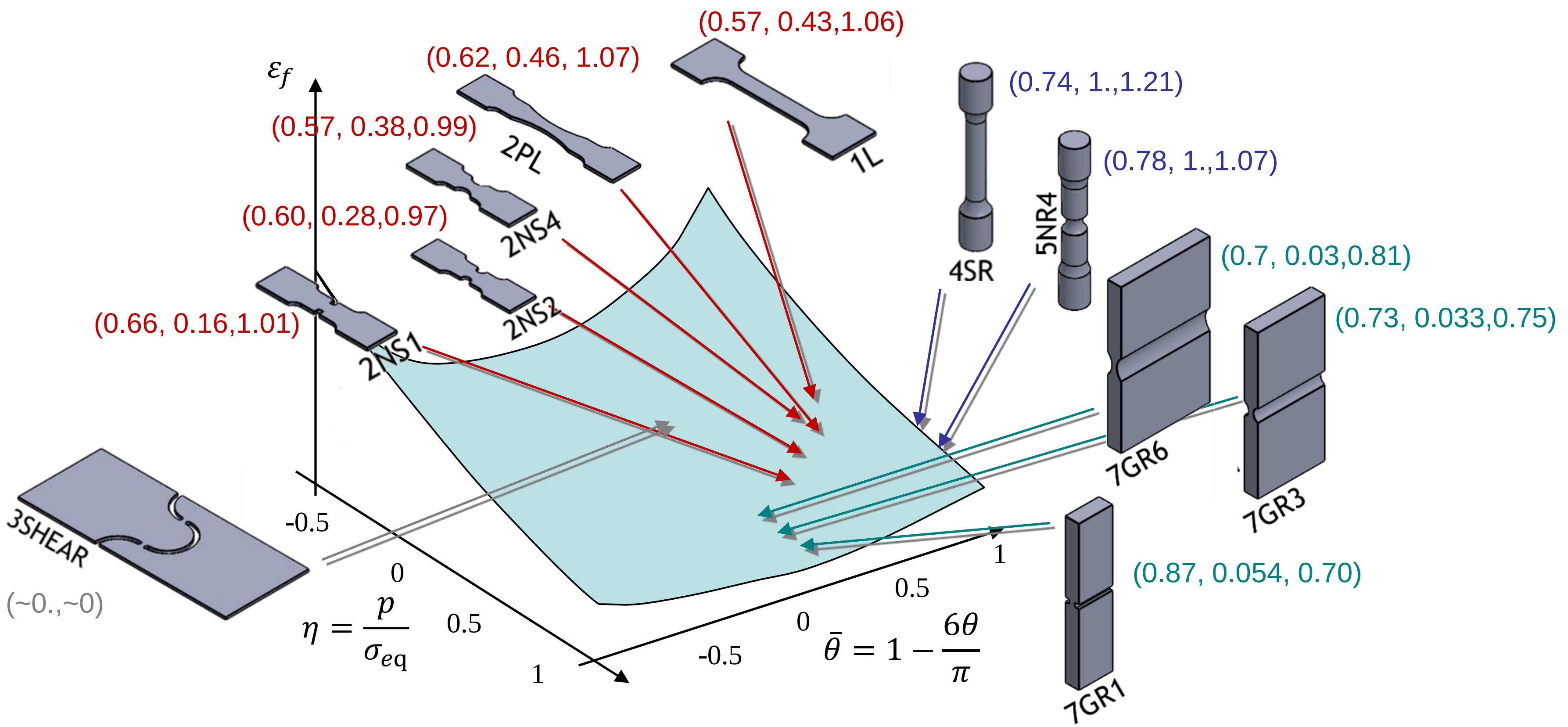

- Identification methodology
  - Porosity evolution
    - No initial porosity
    - Fast nucleation from defects

      ⇒ assume initial f_0

    - Evolution from 2PL

      ⇒ $f_0 = 0.002$

  - Non-local lengths
    - From intervoid spacing

$$\begin{cases} \tilde{\varepsilon}_m - l_c^2\,\Delta\tilde{\varepsilon}_m = \varepsilon_m \\ \tilde{\varepsilon}_v - l_c^2\,\Delta\tilde{\varepsilon}_v = \varepsilon_v \\ \tilde{\varepsilon}_d - l_c^2\,\Delta\tilde{\varepsilon}_d = \varepsilon_d \end{cases}$$

⇒ $l_c = 40\ \mu\text{m}$

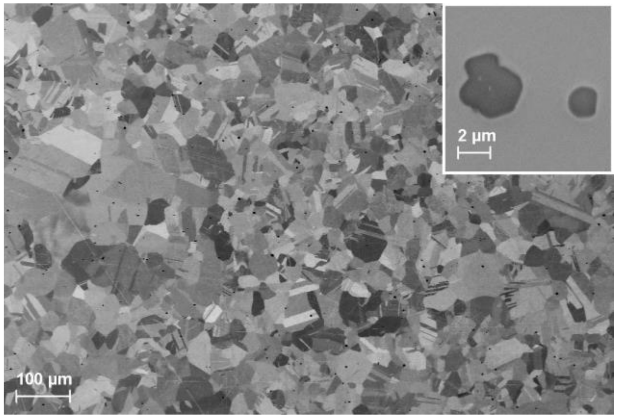

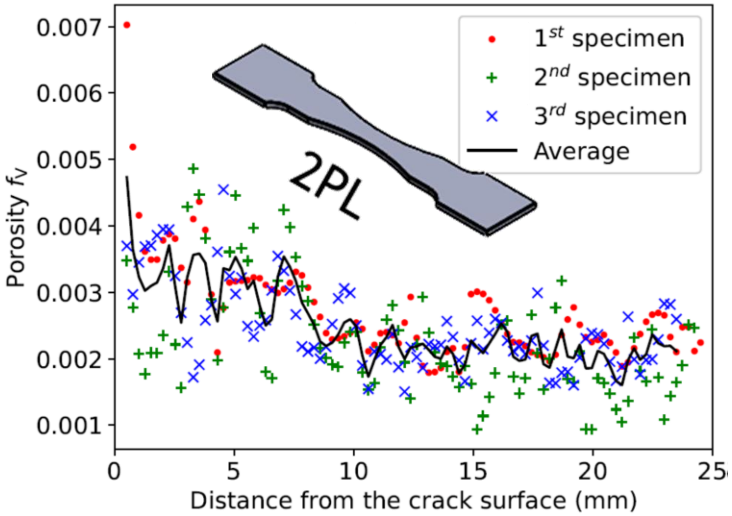

SEM images by A. Hillhorst, UCL

Ductile failure of High-Entropy Alloys (HEA)

- Identification methodology
  - Elasto-plastic matrix
    - Yield surface
      $$\phi_G = \frac{\sigma_{eq}^2}{\sigma_Y^2} + 2q_1 f \cosh\left(\frac{q_2 p}{2\sigma_Y}\right) - 1 - q_3^2 f^2 \leq 0$$
    - Do not consider porosity evolution $f \sim f_0 \sim 0$
    - Hardening law from 1L and 5NR4 samples :

$$\sigma_Y = \begin{cases} \sigma_Y^0 + h_1 \varepsilon_m + h_2 \left[1 - \exp\left(-\frac{\varepsilon_m}{h_{exp}}\right)\right] & \text{if } \varepsilon_m \leq \varepsilon_{mc} \\ \sigma_{Y_c}\left(\frac{\varepsilon_m}{\varepsilon_{mc}}\right)^{n_c} & \text{if } \varepsilon_m > \varepsilon_{mc} \end{cases}$$

  - Porous plasticity parameters of Gurson
    - Classical:

$$\begin{cases} q_1 = 1.5 \\ q_2 = 1 \end{cases}$$

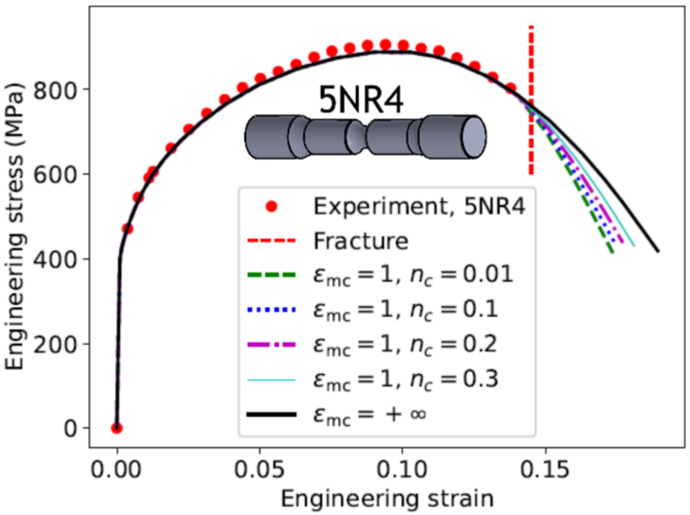

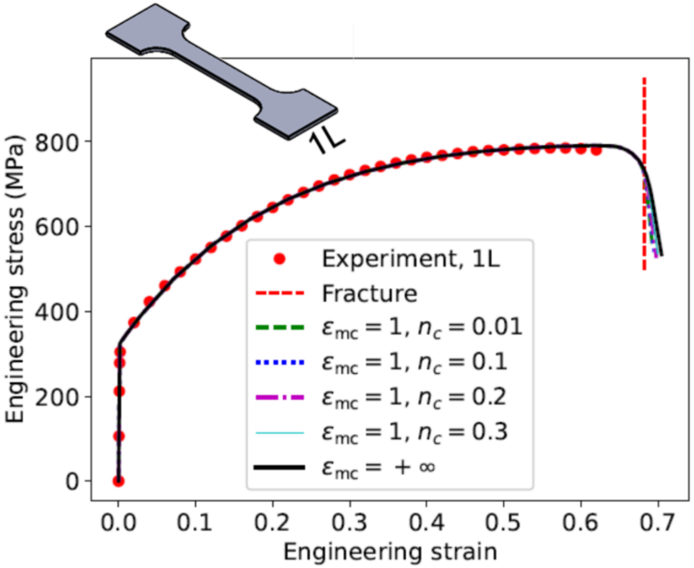

Ductile failure of High-Entropy Alloys (HEA)

- Identification methodology
  - Internal necking
    - Extended Thomason model

$$\phi_{\mathrm{T}} = \frac{2}{3}\sigma_{\mathrm{eq}}\cos\theta \; + |p| - C_{\mathrm{T}}^{f}(\chi, \mathrm{W})\sigma_{\mathrm{Y}} \le 0$$

Max Principal Stress

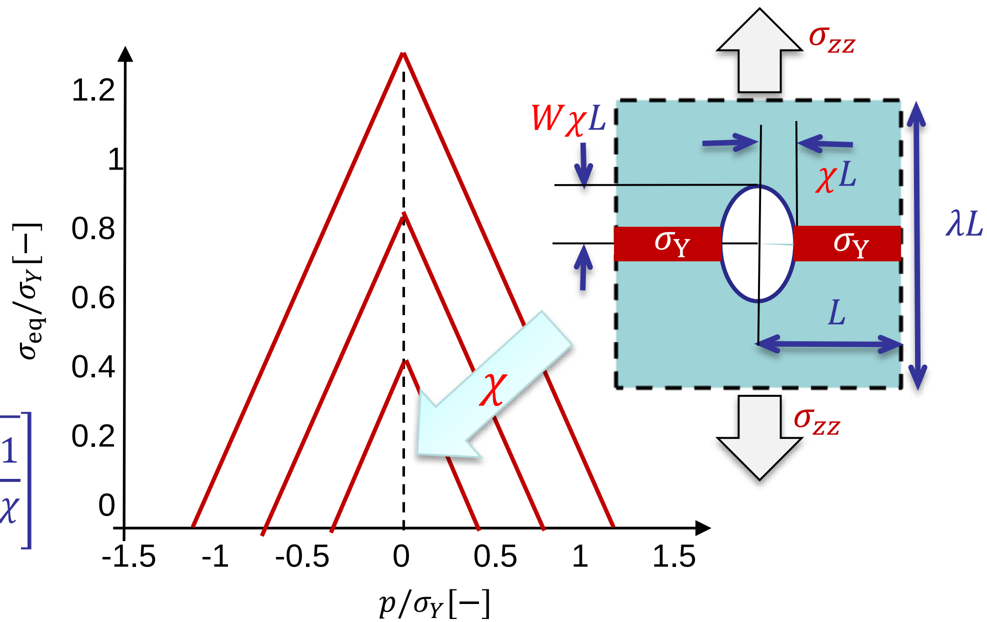

    - With

$$C_{\mathrm{T}}^{f}(\chi, W) = (1-\chi^2)\left[h\left(\frac{1-\chi}{W\chi}\right)^2 + g\sqrt{\frac{1}{\chi}}\right]$$

0.1 1.24

    - 5NR4 fails by internal necking

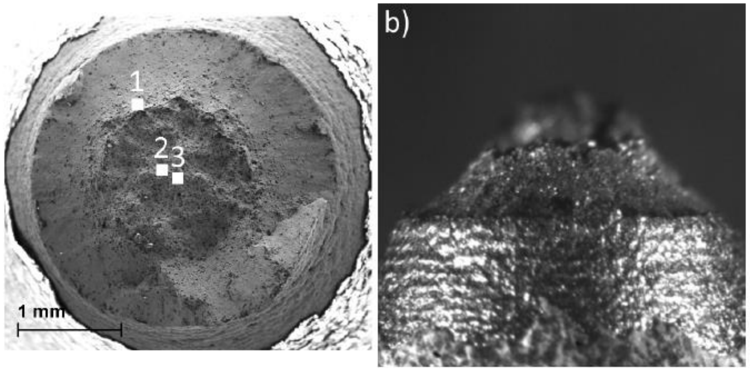

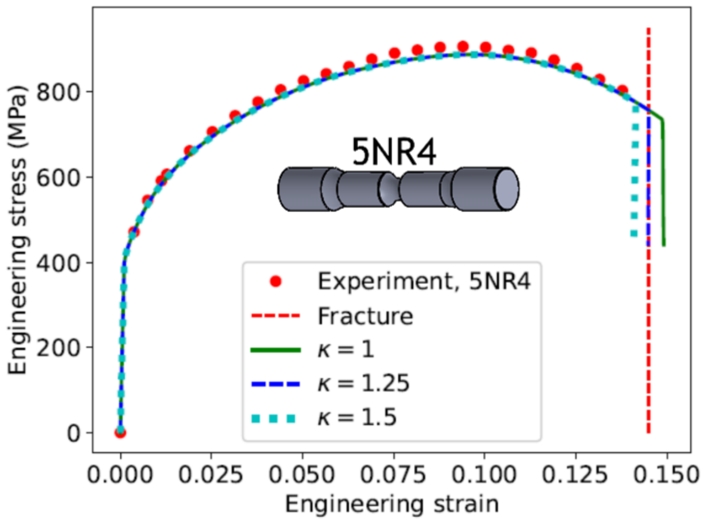

used to calibrate the void spacing factor $\kappa = 1.25$

$$\dot{\lambda} = \kappa\lambda\dot{\bar{\varepsilon}}_d \qquad \dot{\chi} = \frac{3\lambda}{4W}\left(\frac{3}{2\chi^2} - 1\right)\dot{\bar{\varepsilon}}_d$$

Images by A. Hillhorst, UCL

- Identification methodology
  - Porous plasticity parameters
    - $\dot{f} = \dot{f}_{\mathrm{gr}} + \dot{f}_{\mathrm{nu}} + \dot{f}_{\mathrm{sh}}$ with $\dot{f}_{\mathrm{gr}} = (1-f)\dot{\tilde{\varepsilon}}_v$
    - Assume early nucleation $f_0 = 0.002$

$$\dot{f}_{\mathrm{nu}} = A_n(\tilde{\varepsilon}_m)\dot{\tilde{\varepsilon}}_m = 0$$

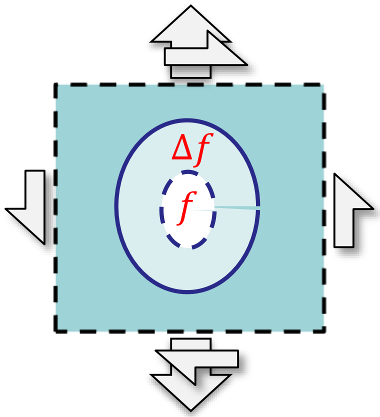

- Shear growth

$$\begin{cases} \dot{f}_{\mathrm{sh}} = k_w \phi_\eta\left(\dfrac{p}{\sigma_{\mathrm{eq}}}\right)\phi_\omega(\cos 3\theta) f \dot{\tilde{\varepsilon}}_d \\ \phi_\eta(\eta) = \exp\left[-\dfrac{1}{2}\left(\dfrac{\eta}{\eta_s}\right)^2\right] \\ \phi_\omega(\omega) = 1 - \omega^2 \end{cases}$$

- For $\eta_s = 0.15$: $\phi_\eta(\eta) \simeq 0$ at high triaxiality

For 7GRx $\dot{f}_{\mathrm{sh}} \simeq 0$

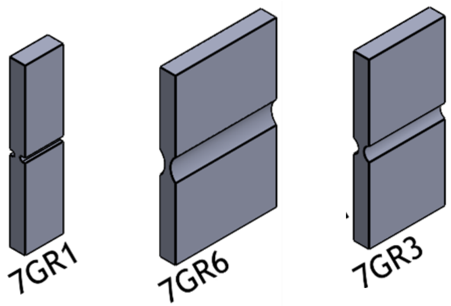

Can be used to characterise remaining parameters

- Identification methodology
  - Coalescence by shearing
    - Shear surface

$$\phi_S = \sqrt{3}\tau - C_S^f(\chi)\sigma_Y = \sigma_{eq}\left(\frac{\sin\theta}{2} + \frac{\sqrt{3}\cos\theta}{2}\right) - C_S^f(\chi)\sigma_Y \leq 0$$

Max Shear Stress

    - With

$$C_S^f(\chi) = \xi(1-\chi^2)$$

    - Ligament evolution

$$\dot{\chi} = K_\chi \dot{\bar{\varepsilon}}_d$$

    - 7GR3 fails by internal necking

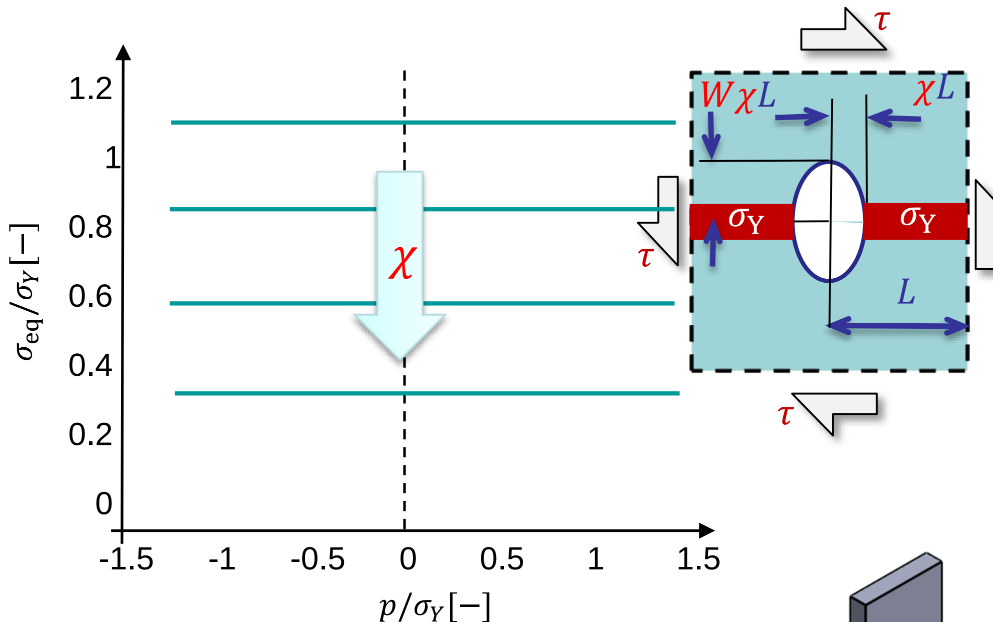

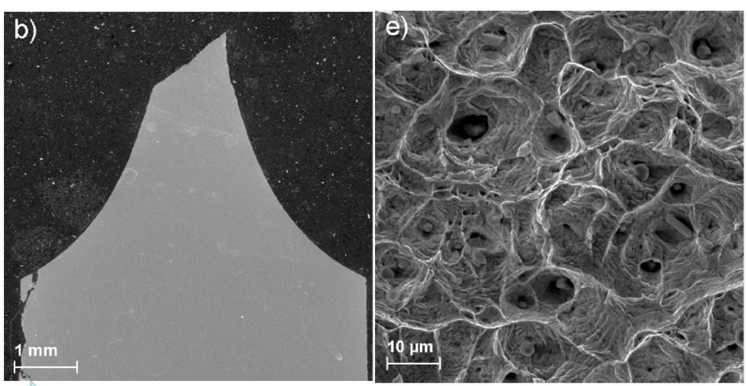

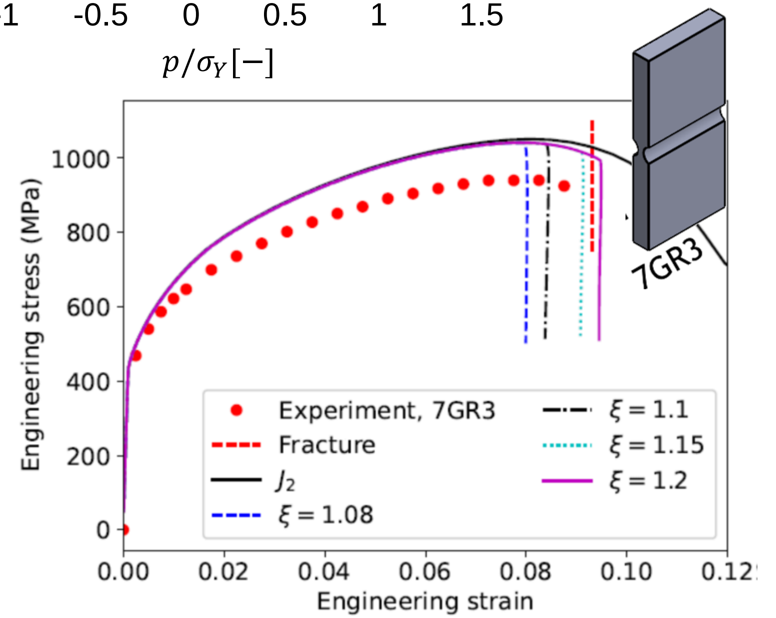

Images by A. Hillhorst, UCL

used to calibrate the shear coalescence parameters $\xi = 1.15$ & $K_\chi = 5$

- Identification methodology
  - Shear-controlled void growth
    - $\dot{f} = \dot{f}_{\mathrm{gr}} + \dot{f}_{\mathrm{nu}} + \dot{f}_{\mathrm{sh}}$ with $\dot{f}_{\mathrm{gr}} = (1-f)\dot{\tilde{\varepsilon}}_v$
    - Assume early nucleation $f_0 = 0.002$

$$\dot{f}_{\mathrm{nu}} = A_n(\tilde{\varepsilon}_m)\dot{\tilde{\varepsilon}}_m = 0$$

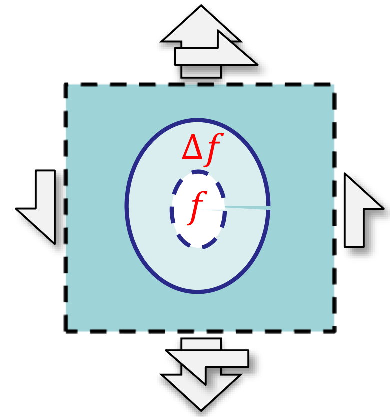

    - Shear growth

$$\begin{cases} \dot{f}_{\mathrm{sh}} = k_w \phi_\eta\left(\dfrac{p}{\sigma_{\mathrm{eq}}}\right)\phi_\omega(\cos 3\theta) f \dot{\tilde{\varepsilon}}_d \\ \phi_\eta(\eta) = \exp\left[-\dfrac{1}{2}\left(\dfrac{\eta}{\eta_s}\right)^2\right] \\ \phi_\omega(\omega) = 1 - \omega^2 \end{cases}$$

    - Last term $k_w = 3.5$ from 3SHEAR

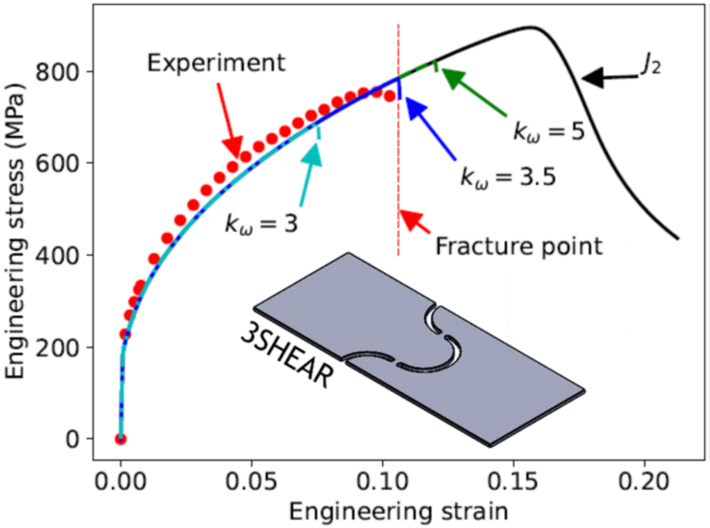

Ductile failure of High-Entropy Alloys (HEA)

- Validation of identified parameters
  - Plates

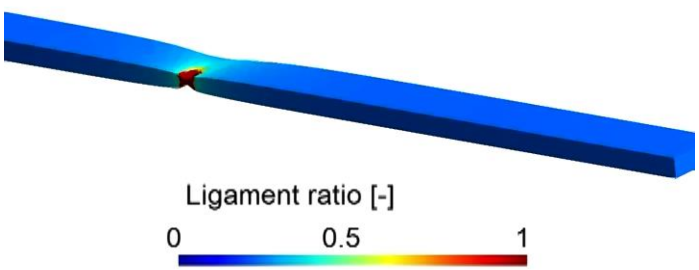

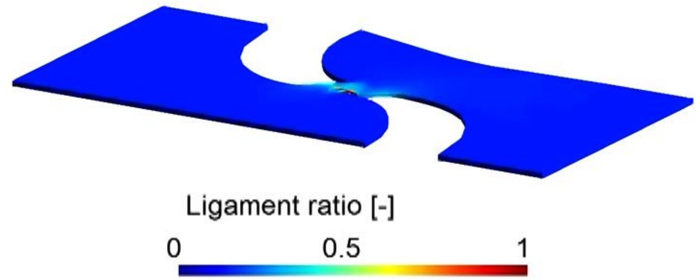

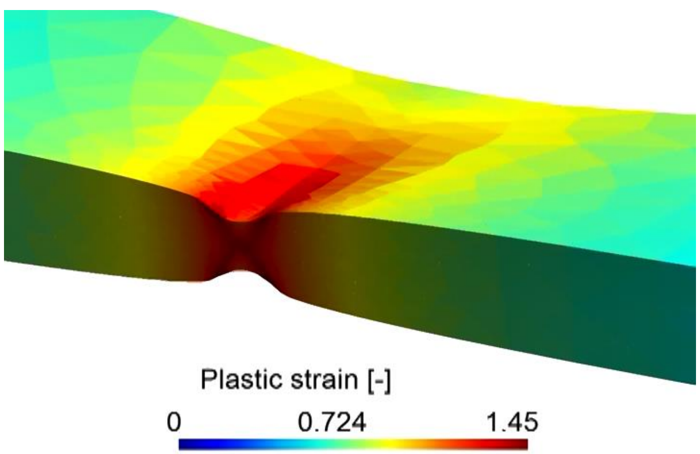

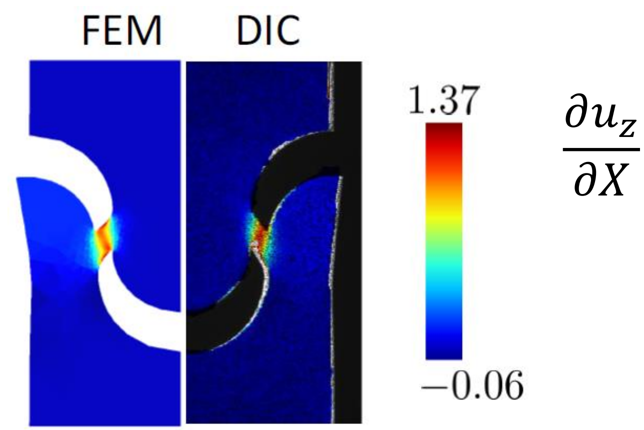

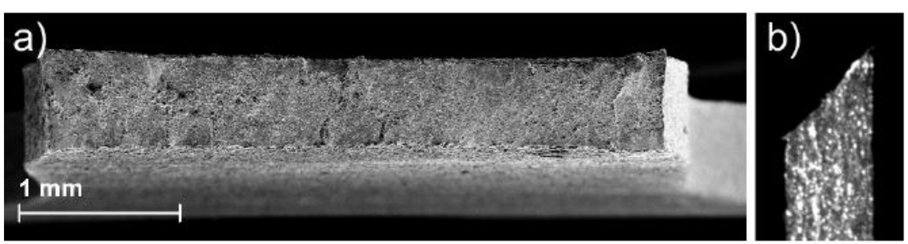

Images by A. Hillhorst, UCL

- Validation of identified parameters
  - Plates (2)

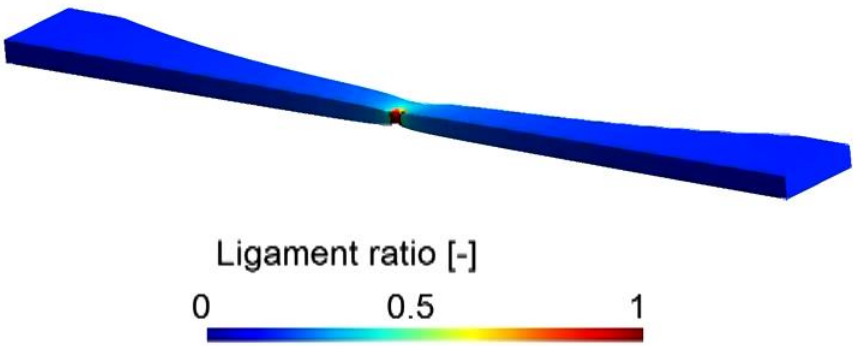

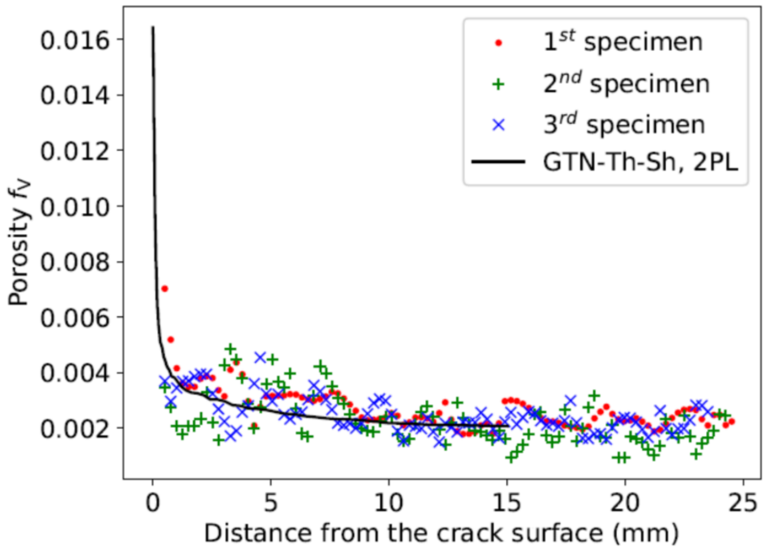

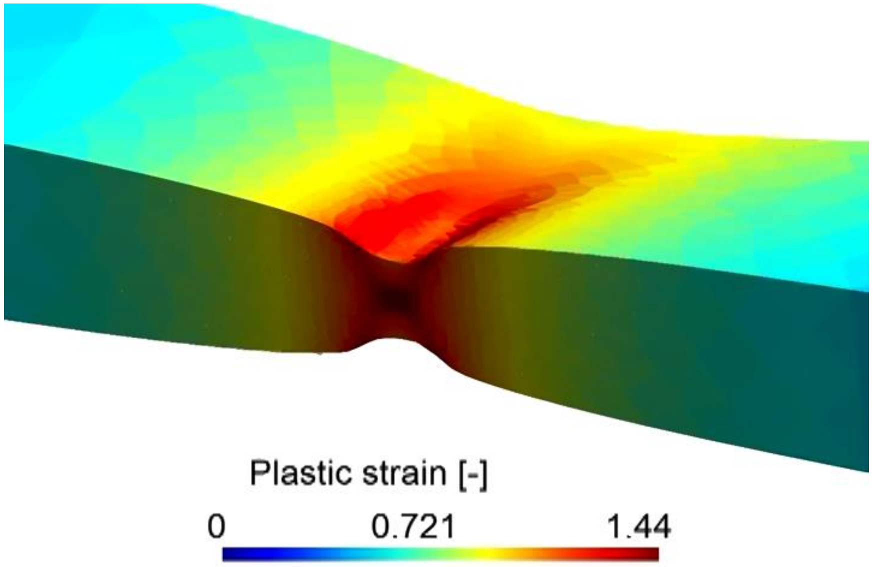

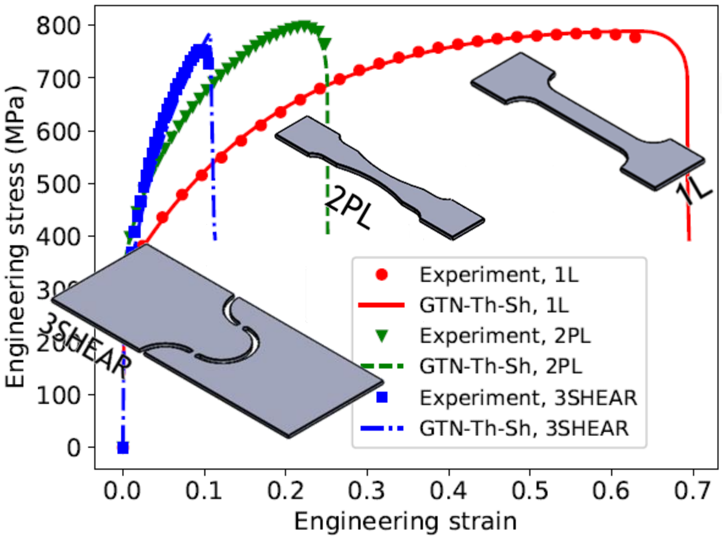

- Validation of identified parameters
  - Notched Plates

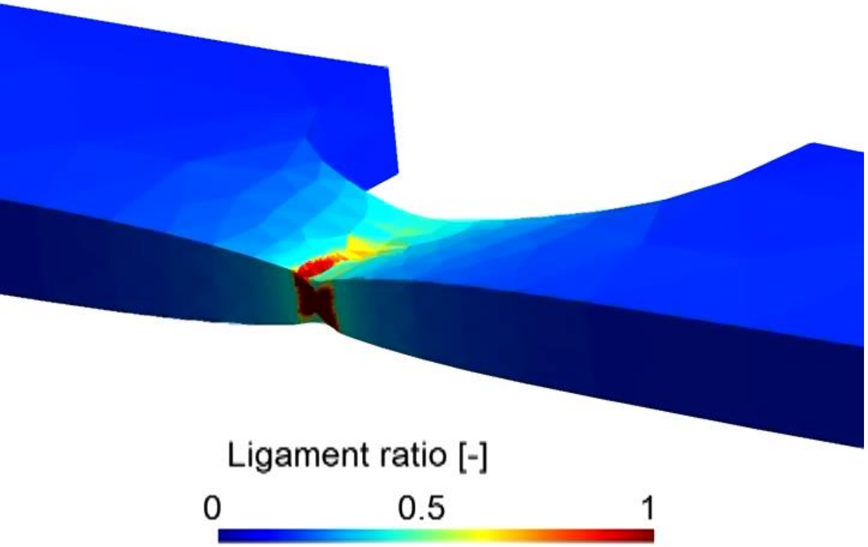

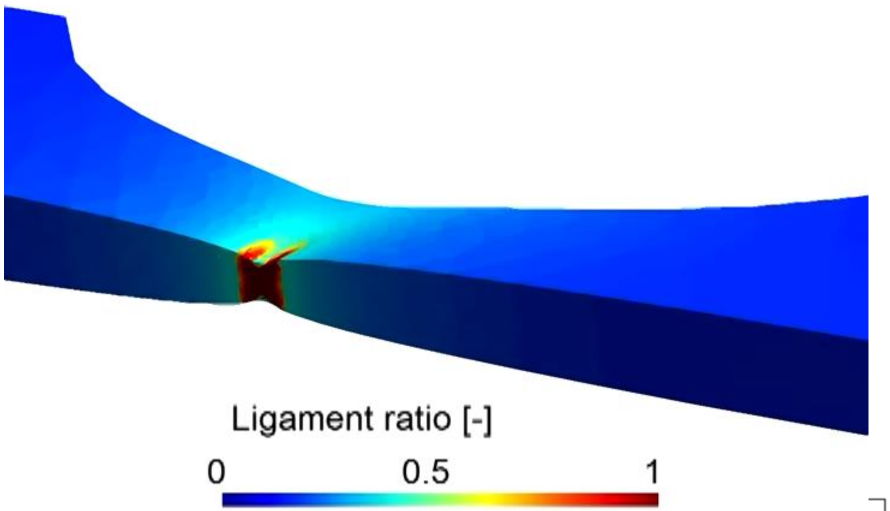

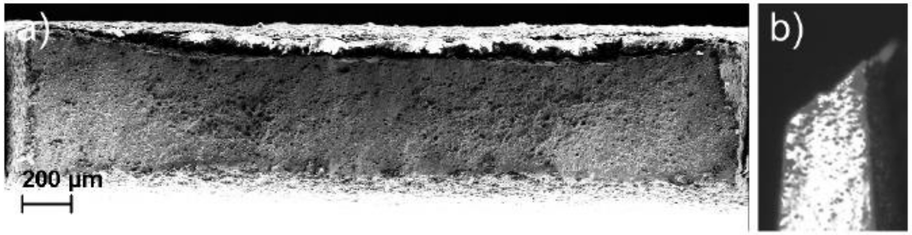

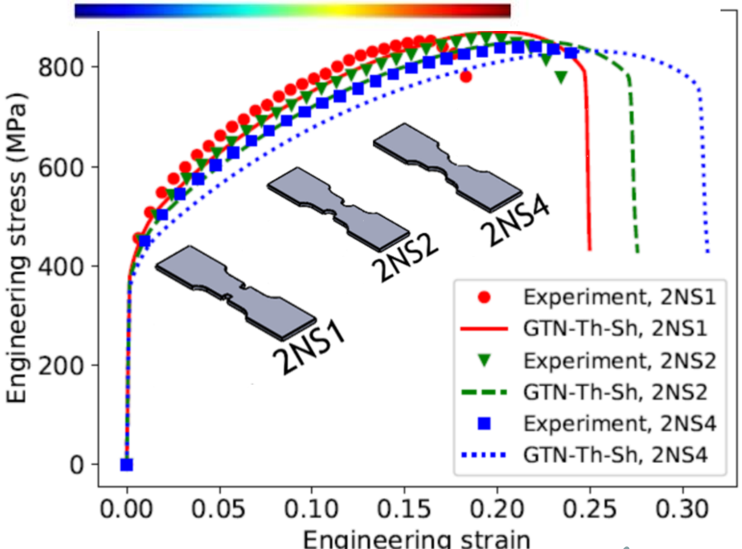

Images by A. Hillhorst, UCL

Ductile failure of High-Entropy Alloys (HEA)

- Validation of identified parameters
  - Axisymmetric bars

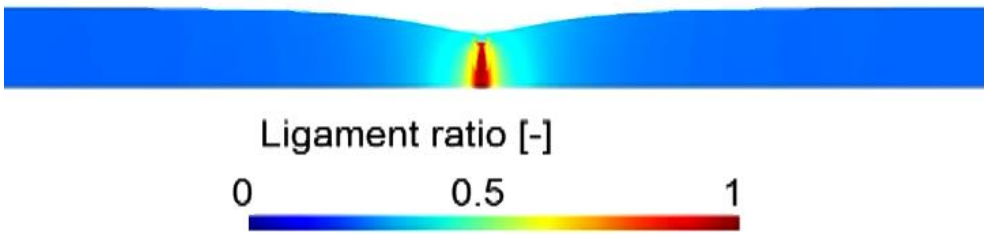

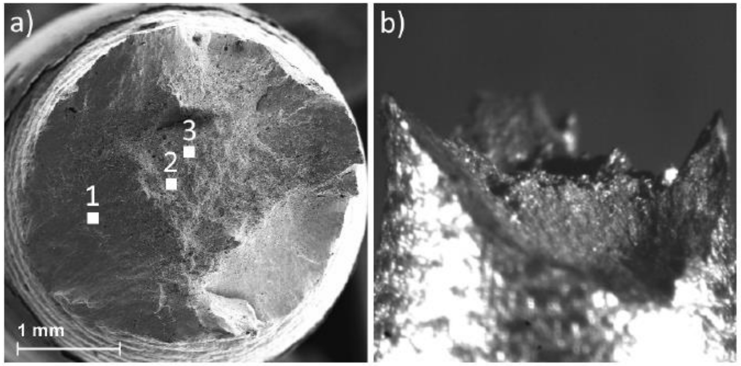

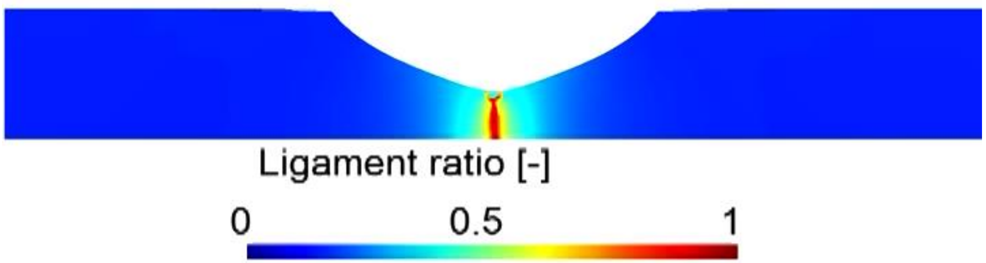

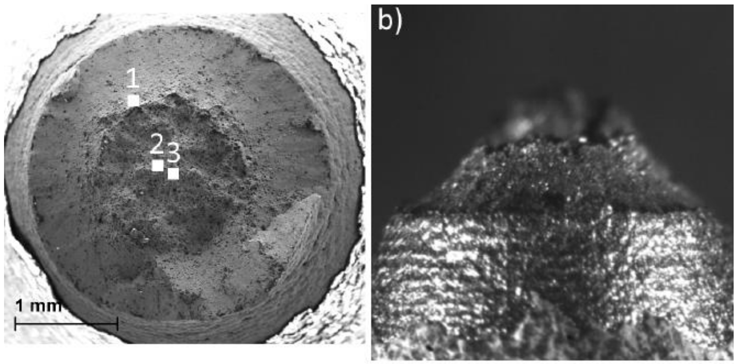

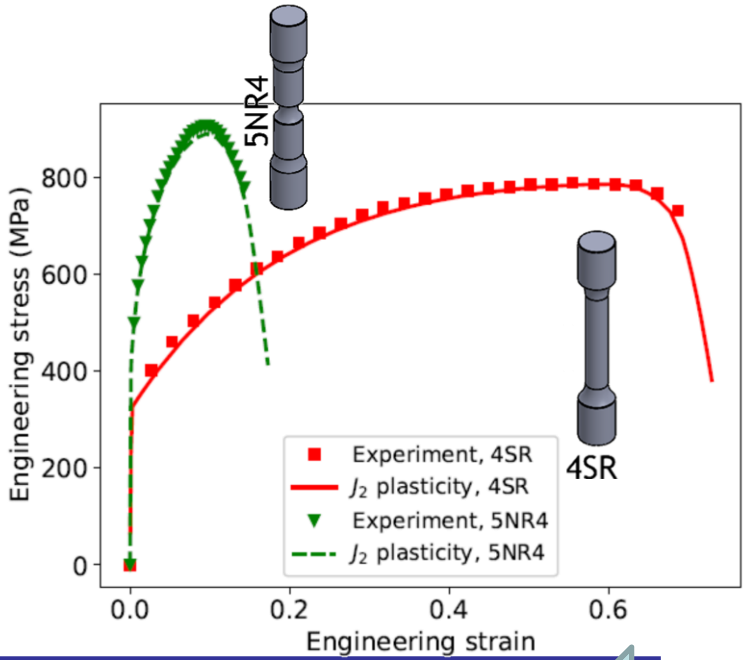

Images by A. Hillhorst, UCL

Ductile failure of High-Entropy Alloys (HEA)

- Validation of identified parameters
  - Grooved plates

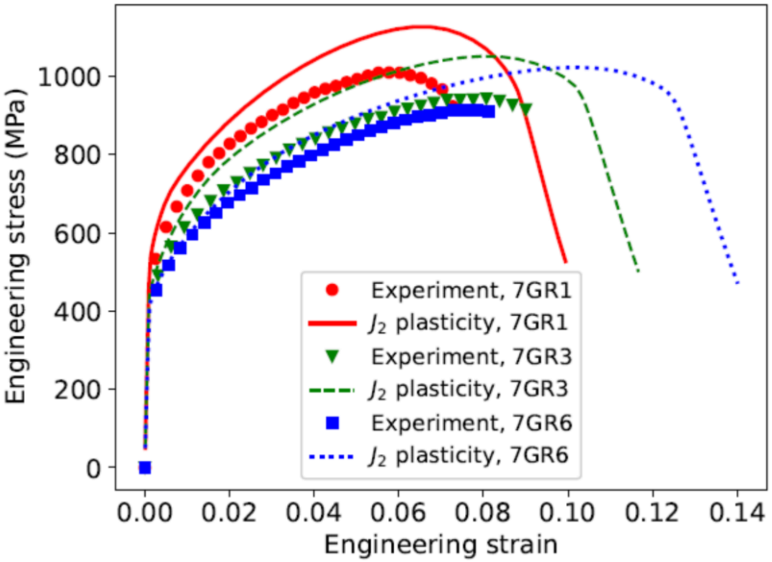

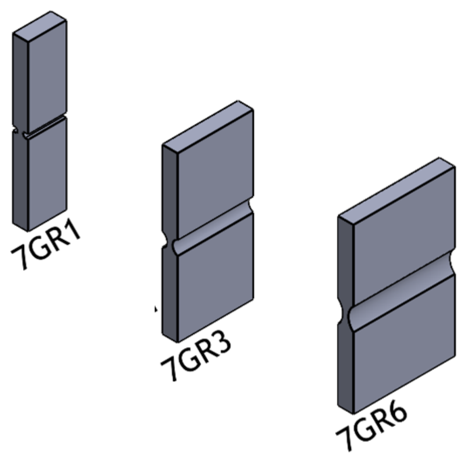

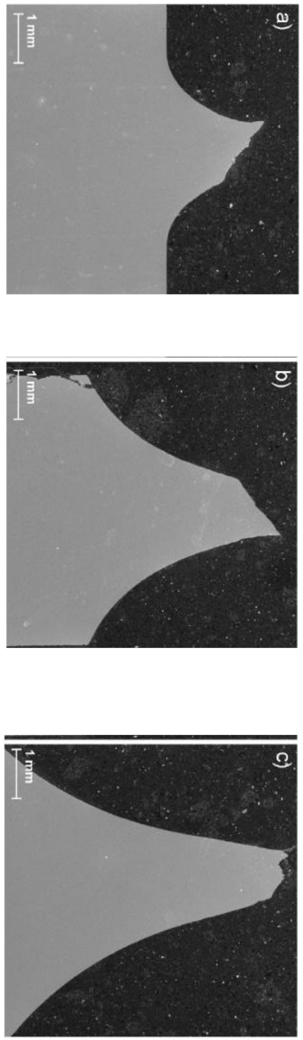

Images by A. Hillhorst, UCL

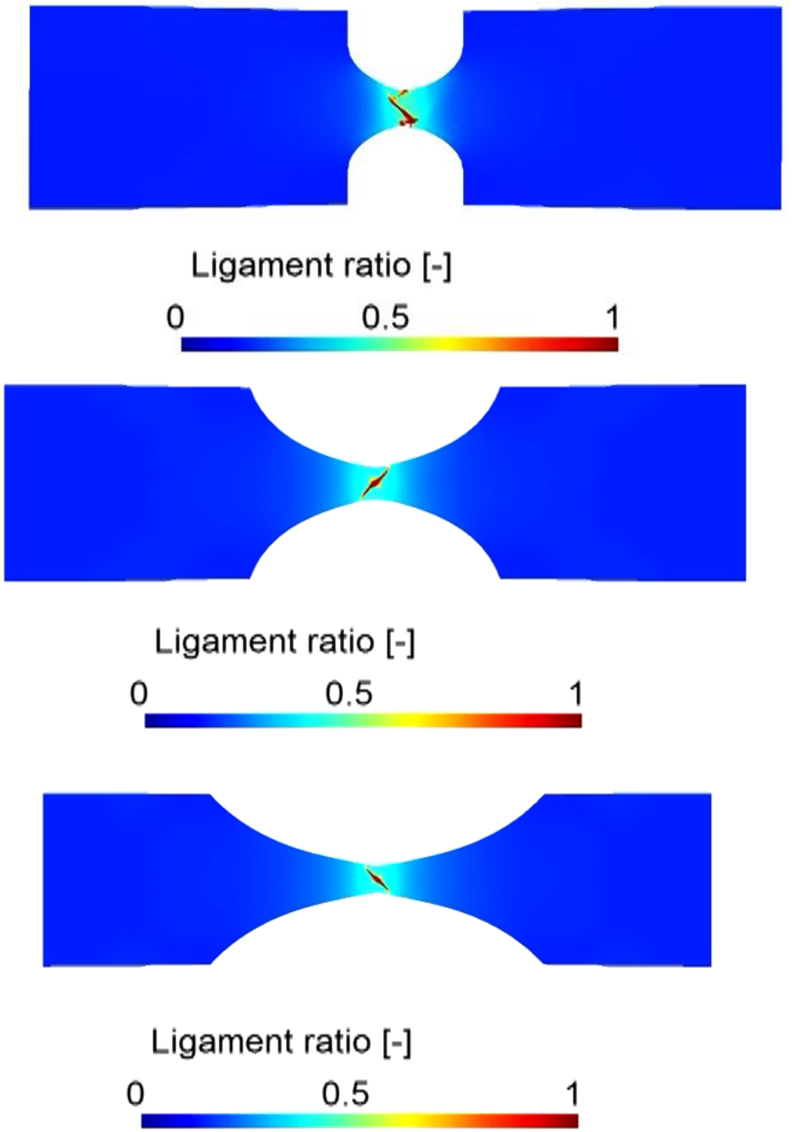

Ductile failure of High-Entropy Alloys (HEA)

- EntroTough WalInnov project
  - UCL, ULB, ULiege (Belgium)
- Publication (doi)
  - 10.1016/j.jmps.2020.103891
  - 10.1016/j.engfracmech.2022.108844

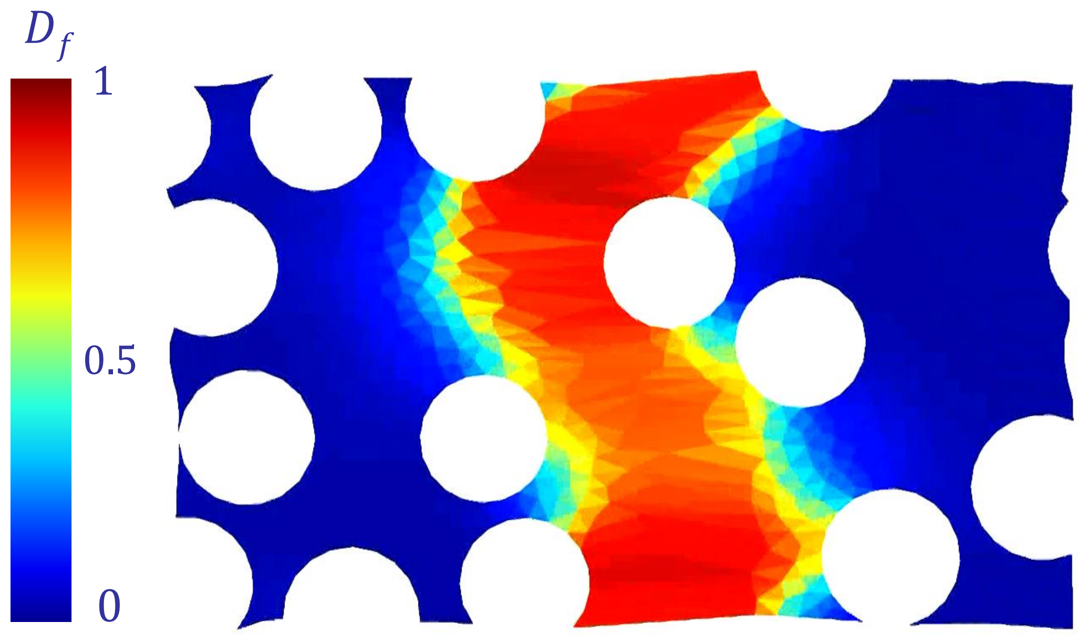

Micro-structural characterization and simulation of fiber-reinforced highly crosslinked epoxy

The authors gratefully acknowledge the nancial support from F.R.S-F.N.R.S. under the project number PDR T.1015.14

Micro-structural simulation of fiber-reinforced highly crosslinked epoxy

- Resin behavior (experiments UCL)
  - Viscoelasto-Viscoplaticity
  - Saturated softening
  - Asymmetry tension-compression
  - Pressure-dependent yield

- To used in micro-structural analysis
  - Behavior in composite is different
  - Introduce a length-scale effect

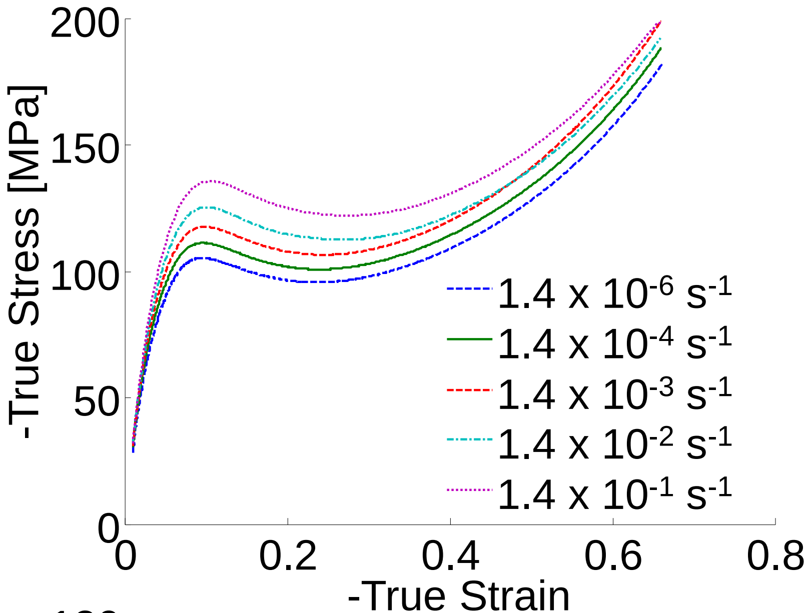

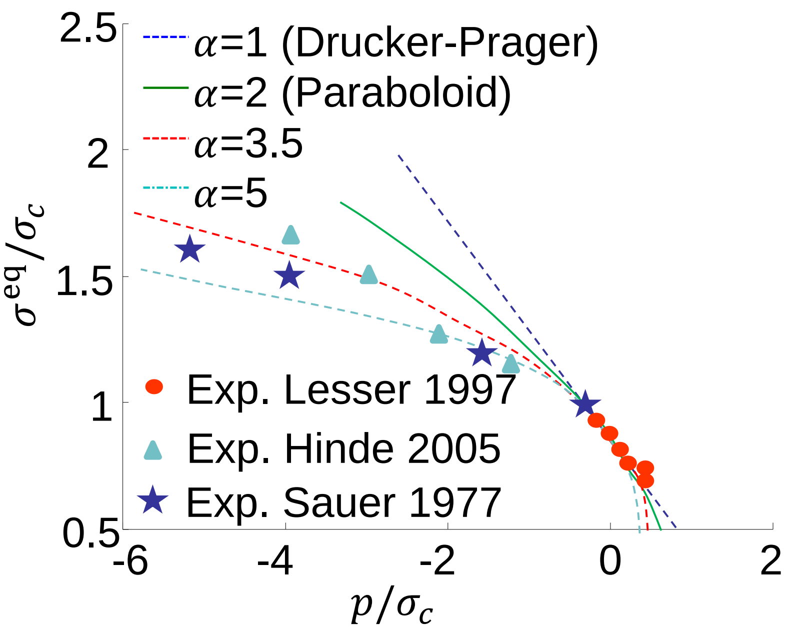

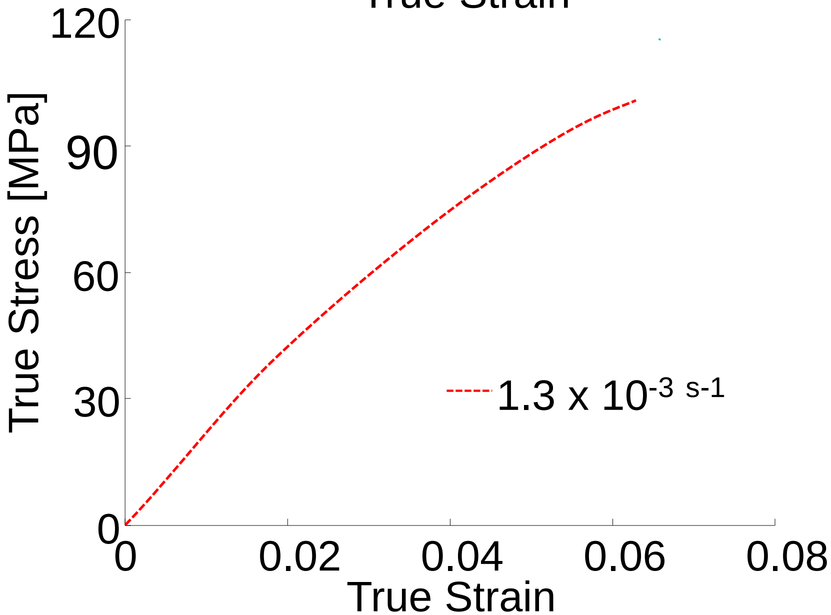

Micro-structural simulation of fiber-reinforced highly crosslinked epoxy

- Material changes represented via internal variables
  - Constitutive law $\mathbf{P}\left(\mathbf{F}; \boldsymbol{Z}(t')\right)$
    - Internal variables $\boldsymbol{Z}(t')$
  - Multi-damage strategy

$$\mathbf{P} = (\mathbf{1} - D_s)(\mathbf{1} - D_f)\widehat{\mathbf{P}}$$

- Resin model implementation:
  - Requires non-local form [Bažant 1988]
    - Introduction of characteristic length l_c
    - Weighted average: $\tilde{Z}(\boldsymbol{x}) = \int_{V_C} W(\boldsymbol{y}; \boldsymbol{x}, l_c)\ Z(\boldsymbol{y}) d\boldsymbol{y}$
  - Implicit form [Peerlings et al. 1998]
    - New degrees of freedom: $\tilde{Z}$
    - New Helmholtz-type equations: $\tilde{Z} - l_c^2\, \Delta\tilde{Z} = Z$
  - Damage evolution laws

$$\begin{cases} \dot{D}_{s/f} = D_{s/f}\left(D_{s/f}, \mathbf{F}(t), \chi_{s/f}(t); Z(\tau), \tau \in [0\ t]\right)\dot{\chi}_{s/f} \\ \chi_{s/f}(t) = \max_{\tau}\left(\tilde{\gamma}_{s/f}(\tau)\right) \\ \tilde{\gamma}_{s/f} - l_{s/f}^2\, \Delta\tilde{\gamma}_{s/f} = \gamma_{s/f} \end{cases}$$

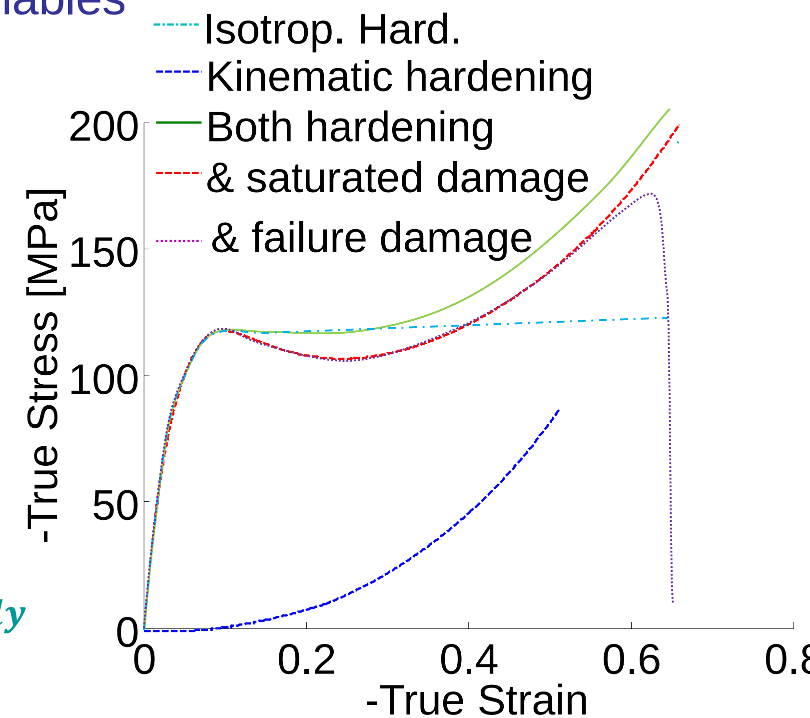

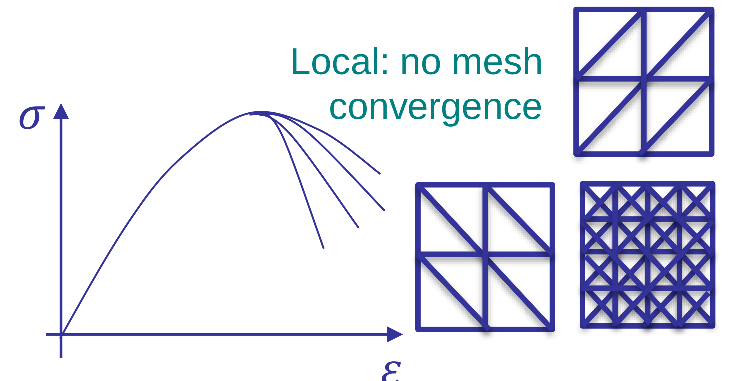

Micro-structural simulation of fiber-reinforced highly crosslinked epoxy

- Resin model: hyperelastic-based formulation
  - Multiplicative decomposition

    $\mathbf{F} = \mathbf{F}^{\mathrm{ve}} \cdot \mathbf{F}^{\mathrm{vp}}, \quad \mathbf{C}^{\mathrm{ve}} = \mathbf{F}^{\mathrm{ve}^T} \cdot \mathbf{F}^{\mathrm{ve}}, \quad J^{\mathrm{ve}} = \det(\mathbf{F}^{\mathrm{ve}})$
  - Undamaged stress tensor definition
    - Elastic potential $\psi(\mathbf{C}^{ve})$
    - Undamaged first Piola-Kirchhoff stress tensor

      $$\hat{\mathbf{P}} = 2\mathbf{F}^{\mathrm{ve}} \cdot \frac{\partial \psi(\mathbf{C}^{\mathrm{ve}})}{\partial \mathbf{C}^{\mathrm{ve}}} \cdot \mathbf{F}^{\mathrm{vp}^{-T}}$$
    - Undamaged Kirchhoff stress tensors
      - In current configuration

        $$\hat{\boldsymbol{\kappa}} = \hat{\mathbf{P}} \cdot \mathbf{F}^T = 2\mathbf{F}^{\mathrm{ve}} \cdot \frac{\partial \psi(\mathbf{C}^{ve})}{\partial \mathbf{C}^{\mathrm{ve}}} \cdot \mathbf{F}^{\mathrm{ve}^T}$$
      - In co-rotational space

        $$\hat{\boldsymbol{\tau}} = \mathbf{C}^{\mathrm{ve}} \cdot \mathbf{F}^{\mathrm{ve}^{-1}} \cdot \hat{\boldsymbol{\kappa}} \cdot \mathbf{F}^{\mathrm{ve}^{-T}} = 2\mathbf{C}^{ve} \cdot \frac{\partial \psi(\mathbf{C}^{\mathrm{ve}})}{\partial \mathbf{C}^{\mathrm{ve}}}$$
  - Apparent stress tensor
    - Piola-Kirchhoff stress

      $$\mathbf{P} = (\mathbf{1} - D_s)(\mathbf{1} - D_f)\hat{\mathbf{P}}$$

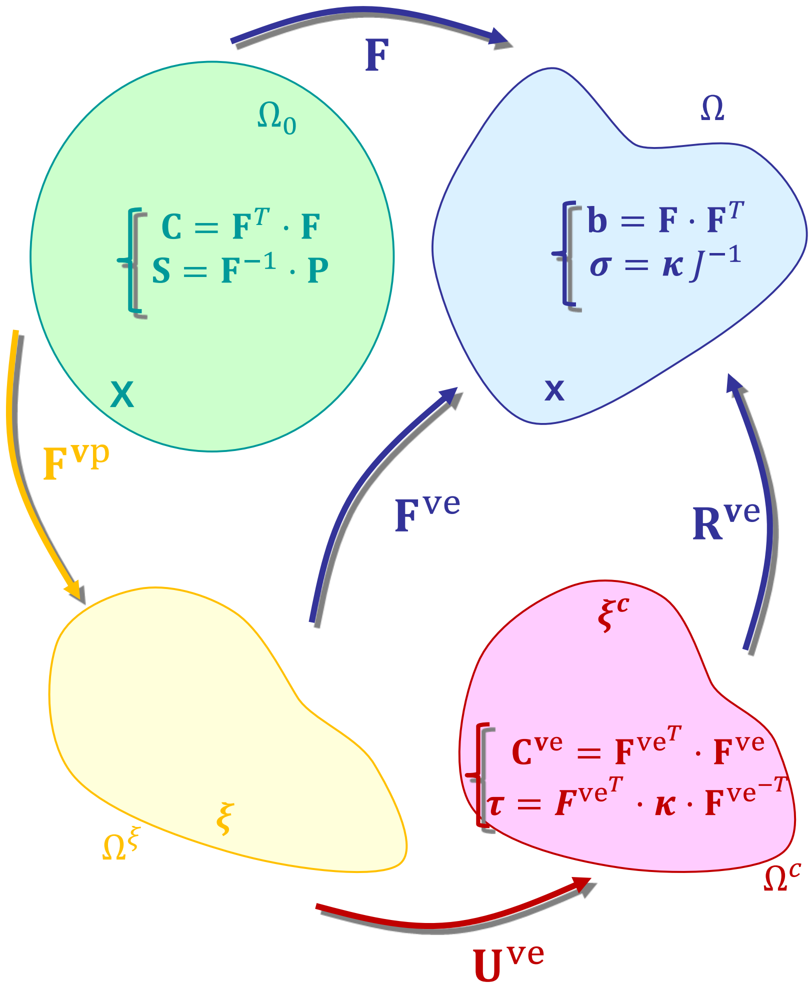

- Resin model: logarithmic visco-elasticity
  - Elastic potentials ψ_i:

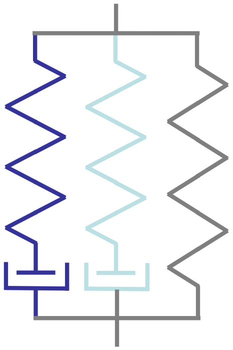

$$\psi_i(\mathbf{C}^{\mathrm{ve}}) = \frac{K_i}{2}\ln^2(J^{\mathrm{ve}}) + \frac{G_i}{4}(\ln(\mathbf{C}^{\mathrm{ve}}))^{\mathrm{dev}}:(\ln(\mathbf{C}^{\mathrm{ve}}))^{\mathrm{dev}}$$

  - Dissipative potentials Υ_i

$$\Upsilon_i(\mathbf{C}^{\mathrm{ve}}, \mathbf{q}_i) = -\mathbf{q}_i : \ln(\mathbf{C}^{\mathrm{ve}}) + \left[\frac{1}{18K_i}\mathrm{tr}^2(\mathbf{q}_i) + \frac{1}{4G_i}\mathbf{q}_i^{\mathrm{dev}} : \mathbf{q}_i^{\mathrm{dev}}\right]$$

$$\begin{cases} \dot{\mathbf{q}}_i^{\mathrm{dev}} = \dfrac{2G_i}{g_i}(\ln(\mathbf{C}^{\mathrm{ve}}))^{\mathrm{dev}} - \dfrac{1}{g_i}\mathbf{q}_i^{\mathrm{dev}} \\ \mathrm{tr}\,(\dot{\mathbf{q}}_i) = \dfrac{3K_i}{k_i}\ln^2(J^{\mathrm{ve}}) - \dfrac{1}{k_i}\mathrm{tr}\,(\mathbf{q}_i) \end{cases}$$

  - Total potential ψ:

$$\begin{cases} \psi(\mathbf{C}^{\mathrm{ve}}; \boldsymbol{q}_i) = \psi_\infty(\mathbf{C}^{\mathrm{ve}}) + \displaystyle\sum_i [\psi_i(\mathbf{C}^{\mathrm{ve}}) + \Upsilon_i(\mathbf{C}^{\mathrm{ve}}, \mathbf{q}_i)] \\ \widehat{\mathbf{P}} = 2\mathbf{F}^{\mathrm{ve}} \cdot \dfrac{\partial\psi(\mathbf{C}^{\mathrm{ve}})}{\partial\mathbf{C}^{\mathrm{ve}}} \cdot \mathbf{F}^{\mathrm{vp}^{-T}} \end{cases}$$

Micro-structural simulation of fiber-reinforced highly crosslinked epoxy

- Resin model: visco-plasticity
  - Stress, back-stress

    $$\boldsymbol{\varphi} = \hat{\boldsymbol{\tau}} - \hat{\boldsymbol{b}}$$

  - Perzina plastic flow rule

    $$\mathbf{D}^{\mathrm{vp}} = \dot{\mathbf{F}}^{\mathrm{v}p} \cdot \mathbf{F}^{\mathrm{v}p} = \frac{1}{\eta}\langle\phi\rangle^{\frac{1}{p}} \frac{\partial P}{\partial \hat{\boldsymbol{\tau}}}$$

  - Pressure dependent yield surface

    $$\begin{cases} \phi = \left(\dfrac{\varphi^{\mathrm{eq}}}{\sigma_c}\right)^{\alpha} - \dfrac{m^{\alpha}-1}{m+1}\dfrac{\mathrm{tr}\boldsymbol{\varphi}}{\sigma_c} - \dfrac{m^{\alpha}+m}{m+1} \le 0 \\ m = \dfrac{\sigma_t}{\sigma_c} \end{cases}$$

  - Non-associated flow potential

    $$P = (\varphi^{\mathrm{eq}})^2 + \beta\left(\frac{\mathrm{tr}\boldsymbol{\varphi}}{3}\right)^2$$

  - Equivalent plastic strain rate:

    $$\begin{cases} \dot{\gamma} = \dfrac{\sqrt{\mathbf{D}^{\mathrm{vp}}:\mathbf{D}^{\mathrm{vp}}}}{\sqrt{\mathbf{1}+\mathbf{2}v_p^2}} \\ v_p = \dfrac{9-2\beta}{18+2\beta} \end{cases}$$

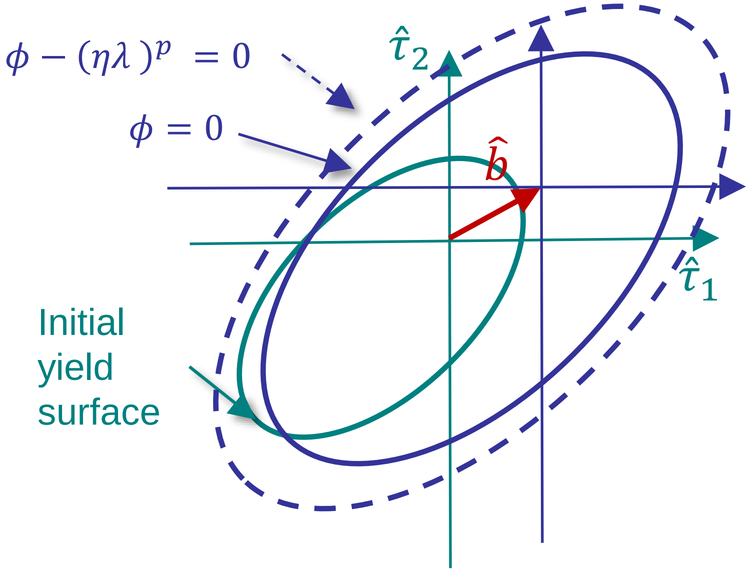

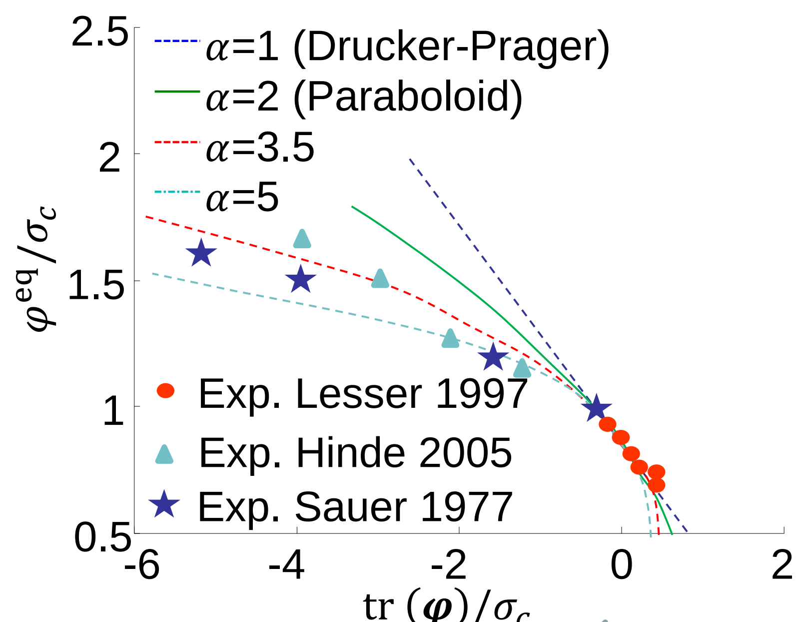

Micro-structural simulation of fiber-reinforced highly crosslinked epoxy

- Resin model: saturated softening
  - Damage evolution

$$\begin{cases} \dot{D}_s = H_s(\chi_s - \chi_{s0})^{\zeta_s}(D_{s\infty} - D_s)\dot{\chi}_s \\ \chi_s = \max_{\tau}\left(\chi_{s0}, \tilde{\gamma}_s(\tau)\right) \\ \tilde{\gamma}_s - l_s^2\, \Delta\tilde{\gamma}_s = \gamma \end{cases}$$

  - Calibration
    - Several hardening/softening combinations
    - Requires composite material tests
      - Length scale effect

$$l_s = 3\mu\text{m}\left(1 - \frac{D_s}{D_{s\infty}}\right)$$

      - Non-local BC at fiber interface $[\![\dot{\tilde{\gamma}}_s]\!] = 0$

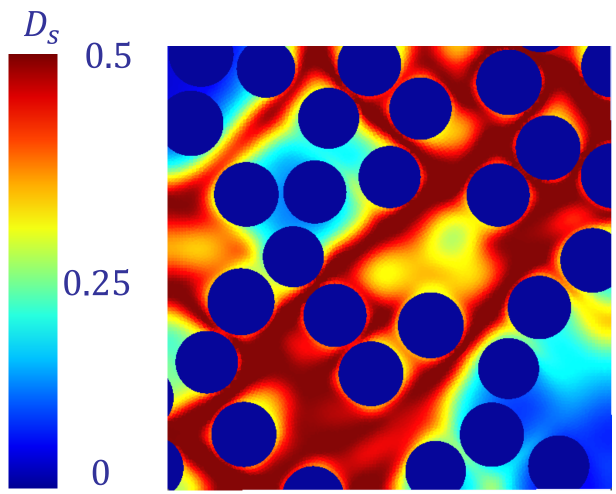

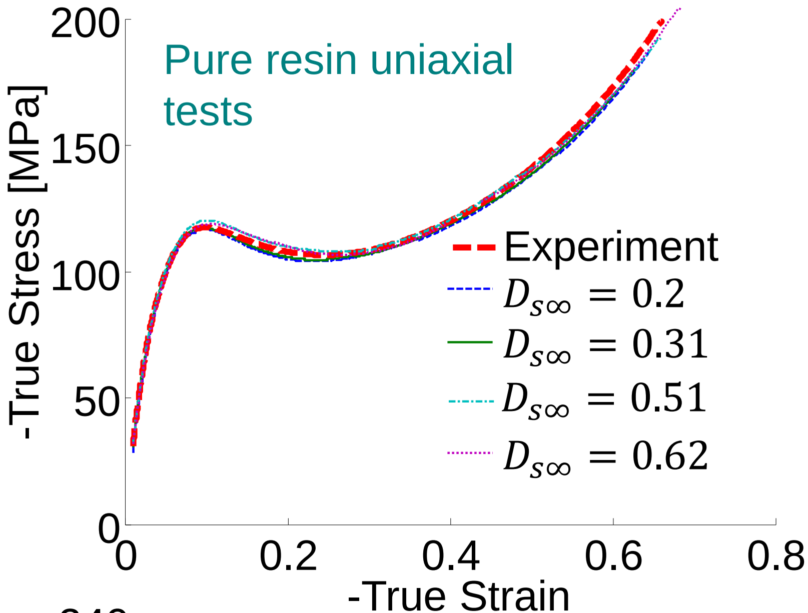

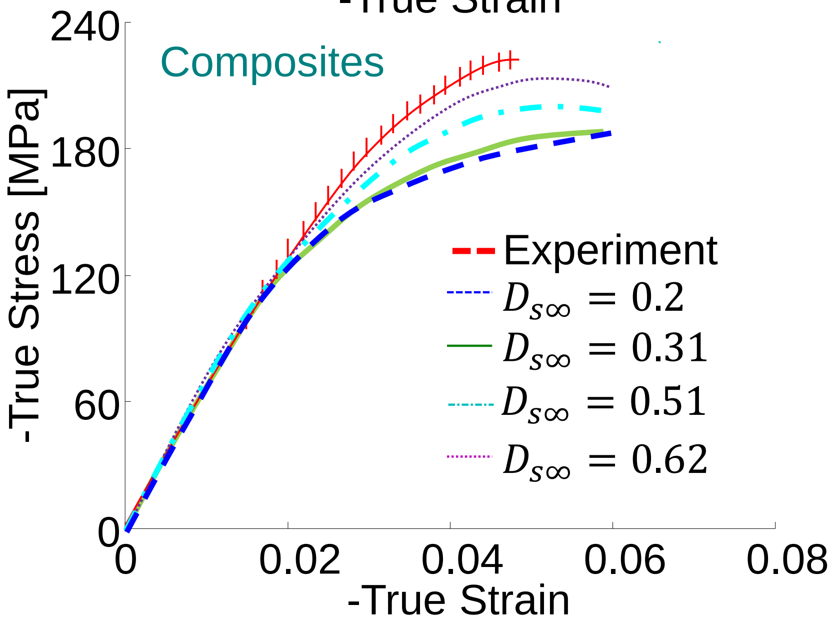

Micro-structural simulation of fiber-reinforced highly crosslinked epoxy

- Resin model: failure softening
  - Failure surface

$$\begin{cases} \phi_f = \gamma - a\exp\left(-b\dfrac{\mathrm{tr}(\hat{\boldsymbol{\tau}})}{3\hat{\tau}^{eq}}\right) - c \\ \phi_f - r \le 0;\ \dot{r} \ge 0; \text{and } \dot{r}\left(\phi_f - r\right) = 0 \\ \dot{\gamma}_f = \dot{r} \end{cases}$$

  - Damage evolution

$$\begin{cases} \dot{D}_f = H_f(\chi_f)^{\zeta_f}(1 - D_f)^{-\zeta_d}\,\dot{\chi}_f \\ \chi_f = \max_{\tau}\left(\tilde{\gamma}_f(\tau)\right) \\ \tilde{\gamma}_f - l_f^2\,\Delta\tilde{\gamma}_f = \gamma_f \\ l_f = 3\ \mu\mathrm{m} \qquad \nabla_0\tilde{\gamma}_f \cdot \mathbf{N} = 0 \end{cases}$$

  - Affect ductility

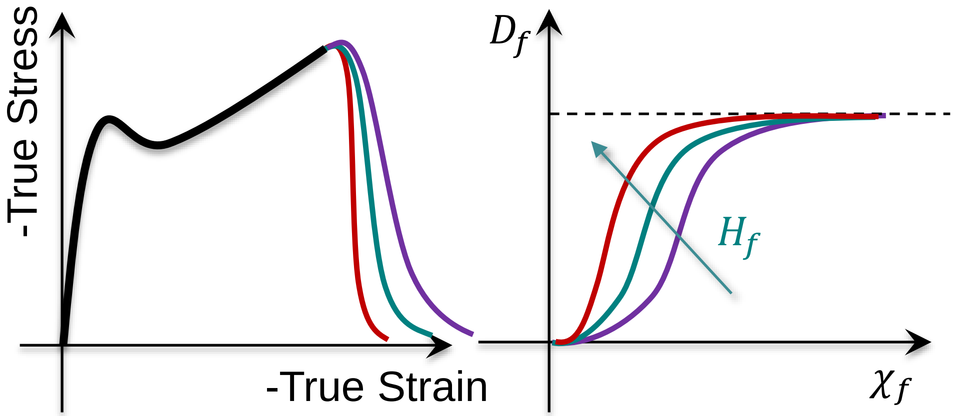

- Resin model: failure softening (2)
  - Damage evolution

$$\dot{D}_f = H_f(\chi_f)^{\zeta_f}(1 - D_f)^{-\zeta_d}\,\dot{\chi}_f$$

$$\tilde{\gamma}_f - l_f^2\,\Delta\tilde{\gamma}_f = \gamma_f$$

  - Calibration
    - Recover the epoxy G_c
    - From localization simulation

$$G_c A = \Upsilon^{\mathrm{end}} - \Upsilon^{\mathrm{loc}}$$

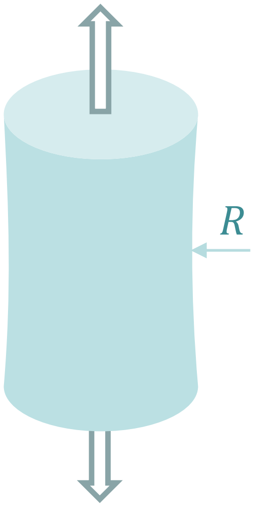

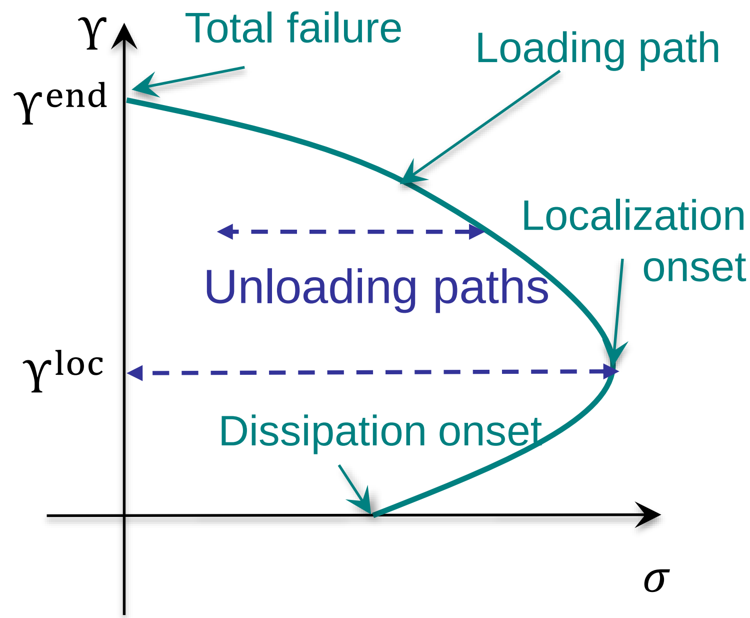

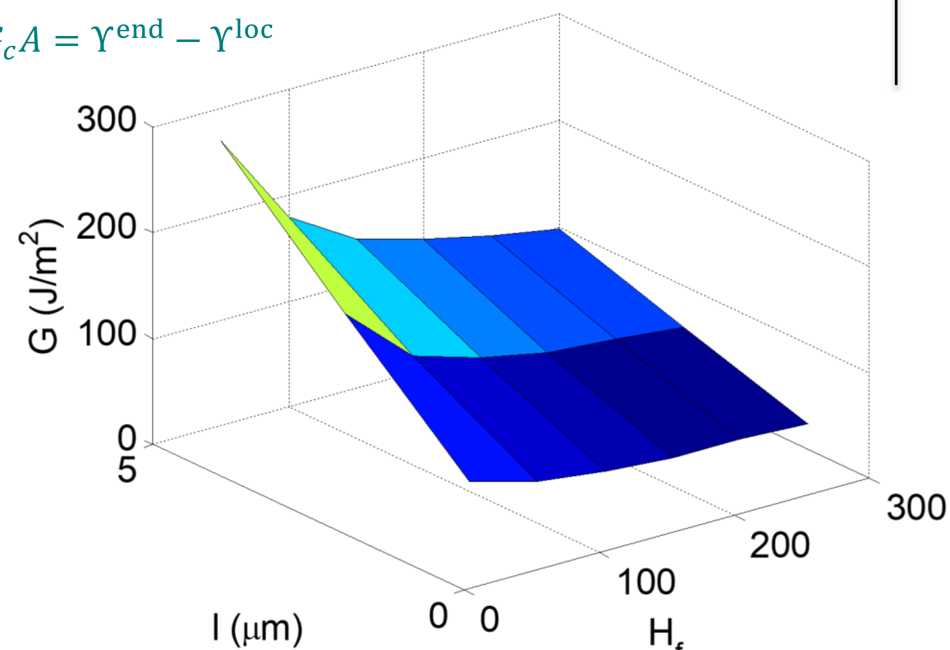

- Resin model: Validation
  - Compression without barrelling effect

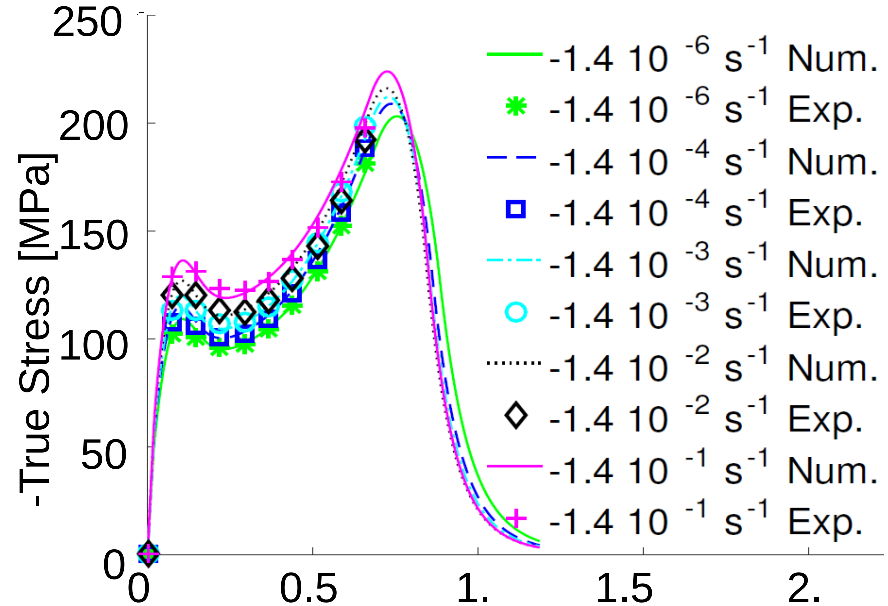

  - With barrelling effect

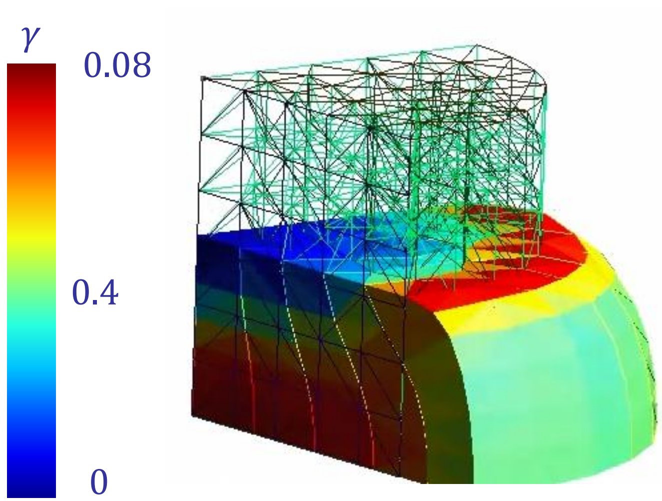

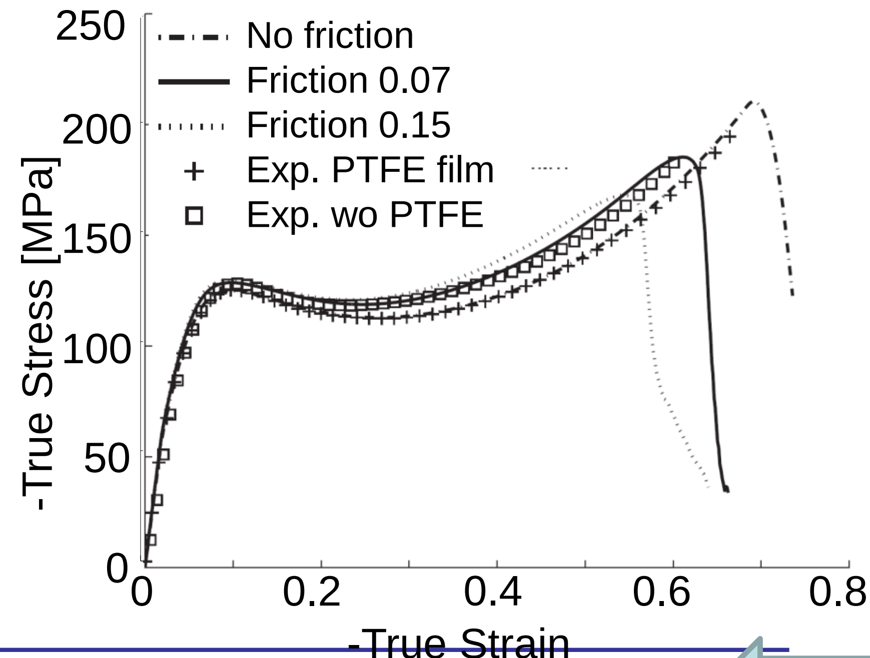

- Composite model: Extraction of G_c

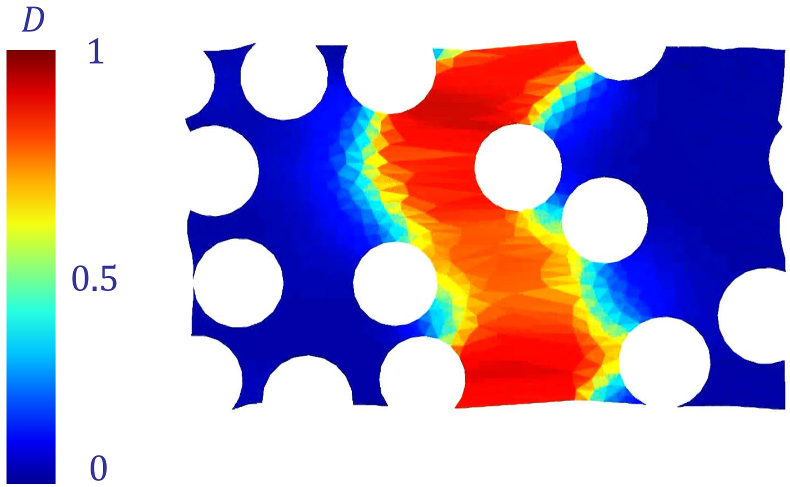

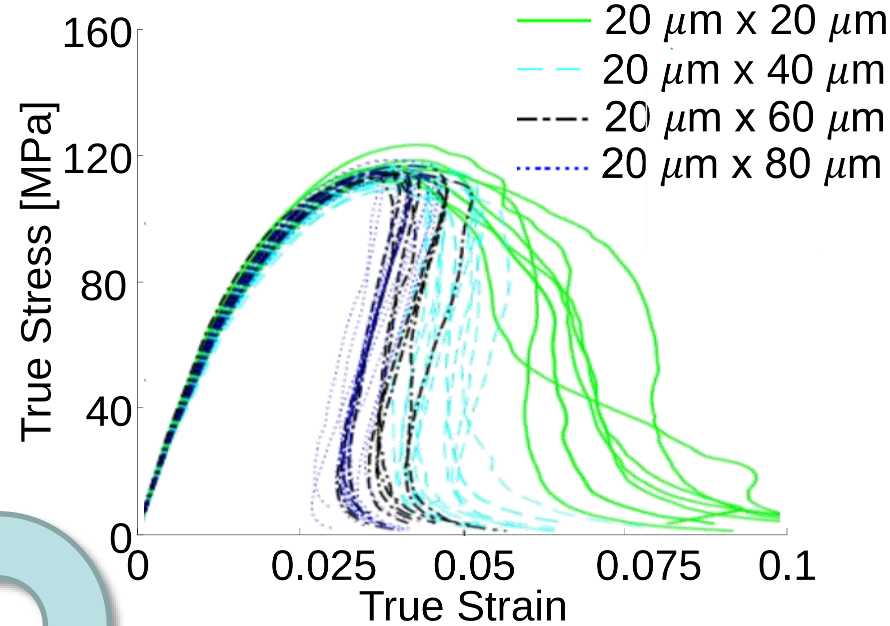

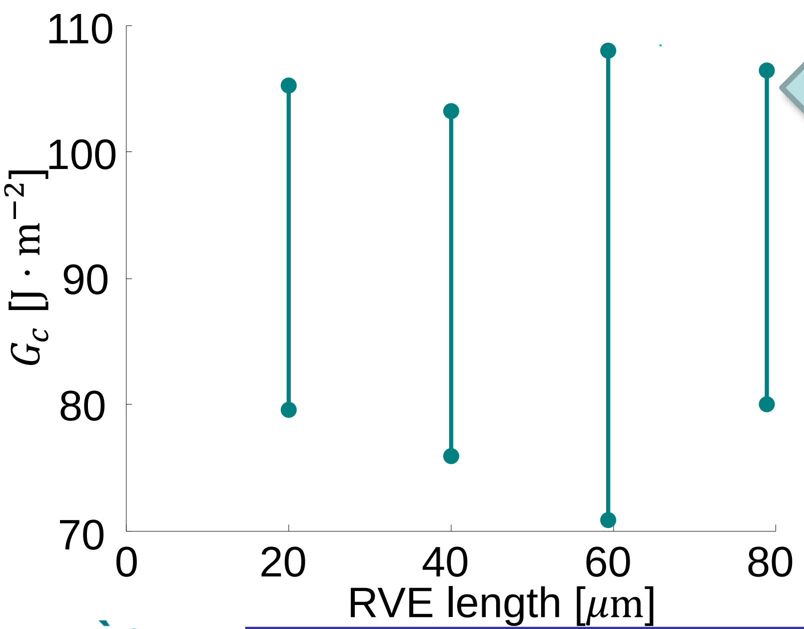

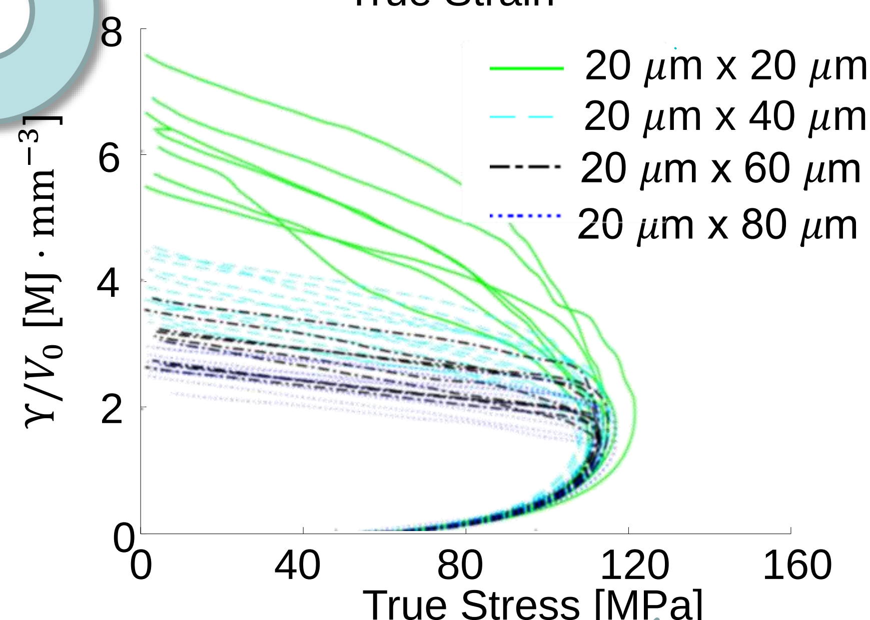

Micro-structural simulation of fiber-reinforced highly crosslinked epoxy

- Composite model: Validation
  - Compression test

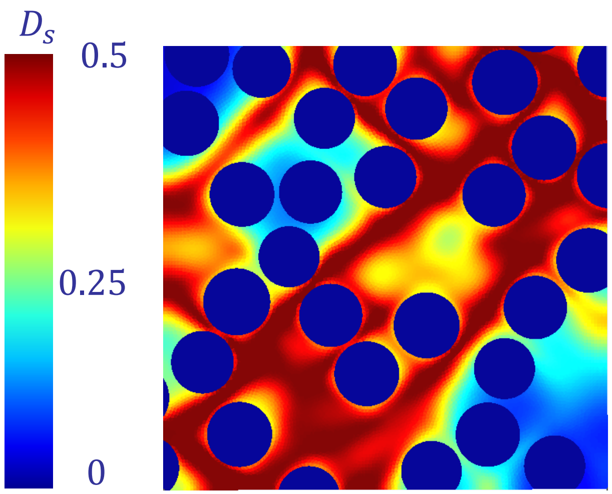

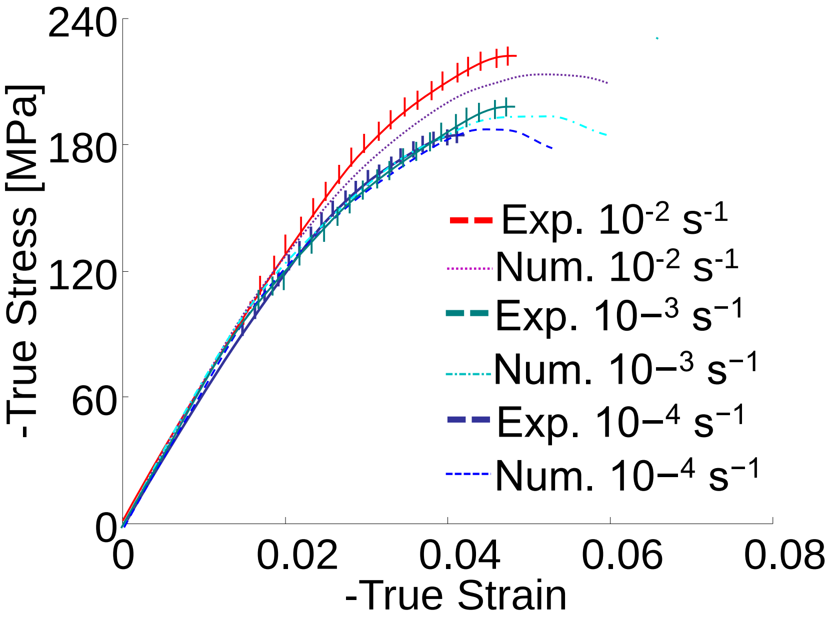

- PDR T.1015.14 project
  - ULiège, UCL (Belgium)

- Publications
  - 10.1016/j.ijsolstr.2016.06.008
  - 10.1016/j.mechmat.2019.02.017

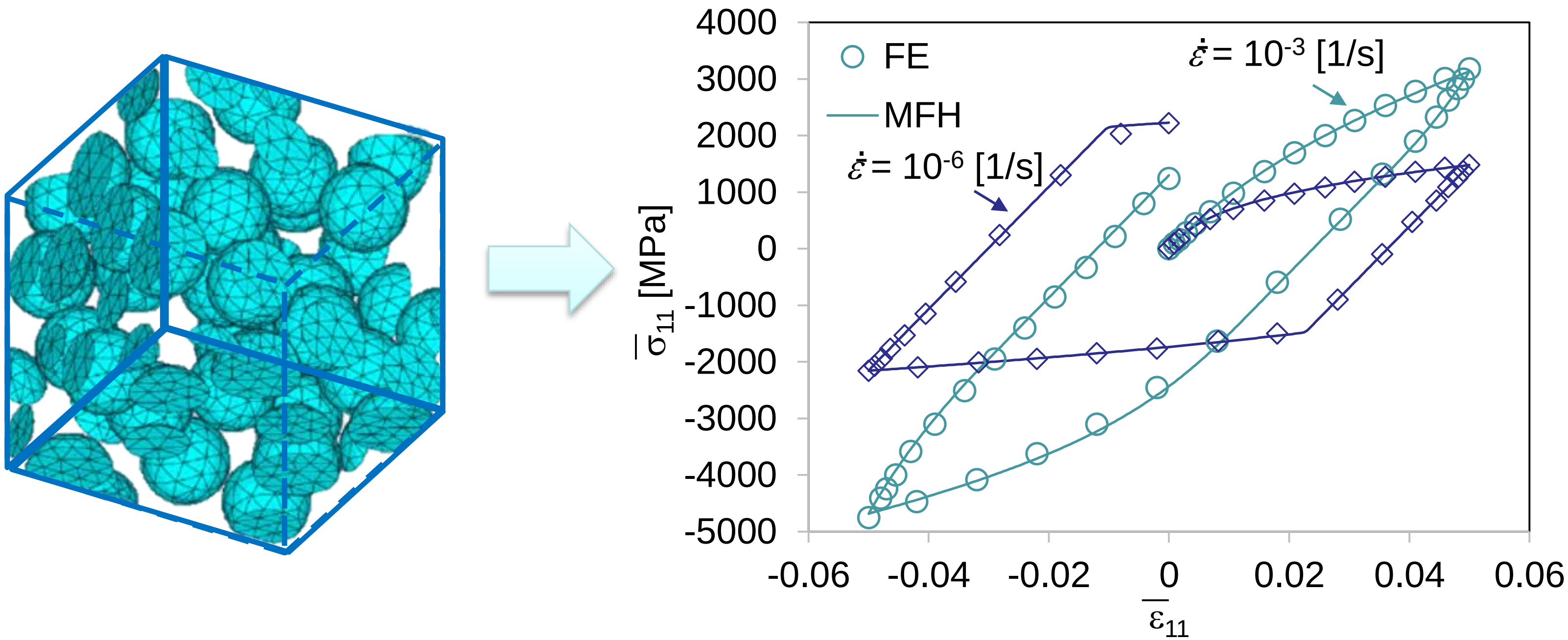

Mean-Field-Homogenization for Elasto-Visco-Plastic Composites

SIMUCOMP The research has been funded by the Walloon Region under the agreement no 1017232 (CT-EUC 2010-10-12) in the context of the ERA-NET +, Matera + framework.
The authors gratefully acknowledge the financial support from F.R.S-F.N.R.S. under the project number PDR T.1015.14
STOMMMAC The research has been funded by the Walloon Region under the agreement no 1410246-STOMMMAC (CT-INT 2013-03-28) in the context of M-ERA.NET Joint Call 2014.

Mean-Field-Homogenization for elasto-visco-plastic composites

- Multi-scale modeling
  - 2 problems are solved concurrently
    - The macro-scale problem
    - The meso-scale problem (on a meso-scale Volume Element)

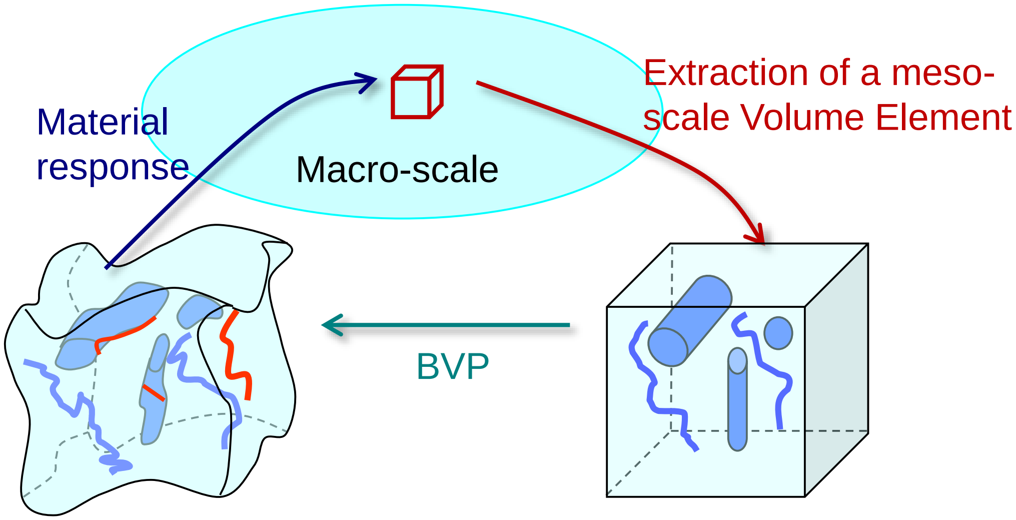

- Length-scales separation

$$L_{\mathrm{macro}} >> L_{\mathrm{VE}} >> L_{\mathrm{micro}}$$

For accuracy: Size of the meso-scale volume element smaller than the characteristic length of the macro-scale loading

To be statistically representative: Size of the meso-scale volume element larger than the characteristic length of the micro-structure

Mean-Field-Homogenization for elasto-visco-plastic composites

- Incremental-secant mean-field-homogenization
  - Linear Comparison Composite material
    - Defined from unloaded state
  - Solve iteratively the system

$$\left\{\begin{aligned} \Delta\bar{\boldsymbol{\varepsilon}}^{\mathrm{r}} &= v_0 \Delta\boldsymbol{\varepsilon}_0^{\mathrm{r}} + v_{\mathrm{I}} \Delta\boldsymbol{\varepsilon}_{\mathrm{I}}^{\mathrm{r}} \\ \Delta\boldsymbol{\varepsilon}_{\mathrm{I}}^{\mathrm{r}} &= \Delta\boldsymbol{\varepsilon}_{\mathrm{I}} + \Delta\boldsymbol{\varepsilon}_{\mathrm{I}}^{\mathrm{unload}} \\ \Delta\boldsymbol{\varepsilon}_0^{\mathrm{r}} &= \Delta\boldsymbol{\varepsilon}_0 + \Delta\boldsymbol{\varepsilon}_0^{\mathrm{unload}} \\ \Delta\boldsymbol{\varepsilon}_{\mathrm{I}}^{\mathrm{r}} &= \mathbf{B}^{\varepsilon}\left(\mathrm{I}, \bar{\mathbf{C}}_0^{\mathrm{Sr}}, \bar{\mathbf{C}}_{\mathrm{I}}^{\mathrm{Sr}}\right) : \Delta\boldsymbol{\varepsilon}_0^{\mathrm{r}} \end{aligned}\right.$$

    - With the stress tensors

$$\left\{\begin{aligned} \bar{\boldsymbol{\sigma}} &= v_0 \boldsymbol{\sigma}_0 + v_{\mathrm{I}} \boldsymbol{\sigma}_{\mathrm{I}} \\ \boldsymbol{\sigma}_{\mathrm{I}} &= \boldsymbol{\sigma}_{\mathrm{I}}^{\mathrm{res}} + \bar{\mathbf{C}}_{\mathrm{I}}^{\mathrm{Sr}} : \Delta\boldsymbol{\varepsilon}_{\mathrm{I}}^{\mathrm{r}} \\ \boldsymbol{\sigma}_0 &= \boldsymbol{\sigma}_0^{\mathrm{res}} + \bar{\mathbf{C}}_0^{\mathrm{Sr}} : \Delta\boldsymbol{\varepsilon}_0^{\mathrm{r}} \end{aligned}\right.$$

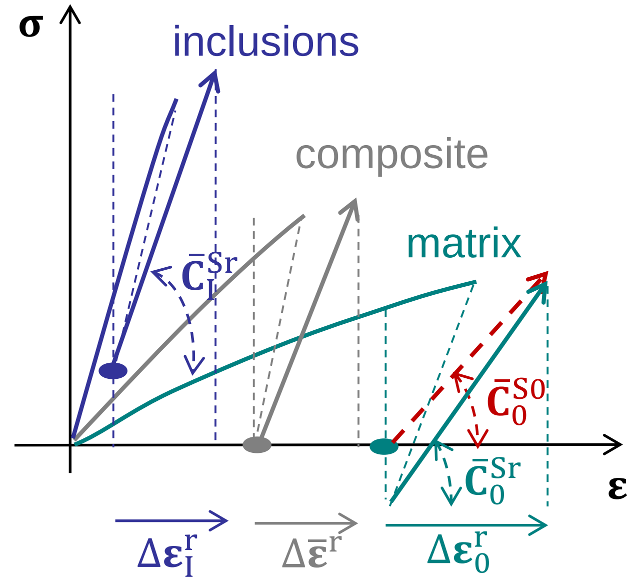

For elasto-plasticity: $f(\sigma^{\mathrm{eq}}, p) = 0$

&

For elasto-visco-plasticity: $\Delta p = g_v(\sigma^{\mathrm{eq}}, p)\Delta t$

  - For soft matrix response
    - Remove residual stress in matrix
    - Or use second moment estimates

$\Delta\boldsymbol{\varepsilon}_{\mathrm{I}}^{\mathrm{r}} = \mathbf{B}^{\varepsilon}\left(\mathrm{I}, \bar{\mathbf{C}}_0^{\mathrm{S0}}, \bar{\mathbf{C}}_{\mathrm{I}}^{\mathrm{Sr}}\right) : \Delta\boldsymbol{\varepsilon}_0^{\mathrm{r}}$ & $\boldsymbol{\sigma}_0 = \bar{\mathbf{C}}_0^{\mathrm{S0}} : \Delta\boldsymbol{\varepsilon}_0^{\mathrm{r}}$

- Incremental-secant mean-field-homogenization
  - Stress tensor (2 forms)

$$\begin{cases} \boldsymbol{\sigma}_{\mathrm{I/0}} = \boldsymbol{\sigma}^{\mathrm{res}}_{\mathrm{I/0}} + \bar{\mathbf{C}}^{\mathrm{Sr}}_{\mathrm{I/0}} : \Delta\boldsymbol{\varepsilon}^{\mathrm{r}}_{\mathrm{I/0}} \\ \boldsymbol{\sigma}_{\mathrm{I/0}} = \bar{\mathbf{C}}^{\mathrm{S0}}_{\mathrm{I/0}} : \Delta\boldsymbol{\varepsilon}^{\mathrm{r}}_{\mathrm{I/0}} \end{cases}$$

  - Radial return direction toward residual stress
    - First order approximation in the strain increment (and not in the total strain)
    - Exact for the zero-incremental-secant method
  - The secant operators are naturally isotropic

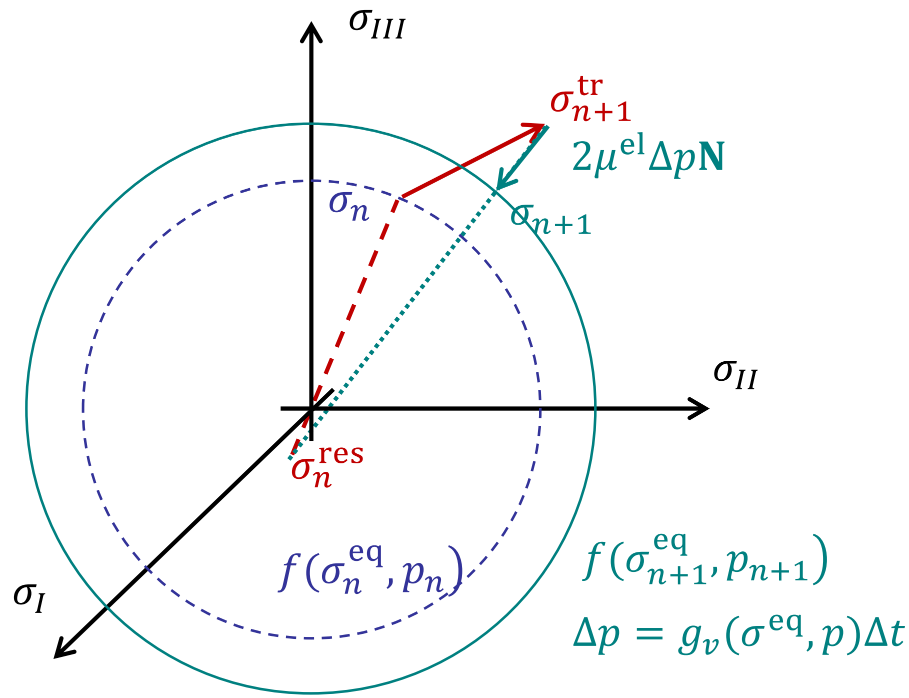

$$\begin{cases} \bar{\mathbf{C}}^{\mathrm{Sr}} = 3\kappa^{\mathrm{el}}\mathbf{I}^{\mathrm{vol}} + 2\left(\mu^{\mathrm{el}} - 3\dfrac{{\mu^{\mathrm{el}}}^2\Delta p}{\left(\boldsymbol{\sigma}_{n+1} - \boldsymbol{\sigma}^{\mathrm{res}}_n\right)^{\mathrm{eq}}}\right)\mathbf{I}^{\mathrm{vol}} \\ \bar{\mathbf{C}}^{\mathrm{S0}} = 3\kappa^{\mathrm{el}}\mathbf{I}^{\mathrm{vol}} + 2\left(\mu^{\mathrm{el}} - 3\dfrac{{\mu^{\mathrm{el}}}^2\Delta p}{\boldsymbol{\sigma}^{\mathrm{eq}}_{n+1}}\right)\mathbf{I}^{\mathrm{vol}} \end{cases}$$

Mean-Field-Homogenization for elasto-visco-plastic composites

- Incremental-secant mean-field-homogenization
  - Second-statistical moment estimation of the von Mises stress
    - First statistical moment (mean value) not fully representative

$$\bar{\sigma}^{\mathrm{eq}}_{\mathrm{I}/0} = \sqrt{\frac{3}{2}\bar{\boldsymbol{\sigma}}^{\mathrm{dev}}_{\mathrm{I}/0} : \bar{\boldsymbol{\sigma}}^{\mathrm{dev}}_{\mathrm{I}/0}}$$

    - Use second statistical moment estimations to define the yield surface

$$\hat{\hat{\sigma}}^{\mathrm{eq}}_{\mathrm{I}/0} = \sqrt{\frac{3}{2}\mathbf{I}^{\mathrm{dev}} :: \langle \boldsymbol{\sigma}_{\mathrm{I}/0} \otimes \boldsymbol{\sigma}_{\mathrm{I}/0} \rangle_{\omega_{\mathrm{I}/0}}} \geq \bar{\sigma}^{\mathrm{eq}}_{\mathrm{I}/0}$$

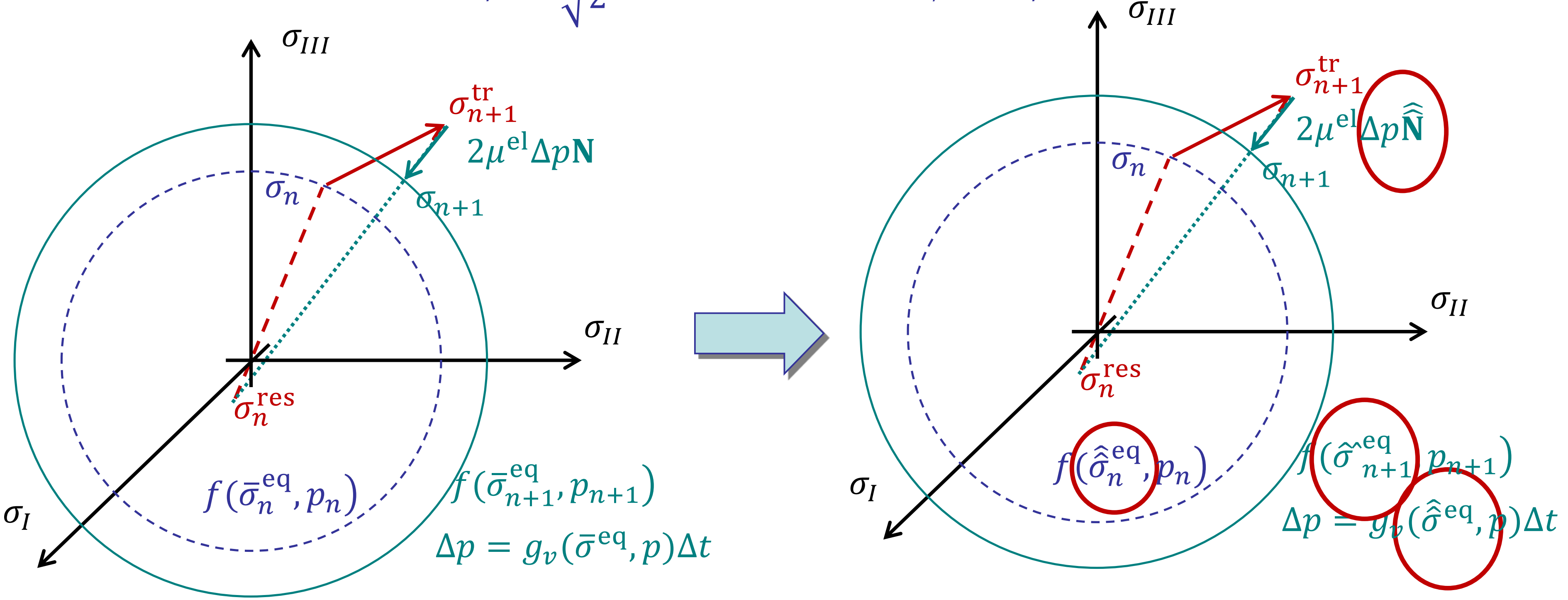

Beginning

Mean-Field-Homogenization for elasto-visco-plastic composites

- Non-proportional loading
  - Spherical inclusions
    - 17 % volume fraction
    - Elastic
  - Elastic-perfectly-plastic matrix

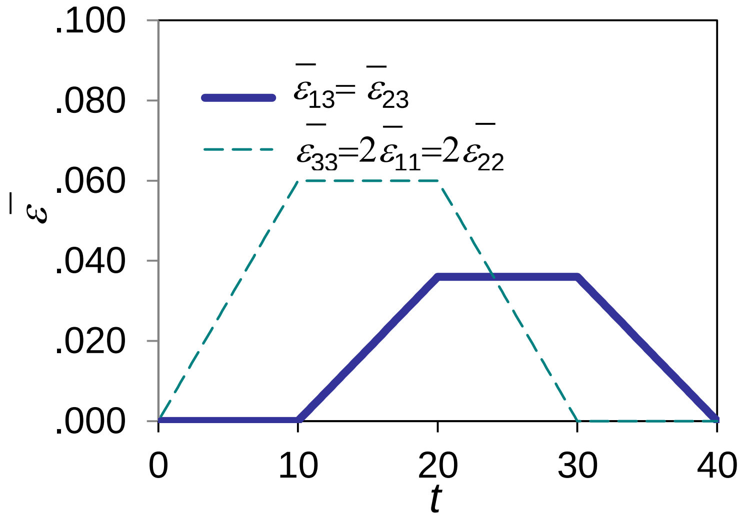

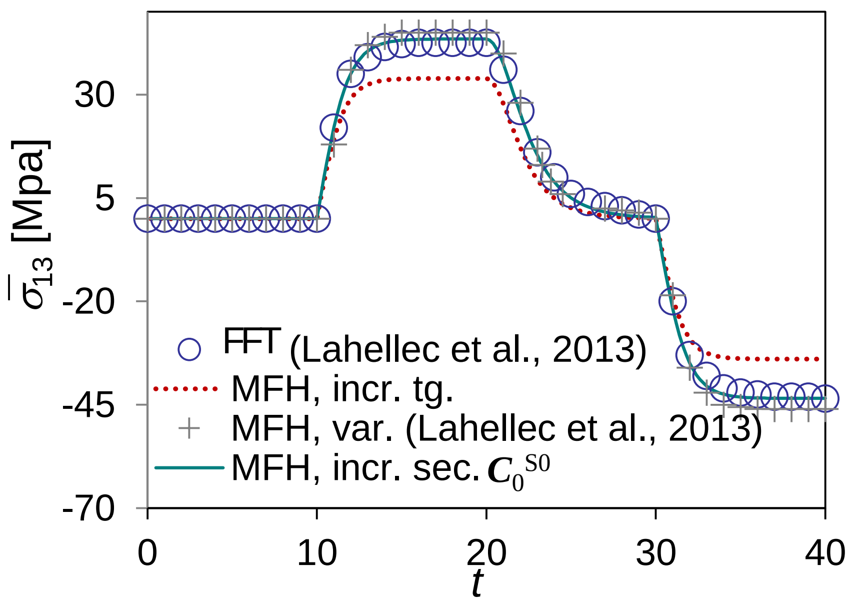

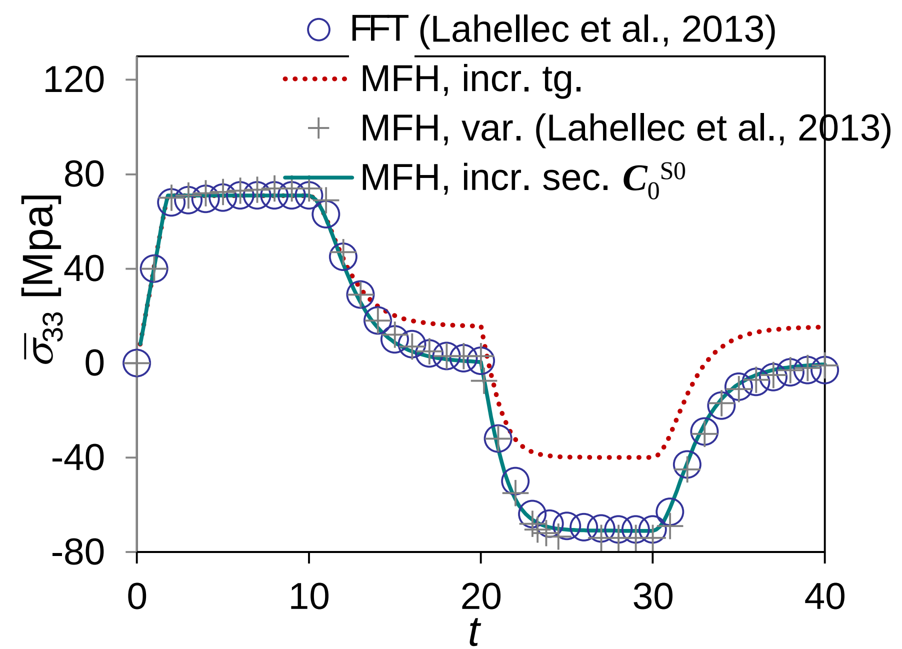

Mean-Field-Homogenization for elasto-visco-plastic composites

- Elasto-visco-plasticity
  - Elasto-visco-plastic short fibres
    - Spherical
    - 30 % volume fraction
  - Elasto-visco-plastic matrix

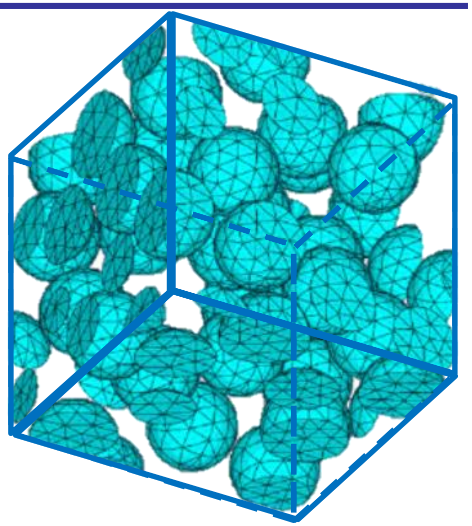

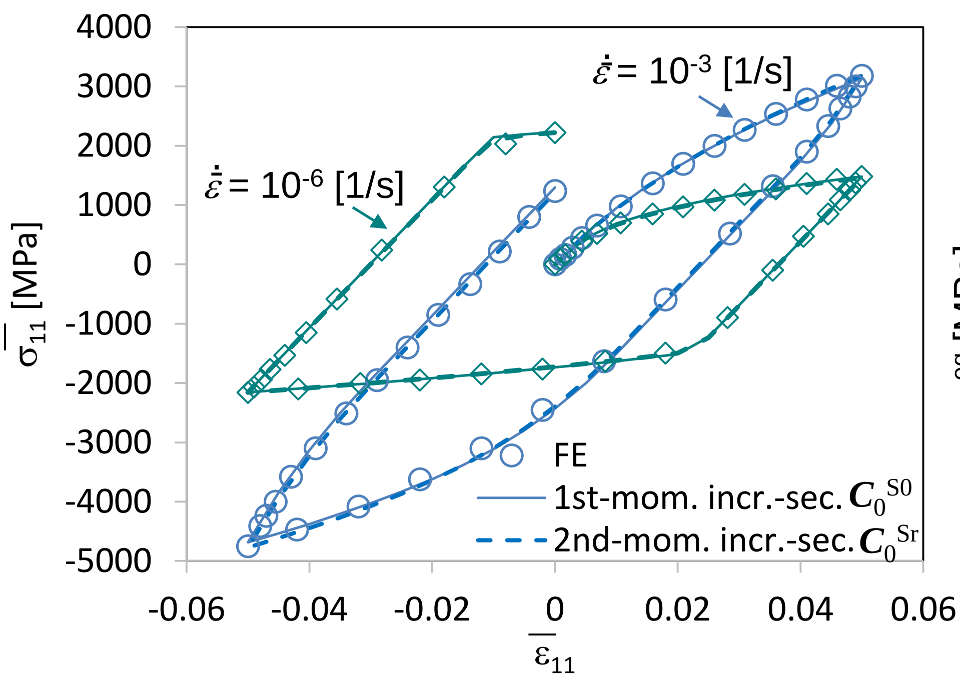

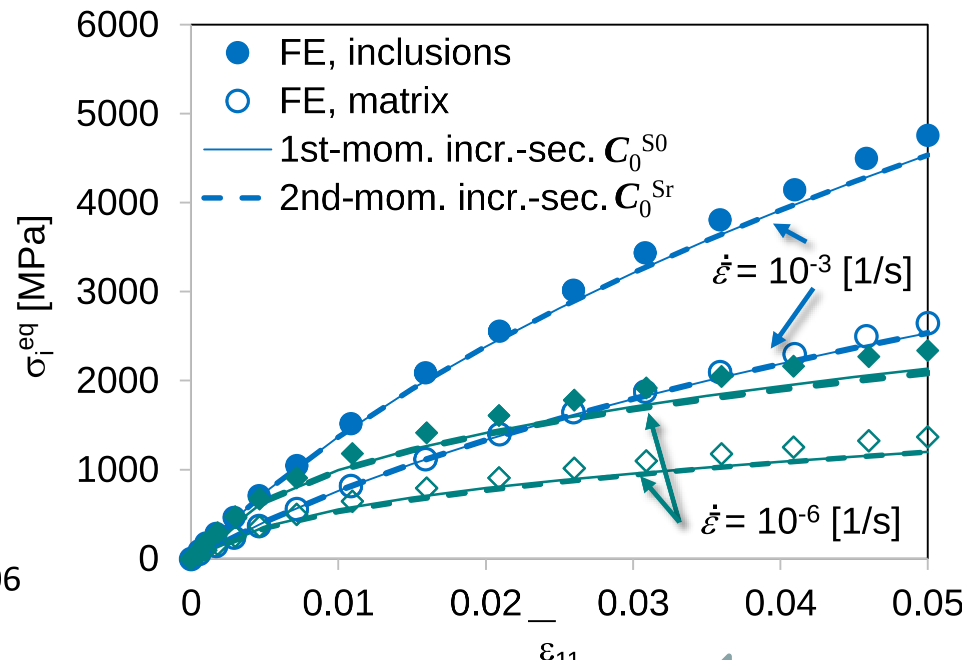

- Extension to finite deformations
  - Formulate everything in terms of elastic left Cauchy-Green tensor

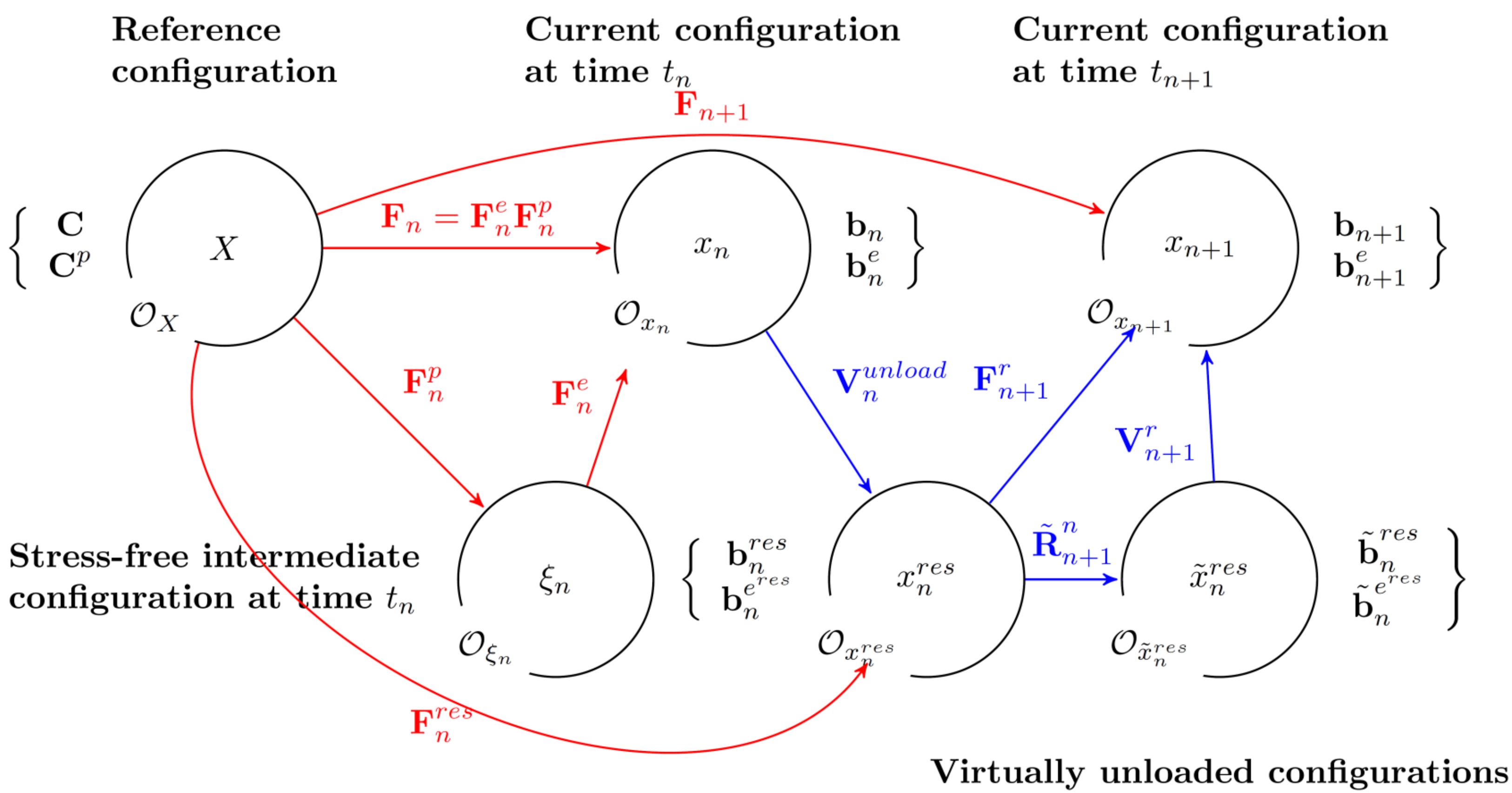

Mean-Field-Homogenization for elasto-visco-plastic composites

- Extension to finite deformations
  - Porous material: homogenized response

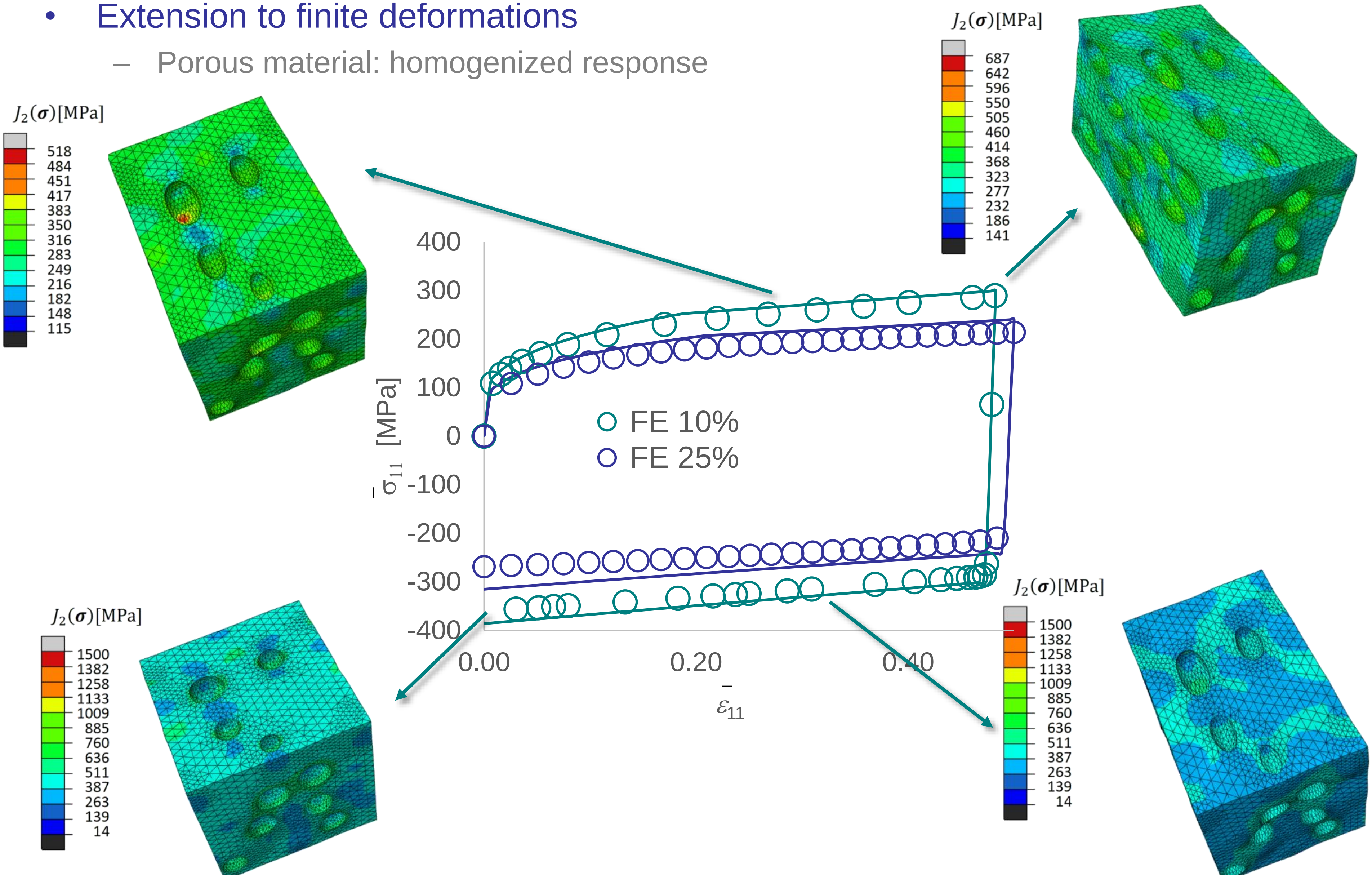

Beginning

Mean-Field-Homogenization for elasto-visco-plastic composites

- Extension to finite deformations
  - Porous material: micro-structure evolution

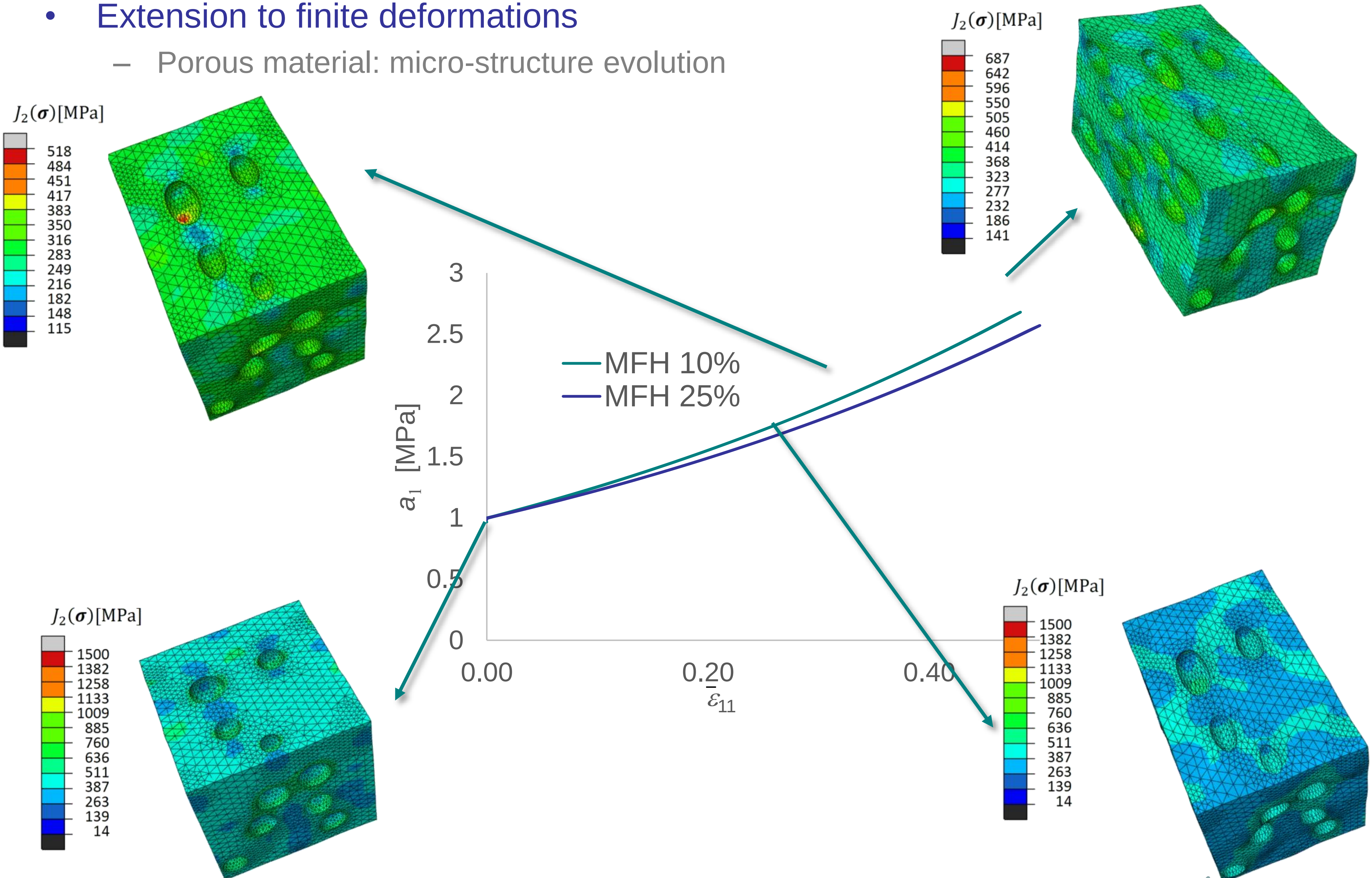

Mean-Field-Homogenization for elasto-visco-plastic composites

- SIMUCOMP ERA-NET project (incremental secant MFH)
  - e-Xstream, CENAERO, ULiège (Belgium)
  - IMDEA Materials (Spain)
  - CRP Henri-Tudor (Luxemburg)

- PDR T.1015.14 project (MFH with second-order moments)
  - ULiège, UCL (Belgium)

- STOMMMAC M.ERA-NET project (MFH for elasto-visco-plastic composites)
  - e-Xstream, ULiège (Belgium)
  - BATZ (Spain)
  - JKU, AC (Austria)
  - U Luxembourg (Luxemburg)

- Publications (doi)
  - 10.1016/j.mechmat.2017.08.006
  - 10.1080/14786435.2015.1087653
  - 10.1016/j.ijplas.2013.06.006
  - 10.1016/j.cma.2018.12.007

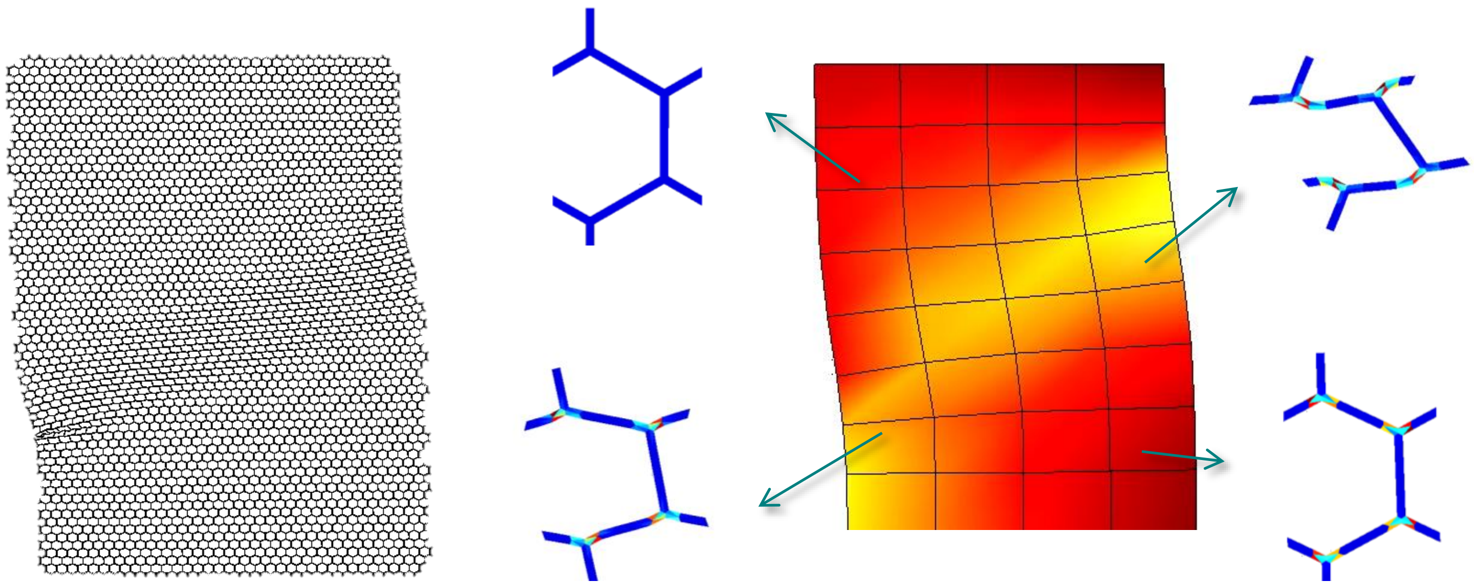

Second order Computational Homogenization for Honeycomb Structures

ARC 09/14-02 BRIDGING - From imaging to geometrical modelling of complex micro structured materials: Bridging computational engineering and material science

Second order Computational Homogenization for Honeycombs

- Multi-scale modeling
  - 2 problems are solved concurrently
    - The macro-scale problem
    - The meso-scale problem (on a meso-scale Volume Element)

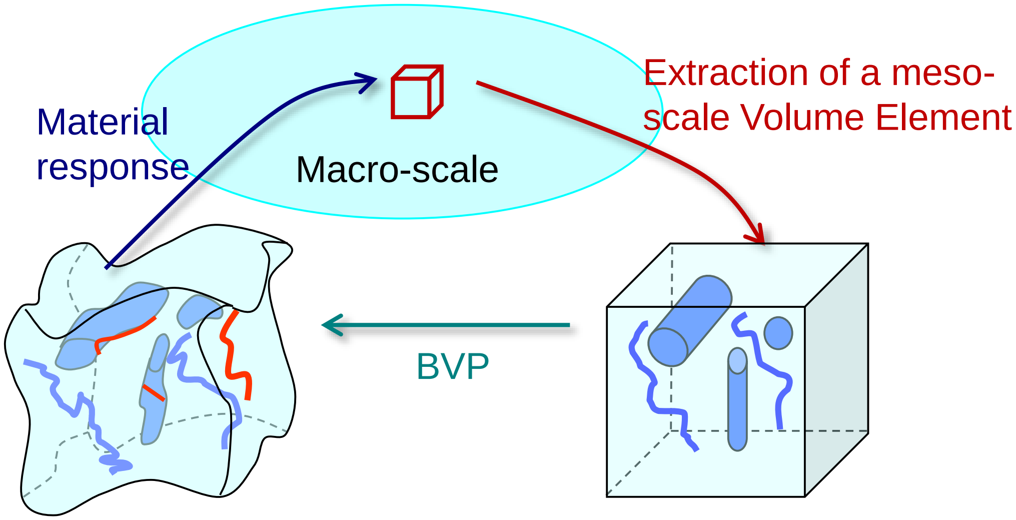

- What if homogenized properties loose ellipticity?
  - Buckling of honeycomb structures

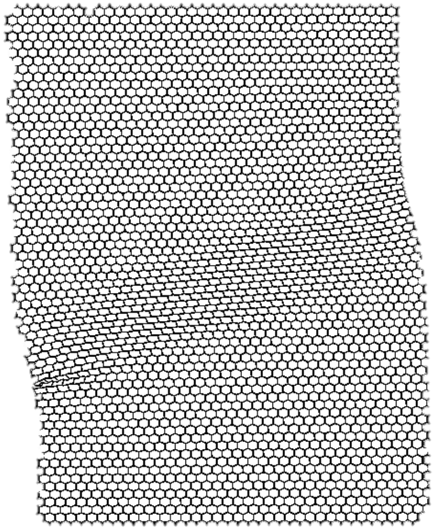

Second order Computational Homogenization for Honeycombs

- DG-based second-order FE²
  - Macro-scale
    - High-order Strain-Gradient formulation
    - C^1 weakly enforced by DG
    - Partitioned mesh (//)
  - Transition
    - Gauss points on different processors
    - Each Gauss point is associated to one mesh and one solver
  - Micro-scale
    - Usual 3D finite elements
    - High-order periodic boundary conditions
      - Non-conforming mesh
      - Use of interpolant functions

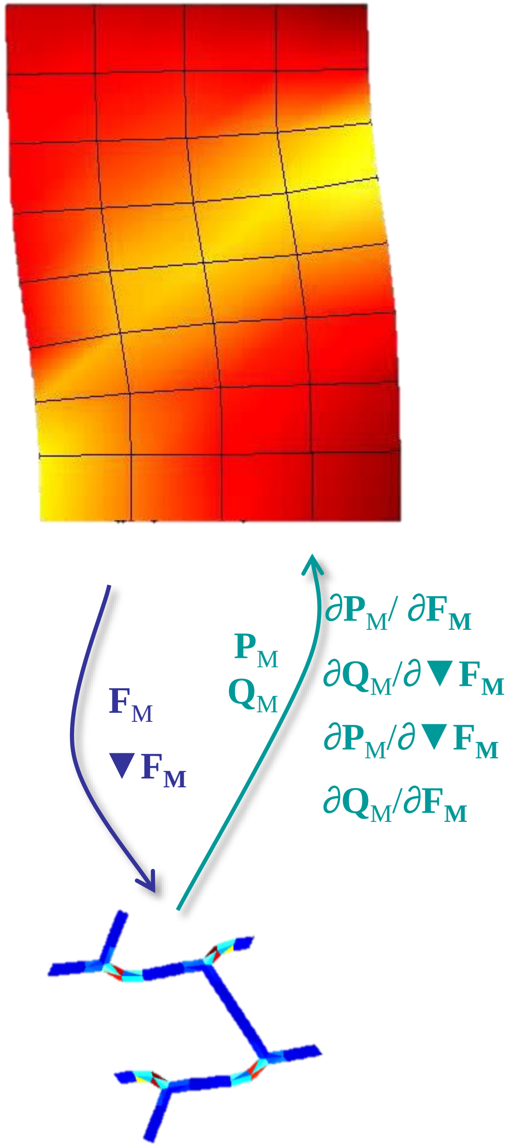

Second order Computational Homogenization for Honeycombs

- Instabilities
  - Micro-scale: buckling
  - Macro-scale: localization bands
  - Captured owing to
    - Second-order homogenization
    - Ad-hoc periodic boundary conditions
    - Path following method

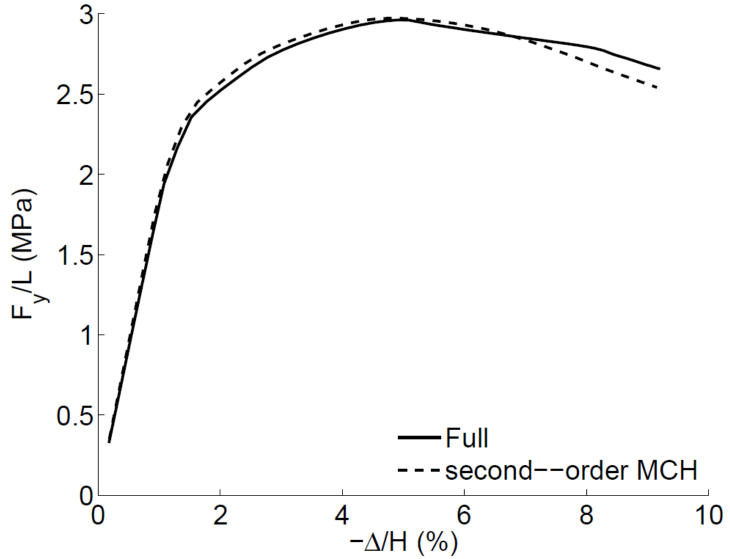

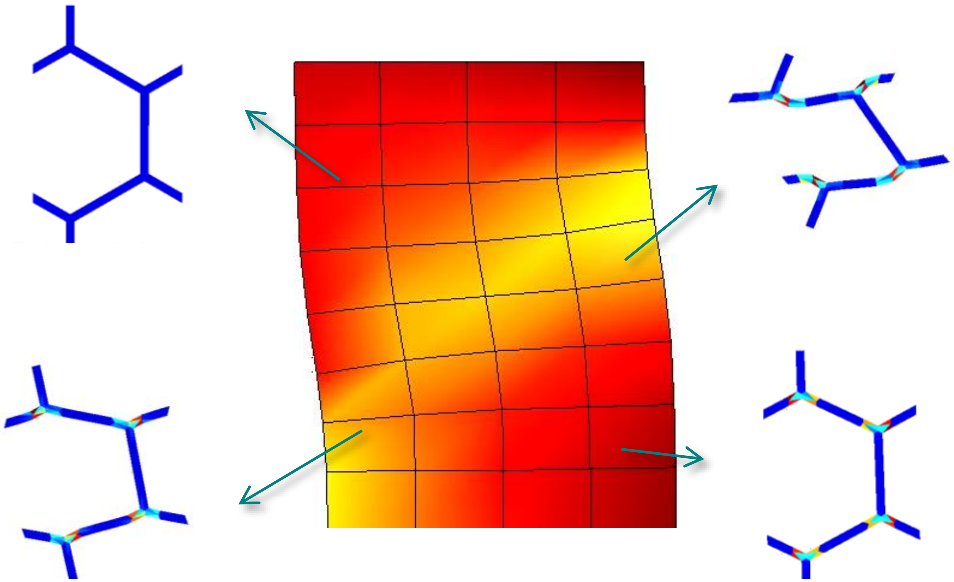

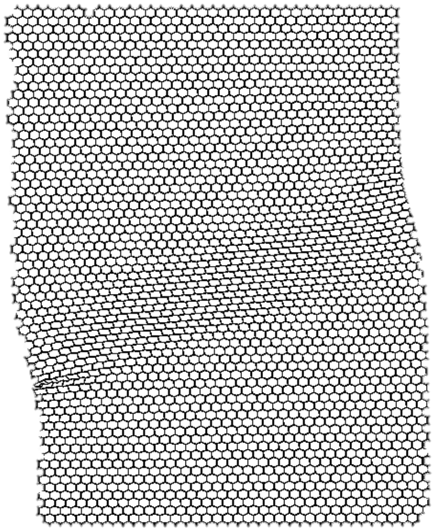

Beginning

Second order Computational Homogenization for Honeycombs

- Open-hole plate

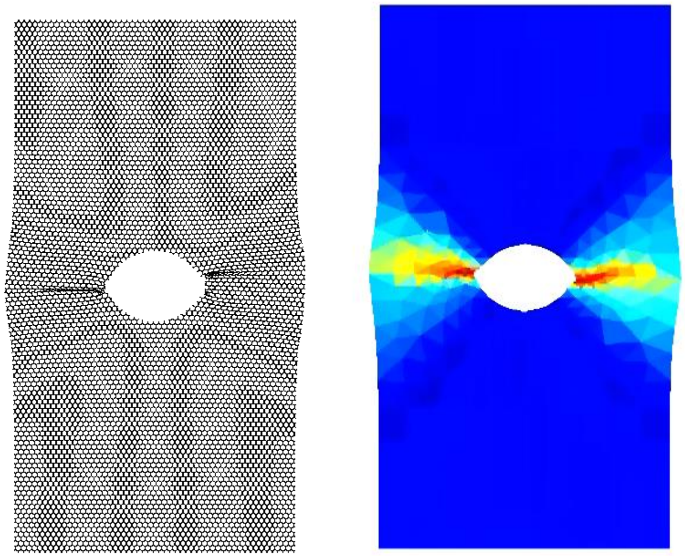

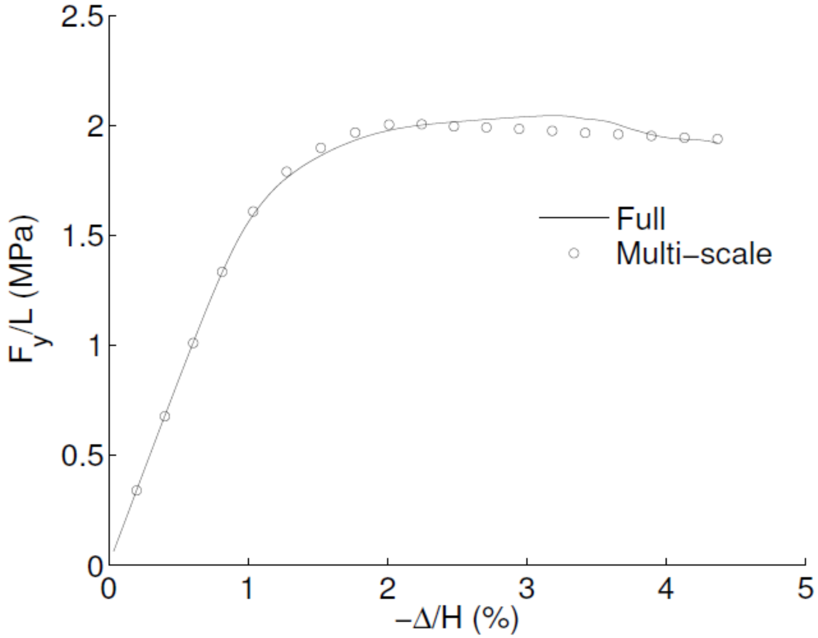

- BRIDGING ARC project
  - ULiège, Applied Sciences (A&M, EEI, ICD)
  - ULiège, Sciences (CERM)
- Publications
  - 10.1016/j.mechmat.2015.07.004
  - 10.1016/j.ijsolstr.2014.02.029
  - 10.1016/j.cma.2013.03.024

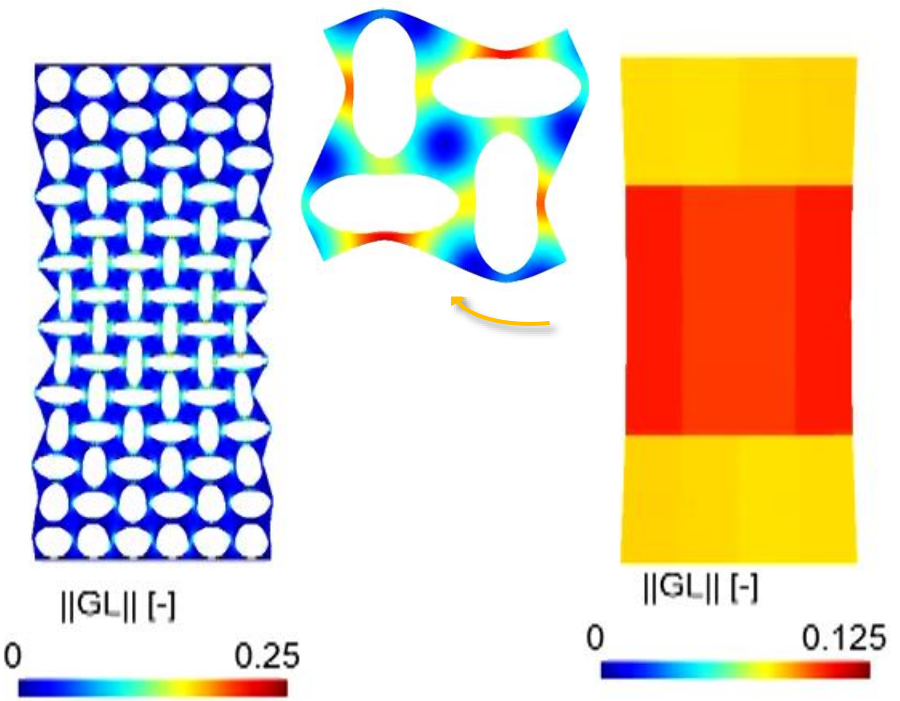

Second order homogenization without RVE size effect for cellular and metamaterials

MOAMMM project has received funding from the European Union's Horizon 2020 research and innovation programme under grant agreement No 862015 for the project Multi-scale Optimisation for Additive Manufacturing of fatigue resistant shock-absorbing MetaMaterials (MOAMMM) of the H2020-EU.1.2.1. - FET Open Programme

MOAMMM

LIÈGE université

- First vs. second order homogenisation
  - First order homogenisation
    - Does not prevent localisation issue
    - No material length-scale
  - Second-order homogenization
    - High order strain $\mathbf{G}_\mathrm{M}$ and stress $\mathbf{Q}_\mathrm{M}$ at macro-scale
    - Material length scale related to the RVE length

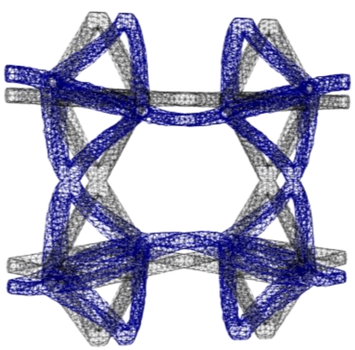

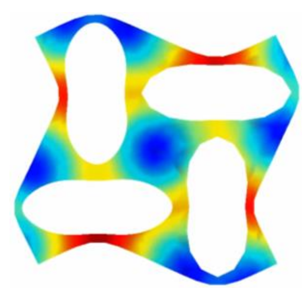

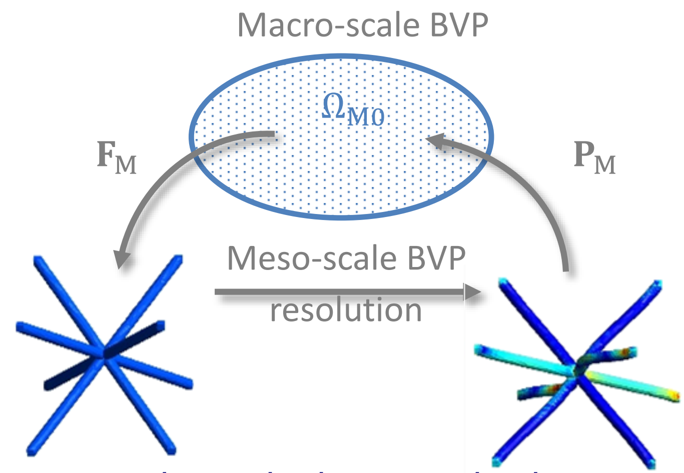

First order homogenisation

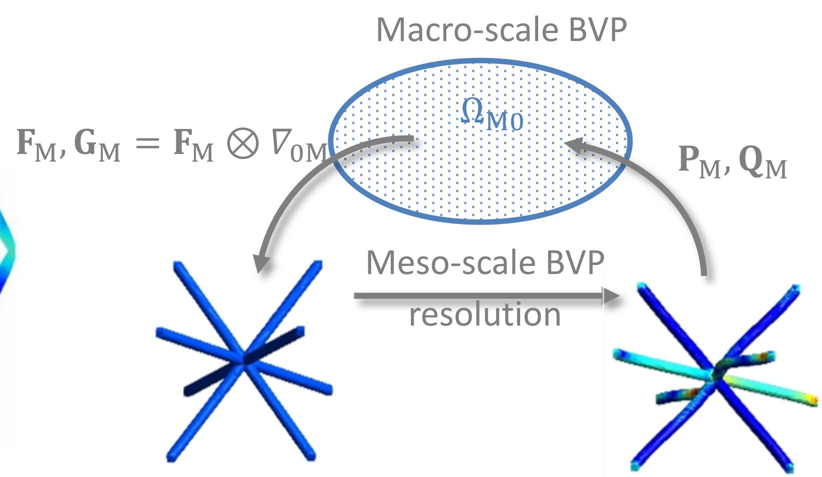

Second order homogenisation

    - Issue for metamaterial: RVE length is larger than unit cell because of patterning change

Second order homogenization for cellular and metamaterials

- Account for patterning change
  - Micromorphic approach
    - Constrain change of patterning modes
    - Developed in elasticity (limited number of modes)
  - Enhanced second-order homogenization
    - Remove cell size dependency using a body-force
    - Arises from asymptotic homogenization in linear elasticity
    - How to account for finite strain, elasto-plasticity etc…?

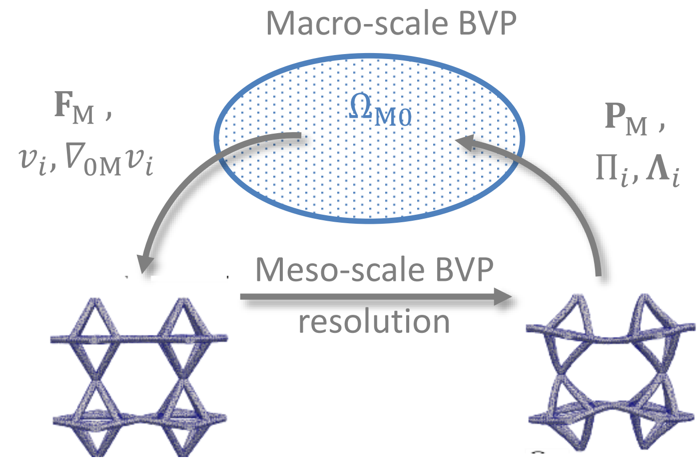

Micromorphic approach

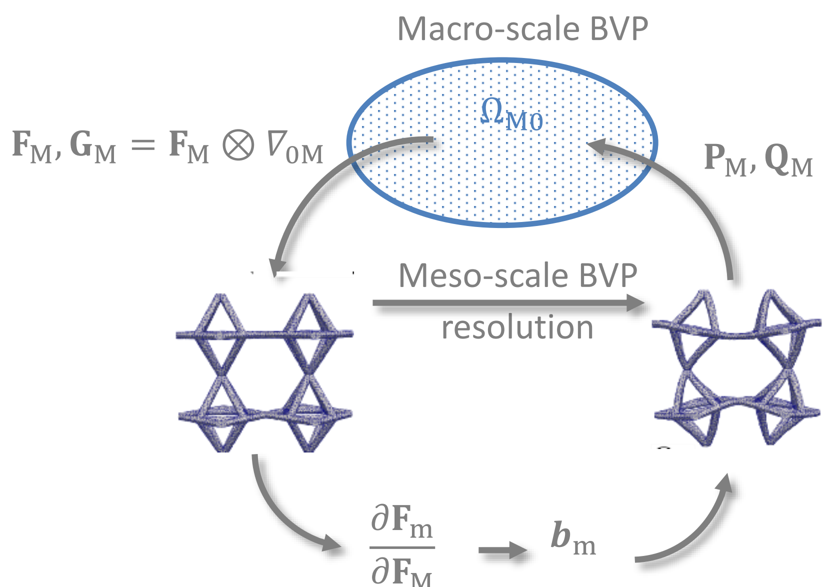

Body-force enhanced second order homogenisation

- Second order homogenization with body force enhancement
  - Consider an equivalent homogeneous volume element
    - Cauchy homogenous — Second order continuum

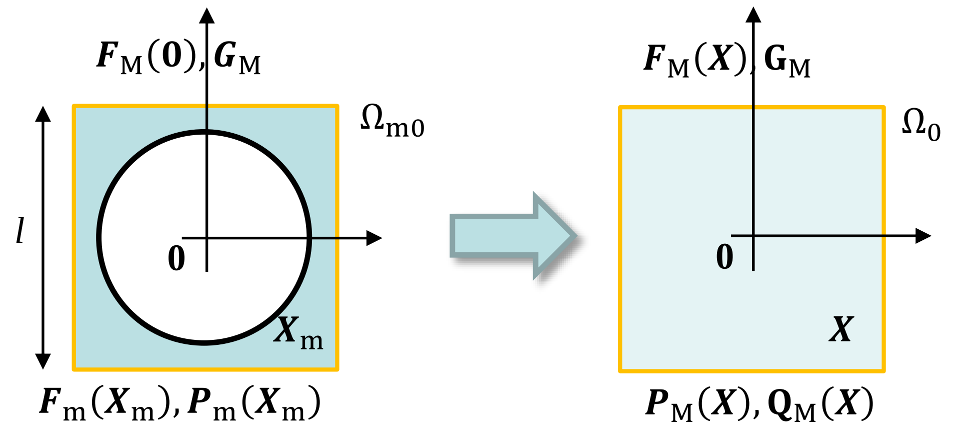

- Development of the (no-longer) homogeneous field

$$\begin{cases} \mathbf{F}_{\mathrm{M}}(\boldsymbol{X}) = \mathbf{F}_{\mathrm{M}}(0) + \mathbf{G}_{\mathrm{M}} \cdot \boldsymbol{X} \\ \mathbf{G}_{\mathrm{M}} = \mathbf{F}_{\mathrm{M}}(\mathbf{0}) \otimes \nabla_{0\mathrm{M}} \\ \mathbf{P}_{\mathrm{M}}(\boldsymbol{X}) = \mathbf{P}_{\mathrm{M}}(0) + \left.\dfrac{\partial \mathbf{P}_{\mathrm{M}}}{\partial \mathbf{F}_{\mathrm{M}}}\right|_0 : \mathbf{G}_{\mathrm{M}} \cdot \boldsymbol{X} \\ \mathbf{Q}_{\mathrm{M}}(\boldsymbol{X}) = \mathbf{Q}_{\mathrm{M}}(0) + \left.\dfrac{\partial \mathbf{Q}_{\mathrm{M}}}{\partial \mathbf{F}_{\mathrm{M}}}\right|_0 : \mathbf{G}_{\mathrm{M}} \cdot \boldsymbol{X} \end{cases}$$

- Second order homogenization with body force enhancement
  - Consider an equivalent homogeneous volume element
    - The equivalence of energy (Hill-Mandel condition) with introduction of body forces $\boldsymbol{b}_m(\boldsymbol{X}_m)$:

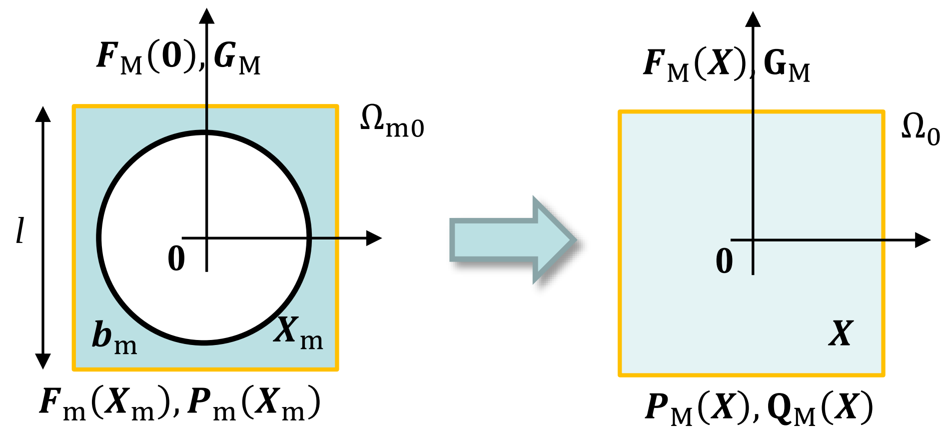

$$\int_{\Omega_{\mathrm{m}0}} [\mathbf{P}_{\mathrm{m}} : \delta \mathbf{F}_{\mathrm{m}} - \mathbf{b}_{\mathrm{m}} \cdot \delta \boldsymbol{u}_{\mathrm{m}}] d\Omega \Leftrightarrow \int_{\Omega_0} (\mathbf{P}_{\mathrm{M}} : \delta \mathbf{F}_{\mathrm{M}} + \mathbf{Q}_{\mathrm{M}} \vdots \delta \mathbf{G}_{\mathrm{M}} - \mathbf{B}_{\mathrm{M}} \cdot \delta \boldsymbol{u}_{\mathrm{M}}) d\Omega$$

- Is satisfied by the following introduction of micro-scale body forces and homogenized stresses

$$\left\{\begin{array}{l}
\mathbf{P}_{\mathrm{M}}(0) = \dfrac{1}{V_0} \displaystyle\int_{\Omega_{\mathrm{m}0}} (\mathbf{P}_{\mathrm{m}} - \boldsymbol{b}_{\mathrm{m}} \otimes \boldsymbol{X}_{\mathrm{m}})\, d\Omega \\[2ex]
\mathbf{Q}_{\mathrm{M}}(0) = \frac{1}{2V_0} \int_{\Omega_{\mathrm{m}0}} [\mathbf{P}_{\mathrm{m}} \otimes \boldsymbol{X}_{\mathrm{m}} + (\mathbf{P}_{\mathrm{m}} \otimes \boldsymbol{X}_{\mathrm{m}})^T]\, d\Omega + \frac{1}{2V_0} \int_{\Omega_{\mathrm{m}0}} [\boldsymbol{b}_{\mathrm{m}} \otimes \boldsymbol{X}_{\mathrm{m}} \otimes \boldsymbol{X}_{\mathrm{m}}]\, d\Omega - \\
\qquad \frac{1}{2\mathrm{V}_0} \left(\left[\frac{\partial \mathbf{P}_{\mathrm{M}}(0)}{\partial \mathbf{F}_{\mathrm{M}}} : \mathbf{G}_{\mathrm{M}} \cdot \boldsymbol{J}_{\mathrm{M}} + \left(\frac{\partial \mathbf{P}_{\mathrm{M}}(0)}{\partial \mathbf{F}_{\mathrm{M}}} : \mathbf{G}_{\mathrm{M}} \cdot \boldsymbol{J}_{\mathrm{M}} \right)^T \right] - \boldsymbol{B}_{\mathrm{M}} \otimes \boldsymbol{J}_{\mathrm{M}} \right) \\[2ex]
\displaystyle\int_{\Omega_{\mathrm{m}0}} \mathbf{b}_{\mathrm{m}} d\Omega = \int_{\Omega_0} \mathbf{B}_{\mathrm{M}} d\Omega = -\int_{\Omega_0} \frac{\partial \mathbf{P}_{\mathrm{M}}}{\partial \mathbf{F}_{\mathrm{M}}} : \mathbf{G}_{\mathrm{M}} : \boldsymbol{I} d\Omega = -\int_{\Omega_{m0}} \frac{\partial \mathbf{P}_{\mathrm{m}}}{\partial \mathbf{F}_{\mathrm{m}}} : \frac{\partial \mathbf{F}_{\mathrm{m}}}{\partial \mathbf{F}_{\mathrm{M}}} : \mathbf{G}_{\mathrm{M}} : \boldsymbol{I} d\Omega
\end{array}\right.$$

- Remove boundary effect
  - Apply $\mathrm{G}_{\mathrm{M}_{\mathrm{xxx}}} = 0.05\ /mm$

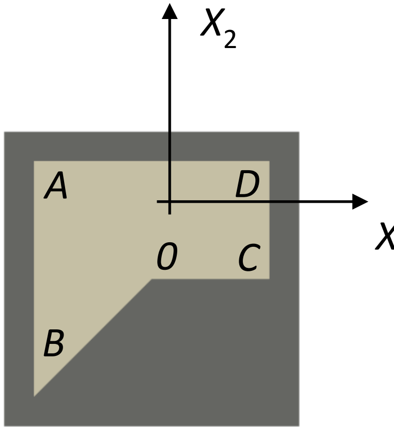

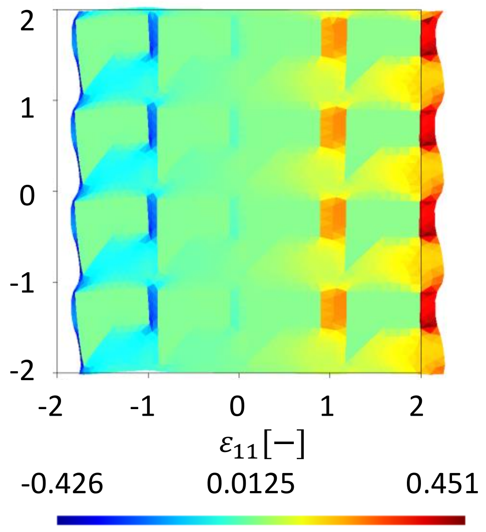

Body-force enhanced second order homogenization

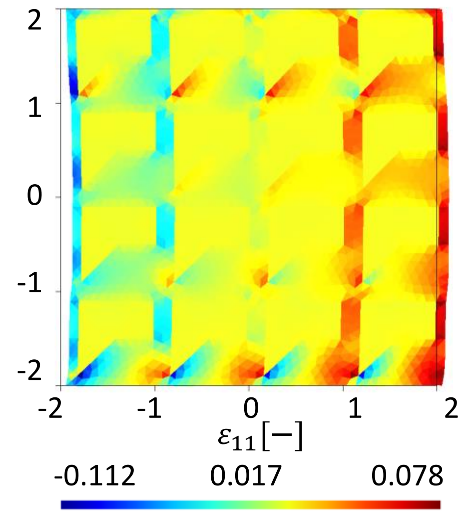

Classical second order homogenization

- Converges toward DNS
  - Linear elasticity: Beam bending

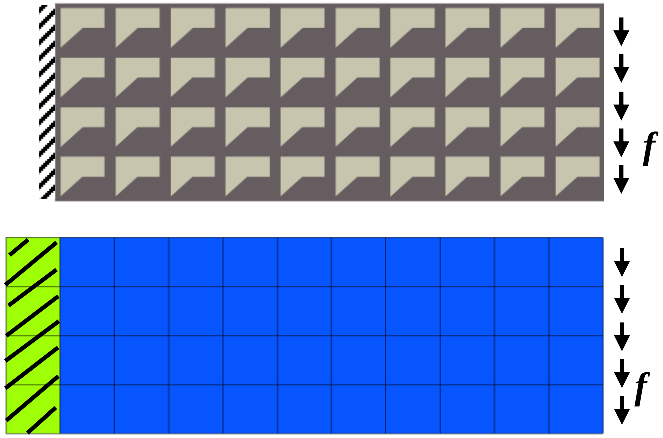

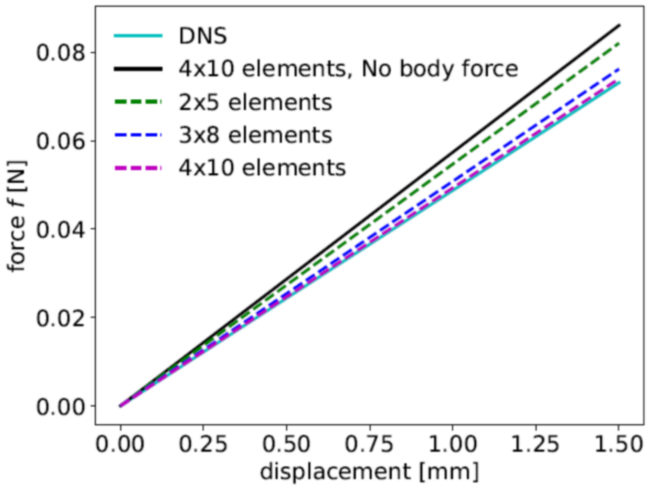

  - Linear elasticity: Beam shearing

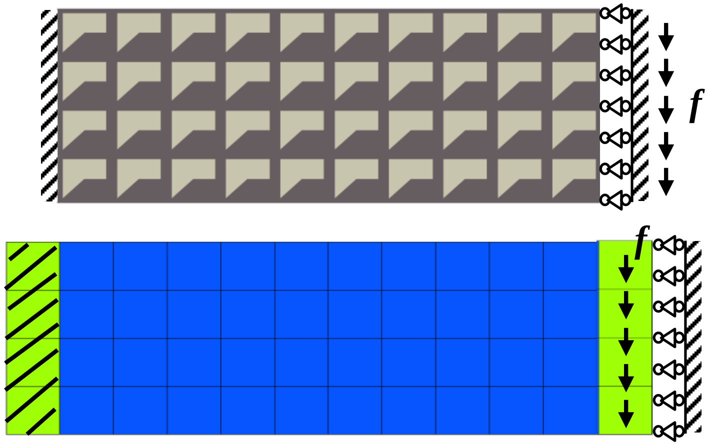

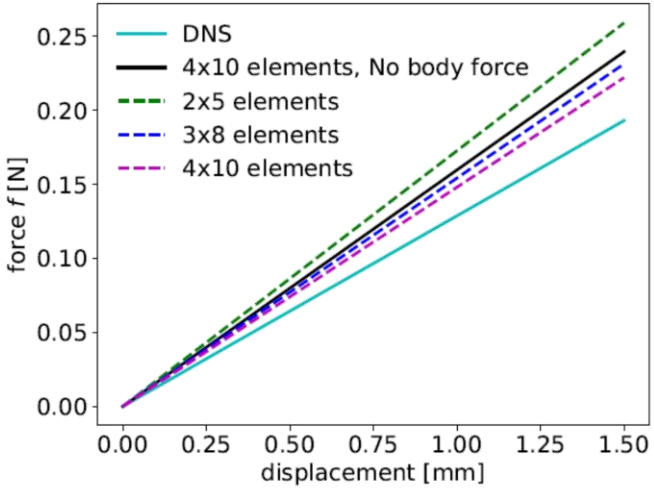

- Multiscale simulation on honeycomb structures
  - Effect of RVE size disappears when considering body forces

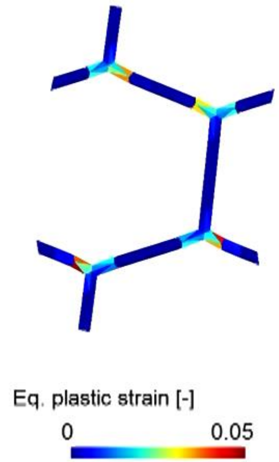

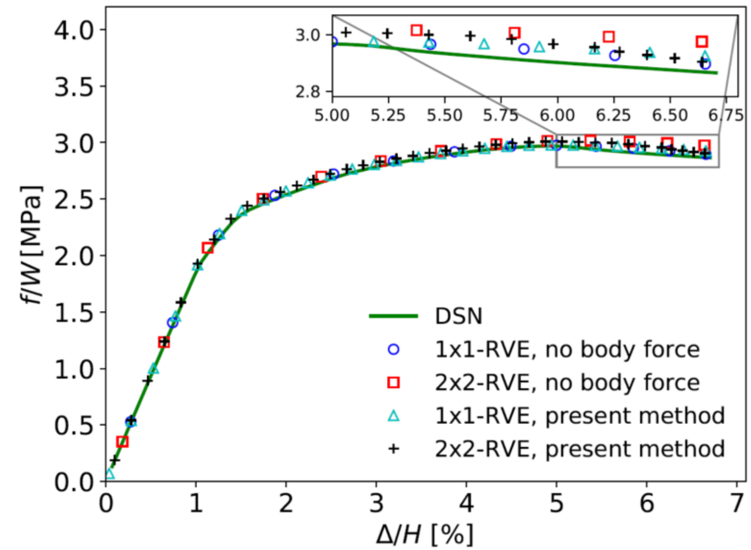

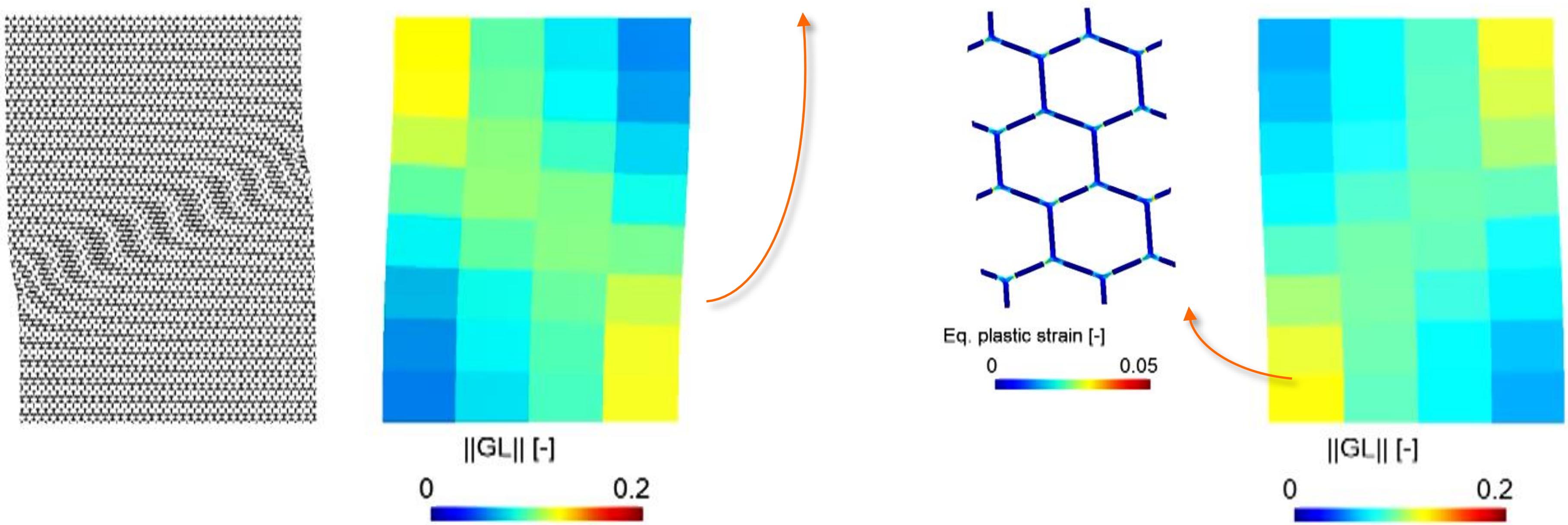

Second order homogenization for cellular and metamaterials

- Multiscale simulation on meta-structures
  - Compression samples of different sizes
    - 6x14 holes ➔ local instability
    - 6x34 holes ➔ global instability

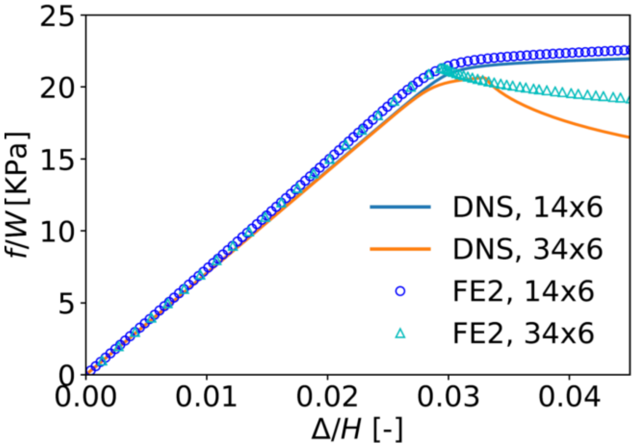

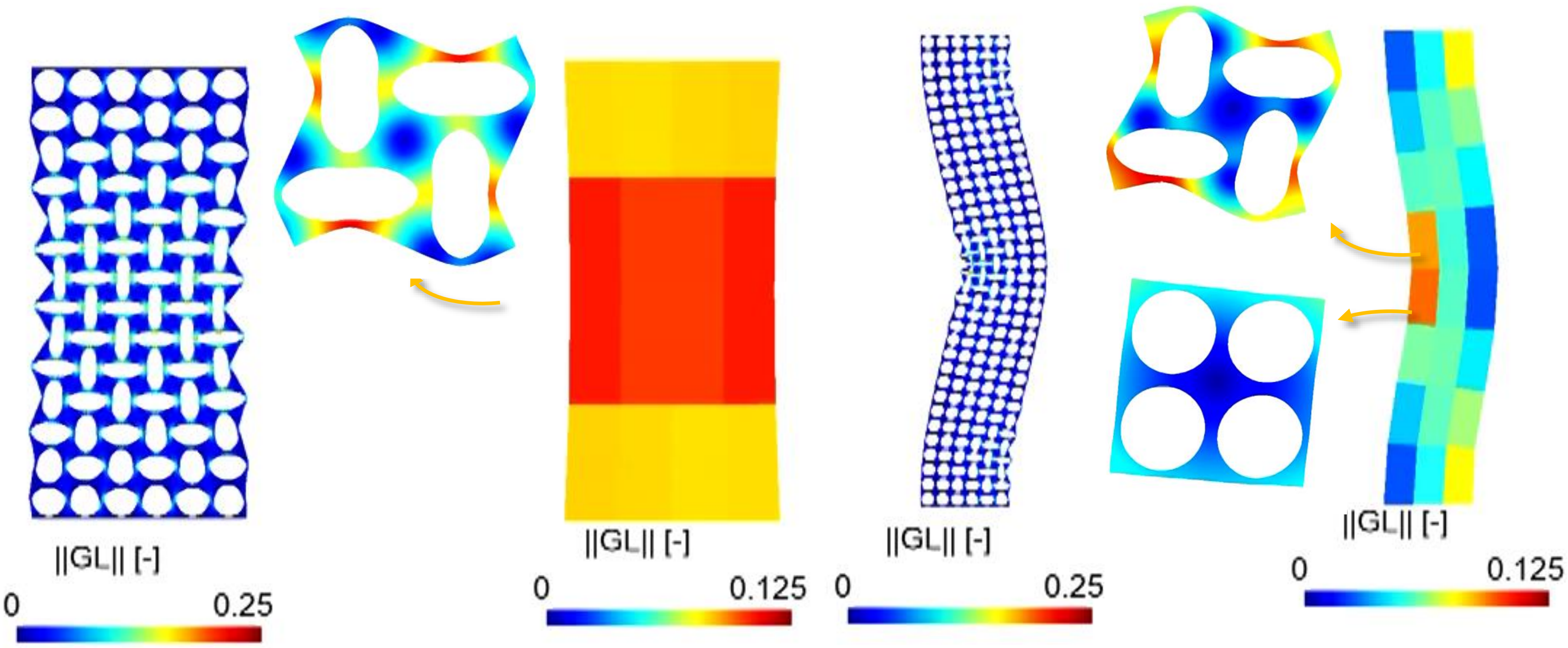

Second order homogenization for cellular and metamaterials

- MOAMMM FET-OPEN project (https://www.moammm.eu/)
  - ULiège, UCL (Belgium)
  - IMDEA Materials (Spain)
  - JKU (Austria)
  - cirp GmbH (Germany)

- Publications (doi)
  - Submitted

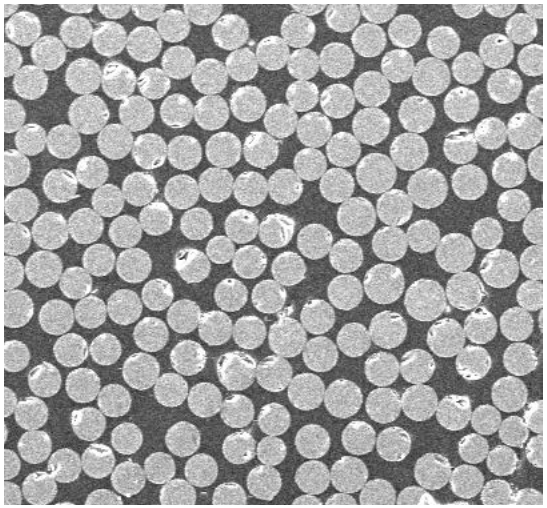

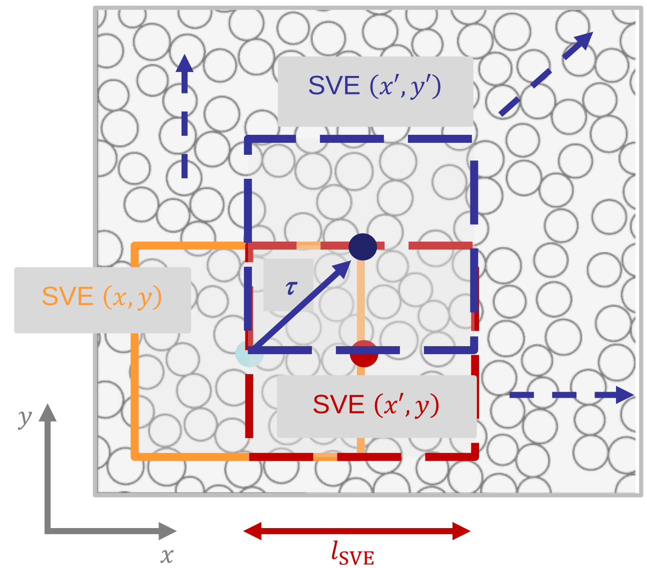

Stochastic Homogenization of Composite Materials

STOMMMAC The research has been funded by the Walloon Region under the agreement no 1410246-STOMMMAC (CT-INT 2013-03-28) in the context of M-ERA.NET Joint Call 2014.

Stochastic Homogenization of Composite Materials

- Multi-scale modeling
  - 2 problems are solved concurrently
    - The macro-scale problem
    - The meso-scale problem (on a meso-scale Volume Element)

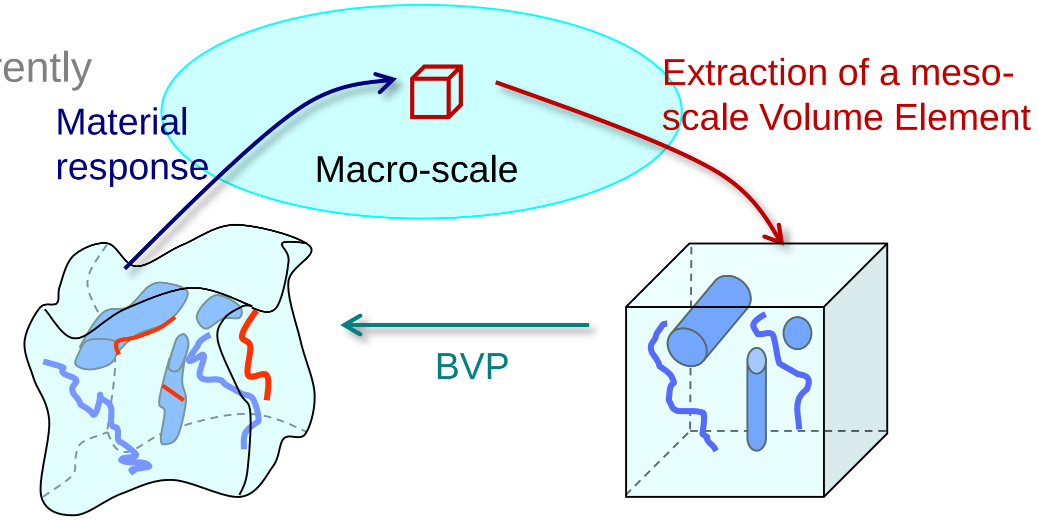

- For structures not several orders larger than the micro-structure size

$L_{\text{macro}} >> L_{\text{VE}} >\sim L_{\text{micro}}$

For accuracy: Size of the meso-scale volume element smaller than the characteristic length of the macro-scale loading

Meso-scale volume element no longer statistically representative:
- **Stochastic Volume Elements**

- Material uncertainties affect structural behaviors

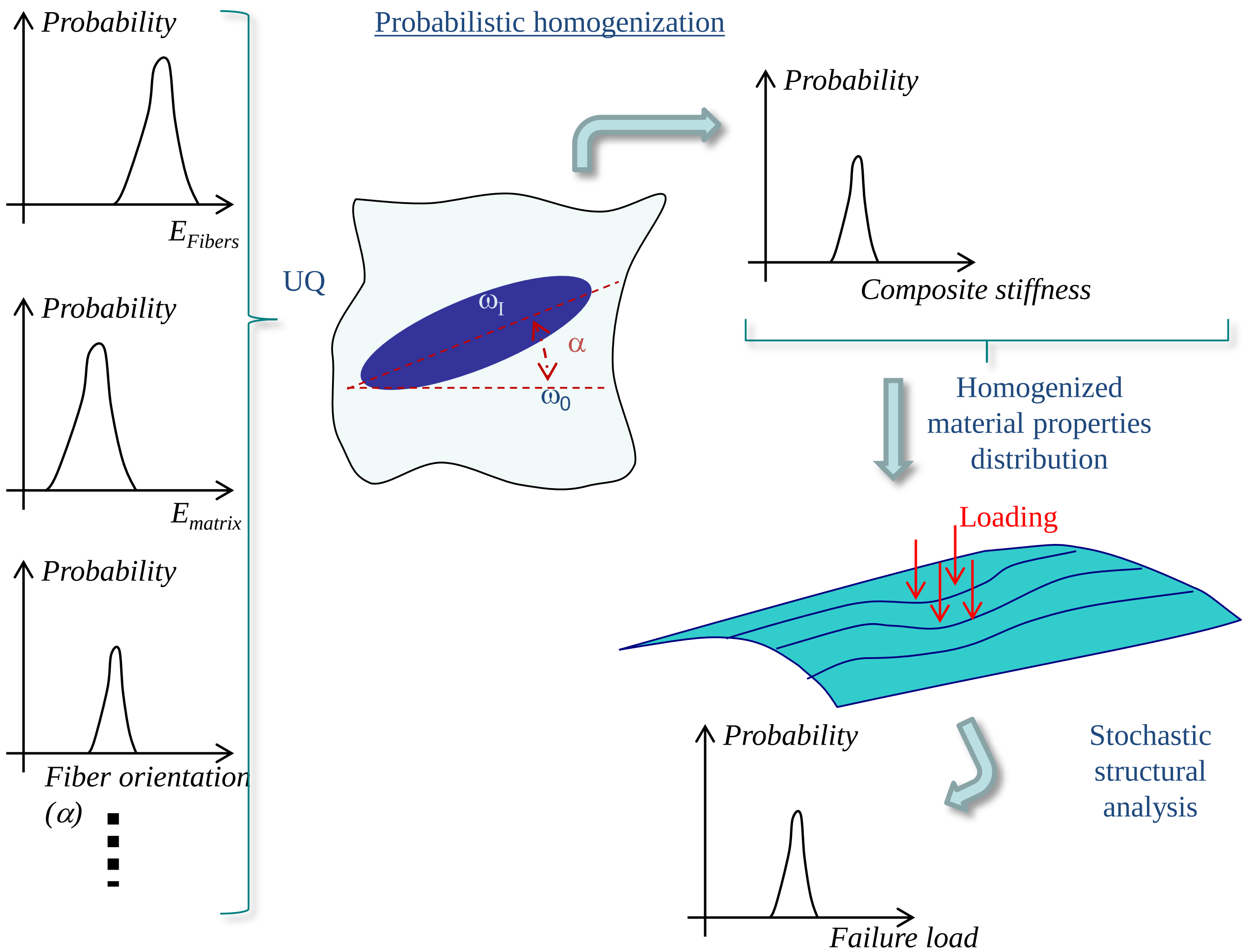

Stochastic Homogenization of Composite Materials

- Proposed methodology for material:
  - To develop a stochastic Mean Field Homogenization method able to predict the probabilistic distribution of material response at an intermediate scale from micro-structural constituents characterization

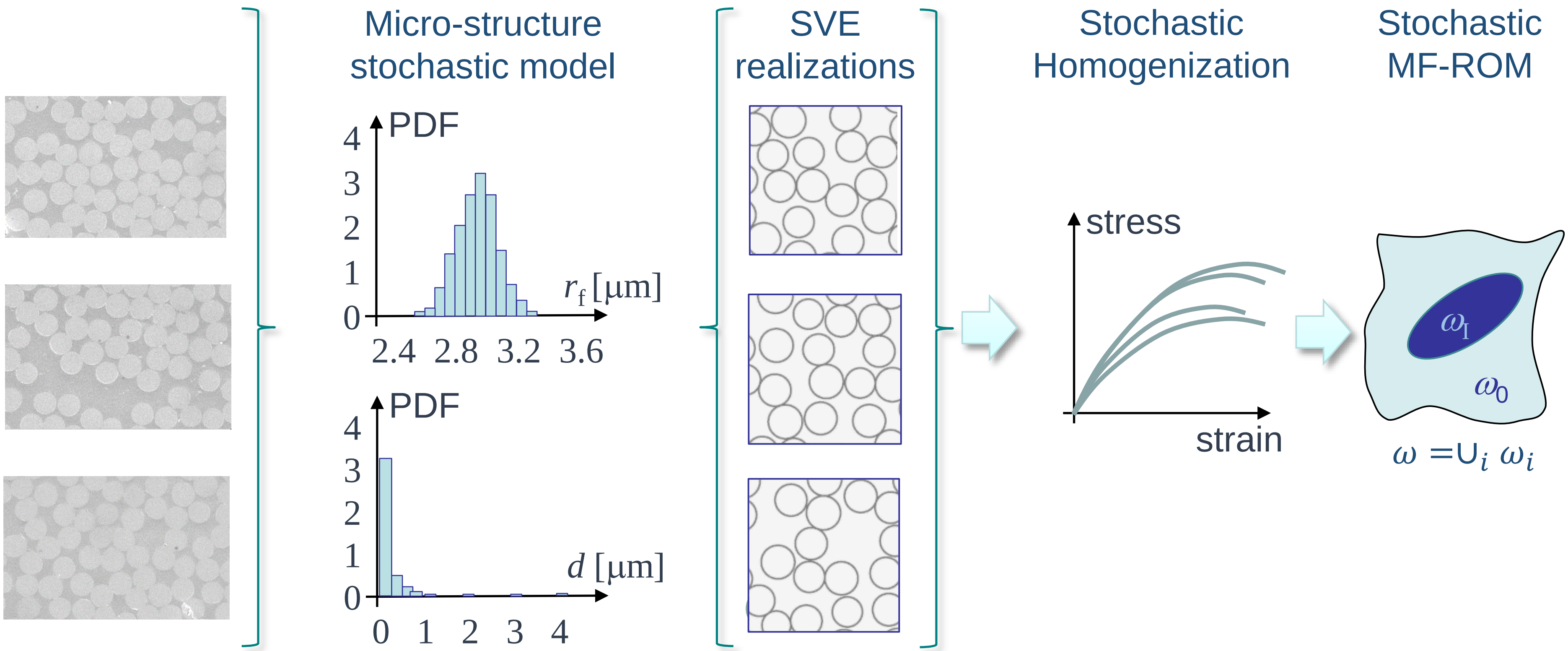

Stochastic Homogenization of Composite Materials

- Micro-structure stochastic model
  - 2000x and 3000x SEM images

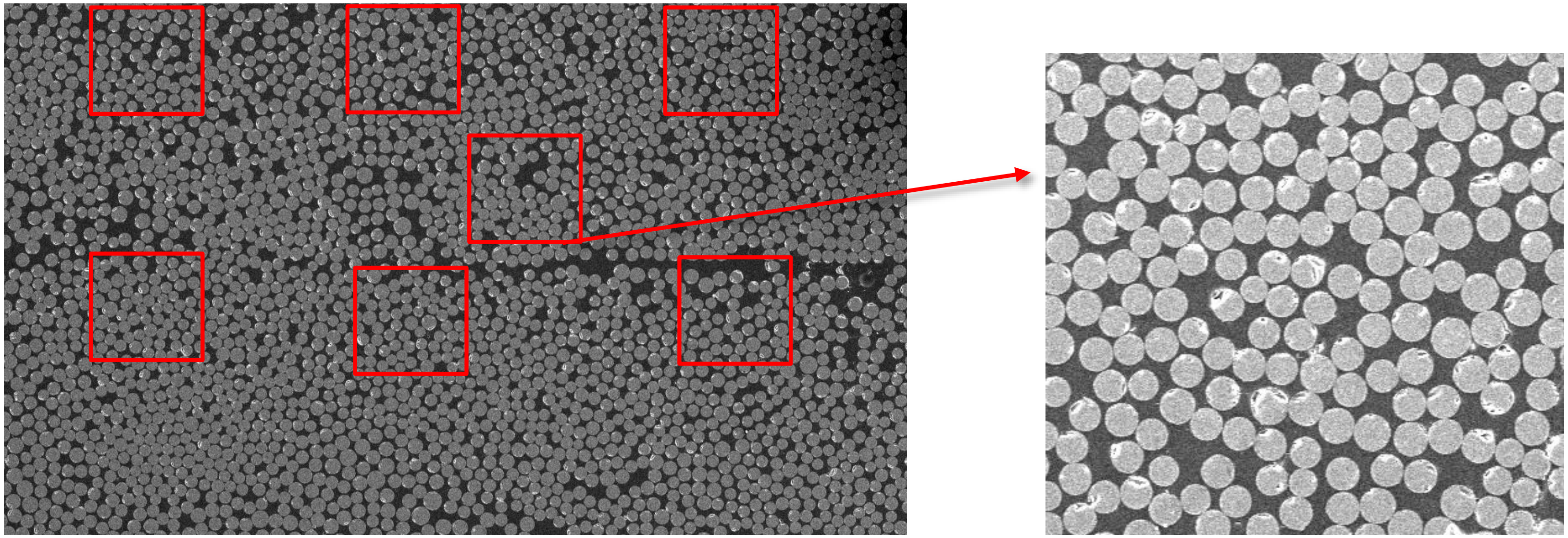

  - Fibers detection

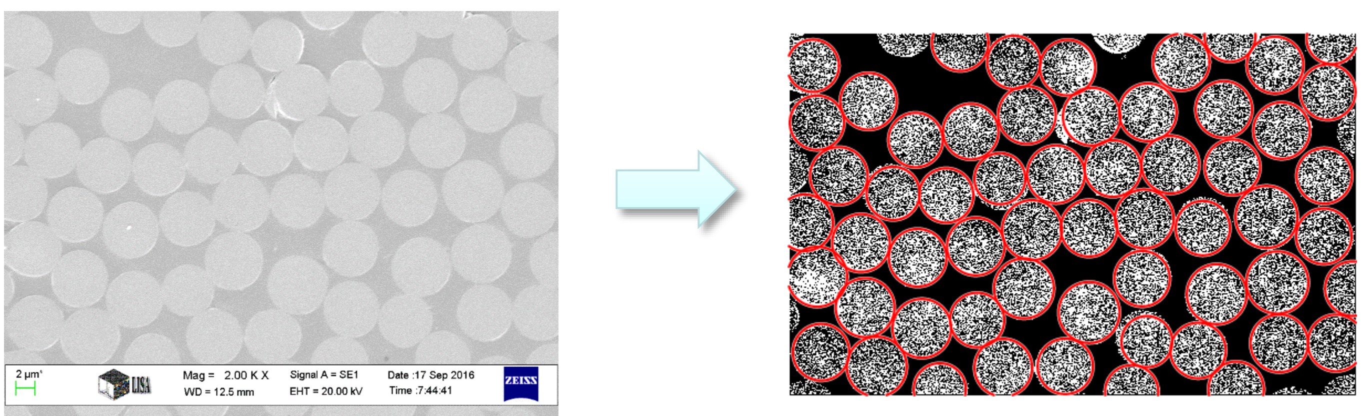

- Micro-structure stochastic model
  - Histograms of random micro-structures' descriptors

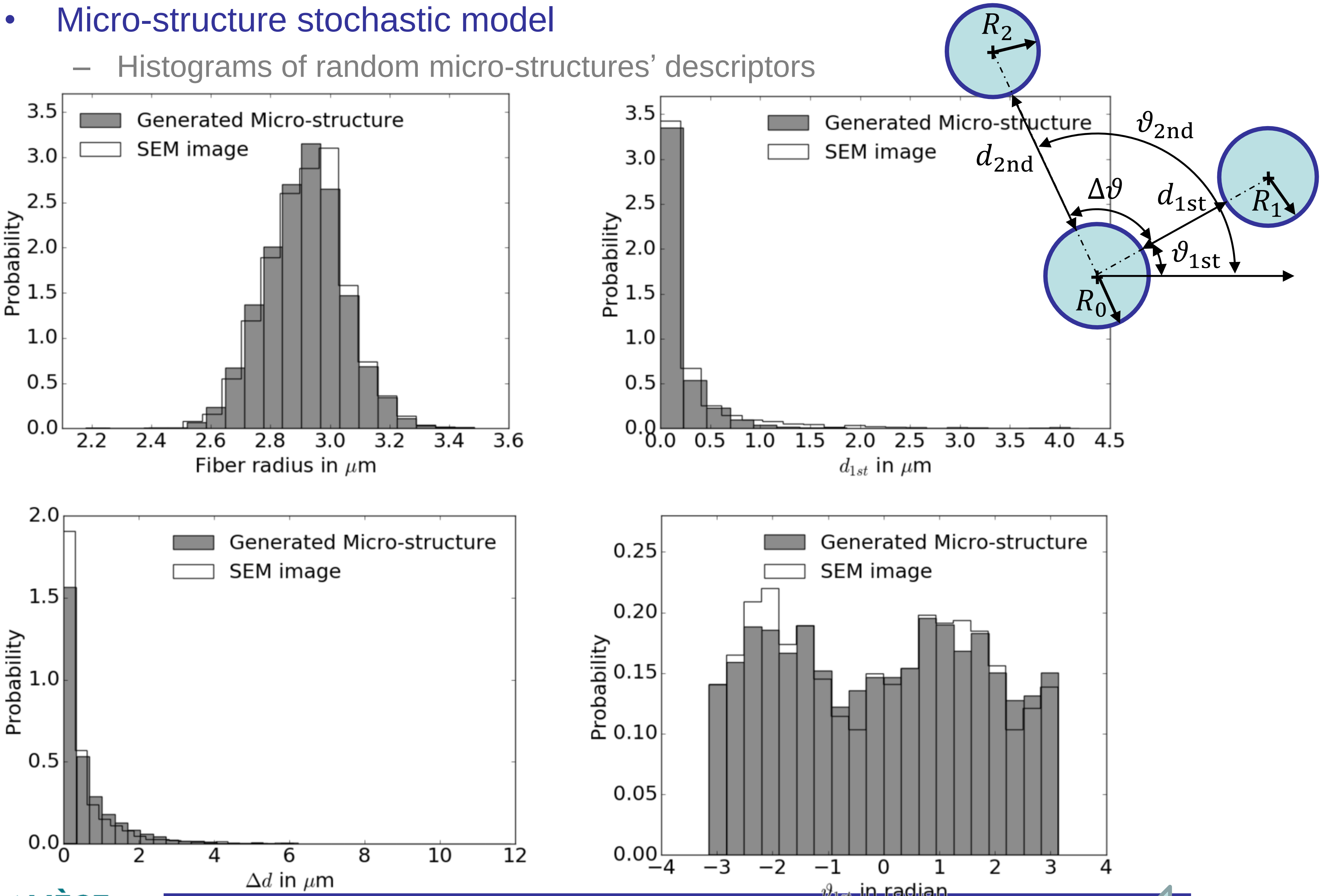

- Micro-structure stochastic model
  - Dependent variables generated using their empirical copula

SEM sample

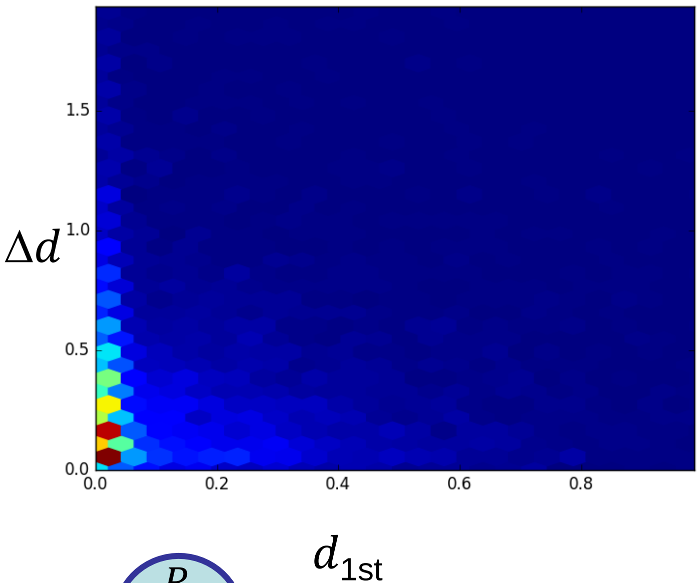

Generated sample

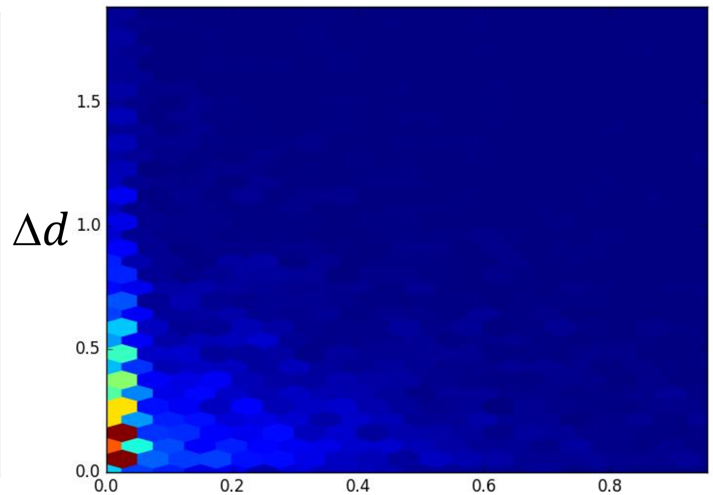

Directly from copula generator

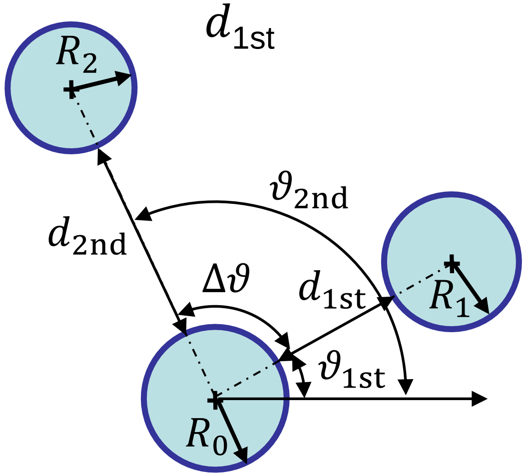

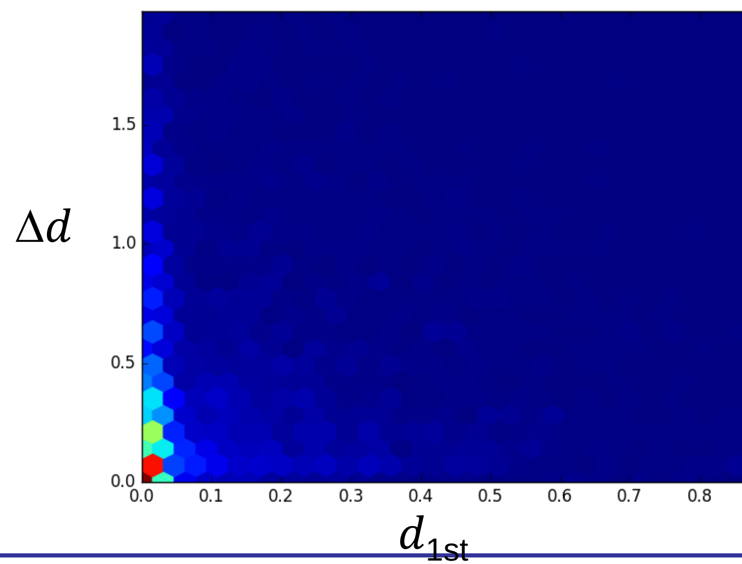

Statistic result from generated SVE

- Micro-structure stochastic model
  - Dependent variables generated using their empirical copula
  - Fiber additive process
    1) Define N seeds with first and second neighbors distances
    2) Generate first neighbor with its own first and second neighbors distances
    3) Generate second neighbor with its own first and second neighbors distances
    4) Change seeds & then change central fiber of the seeds

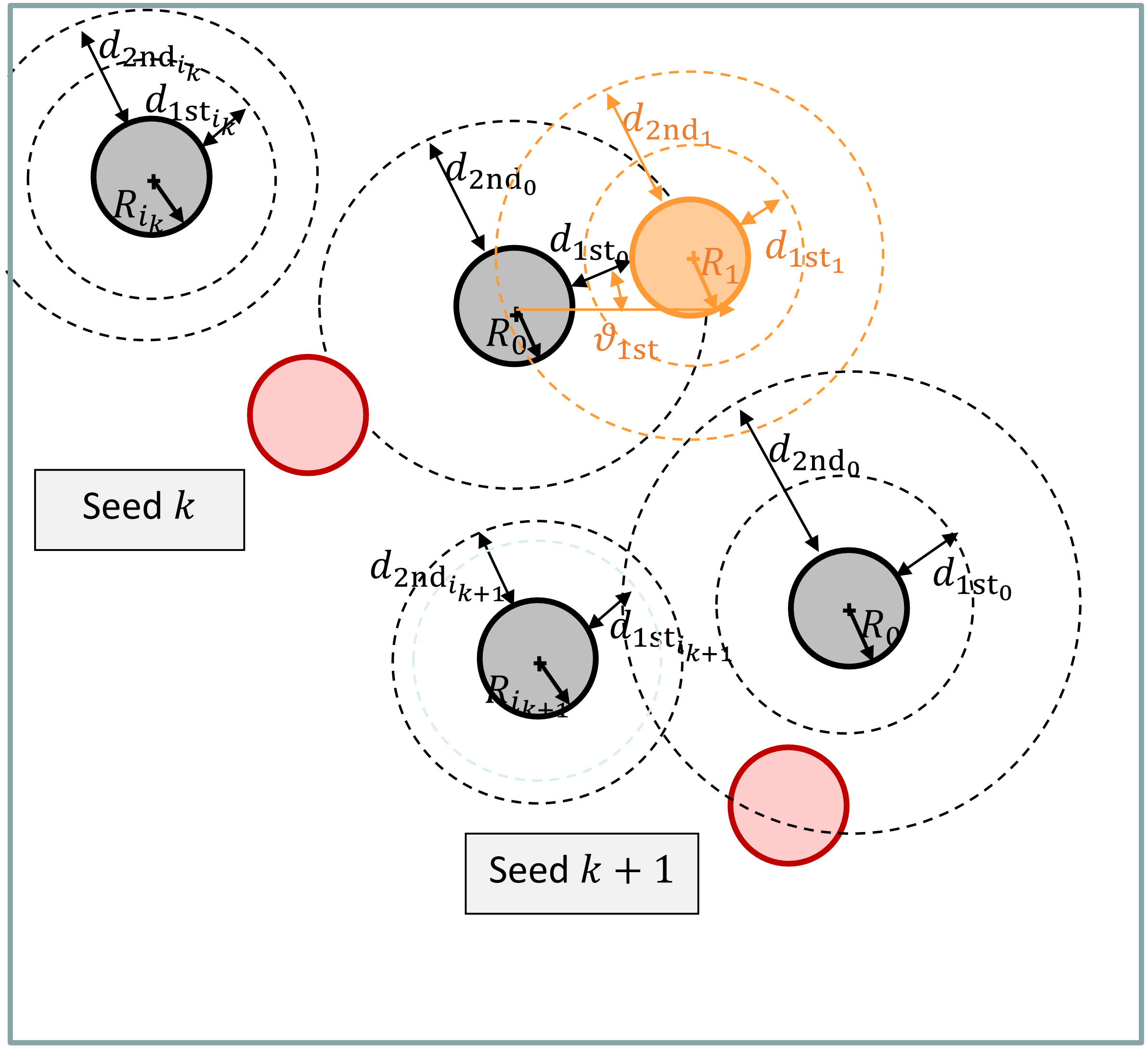

- Micro-structure stochastic model
  - Arbitrary size
  - Arbitrary number

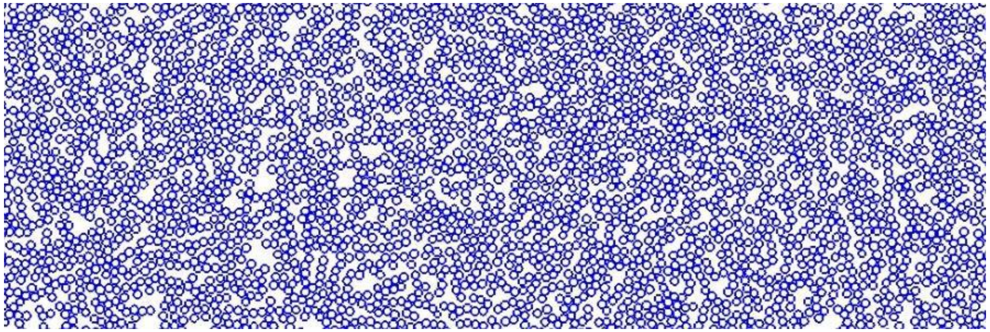

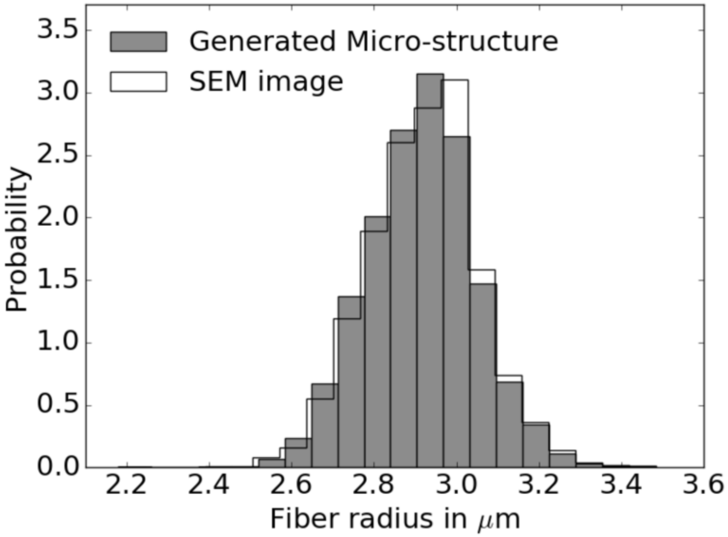

  - Possibility to generate non-homogenous distributions

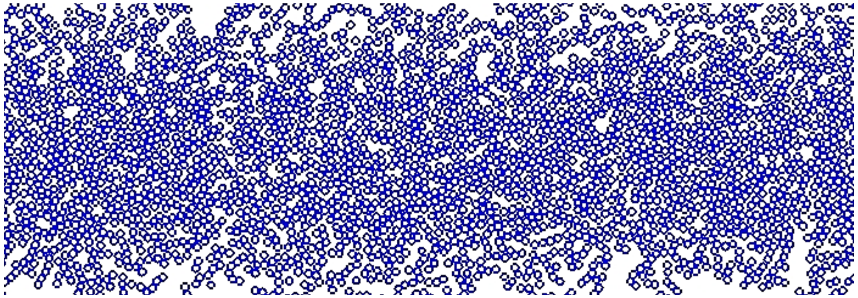

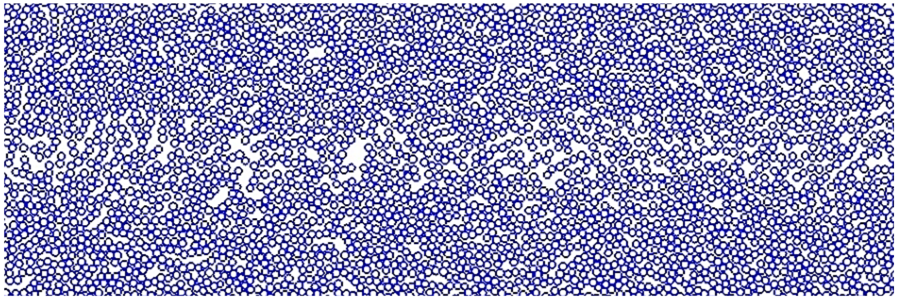

- Stochastic homogenization of SVEs
  - Extraction of Stochastic Volume Elements
    - 2 sizes considered: $l_{\mathrm{SVE}} = 10\ \mu m$ & $l_{\mathrm{SVE}} = 25\ \mu m$
    - Window technique to capture correlation

$$R_{\mathbf{rs}}(\boldsymbol{\tau}) = \frac{\mathbb{E}\left[\left(r(\boldsymbol{x}) - \mathbb{E}(r)\right)\left(s(\boldsymbol{x}+\boldsymbol{\tau}) - \mathbb{E}(s)\right)\right]}{\sqrt{\mathbb{E}\left[\left(r - \mathbb{E}(r)\right)^2\right]}\sqrt{\mathbb{E}\left[\left(s - \mathbb{E}(s)\right)^2\right]}}$$

  - For each SVE
    - Extract apparent homogenized material tensor $\mathbb{C}_{\mathrm{M}}$

$$\begin{cases} \boldsymbol{\varepsilon}_{\mathrm{M}} = \dfrac{1}{V(\omega)} \displaystyle\int_{\omega} \boldsymbol{\varepsilon}_{\mathrm{m}} d\omega \\ \boldsymbol{\sigma}_{\mathrm{M}} = \dfrac{1}{V(\omega)} \displaystyle\int_{\omega} \boldsymbol{\sigma}_{\mathrm{m}} d\omega \\ \mathbb{C}_{\mathrm{M}} = \dfrac{\partial \boldsymbol{\sigma}_{\mathrm{M}}}{\partial \boldsymbol{u}_{\mathrm{M}} \otimes \boldsymbol{\nabla}_{\mathrm{M}}} \end{cases}$$

    - Consistent boundary conditions:
      - Periodic (PBC)
      - Minimum kinematics (SUBC)
      - Kinematic (KUBC)

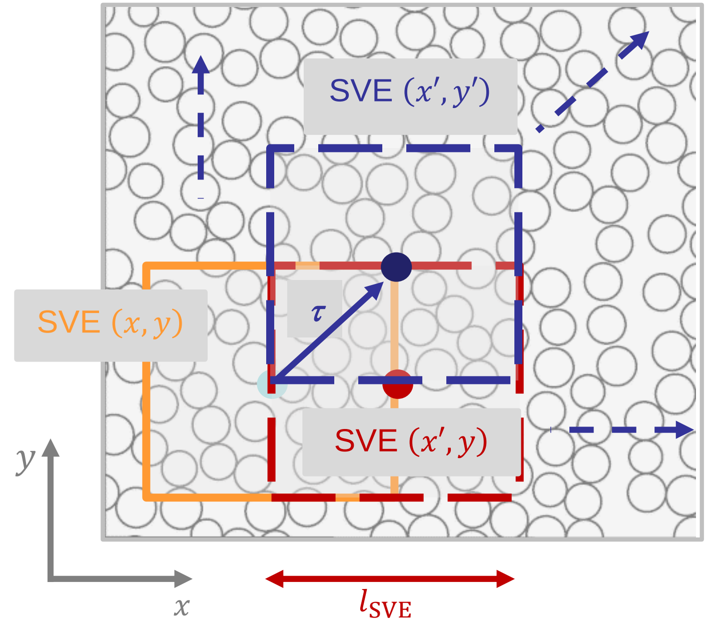

- Stochastic homogenization of SVEs
  - Apparent properties

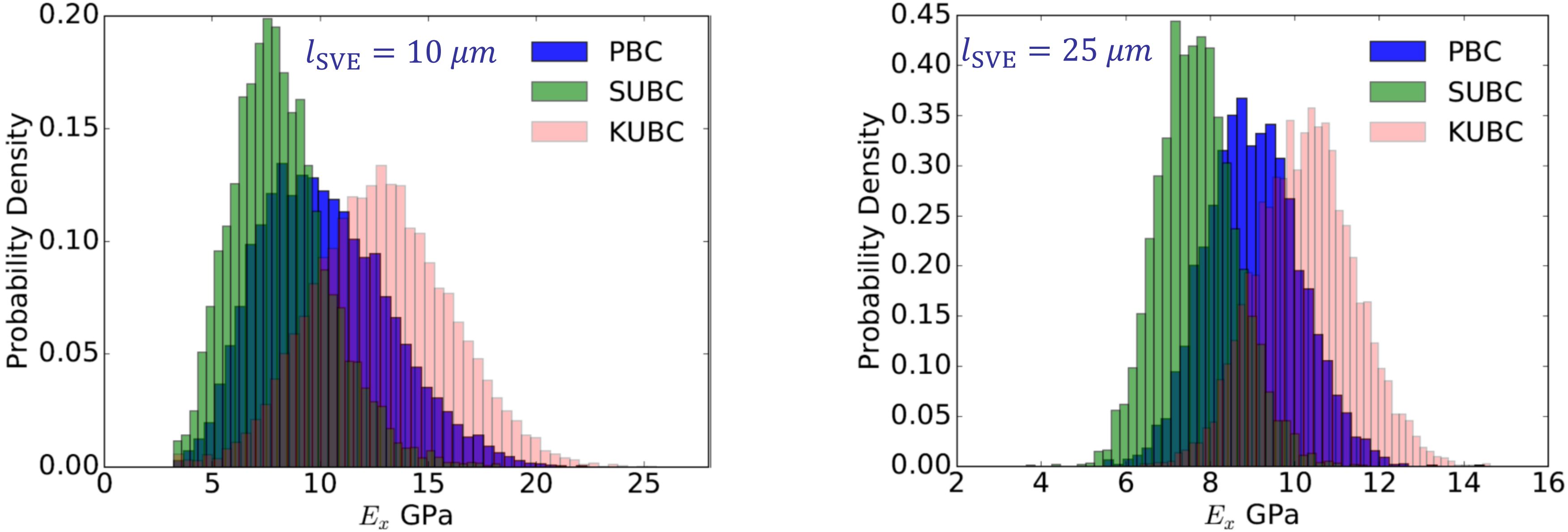

Increasing l_{SVE}

When l_{SVE} increases
- Average values for different BCs get closer (to PBC one)
- Distributions narrow
- Distributions get closer to normal

- Stochastic homogenization of SVEs
  - Correlation study

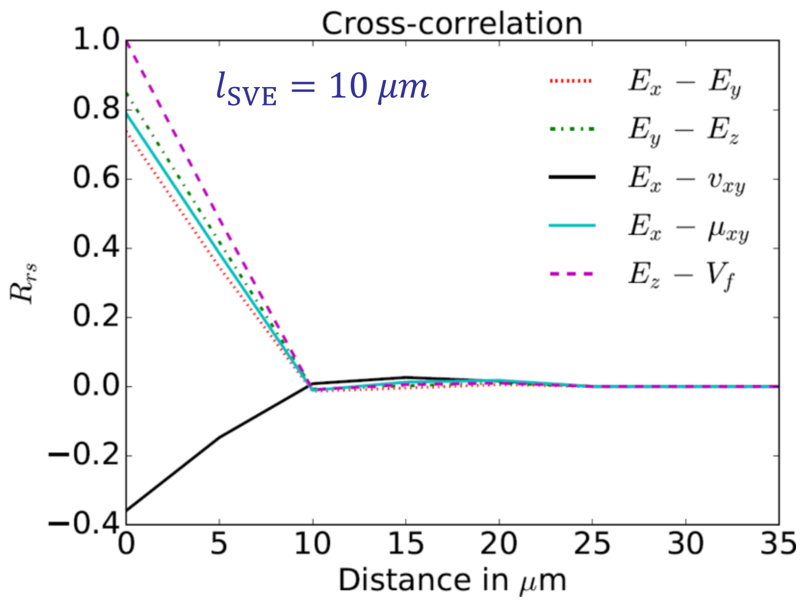

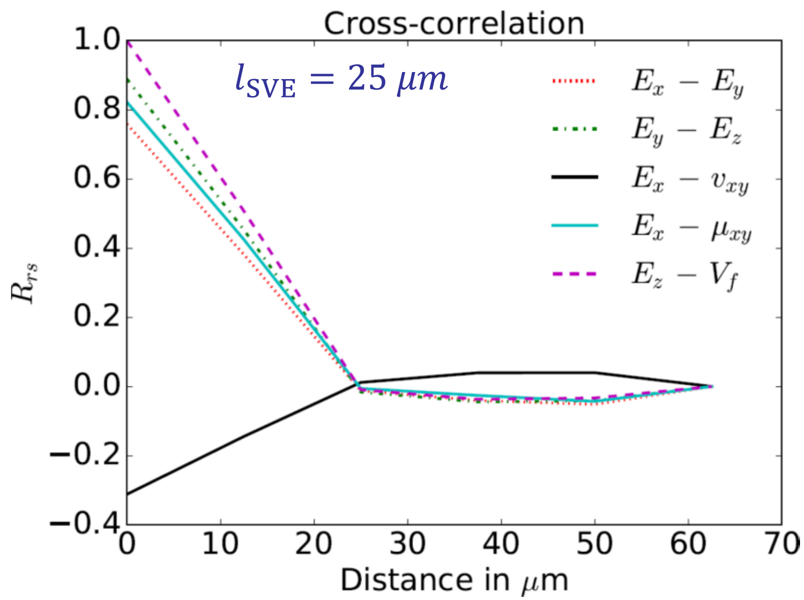

Increasing l_{SVE}

(1) Auto/cross correlation vanishes at $\tau = l_{\mathrm{SVE}}$
(2) When l_{SVE} increases, distributions get closer to normal

(1)+(2) Apparent properties are independent random variables
However the distribution depend on

- l_{SVE}
- The boundary conditions

Stochastic Homogenization of Composite Materials

- Mean-Field-homogenization (MFH)
  - Linear composites

$$\begin{cases} \boldsymbol{\sigma}_{\mathrm{M}} = \overline{\boldsymbol{\sigma}} = v_0 \boldsymbol{\sigma}_0 + v_{\mathrm{I}} \boldsymbol{\sigma}_{\mathrm{I}} \\ \boldsymbol{\varepsilon}_{\mathrm{M}} = \overline{\boldsymbol{\varepsilon}} = v_0 \boldsymbol{\varepsilon}_0 + v_{\mathrm{I}} \boldsymbol{\varepsilon}_{\mathrm{I}} \\ \boldsymbol{\varepsilon}_{\mathrm{I}} = \mathbb{B}^{\varepsilon}\left(\mathrm{I}, \mathbb{C}_0, \mathbb{C}_{\mathrm{I}}\right) : \boldsymbol{\varepsilon}_0 \end{cases}$$

$$\hat{\mathbb{C}}_{\mathrm{M}} = \hat{\mathbb{C}}_{\mathrm{M}}\left(\mathrm{I}, \mathbb{C}_0, \mathbb{C}_{\mathrm{I}}, v_{\mathrm{I}}\right)$$

Defined as random variables

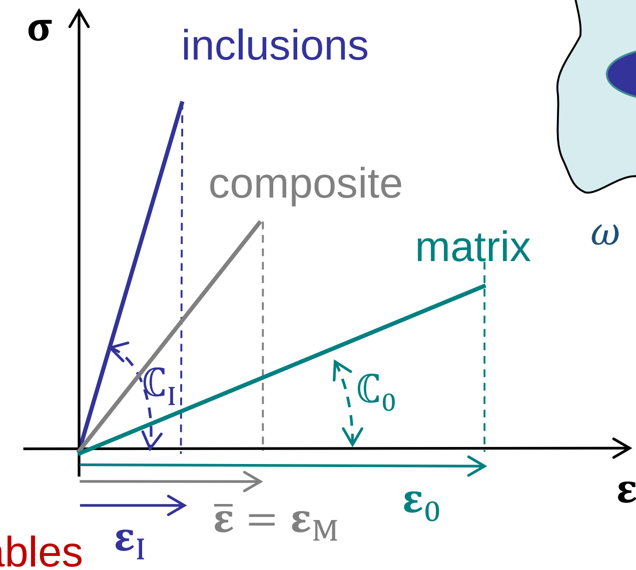

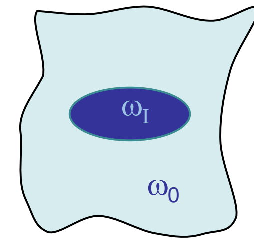

$\omega = \cup_i \, \omega_i$

- Consider an equivalent system
  - For each SVE realization i:
    - $\mathbb{C}_{\mathrm{M}}$ and v_{I} known
  - Anisotropy from $\mathbb{C}_{\mathrm{M}}^{i}$
    - θ is evaluated
  - Fiber behavior uniform
    - $\hat{\mathbb{C}}_{\mathrm{I}}$ for one SVE

$$\mathbb{C}_{\mathrm{M}} \simeq \hat{\mathbb{C}}_{\mathrm{M}}\left(\hat{\mathrm{I}}, \hat{\mathbb{C}}_0, \hat{\mathbb{C}}_{\mathrm{I}}, v_{\mathrm{I}}, \theta\right)$$

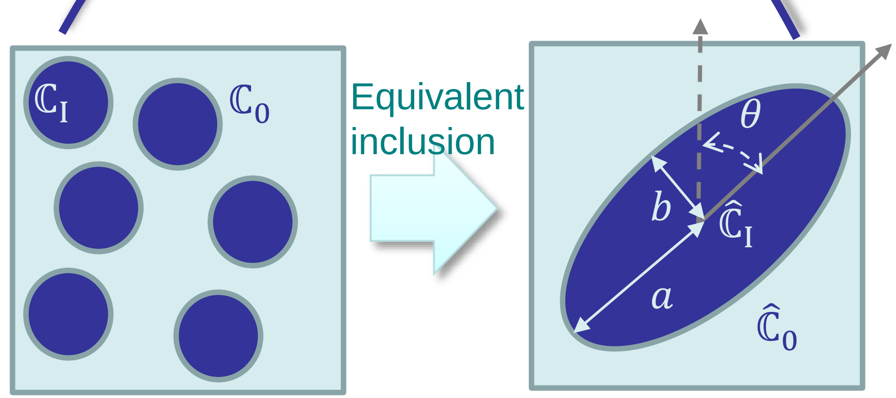

  - Remaining optimization problem:

$$\min_{\frac{a}{b}, \hat{E}_0, \hat{\nu}_0} \left\| \mathbb{C}_{\mathrm{M}} - \hat{\mathbb{C}}_{\mathrm{M}}\left(\frac{a}{b}, \hat{E}_0, \hat{\nu}_0 ; v_{\mathrm{I}}, \theta, \hat{\mathbb{C}}_{\mathrm{I}}\right) \right\|$$

- Inverse stochastic identification
  - Comparison of homogenized properties from SVE realizations and stochastic MFH

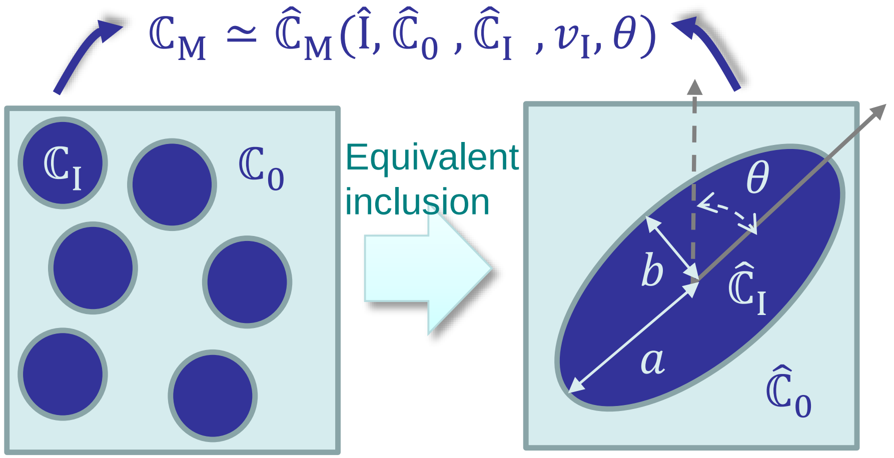

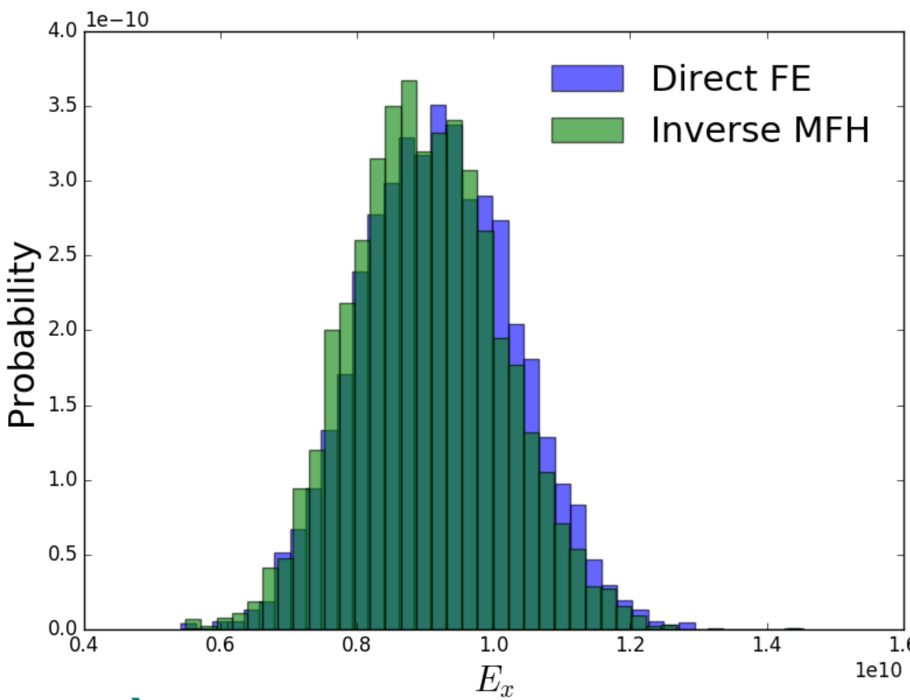

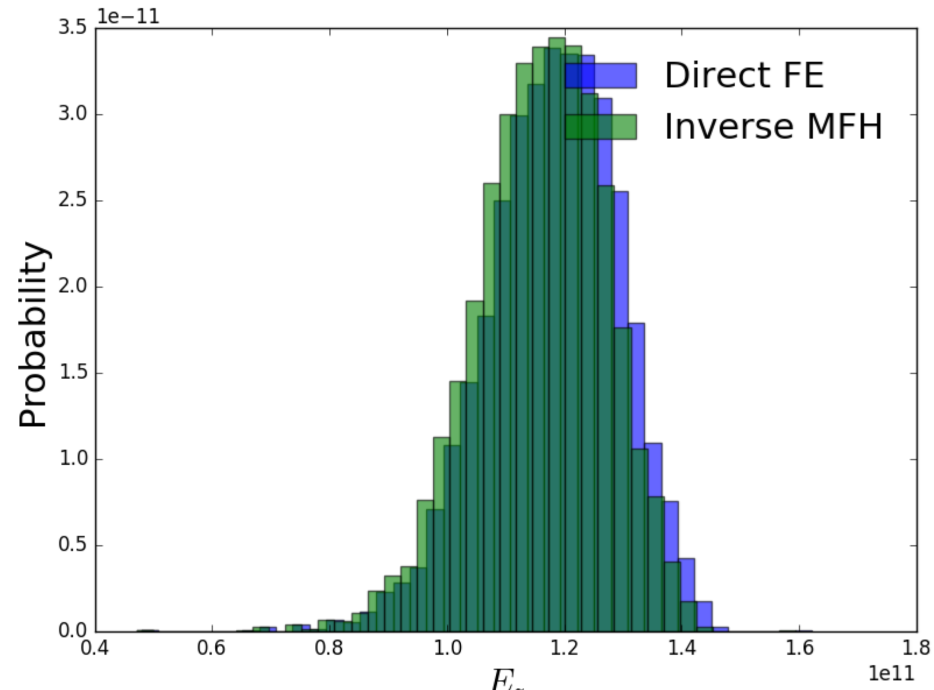

- Incremental-secant Mean-Field-homogenization
  - Virtual elastic unloading from previous state
    - Composite material unloaded to reach the stress-free state
    - Residual stress in components
  - Define Linear Comparison Composite
    - From unloaded state

$$\Delta\boldsymbol{\varepsilon}^{\mathbf{r}}_{\mathrm{I}/0} = \Delta\boldsymbol{\varepsilon}_{\mathrm{I}/0} + \Delta\boldsymbol{\varepsilon}^{\mathrm{unload}}_{\mathrm{I}/0}$$

    - Incremental-secant loading

$$\begin{cases} \boldsymbol{\sigma}_{\mathrm{M}} = \bar{\boldsymbol{\sigma}} = v_0\boldsymbol{\sigma}_0 + v_{\mathrm{I}}\boldsymbol{\sigma}_{\mathrm{I}} \\ \Delta\boldsymbol{\varepsilon}^{\mathbf{r}}_{\mathrm{M}} = \overline{\Delta\boldsymbol{\varepsilon}} = v_0\Delta\boldsymbol{\varepsilon}^{\mathbf{r}}_0 + v_{\mathrm{I}}\Delta\boldsymbol{\varepsilon}^{\mathbf{r}}_{\mathrm{I}} \\ \Delta\boldsymbol{\varepsilon}^{\mathbf{r}}_{\mathrm{I}} = \mathbb{B}^{\varepsilon}\left(\mathrm{I}, \mathbb{C}^{\mathrm{S}}_0, \mathbb{C}^{\mathrm{S}}_{\mathrm{I}}\right) : \Delta\boldsymbol{\varepsilon}^{\mathbf{r}}_0 \end{cases}$$

    - Incremental secant operator

$$\Rightarrow \quad \Delta\boldsymbol{\sigma}_{\mathrm{M}} = \mathbb{C}^{\mathrm{S}}_{\mathrm{M}}\left(\mathrm{I}, \mathbb{C}^{\mathrm{S}}_0, \mathbb{C}^{\mathrm{S}}_{\mathrm{I}}, v_{\mathrm{I}}\right) : \Delta\boldsymbol{\varepsilon}^{\mathbf{r}}_{\mathrm{M}}$$

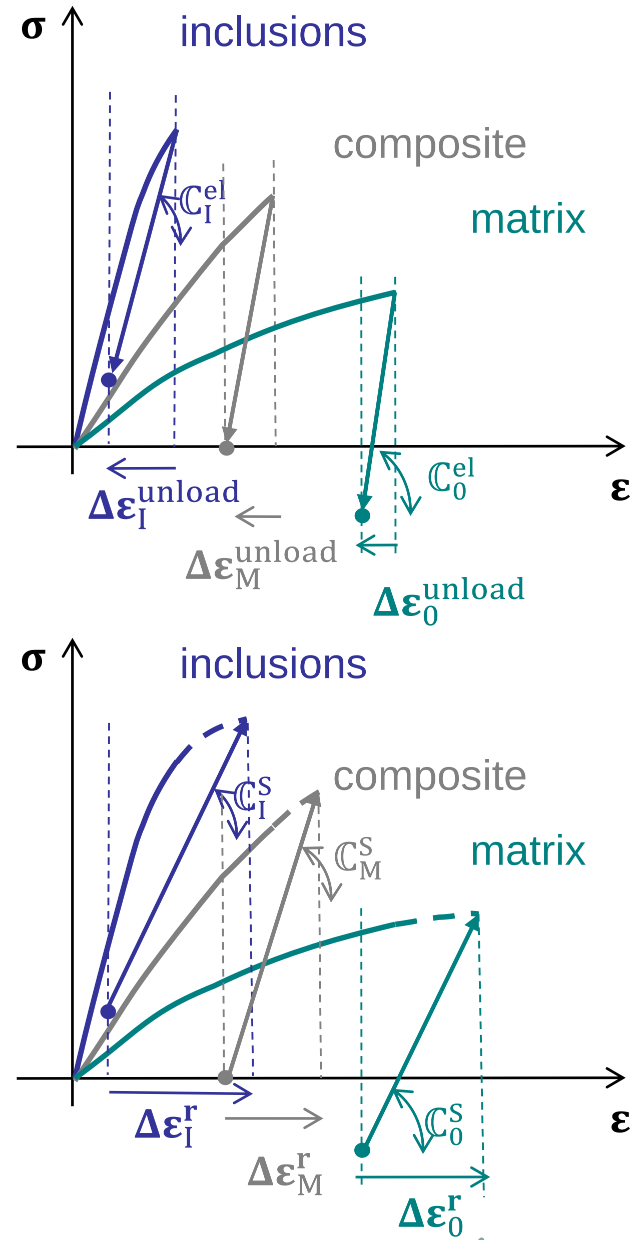

- Non-linear inverse identification
  - First step from elastic response

$$\mathbb{C}_{\mathrm{M}}^{\mathrm{el}} \simeq \hat{\mathbb{C}}_{\mathrm{M}}^{\mathrm{el}}(\hat{\mathrm{I}}, \hat{\mathbb{C}}_{0}^{\mathrm{el}}, \hat{\mathbb{C}}_{\mathrm{I}}^{\mathrm{el}}, v_{\mathrm{I}}, \theta)$$

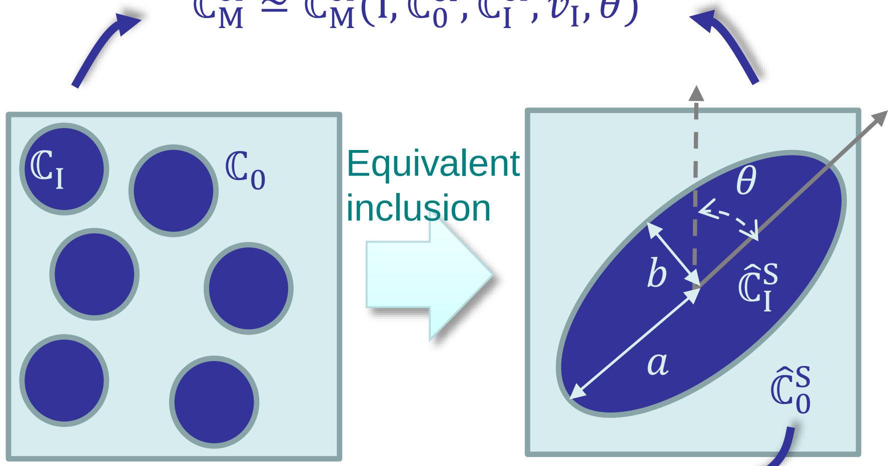

$$\mathbb{C}_{0}^{\mathrm{S}} \simeq \hat{\mathbb{C}}_{0}^{\mathrm{S}}(\hat{R}(\hat{p}_0); \hat{\mathbb{C}}_{0}^{\mathrm{el}})$$

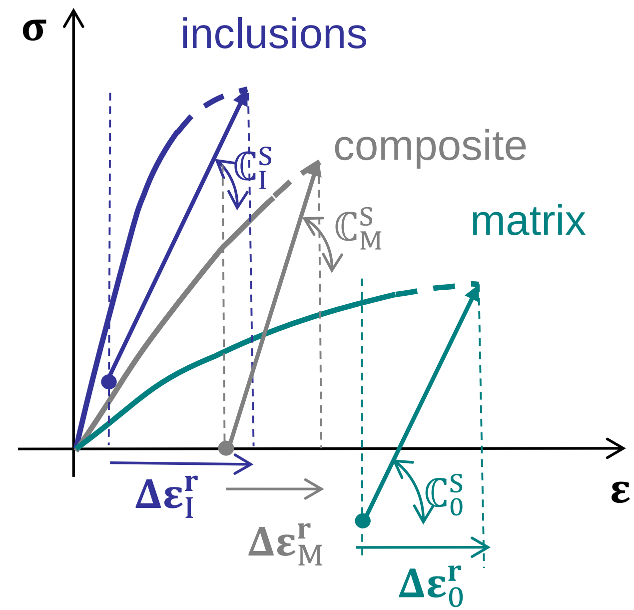

  - Second step from the LCC
    - New optimization problem

$$\boldsymbol{\Delta\sigma}_{\mathrm{M}} \simeq \hat{\mathbb{C}}_{\mathrm{M}}^{\mathrm{S}}\left(\hat{\mathrm{I}}, \hat{\mathbb{C}}_{0}^{\mathrm{S}}, \mathbb{C}_{\mathrm{I}}^{\mathrm{S}}, v_{\mathrm{I}}, \theta\right): \boldsymbol{\Delta\varepsilon}_{\mathrm{M}}^{\mathrm{r}}$$

    - Extract the equivalent hardening $\hat{R}(\hat{p}_0)$ from the incremental secant tensor

$$\mathbb{C}_{0}^{\mathrm{S}} \simeq \hat{\mathbb{C}}_{0}^{\mathrm{S}}(\hat{R}(\hat{p}_0); \hat{\mathbb{C}}_{0}^{\mathrm{el}})$$

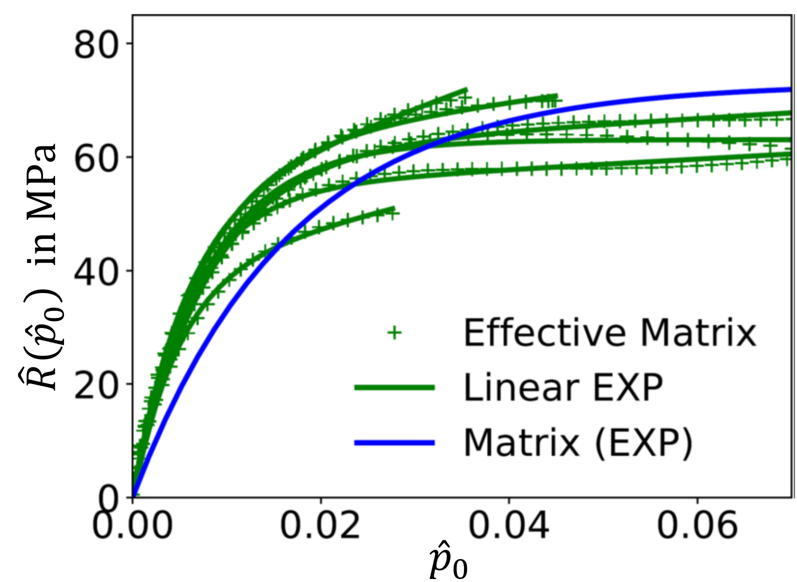

- Non-linear inverse identification
  - Comparison SVE vs. MFH

$\mathbb{C}_{\mathrm{M}}^{\mathrm{el}} \simeq \hat{\mathbb{C}}_{\mathrm{M}}^{\mathrm{el}}(\hat{\mathrm{I}}, \hat{\mathbb{C}}_0^{\mathrm{el}}, \hat{\mathbb{C}}_{\mathrm{I}}^{\mathrm{el}}, v_{\mathrm{I}}, \theta)$

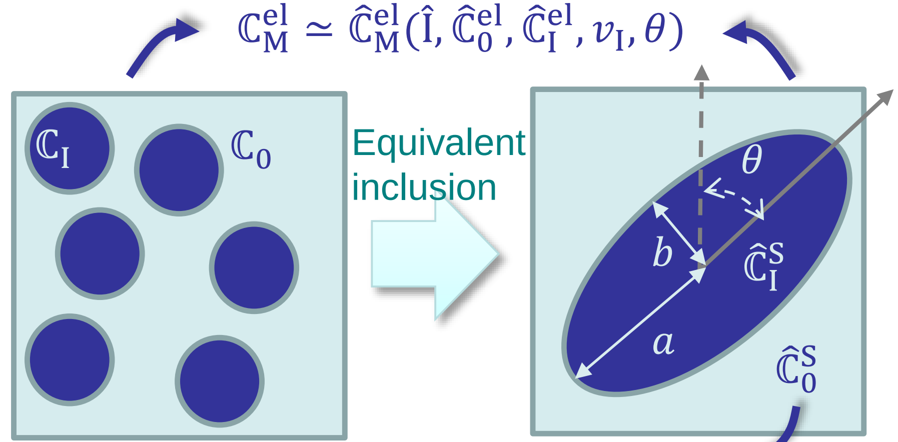

$\mathbb{C}_0^{\mathrm{S}} \simeq \hat{\mathbb{C}}_0^{\mathrm{S}}(\hat{R}(\hat{p}_0); \hat{\mathbb{C}}_0^{\mathrm{el}})$

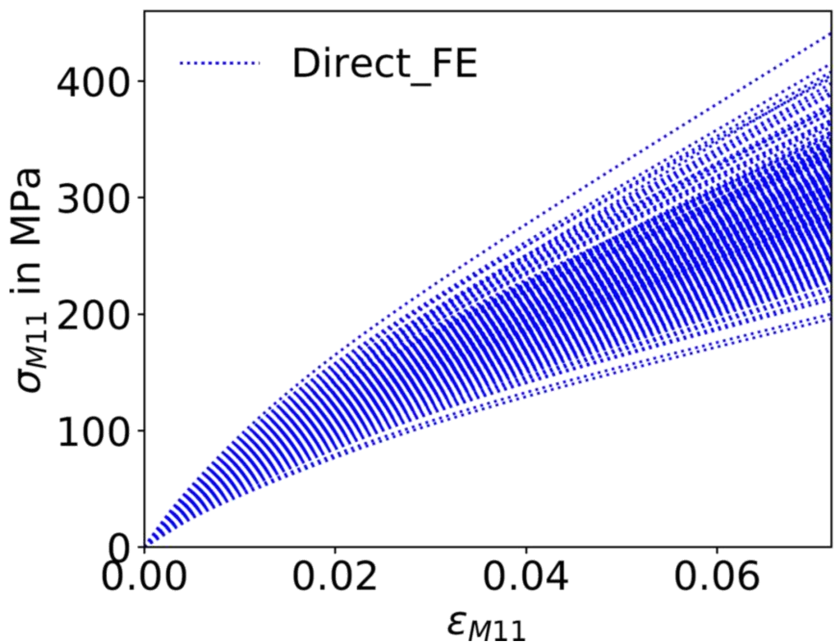

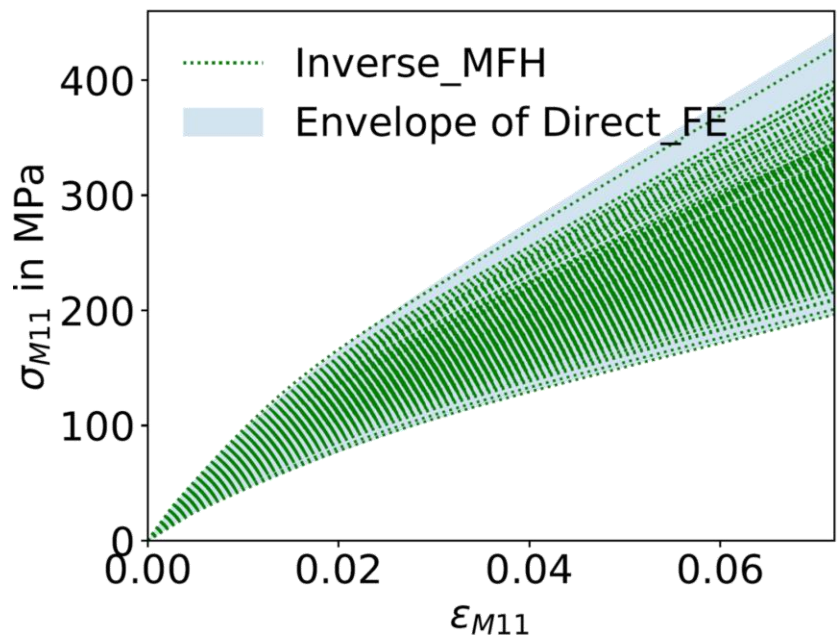

- Damage-enhanced Mean-Field-homogenization
  - Virtual elastic unloading from previous state
    - Composite material unloaded to reach the stress-free state
    - Residual stress in components
  - Define Linear Comparison Composite
    - From elastic state

$$\boldsymbol{\Delta\varepsilon}^{\mathrm{r}}_{\mathrm{I}/0} = \boldsymbol{\Delta\varepsilon}_{\mathrm{I}/0} + \boldsymbol{\Delta\varepsilon}^{\mathrm{unload}}_{\mathrm{I}/0}$$

    - Incremental-secant loading

$$\begin{cases} \boldsymbol{\sigma}_{\mathrm{M}} = \bar{\boldsymbol{\sigma}} = v_0\boldsymbol{\sigma}_0 + v_{\mathrm{I}}\boldsymbol{\sigma}_{\mathrm{I}} \\ \boldsymbol{\Delta\varepsilon}^{\mathrm{r}}_{\mathrm{M}} = \overline{\boldsymbol{\Delta\varepsilon}} = v_0\boldsymbol{\Delta\varepsilon}^{\mathrm{r}}_0 + v_{\mathrm{I}}\boldsymbol{\Delta\varepsilon}^{\mathrm{r}}_{\mathrm{I}} \\ \boldsymbol{\Delta\varepsilon}^{\mathrm{r}}_{\mathrm{I}} = \mathbb{B}^{\varepsilon}\left(\mathrm{I}, (1-D_0)\mathbb{C}^{\mathrm{S}}_0, \mathbb{C}^{\mathrm{S}}_{\mathrm{I}}\right) : \boldsymbol{\Delta\varepsilon}^{\mathrm{r}}_0 \end{cases}$$

    - Incremental secant operator

$$\Rightarrow \quad \boldsymbol{\Delta\sigma}_{\mathrm{M}} = \mathbb{C}^{\mathrm{S}}_{\mathrm{M}}\left(\mathrm{I}, (1-D_0)\mathbb{C}^{\mathrm{S}}_0, \mathbb{C}^{\mathrm{S}}_{\mathrm{I}}, v_{\mathrm{I}}\right) : \boldsymbol{\Delta\varepsilon}^{\mathrm{r}}_{\mathrm{M}}$$

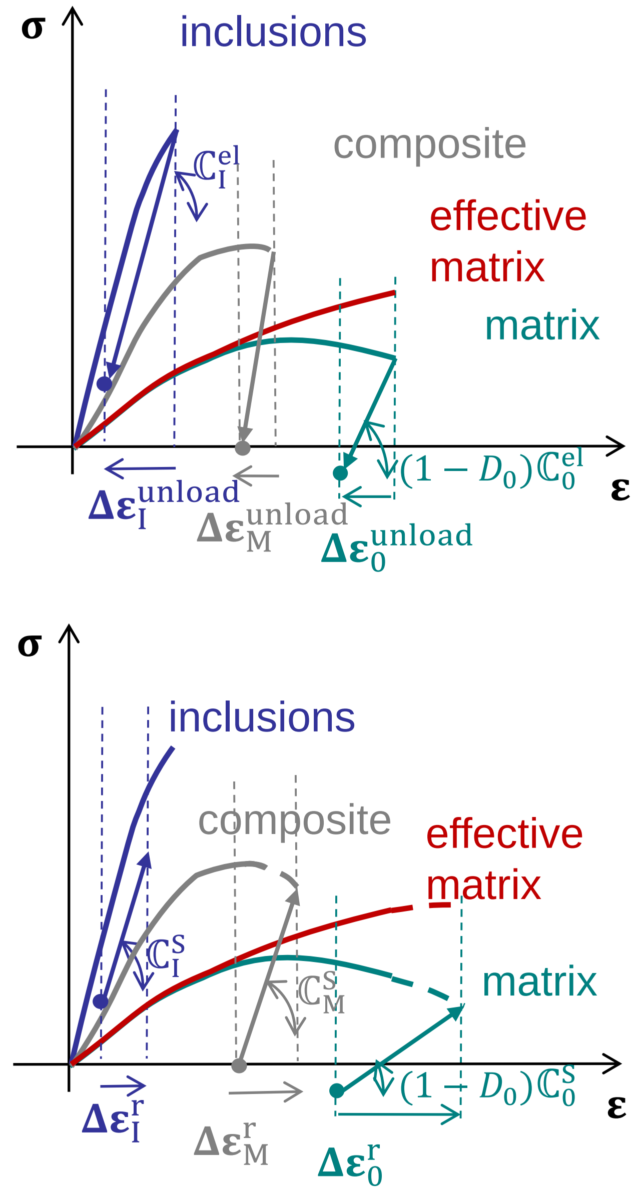

- Damage-enhanced inverse identification
  - Comparison SVE vs. MFH

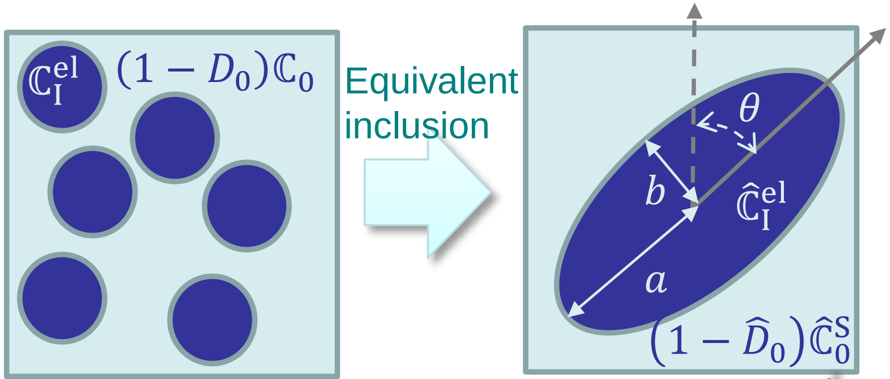

$$(1-\mathrm{D}_0)\mathbb{C}_0^S \simeq \left(1-\hat{\mathrm{D}}_0(\hat{p}_0)\right)\hat{\mathbb{C}}_0^S(\hat{R}(\hat{p}_0);\hat{\mathbb{C}}_0^{\mathrm{el}})$$

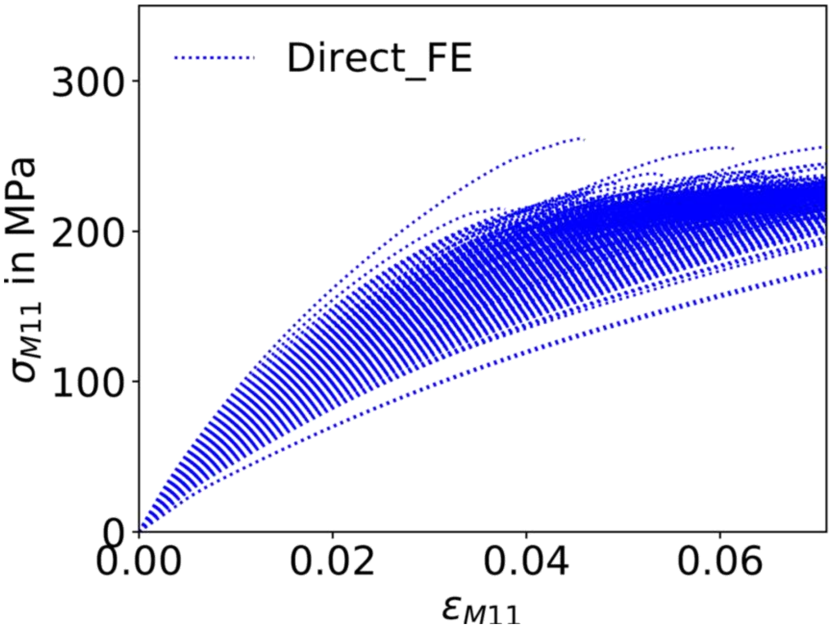

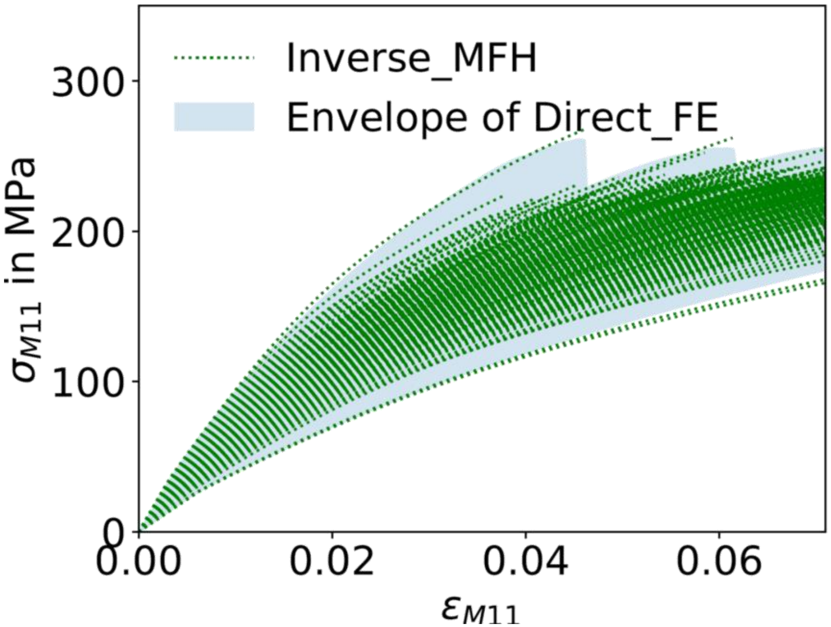

- Generation of random field
  - Comparison inverse identification vs. diffusion map –based generator

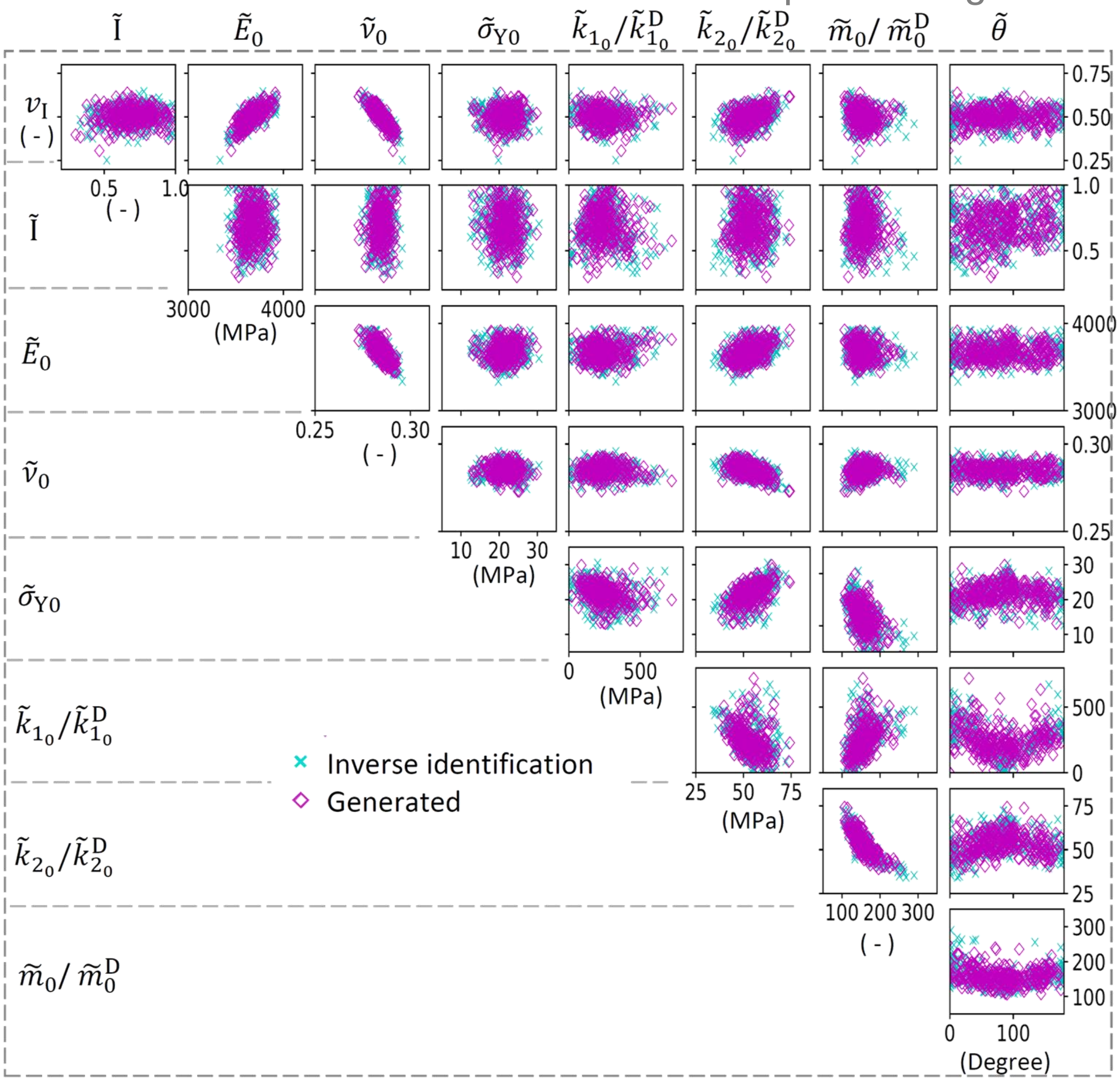

Beginning

Stochastic Homogenization of Composite Materials

- One single ply loading realization
  - Random field and finite elements discretizations
  - Non-uniform homogenized stress distributions
  - Creates damage localization

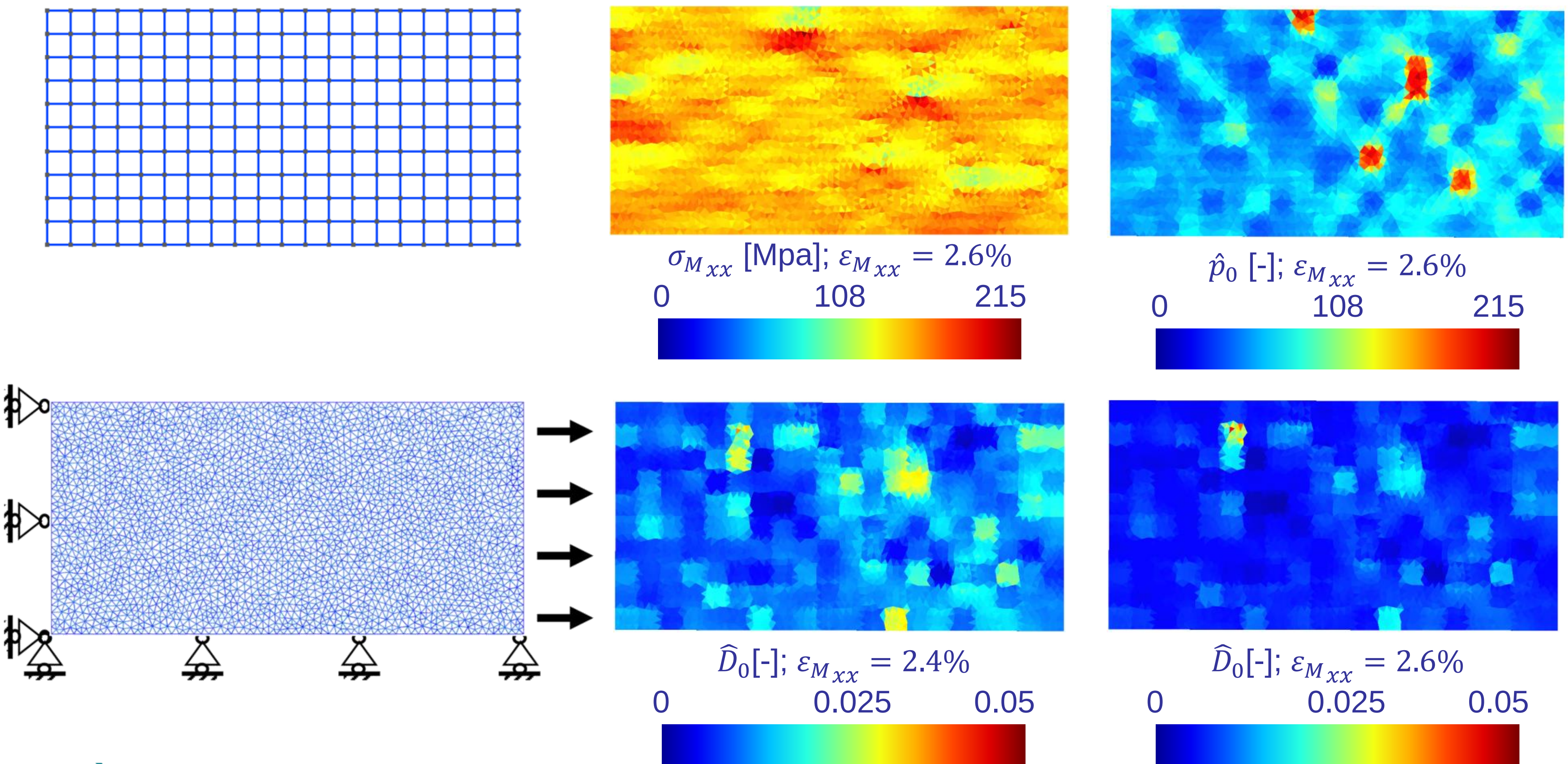

- Ply loading realizations
  - Simple failure criterion at (homogenized stress) loss of ellipticity
  - Discrepancy in failure point

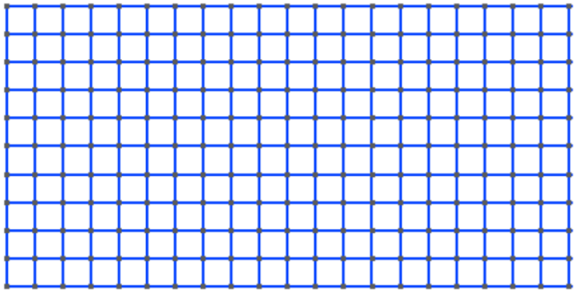

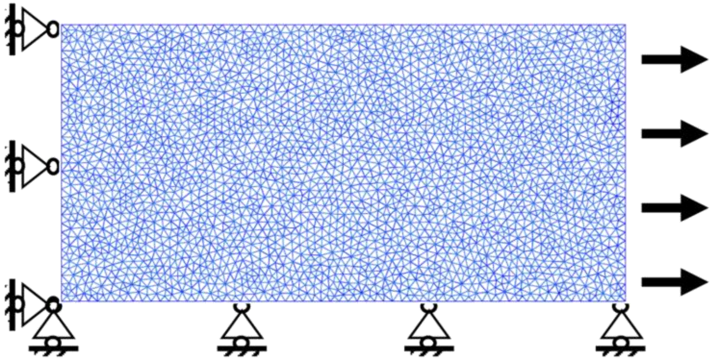

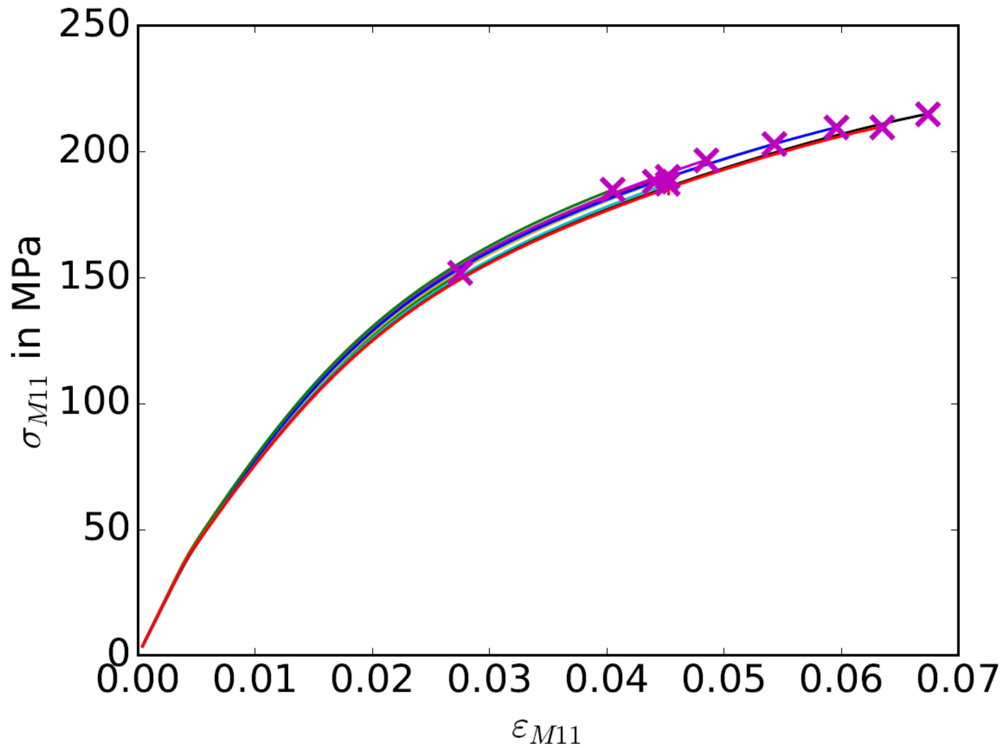

Stochastic Homogenization of Composite Materials

- STOMMMAC M.ERA-NET project (MFH for elasto-visco-plastic composites)
  - e-Xstream, ULiège (Belgium)
  - BATZ (Spain)
  - JKU, AC (Austria)
  - U Luxembourg (Luxemburg)

- Publications (doi)
  - 10.1016/j.compstruct.2018.01.051
  - 10.1002/nme.5903
  - 10.1016/j.cma.2019.01.016

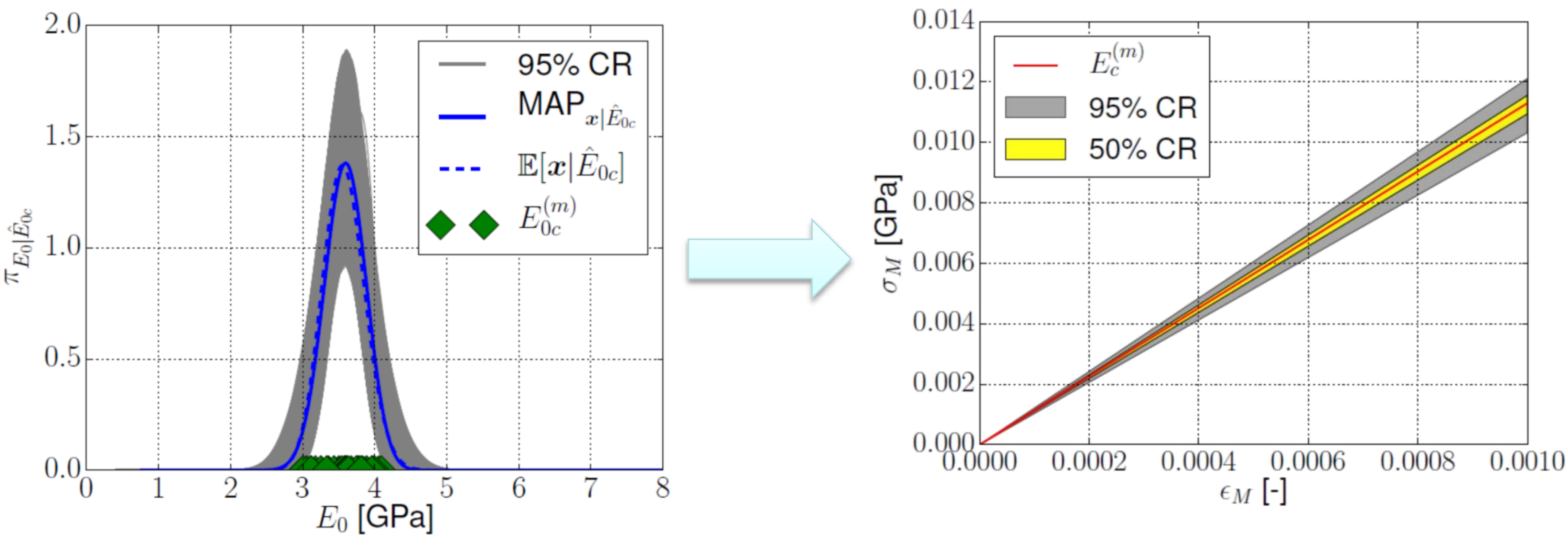

Bayesian identification of stochastic Mean-Field Homogenization model parameters

STOMMMAC The research has been funded by the Walloon Region under the agreement no 1410246-STOMMMAC (CT-INT 2013-03-28) in the context of M-ERA.NET Joint Call 2014.

- Multi-scale modeling
  - 2 problems are solved concurrently
    - The macro-scale problem
    - The meso-scale problem (on a meso-scale Volume Element)

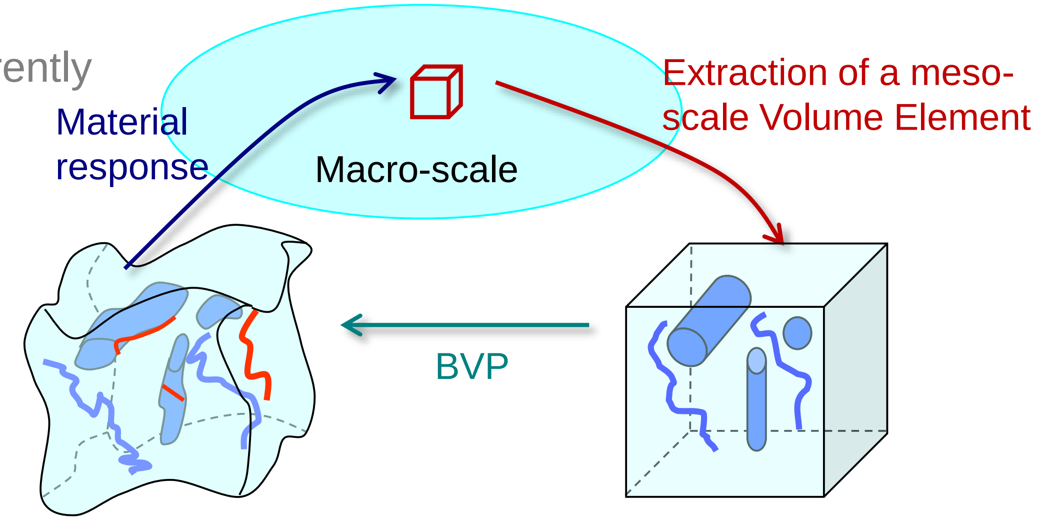

Identification: Requires identification of micro-scale geometrical and material model parameters

Bayesian identification of stochastic MFH model parameters

- Proposed methodology
  - To develop a stochastic Mean Field Homogenization method whose missing micro-constituents properties are inferred from coupons tests

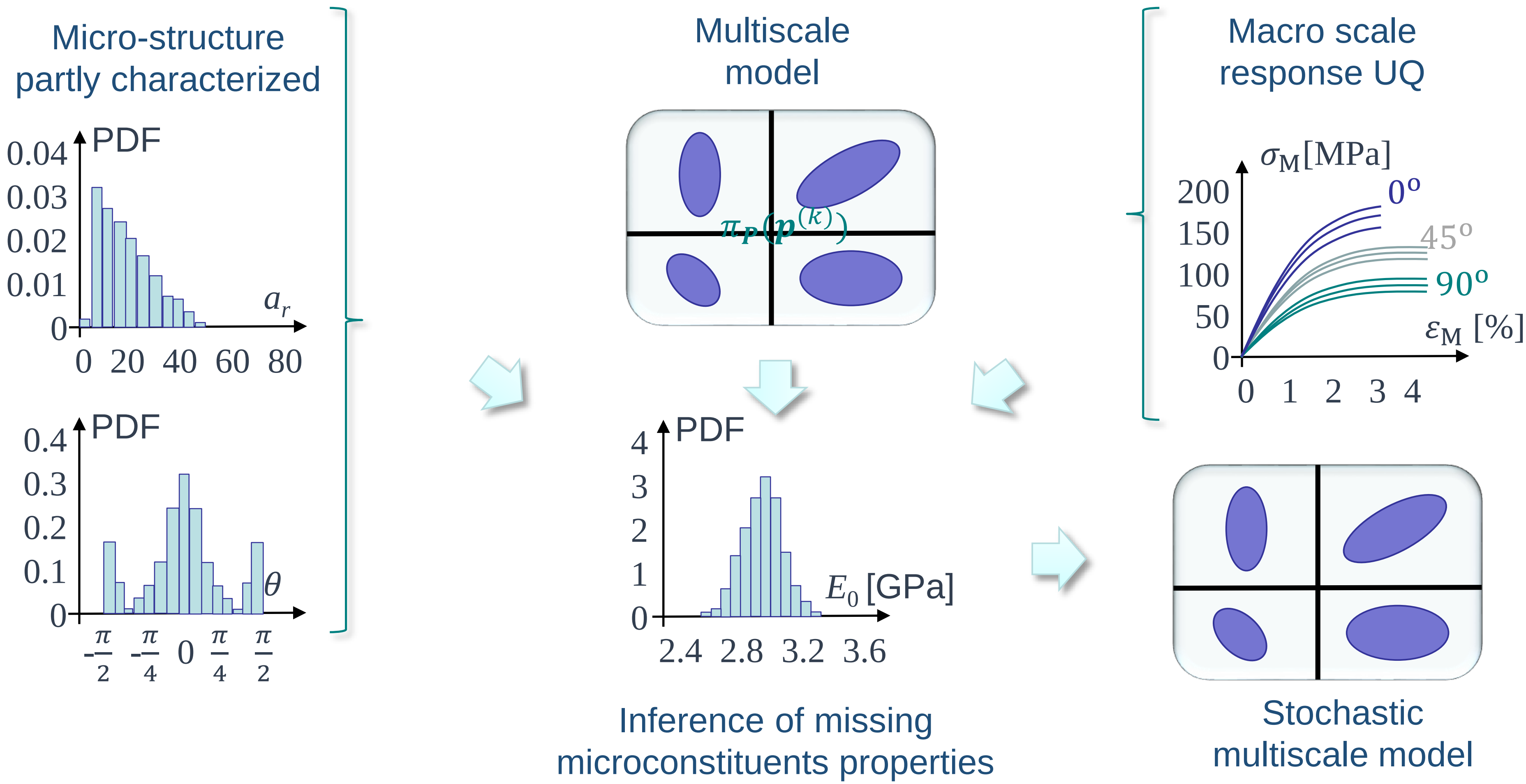

- Fibre distribution effect
  - 2-step homogenization

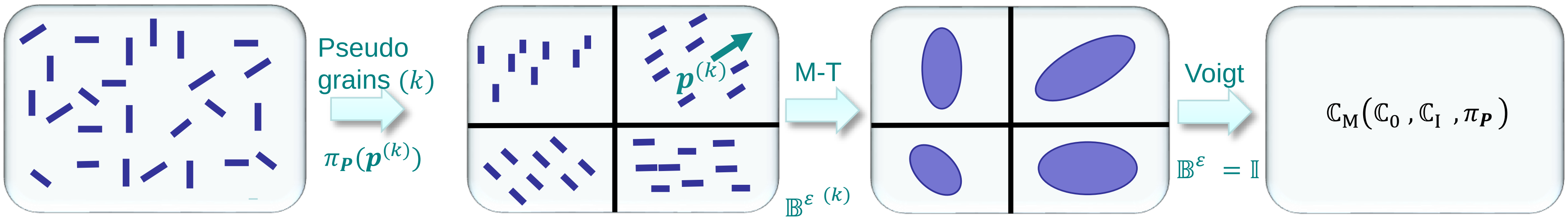

  - For uniaxial tests along direction θ: $\sigma_{\mathrm{M}} = \sigma_{\mathrm{M}}\left(\mathrm{I}(\psi(\boldsymbol{p})), \mathbb{C}_0, \mathbb{C}_{\mathrm{I}}; \theta, \varepsilon_{\mathrm{M}}\right)$

- Fibre distribution effect
  - Skin-core effect

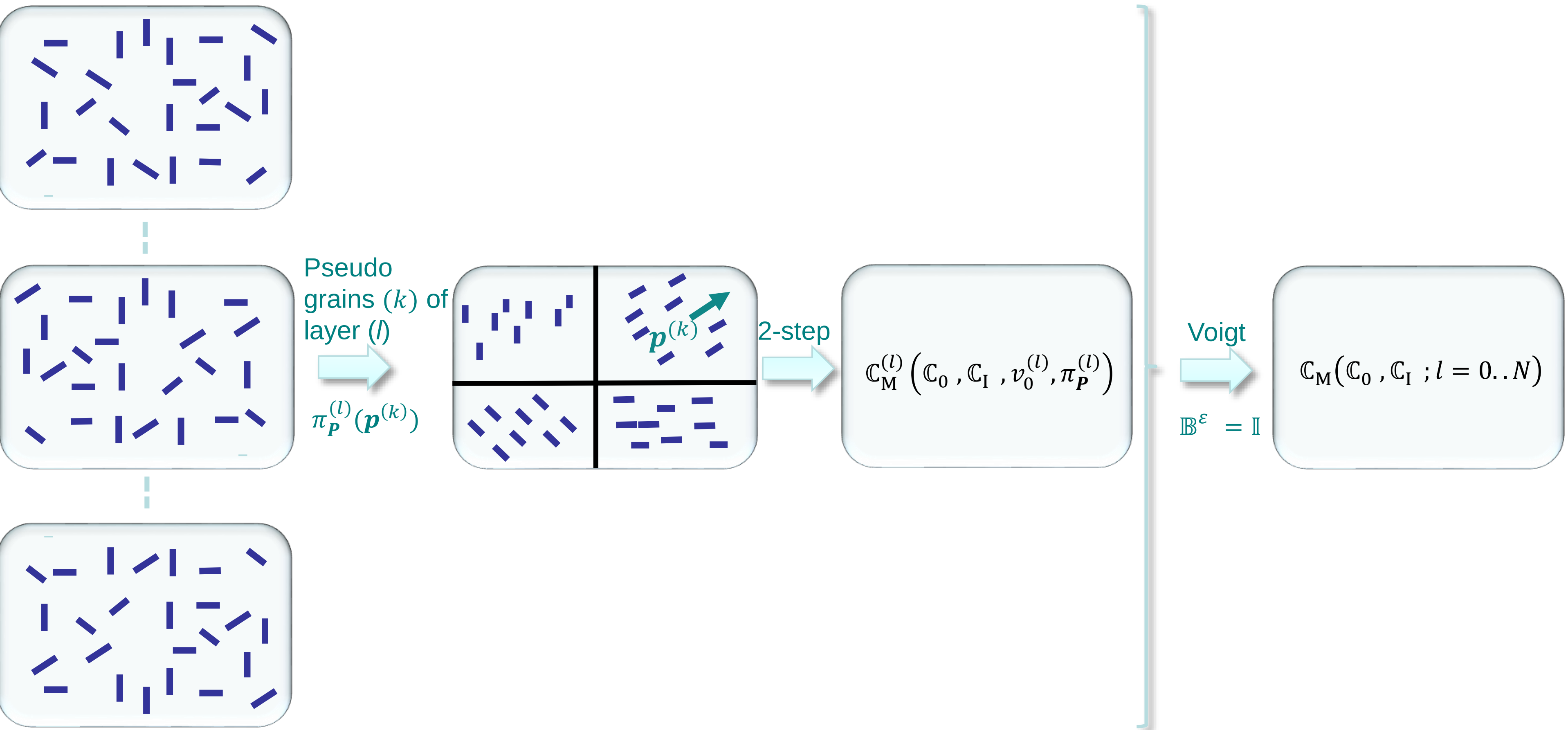

  - For uniaxial tests along direction θ: $\sigma_{\mathrm{M}} = \sigma_{\mathrm{M}}\left(\mathrm{I}(\psi(\boldsymbol{p})), \mathbb{C}_0, \mathbb{C}_{\mathrm{I}}; \theta, \varepsilon_{\mathrm{M}}\right)$

Bayesian identification of stochastic MFH model parameters

- Experimental characterization

Fiber orientation and aspect ratio (JKU)

Composite material response (BATZ)

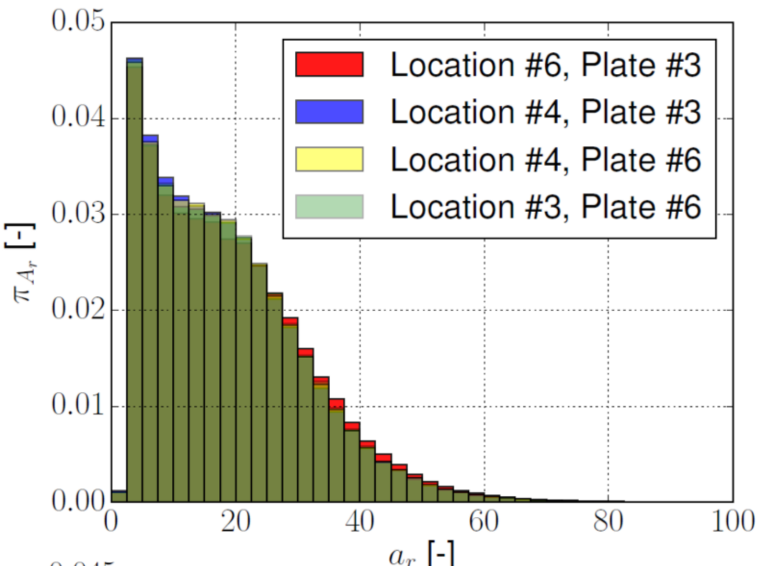

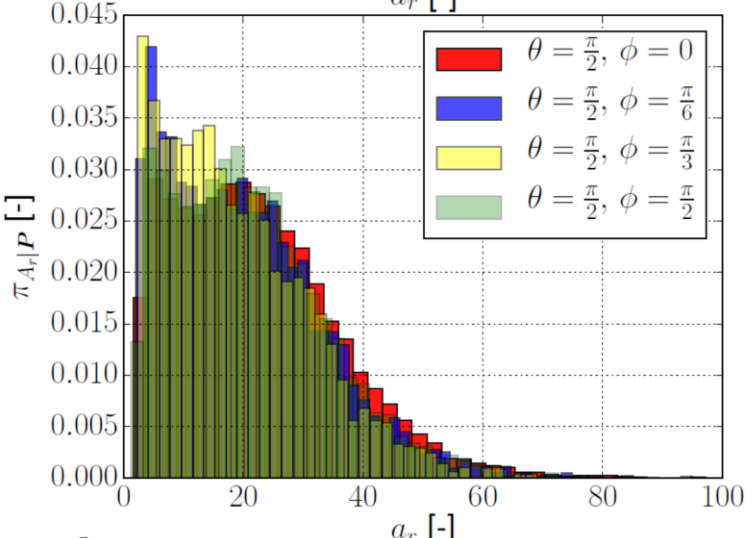

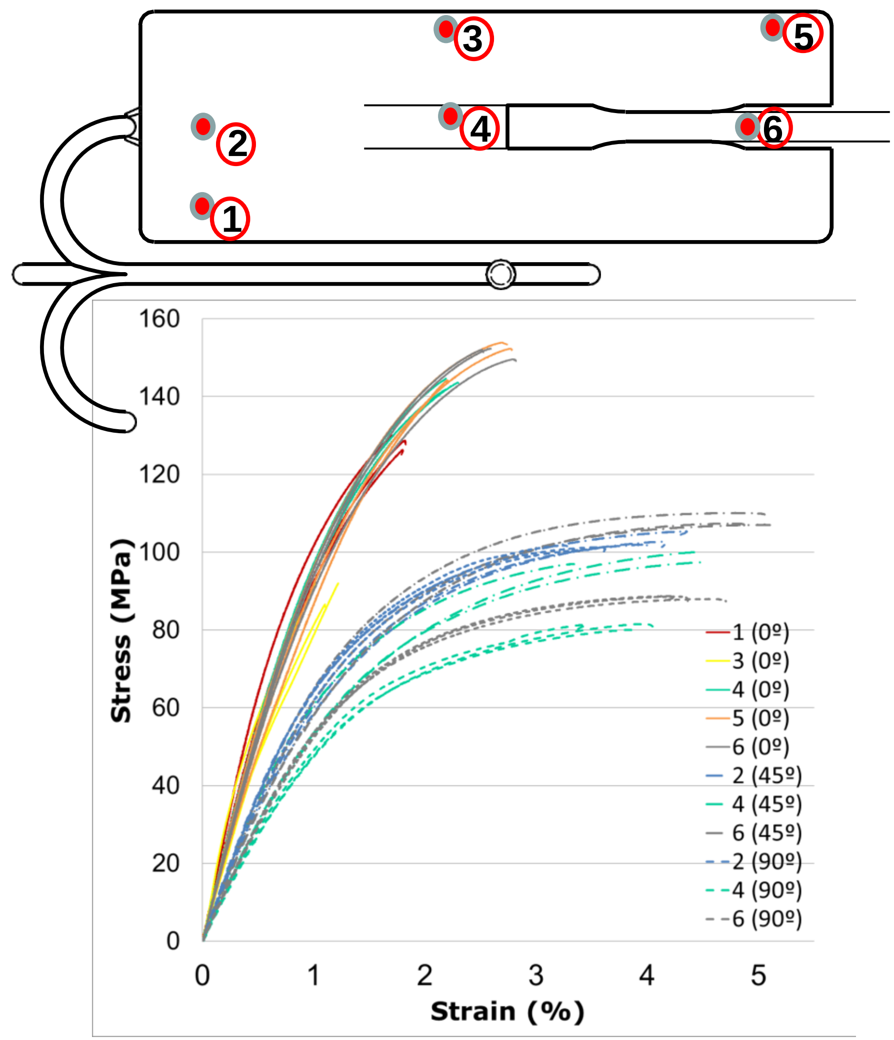

- Assume a distribution of the matrix Young's modulus
  - Beta distribution $E_0 \sim \beta_{\alpha,\beta,a,b}$ with $\beta_{\alpha,\beta,a,b}(y) = \dfrac{(y-a)^{\alpha-1}(y-b)^{\beta-1}}{(b-a)^{\alpha+\beta+1}B(\alpha,\beta)}$
  - Matrix Young 's modulus corresponding to experimental measurements
    - $E_{0c}^{(n)}$ with $n = 1..n_{\text{total}}$, for all directions and positions
  - Bayes' theorem

$$\pi_{\text{post}}\left(\alpha,\beta,a,b|\hat{E}_{0c}\right) \propto \pi\left(\hat{E}_{0c}|\alpha,\beta,a,b\right)\pi_{\text{prior}}(\alpha)\pi_{\text{prior}}(\beta)\pi_{\text{prior}}(a)\pi_{\text{prior}}(b)$$

- Priors: $\pi_{\text{prior}}(x) = \Gamma_{\alpha,\beta,\,a,c}$ with $\Gamma_{\alpha,\beta,\,a,\,c}(y) = \dfrac{\left(\frac{y-a}{c}\right)^{\alpha-1}\beta^{\alpha}e^{-\beta\left(\frac{y-a}{c}\right)}}{c\Gamma(\alpha)}$

- Likelihood: $\pi\left(\hat{E}_{\,0c}|\alpha,\beta,a,b\right) = \prod_{n=1}^{n_{\text{total}}}\beta_{\alpha,\beta,a,b}\left(E_{0c}^{(n)}\right)$

$$\Rightarrow \quad \pi_{\text{post}}\left(\alpha,\beta,a,b|\hat{E}_{0c}\right) \propto \prod_{n=1}^{n_{\text{total}}}\beta_{\alpha,\beta,a,c}\left(E_{0c}^{(n)}\right)\pi_{\text{prior}}(\alpha)\pi_{\text{prior}}(\beta)\pi_{\text{prior}}(a)\pi_{\text{prior}}(b)$$

Bayesian identification of stochastic MFH model parameters

- Assume a distribution of the matrix Young's modulus
  - Inference: $\pi_{\text{post}}\left(\alpha, \beta, a, b | \hat{E}_{0c}\right) \propto \prod_{n=1}^{n_{\text{total}}} \beta_{\alpha,\beta,a,c}\left(E_{0c}^{(n)}\right) \pi_{\text{prior}}(\alpha\ )\pi_{\text{prior}}(\beta)\pi_{\text{prior}}(a)\pi_{\text{prior}}(b)$
    - $i = 1..n_{\text{pos}}$, with n_{pos} the number of positions tested (5, positions #1-#5)

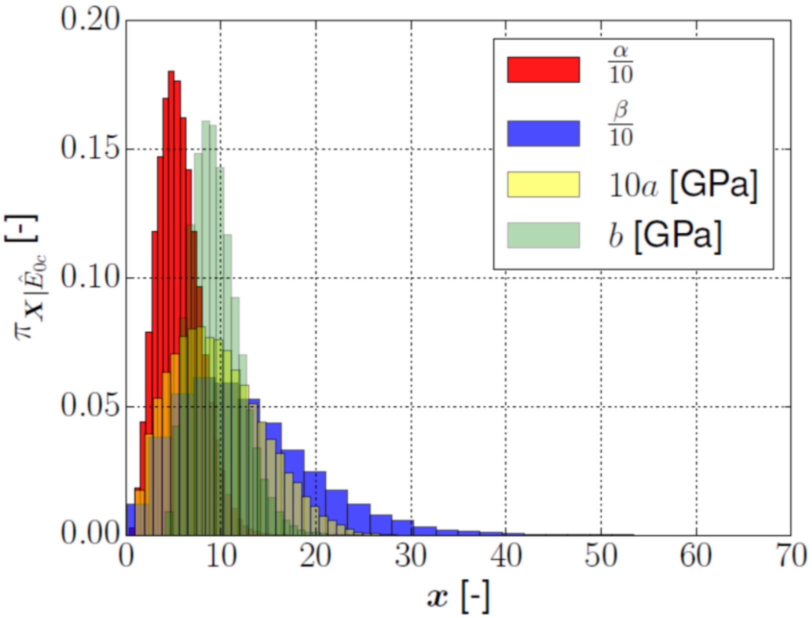

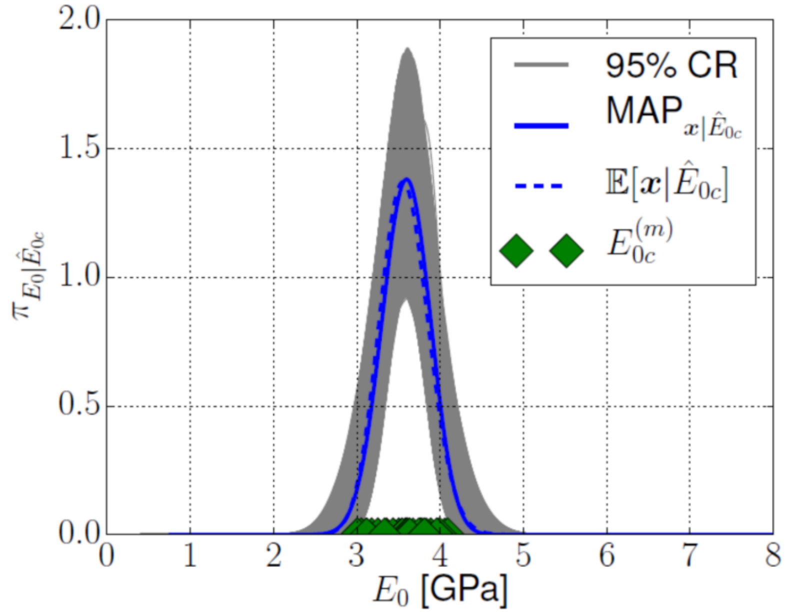

- Validation
  - Evaluate stochastic response at Position 6
    - Perform stochastic homogenization from

      $\pi_{\text{post}}(\alpha, \beta, a, b | \hat{E}_{0c})$

    - From sampling of $[\alpha, \beta, a, b]$, evaluate

      $E_0 \sim \beta_{\alpha,\beta,a,b}$

    - From sampling of $[E_0]$, evaluate composite response

$$E_{\text{MFH}} = E_{\text{MFH}}\big(\mathrm{I}(\psi(\boldsymbol{p}), a_r), E_0\ , \mathbb{C}_{\mathrm{I}}\ ; \theta\big)$$

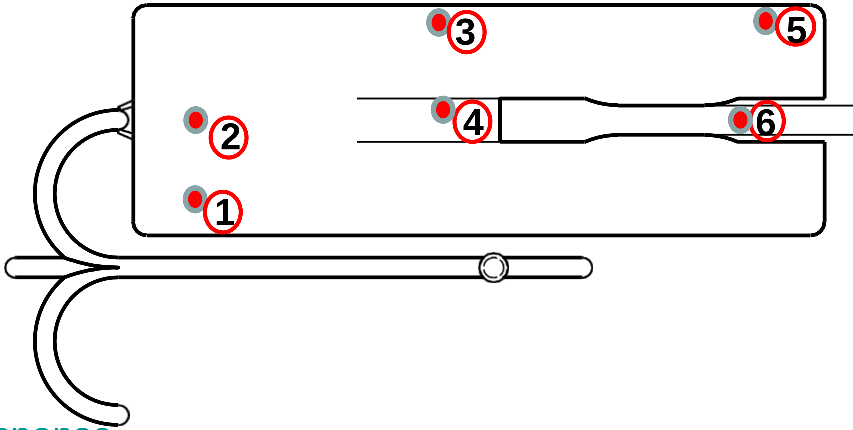

    - Compare with experimental measurements $\hat{E}_c^{(6,j)}$

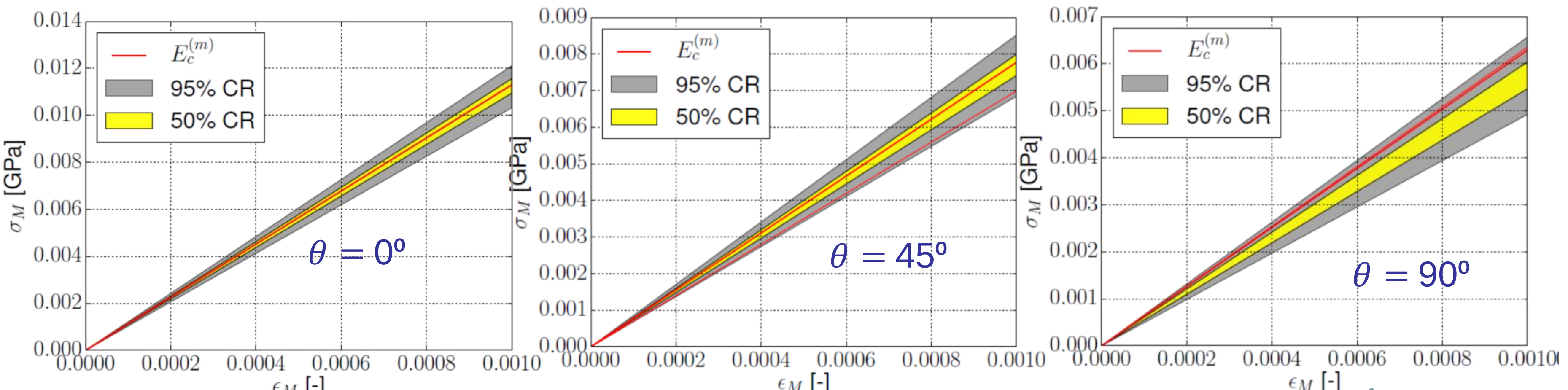

Bayesian identification of stochastic MFH model parameters

- Extension to non-linear behavior
  - More parameters to infer
    - Matrix Young's modulus E_0
    - Matrix yield stress $\sigma_{Y\,0}$
    - Matrix hardening law
      $R(p_0) = h\, p_0^{m_1}(1 - \exp(-m_2 p_0))$
    - Effective aspect ratio a_r
  - 2-Step MFH model requires many iterations
    - Incremental secant approach

$$\begin{cases} \boldsymbol{\sigma}_{\mathrm{M}} = \overline{\boldsymbol{\sigma}} = v_0 \boldsymbol{\sigma}_0 + v_{\mathrm{I}} \boldsymbol{\sigma}_{\mathrm{I}} \\ \Delta\boldsymbol{\varepsilon}_{\mathrm{M}}^{\mathrm{r}} = \overline{\Delta\boldsymbol{\varepsilon}} = v_0 \Delta\boldsymbol{\varepsilon}_0^{\mathrm{r}} + v_{\mathrm{I}} \Delta\boldsymbol{\varepsilon}_{\mathrm{I}}^{\mathrm{r}} \\ \Delta\boldsymbol{\varepsilon}_{\mathrm{I}}^{\mathrm{r}} = \mathbb{B}^{\varepsilon}\left(\mathrm{I}, \mathbb{C}_0^{\mathrm{S}}, \mathbb{C}_{\mathrm{I}}^{\mathrm{S}}\right) : \Delta\boldsymbol{\varepsilon}_0^{\mathrm{r}} \end{cases}$$

Too expensive for BI

  - Definition of parameters

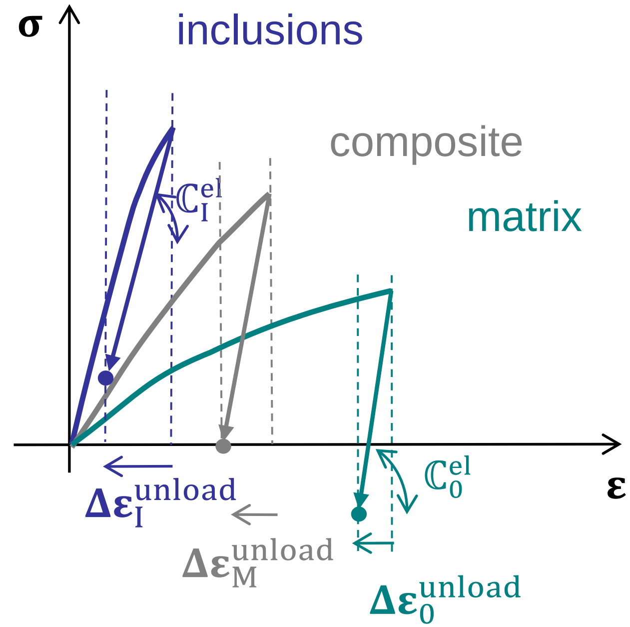

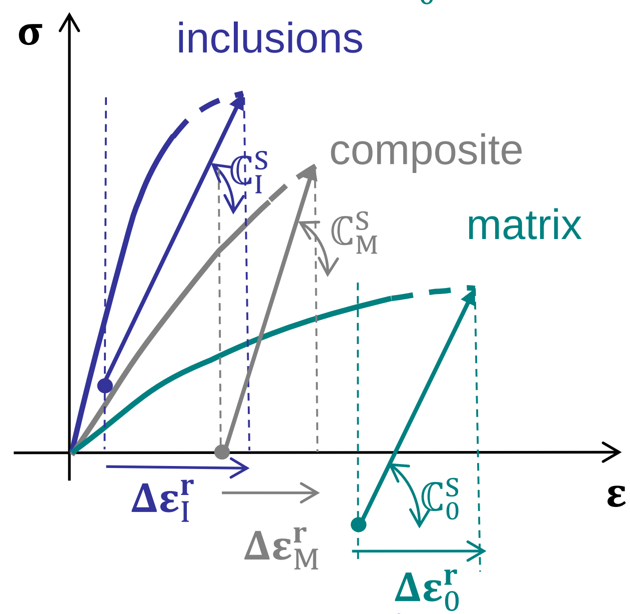

Bayesian identification of stochastic MFH model parameters

- Speed up the evaluation of the likelihood
  - Likelihood
    - $\pi(\hat{\sigma}_{\mathrm{M}}(t)|[\varepsilon_{\mathrm{M}}(t' \leq t), \boldsymbol{\vartheta}])$
    - With $\boldsymbol{\vartheta} = [E_0, \sigma_{Y_0}, h, m_1, m_2, a_r]$
    - 2-Step MFH model

      $\sigma_{\mathrm{MFH}}(t) = \sigma_{\mathrm{MFH}}\big(\mathrm{I}(\psi(\boldsymbol{p}), a_r), E_0$

      Too expensive for BI
  - Use of a surrogate
    - $\sigma_{\mathrm{NNW}}(t) = \sigma_{\mathrm{NNW}}\big(\boldsymbol{\varepsilon}_{\mathbf{M}}(t), \boldsymbol{\vartheta}, \mathbb{C}_{\mathrm{I}}\ ; \theta\big)$
    - Constructed using artificial Neural Network
    - Trained fusing the 2-Step MFH model

      $\sigma_{\mathrm{MFH}}(t) = \sigma_{\mathrm{MFH}}\big(\mathrm{I}(\psi(\boldsymbol{p}), a_r), E_0 , \quad \mathbb{C}_{\mathrm{I}}\ , \varepsilon_{\mathrm{M}}(t'$

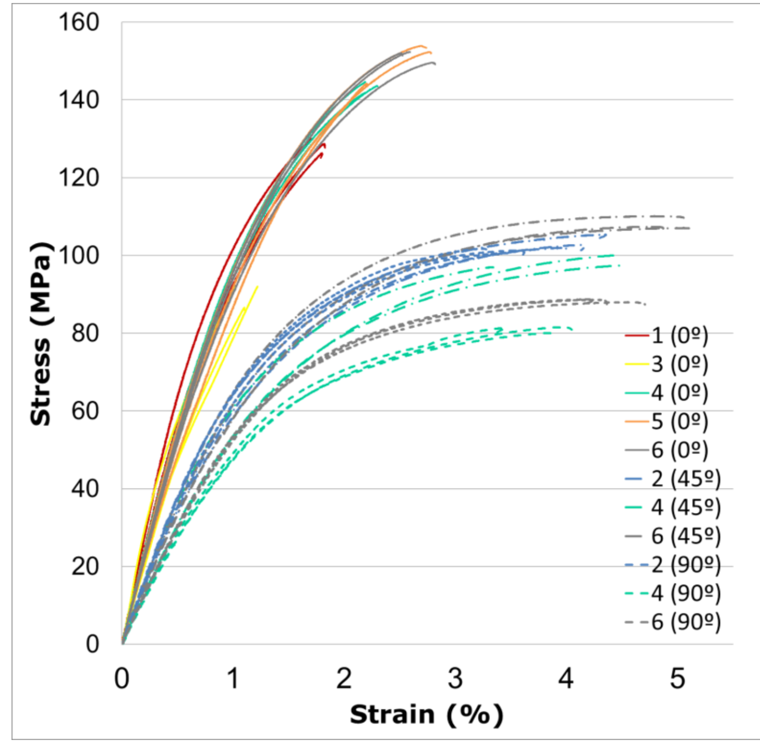

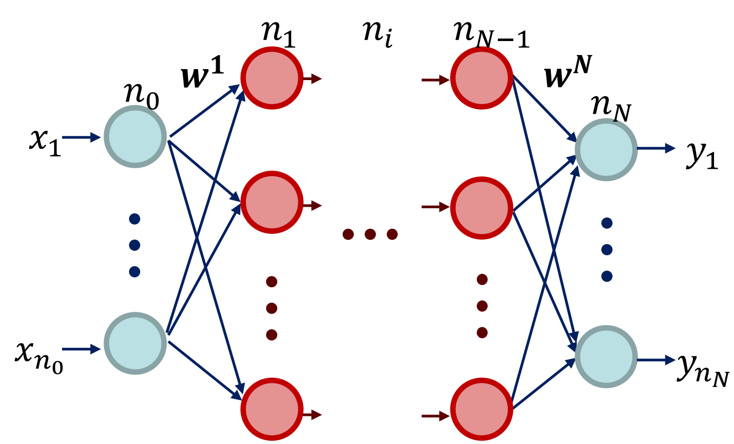

Bayesian identification of stochastic MFH model parameters

- Assume a noise in the measurements & use surrogate model
  - Measurements at strain i in direction θ_j:

$$\Sigma_c^{(i,j,k)} = \sigma_{\mathrm{NNW}}^{(i,j)}\left(\boldsymbol{\varepsilon}_{\mathbf{M}}^{(\boldsymbol{i},\boldsymbol{j})}, \boldsymbol{\vartheta}, \mathbb{C}_{\mathrm{I}}\ ; \theta_j\right) + \mathrm{noise}^{(i,j)}$$

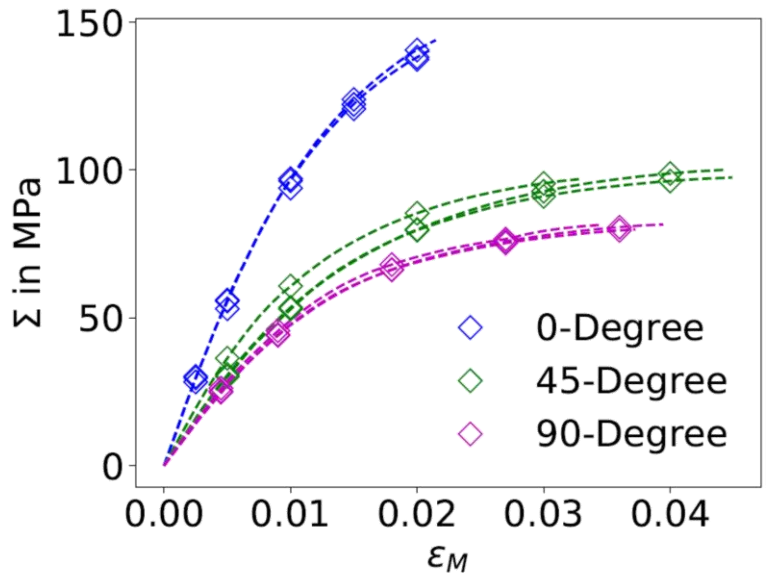

$$\pi\left(\Sigma_c^{(i,j,k)} \middle| \left[\boldsymbol{\varepsilon}_{\mathbf{M}}^{(\boldsymbol{i},\boldsymbol{j})}, \boldsymbol{\vartheta}\right]\right) = \pi_{\mathrm{noise}}^{(i,j)}\left(\Sigma_c^{(i,j,k)} - \sigma_{\mathrm{NNW}}^{(i,j)}\left(\boldsymbol{\varepsilon}_{\mathbf{M}}^{(\boldsymbol{i},\boldsymbol{j})}, \boldsymbol{\vartheta}, \mathbb{C}_{\mathrm{I}}\ ; \theta_j\right)\right)$$

- $j = 1..n_{\mathrm{dir}}$, with
  n_{dir} the number of directions θ_j tested
- $i = 1..n_{\varepsilon}^{(j)}$, with
  n_{ε} the number of stress-strain points
- $k = 1..n_{\mathrm{test}}^{(i,j)}$, with
  $n_{\mathrm{test}}^{(i,j)}$ the number of samples tested at point i along direction θ_j

  - Noise function from $n_{\mathrm{test},i,j}$ measurements at strain i in direction θ_j:

$$\pi_{\mathrm{noise}^{(i,j)}}(y) = \frac{1}{\sqrt{2\pi}\,\sigma_{\Sigma_c^{(i,j)}}} \exp\left(-\frac{y^2}{2\sigma^2_{\Sigma_c^{(i,j)}}}\right)$$

  - Bayes' theory:

$$\pi_{\mathrm{post}}\left(\boldsymbol{\vartheta} \middle| \hat{\boldsymbol{\varepsilon}}_{\mathbf{M}}, \hat{\boldsymbol{\Sigma}}_{\mathrm{c}}\ \right) \propto \pi_{\mathrm{prior}}(\boldsymbol{\vartheta})\ \prod_{j=1}^{n_{\mathrm{dir}}} \prod_{i=1}^{n_{\varepsilon}^{(j)}} \prod_{k=1}^{n_{\mathrm{test}}^{(i,j)}} \pi_{\mathrm{noise}}^{(i,j)}\left(\Sigma_c^{(i,j,k)} - \sigma_{\mathrm{NNW}}^{(i,j)}\left(\boldsymbol{\varepsilon}_{\mathbf{M}}^{(\boldsymbol{i},\boldsymbol{j})}, \boldsymbol{\vartheta}, \mathbb{C}_{\mathrm{I}}\ ; \theta_j\right)\right)$$

- Results

$$\pi_{\text{post}}\left(\boldsymbol{\vartheta}|\hat{\boldsymbol{\varepsilon}}_{\mathbf{M}},\hat{\boldsymbol{\Sigma}}_{\text{c}}\right) \propto \pi_{\text{prior}}(\boldsymbol{\vartheta}) \prod_{j=1}^{n_{\text{dir}}} \prod_{i=1}^{n_{\varepsilon}^{(j)}} \prod_{k=1}^{n_{\text{test}}^{(i,j)}} \pi_{\text{noise}}^{(i,j)}\left(\Sigma_{c}^{(i,j,k)} - \sigma_{\text{NNW}}^{(i,j)}\left(\boldsymbol{\varepsilon}_{\mathbf{M}}^{(\boldsymbol{i},\boldsymbol{j})},\boldsymbol{\vartheta},\mathbb{C}_{\text{I}}\ ;\theta_j\right)\right)$$

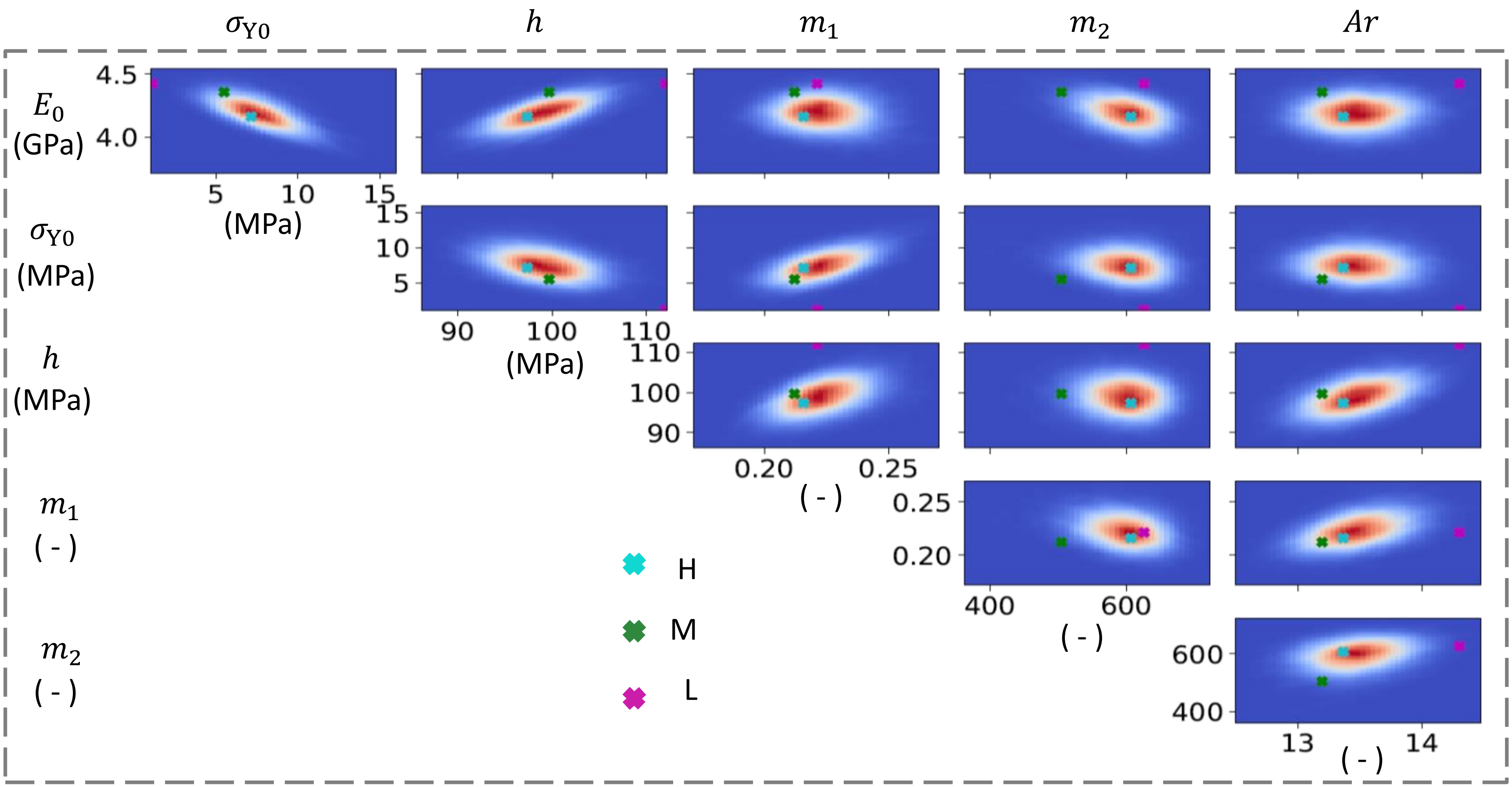

Beginning

- Verification

$$\pi_{\mathrm{post}}\left(\boldsymbol{\vartheta}|\hat{\boldsymbol{\varepsilon}}_{\mathbf{M}},\widehat{\boldsymbol{\Sigma}}_{\mathrm{c}}\right) \propto \pi_{\mathrm{prior}}(\boldsymbol{\vartheta}) \prod_{j=1}^{n_{\mathrm{dir}}} \prod_{i=1}^{n_{\varepsilon}^{(j)}} \prod_{k=1}^{n_{\mathrm{test}}^{(i,j)}} \pi_{\mathrm{noise}}^{(i,j)}\left(\Sigma_c^{(i,j,k)} - \sigma_{\mathrm{NNW}}^{(i,j)}\left(\boldsymbol{\varepsilon}_{\mathbf{M}}^{(\boldsymbol{i},\boldsymbol{j})},\boldsymbol{\vartheta},\mathbb{C}_{\mathrm{I}}\ ;\theta_j\right)\right)$$

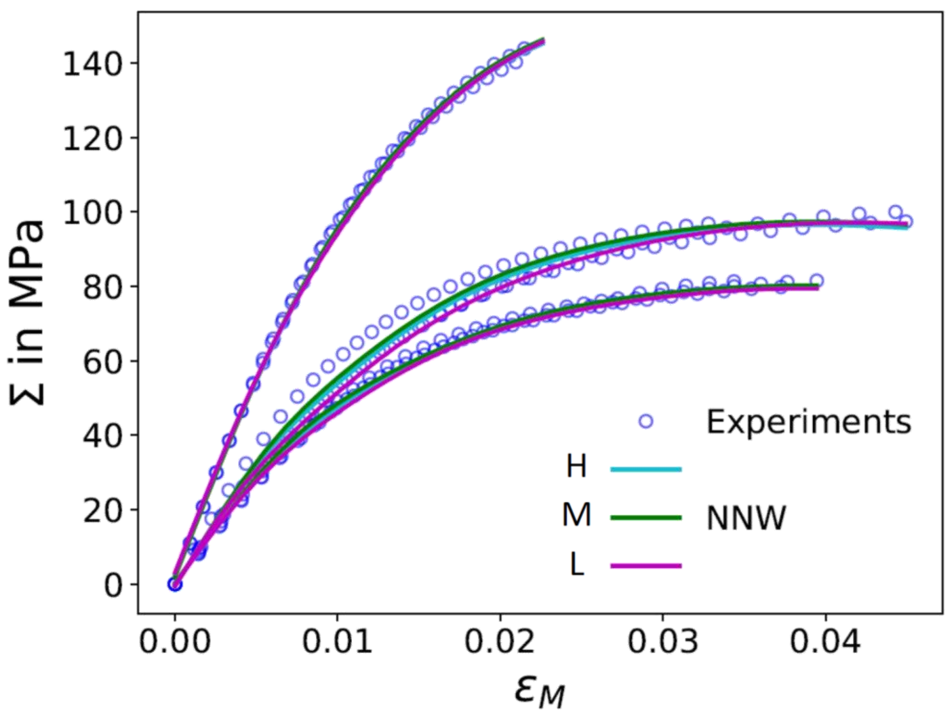

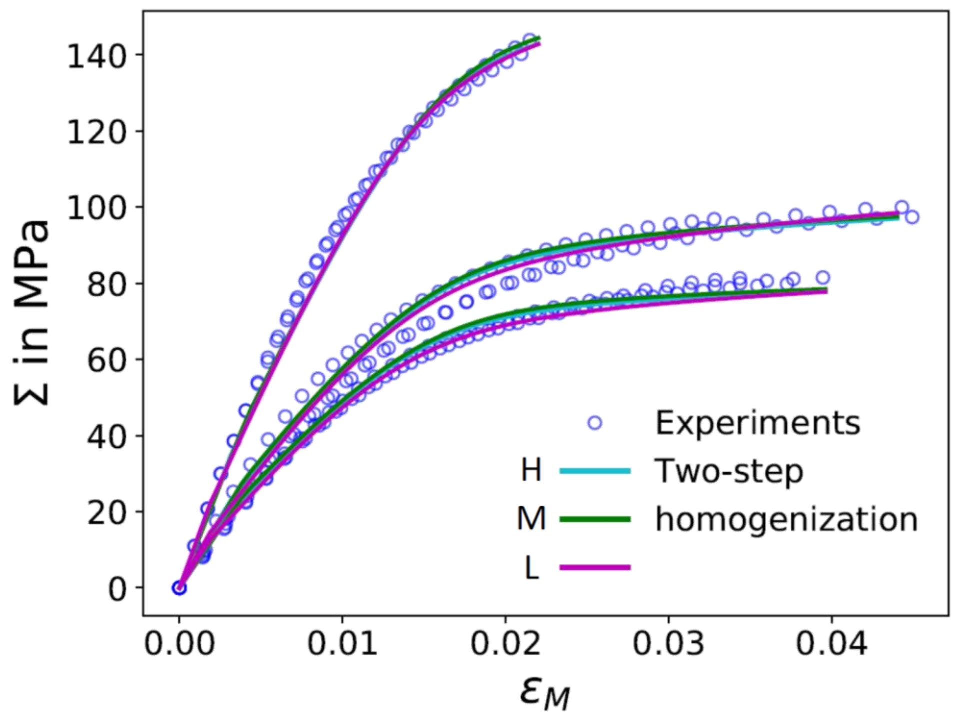

Bayesian identification of stochastic MFH model parameters

- STOMMMAC M.ERA-NET project (MFH for elasto-visco-plastic composites)
  - e-Xstream, ULiège (Belgium)
  - BATZ (Spain)
  - JKU, AC (Austria)
  - U Luxembourg (Luxemburg)

- Publications (doi)
  - 10.1016/j.cma.2019.112693 data on 10.5281/zenodo.3740410
  - 10.1016/j.compstruct.2019.03.066

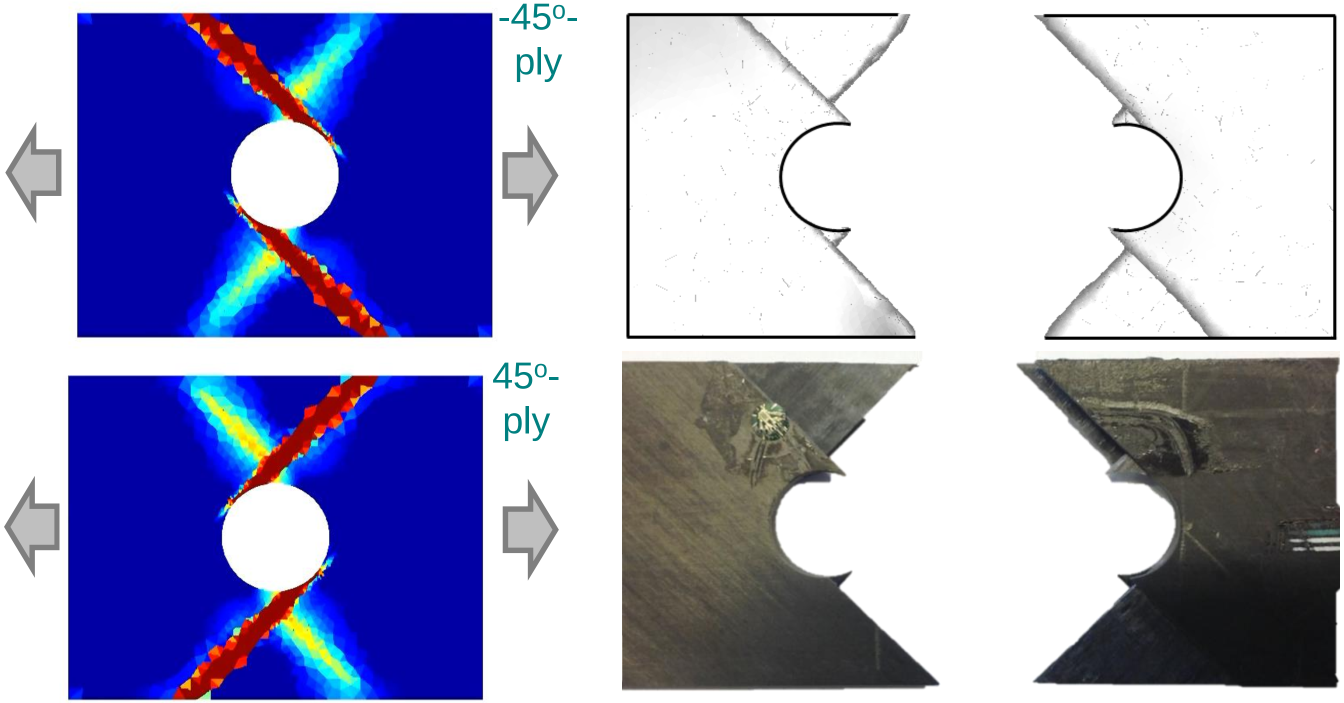

Non-Local Damage & Phase-Field Enhanced Mean-Field-Homogenization

SIMUCOMP The research has been funded by the Walloon Region under the agreement no 1017232 (CT-EUC 2010-10-12) in the context of the ERA-NET +, Matera + framework.

Non-Local Damage Mean-Field-Homogenization

- Multi-scale modeling
  - 2 problems are solved concurrently
    - The macro-scale problem
    - The meso-scale problem (on a meso-scale Volume Element)

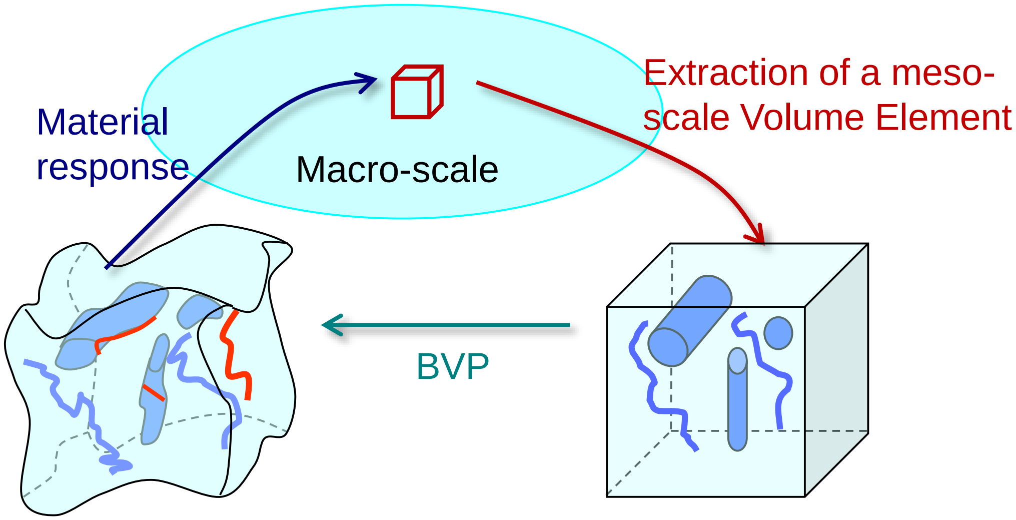

- Length-scales separation

$$L_{macro} >> L_{VE} >> L_{micro}$$

For accuracy: Size of the meso-scale volume element smaller than the characteristic length of the macro-scale loading

To be statistically representative: Size of the meso-scale volume element larger than the characteristic length of the micro-structure

- Materials with strain softening
  - Incremental forms
    - Strain increments in the same direction

$$\Delta\boldsymbol{\varepsilon}_{\mathrm{I}} = \mathbf{B}^{\varepsilon}\left(\mathrm{I}, \bar{\mathbf{C}}_0^{\mathrm{alg}}, \bar{\mathbf{C}}_{\mathrm{I}}^{\mathrm{alg}}\right) : \Delta\boldsymbol{\varepsilon}_0$$

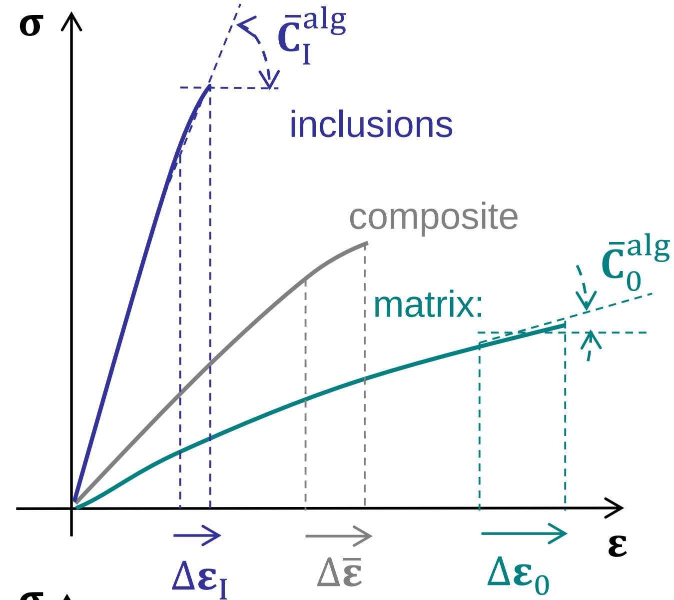

  - Because of the damaging process, the fiber phase is elastically unloaded during matrix softening

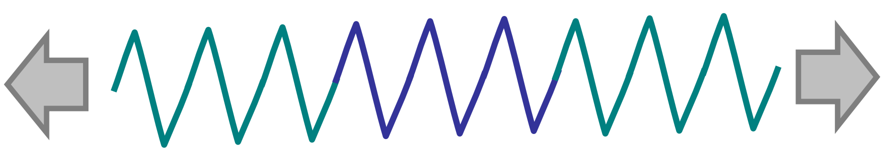

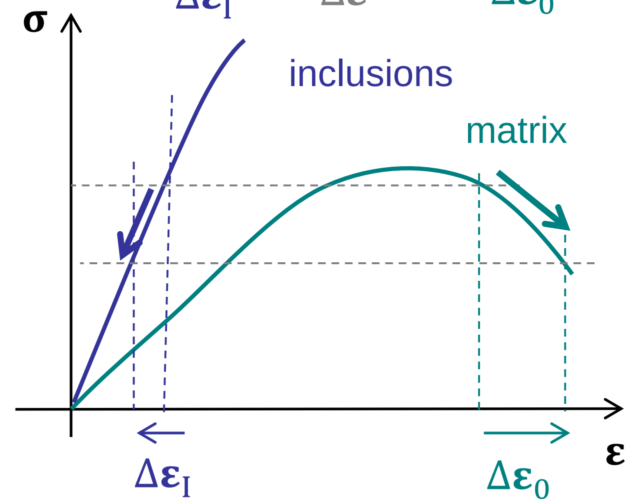

- Solution: new incremental-secant method
  - We need to define the LCC from another stress state

- Based on the incremental-secant approach
  - Perform a virtual elastic unloading from previous solution
    - Composite material unloaded to reach the stress-free state
    - Residual stress in components
  - Apply MFH from unloaded state
    - New strain increments (>0)

$$\Delta\boldsymbol{\varepsilon}^{\mathrm{r}}_{\mathrm{I}/0} = \Delta\boldsymbol{\varepsilon}_{\mathrm{I}/0} + \Delta\boldsymbol{\varepsilon}^{\mathrm{unload}}_{\mathrm{I}/0}$$

    - Use of secant operators

$$\Delta\boldsymbol{\varepsilon}^{\mathrm{r}}_{\mathrm{I}} = \mathbf{B}^{\varepsilon}\left(\mathrm{I},(1-D)\bar{\mathbf{C}}^{\mathrm{Sr}}_{0},\bar{\mathbf{C}}^{\mathrm{S0}}_{\mathrm{I}}\right):\Delta\boldsymbol{\varepsilon}^{\mathrm{r}}_{0}$$

    - Possibility of unloading

$$\begin{cases} \Delta\boldsymbol{\varepsilon}^{\mathrm{r}}_{\mathrm{I}} > \mathbf{0} \\ \Delta\boldsymbol{\varepsilon}_{\mathrm{I}} \ \ < \mathbf{0} \end{cases}$$

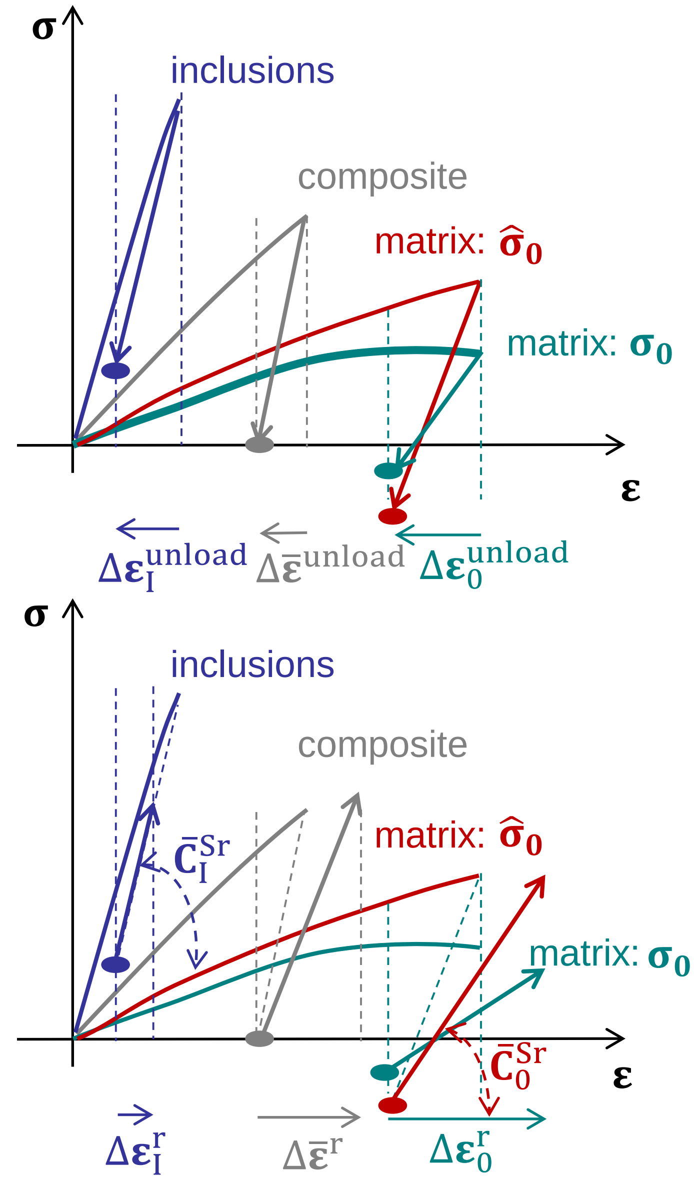

- New results for damage
  - Fictitious composite
    - 50%-UD fibres
  - Elasto-plastic matrix with damage

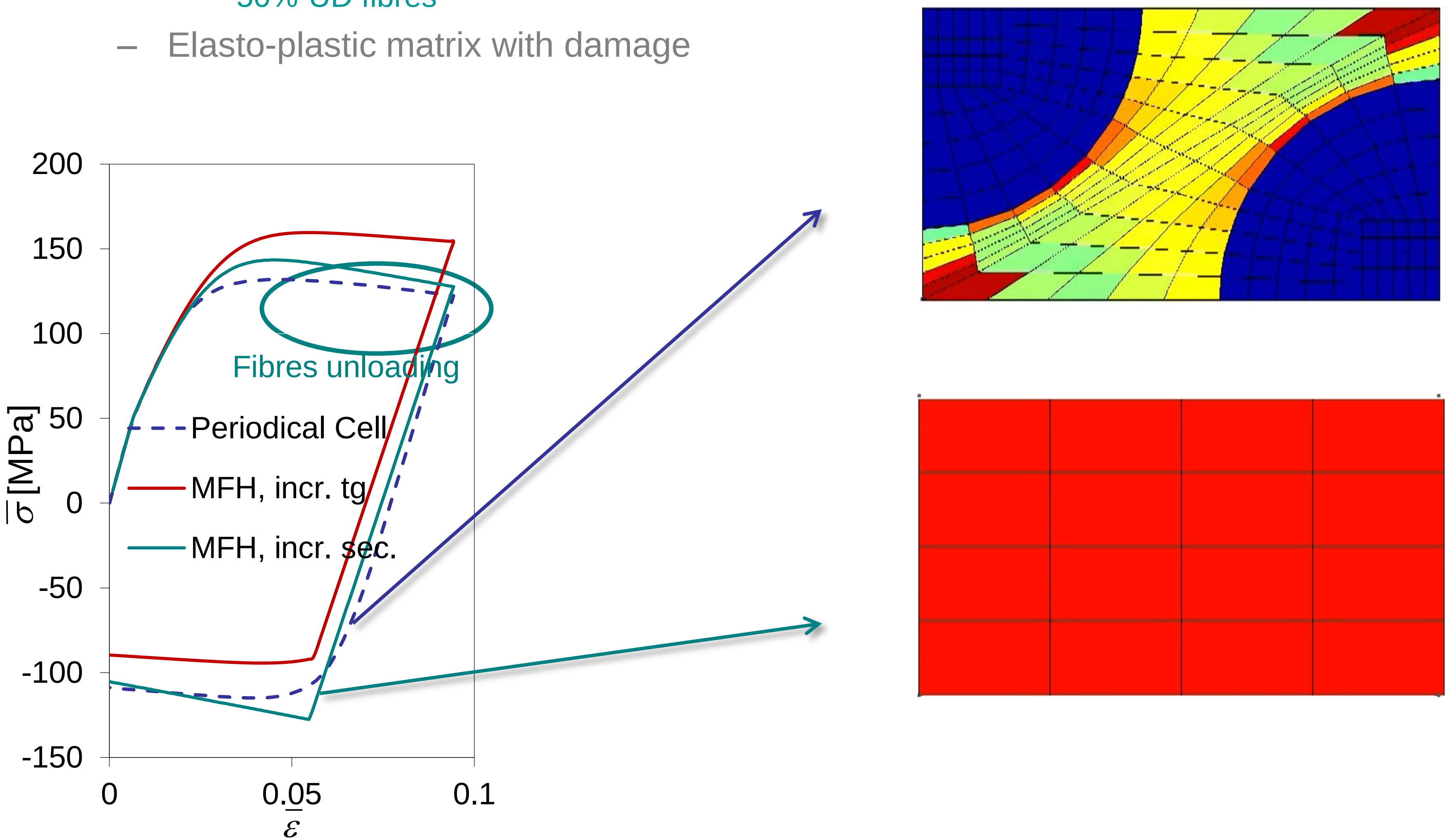

- Material models
  - Elasto-plastic material
    - Stress tensor $\boldsymbol{\sigma} = \mathbf{C}^{\mathrm{el}} : (\boldsymbol{\varepsilon} - \boldsymbol{\varepsilon}^{\mathrm{pl}})$
    - Yield surface $f(\boldsymbol{\sigma}, p) = \boldsymbol{\sigma}^{\mathrm{eq}} - \sigma^{Y} - R(p) \leq 0$
    - Plastic flow $\Delta\boldsymbol{\varepsilon}^{\mathbf{pl}} = \Delta p \mathbf{N}$ & $\mathbf{N} = \frac{\partial f}{\partial \boldsymbol{\sigma}}$
  - Local damage model
    - Apparent-effective stress tensors $\boldsymbol{\sigma} = (1 - D)\hat{\boldsymbol{\sigma}}$
    - Plastic flow in the effective stress space
    - Damage evolution $\Delta D = F_D(\boldsymbol{\varepsilon}, \Delta p)$
  - Non-Local damage model [Peerlings et al., 1996]
    - Damage evolution $\Delta D = F_D(\boldsymbol{\varepsilon}, \Delta \tilde{p})$
    - Anisotropic governing equation $\tilde{p} - \nabla \cdot \left(\mathbf{c}_{\mathrm{g}} \cdot \nabla \tilde{p}\right) = p$

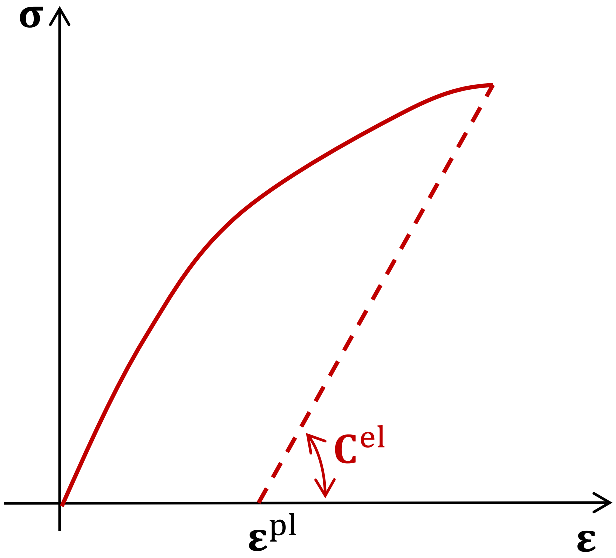

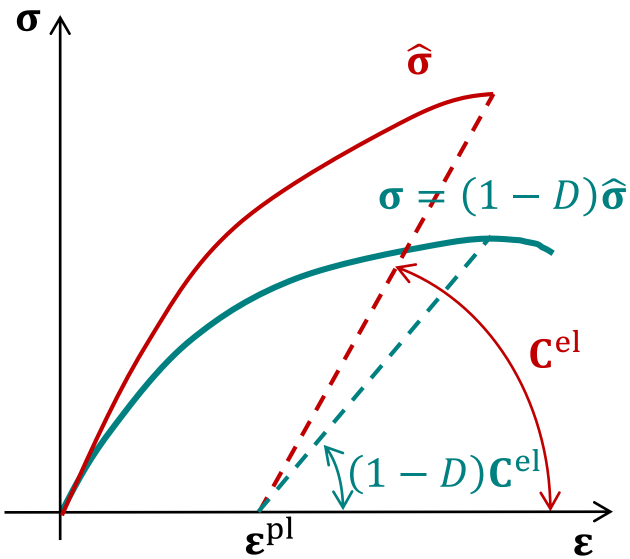

- Laminate studies
  - Bulk material law
    - Non-local damage-enhanced MFH
    - Intra-laminar failure
    - Account for anisotropy
  - Interface
    - DG/Cohesive zone model
    - Inter-laminar failure

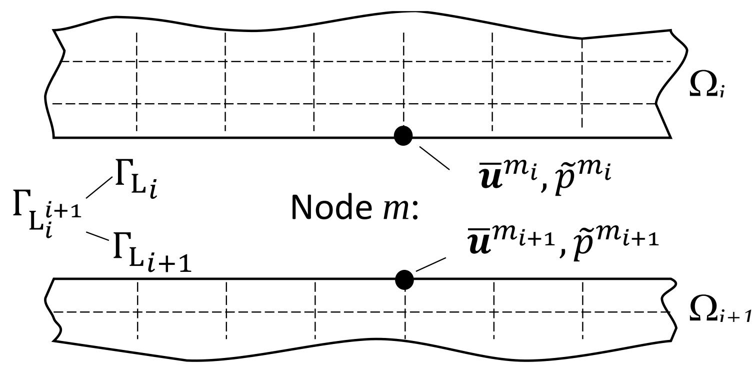

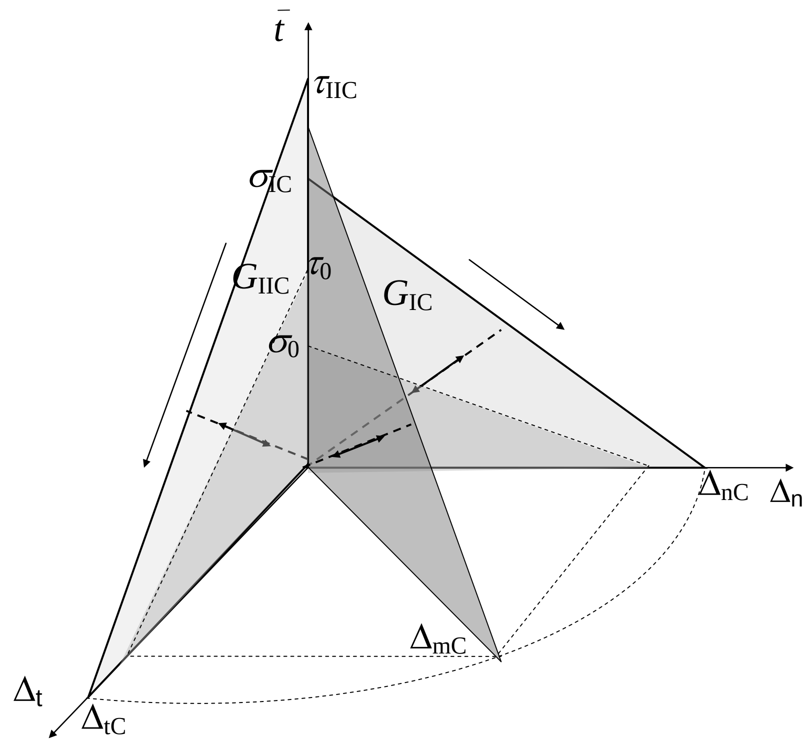

Non-Local Damage Mean-Field-Homogenization

- $[45^o{}_4 / -45^o{}_4]_S$- open hole laminate (epoxy- with 60% UD CF)

Intra-laminar failure along fiber directions

Inter-laminar failure matches experimental results

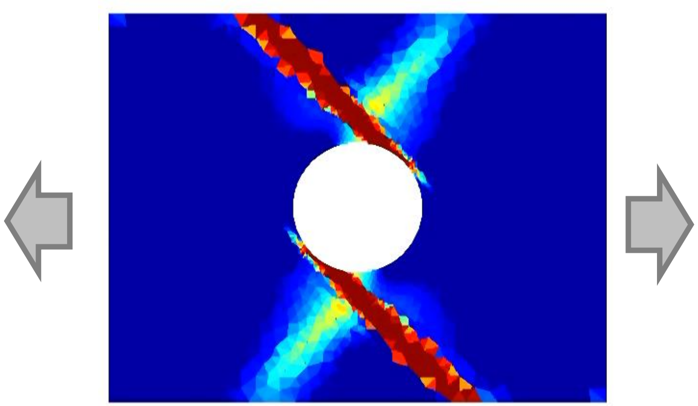

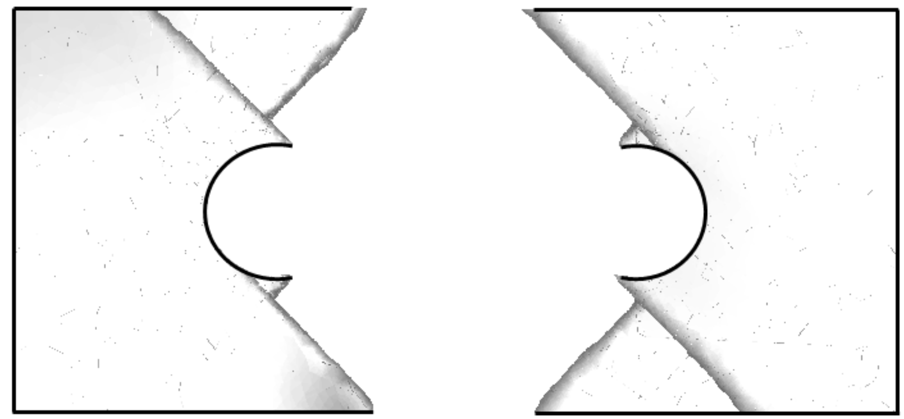

-45o-ply

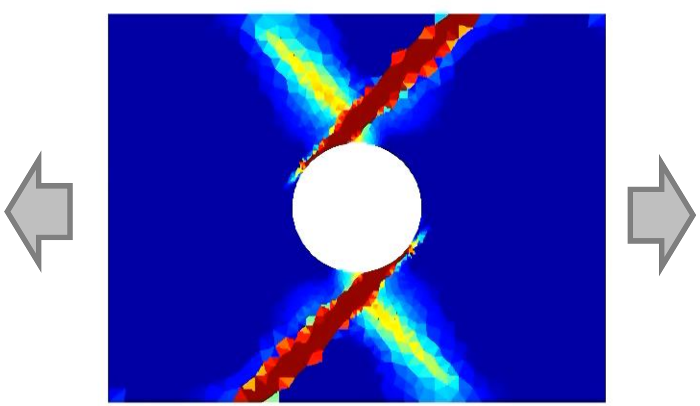

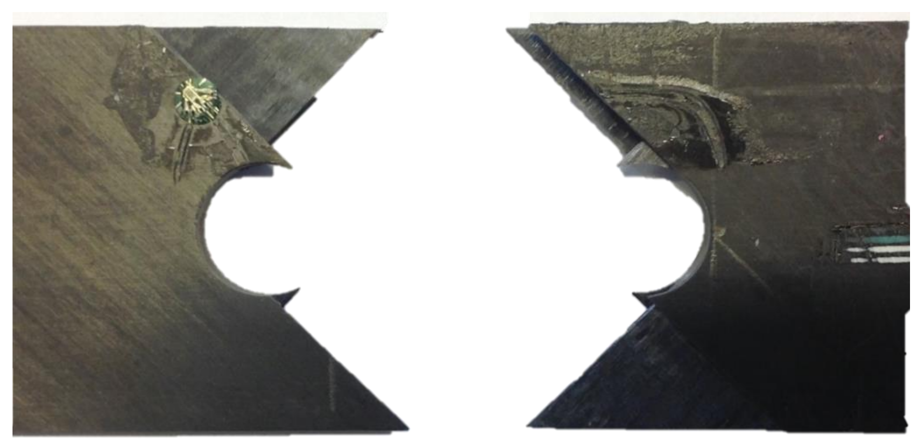

45o-ply

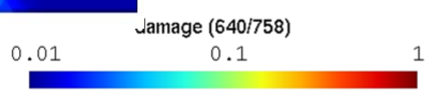

Non-Local Damage Mean-Field-Homogenization

- $[90^o / 45^o / -45^o / 90^o / 0^o]_S$- open hole laminate
  - Intra-laminar failure along fiber directions (experiments: IMDEA Materials)

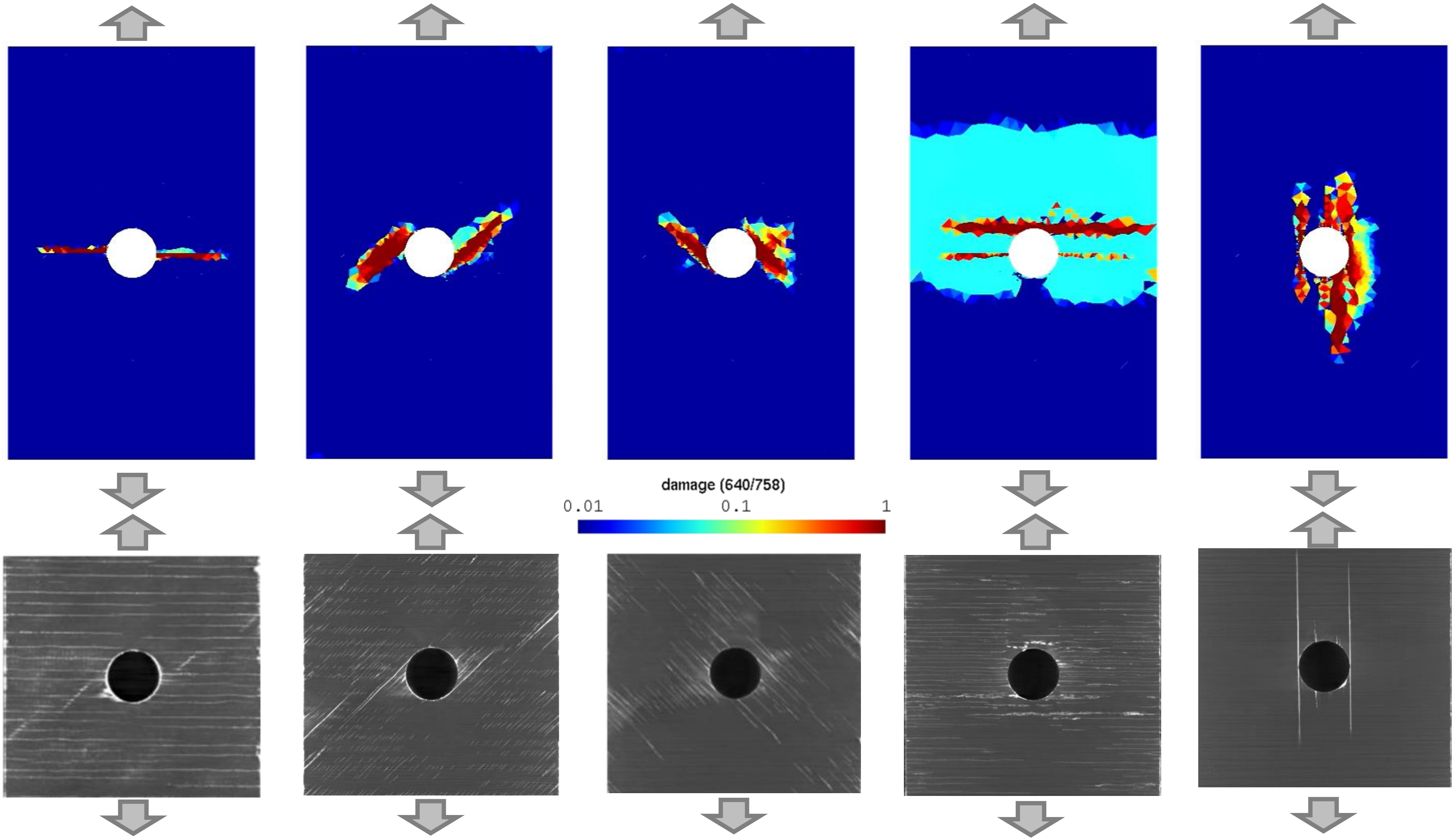

90º-ply (out) 45º-ply -45º-ply 90º-ply (in) 0º-ply

Non-Local Damage Mean-Field-Homogenization

- $[90^o / 45^o / -45^o / 90^o / 0^o]_S$- open hole laminate
  - Inter-laminar failure compared to experimental results (experiments: IMDEA Materials)

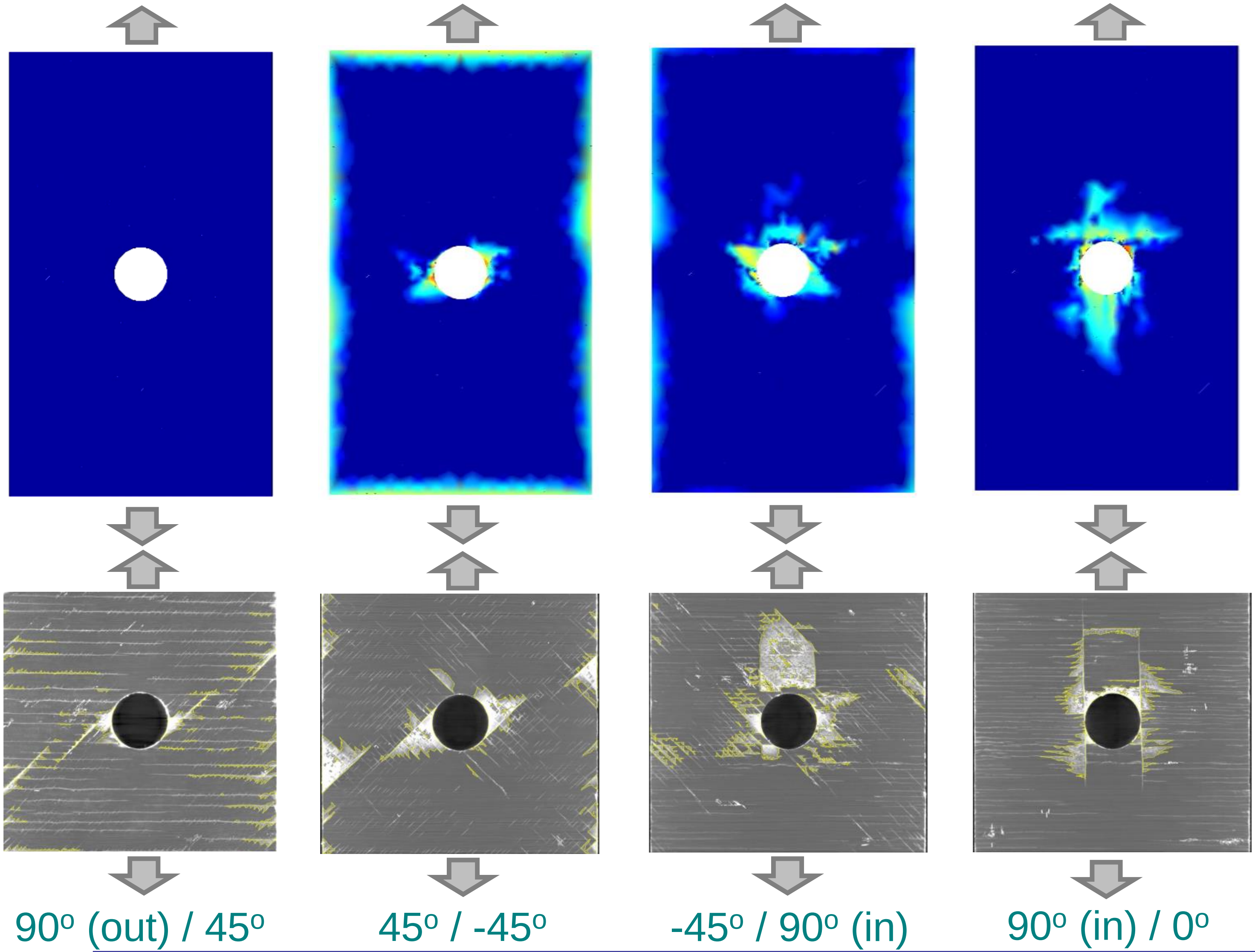

Non-Local Damage Mean-Field-Homogenization

- SIMUCOMP ERA-NET project
  - e-Xstream, CENAERO, ULiège (Belgium), IMDEA Materials (Spain), CRP Henri-Tudor (Luxemburg)
- Publications (doi)
  - 10.1016/j.compstruct.2015.02.070
  - 10.1016/j.ijsolstr.2013.07.022
  - 10.1016/j.ijplas.2013.06.006
  - 10.1016/j.cma.2012.04.011
  - 10.1007/978-1-4614-4553-1_13

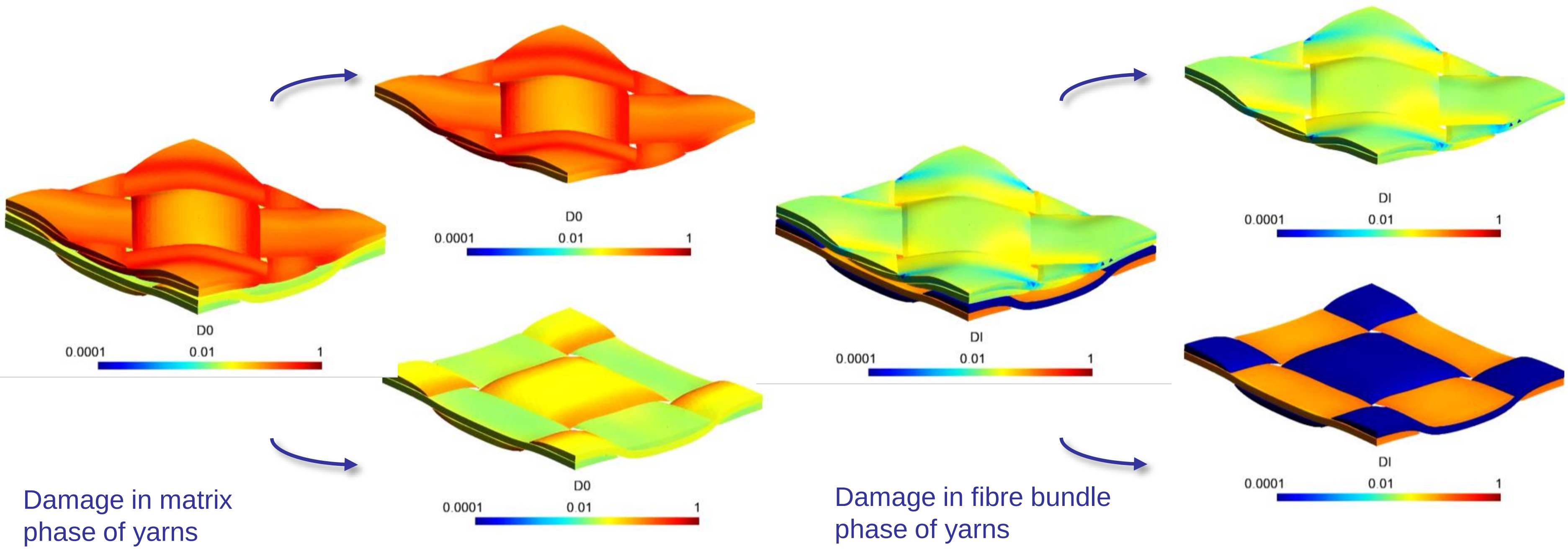

Non-Local Damage & Phase-Field Enhanced Mean-Field-Homogenization

The research has been funded by the Walloon Region under the agreement no.7911-VISCOS in the context of the 21st SKYWIN call.

LIÈGE université

- Probabilistic damage model of fibre bundle
  - Failure probability for one fibre of length L at stress σ

$$P(\sigma, L) = 1.0 - \exp\left\{-\left(\frac{L}{L_0}\right)^{\alpha}\left(\frac{\sigma}{\sigma_0}\right)^{m}\right\}$$

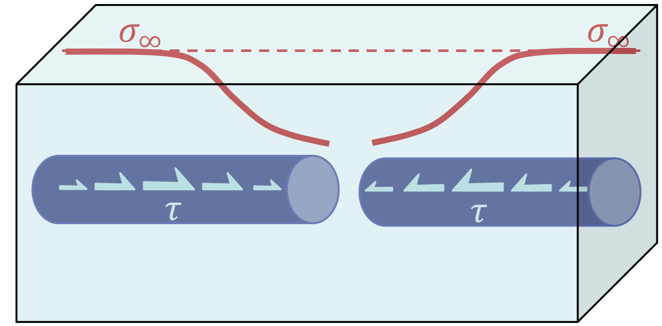

  - Damage of bundle: failure of k fibres of a bundle of N fibres

$$\left.\begin{aligned} D &= \frac{k}{N} \\ \hat{\sigma} &= \frac{\sigma}{(1-D)} \end{aligned}\right\} \Rightarrow \left\{\begin{aligned} &P(D|\hat{\sigma}, L) \approx N\left(p, \frac{p(1-p)}{N}\right) \\ &p = P(\hat{\sigma}\,; L) \end{aligned}\right.$$

  - Length effect

$$\left.\begin{aligned} \sigma(x) &= \sigma_\infty\left(1 - \exp\left(-\frac{|x|}{cl}\right)\right)^n \\ \tau &= \frac{r}{2}\frac{\mathrm{d}\sigma}{\mathrm{d}x} \end{aligned}\right\} \Rightarrow \left\{\begin{aligned} &L \text{ such that} \\ &\sigma(L) = 0.99\,\sigma_\infty \end{aligned}\right.$$

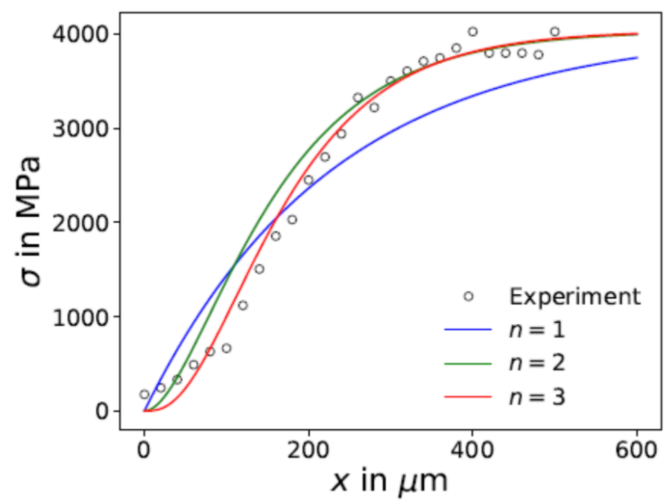

- Phase-field damage model of fibre bundle
  - Stress σ build up from failure

$$\sigma(x) = \sigma_\infty \left(1 - \exp\left(-\frac{|x|}{cl}\right)\right)^n$$

  - Definition of an auxiliary damage variable

$$d_{\mathrm{I}}(x) = \exp\left(-\frac{|x|}{cl}\right) \Rightarrow D_{\mathrm{I}}(x) = 1.0 - [1 - d_{\mathrm{I}}(x)]^n$$

  - Auxiliary governing equation in terms of fracture energy G_{IC}

$$d_{\mathrm{I}} - cl^2 \nabla^2 d_I - \frac{cl}{G_{IC}} = -\frac{cl}{G_{Ic}} \frac{\partial \psi_{\mathrm{I}}^+}{\partial d_{\mathrm{I}}}$$

  - Material law

$$\psi(\boldsymbol{\varepsilon}, D_{\mathrm{I}}) = \frac{1}{2} \varepsilon : \mathbb{C}_{\mathrm{I}}^{\mathrm{el\ D}}(D_{\mathrm{I}}) \Rightarrow \boldsymbol{\sigma} = \frac{\partial \psi}{\partial \boldsymbol{\varepsilon}}$$

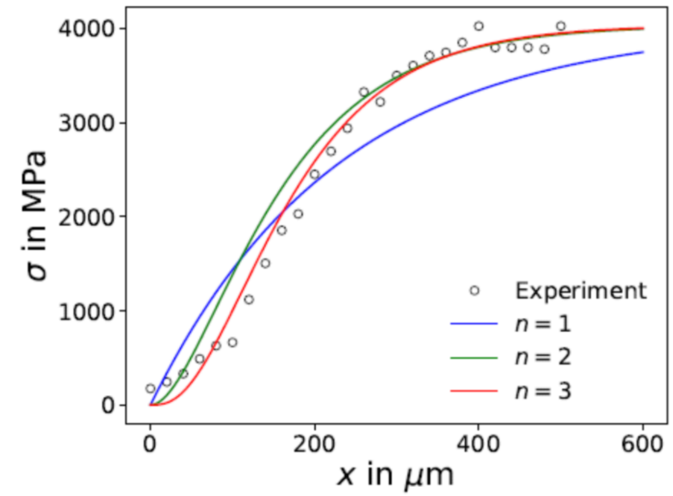

- Damage transverse isotropic model
  - Material law

$$\psi(\boldsymbol{\varepsilon}, D_{\mathrm{I}}) = \frac{1}{2}\varepsilon : \mathbb{C}_{\mathrm{I}}^{\mathrm{el\,D}}(D_{\mathrm{I}}) \qquad \boldsymbol{\sigma} = \frac{\partial \psi}{\partial \boldsymbol{\varepsilon}}$$

$$\begin{cases} \nu_{\mathrm{I}}^{\mathrm{LT\,D}} = (1 - D_{\mathrm{I}})\nu_{\mathrm{I}}^{\mathrm{LT}} \\ E_{\mathrm{I}}^{\mathrm{L\,D}} = (1 - D_{\mathrm{I}})E_{\mathrm{I}}^{\mathrm{L}} \end{cases}$$

$$\mathbb{C}_{\mathrm{I}}^{\mathrm{LCC}} = \mathbb{C}_{\mathrm{I}}^{\mathrm{el\,D}} = \left[\begin{array}{ccc|ccc} \frac{E_{\mathrm{I}}^{\mathrm{T}}\left(1-\nu_{\mathrm{I}}^{\mathrm{LT\,D}}\nu_{\mathrm{I}}^{\mathrm{TL}}\right)}{\Delta^{\mathrm{D}}} & \frac{E_{\mathrm{I}}^{\mathrm{T}}\left(\nu_{\mathrm{I}}^{\mathrm{TT}}+\nu_{\mathrm{I}}^{\mathrm{LT\,D}}\nu_{\mathrm{I}}^{\mathrm{TL}}\right)}{\Delta^{\mathrm{D}}} & \frac{E_{\mathrm{I}}^{\mathrm{T}}\left(\nu_{\mathrm{I}}^{\mathrm{LT\,D}}+\nu_{\mathrm{I}}^{\mathrm{TT}}\nu_{\mathrm{I}}^{\mathrm{LT\,D}}\right)}{\Delta^{\mathrm{D}}} & & & \\ \mathrm{Sim} & \Delta^{\mathrm{D}} & \frac{E_{\mathrm{I}}^{\mathrm{T}}\left(\nu_{\mathrm{I}}^{\mathrm{LT\,D}}+\nu_{\mathrm{I}}^{\mathrm{TT}}\nu_{\mathrm{I}}^{\mathrm{LT\,D}}\right)}{\Delta} & & 0 & \\ \mathrm{Sim} & \mathrm{Sim} & \frac{E_{\mathrm{I}}^{\mathrm{L\,D}}\left(1-\nu_{\mathrm{I}}^{\mathrm{TT}}\nu_{\mathrm{I}}^{\mathrm{TT}}\right)}{\Delta^{\mathrm{D}}} & & & \\ \hline & & & 2\mu_{\mathrm{I}}^{\mathrm{LT}} & 0 & 0 \\ & 0 & & 0 & 2\mu_{\mathrm{I}}^{\mathrm{LT}} & 0 \\ & & & 0 & 0 & \frac{E_{\mathrm{I}}^{\mathrm{T}}}{1+\nu_{\mathrm{I}}^{\mathrm{TT}}} \end{array}\right]$$

- Matrix damage model for MFH
  - Lemaitre Chaboche

$$\dot{D}_{0=}\left(\frac{\psi}{S_0}\right)^{s_0}\dot{\chi},\ \text{for}\ (\chi - p_{C0})\dot{\chi} > 0$$

$$\psi = \frac{1}{2}\boldsymbol{\varepsilon} : \mathbb{C}_0^{\mathrm{el}} : \boldsymbol{\varepsilon}$$

  - Saturated damage

$$D_{0=}D_{\max_0}\left(\frac{1}{1+\exp(-\beta_0(\chi-p_{c0}))} - \frac{1}{1+\exp(\beta_0 p_{c0})}\right)\frac{1}{1-\frac{1}{1+\exp(\beta_0 p_{c0})}},$$

for $\dot{\chi} > 0.$

  - Anisotropic non-local form

$$\begin{cases} \chi = \max_t \tilde{p}_0(t) \\ \tilde{p}_0 - \nabla\cdot\left(\boldsymbol{c}_g \cdot \nabla\tilde{p}_0\right) = p_0 \end{cases}$$

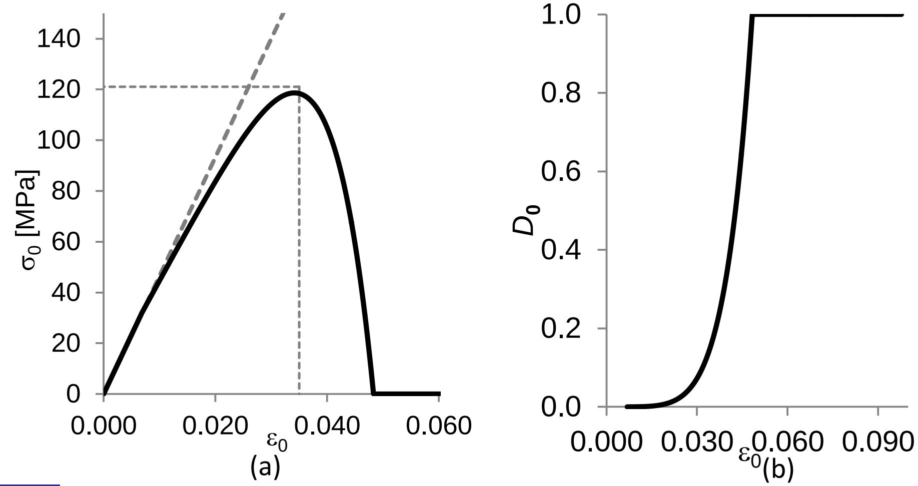

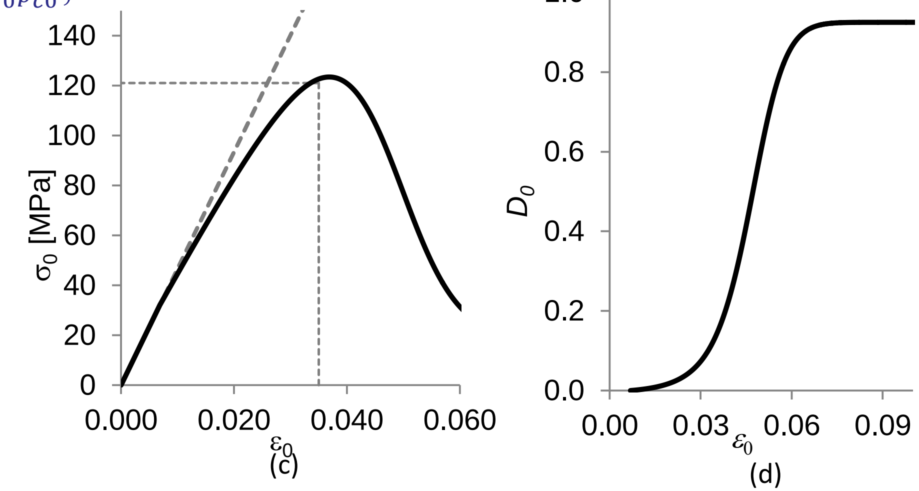

- MFH with matrix and fibre bundle damage models
  - Incremental-secant MFH
    - Unloading step

$$\Delta\boldsymbol{\sigma}_0 = -\mathbb{C}_0^{\mathrm{el\,D}} : \Delta\boldsymbol{\varepsilon}_0^{\mathbf{unload}}$$

$$\Delta\boldsymbol{\sigma}_\mathrm{I} = -\mathbb{C}_\mathrm{I}^{\mathrm{el\,D}} : \Delta\boldsymbol{\varepsilon}_\mathrm{I}^{\mathbf{unload}}$$

$$\Delta\boldsymbol{\varepsilon}_\mathrm{I}^{\mathbf{unload}} = \mathbb{B}^{\epsilon}\left(\mathrm{I}, \mathbb{C}_0^{\mathrm{elD}}, \mathbb{C}_\mathrm{I}^{\mathrm{elD}}\right) : \Delta\boldsymbol{\varepsilon}_0^{\mathbf{unload}}$$

    - Followed by reloading

$$\Delta\boldsymbol{\varepsilon}_\mathrm{I}^\mathrm{r} = \mathbf{B}^{\varepsilon}\left(\mathrm{I}, \mathbb{C}_0^{\mathrm{SD}}, \mathbb{C}_\mathrm{I}^{\mathrm{Sr}}\right) : \Delta\boldsymbol{\varepsilon}_0^\mathrm{r}$$

$$\Delta\boldsymbol{\varepsilon}_{\mathrm{I}/0}^\mathrm{r} = \Delta\boldsymbol{\varepsilon}_{\mathrm{I}/0} + \Delta\boldsymbol{\varepsilon}_{\mathrm{I}/0}^{\mathrm{unload}}$$

$$\begin{cases} \Delta\boldsymbol{\varepsilon}_\mathrm{I}^\mathrm{r} > \mathbf{0} \\ \Delta\boldsymbol{\varepsilon}_\mathbf{I} < \mathbf{0} \end{cases}$$

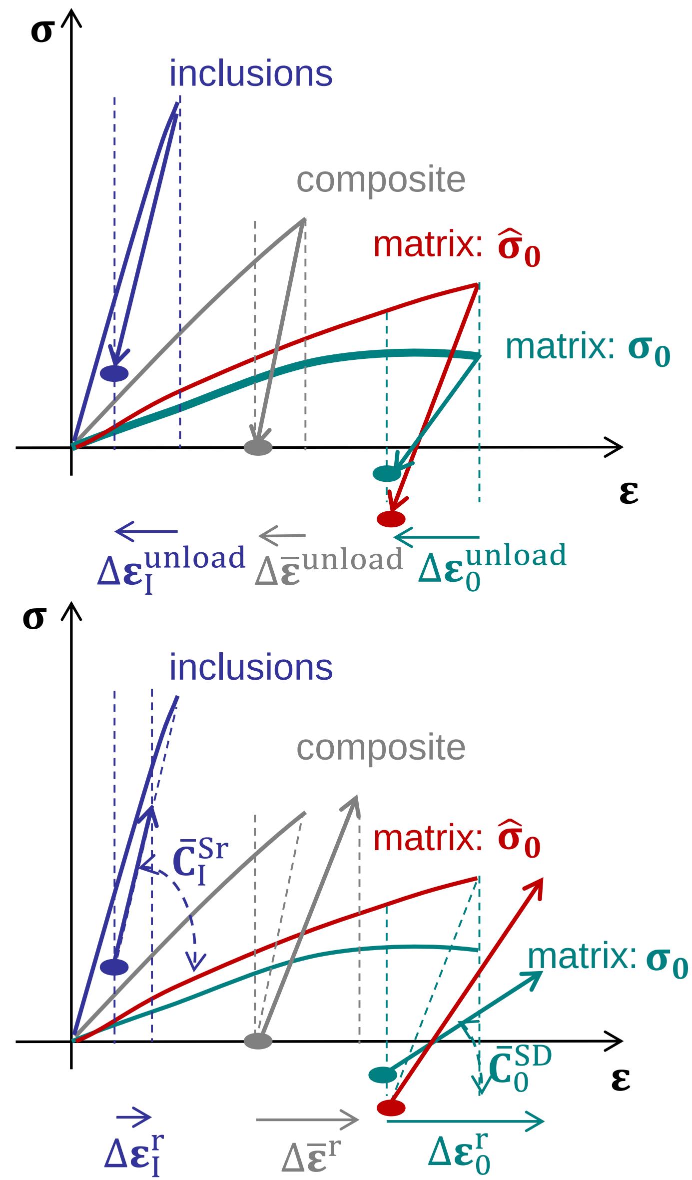

Non-Local Damage & Phase-Field Mean-Field-Homogenization

- MFH with matrix and fibre bundle damage models
  - Incremental-secant MFH
    - Damage in matrix

$$\left\{\begin{array}{l} \hat{\boldsymbol{\sigma}}_0 - \hat{\boldsymbol{\sigma}}_0^{\mathrm{res}} = \bar{\mathbb{C}}_0^{\mathrm{S}} : \Delta\boldsymbol{\varepsilon}_0^{\mathrm{r}} \\ \text{or } \hat{\boldsymbol{\sigma}}_0 = \bar{\mathbb{C}}_0^{\mathrm{S0}} : \Delta\boldsymbol{\varepsilon}_0^{\mathrm{r}} \\ \bar{\mathbb{C}}_0^{\mathrm{LCC}} = \bar{\mathbb{C}}_0^{\mathrm{SD}} = (1 - D_0)\bar{\mathbb{C}}_0^{\mathrm{S}} \end{array}\right.$$

    - Damage in Fibre bundle

$$\left\{\begin{array}{l} \hat{\boldsymbol{\sigma}}_{\mathrm{I}} - \hat{\boldsymbol{\sigma}}_{\mathrm{I}}^{\mathrm{res}} = \bar{\mathbb{C}}_{\mathrm{I}}^{\mathrm{S}} : \Delta\boldsymbol{\varepsilon}_I^{\mathrm{r}} \\ \bar{\mathbb{C}}_{\mathrm{I}}^{\mathrm{LCC}} = \bar{\mathbb{C}}_{\mathrm{I}}^{\mathrm{SD}} = \bar{\mathbb{C}}_{\mathrm{I}}^{\mathrm{el\,D}}(D_{\mathrm{I}}) \end{array}\right.$$

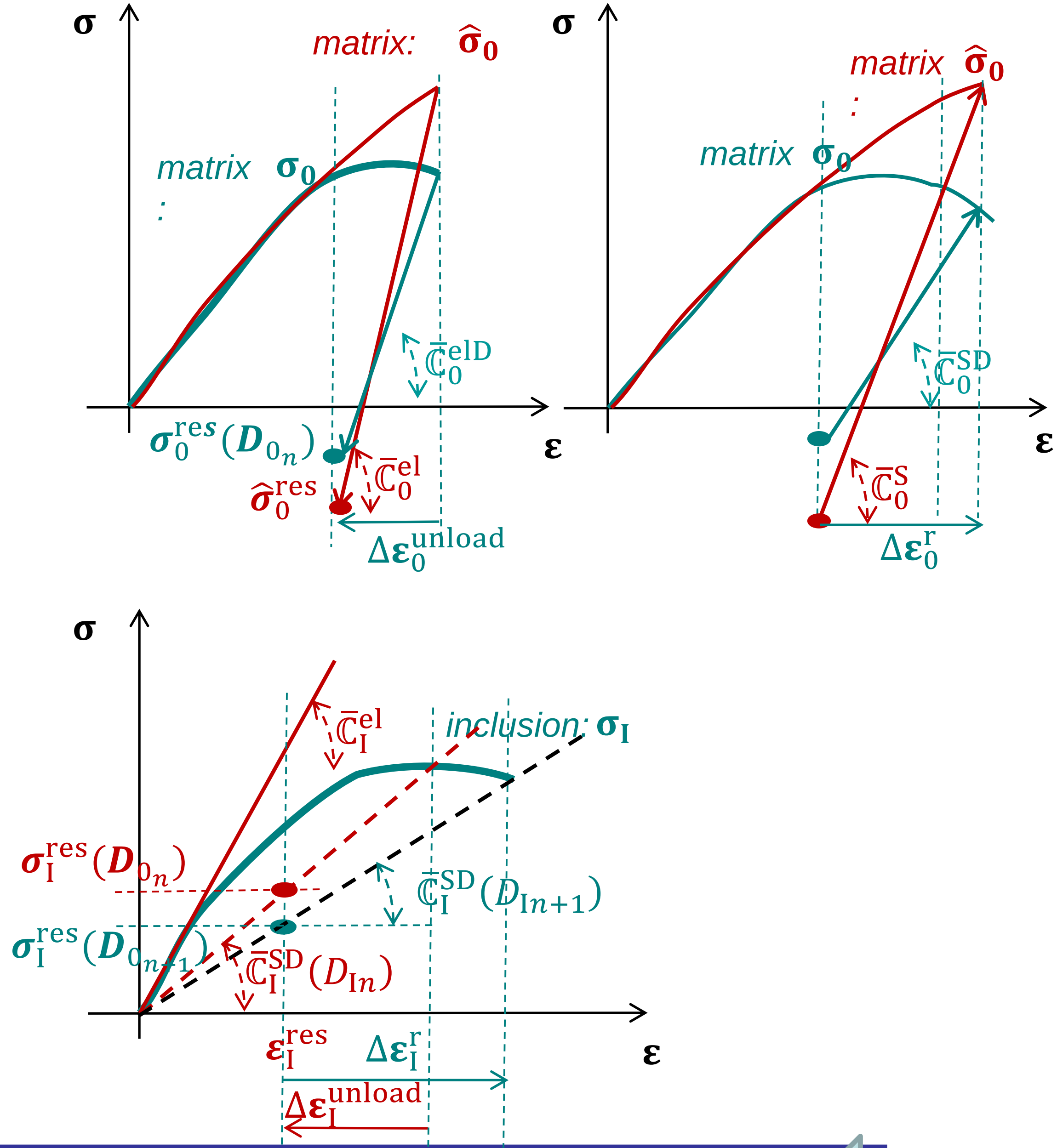

- Test of Phase-Field formulation
  - Axial loading on composite

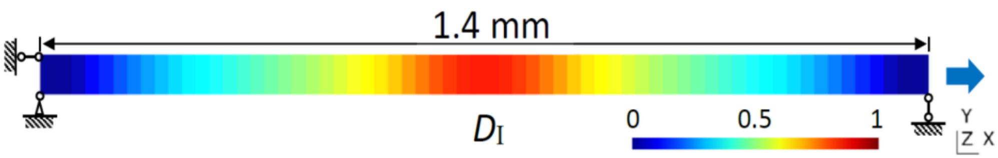

(a) Damage in fibres, configuration 1

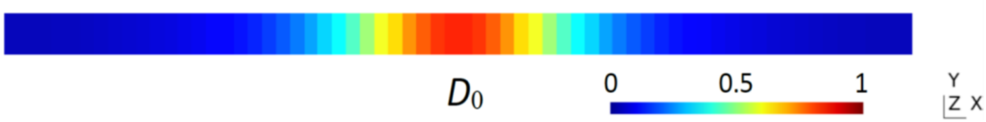

(b) Damage in matrix, configuration 1

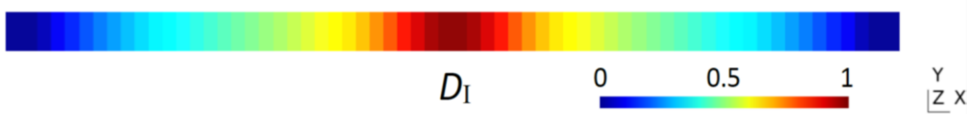

(c) Damage in fibres, configuration 2

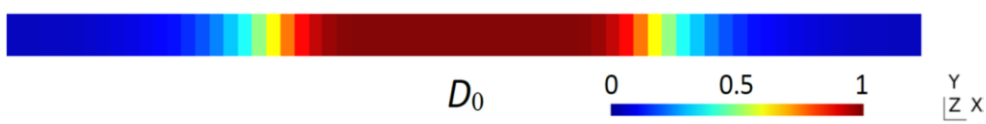

(d) Damage in matrix, configuration 2

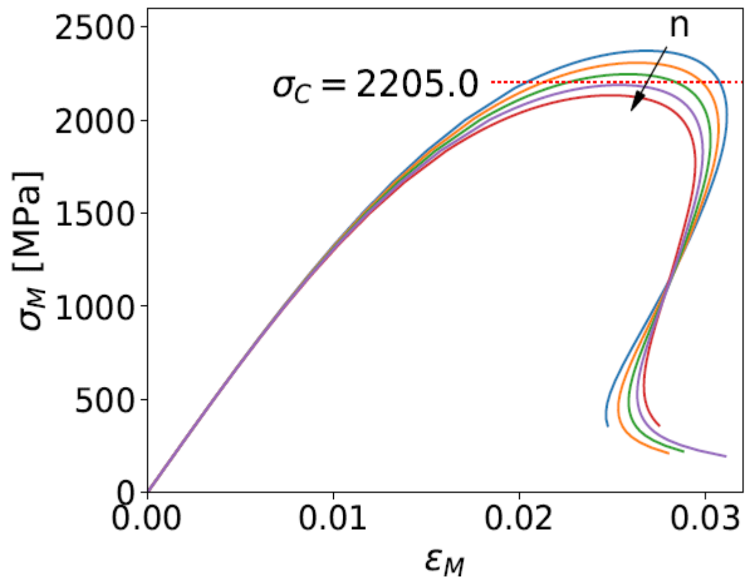

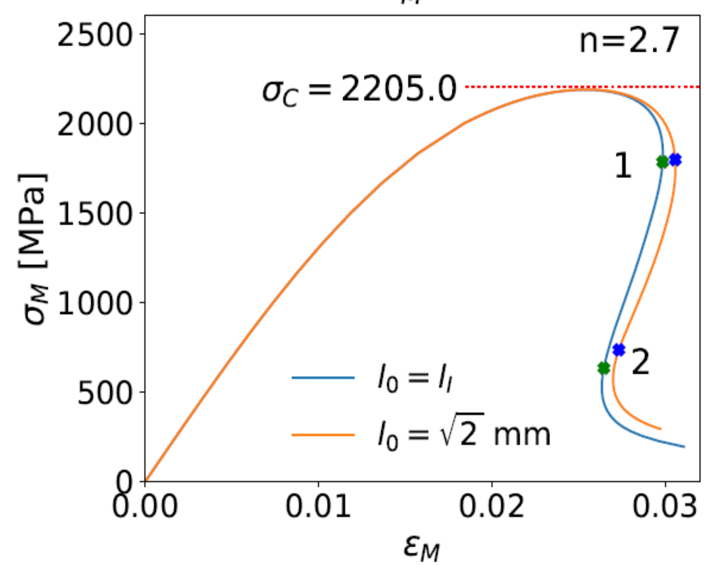

Non-Local Damage & Phase-Field Mean-Field-Homogenization

- Laminate study
  - AS4/8552 – Notched Specimen

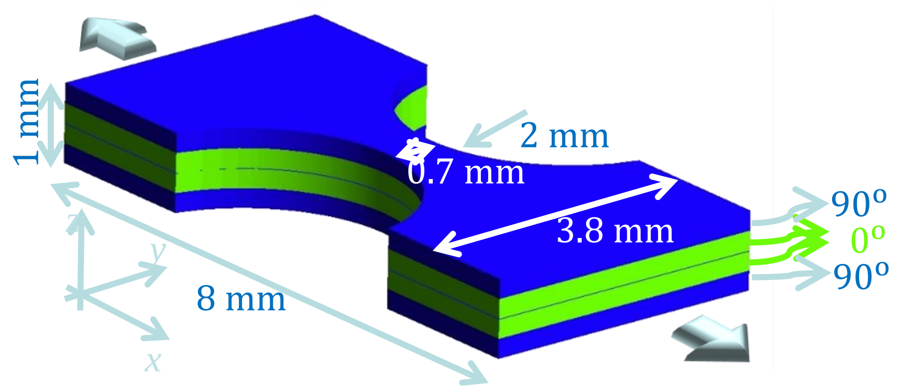

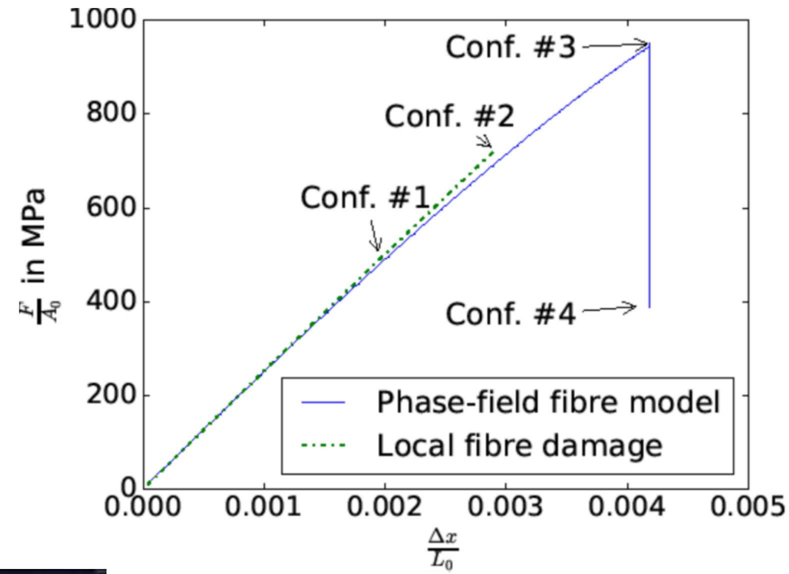

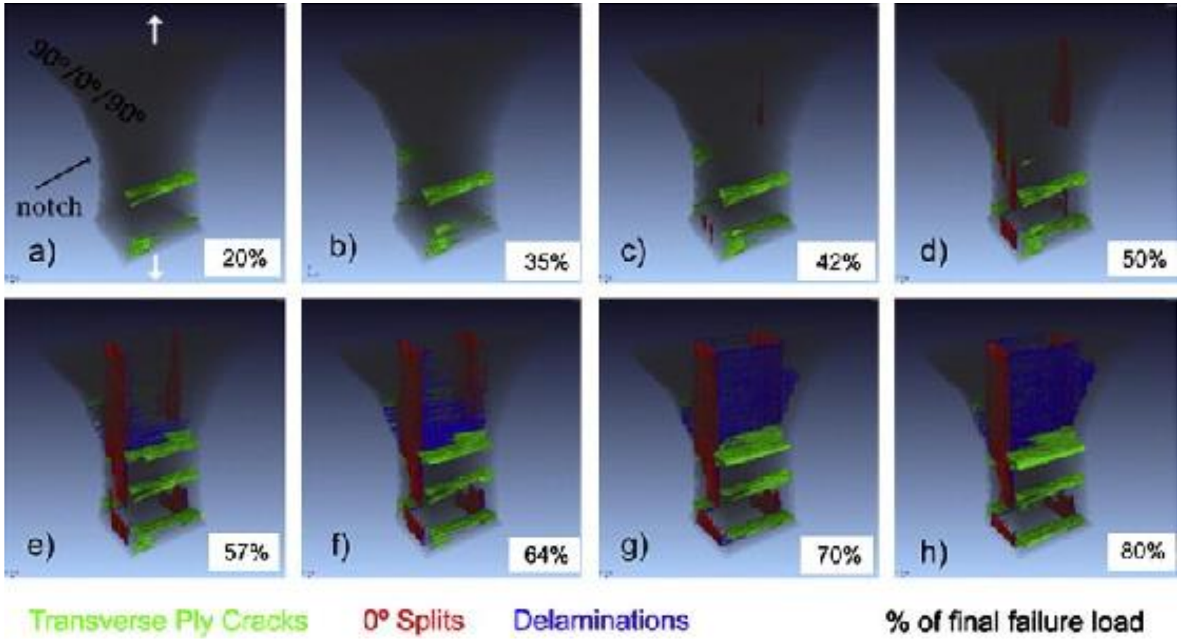

Composites Science and Technology, 71/12, A.E. Scott and M. Mavrogordato and P. Wright and I. Sinclair and S.M. Spearing, In situ fibre fracture measurement in carbonepoxy laminates using high resolution computed tomography, 1471-1477, 2011

- Laminate study
  - AS4/8552 – Notched Specimen: Configuration 1

Local fibre damage

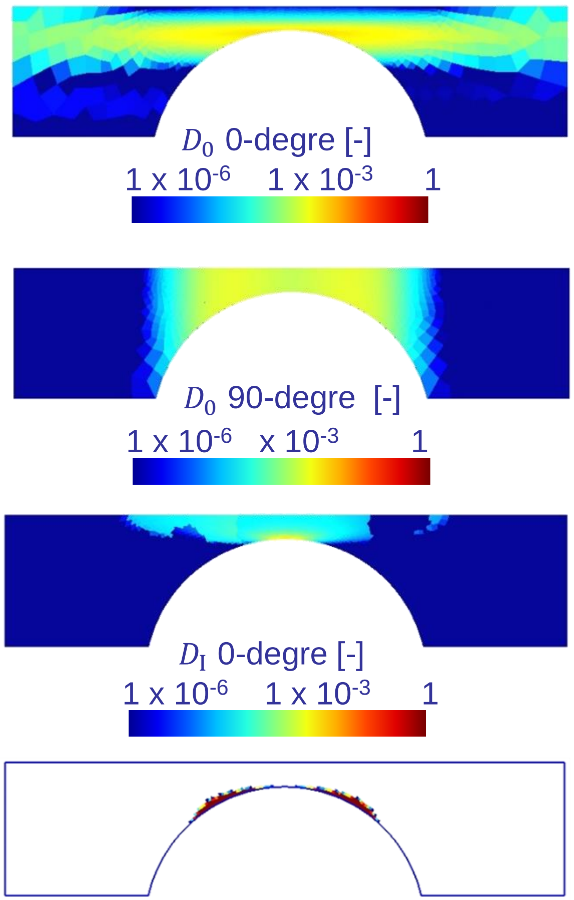

Active delamination

Phase-field fibre damage

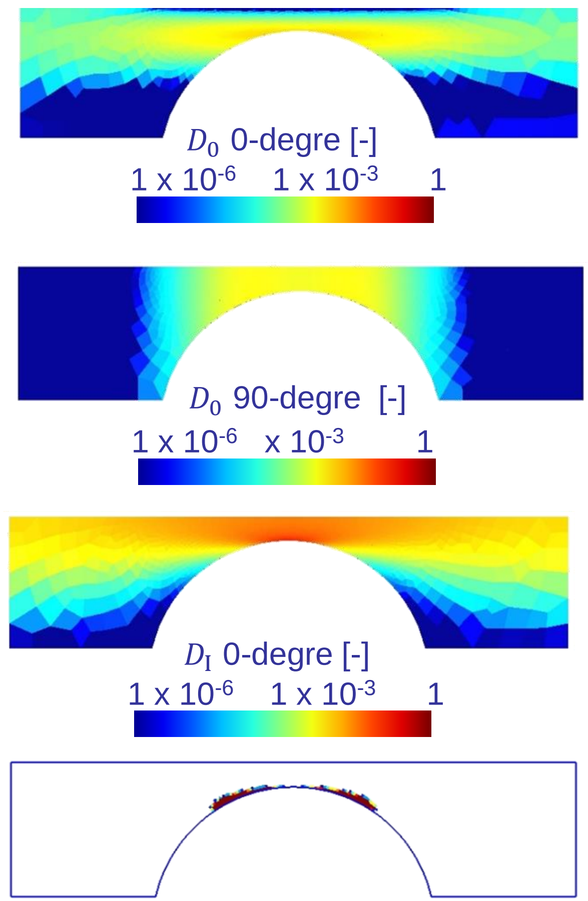

Active delamination

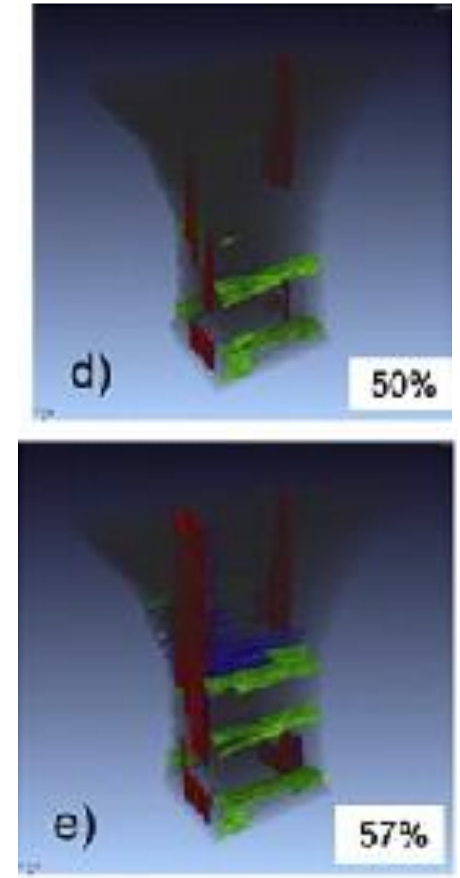

Composites Science and Technology, 71/12, A.E. Scott and M. Mavrogordato and P. Wright and I. Sinclair and S.M. Spearing, In situ fibre fracture measurement in carbonepoxy laminates using high resolution computed tomography, 1471-1477, 2011

Non-Local Damage & Phase-Field Mean-Field-Homogenization

- Laminate study
  - AS4/8552 – Notched Specimen: Configuration 2

Local fibre damage

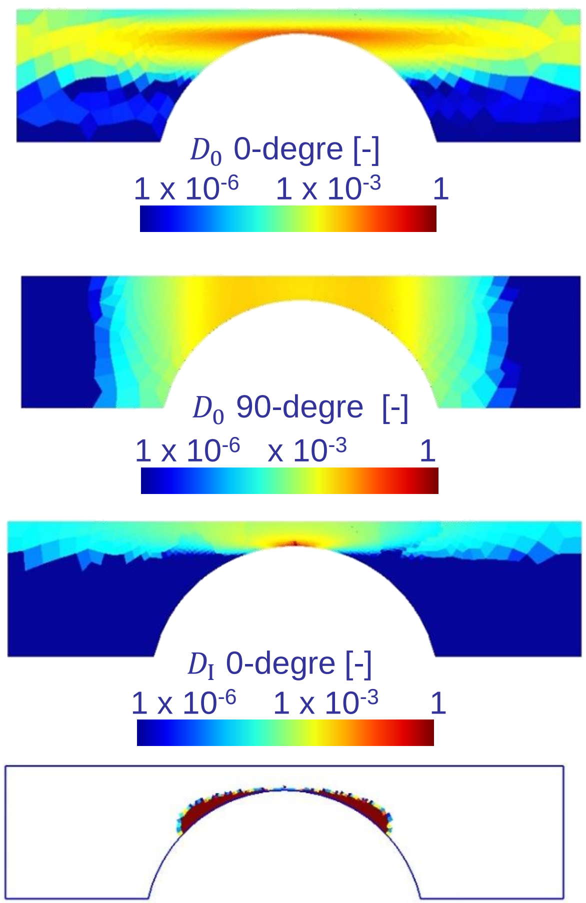

Active delamination

Phase-field fibre damage

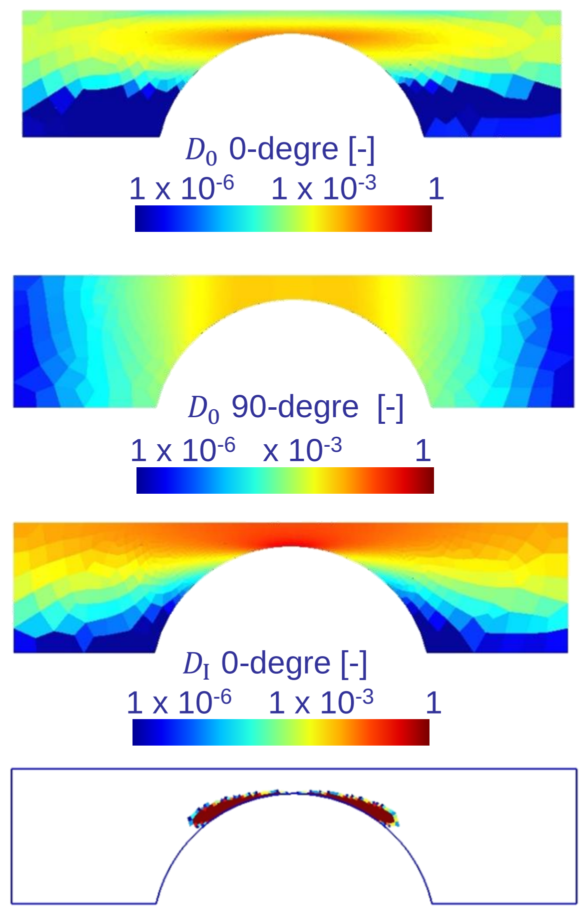

Active delamination

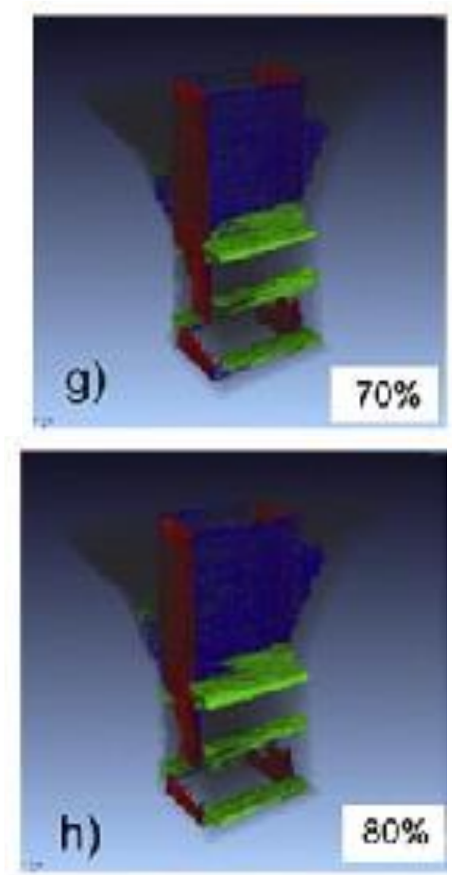

Composites Science and Technology, 71/12, A.E. Scott and M. Mavrogordato and P. Wright and I. Sinclair and S.M. Spearing, In situ fibre fracture measurement in carbonepoxy laminates using high resolution computed tomography, 1471-1477, 2011

Non-Local Damage & Phase-Field Mean-Field-Homogenization

- Laminate study
  - AS4/8552 – Notched Specimen: Configuration 3 & Configuration 4

Phase-field fibre damage, #3

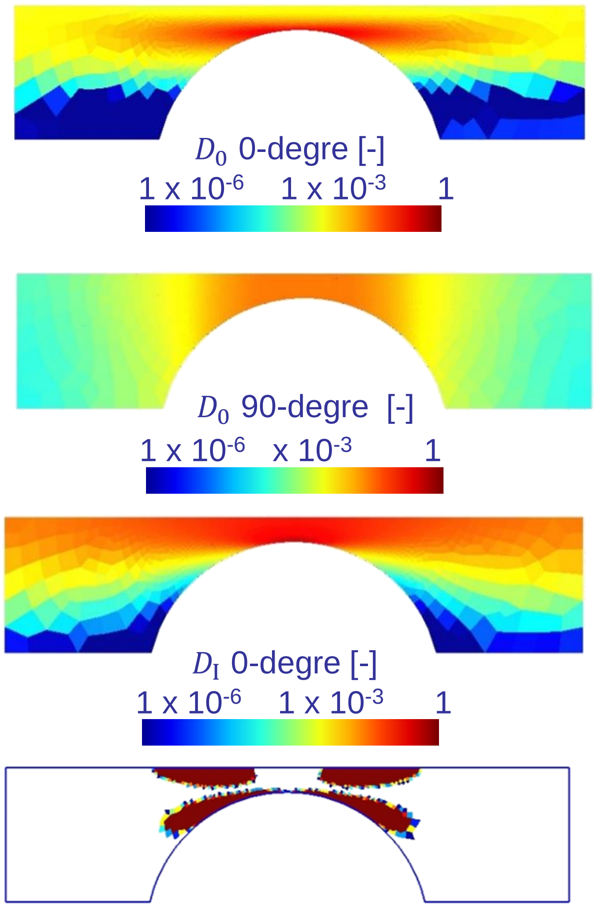

Active delamination

Phase-field fibre damage, #4

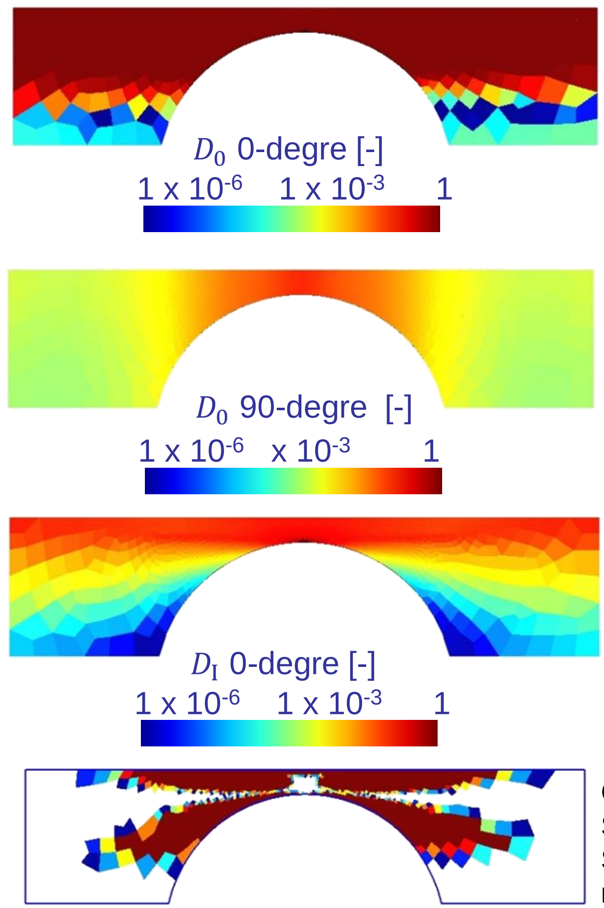

Active delamination

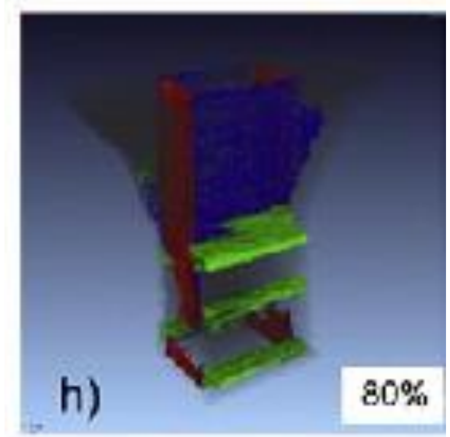

Composites Science and Technology, 71/12, A.E. Scott and M. Mavrogordato and P. Wright and I. Sinclair and S.M. Spearing, In situ fibre fracture measurement in carbonepoxy laminates using high resolution computed tomography, 1471-1477, 2011

- Laminate study
  - AS4/8552 – Notched Specimen

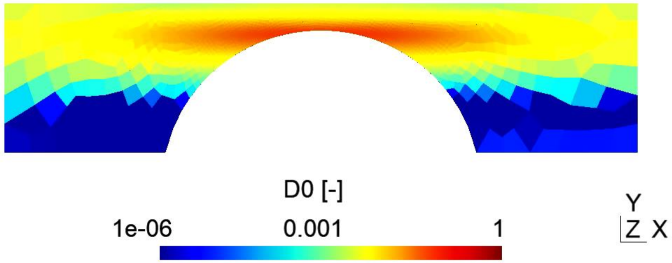

D_0 0-degre [-]

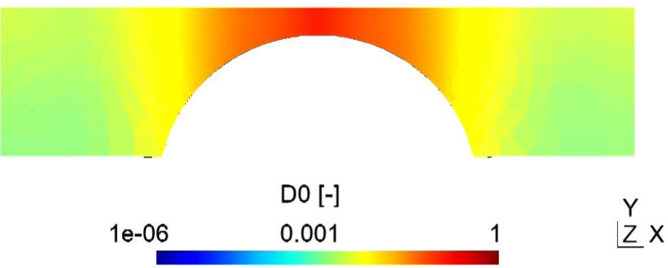

D_0 90-degre [-]

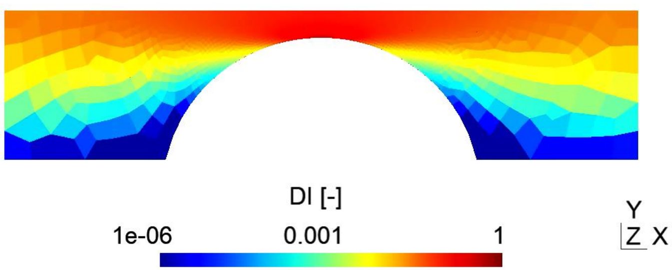

D_I 0-degre [-]

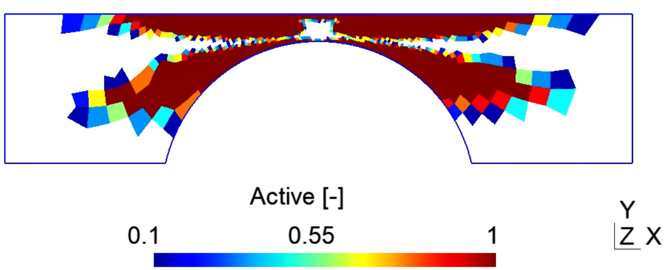

Active delamination

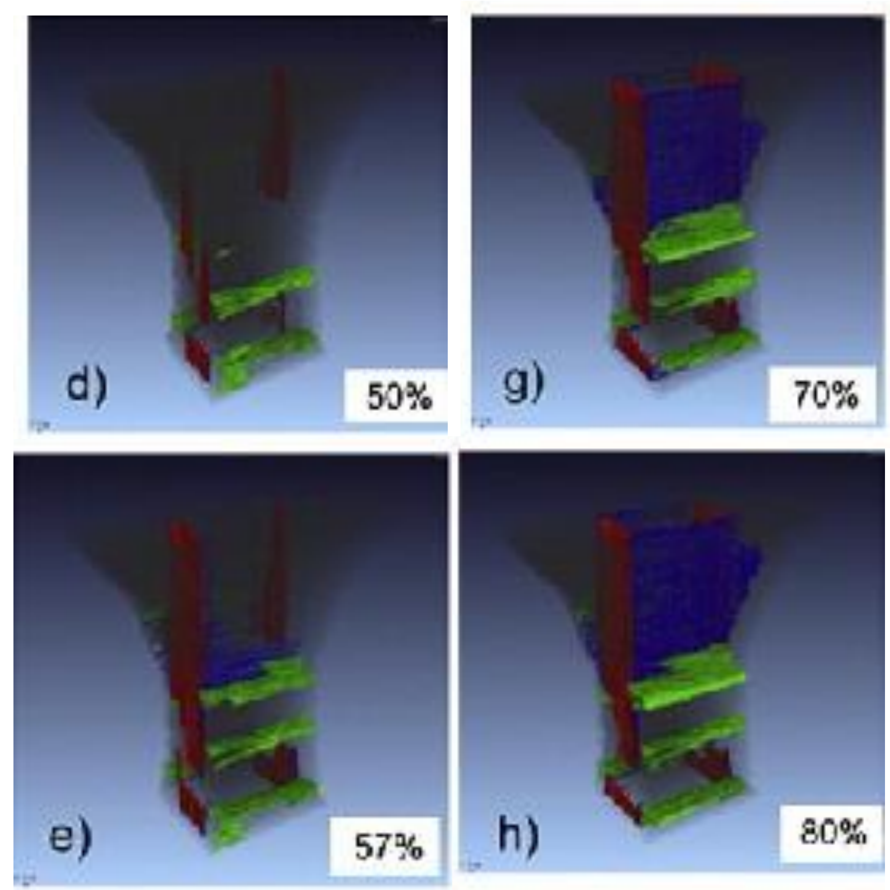

Composites Science and Technology, 71/12, A.E. Scott and M. Mavrogordato and P. Wright and I. Sinclair and S.M. Spearing, In situ fibre fracture measurement in carbonepoxy laminates using high resolution computed tomography, 1471-1477, 2011

Non-Local Damage & Phase-Field Mean-Field-Homogenization

- Geometry
  - Yarns:
    - Non-local damage & Phase-field MFH following yarn direction
  - Matrix
    - Non-local damage

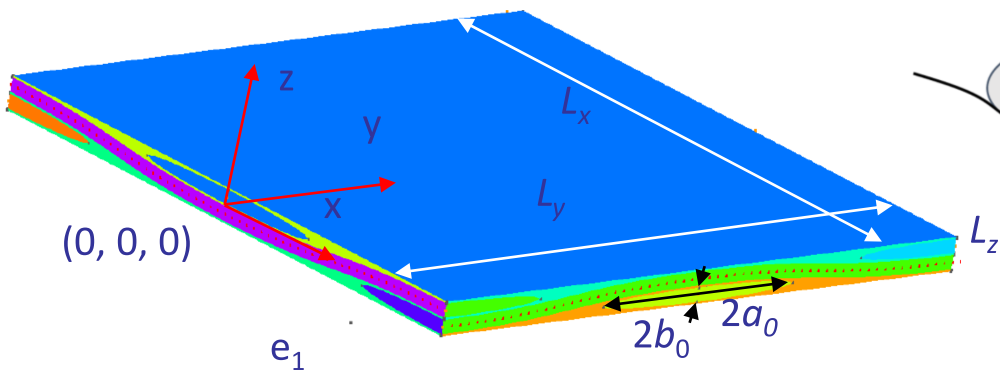

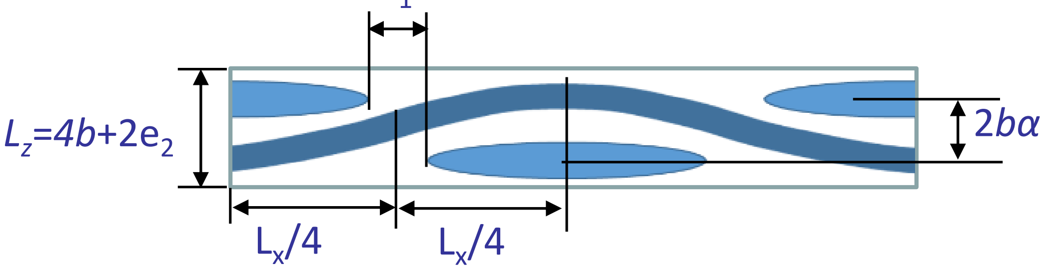

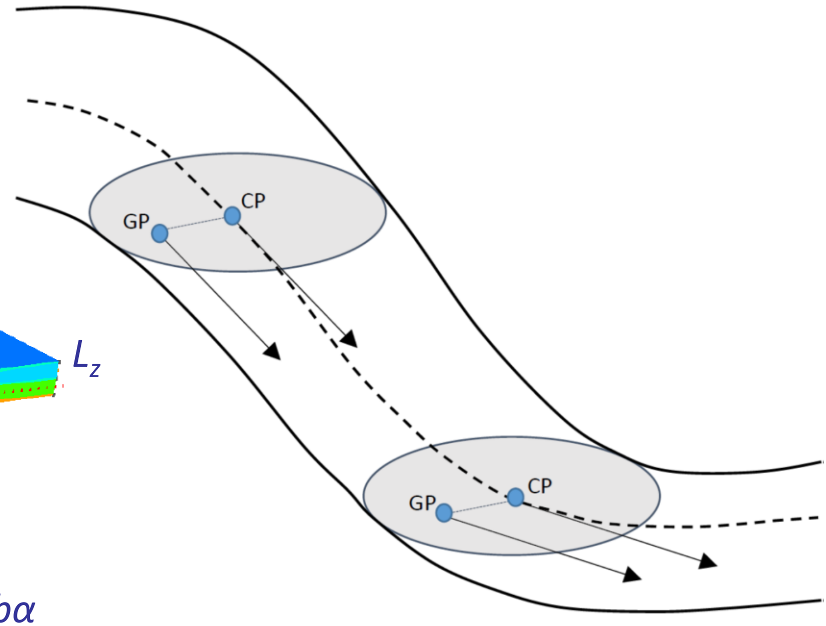

$$z = b\left[\frac{2}{1+e^{-\frac{l}{2}\left(2x-\frac{L_x}{2}\right)}}-1\right]$$

Non-Local Damage & Phase-Field Mean-Field-Homogenization

- Damage distribution for uniaxial loading
  - Yarns:
    - Non-local damage & Phase-field MFH following yarn direction
  - Matrix
    - Non-local damage

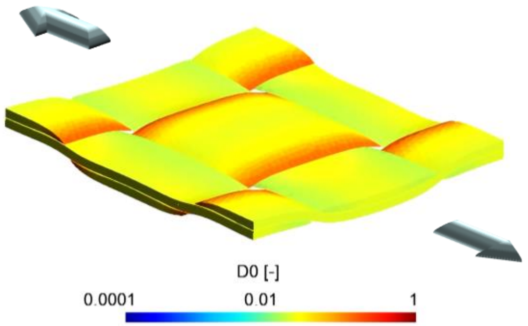

Damage in matrix phase out of yarns

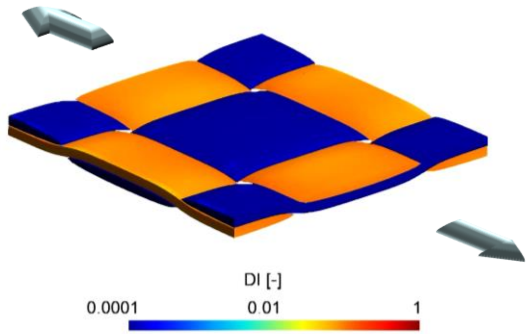

Damage in fibre bundle phase of yarns

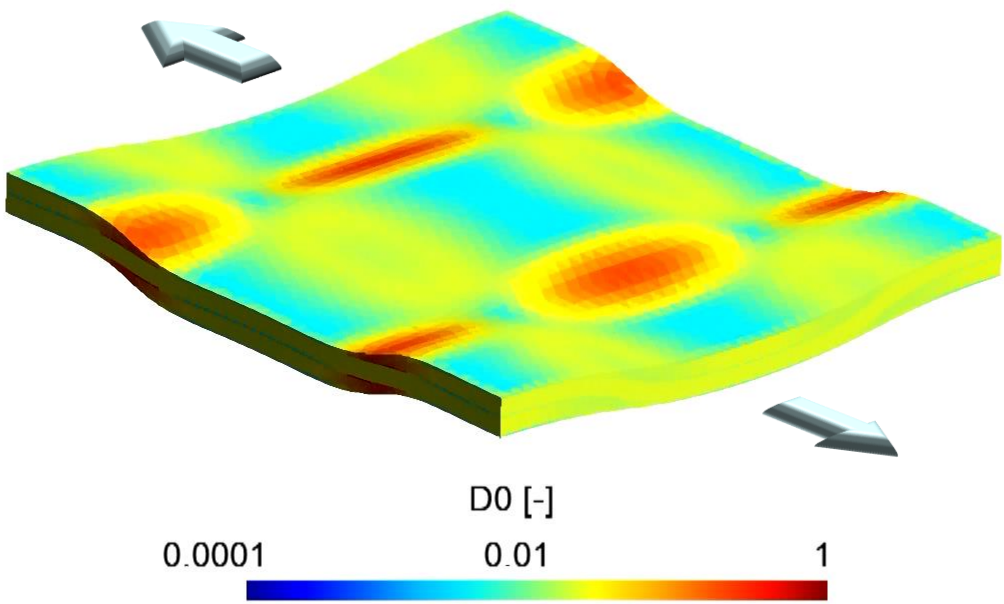

Damage in matrix (in & out of yarns)

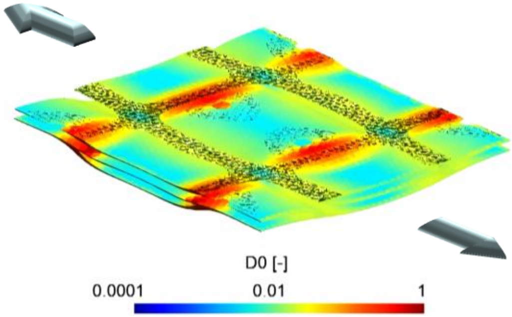

Damage in matrix phase of yarns

- Effect of boundary conditions
  - Side faces periodic and upper/lower faces flat (MBC/KUBC) vs. full PBC

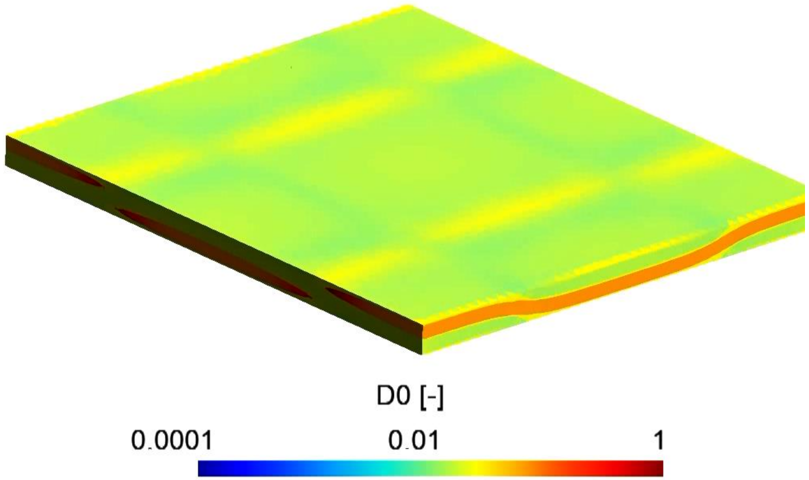

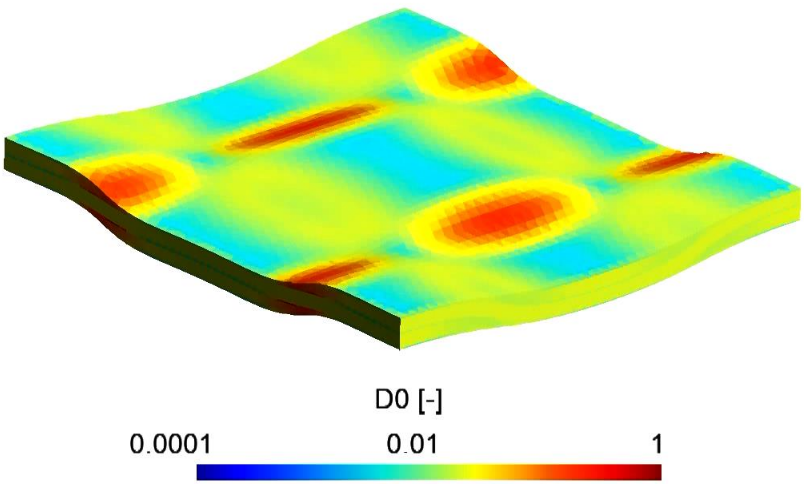

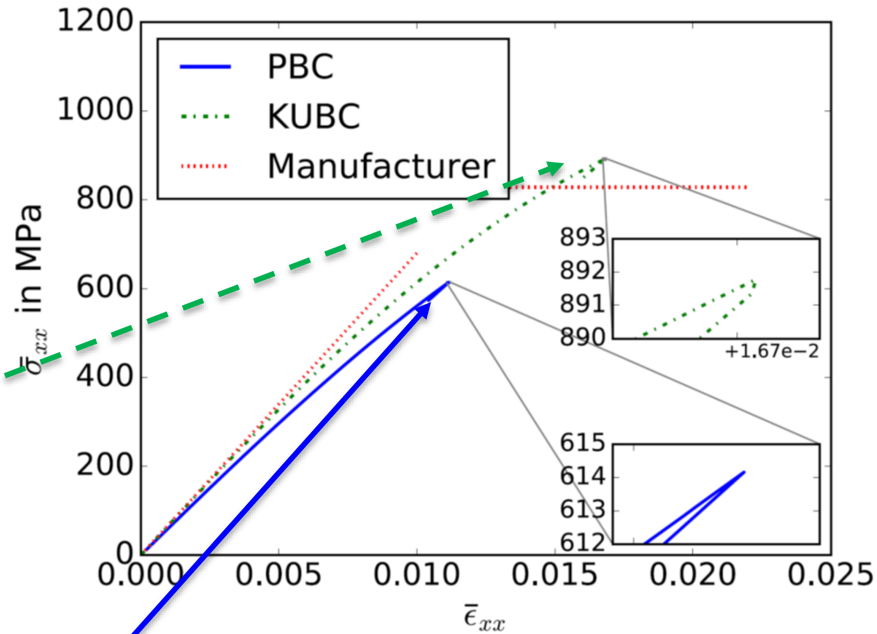

Non-Local Damage & Phase-Field Mean-Field-Homogenization

- Effect of boundary conditions
  - 2-ply layout with full periodic BC

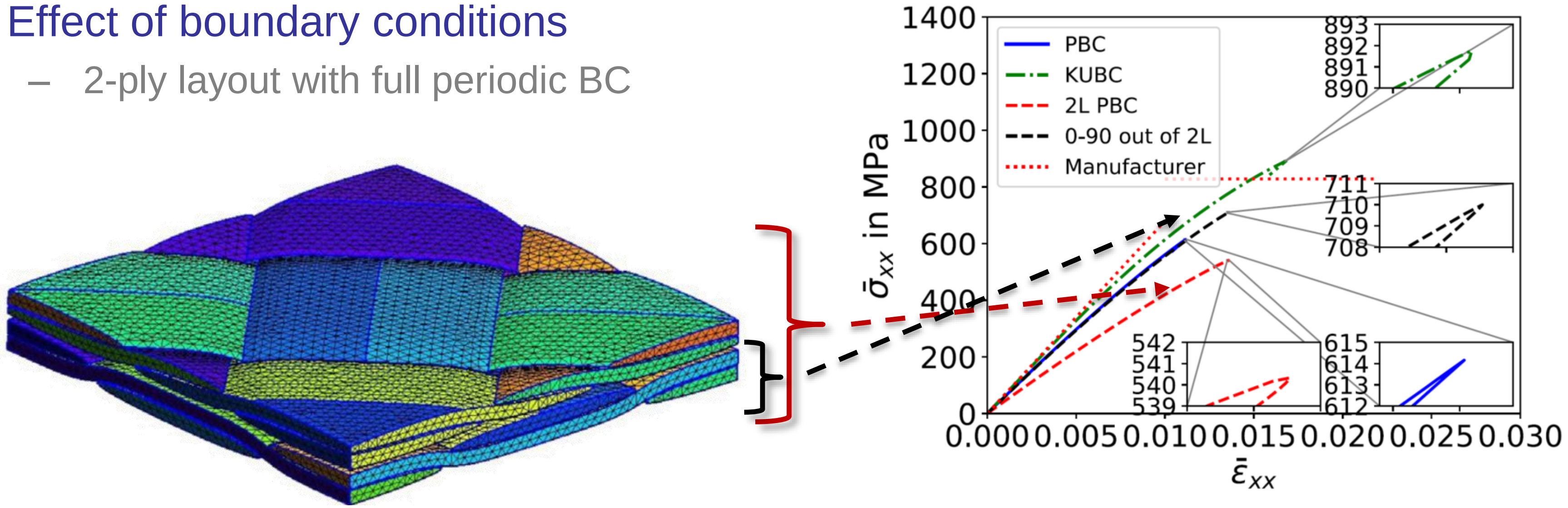

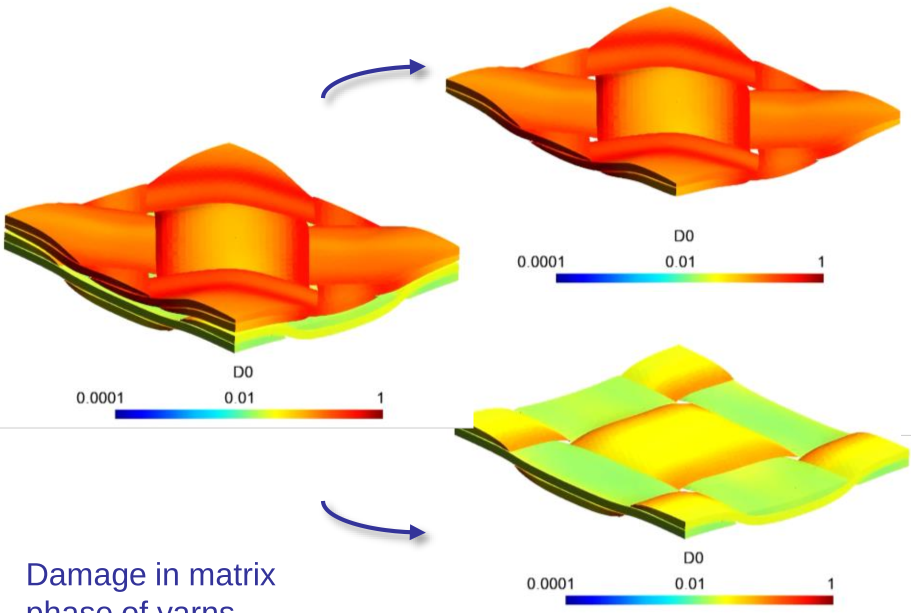

Damage in matrix phase of yarns

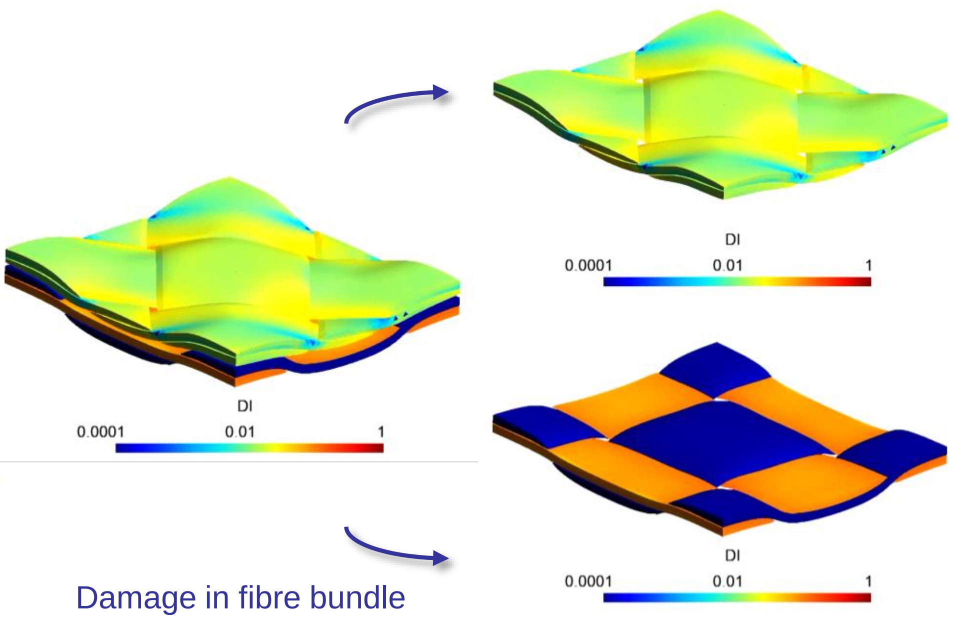

Damage in fibre bundle phase of yarns

Non-Local Damage & Phase-Field Mean-Field-Homogenization

- VISCOS project, 21st Call of Skywin
  - SONACA S.A., e-Xstream (Hexagon S.A.), Isomatex S.A., UCL, ULiege
- Publications (doi)
  - 10.1016/j.compstruc.2021.106650
  - 10.1016/j.compstruct.2021.114270
  - 10.1016/j.compstruct.2021.114058
    - Open data

Boundary conditions and tangent operator in multi-physics computational homogenization

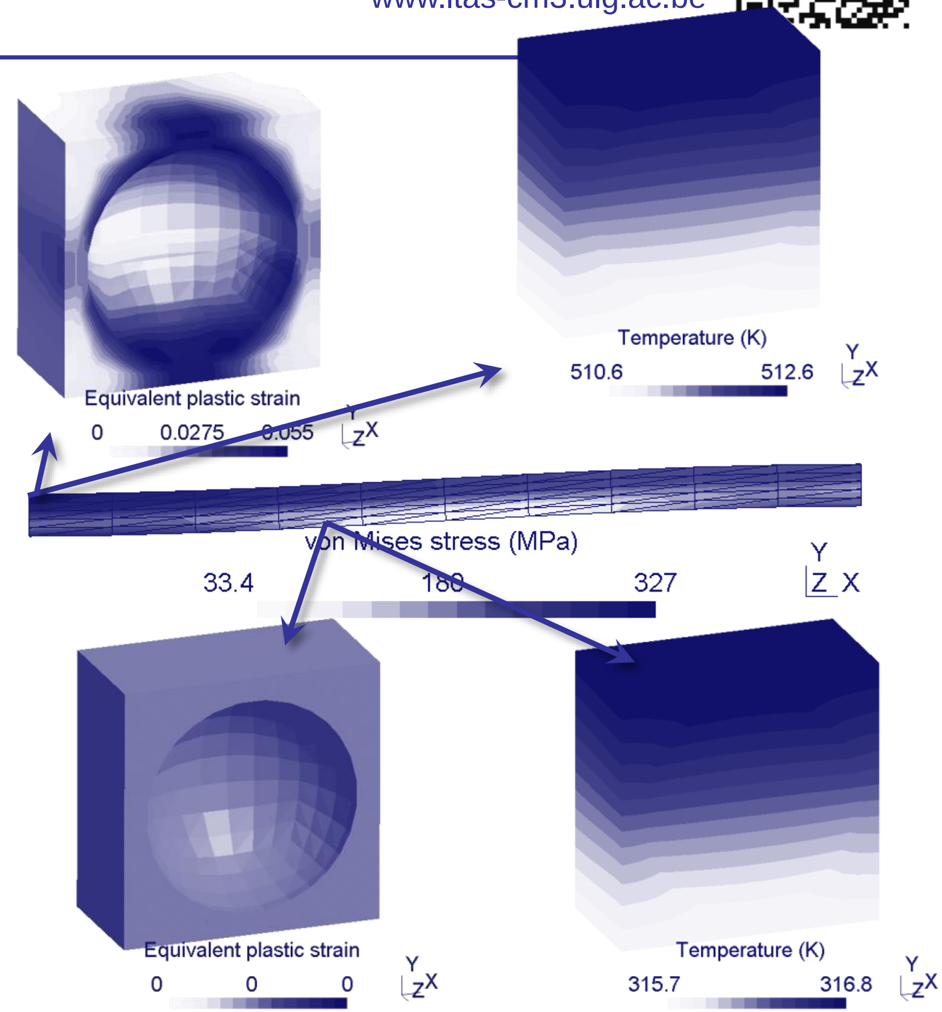

ARC 09/14-02 BRIDGING - From imaging to geometrical modelling of complex micro structured materials: Bridging computational engineering and material science
The authors gratefully acknowledge the financial support from F.R.S-F.N.R.S. under the project number PDR T.1015.14

Boundary conditions and tangent operator in FE²

- Multi-scale modeling
  - 2 problems are solved concurrently
    - The macro-scale problem
    - The meso-scale problem (on a meso-scale Volume Element)

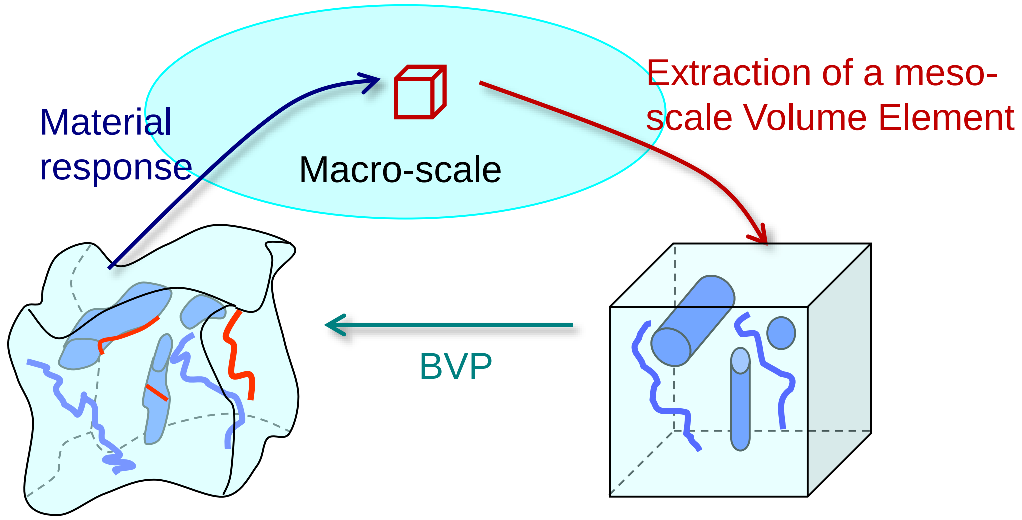

- Length-scales separation

$$L_{\text{macro}} >> L_{\text{VE}} >> L_{\text{micro}}$$

For accuracy: Size of the meso-scale volume element smaller than the characteristic length of the macro-scale loading

To be statistically representative: Size of the meso-scale volume element larger than the characteristic length of the micro-structure

- Generalized multi-physics representation
  - Strong form $\mathcal{P}\cdot\nabla_0 = 0$
  - Fully-coupled constitutive law $\mathcal{P} = \mathcal{P}\left(\mathcal{X}^C, \mathcal{F}; \mathcal{Z}\right)$
    - $\mathcal{F}$: generalized deformation gradient, $\mathcal{X}^C$: fields appearing in the constitutive relations
    - $\mathcal{Z}$: internal variables
    - Tangent operators $\mathcal{L} = \frac{\partial\mathcal{P}}{\partial\mathcal{F}}$ & $\mathcal{J} = \frac{\partial\mathcal{P}}{\partial\mathcal{X}^C}$ but also $\mathcal{Y}_{\mathcal{F}} = \frac{\partial\mathcal{Z}}{\partial\mathcal{F}}$ & $\mathcal{Y}_{\mathcal{X}^C} = \frac{\partial\mathcal{Z}}{\partial\mathcal{X}^C}$
- Two-scale procedure

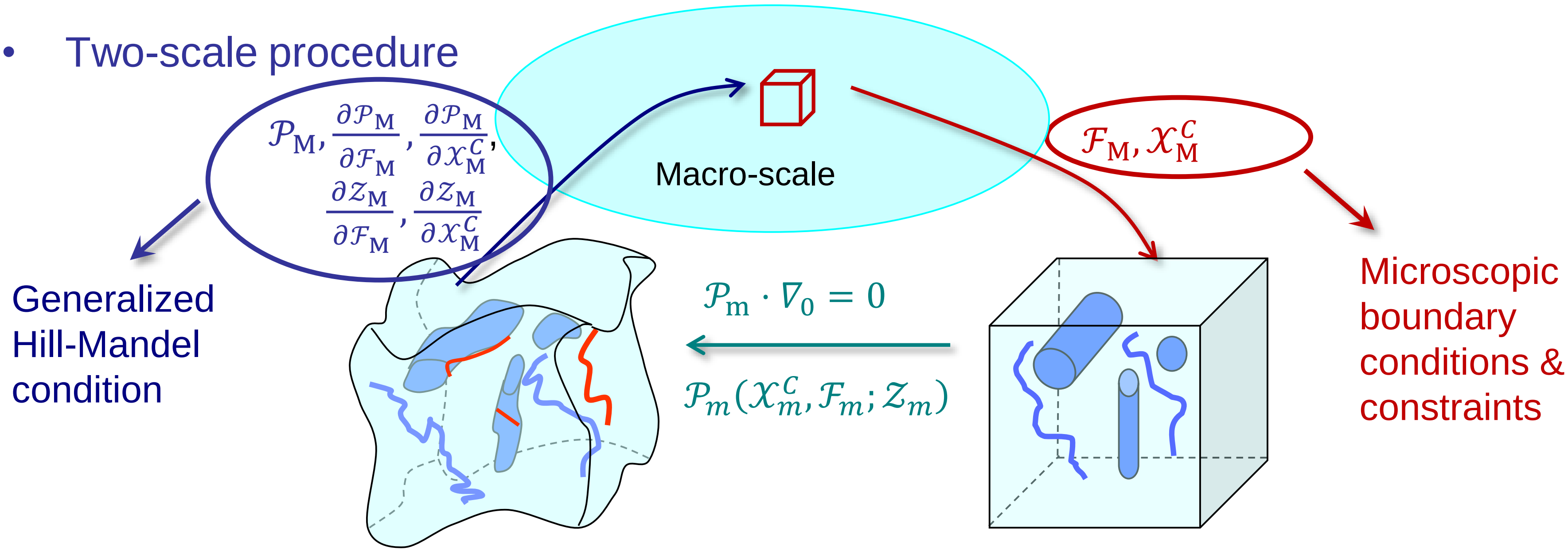

- Generalized microscopic boundary conditions
  - Arbitrary field k kinematics: $\mathcal{X}^k_{\mathrm{m}} = \mathcal{X}^k_{\mathrm{M}} + \mathcal{F}^k_{\mathrm{M}} \cdot \mathrm{X}_{\mathrm{m}} + \mathcal{W}^k_{\mathrm{m}}$

    Fluctuation
  - Constrained field k equivalence: $\int_{\omega_0} C^k_m \mathcal{X}^{C^k}_{\mathrm{m}}\, d\omega = \int_{\omega_0} C^k_m d\omega\, \mathcal{X}^{C^k}_{\mathrm{M}}$
  - E.g. periodic boundary conditions

    Define an interpolant map

    $$\mathbb{S}^i = \sum \mathbb{N}^i_k(\boldsymbol{X}_m) a^i_k$$

    Substitute fluctuation fields

    $$W^k_m(\boldsymbol{X}^+_m) = \mathbb{S}^i(\boldsymbol{X}^-_m) = W^k_m(\boldsymbol{X}^-_m)$$

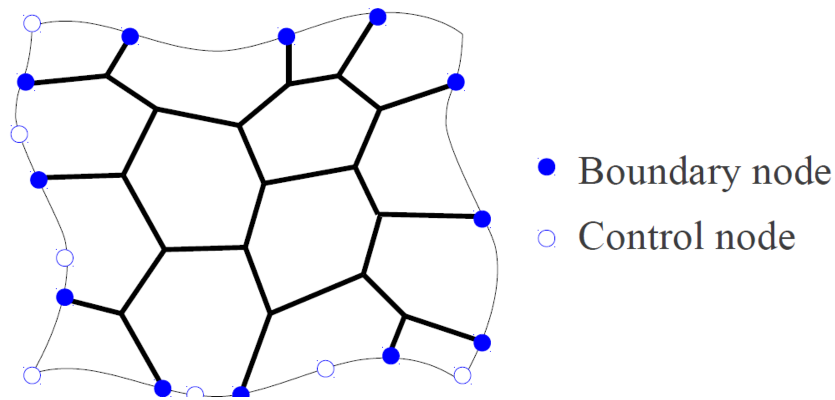

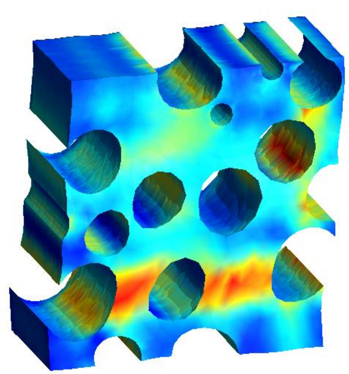

- Microscale BVP
  - Weak formulation

$$\begin{cases} \mathcal{P}_{\mathrm{m}} \cdot \nabla_0 = 0 \qquad \text{with } \mathcal{P}_m(\mathcal{X}_m^C, \mathcal{F}_m; \mathcal{Z}_m) \\ \mathcal{X}_{\mathrm{m}}^k = \mathcal{X}_{\mathrm{M}}^k + \mathcal{F}_{\mathrm{M}}^k \cdot \mathrm{X}_{\mathrm{m}} + \mathcal{W}_{\mathrm{m}}^k \\ \int_{\omega_0} C_m^k \mathcal{X}_{\mathrm{m}}^{C\,k} \, d\omega = \int_{\omega_0} C_m^k d\omega \, \mathcal{X}_{\mathrm{M}}^{C\,k} \end{cases}$$

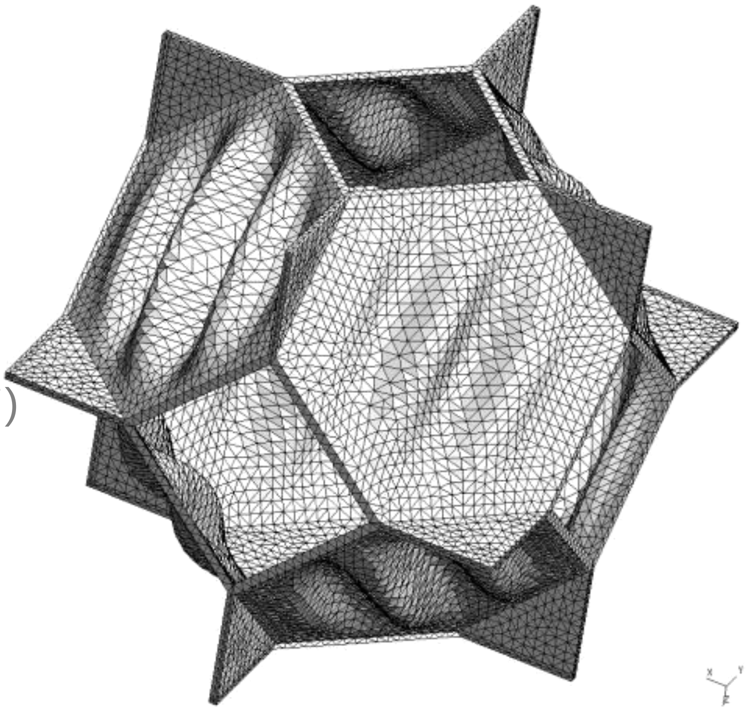

  - Weak finite element constrained form ($\omega_0 = \cup_e \, \omega^e$)

$$\begin{cases} \mathbf{f}_{\mathrm{m}}(\boldsymbol{\mathcal{U}}_m) - \mathbf{C}^{\mathrm{T}} \boldsymbol{\lambda} = 0 \\ \mathbf{C}\boldsymbol{\mathcal{U}}_m - \mathbf{S} \begin{bmatrix} \mathcal{F}_{\mathrm{M}} \\ \mathcal{X}_{\mathrm{M}}^C \end{bmatrix} = 0 \end{cases}$$

  - System linearization

$$\begin{cases} \mathbf{Q}^{\mathrm{T}} \dfrac{\partial \mathbf{f}_{\mathrm{m}}}{\partial \boldsymbol{\mathcal{U}}_m} \mathbf{Q} \delta \boldsymbol{\mathcal{U}}_m + \mathbf{r} - \mathbf{Q}^{\mathrm{T}} \dfrac{\partial \mathbf{f}_{\mathrm{m}}}{\partial \boldsymbol{\mathcal{U}}_m} \mathbf{C}^{\mathrm{T}} (\mathbf{C}\mathbf{C}^{\mathrm{T}})^{-1} \left(\mathbf{r}_c - \mathbf{S} \begin{bmatrix} \delta\mathcal{F}_{\mathrm{M}} \\ \delta\mathcal{X}_{\mathrm{M}}^C \end{bmatrix} \right) = 0 \\ \mathbf{C}\delta\boldsymbol{\mathcal{U}}_m + \mathbf{r}_{\mathrm{c}} - \mathbf{S} \begin{bmatrix} \delta\mathcal{F}_{\mathrm{M}} \\ \delta\mathcal{X}_{\mathrm{M}}^C \end{bmatrix} = 0 \qquad \& \qquad \mathbf{Q} = \mathbf{I} - \mathbf{C}^{\mathrm{T}}(\mathbf{C}\mathbf{C}^{\mathrm{T}})^{-1}\mathbf{C} \end{cases}$$

- Multi-scale resolution
  - System linearization

$$\begin{cases} \mathbf{Q}^{\mathrm{T}}\dfrac{\partial \mathbf{f}_{\mathrm{m}}}{\partial \boldsymbol{\mathcal{U}}_m}\mathbf{Q}\delta\boldsymbol{\mathcal{U}}_m + \mathbf{r} - \mathbf{Q}^{\mathrm{T}}\dfrac{\partial \mathbf{f}_{\mathrm{m}}}{\partial \boldsymbol{\mathcal{U}}_m}\mathbf{C}^{\mathrm{T}}\left(\mathbf{C}\mathbf{C}^{\mathrm{T}}\right)^{-1}\left(\mathbf{r}_c - \mathbf{S}\begin{bmatrix}\delta\mathcal{F}_{\mathrm{M}}\\ \delta\mathcal{X}_{\mathrm{M}}^{C}\end{bmatrix}\right) = 0 \\ \mathbf{C}\delta\boldsymbol{\mathcal{U}}_m + \mathbf{r}_{\mathrm{c}} - \mathbf{S}\begin{bmatrix}\delta\mathcal{F}_{\mathrm{M}}\\ \delta\mathcal{X}_{\mathrm{M}}^{C}\end{bmatrix} = 0 \qquad \& \qquad \mathbf{Q} = \mathbf{I} - \mathbf{C}^{\mathrm{T}}\left(\mathbf{C}\mathbf{C}^{\mathrm{T}}\right)^{-1}\mathbf{C} \end{cases}$$

  - FEM resolution: $\delta\mathcal{F}_{\mathrm{M}}=\delta\mathcal{X}_{\mathrm{M}}^{C}=0$

$$\delta\boldsymbol{\mathcal{U}}_m = -\widetilde{\mathbf{K}}^{-1}\left(\mathbf{r} + \left(\mathbf{C}^{\mathrm{T}} - \mathbf{Q}^{\mathrm{T}}\frac{\partial \mathbf{f}_{\mathrm{m}}}{\partial \boldsymbol{\mathcal{U}}_m}\mathbf{C}^{\mathrm{T}}\left(\mathbf{C}\mathbf{C}^{\mathrm{T}}\right)^{-1}\right)\mathbf{r}_c\right)$$

Only one matrix to factorize

$$\widetilde{\mathbf{K}} = \mathbf{C}^{\mathrm{T}}\mathbf{C} + \mathbf{Q}^{\mathrm{T}}\frac{\partial \mathbf{f}_{\mathrm{m}}}{\partial \boldsymbol{\mathcal{U}}_m}\mathbf{Q}$$

  - Constraints effect: $\mathbf{r} = \mathbf{r}_c=0$

$$\frac{\partial \boldsymbol{\mathcal{U}}_m}{\partial\left[\mathcal{F}_{\mathrm{M}} \quad \mathcal{X}_{\mathrm{M}}^{C}\right]^{T}} = \widetilde{\mathbf{K}}^{-1}\left(\mathbf{C}^{\mathrm{T}} - \mathbf{Q}^{\mathrm{T}}\frac{\partial \mathbf{f}_{\mathrm{m}}}{\partial \boldsymbol{\mathcal{U}}_m}\mathbf{C}^{\mathrm{T}}\left(\mathbf{C}\mathbf{C}^{\mathrm{T}}\right)^{-1}\right)\mathbf{S}$$

  - Macro-scale operators at low cost

$$\begin{bmatrix} \dfrac{\partial \mathcal{P}_{\mathrm{M}}}{\partial \mathcal{F}_{\mathrm{M}}} & \dfrac{\partial \mathcal{P}_{\mathrm{M}}}{\partial \mathcal{X}_{\mathrm{M}}^{C}} \\ \dfrac{\partial \mathcal{Z}_{\mathrm{M}}}{\partial \mathcal{F}_{\mathrm{M}}} & \dfrac{\partial \mathcal{Z}_{\mathrm{M}}}{\partial \mathcal{X}_{\mathrm{M}}^{C}} \end{bmatrix} = \left(\bigwedge_{\omega^e}\frac{1}{V(\omega_0)}\int_{\omega_0^e}\begin{bmatrix} \dfrac{\partial \mathcal{P}_{\mathrm{m}}}{\partial \mathcal{F}_{\mathrm{m}}}\mathbf{B}^e & \dfrac{\partial \mathcal{P}_{\mathrm{m}}}{\partial \mathcal{X}_{\mathrm{m}}^{C}}\mathbf{N}^e \\ \dfrac{\partial \mathcal{Z}_{\mathrm{m}}}{\partial \mathcal{F}_{\mathrm{m}}}\mathbf{B}^e & \dfrac{\partial \mathcal{Z}_{\mathrm{m}}}{\partial \mathcal{X}_{\mathrm{m}}^{C}}\mathbf{N}^e \end{bmatrix}d\omega\right)\frac{\partial \boldsymbol{\mathcal{U}}_m}{\partial\left[\mathcal{F}_{\mathrm{M}} \quad \mathcal{X}_{\mathrm{M}}^{C}\right]^{T}}$$

- Thermo-elasto-plasticity

$$\begin{cases} \mathbf{P}_\mathrm{M} \cdot \boldsymbol{\nabla}_0 = 0 \\ \rho_\mathrm{M} C_{v\mathrm{M}} \dot{\vartheta}_\mathrm{M} - \mathcal{D}_\mathrm{M} + \mathbf{q}_\mathrm{M} \cdot \boldsymbol{\nabla}_0 = 0 \end{cases}$$

$$\begin{cases} \mathbf{P}_\mathrm{M} = \dfrac{1}{V(\omega_0)} \displaystyle\int_{\omega_0} \mathbf{P}_\mathrm{m} d\omega \\ \boldsymbol{q}_\mathrm{M} = \dfrac{1}{V(\omega_0)} \displaystyle\int_{\omega_0} \boldsymbol{q}_\mathrm{m} d\omega \\ \rho_\mathrm{M} C_{v\mathrm{M}} = \dfrac{1}{V(\omega_0)} \displaystyle\int \rho_\mathrm{m} C_{v\mathrm{m}} d\omega \\ \mathcal{D}_\mathrm{M} = \dfrac{1}{V(\omega_0)} \displaystyle\int \mathcal{D}_\mathrm{m} d\omega \\ \& \\ \dfrac{\partial \mathbf{P}_\mathrm{M}}{\partial \mathbf{F}_\mathrm{M}}, \dfrac{\partial \mathbf{P}_\mathrm{M}}{\partial \vartheta_\mathrm{M}}, \dfrac{\partial \mathbf{P}_\mathrm{M}}{\partial \boldsymbol{\nabla}_0 \vartheta_\mathrm{M}}, \\ \dfrac{\partial \mathbf{q}_\mathrm{M}}{\partial \mathbf{F}_\mathrm{M}}, \dfrac{\partial \mathbf{q}_\mathrm{M}}{\partial \vartheta_\mathrm{M}}, \dfrac{\partial \mathbf{q}_\mathrm{M}}{\partial \boldsymbol{\nabla}_0 \vartheta_\mathrm{M}}, \\ \dfrac{\partial \mathcal{D}_\mathrm{M}}{\partial \mathbf{F}_\mathrm{M}}, \dfrac{\partial \mathcal{D}_\mathrm{M}}{\partial \vartheta_\mathrm{M}}, \dfrac{\partial \mathcal{D}_\mathrm{M}}{\partial \boldsymbol{\nabla}_0 \vartheta_\mathrm{M}} \end{cases}$$

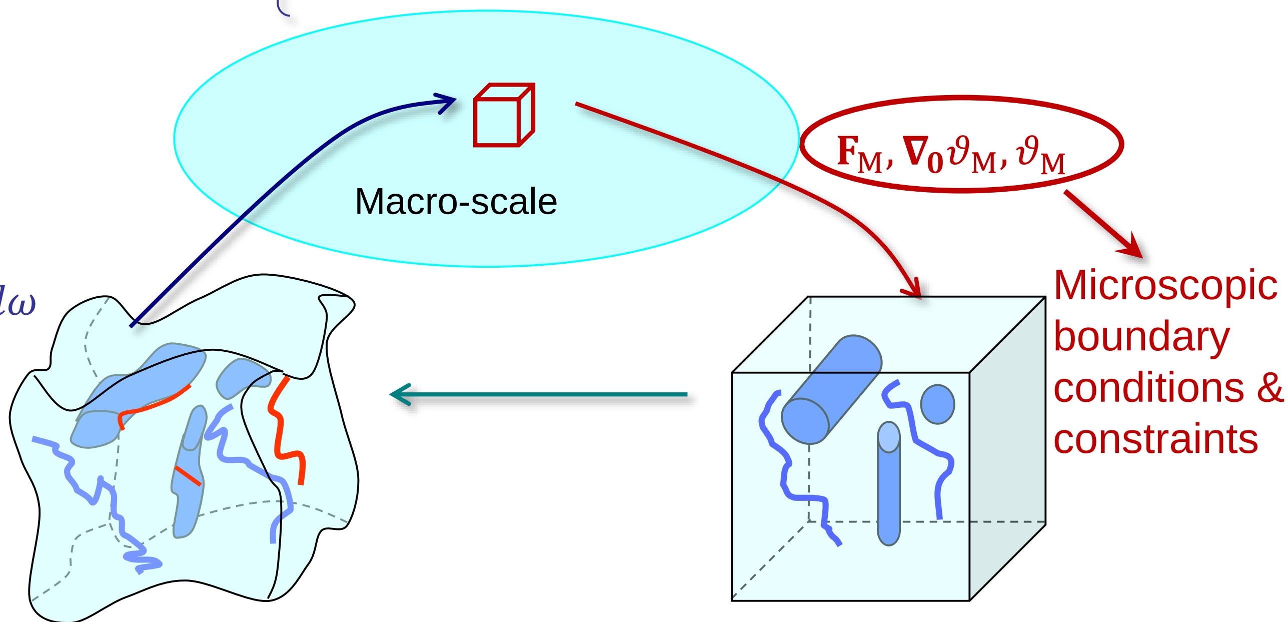

$$\begin{cases} \mathbf{P}_\mathrm{m} = \mathbf{P}_\mathrm{m}\left(\mathbf{F}_\mathrm{m}, \boldsymbol{\nabla}_\mathbf{0} \vartheta_\mathrm{m}, \vartheta_\mathrm{m}; p, \mathbf{F}_\mathrm{m}^\mathbf{p}\right) \\ \mathbf{q}_\mathrm{m} = \mathbf{q}_\mathrm{m}\left(\mathbf{F}_\mathrm{m}, \boldsymbol{\nabla}_\mathbf{0} \vartheta_\mathrm{m}, \vartheta_\mathrm{m}; p, \mathbf{F}_\mathrm{m}^\mathbf{p}\right) \\ \mathcal{D}_\mathrm{m} = \beta \dot{p} \tau + \vartheta \dfrac{\partial \dot{W}^\mathrm{el}}{\partial \vartheta} \\ \mathbf{P}_\mathrm{m} \cdot \boldsymbol{\nabla}_0 = 0 \\ \mathbf{q}_\mathrm{m} \cdot \boldsymbol{\nabla}_0 = 0 \end{cases}$$

Boundary conditions and tangent operator in FE^2

- Thermo-elasto-plasticity
  - Thermal-softening hardening
    $$\tau = (\sigma_0 + Hp)(1 - \omega_T(T - T_0))$$

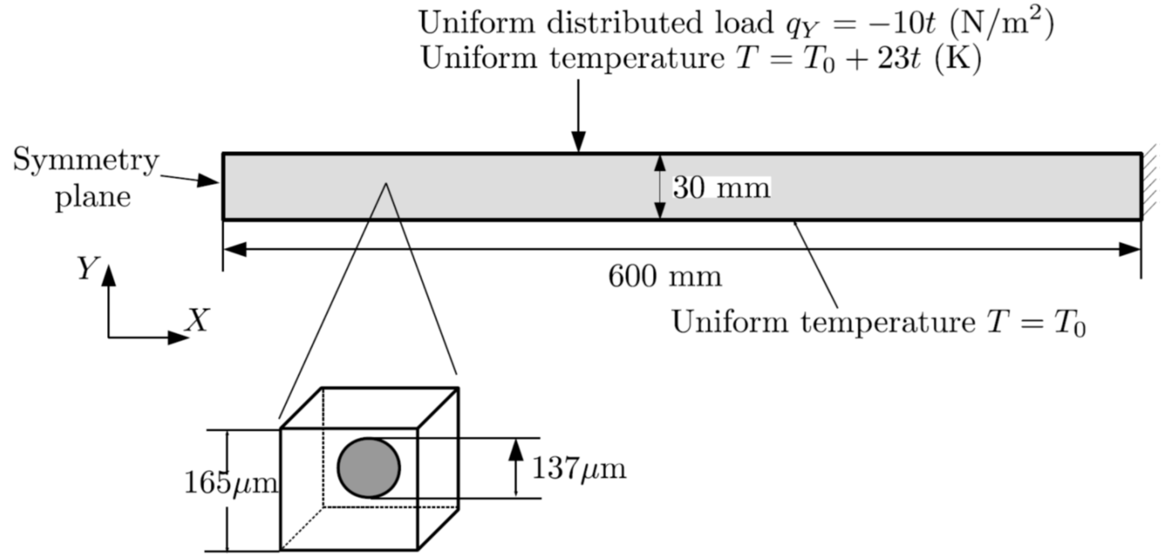

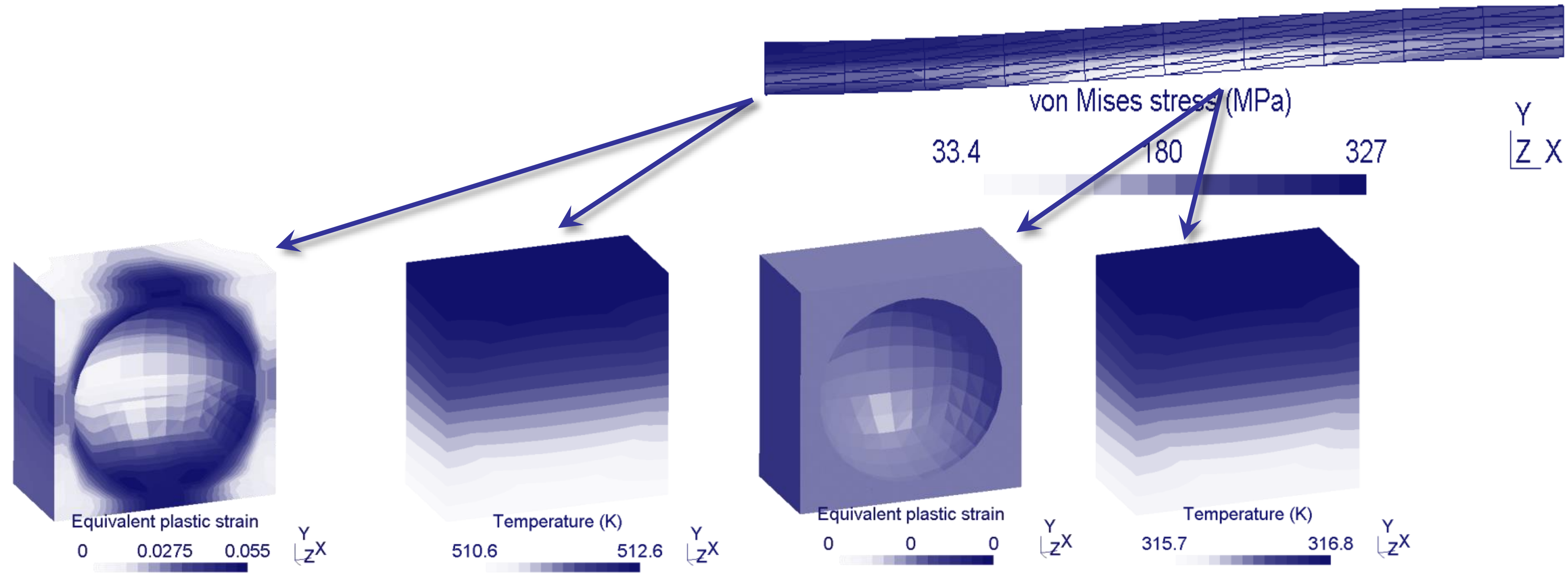

Boundary conditions and tangent operator in FE^2

- BRIDGING ARC project (Periodic boundary conditions)
  - ULiège, Applied Sciences (A&M, EEI, ICD)
  - ULiège, Sciences (CERM)

- PDR T.1015.14 project (MFH with second-order moments)
  - ULiège, UCL (Belgium)

- Publications
  - 10.1007/s00466-016-1358-z
  - 10.1016/j.commatsci.2011.10.017

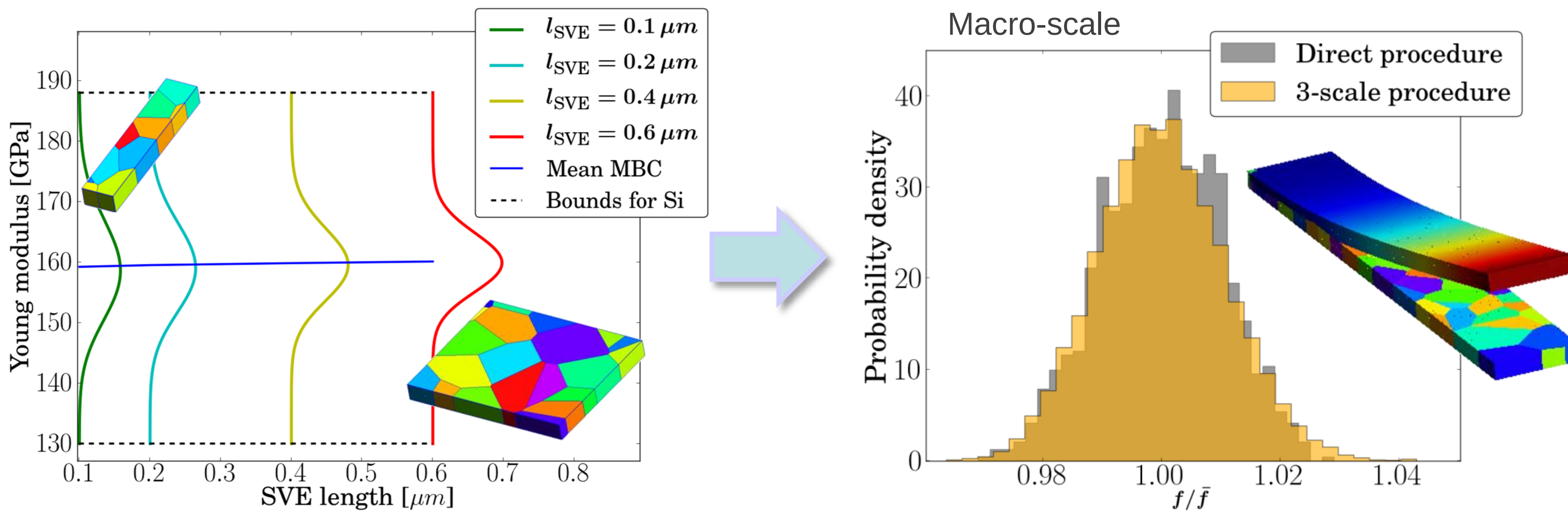

Stochastic 3-Scale Models for Polycrystalline Materials

3SMVIB: The research has been funded by the Walloon Region under the agreement no 1117477 (CT-INT 2011-11-14) in the context of the ERA-NET MNT framework.

- Multi-scale modeling
  - 2 problems are solved concurrently
    - The macro-scale problem
    - The meso-scale problem (on a meso-scale Volume Element)

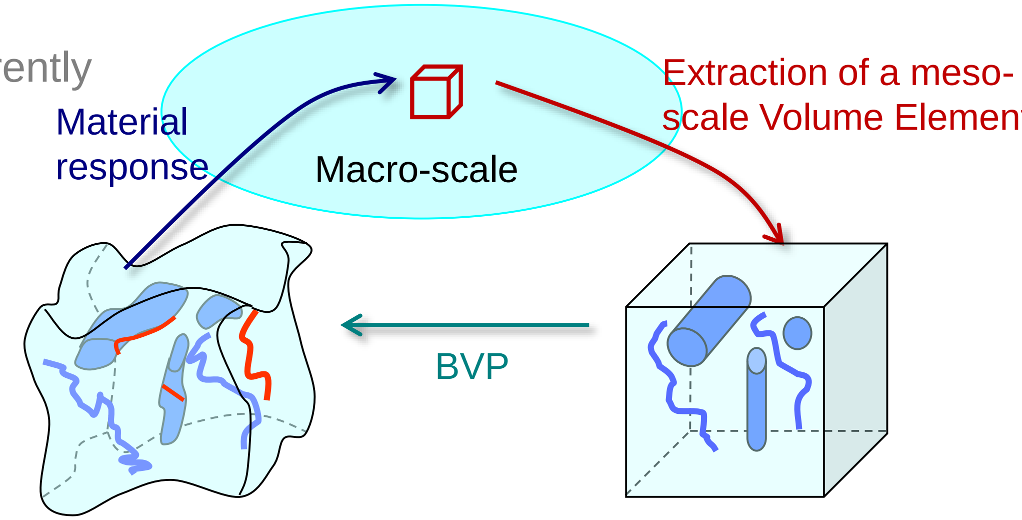

- For structures not several orders larger than the micro-structure size

$L_{\mathrm{macro}} >> L_{\mathrm{VE}} >\sim L_{\mathrm{micro}}$

For accuracy: Size of the meso-scale volume element smaller than the characteristic length of the macro-scale loading

Meso-scale volume element no longer statistically representative:
- **Stochastic Volume Elements**

Stochastic 3-Scale Models

- Key idea

Micro-scale	Meso-scale	Macro-scale
➢ Samples of stochastic volume elements ➢ Random microstructure	➢ Intermediate scale ➢ The distribution of the material property $\mathbb{P}(C)$ is defined	➢ Uncertainty quantification of the macro-scale quantity ➢ Quantity of interest distribution $\mathbb{P}(Q)$

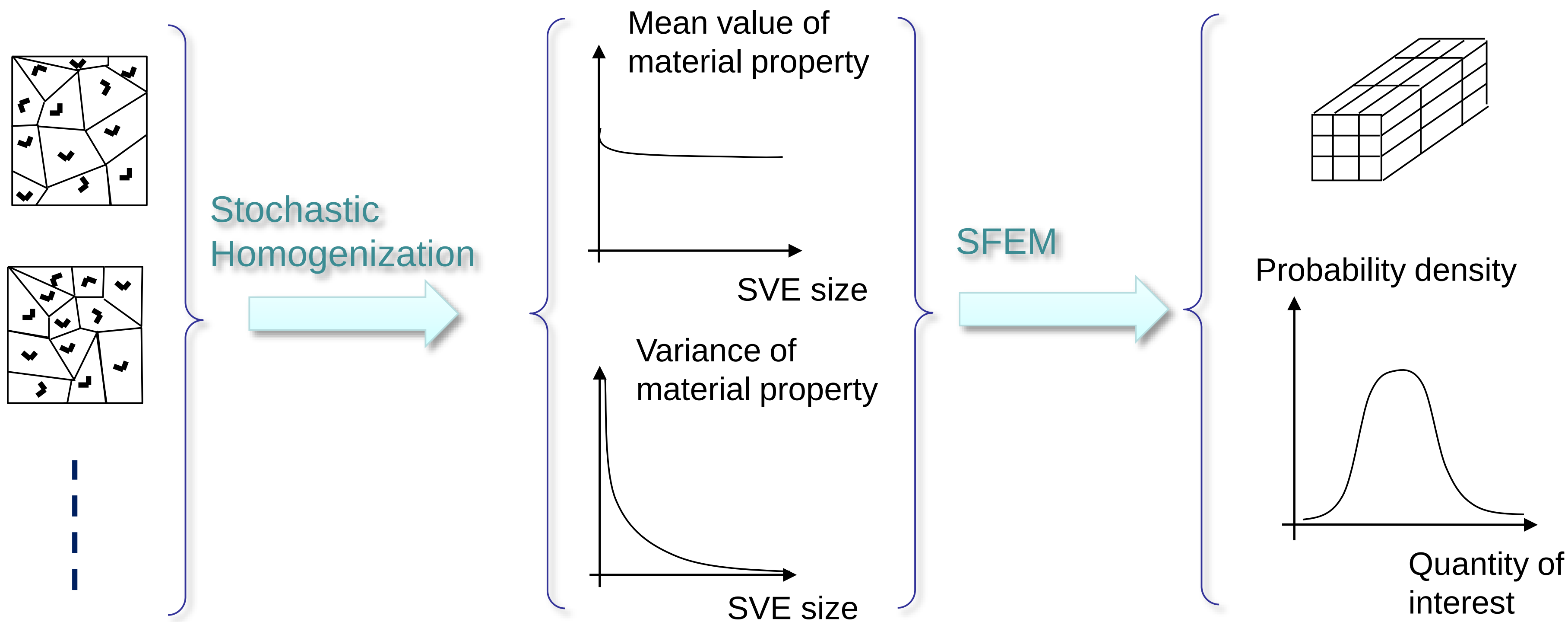

Stochastic 3-Scale Models

- Material structure: grain orientation distribution
  - Grain orientation by XRD (X-ray Diffraction) measurements on 2 µm-thick poly-silicon films

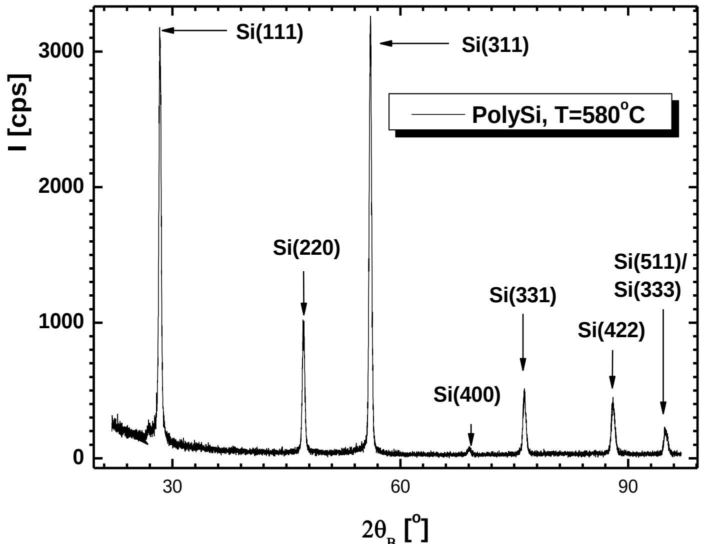

Deposition temperature: 580 °C

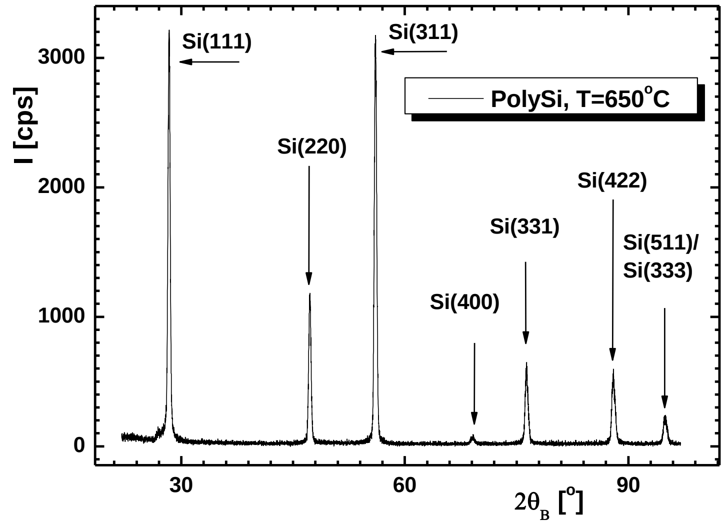

Deposition temperature: 630 °C

Deposition temperature [°C]	580	610	630	650
<111> [%]	12.57	19.96	12.88	11.72
<220> [%]	7.19	13.67	7.96	7.59
<311> [%]	42.83	28.83	39.08	38.47
<400> [%]	4.28	5.54	3.13	3.93
<331> [%]	17.97	18.14	21.32	20.45
<422> [%]	15.15	13.86	15.63	17.84

XRD images provided by IMT Bucharest, Rodica Voicu, Angela Baracu, Raluca Muller

- Application to polycrystalline materials: The micro-scale to meso-scale transition
  - Stochastic homogenization

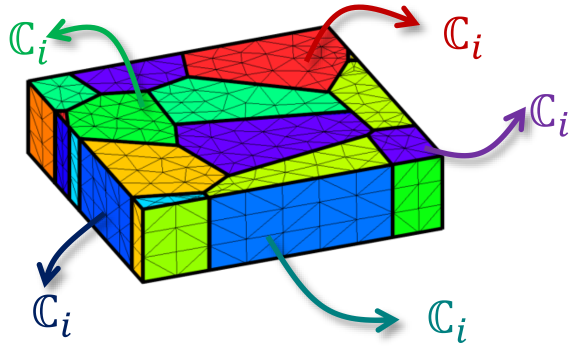

$$\boldsymbol{\sigma}_{m^i} = \mathbb{C}_i : \boldsymbol{\epsilon}_{m^i} \quad , \forall i$$

Stochastic Homogenization

$$\boldsymbol{\sigma}_M = \mathbb{C}_M : \boldsymbol{\epsilon}_M$$

Samples of the meso-scale homogenized elasticity tensors

  - Homogenized Young's modulus distribution

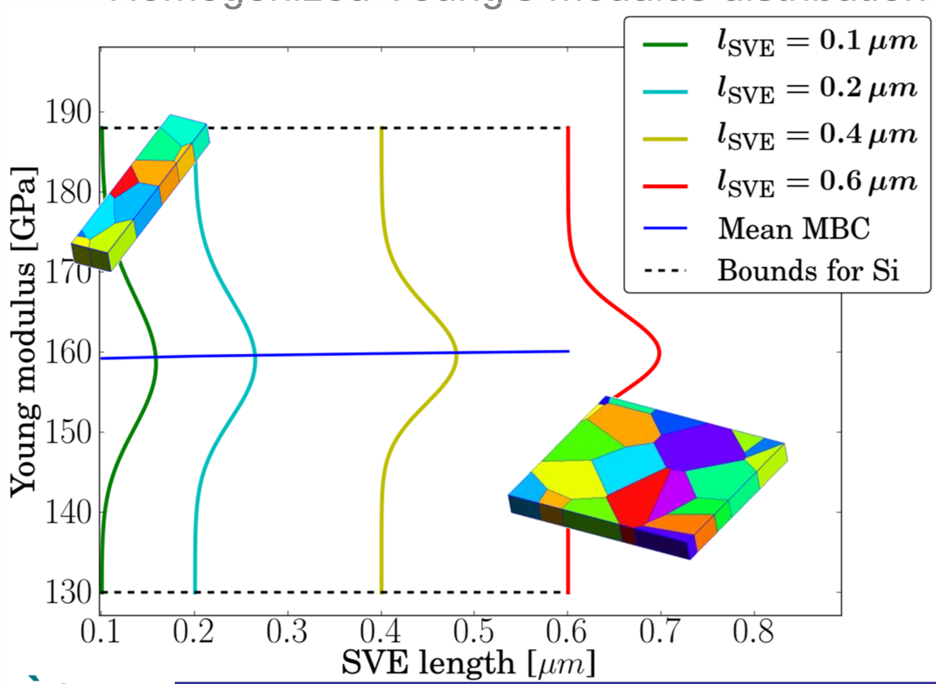

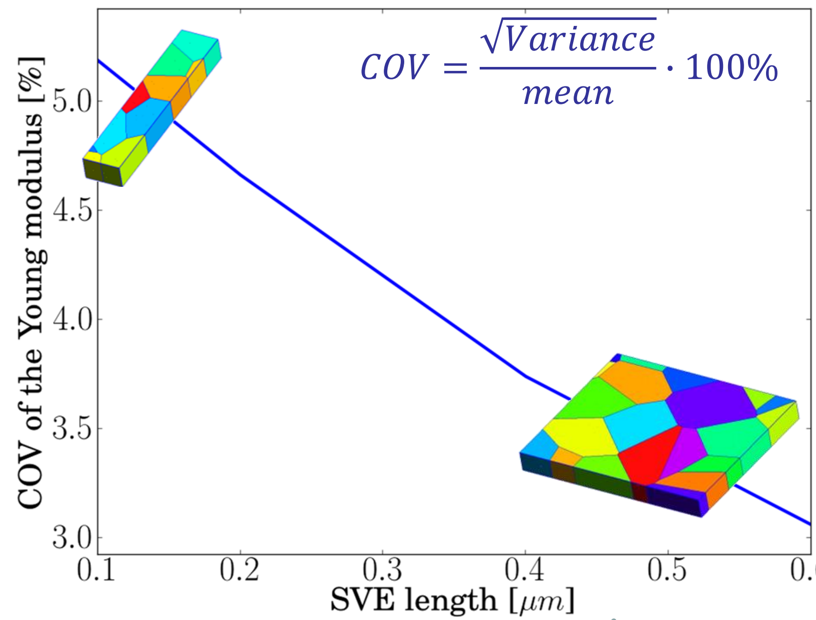

- Application to polycrystalline materials: The meso-scale spatial correlation
  - Use of the window technique

$$R_{\mathbb{C}}^{(rs)}(\boldsymbol{\tau}) = \frac{\mathbb{E}\left[\left(\mathbb{C}^{(r)}(\boldsymbol{x}) - \mathbb{E}\left(\mathbb{C}^{(r)}\right)\right)\left(\mathbb{C}^{(s)}(\boldsymbol{x}+\boldsymbol{\tau}) - \mathbb{E}\left(\mathbb{C}^{(s)}\right)\right)\right]}{\sqrt{\mathbb{E}\left[\left(\mathbb{C}^{(r)} - \mathbb{E}\left(\mathbb{C}^{(r)}\right)\right)^2\right]\mathbb{E}\left[\left(\mathbb{C}^{(s)} - \mathbb{E}\left(\mathbb{C}^{(s)}\right)\right)^2\right]}}$$

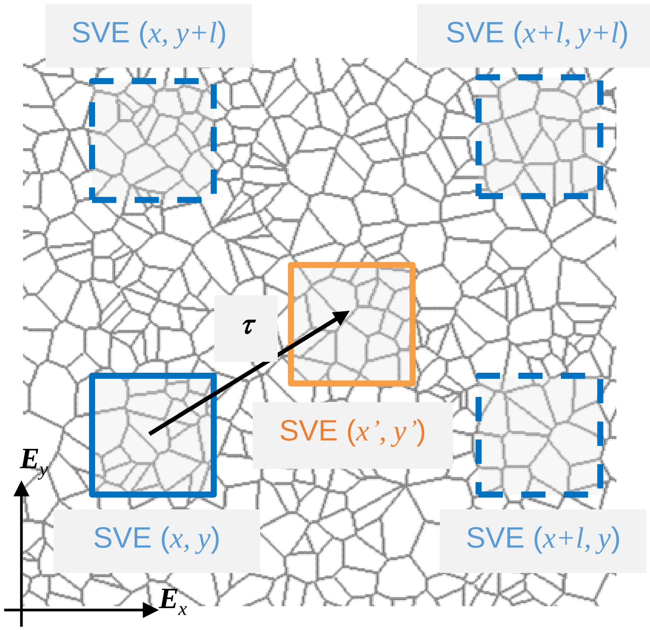

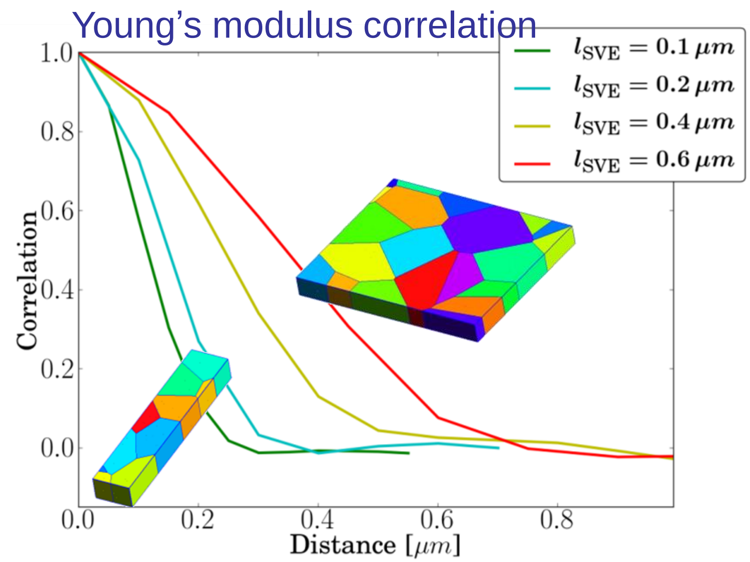

  - Definition of the correlation length

$$L_{\mathbb{C}}^{(rs)} = \frac{\int_{-\infty}^{\infty} R_{\mathbb{C}}^{(rs)}}{R_{\mathbb{C}}^{(rs)}(0)}$$

- Application to polycrystalline materials: The meso-scale random field
  - Accounts for the meso-scale distribution & spatial correlation

Random field with different SVEs sizes

$l_{\mathrm{SVE}} = 0.1\ \mu m$

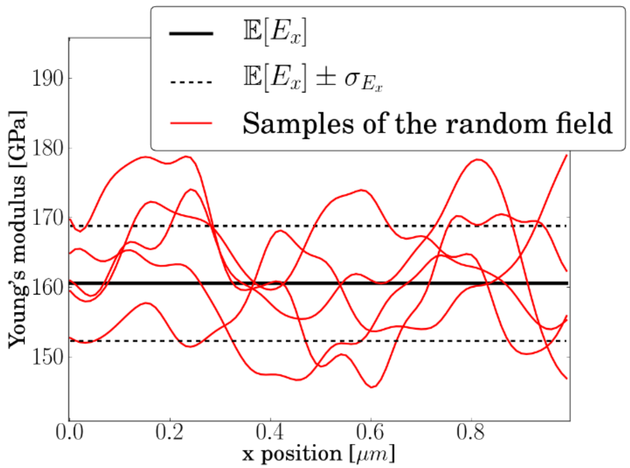

$l_{\mathrm{SVE}} = 0.4\ \mu m$

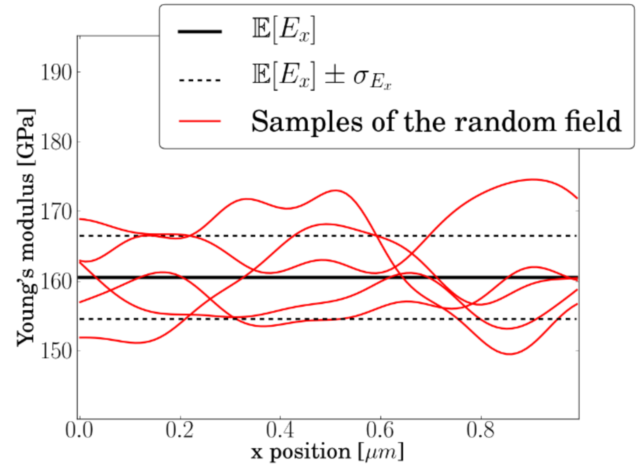

  - Needs to be generated using a stochastic model

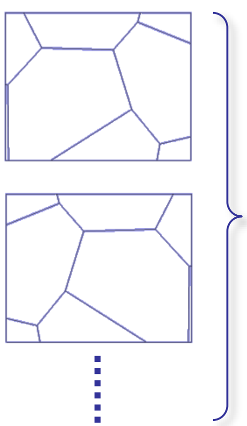

Stochastic model

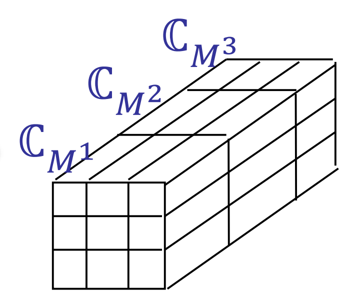

- Stochastic model of Gaussian meso-scale random fields
  - Define the homogenous zero-mean random field $\mathcal{A}'(\boldsymbol{x},\boldsymbol{\theta})$
    - Elasticity tensor $\mathbb{C}_{\mathrm{M}}(x,\theta)$ (matrix form $\boldsymbol{C}_M$) is bounded

$$\boldsymbol{\varepsilon}:(\mathbb{C}_{\mathrm{M}}-\mathbb{C}_{\mathrm{L}}):\boldsymbol{\varepsilon}>0 \qquad \forall\boldsymbol{\varepsilon}$$

    - Use a Cholesky decomposition

$$\boldsymbol{C}_{\mathrm{M}}(\boldsymbol{x},\boldsymbol{\theta})=\boldsymbol{C}_{\mathrm{L}}+\left(\bar{\mathcal{A}}+\mathcal{A}'(\boldsymbol{x},\boldsymbol{\theta})\right)^T\left(\bar{\mathcal{A}}+\mathcal{A}'(\boldsymbol{x},\boldsymbol{\theta})\right)$$

  - Evaluate the covariance function

$$\tilde{R}^{(rs)}_{\mathcal{A}'}(\boldsymbol{\tau})=\sigma_{\mathcal{A}'^{(r)}}\sigma_{\mathcal{A}'^{(s)}}R^{(rs)}_{\mathcal{A}'}(\boldsymbol{\tau})$$
$$=\mathbb{E}\left[\left(\mathcal{A}'^{(r)}(\boldsymbol{x})\right)\left(\mathcal{A}'^{(s)}(\boldsymbol{x}+\boldsymbol{\tau})\right)\right]$$

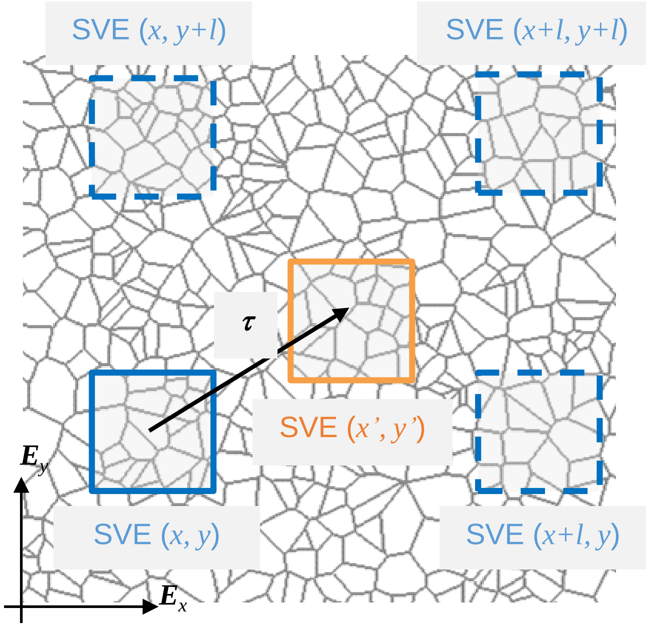

  - Evaluate the spectral density matrix from periodized zero-padded matrix $\tilde{\boldsymbol{R}}^{\mathrm{P}}_{\mathcal{V}'}(\boldsymbol{\tau})$

$$\boldsymbol{S}^{(rs)}_{\mathcal{A}'}\left[\boldsymbol{\omega}^{(\boldsymbol{m})}\right]=\sum_{n}\tilde{R}^{\mathrm{P}}_{\mathcal{A}'}{}^{(rs)}\left[\boldsymbol{\tau}^{(\boldsymbol{n})}\right]e^{-2\pi i\boldsymbol{\tau}^{(\boldsymbol{n})}\cdot\boldsymbol{\omega}^{(\boldsymbol{m})}} \quad \& \quad \boldsymbol{S}_{\mathcal{A}'}\left[\boldsymbol{\omega}^{(\boldsymbol{m})}\right]=\boldsymbol{H}_{\mathcal{A}'}\left[\boldsymbol{\omega}^{(\boldsymbol{m})}\right]\boldsymbol{H}^{*}_{\mathcal{A}'}\left[\boldsymbol{\omega}^{(\boldsymbol{m})}\right]$$

  - Generate a Gaussian random field $\mathcal{A}'(\boldsymbol{x},\boldsymbol{\theta})$

$$\mathcal{A}'^{(r)}(\boldsymbol{x},\boldsymbol{\theta})=\sqrt{2\Delta\omega}\,\Re\left(\sum_{s}\sum_{\boldsymbol{m}}\boldsymbol{H}^{(rs)}_{\mathcal{A}'}\left[\boldsymbol{\omega}^{(\boldsymbol{m})}\right]\eta^{(s,\boldsymbol{m})}\,e^{2\pi i\left(\boldsymbol{x}\cdot\boldsymbol{\omega}^{(\boldsymbol{m})}+\boldsymbol{\theta}^{(s,\boldsymbol{m})}\right)}\right)$$

- Stochastic model of non-Gaussian meso-scale random fields
  - Start from micro-sampling of the stochastic homogenization
    - The continuous form of the targeted PSD function

$$\boldsymbol{S}^{\mathrm{T}^{(rs)}}(\boldsymbol{\omega}) = \Delta\boldsymbol{\tau}\boldsymbol{S}^{(rs)}_{\boldsymbol{\mathcal{V}}'}\left[\boldsymbol{\omega}^{(m)}\right] = \Delta\boldsymbol{\tau}\sum_{n} \widetilde{R}^{\mathrm{P}}_{\mathcal{A}'}{}^{(rs)}\left[\boldsymbol{\tau}^{(n)}\right]e^{-2\pi i\boldsymbol{\tau}^{(n)}\cdot\boldsymbol{\omega}^{(m)}}$$

    - The targeted marginal distribution density function $\boldsymbol{F}^{\mathrm{NG}(\boldsymbol{r})}$ of the random variable $\mathcal{A}'^{(\boldsymbol{r})}$
    - A marginal Gaussian distribution $\boldsymbol{F}^{\boldsymbol{G}(\boldsymbol{r})}$ of zero-mean and targeted variance $\boldsymbol{\sigma}_{\mathcal{A}'^{(r)}}$
  - Iterate

Generate Gaussian random vector $\mathcal{A}'^{\mathrm{G}}(\boldsymbol{x})$ from $\boldsymbol{S}^{(rs)}(\boldsymbol{\omega})$

Map $\mathcal{A}'^{\boldsymbol{G}}(\boldsymbol{x})$ to a non-Gaussian field:

$$\mathcal{A}'^{\mathrm{NG}^{(r)}}(\boldsymbol{x}) = \boldsymbol{F}^{\mathrm{NG}(\boldsymbol{r})^{-1}}\left(\boldsymbol{F}^{\mathrm{G}(\boldsymbol{r})}\left(\mathcal{A}'^{\mathrm{G}^{(r)}}(\boldsymbol{x})\right)\right)$$

Evaluate the PSD $\boldsymbol{S}^{\mathrm{NG}^{(rs)}}(\boldsymbol{\omega})$ of $\boldsymbol{\mathcal{V}}^{\mathrm{NG}}(\boldsymbol{x})$

$$\boldsymbol{S}^{\mathrm{NG}^{(rs)}} \simeq \boldsymbol{S}^{\mathrm{T}^{(rs)}}?$$

No

$$\boldsymbol{S}^{(rs)}(\boldsymbol{\omega}) \leftarrow \boldsymbol{S}^{(rs)}(\boldsymbol{\omega})\frac{\boldsymbol{S}^{\mathrm{T}^{(rr)}}(\boldsymbol{\omega})\boldsymbol{S}^{\mathrm{T}^{(ss)}}(\boldsymbol{\omega})}{\boldsymbol{S}^{\mathrm{NG}^{(rr)}}(\boldsymbol{\omega})\boldsymbol{S}^{\mathrm{NG}^{(ss)}}(\boldsymbol{\omega})}$$

- The meso-scale stochastic model
  - Application to film deposited at 610 ºC:
  - Comparison between micro-samples and generated fields

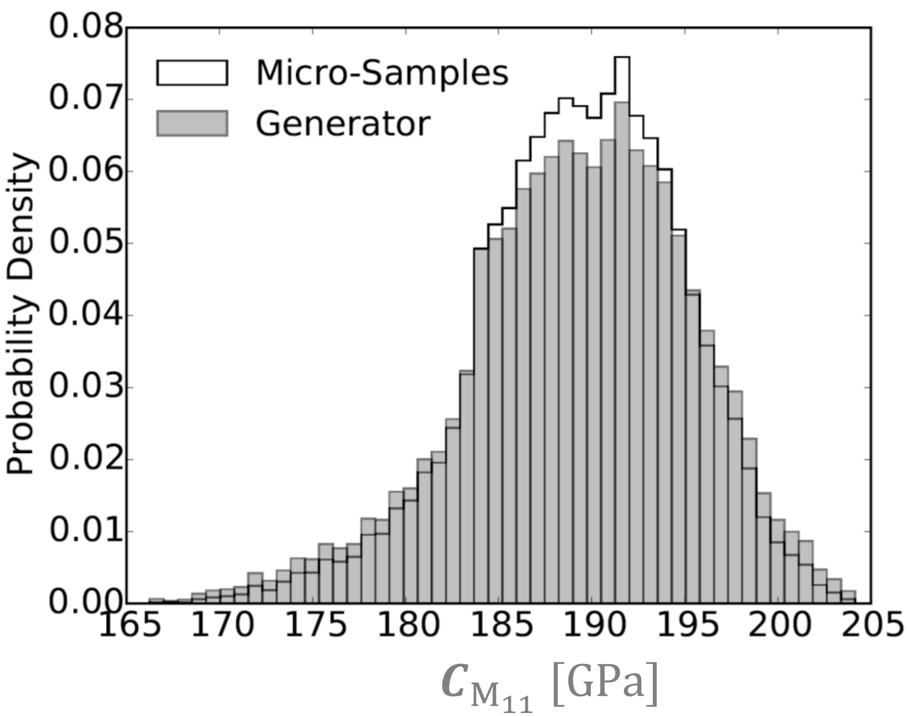

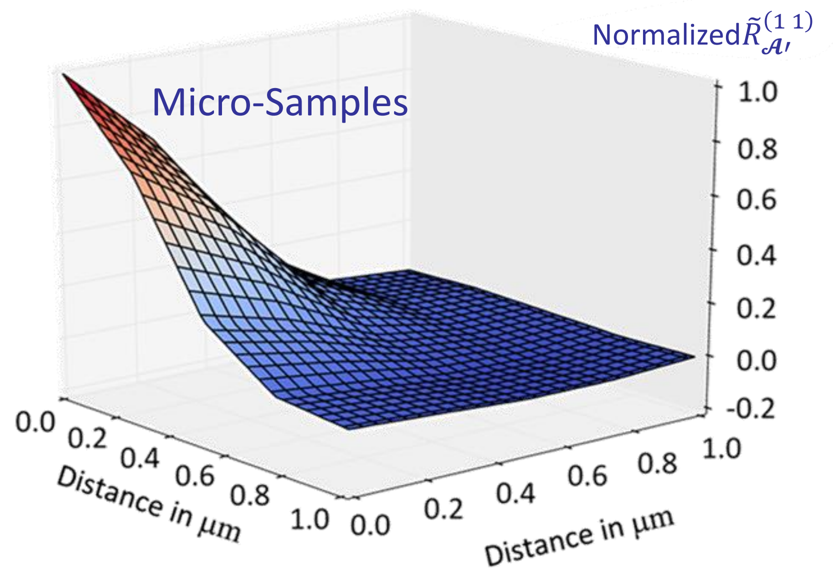

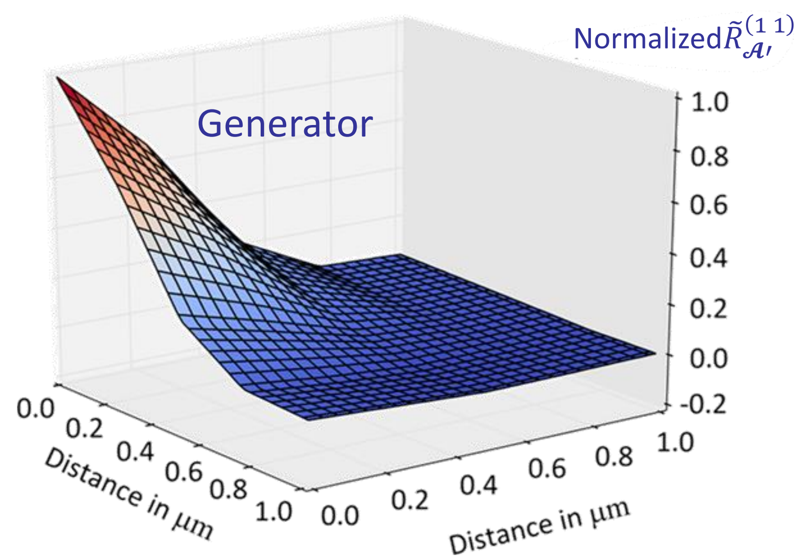

- Application to polycrystalline materials: The meso-scale to macro-scale transition
  - Convergence in terms of $\alpha = \frac{l_{\mathbb{C}}}{l_{\text{mesh}}}$, the correlation length and macro-mesh ratio
  - The results converge
    - With the mesh size for all the SVE sizes
    - Toward the direct Monte Carlo simulations results

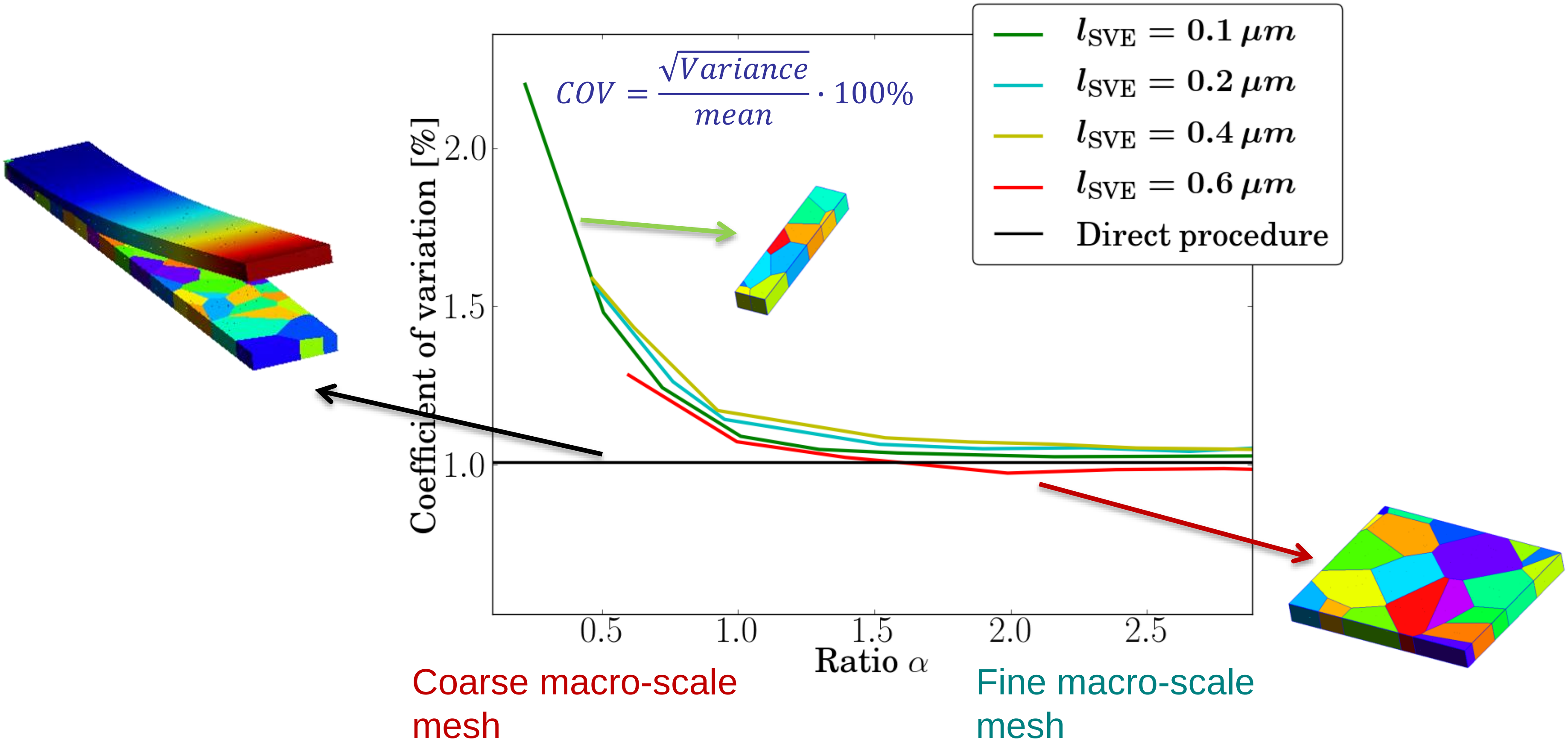

- Application to polycrystalline materials: The meso-scale to macro-scale transition
  - Comparison with direct Monte Carlo simulations

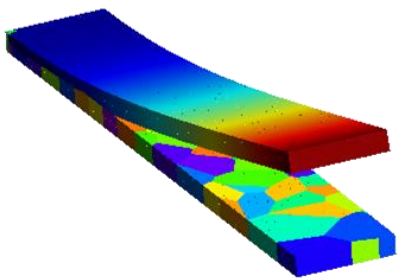

Relative difference in the mean: 0.57 %

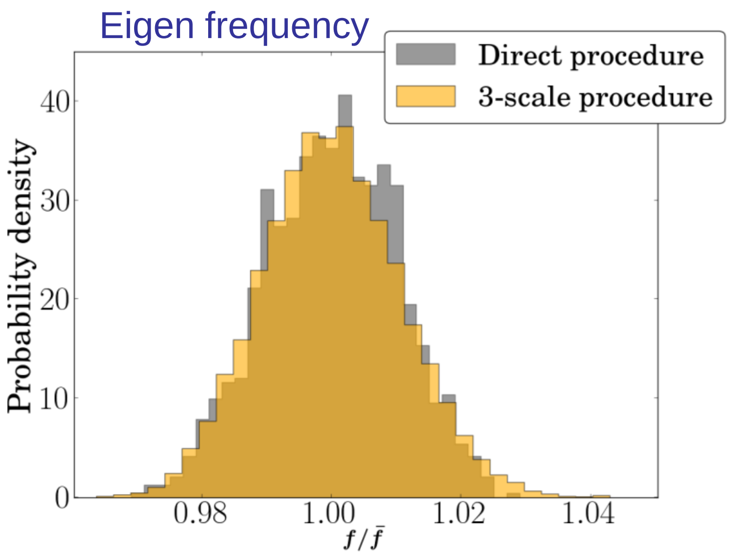

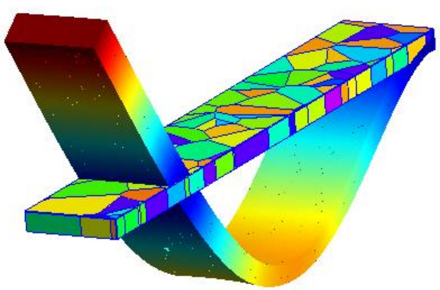

Relative difference in the mean: 0.44 %

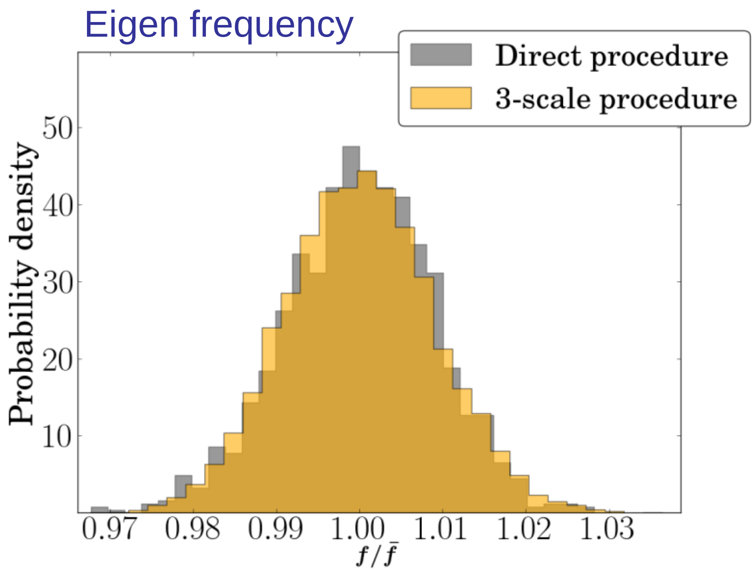

- Thermo-mechanical homogenization
  - Down-scaling

$$\begin{cases} \boldsymbol{\varepsilon}_{\mathrm{M}} = \dfrac{1}{V(\omega)} \displaystyle\int_{\omega} \boldsymbol{\varepsilon}_{\mathrm{m}} d\omega \\ \nabla_{\mathrm{M}} \vartheta_{\mathrm{M}} = \dfrac{1}{V(\omega)} \displaystyle\int_{\omega} \nabla_{\mathrm{m}} \vartheta_{\mathrm{m}} d\omega \\ \vartheta_{\mathrm{M}} = \dfrac{1}{V(\omega)} \displaystyle\int_{\omega} \dfrac{\rho_{\mathrm{m}} C_{v\mathrm{m}}}{\rho_{\mathrm{M}} C_{v\mathrm{M}}} \vartheta_{\mathrm{m}} d\omega \end{cases}$$

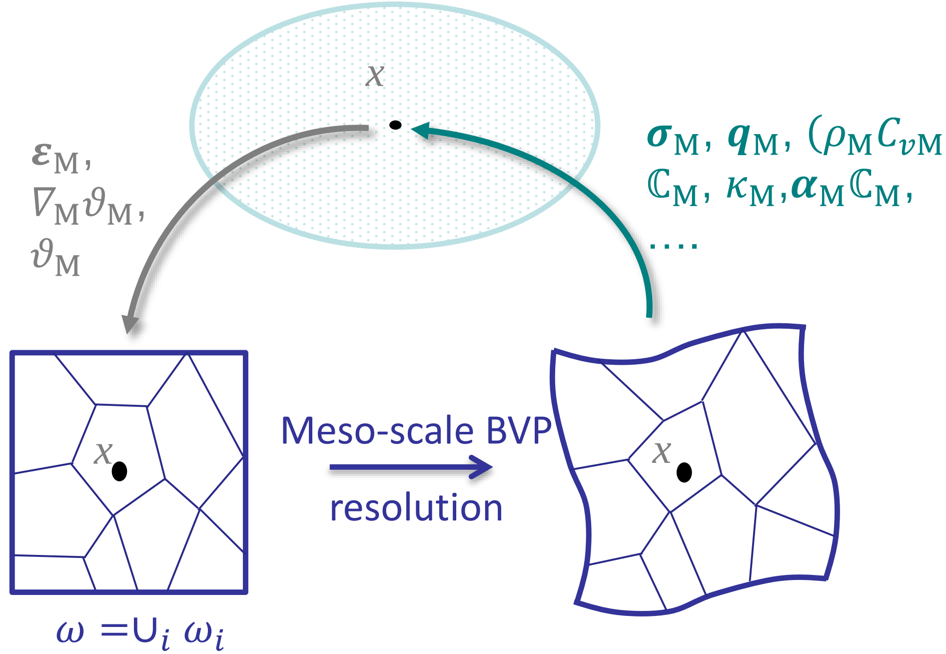

  - Up-scaling

$$\begin{cases} \boldsymbol{\sigma}_{\mathrm{M}} = \dfrac{1}{V(\omega)} \displaystyle\int_{\omega} \boldsymbol{\sigma}_{\mathrm{m}} d\omega \\ \boldsymbol{q}_{\mathrm{M}} = \dfrac{1}{V(\omega)} \displaystyle\int_{\omega} \boldsymbol{q}_{\mathrm{m}} d\omega \\ \rho_{\mathrm{M}} C_{v\mathrm{M}} = \dfrac{1}{V(\omega)} \displaystyle\int \rho_{\mathrm{m}} C_{v\mathrm{m}} dV \end{cases} \longrightarrow \begin{cases} \mathbb{C}_{\mathrm{M}} = \dfrac{\partial \boldsymbol{\sigma}_{\mathrm{M}}}{\partial \boldsymbol{u}_{\mathrm{M}} \otimes \boldsymbol{\nabla}_{\mathrm{M}}} \quad \& \quad \boldsymbol{\alpha}_{\mathrm{M}} : \mathbb{C}_{\mathrm{M}} = -\dfrac{\partial \boldsymbol{\sigma}_{\mathrm{M}}}{\partial \vartheta_{\mathrm{M}}} \\ \boldsymbol{\kappa}_{\mathrm{M}} = -\dfrac{\partial \boldsymbol{q}_{\mathrm{M}}}{\partial \nabla_{\mathrm{M}} \vartheta_{\mathrm{M}}} \end{cases}$$

  - Consistency $\longrightarrow$ Satisfied by periodic boundary conditions

- Quality factor
  - Micro-resonators
    - Temperature changes with compression/traction
    - Energy dissipation

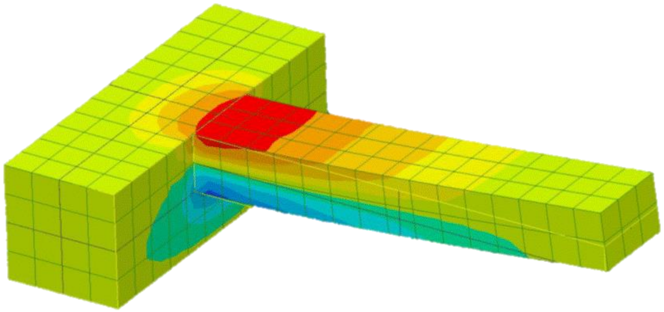

  - Eigen values problem
    - Governing equations

$$\begin{bmatrix}\mathbf{M} & \mathbf{0}\\ \mathbf{0} & \mathbf{0}\end{bmatrix}\begin{bmatrix}\ddot{\mathbf{u}}\\ \ddot{\boldsymbol{\vartheta}}\end{bmatrix}+\begin{bmatrix}\mathbf{0} & \mathbf{0}\\ \mathbf{D}_{\mathrm{u}\vartheta}(\boldsymbol{\theta}) & \mathbf{D}_{\vartheta\vartheta}\end{bmatrix}\begin{bmatrix}\dot{\mathbf{u}}\\ \dot{\boldsymbol{\vartheta}}\end{bmatrix}+\begin{bmatrix}\mathbf{K}_{\mathrm{uu}}(\boldsymbol{\theta}) & \mathbf{K}_{\mathrm{u}\vartheta}(\boldsymbol{\theta})\\ \mathbf{0} & \mathbf{K}_{\vartheta\vartheta}(\boldsymbol{\theta})\end{bmatrix}\begin{bmatrix}\mathbf{u}\\ \boldsymbol{\vartheta}\end{bmatrix}=\begin{bmatrix}\boldsymbol{F}_{\mathrm{u}}\\ \boldsymbol{F}_{\vartheta}\end{bmatrix}$$

    - Free vibrating problem

$$\begin{bmatrix}\mathbf{u}(t)\\ \boldsymbol{\vartheta}(t)\end{bmatrix}=\begin{bmatrix}\mathbf{u}_0\\ \boldsymbol{\vartheta}_0\end{bmatrix}e^{i\omega t}$$

$$\hookrightarrow \begin{bmatrix}-\mathbf{K}_{\mathrm{uu}}(\boldsymbol{\theta}) & -\mathbf{K}_{\mathrm{u}\vartheta}(\boldsymbol{\theta}) & \mathbf{0}\\ \mathbf{0} & -\mathbf{K}_{\vartheta\vartheta}(\boldsymbol{\theta}) & \mathbf{0}\\ \mathbf{0} & \mathbf{0} & \mathbf{I}\end{bmatrix}\begin{bmatrix}\mathbf{u}\\ \boldsymbol{\vartheta}\\ \dot{\mathbf{u}}\end{bmatrix}=i\omega\begin{bmatrix}\mathbf{0} & \mathbf{0} & \mathbf{M}\\ \mathbf{D}_{\vartheta\mathrm{u}}(\boldsymbol{\theta}) & \mathbf{D}_{\vartheta\vartheta} & \mathbf{0}\\ \mathbf{I} & \mathbf{0} & \mathbf{0}\end{bmatrix}\begin{bmatrix}\mathbf{u}\\ \boldsymbol{\vartheta}\\ \dot{\mathbf{u}}\end{bmatrix}$$

  - Quality factor
    - From the dissipated energy per cycle
    - $Q^{-1}=\dfrac{2|\Im\omega\,|}{\sqrt{(\Im\omega)^2+(\Re\omega)^2}}$

- Application of the 3-Scale method to extract the quality factor distribution
  - 3D models readily available
  - The effect of the anchor can be studied

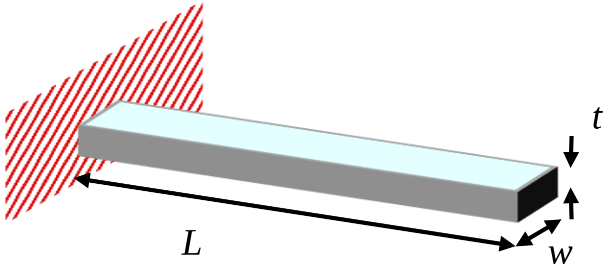

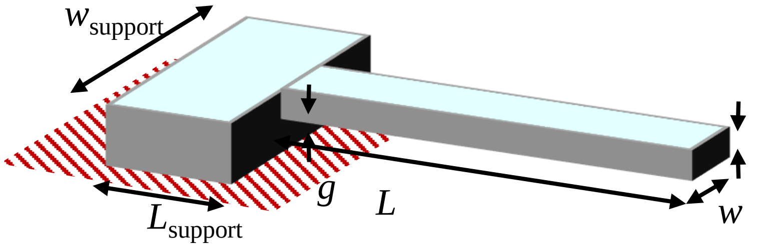

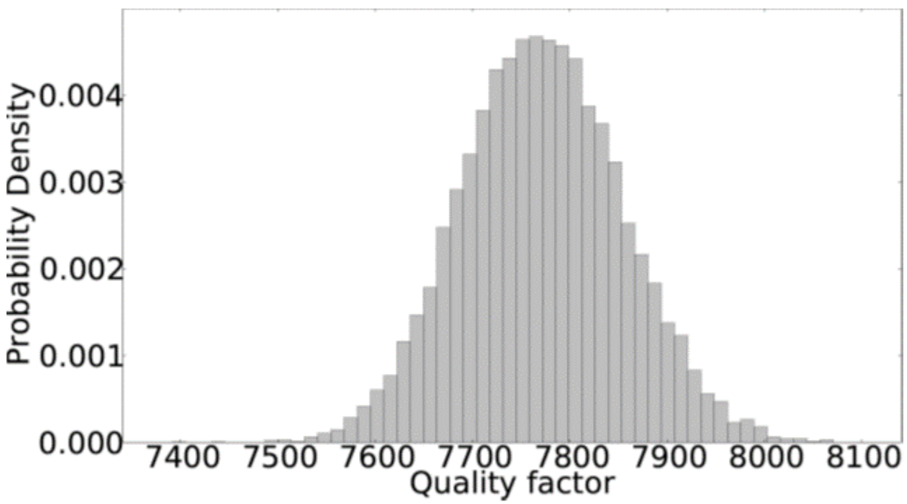

15 x 3 x 2 μm^3-beam,

deposited at 610 ºC

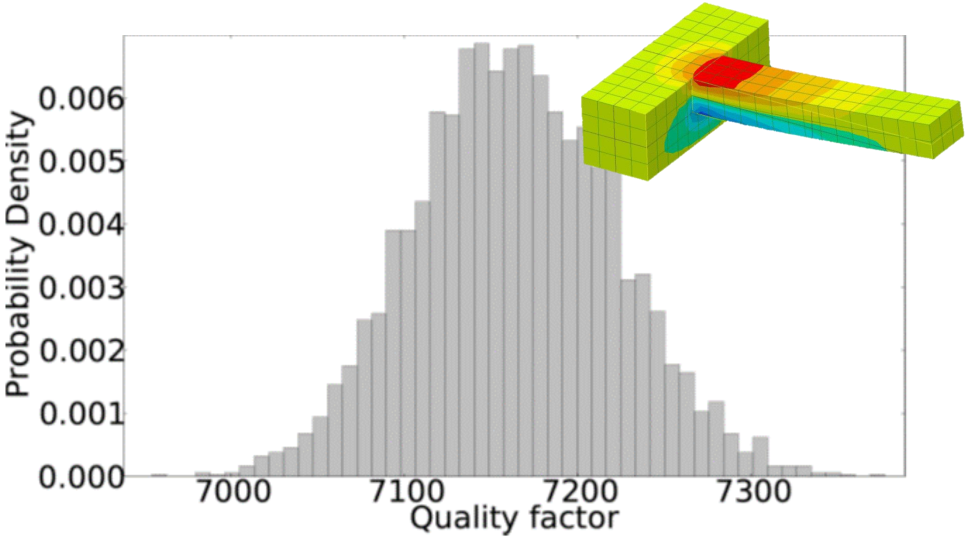

15 x 3 x 2 μm^3-beam & anchor,

deposited at 610 ºC

- Surface topology: asperity distribution
  - Upper surface topology by AFM (Atomic Force Microscope) measurements on 2 µm-thick poly-silicon films

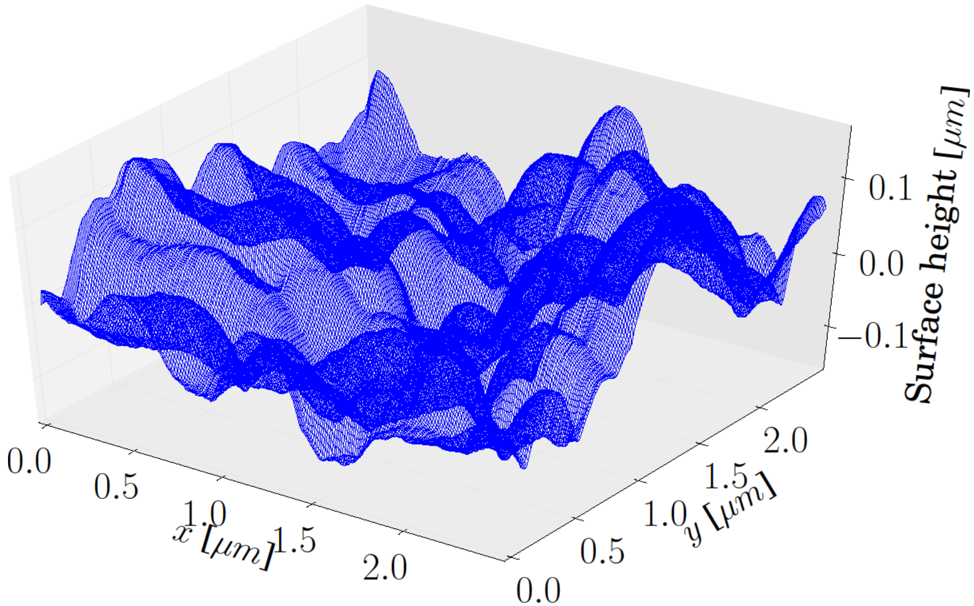

Deposition temperature [ºC]	580	610	630	650
Std deviation [nm]	35.6	60.3	90.7	88.3

AFM data provided by IMT Bucharest, Rodica Voicu, Angela Baracu, Raluca Muller

Stochastic 3-Scale Models

- Accounting for roughness
  - Second-order homogenization

$$\begin{cases} \tilde{\boldsymbol{n}}_{\mathrm{M}} = \mathbb{C}_{\mathrm{M}_1} : \boldsymbol{\varepsilon}_{\mathrm{M}} + \mathbb{C}_{\mathrm{M}_2} : \boldsymbol{\kappa}_{\mathrm{M}} \\ \tilde{\boldsymbol{m}}_{\mathrm{M}} = \mathbb{C}_{\mathrm{M}_3} : \boldsymbol{\varepsilon}_{\mathrm{M}} + \mathbb{C}_{\mathrm{M}_4} : \boldsymbol{\kappa}_{\mathrm{M}} \end{cases}$$

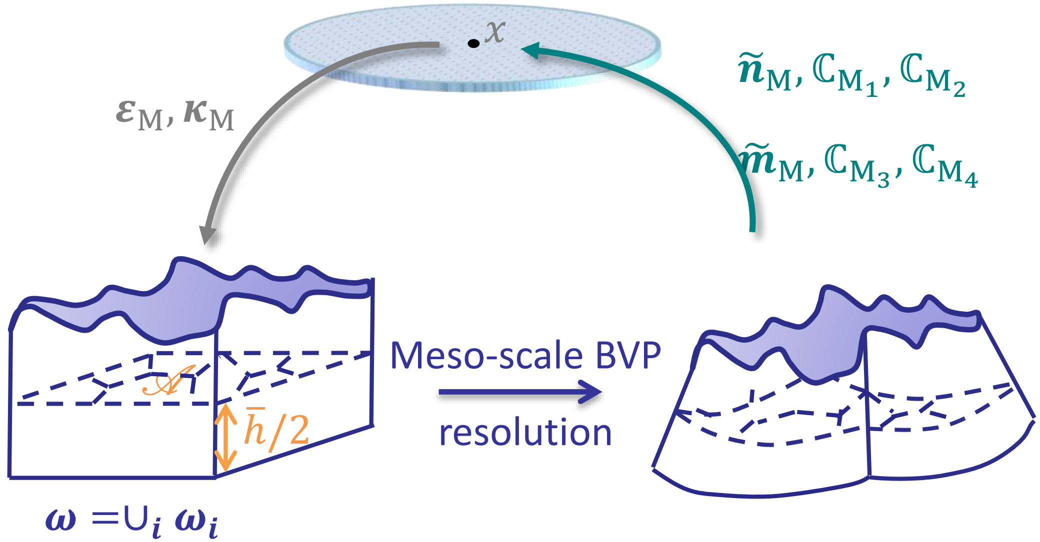

  - Stochastic homogenization
    - Several SVE realizations
    - For each SVE $\omega_j = \cup_i \omega_i$
    - The density per unit area is now non-constant

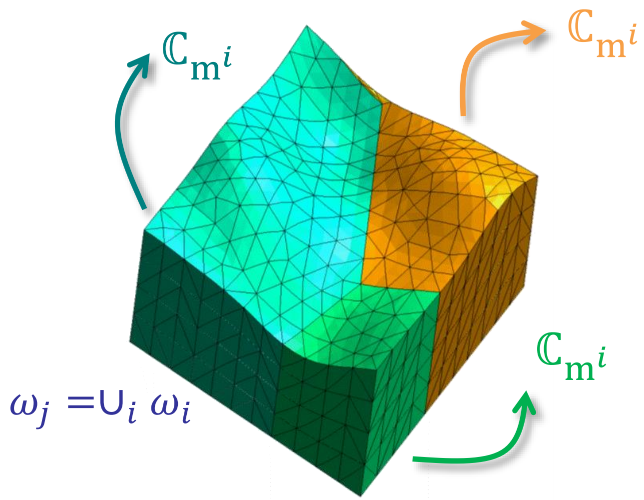

$\mathbb{C}_{\mathrm{m}^i}\ \forall i \longrightarrow \mathbb{C}_{\mathrm{M}_1^j}, \mathbb{C}_{\mathrm{M}_2^j}, \mathbb{C}_{\mathrm{M}_3^j}, \mathbb{C}_{\mathrm{M}_4^j} \longrightarrow \mathrm{U}_{\mathrm{M}^j}$

Computational homogenization

$\bar{\boldsymbol{\rho}}_{\mathrm{M}^j}$

Samples of the meso-scale homogenized elasticity matrix U_{M} & density $\bar{\boldsymbol{\rho}}_{\mathrm{M}}$

Stochastic 3-Scale Models

- Accounting for roughness
  - Cantilever of 8 x 3 x t $\mu\mathrm{m}^3$ deposited at 610 ºC

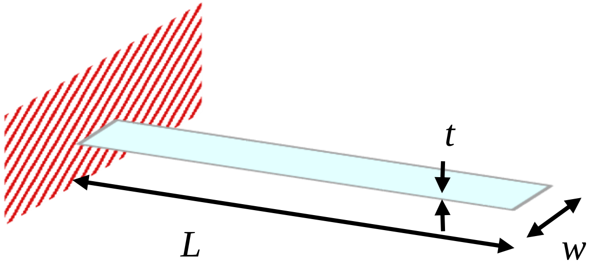

Flat SVEs (no roughness) - F
Rough SVEs (Polysilicon film deposited at 610 ºC) - R
Grain orientation following XRD measurements – Si_{pref}
Grain orientation uniformly distributed – Si_{uni}
Reference isotropic material – Iso

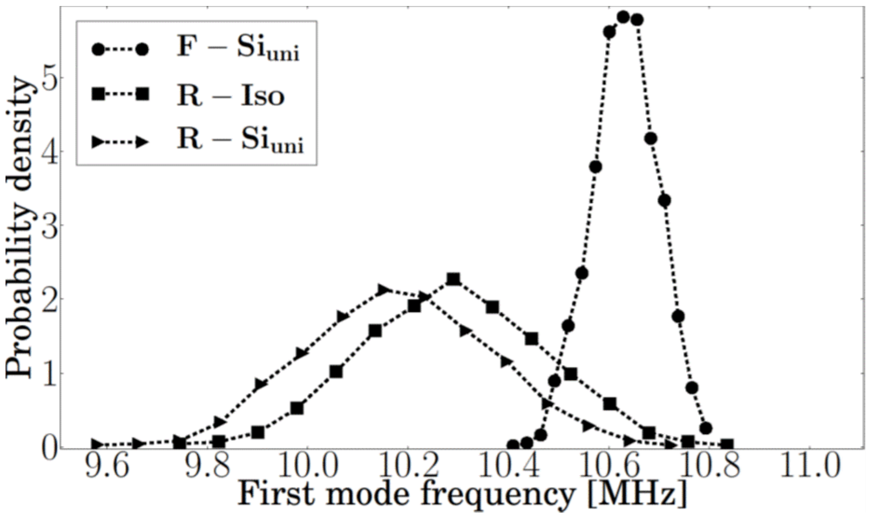

Roughness effect is the most important for 8 x 3 x 0.5 $\mu\mathrm{m}^3$ cantilevers

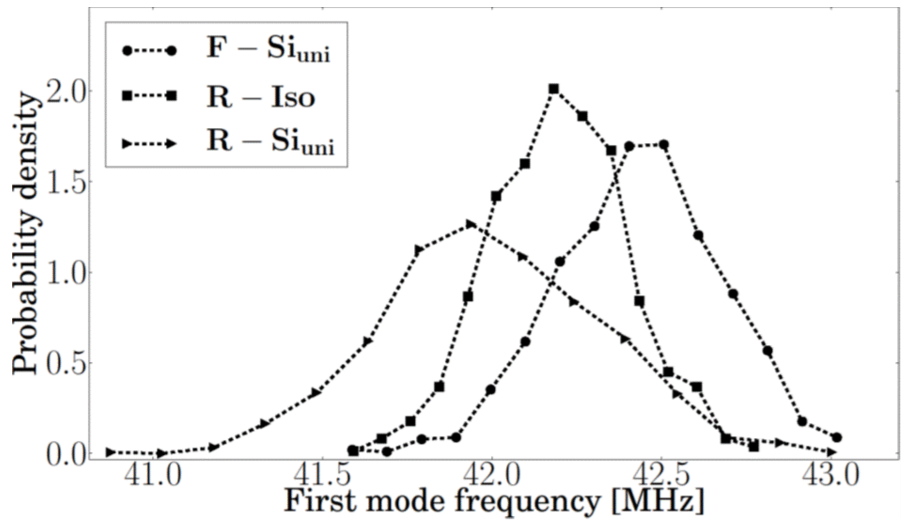

Roughness effect is of same importance as orientation for 8 x 3 x 2 $\mu\mathrm{m}^3$ cantilevers

- Application to robust design
  - Determination of probabilistic meso-scale properties
  - Propagate uncertainties to higher scale
  - Vibro-meter sensors:
    - Uncertainties in resonance frequency / Q factor

- 3SMVIB MNT.ERA-NET project
  - Open-Engineering, V2i, ULiège (Belgium)
  - Polit. Warszawska (Poland)
  - IMT, Univ. Cluj-Napoca (Romania)

- Publications (doi)
  - 10.1002/nme.5452
  - 10.1016/j.cma.2016.07.042
  - 10.1016/j.cma.2015.05.019

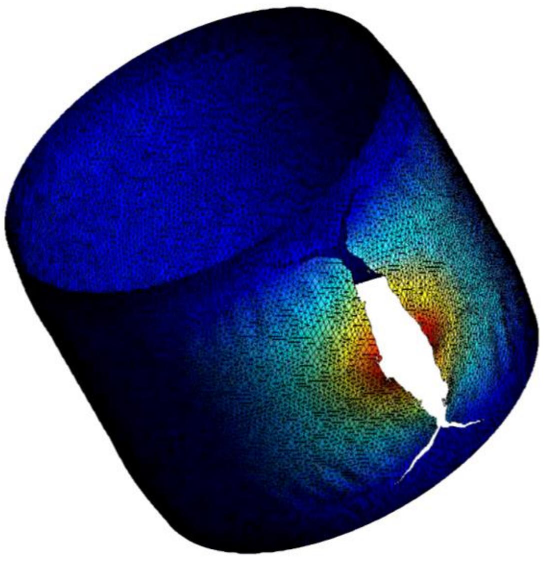

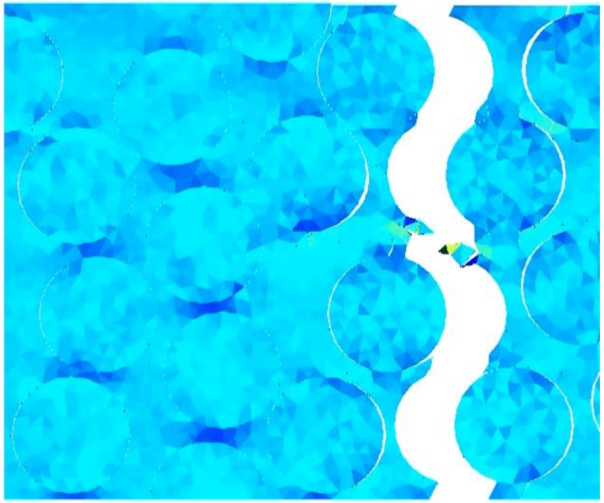

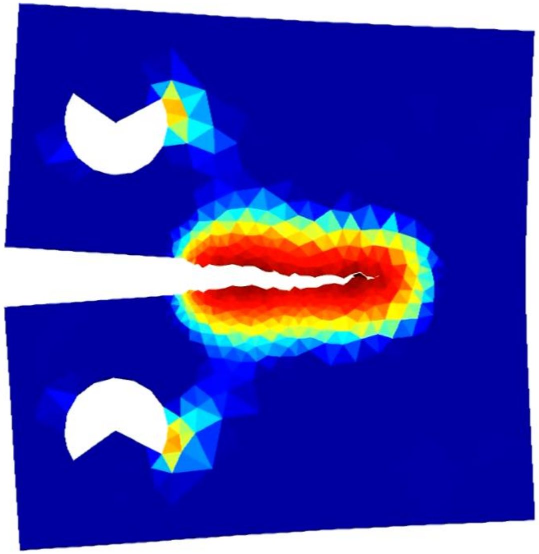

DG-Based (Multi-Scale) Fracture

The research has been funded by the Belgian National Fund for Education at the Research in Industry and Farming.
SIMUCOMP The research has been funded by the Walloon Region under the agreement no 1017232 (CT-EUC 2010-10-12) in the context of the ERA-NET +, Matera + framework.
The research has been funded by the Walloon Region under the agreement no.7581-MRIPF in the context of the 16th MECATECH call.

DG-Based Fracture

- Hybrid DG/cohesive law formulation
  - Discontinuous Galerkin method
    - Finite-element discretization
    - Same **discontinuous** polynomial approximations for the
      - **Test** functions φ_h and
      - **Trial** functions $\delta\varphi$

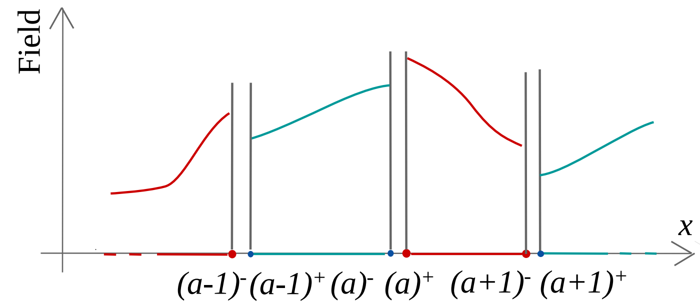

  - Can easily be combined with a cohesive law for fracture analyses
    - Interface elements already exist
    - Easy to shift from un-fractured to fractured states
    - Remains accurate before fracture onset (DG formulation)
    - Efficient // implementation

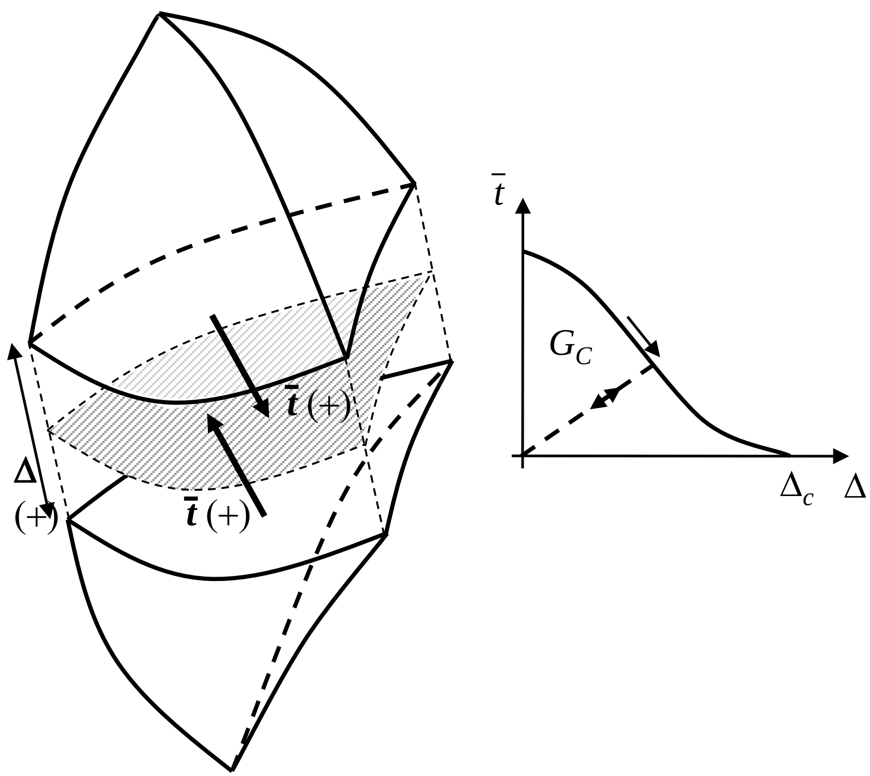

- Publications (doi)
  - [10.1016/j.cma.2010.08.014](10.1016/j.cma.2010.08.014)

DG-Based Multi-Scale Fracture

- Multi-scale modeling
  - 2 problems are solved concurrently
    - The macro-scale problem
    - The meso-scale problem (on a meso-scale Volume Element)

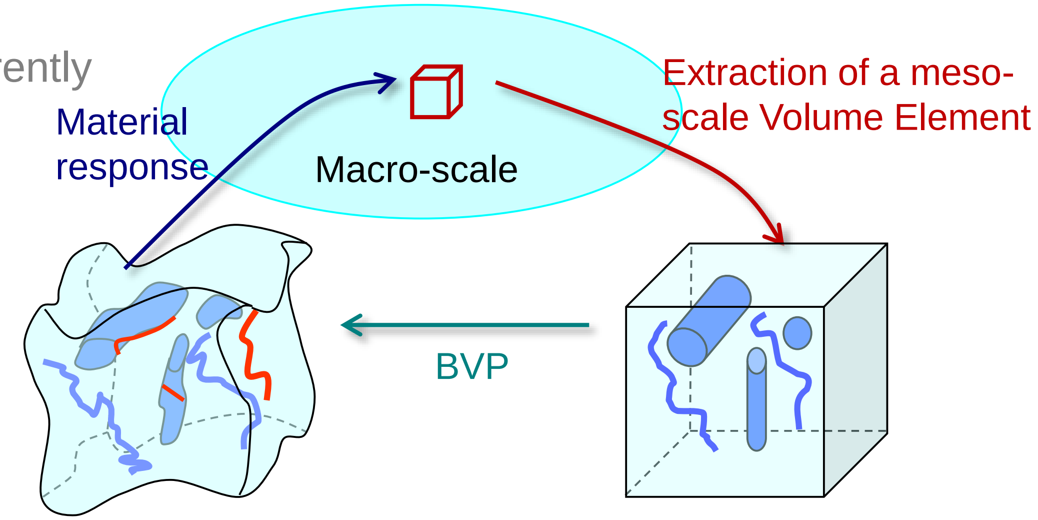

- For meso-scale volume elements embedding crack propagation

$L_{\text{macro}} >> L_{\text{VE}} \; ? \; L_{\text{micro}}$

For accuracy: Size of the meso-scale volume element smaller than the characteristic length of the macro-scale loading

The crack induces a loss of statistical representativeness
- **Should recover consistency lost due to the discontinuity**

DG-Based Multi-Scale Fracture

- Micro-Meso fracture model for intra-laminar failure
  - Epoxy-CF (60%), transverse loading
  - 3 stages captured

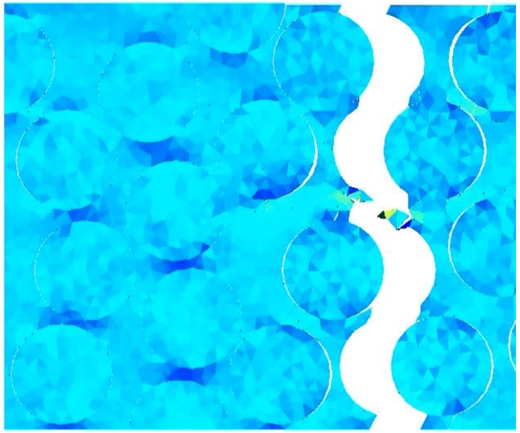

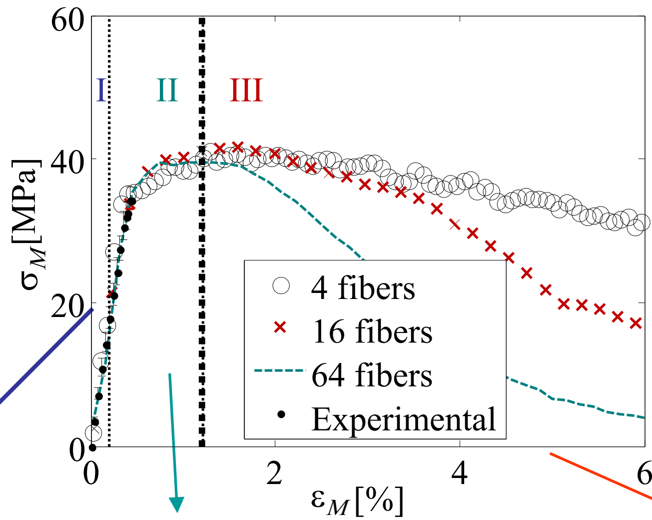

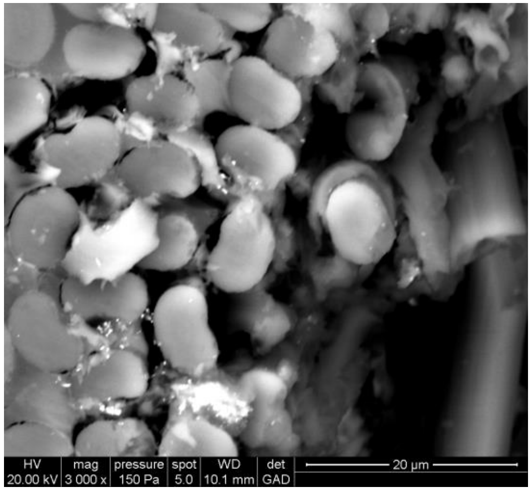

Elastic response

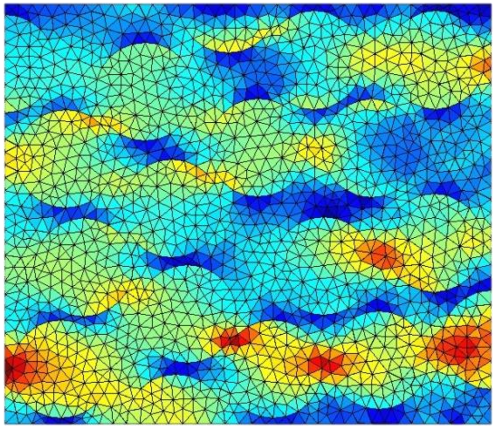

Damage due to debonding

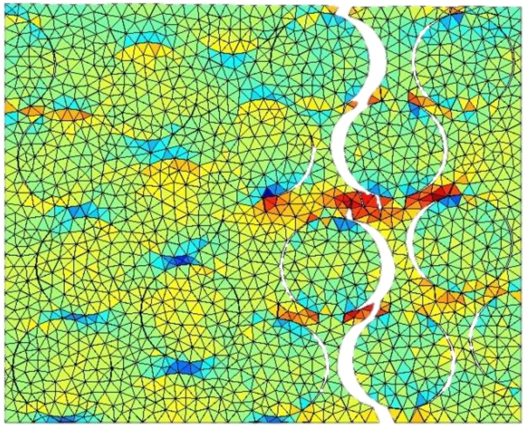

Meso-crack

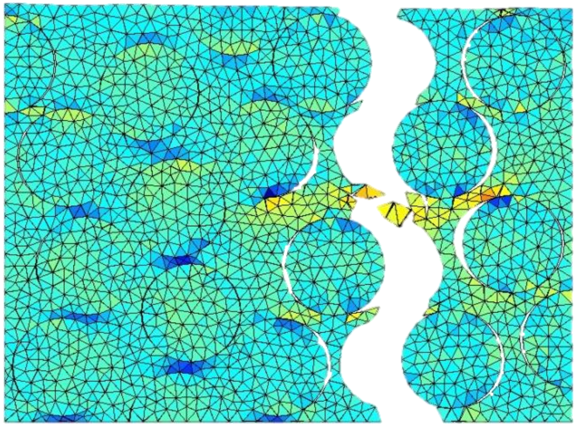

- Micro-Meso fracture model for intra-laminar failure (2)
  - Scale transition after softening onset
    - Should not depend on the RVE size
    - Extraction of the meso-scale TSL ($\bar{t}_M$ vs. Δ_M)

[Verhoosel et al., IJNME 2010]

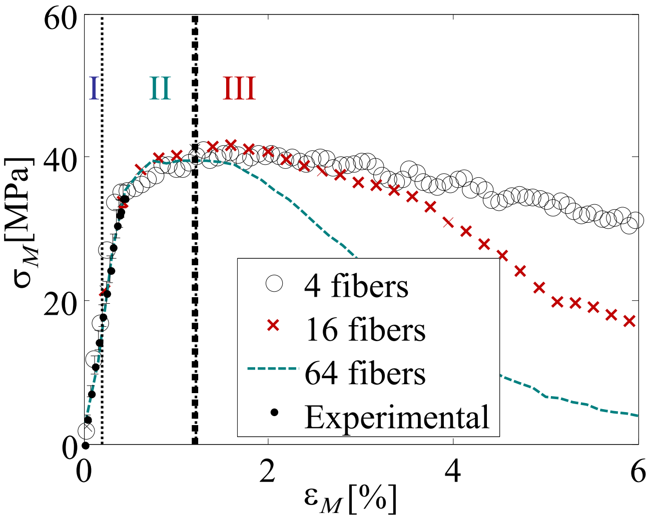

$$\delta\bar{\boldsymbol{t}}_M = \boldsymbol{\delta\sigma_M} \cdot \boldsymbol{e}_X$$

$$\delta\boldsymbol{\Delta}_M = \delta\boldsymbol{u}^m - L_{\text{cell}}\boldsymbol{C_M}^{-1}: \boldsymbol{e}_X \otimes \boldsymbol{e}_X \cdot \boldsymbol{\delta\bar{t}}_M$$

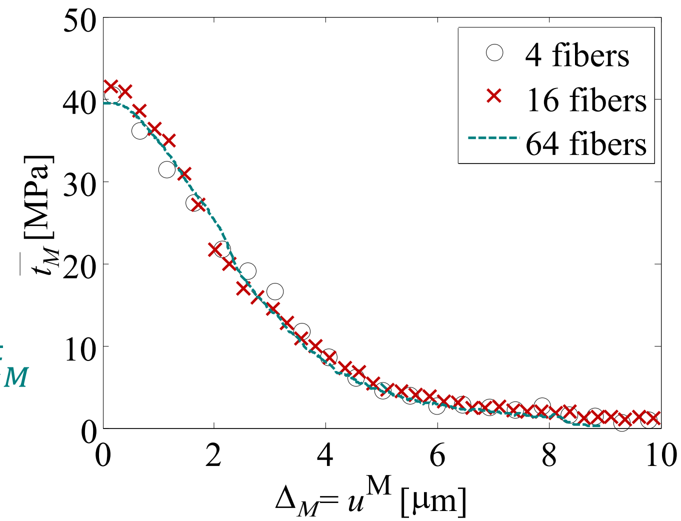

- SIMUCOMP ERA-NET project
  - e-Xstream, CENAERO, ULiège (Belgium)
  - IMDEA Materials (Spain)
  - CRP Henri-Tudor (Luxemburg)
- Publication (doi)
  - [10.1016/j.engfracmech.2013.03.018](https://doi.org/10.1016/j.engfracmech.2013.03.018)

- Fracture of thin structures

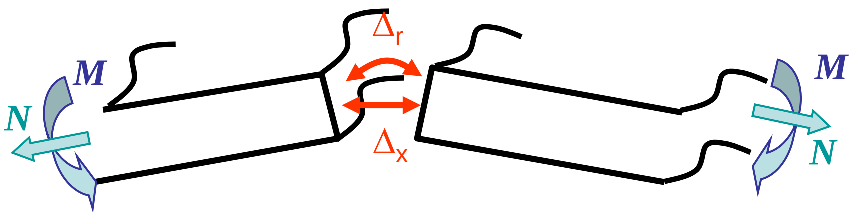

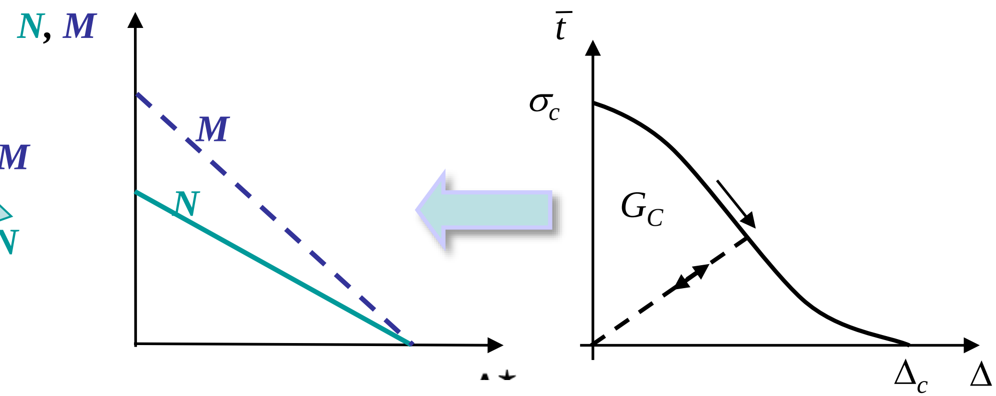

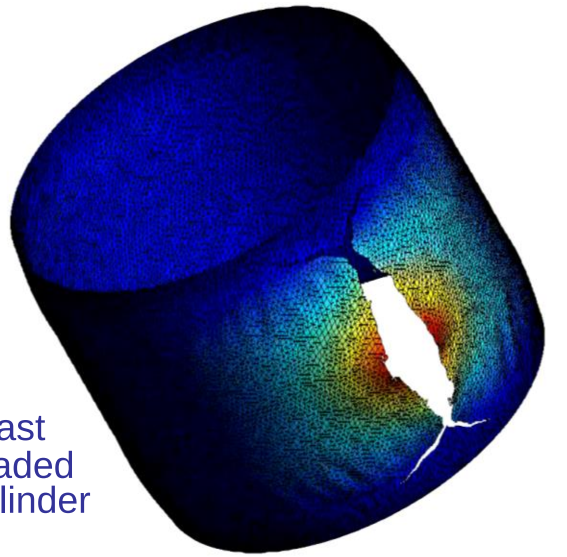
Blast loaded cylinder

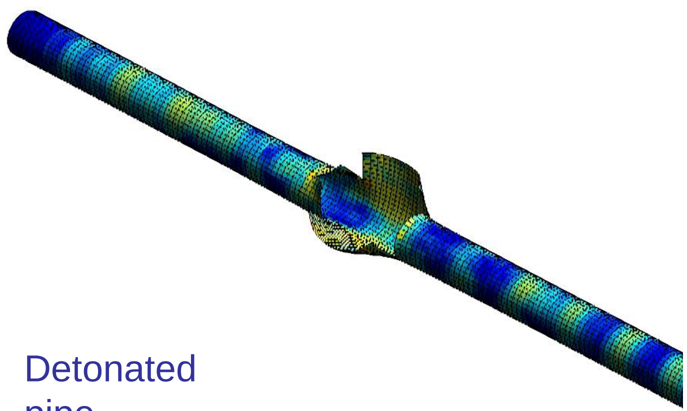
Detonated pipe

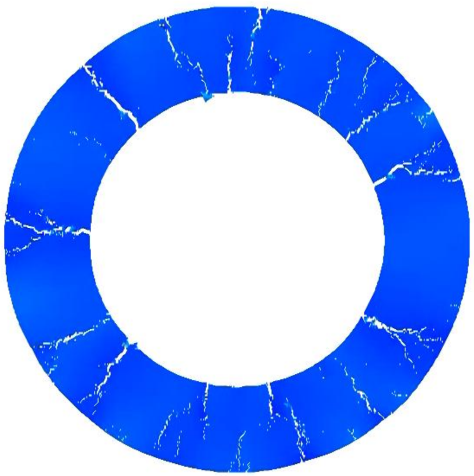
Fragmented disk

- FNRS-FRIA fellowship
- Publications (doi)
  - [10.1002/nme.4381]
  - [10.1007/s10704-012-9748-5]
  - [10.1016/j.cma.2011.07.008]
  - [10.1002/nme.3008]

- Capture triaxiality effects: Cohesive Band Model (CBM)
  - Introduction of a uniform band of given thickness h_b [Remmers et al. 2013]

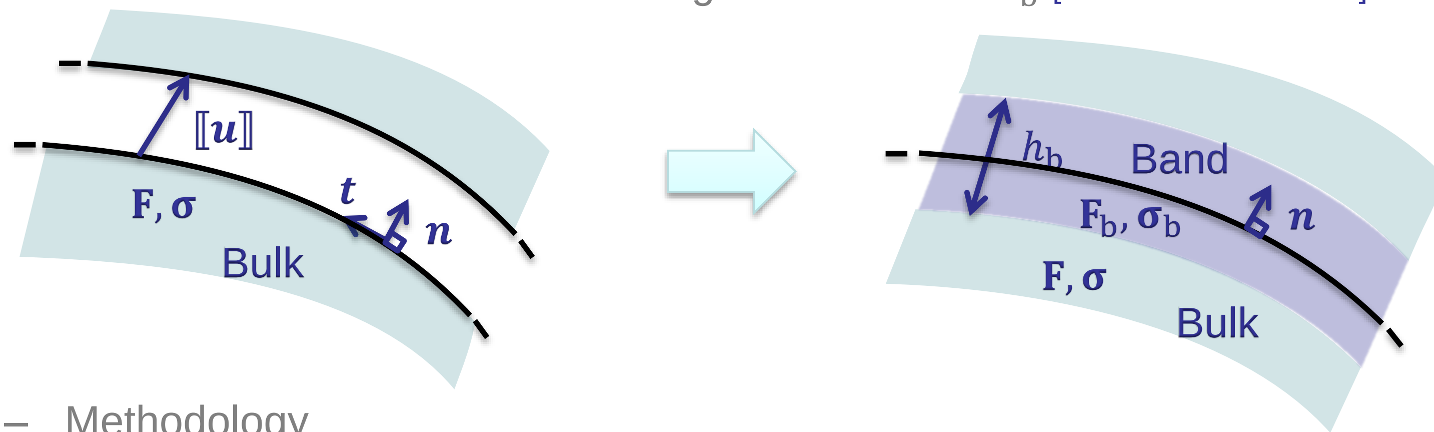

  - Methodology
    1. Bulk stress $\boldsymbol{\sigma}$ using non-local damage law
    2. Compute a "band" deformation gradient

$$\mathbf{F}_\mathrm{b} = \mathbf{F} + \frac{[\![\boldsymbol{u}]\!] \otimes \boldsymbol{N}}{h_\mathrm{b}} + \frac{1}{2}\boldsymbol{\nabla}_T [\![\boldsymbol{u}]\!]$$

    3. Band stress $\boldsymbol{\sigma}_\mathrm{b}$ using the (local) damage law
    4. Recover traction forces $\boldsymbol{t}([\![\boldsymbol{u}]\!], \mathbf{F}) = \boldsymbol{\sigma}_\mathrm{b}.\boldsymbol{n}$

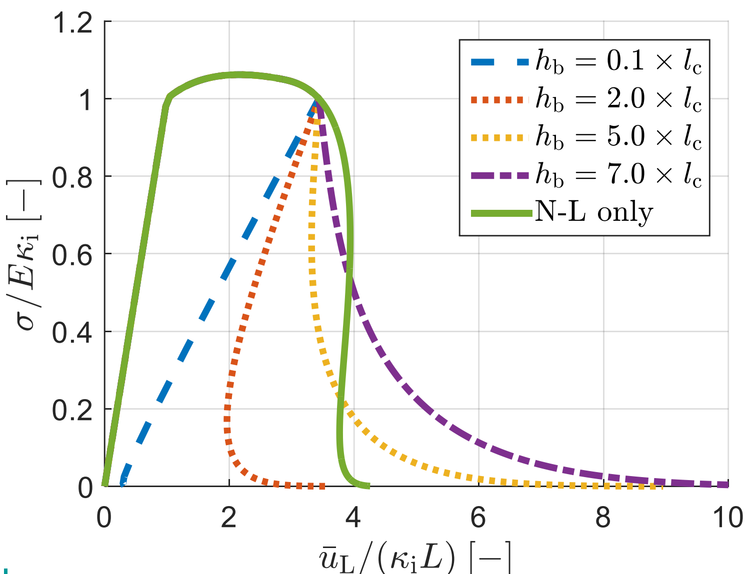

  - The cohesive band thickness
    - Evaluated to ensure energy consistency
    - Same dissipated energy as with a damage model

DG-Based elastic damage to crack transition

- Slit plate

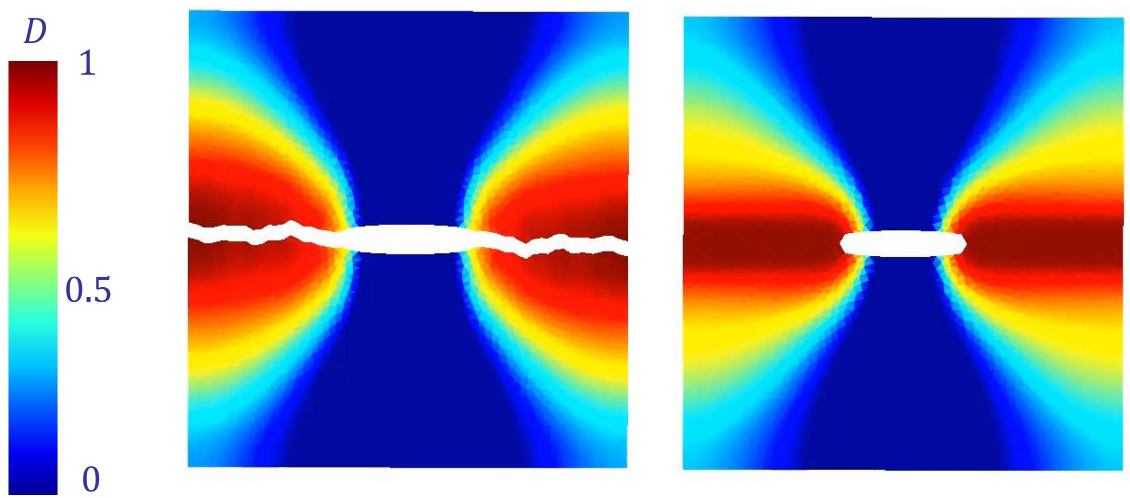

Non-Local+ CBM Non-Local

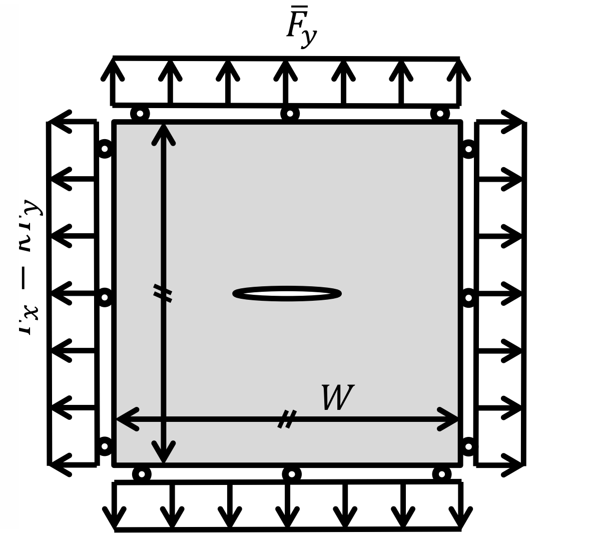

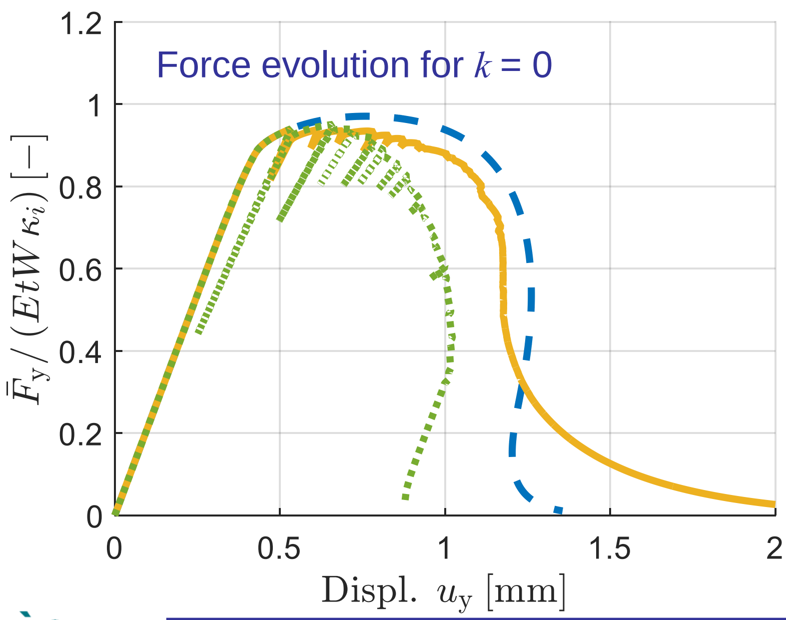

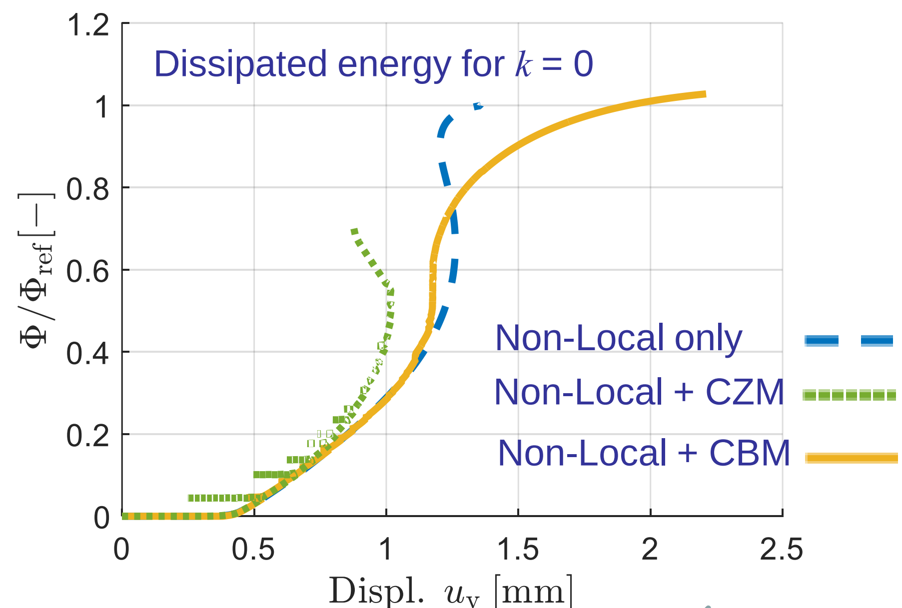

DG-Based elastic damage to crack transition

- Slit plate
  - Triaxiality effect through ratio k

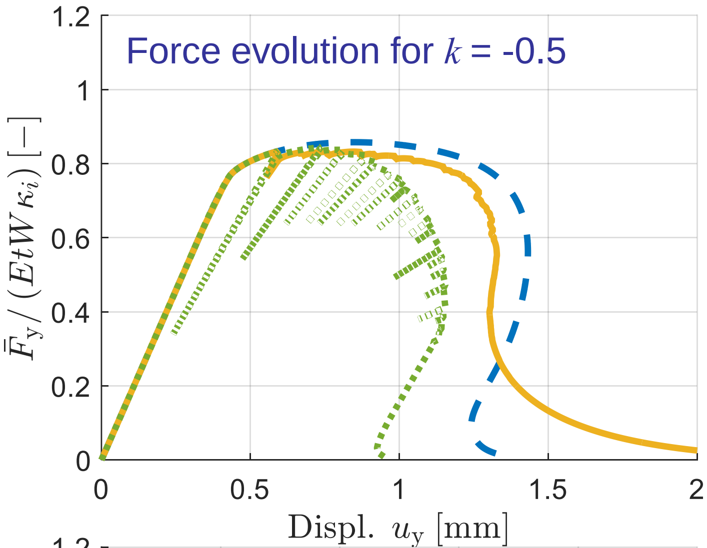

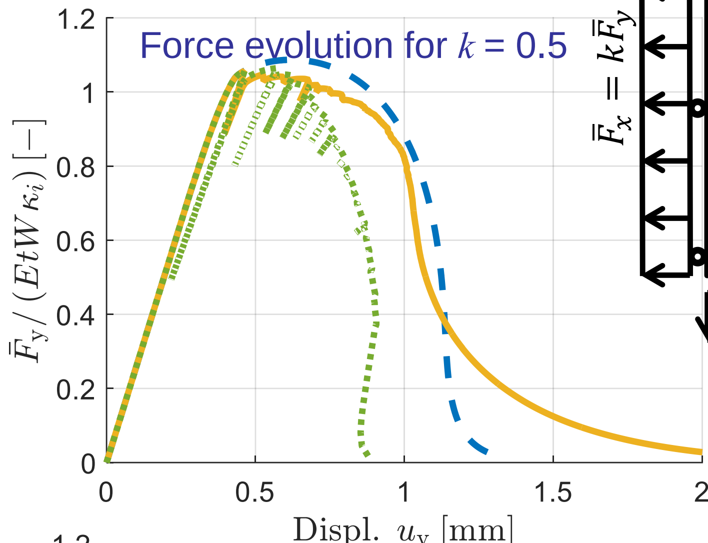

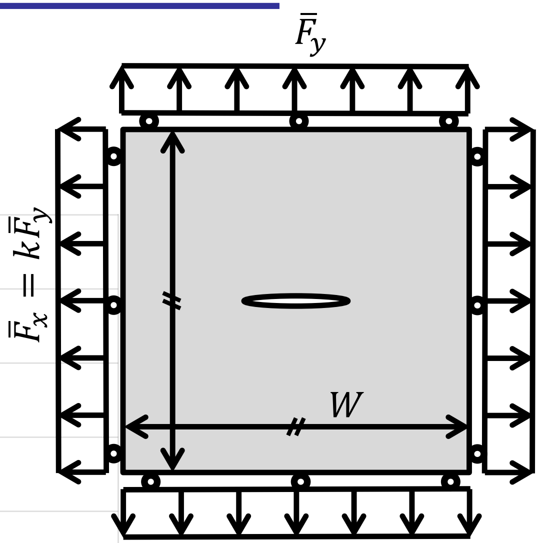

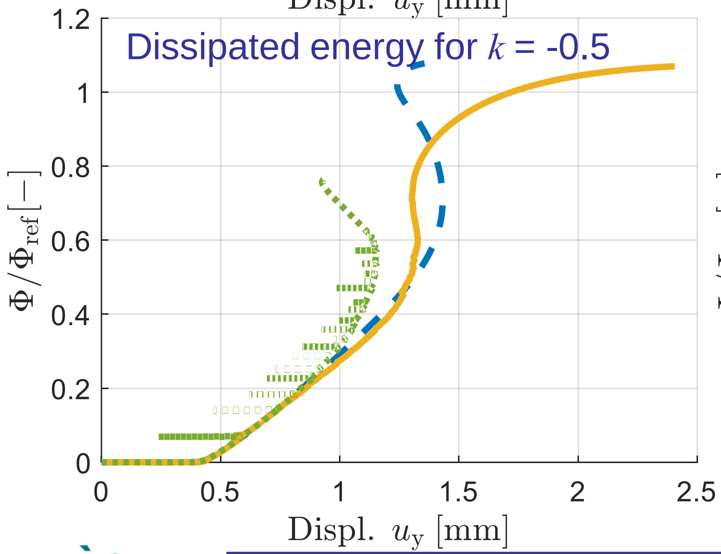

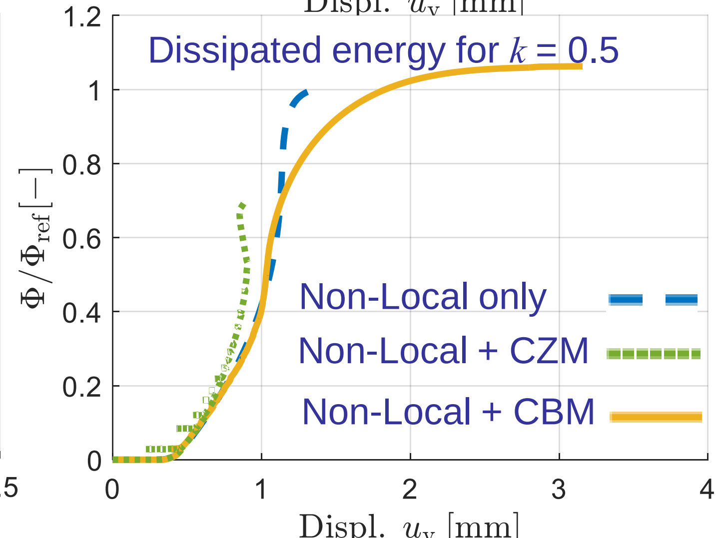

- Comparison with phase field
  - Single edge notched specimen [Miehe et al. 2010]
    - Calibration of damage and CBM parameters with 1D case [Leclerc et al. 2018]

Non-local model | Cohesive band model | Force-displacement curve

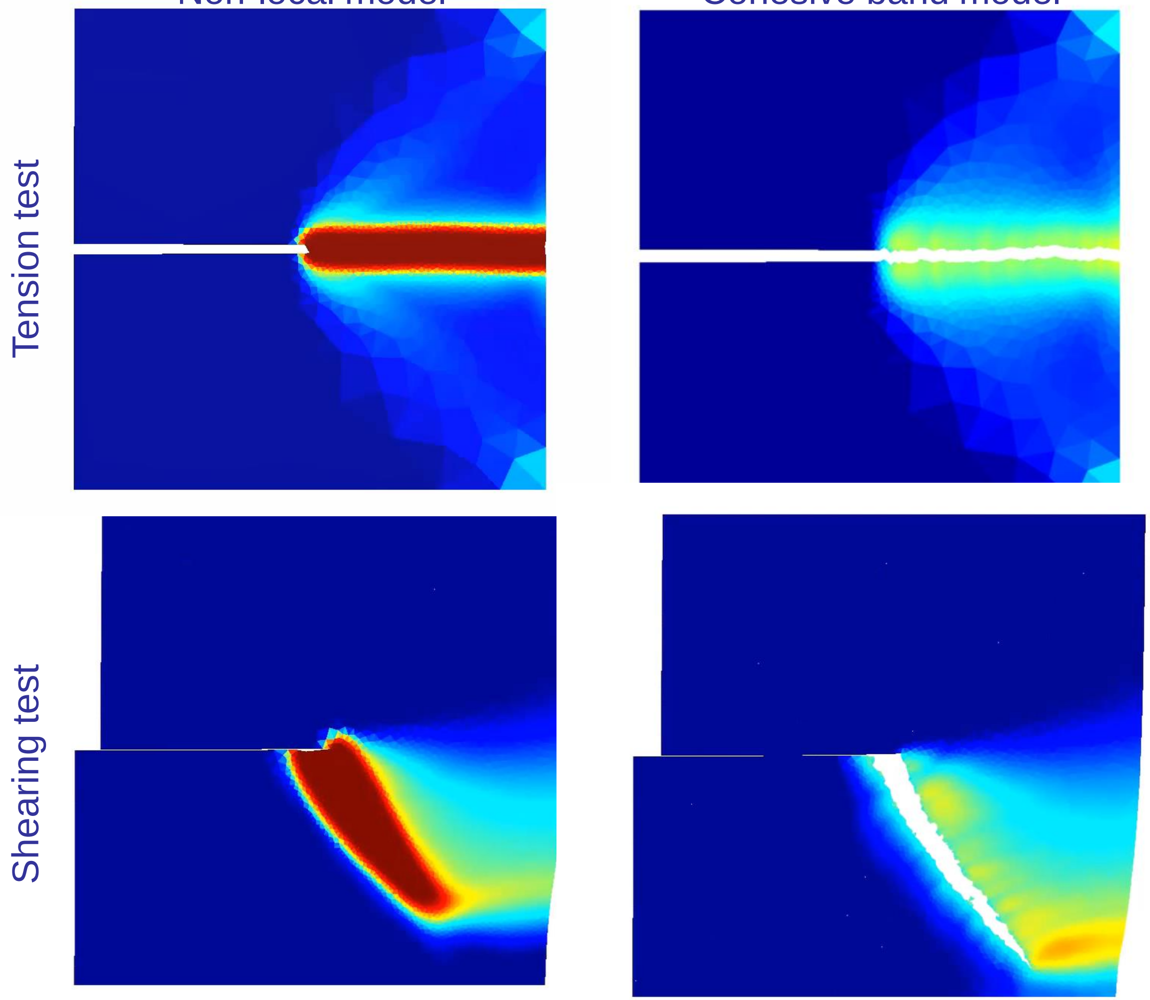

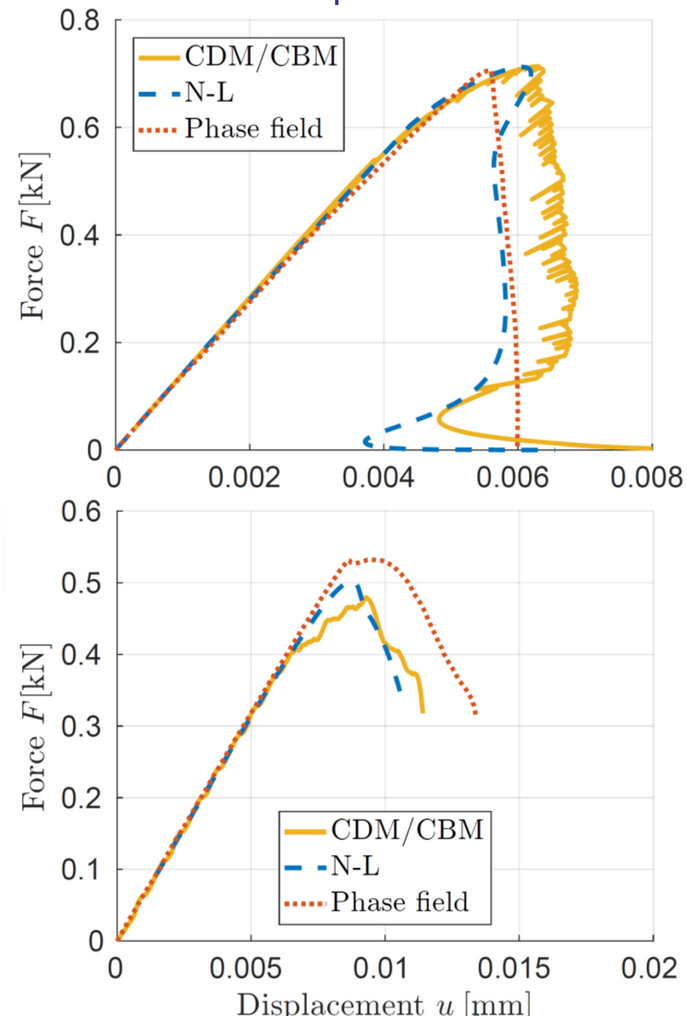

Beginning

DG-Based elastic damage to crack transition

- Compact Tension Specimen:
  - Non-Local damage law combined to cohesive band model improves accuracy

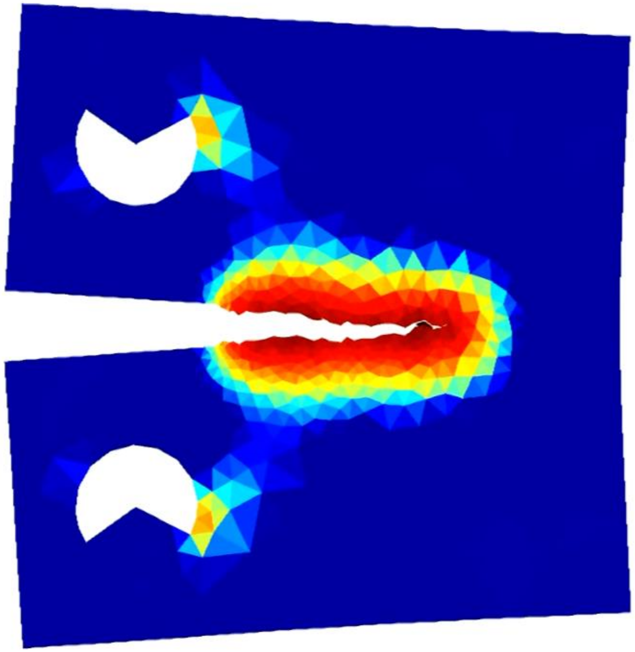

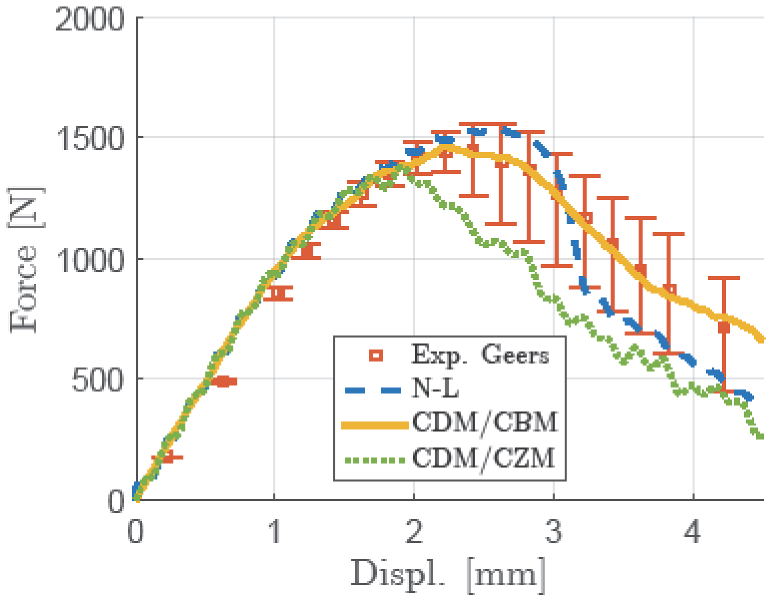

- MRIPF MECATECH project
  - GDTech, UCL, FZ, MECAR, Capital People (Belgium)
- Publication (doi)
  - [10.1002/nme.5618]
  - [10.1016/j.cma.2014.06.031]

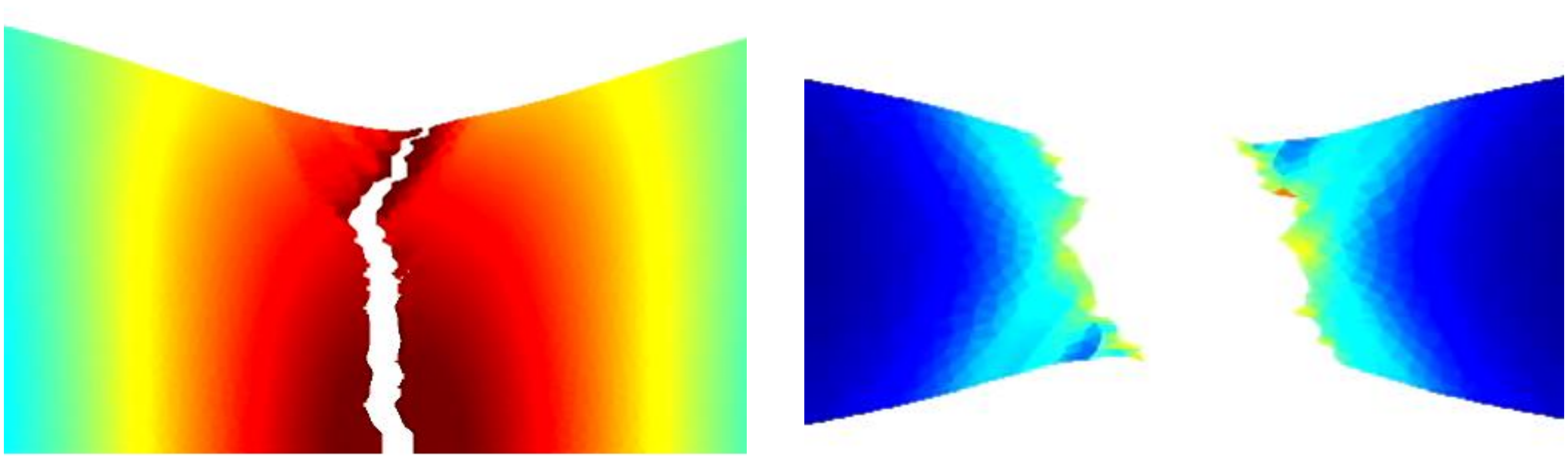

Non-local Gurson damage model to crack transition

The research has been funded by the Walloon Region under the agreement no.7581-MRIPF in the context of the 16th MECATECH call.

Non-local Gurson damage model to crack transition

- Objective:
  - To develop high fidelity numerical methods for ductile failure

- Numerical approach:
  - Combination of 2 complementary methods in a single finite element framework:
    - continuous (damage model)
      + transition to
    - discontinuous (cohesive band model including triaxiality / strain rate effects)

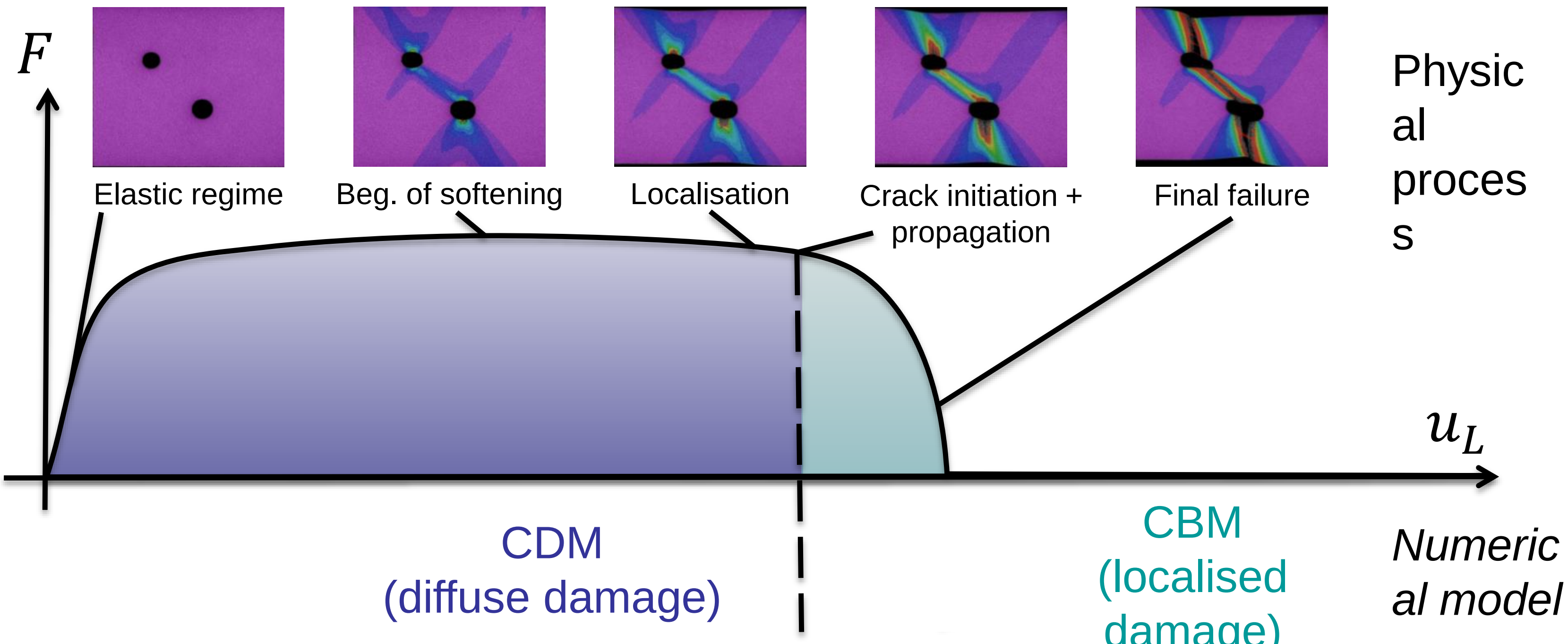

Non-local Gurson damage model to crack transition

- Material changes represented via internal variables
  - Constitutive law $\boldsymbol{\sigma}\left(\boldsymbol{\varepsilon}; \boldsymbol{Z}(t')\right)$
    - Internal variables $\boldsymbol{Z}(t')$
  - Different models
    - Lemaitre-Chaboche (degraded properties)
    - Gurson model (yield surface in terms of porosity f)

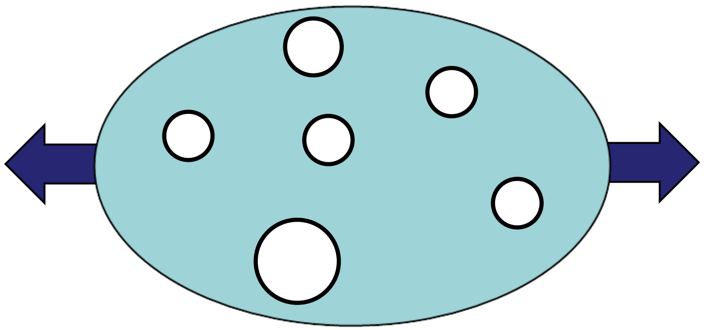

- Model implementation:
  - Local form
    - Mesh dependency
  - Requires non-local form [Bažant 1988]
    - Introduction of characteristic length l_c
    - Weighted average: $\tilde{Z}(\boldsymbol{x}) = \int_{V_C} W(\boldsymbol{y}; \boldsymbol{x}, l_c)\ Z(\mathbf{y}) d\boldsymbol{y}$
  - Implicit form [Peerlings et al. 1998]
    - New degrees of freedom: $\tilde{Z}$
    - New Helmholtz-type equations: $\tilde{Z} - l_c^2\ \Delta\tilde{Z} = Z$

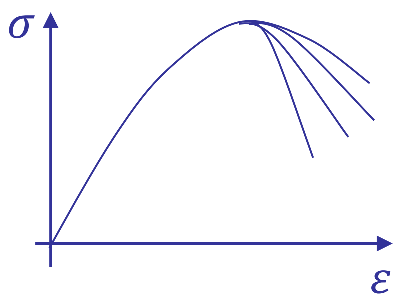

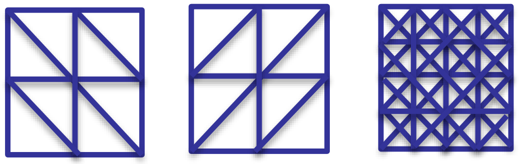

The numerical results change without convergence

Non-local Gurson damage model to crack transition

- Hyperelastic-based formulation
  - Multiplicative decomposition

    $\mathbf{F} = \mathbf{F}^{\mathrm{e}} \cdot \mathbf{F}^{\mathrm{p}}, \quad \mathbf{C}^{\mathrm{e}} = \mathbf{F}^{\mathrm{e}^{T}} \cdot \mathbf{F}^{\mathrm{e}}, \quad J^{e} = \det(\mathbf{F}^{\mathrm{e}})$
  - Stress tensor definition
    - Elastic potential $\psi(\mathbf{C}^{\mathrm{e}})$
    - First Piola-Kirchhoff stress tensor

      $$\mathbf{P} = 2\mathbf{F}^{\mathrm{e}} \cdot \frac{\partial \psi(\mathbf{C}^{\mathrm{e}})}{\partial \mathbf{C}^{\mathrm{e}}} \cdot \mathbf{F}^{\mathrm{p}^{-T}}$$
    - Kirchhoff stress tensors
      - In current configuration

        $$\boldsymbol{\kappa} = \mathbf{P} \cdot \mathbf{F}^{T} = 2\mathbf{F}^{\mathrm{e}} \cdot \frac{\partial \psi(\mathbf{C}^{\mathrm{e}})}{\partial \mathbf{C}^{\mathrm{e}}} \cdot \mathbf{F}^{\mathrm{e}^{T}}$$
      - In co-rotational space

        $$\boldsymbol{\tau} = \mathbf{C}^{\mathrm{e}} \cdot \mathbf{F}^{\mathrm{e}^{-1}} \cdot \boldsymbol{\kappa} \cdot \mathbf{F}^{\mathrm{e}^{-T}} = 2\mathbf{C}^{\mathrm{e}} \cdot \frac{\partial \psi(\mathbf{C}^{\mathrm{e}})}{\partial \mathbf{C}^{\mathrm{e}}}$$
- Logarithmic deformation
  - Elastic potential ψ:

    $$\psi(\mathbf{C}^{\mathrm{e}}) = \frac{K}{2} \ln^{2}(J^{e}) + \frac{G}{4} (\ln(\mathbf{C}^{\mathrm{e}}))^{\mathrm{dev}} : (\ln(\mathbf{C}^{\mathrm{e}}))^{\mathrm{dev}}$$
  - Stress tensor in co-rotational space

    $$\boldsymbol{\tau} = \underbrace{K \ln(J^{e})}_{p}\, \mathbf{I} + G(\ln(\mathbf{C}^{\mathrm{e}}))^{\mathrm{dev}}$$

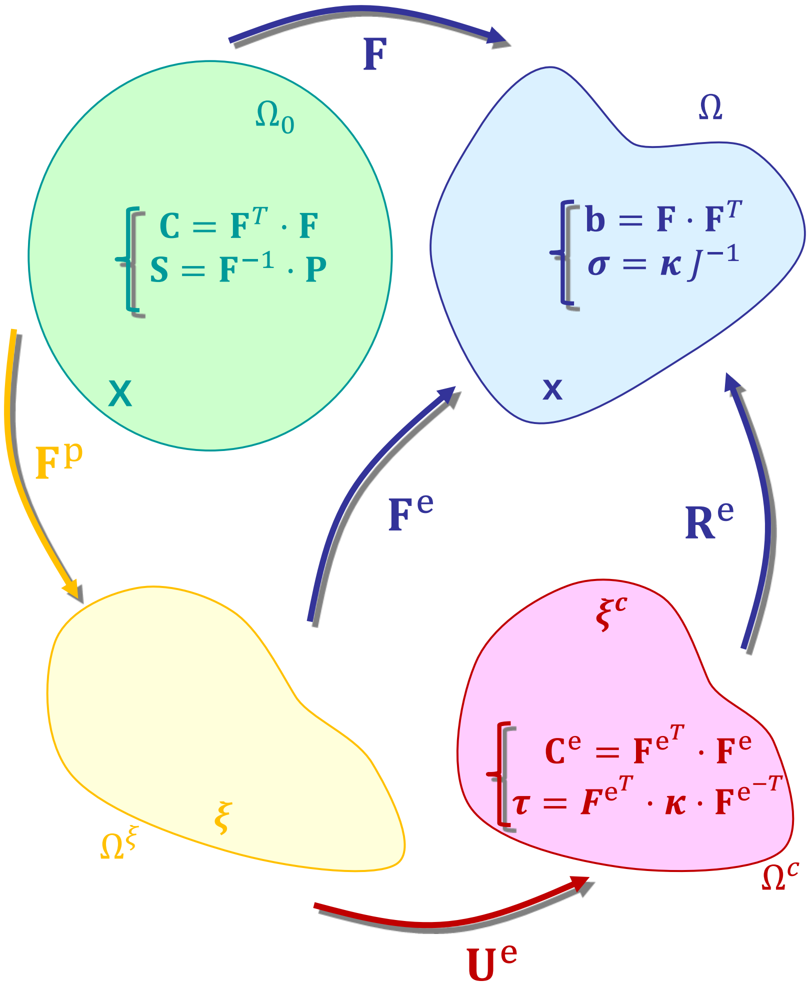

- Porous plasticity (or Gurson) approach
  - Competition between 2 plastic modes:

Growth mode:
Gurson model

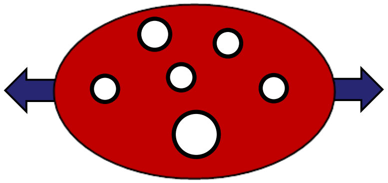

Coalescence mode:
Thomason model

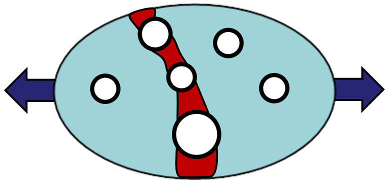

$$\phi_{\mathrm{G}} = \frac{\tau_{\mathrm{eq}}^2}{\tau_{\mathrm{Y}}^2} + 2q_1\tilde{f}\cosh\left(\frac{q_2 p}{2\tau_{\mathrm{Y}}}\right) - 1 - q_3^2\tilde{f}^2 \le 0$$

vs

$$\phi_{\mathrm{T}} = \frac{2}{3}\tau_{\mathrm{eq}} + |p| - C_{\mathrm{T}}^{f}(\chi)\tau_{\mathrm{Y}} \le 0$$

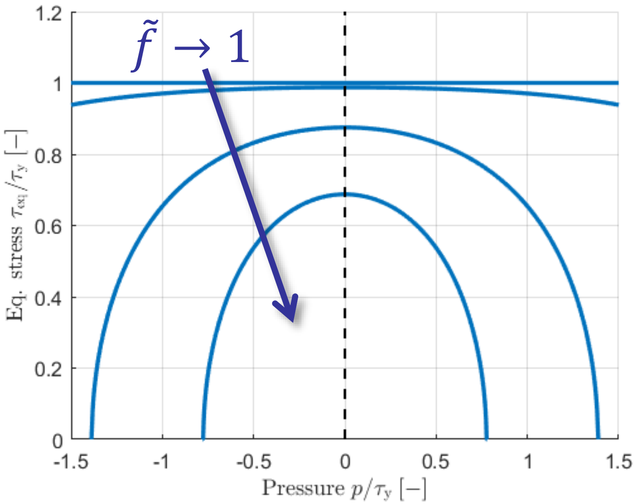

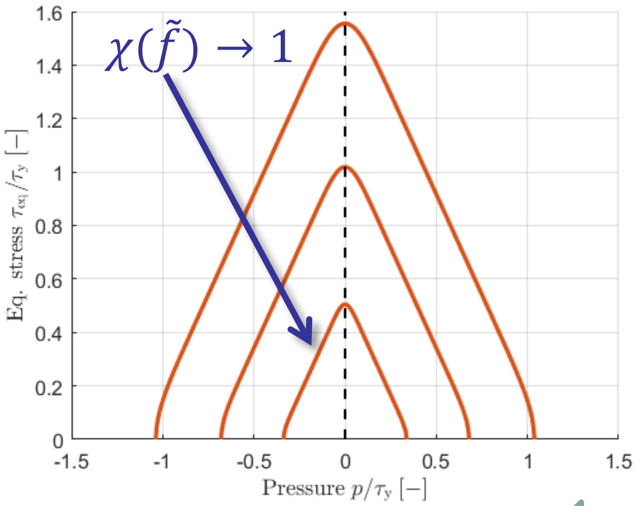

- Hybrid DG model: use of a Cohesive Band Model (CBM)
  - Principles
    - Substitute TSL of CZM by the behavior of a uniform band of thickness h_{b} [Remmers et al. 2013]

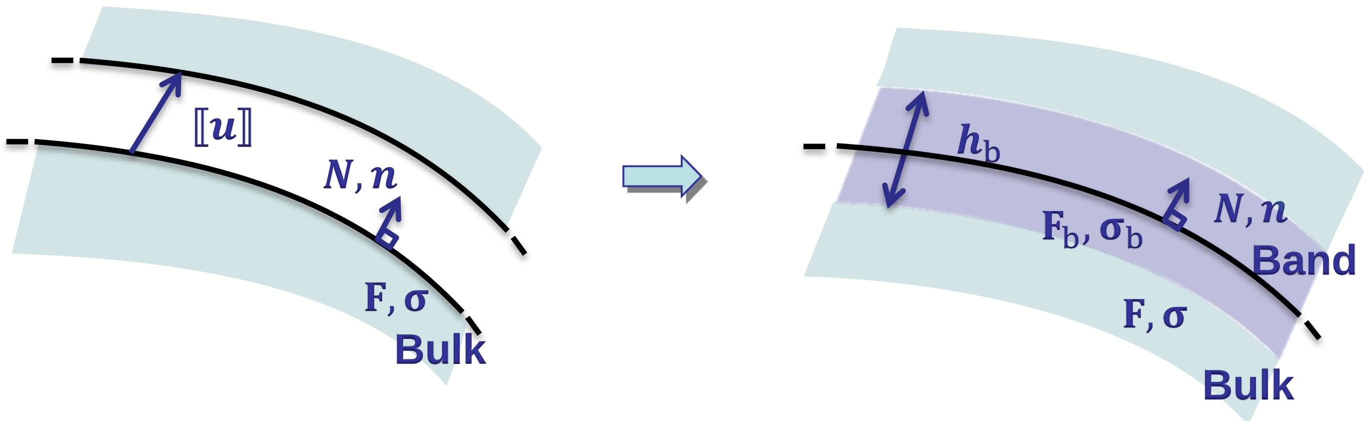

  - Localization criterion
    - Thomason: $\boldsymbol{N}\cdot\boldsymbol{\tau}\cdot\boldsymbol{N} - C_I^f\tau_y \geq 0$
  - Methodology [Leclerc et al. 2018]
    1. Compute a band strain tensor $\mathbf{F}_{\mathrm{b}} = \mathbf{F} + \frac{[\![\boldsymbol{u}]\!]\otimes\boldsymbol{N}}{h_b} + \frac{1}{2}\boldsymbol{\nabla}_T[\![\boldsymbol{u}]\!]$
    2. Compute a band stress tensor $\boldsymbol{\sigma}_{\mathrm{b}}\big(\mathbf{F}_{\mathrm{b}};\mathrm{Z}(\tau)\big)$ using the same CDM as bulk elements
    3. Recover a surface traction $\boldsymbol{t}([\![\boldsymbol{u}]\!],\mathbf{F}) = \boldsymbol{\sigma}_{\mathrm{b}}.\boldsymbol{n}$
  - What is the effect of h_{b} (band thickness)
    - Recover the fracture energy

Non-local Gurson damage model to crack transition

- Comparison with literature [Huespe2012,Besson2003]

Slanted plane strain specimen

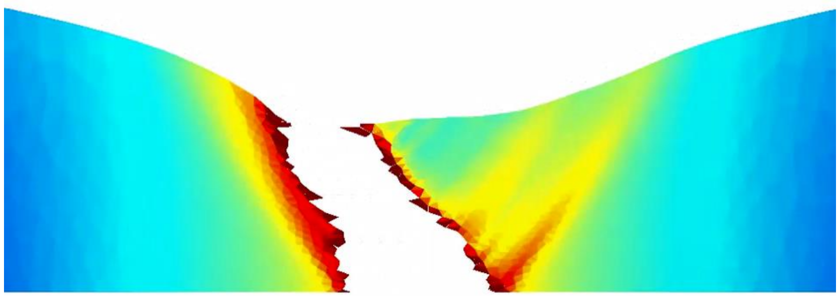

Cup-cone in round bar

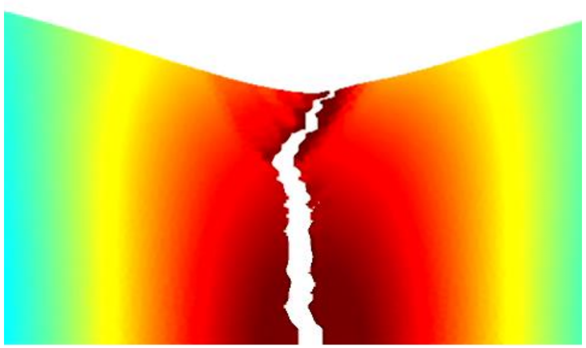

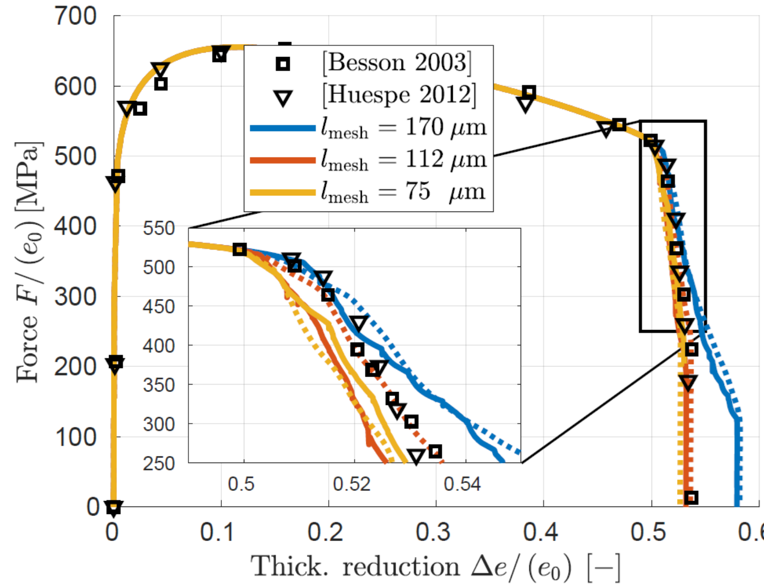

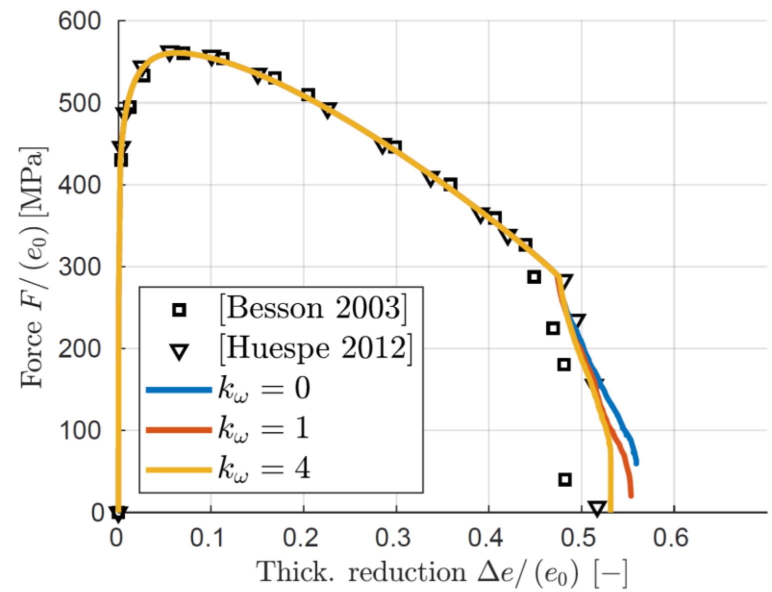

Non-local Gurson damage model to crack transition

- Grooved plate

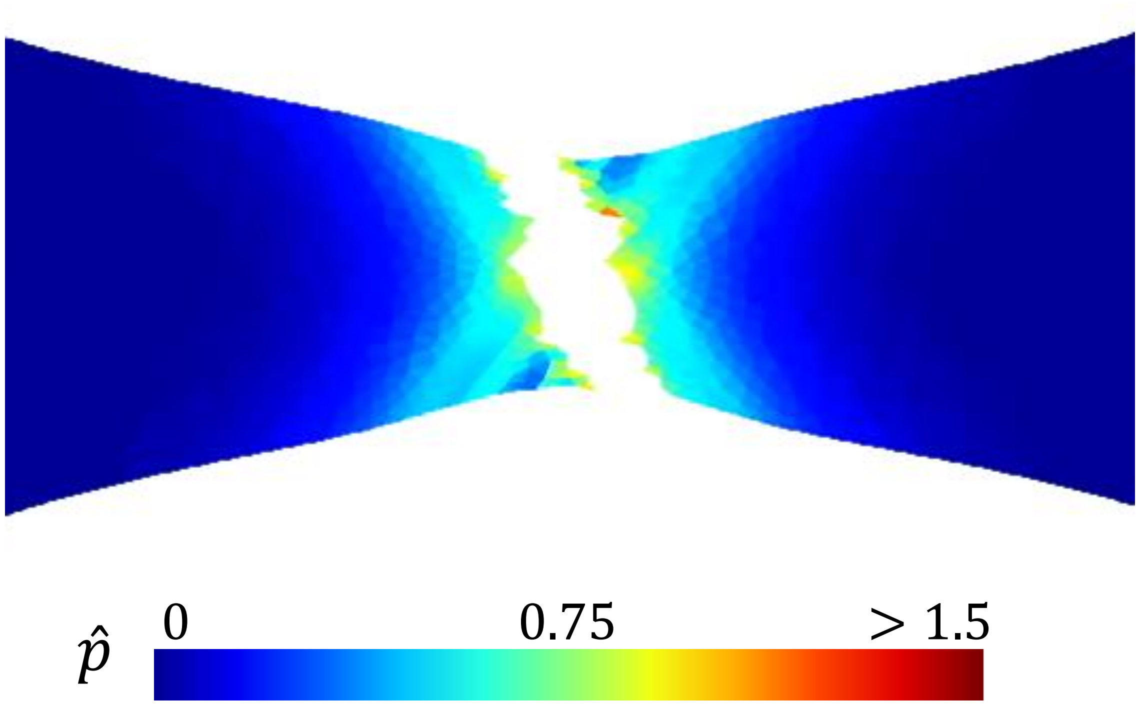

- MRIPF MECATECH project
  - GDTech, UCL, FZ, MECAR, Capital People (Belgium)
- Publication (doi)
  - [10.1002/nme.5618](https://doi.org/10.1002/nme.5618)
  - [10.1016/j.ijplas.2019.11.010](https://doi.org/10.1016/j.ijplas.2019.11.010)

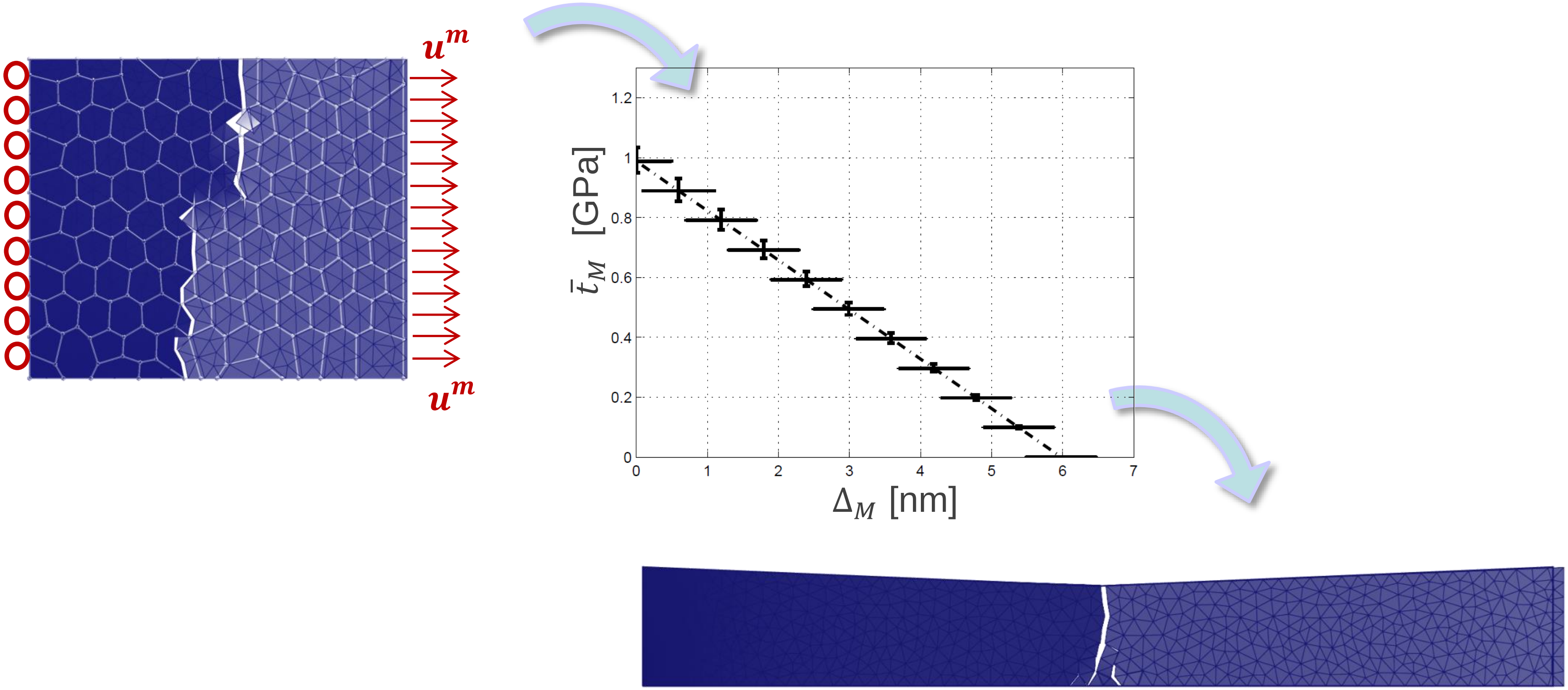

Stochastic Multi-Scale Fracture of Polycrystalline Films

Robust design of MEMS: Financial support from F. R. S. - F. N. R. S. under the project number FRFC 2.4508.11

Stochastic Multi-Scale Fracture of Polycrystalline Films

- Multi-scale modeling
  - 2 problems are solved concurrently
    - The macro-scale problem
    - The meso-scale problem (on a meso-scale Volume Element)

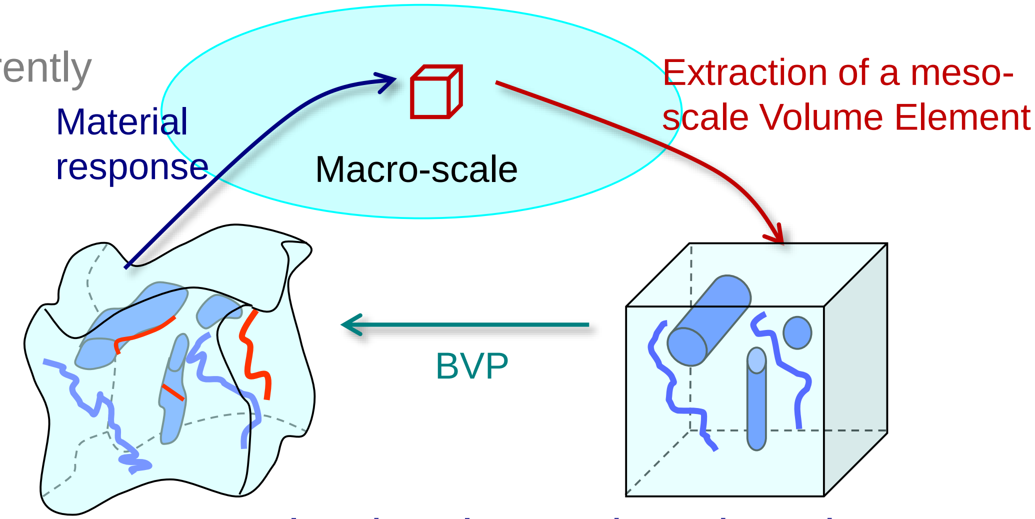

- For meso-scale volume elements not several orders larger than the micro-structure size and embedding crack propagations

$$L_{\mathrm{macro}} >> L_{\mathrm{VE}} \sim ?\ L_{\mathrm{micro}}$$

For accuracy: Size of the meso-scale volume element smaller than the characteristic length of the macro-scale loading

Meso-scale volume element no longer statistically representative:
- **Stochastic Volume Elements**
- **Should recover consistency lost due to the discontinuity**

- Micro-scale model: Silicon crystal
  - Different fracture strengths and critical energy release rates

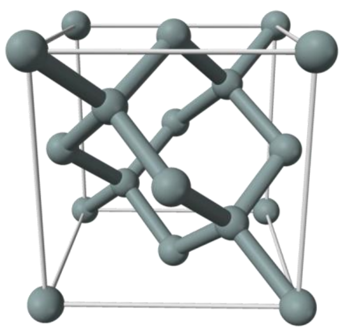

{1 0 0}

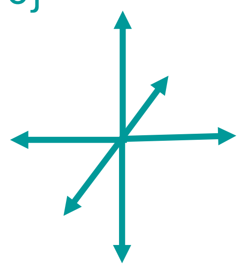

{1 1 0}

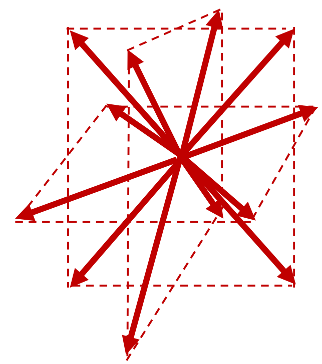

{1 1 1}

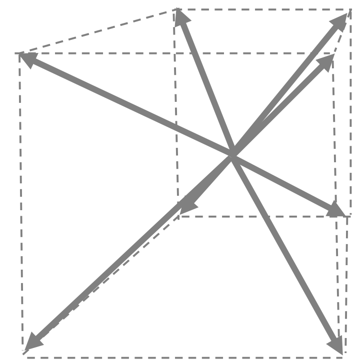

  - Define a “continuous” strength mapping

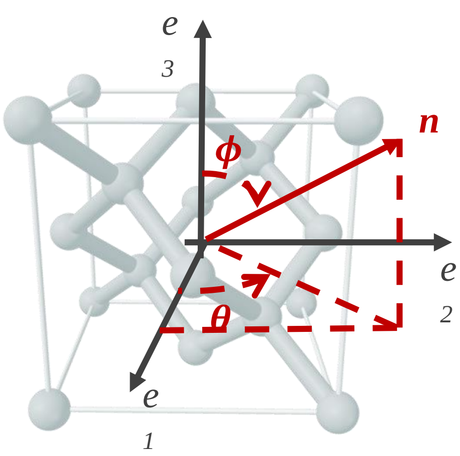

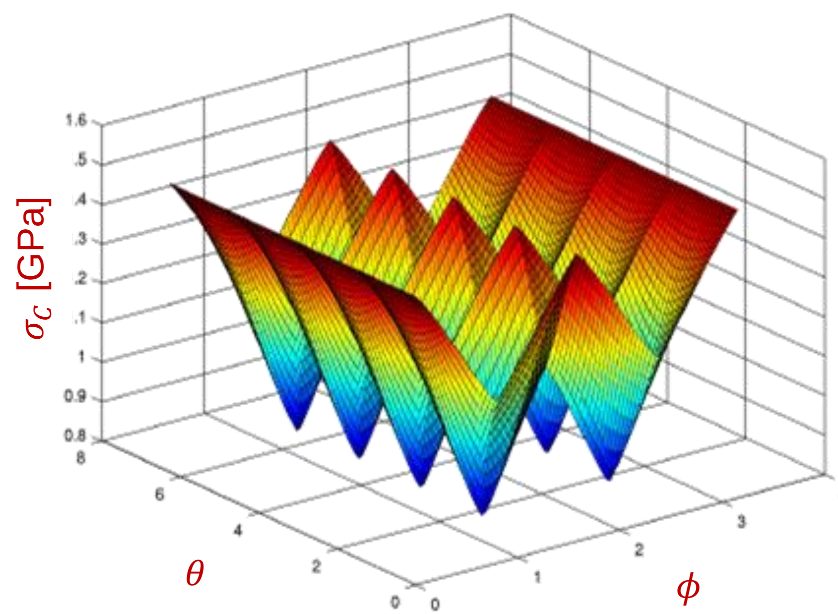

- Micro-scale model: Polycrsytalline films
  - [Discontinuous Galerkin method]
  - Extrinsic cohesive law
  - Intra/Inter granular fracture
  - Accounts for interface orientation

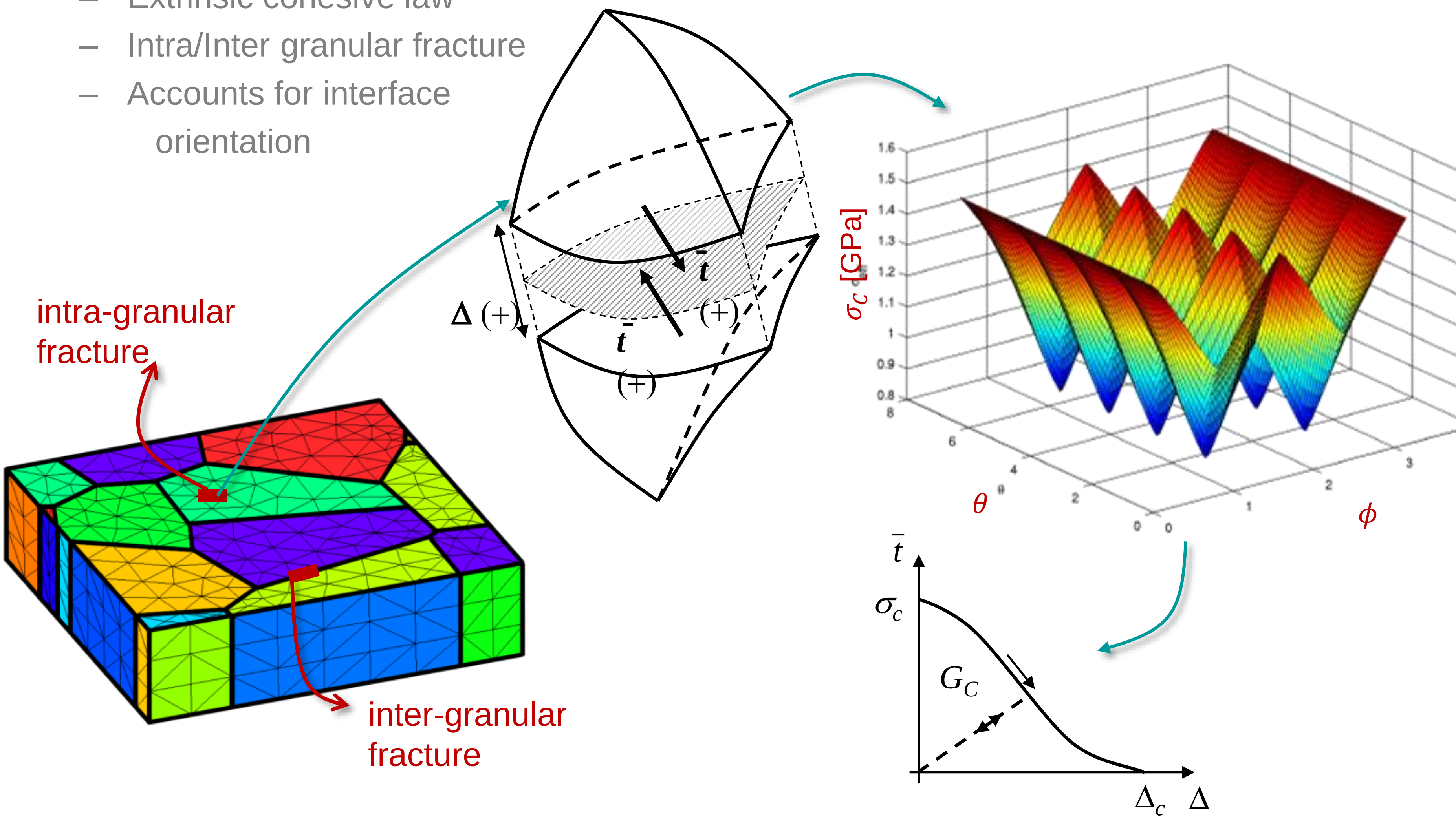

- Stochastic micro-scale to meso-scale model
  - Several SVE realizations (random grain orientation)
  - Extraction of consistent meso-scale cohesive laws
    - $\bar{t}_M$ vs. Δ_M
    - for each SVE sample
  - Resulting meso-scale cohesive law distribution

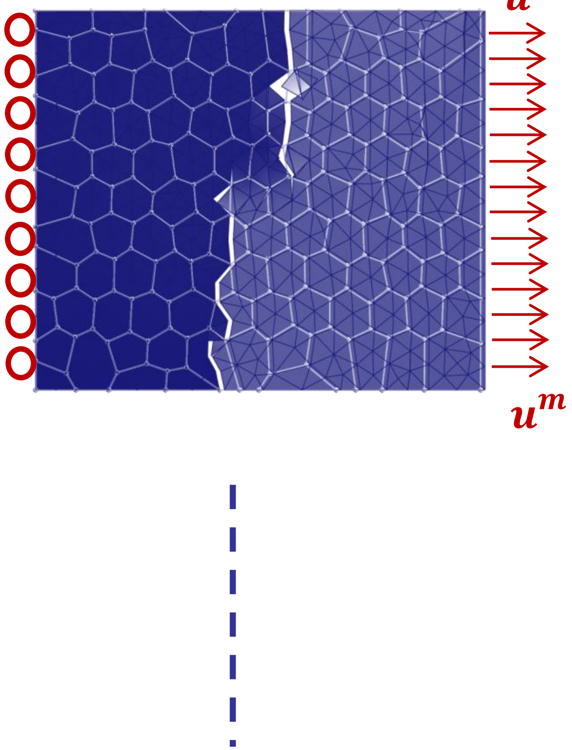

$$\delta\bar{t}_M = \delta\boldsymbol{\sigma}_M \cdot \boldsymbol{e}_X$$

$$\delta\boldsymbol{\Delta}_M = \delta\boldsymbol{u}^m - L_{\text{cell}}\boldsymbol{C}_M{}^{-1} : \boldsymbol{e}_X \otimes \boldsymbol{e}_X \cdot \delta\bar{\boldsymbol{t}}_M$$

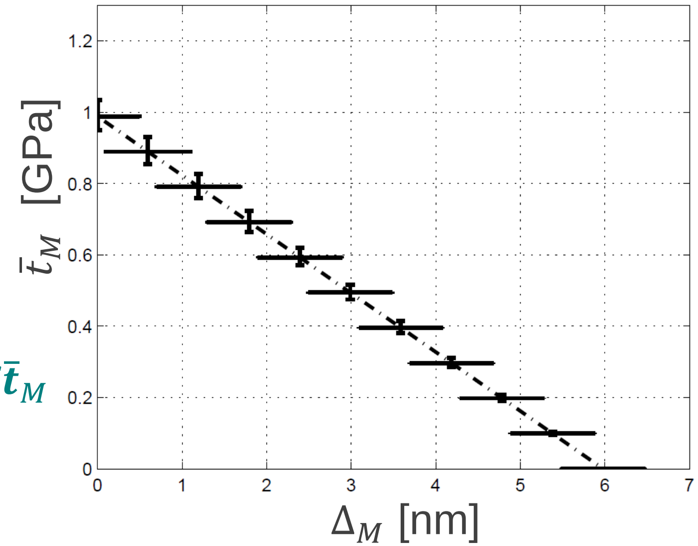

Beginning

Stochastic Multi-Scale Fracture of Polycrystalline Films

- Macro-scale simulation
  - Finite element model non-conforming to the grains
  - Use homogenized (random) meso-scale cohesive laws as input

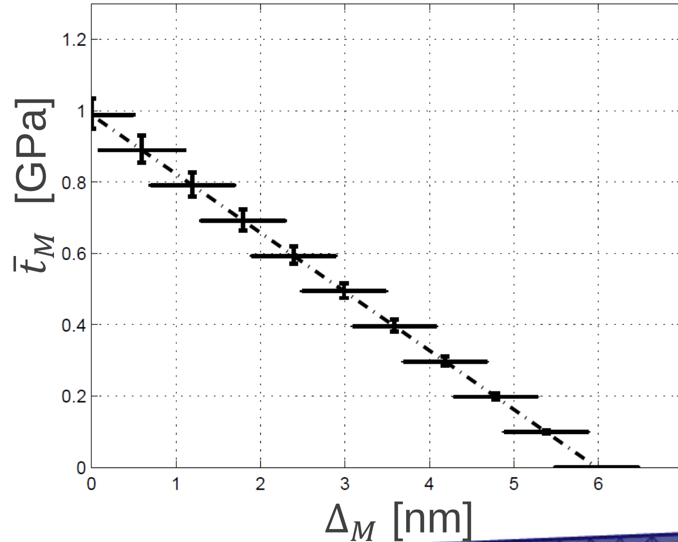

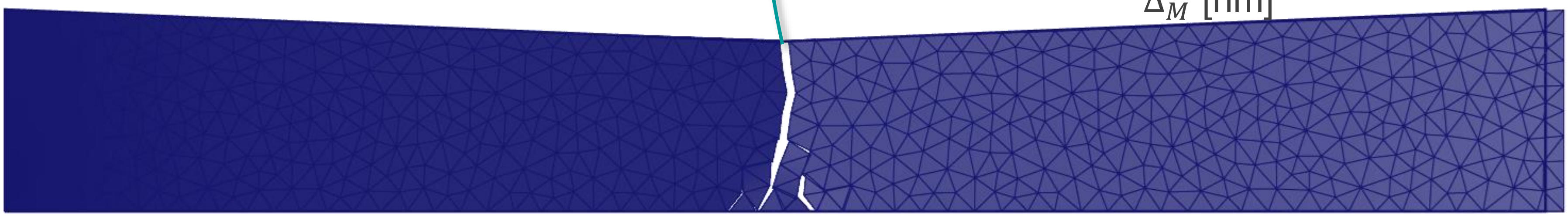

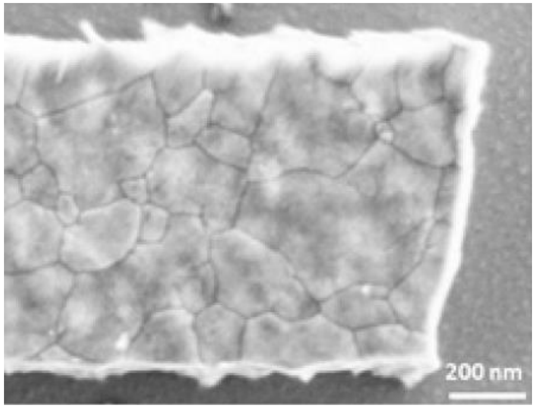

- Collaboration for experiments
  - UcL (T. Pardoen, J.-P Raskin)
- Publications
  - 10.1007/s00466-014-1083-4

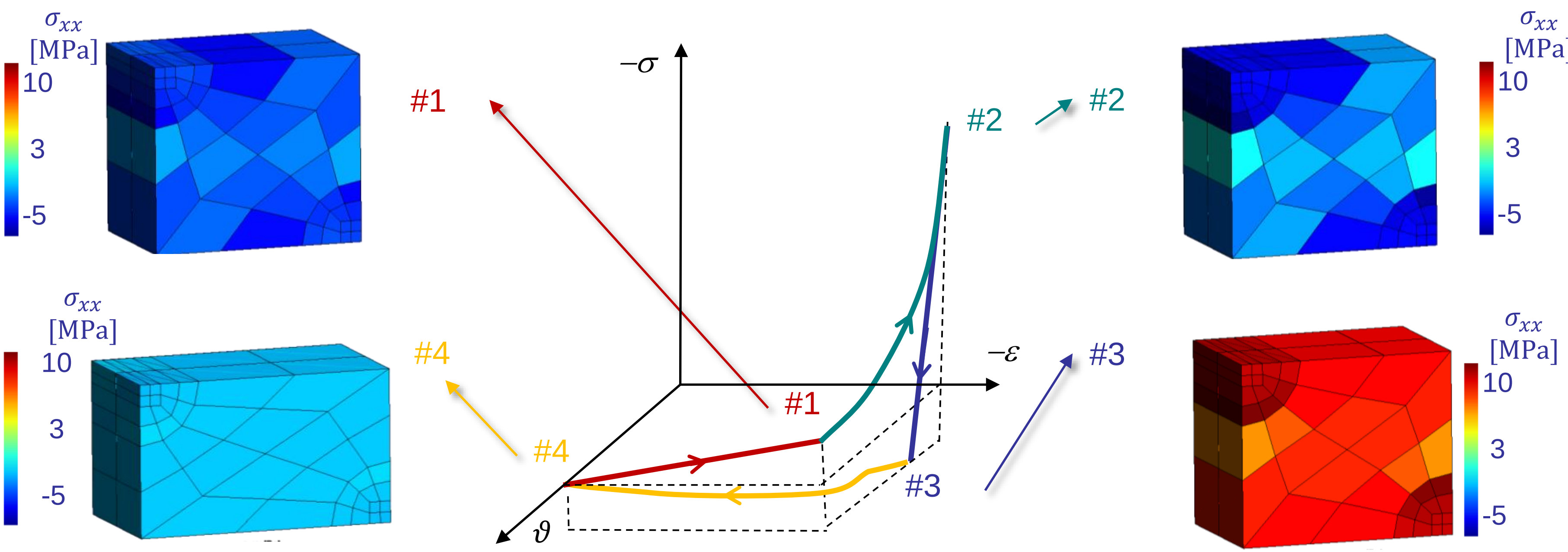

Smart Composite Materials

This project has been funded with support of the European Commission under the grant number 2012-2624/001-001-EM. This publication reflects the view only of the author, and the Commission cannot be held responsible for any use which may be made of the information contained therein.

- Electro-thermo-mechanical coupling
  - Finite field variation formulation
  - Strong coupling

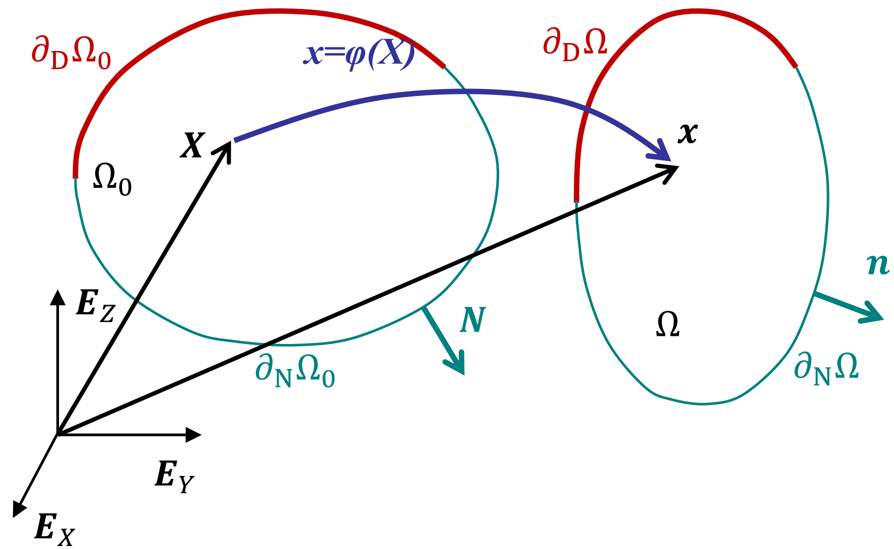

Conservation of electric charge	Conservation of energy	Conservation of momentum balance
$\mathbf{J}_e \cdot \boldsymbol{\nabla}_0 = 0$ $\mathbf{J}_e = \mathbf{J}_e(\mathbf{F}, \boldsymbol{\nabla}_0 V, V, \boldsymbol{\nabla}_0\vartheta, \vartheta; \boldsymbol{Z})$	$\rho C_v \dot{\vartheta} - \mathcal{D} + \mathbf{J}_y \cdot \boldsymbol{\nabla}_0 = 0$ $\mathbf{J}_y = \mathbf{q} + V\mathbf{J}_e$ $\mathbf{q} = \mathbf{q}(\mathbf{F}, V, \boldsymbol{\nabla}_0\vartheta, \vartheta; \boldsymbol{Z})$	$\mathbf{P} \cdot \boldsymbol{\nabla}_0 = 0$ $\mathbf{P} = \mathbf{P}(\mathbf{F}, \vartheta; \boldsymbol{Z})$ $\mathcal{D} = \beta \dot{p} \tau + \vartheta \dfrac{\partial \dot{W}^{\mathrm{el}}}{\partial \vartheta}$

- Two-way electro-thermal coupling
  - Seebeck coefficient α
  - Finite strain conductivities $\mathbf{K}(V,\vartheta)=\mathbf{F}^{-1}\cdot\mathbf{k}(V,\vartheta)\cdot\mathbf{F}^{-T}J$ & $\mathbf{L}(V,\vartheta)=\mathbf{F}^{-1}\cdot\mathbf{l}(V,\vartheta)\cdot\mathbf{F}^{-T}J$

$$\begin{pmatrix}\mathbf{J}_e\\ \mathbf{J}_y\end{pmatrix}=\begin{pmatrix}\mathbf{L}(V,\vartheta) & \alpha\mathbf{L}(V,\vartheta)\\ V\mathbf{L}(V,\vartheta)+\alpha T\mathbf{L}(V,\vartheta) & \mathbf{K}(V,\vartheta)+\alpha V\mathbf{L}(V,\vartheta)+\alpha^2 T\mathbf{L}(V,\vartheta)\end{pmatrix}\begin{pmatrix}-\boldsymbol{\nabla}_0 V\\ -\boldsymbol{\nabla}_0\vartheta\end{pmatrix}$$

Non energetically conjugated

[Liu IJES, 2012]

Change of variables

$$\begin{cases} f_V=-\dfrac{V}{\vartheta}\\ f_\vartheta=\dfrac{1}{\vartheta}\end{cases}$$

$$\begin{pmatrix}\mathbf{J}_e\\ \mathbf{J}_y\end{pmatrix}=\mathbf{Z}(\mathbf{F},f_V,f_\vartheta)\begin{pmatrix}\boldsymbol{\nabla}_0 f_V\\ \boldsymbol{\nabla}_0 f_\vartheta\end{pmatrix}$$

  - The coefficients matrix $\mathbf{Z}(\mathbf{F},f_V,f_\vartheta)$ is symmetric and definite positive

- Thermo-mechanical shape memory polymer
  - Deformations above glass transition temperature ϑ_g (1)
  - Fixed once cooled down below ϑ_g (2 & 3)
  - Recovery once heated up (4)

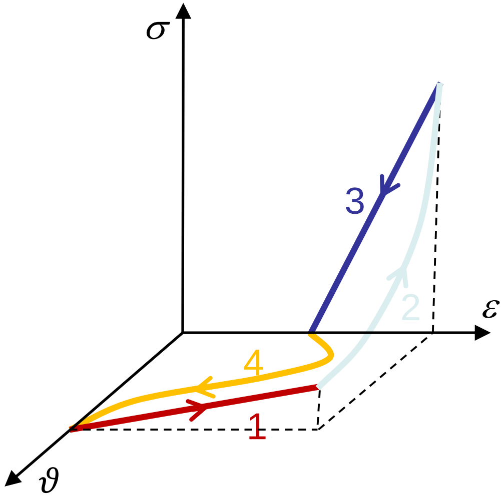

- Elasto-visco-plastic model constitutive behavior
  - Different mechanisms (α)
    - Multiplicative decomposition
      $\mathbf{F}^{(\alpha)} = \mathbf{F}^{\mathrm{e}(\alpha)}\mathbf{F}^{\mathrm{p}(\alpha)}$
    - Free energy
      $$\psi = \sum_{\alpha} \psi^{(\alpha)}\left(\mathbf{C}^{\mathrm{e}(\alpha)}, \vartheta\right)$$
    - Thermo-visco-plasticity
      $$\tau^{(\alpha)} = \mathcal{T}\left(\mathbf{C}^{\mathrm{e}(\alpha)}, \mathbf{F}^{\mathrm{p}(\alpha)}, \dot{p}^{(\alpha)}, \vartheta, \xi^{(\alpha)}\right)$$
  - Stress and dissipation
    $$\begin{cases} \mathbf{P} = \mathbf{P}\left(\mathbf{F}, \vartheta; \mathbf{F}^{\mathrm{p}(\alpha)}, p^{(\alpha)}, \xi^{(\alpha)}\right) \\ \mathcal{D} = \beta \dot{p}^{(\alpha)} \tau^{(\alpha)} \end{cases}$$

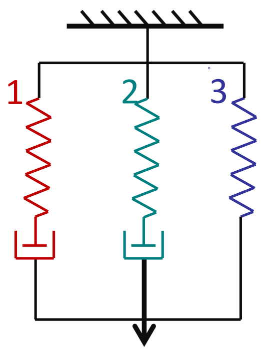

[V. Srivastav et. al, 2010]

- Elasto-visco-plastic behavior of thermo-mechanical shape memory polymer

Refs. by [V. Srivastav et. al, 2010]

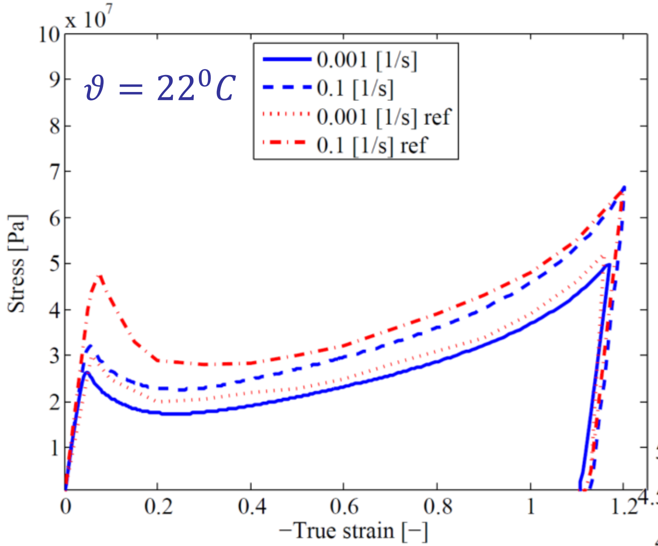

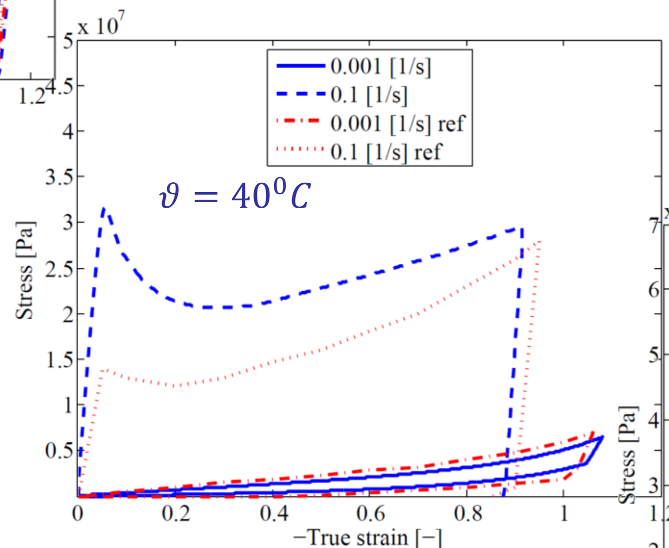

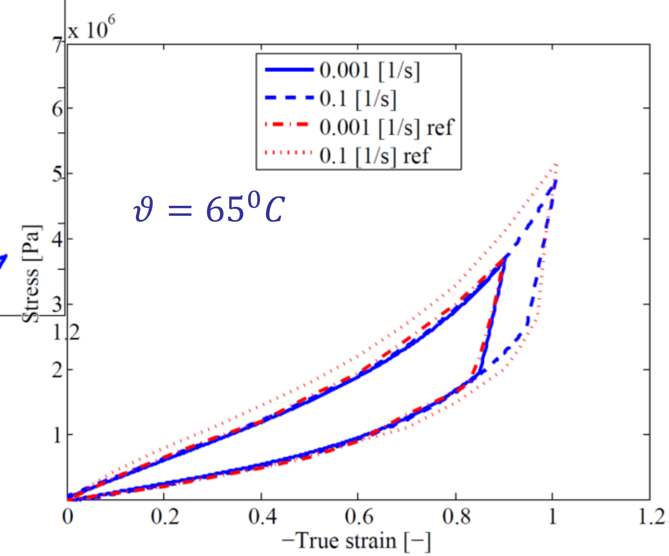

- Recovery of a shape memory composite unit cell
  - Carbon Fiber reinforced SMP
  - Shape memory effect triggered by Joule effect
  - Test with compressive force recovery:
    - #1: Compression deformation obtained above ϑ_g
    - #2: Fixation of the deformation above ϑ_g
    - #3: Reheat above ϑ_g at constant deformation:
      → recovery force, the cell wants to expend
    - #4: Release deformation/stress
      → recovery force vanishes

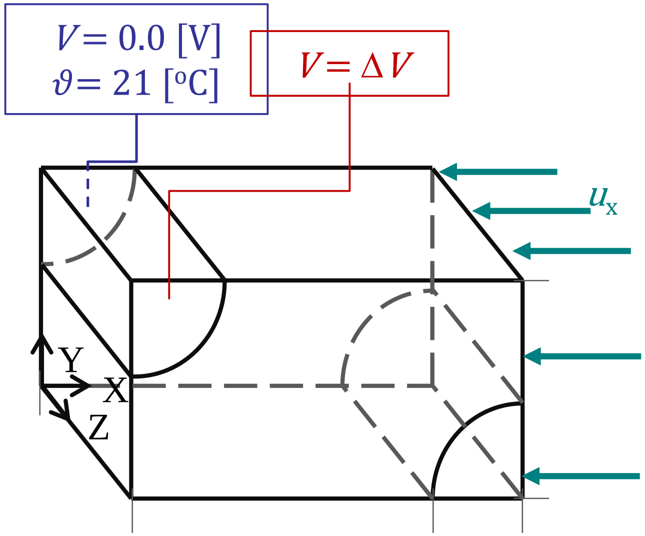

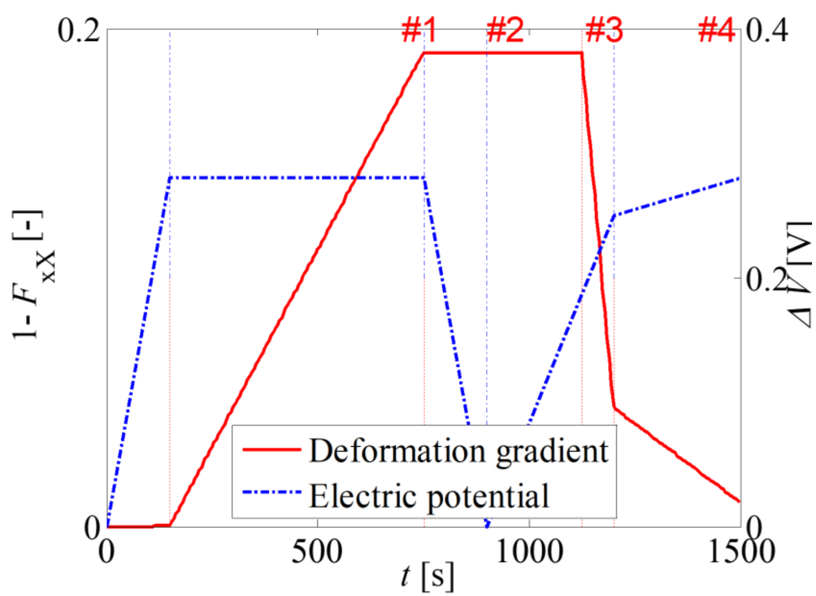

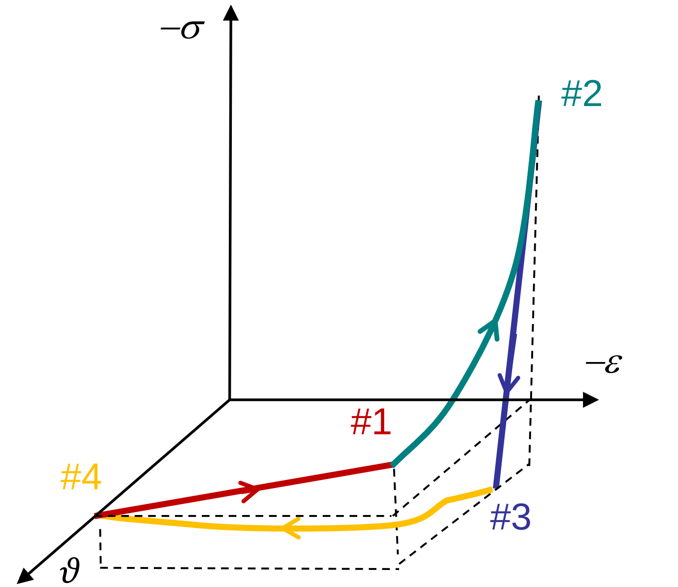

- Recovery of a shape memory composite unit cell
  - Carbon Fiber reinforced SMP
  - Triggered by Joule effecy

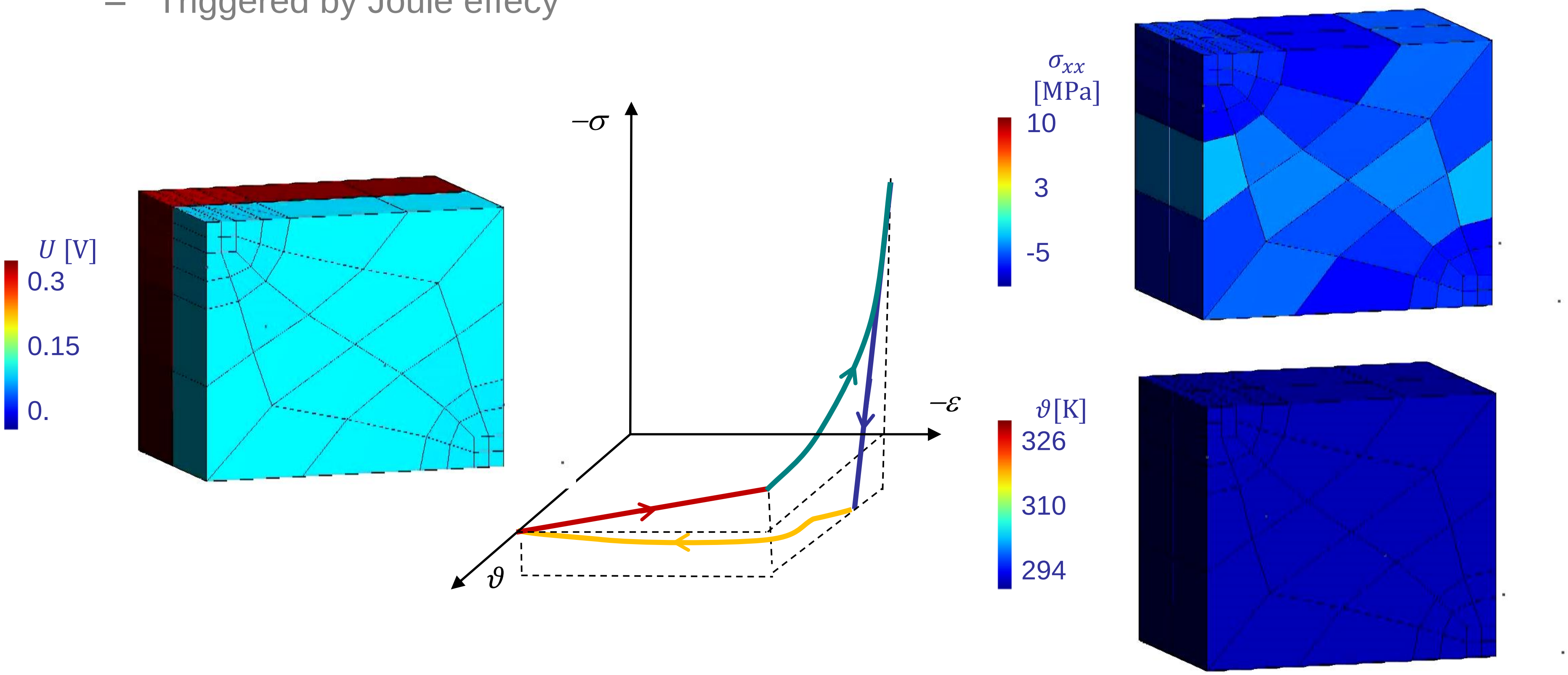

- Discontinuous Galerkin implementation
  - Finite-element discretization
  - Same **discontinuous** polynomial approximations for the
    - **Test** functions φ_h and
    - **Trial** functions $\delta\varphi$

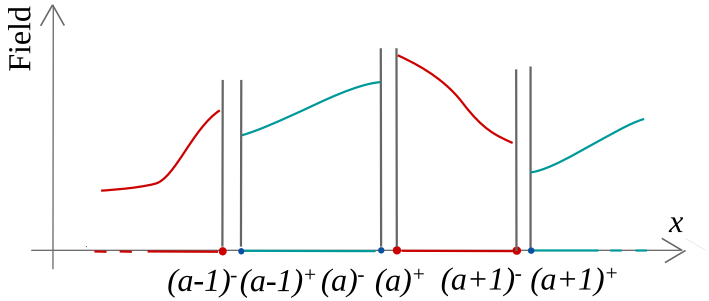

  - Extended to non-linear electro-thermo-mechanical coupling

- Publication (doi)
  - 10.1007/s11012-017-0743-9
  - 10.1016/j.jcp.2017.07.028

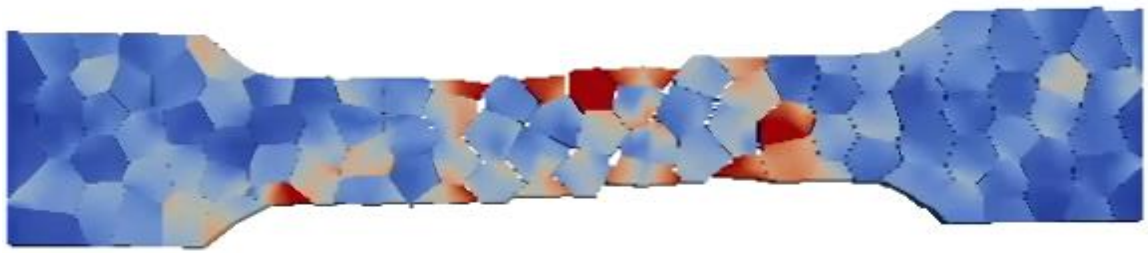

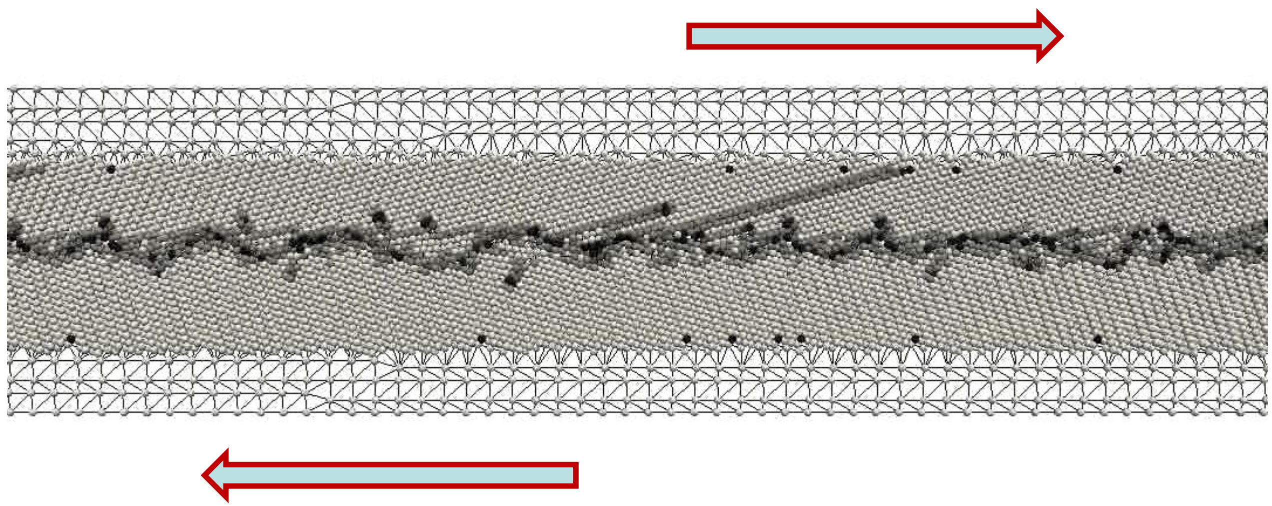

Multi-Scale Modeling of Nano-Crystal Grain Boundary Sliding

Multi-Scale Modeling of Nano-Crystal Grain Boundary Sliding

- 2-scale framework
  - Macro-scale: Finite Elements
  - Micro-scale: Quasi-Continuum

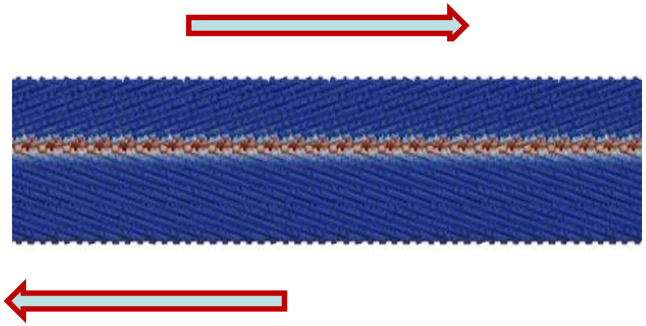

Grain-boundary sliding/opening characterization

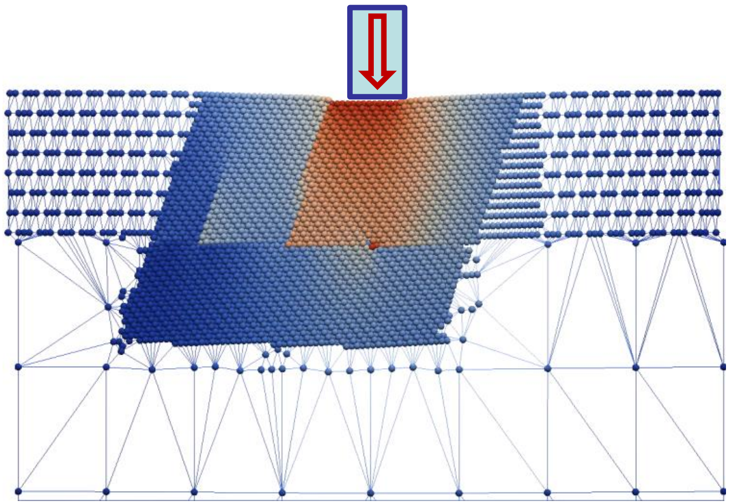

Crystal plasticity characterization by nano-indentation

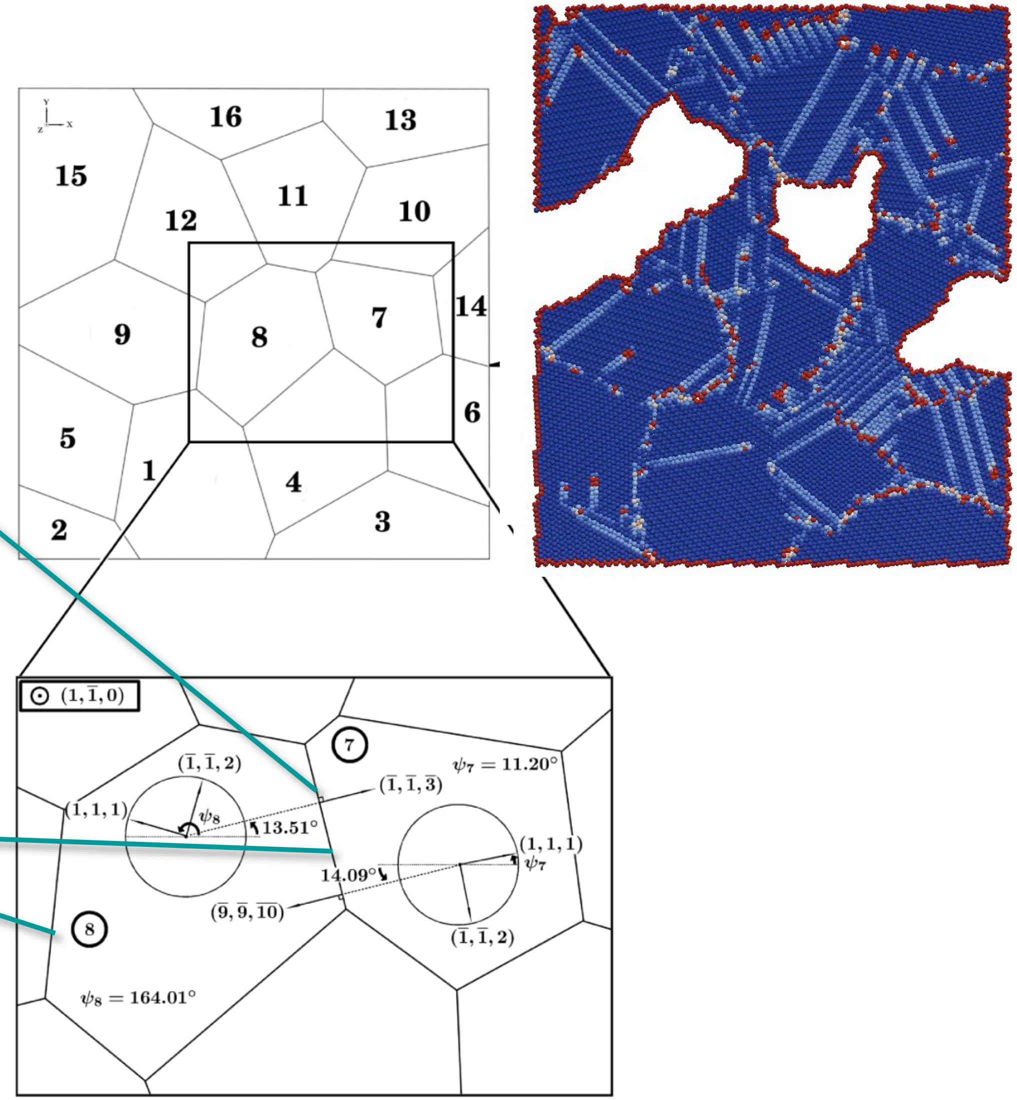

Multi-Scale Modeling of Nano-Crystal Grain Boundary Sliding

- Grain size effect
  - Competition between inter-intra granular

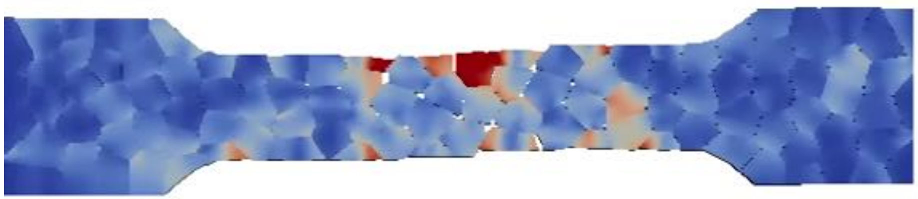

Grain size: 6.56 nm

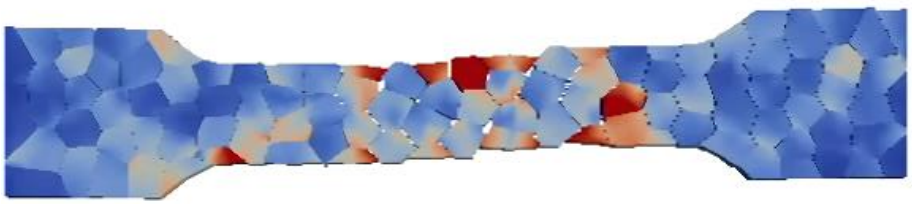

Grain size: 3.28 nm

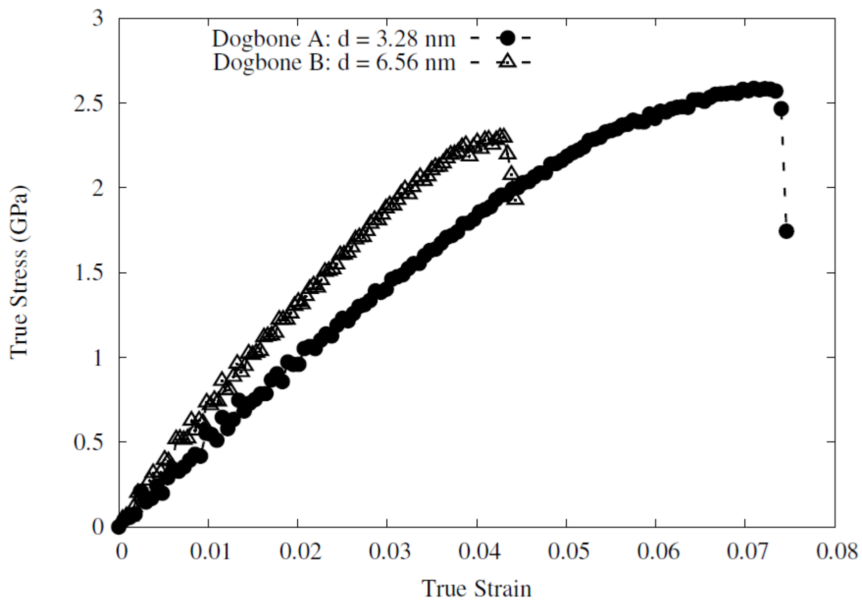

- Effect of nano-voids in the grain boundaries
  - Different deformation mechanism
  - Lower yield stress
- Collaboration
  - EC Nantes, Univ. of Vermont, Oxford
- Publications
  - 10.1016/j.commatsci.2014.03.070
  - 10.1016/j.actamat.2013.10.056
  - 10.1016/j.jmps.2013.04.009

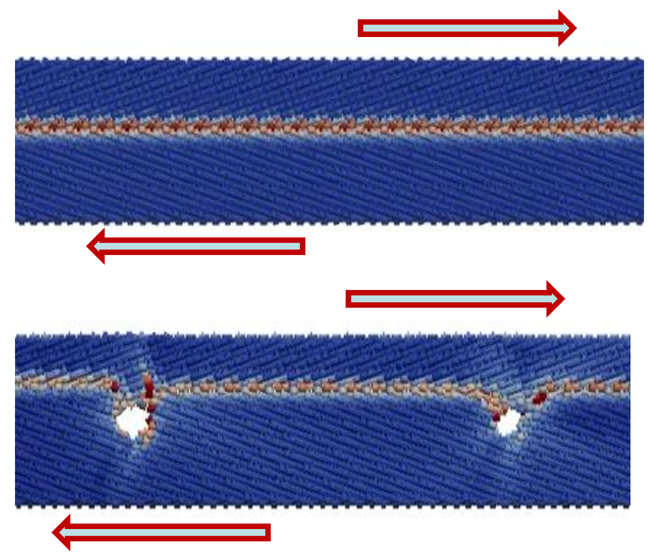

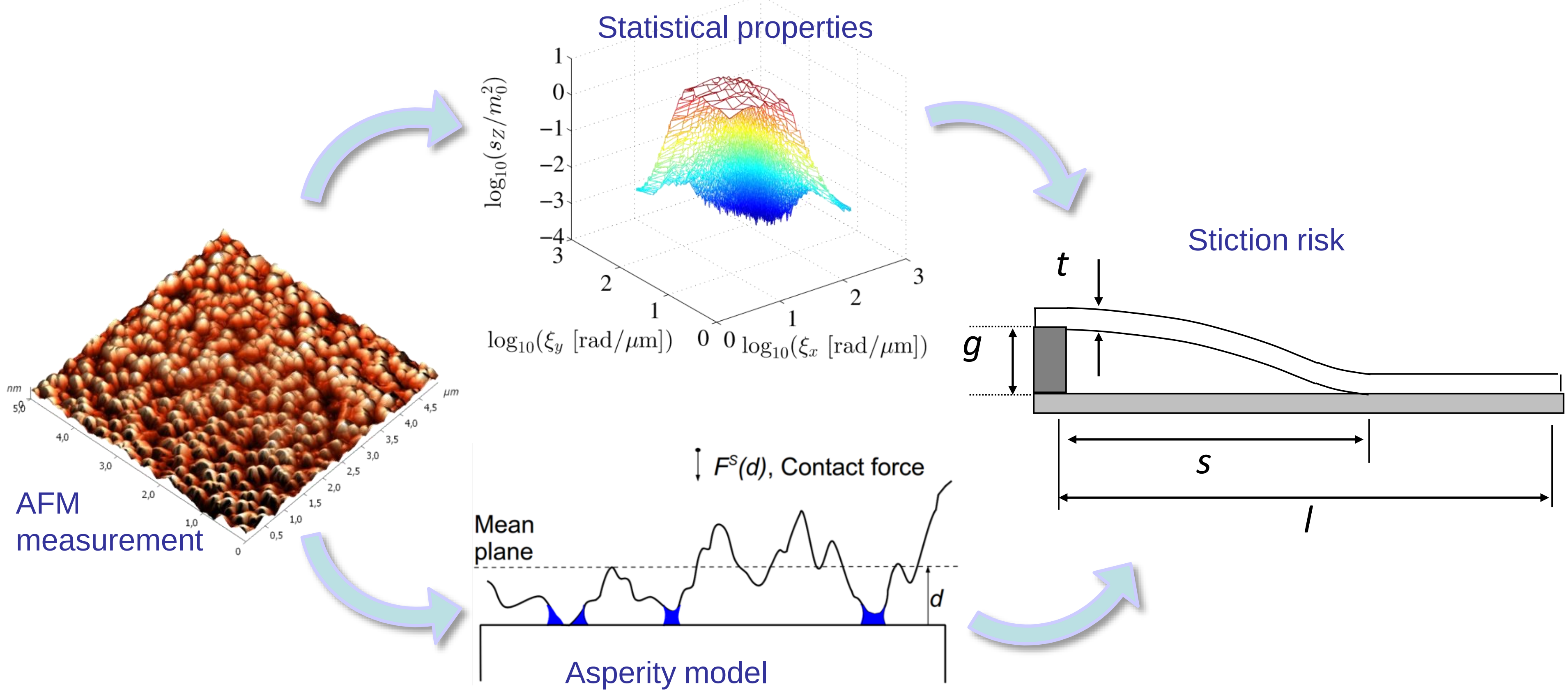

Stochastic Multi-Scale Model to Predict MEMS Stiction

3SMVIB: The research has been funded by the Walloon Region under the agreement no 1117477 (CT-INT 2011-11-14) in the context of the ERA-NET MNT framework.
The research has been funded by the Belgian National Fund for Education at the Research in Industry and Farming.

Stochastic Multi-Scale Model to Predict MEMS Stiction

- Stiction (adhesion of MEMS)
  - Different physics at the different scales
  - Elastic or Elasto-plastic behaviors
  - Due to van der Waals (dry environment) and/or capillary (humid environment) forces

- Requires surfaces topology knowledge (AFM measures)
  - Subject to uncertainties

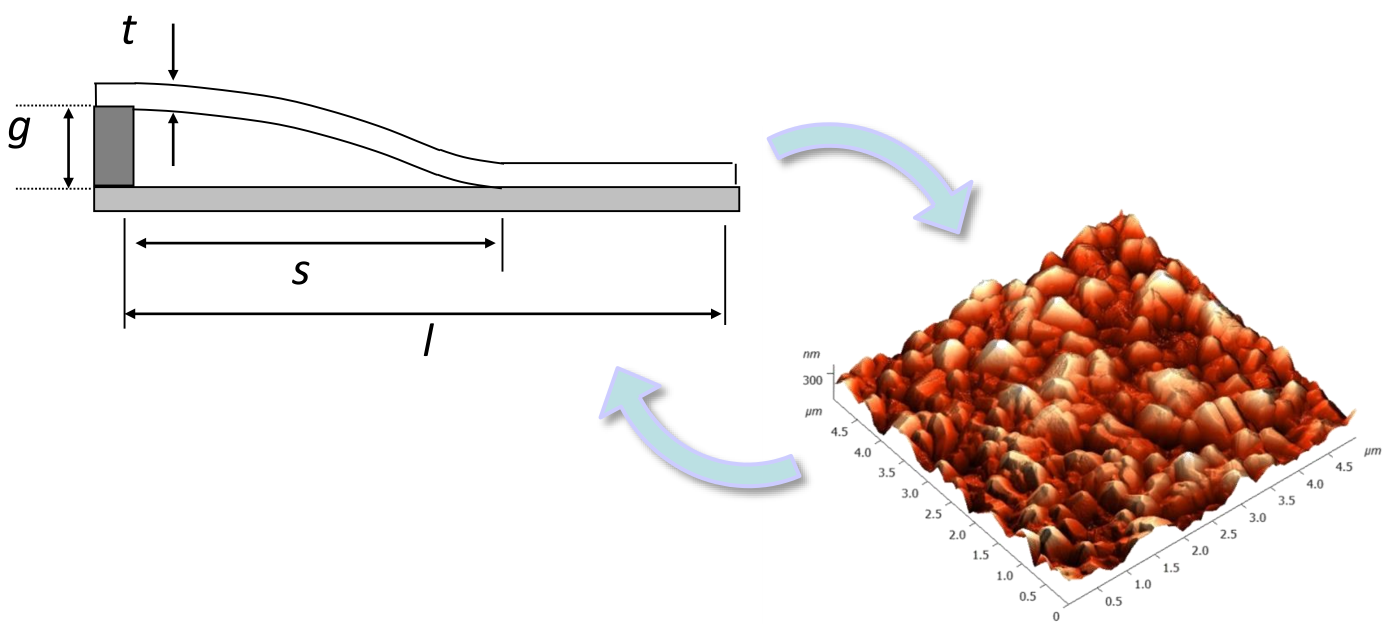

Stochastic Multi-Scale Model to Predict MEMS Stiction

- Deterministic multi-scale models for van der Waals forces
  - Extraction of meso-scale adhesive-forces
  - Using statistical representations of the rough surface (average solution)
  - Account for induced elasto-plasticity (cyclic loading)

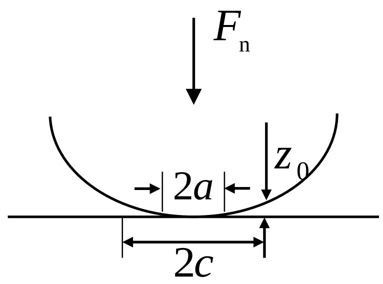

van der Waals/Hertz forces at the asperity level

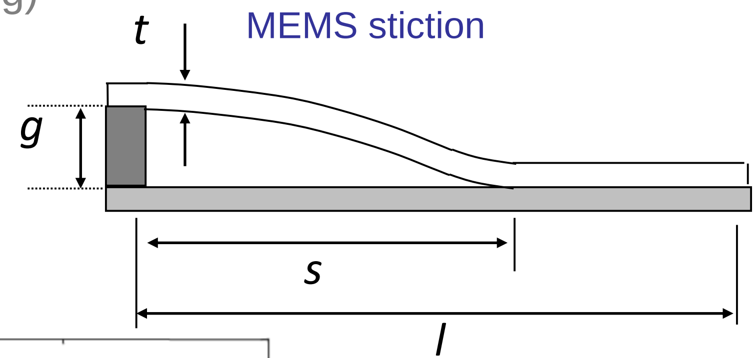

MEMS stiction

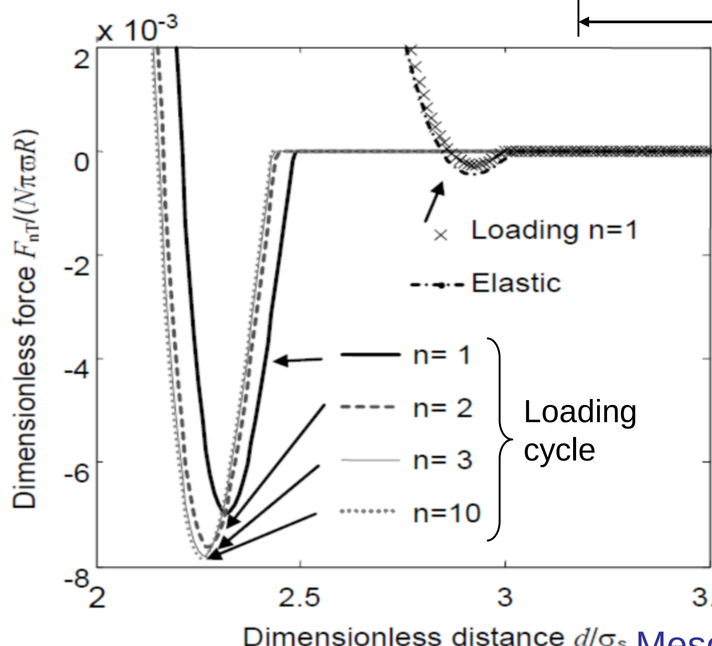

Meso-scale adhesive forces in terms of loading cycle

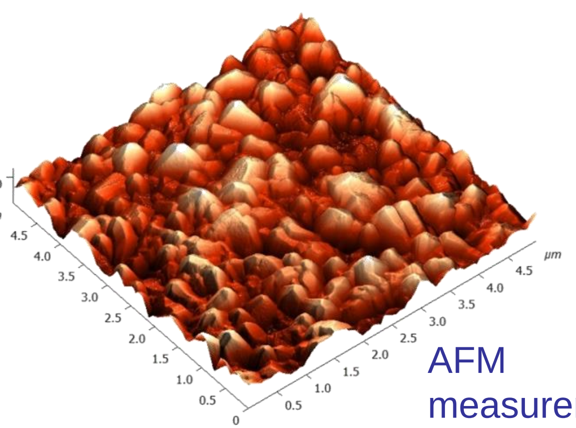

AFM measurement

- New multi-scale models with capillary effect
  - Extraction of meso-scale adhesive-forces from a single surface measurement
  - Depends on the surface sample measurement location
  - Motivates the development of a stochastic multi-scale method

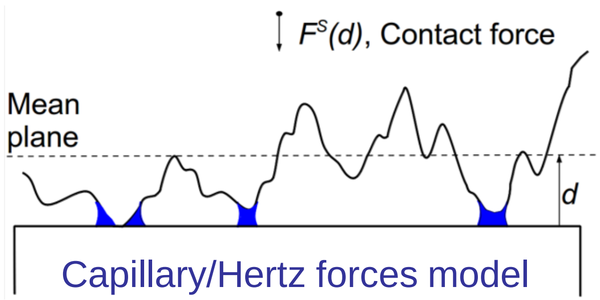

Capillary/Hertz forces model

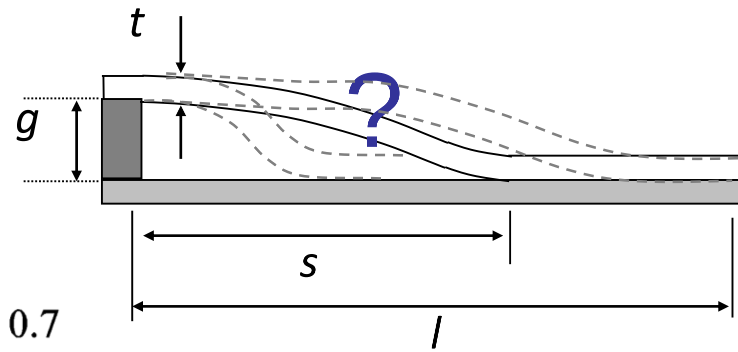

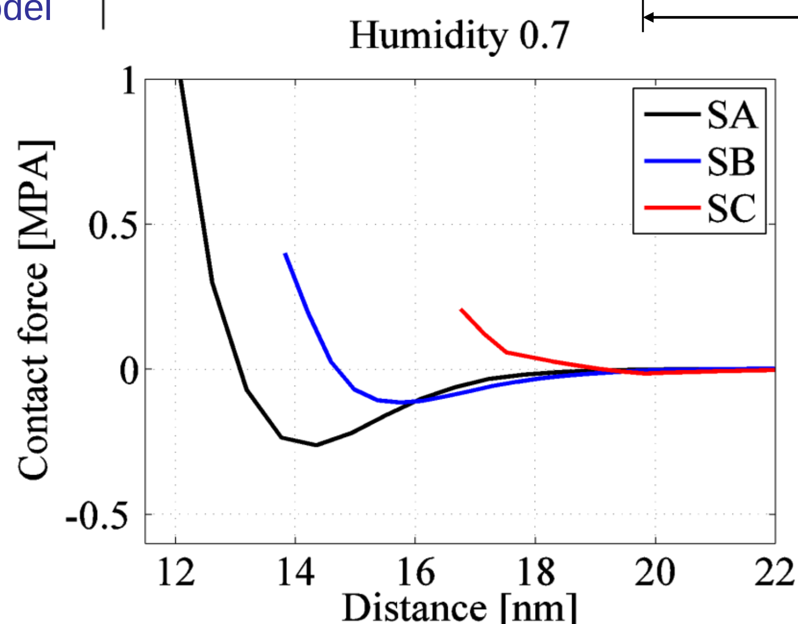

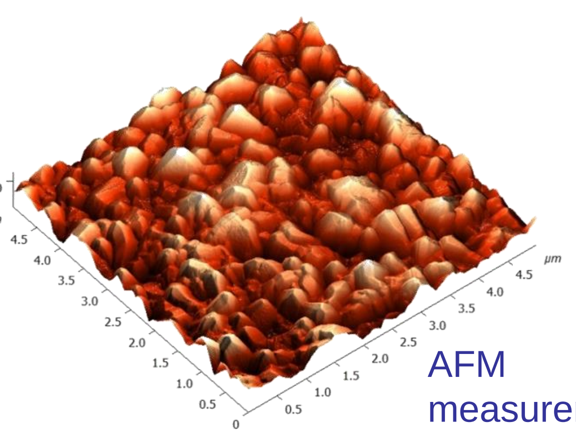

AFM measurement

Meso-scale adhesive forces in terms of surface sample

Stochastic Multi-Scale Model to Predict MEMS Stiction

- Stochastic multi-scale model: From the AFM to virtual surfaces

Enforce statistical moments with maximum entropy method

$$m_i = \int_R z^i \mathrm{p}_Z(z)\, dz$$

$$\mathrm{p}_Z = \arg\max - \int_R \mathrm{p}_Z(z)\, \ln(\mathrm{p}_Z(z))\, dz$$

Evaluate PSD from covariance

$$\tilde{R}(\boldsymbol{\tau}) = \mathbb{E}[z(\boldsymbol{x}), z(\boldsymbol{x}+\boldsymbol{\tau})]$$

$$S_Z(\boldsymbol{\tau}) = \int_{R^2} \exp(-i\boldsymbol{\zeta}\cdot\boldsymbol{\tau}) \tilde{R}_Z(\boldsymbol{\tau}) d\boldsymbol{\zeta}$$

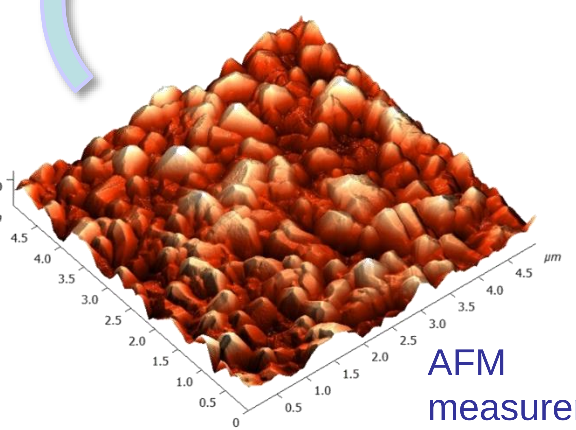

AFM measurement

Height Probability Density Function

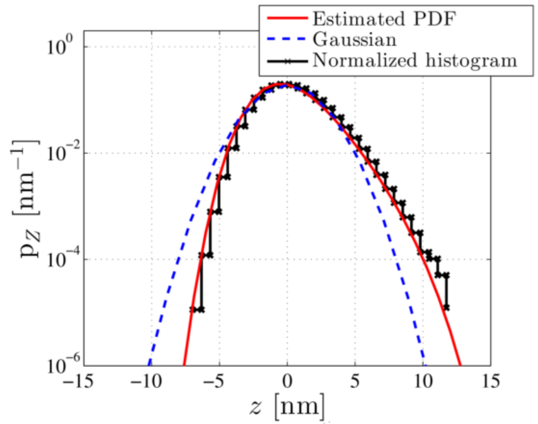

Power spectrum density

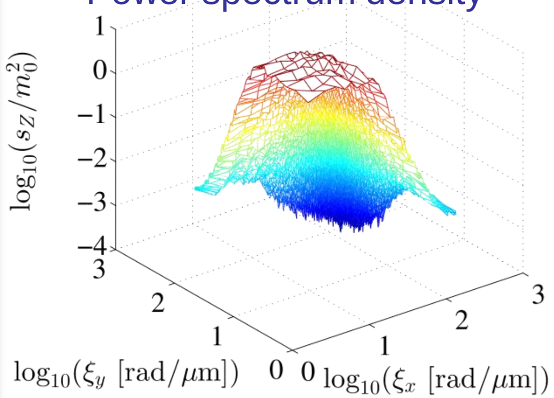

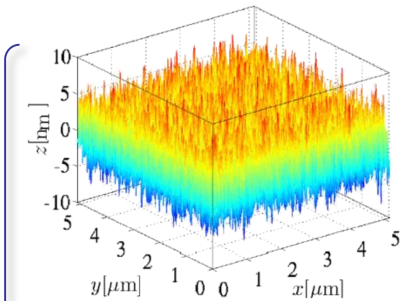

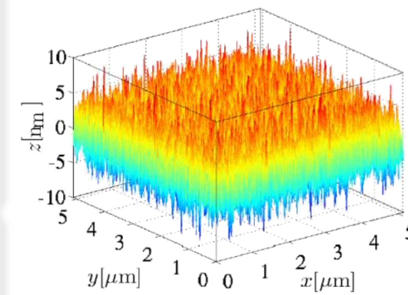

Generated non-Gaussian surface samples

- Stochastic multi-scale model: Evaluate meso-scale surface forces

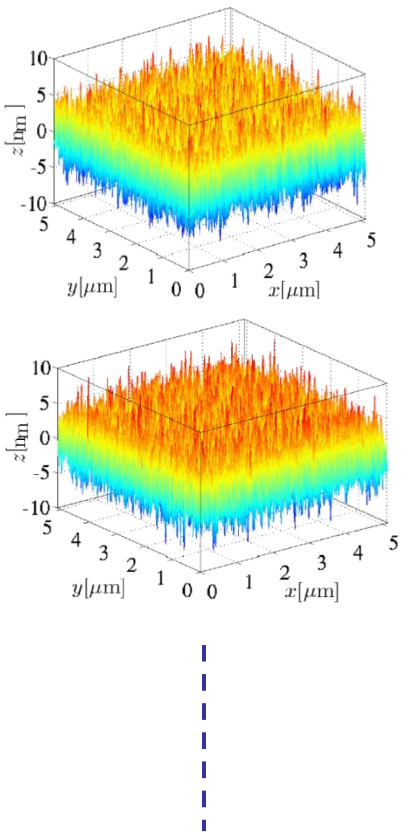

Generated non-Gaussian surface samples

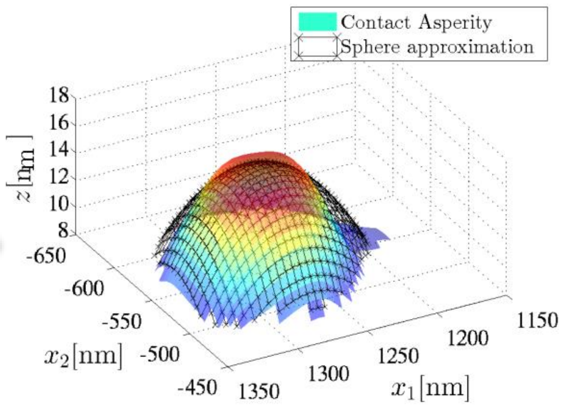

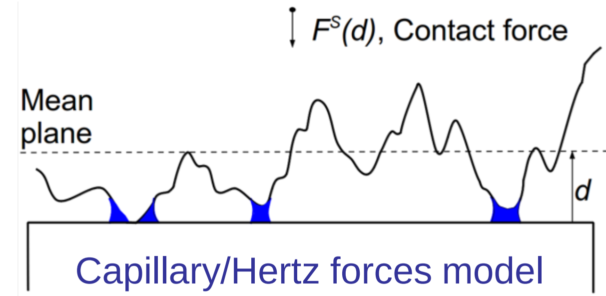

Capillary/Hertz forces model

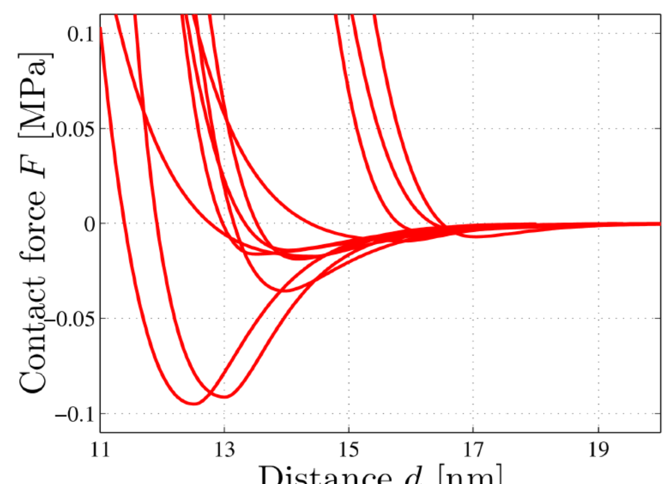

Computed meso-scale adhesive forces

- Stochastic multi-scale model: Stochastic model of meso-scale adhesion forces

Definition of parameter vector $\boldsymbol{v}$

$$\bar{f}(\bar{d}) = \Phi(\bar{d}, \boldsymbol{v})$$

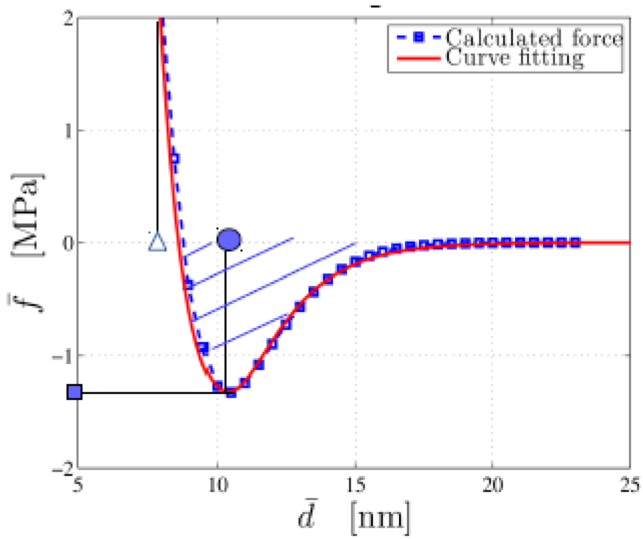

Enforce physical constraints

$$\boldsymbol{v}^{(i)} \rightarrow \boldsymbol{q}^{(i)}$$

Principal component analysis from covariance matrix $[\tilde{R}_Q]$ of vectors $\boldsymbol{q}^{(i)}$

$$\boldsymbol{\eta}^T = (\boldsymbol{q} - \bar{\boldsymbol{q}})^T [A][\lambda]^{-1/2}$$

Polynomial chaos expansion

$$\boldsymbol{\eta}^{\mathrm{PC}} = \sum c_\alpha \Psi_\alpha(\boldsymbol{\xi})$$

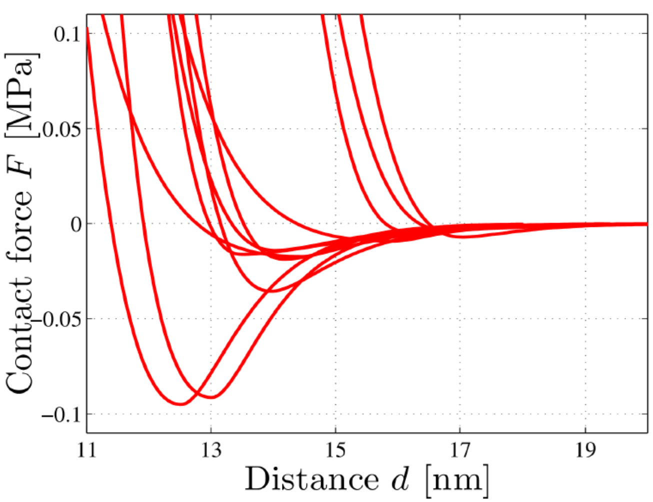

Computed meso-scale adhesive forces

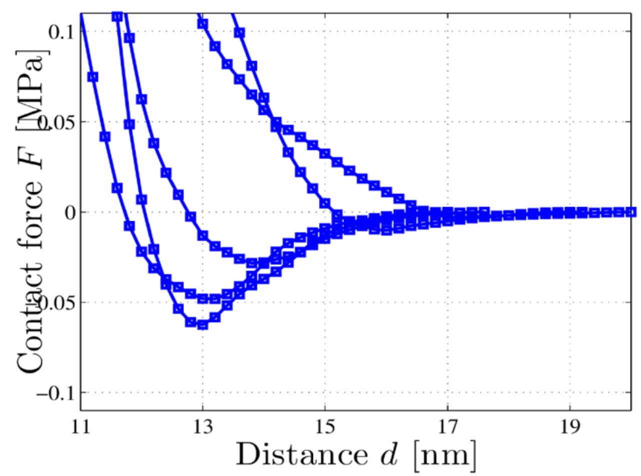

Generated adhesive forces

- Stochastic multi-scale model: Stochastic MEMS stiction analyzes

Stochastic finite elements (random contact law variable)

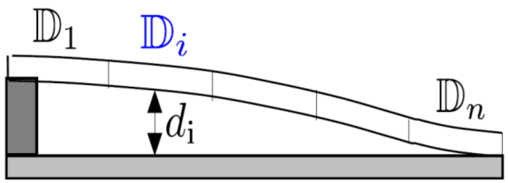

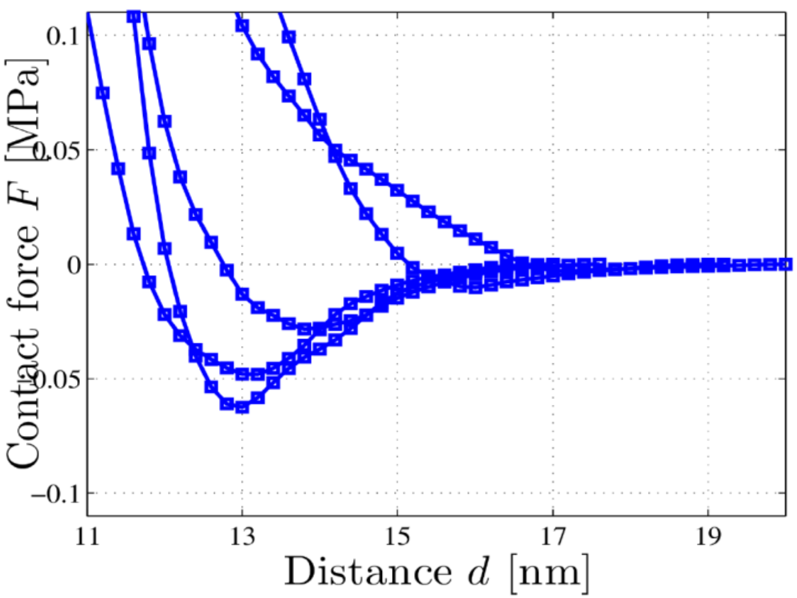

Generated meso-scale adhesive forces

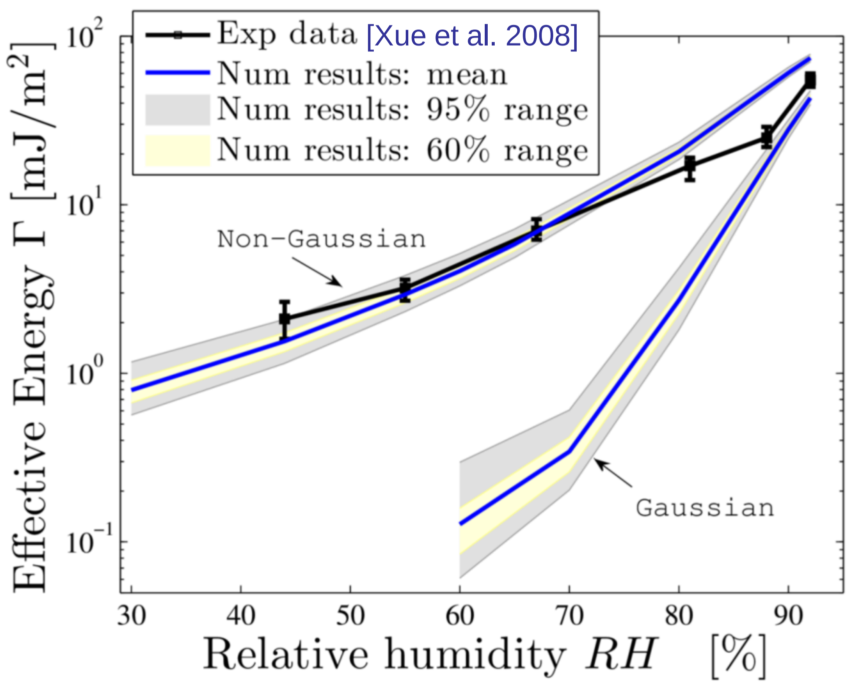

Stiction risk

Stochastic Multi-Scale Model to Predict MEMS Stiction

- Application to robust design
  - Determination of probabilistic meso-scale properties
  - Propagate uncertainties to higher scale
  - Vibro-meter sensors:
    - Uncertainties in stiction risk

- 3SMVIB MNT.ERA-NET project
  - Open-Engineering, V2i, ULiège (Belgium)
  - Polit. Warszawska (Poland)
  - IMT, Univ. Cluj-Napoca (Romania)

- FNRS-FRIA fellowship

- Publications (doi)
  - 10.1109/JMEMS.2018.2797133
  - 10.1016/j.triboint.2016.10.007
  - 10.1007/978-3-319-42228-2_1
  - 10.1016/j.cam.2015.02.022
  - 10.1016/j.triboint.2012.08.003
  - 10.1007/978-1-4614-4436-7_11
  - 10.1109/JMEMS.2011.2153823
  - 10.1063/1.3260248